Marine Fragrance Chemistry: Synthesis, Olfactory Characterisation and Structure-Odour-Relationships of Benzodioxepinone Analogues

A thesis submitted in fulfillment of the requirements for the degree of Doctor of Philosophy

Britta Drevermann

August 2007

Department of Applied Chemistry
RMIT University
Melbourne, Australia

Declaration

I certify that except where due acknowledgement has been made, the work is that of the author alone; the work has not been submitted previously, in whole or in part, to qualify for any other academic award; the content of the thesis is the result of work which has been carried out since the official commencement date of the approved research program; and, any editorial work, paid or unpaid, carried out by a third party is acknowledged.

Britta Drevermann

"…kein Atom ist ohne Leben, das heiβt, in jedem wohnt ein von Mir hineingelegter Geist, welcher von dort an seine Rundreise antreten muβ, um einst zu Mir zurückgelangen zu können mit dem Bewuβtsein seiner göttlichen Abkunft."

-Gottfried Mayerhofer

"Where we are going and why it smells the way it does."[1]

---

[1] Robbins, T. *Jitterbug Perfume*, Bantam Books, New York, **2003**, p 320.

Publications

Drevermann, B.; Lingham, A.; Hügel, H.; Marriott, P. J. "Microwave assisted synthesis of the fragrant compound Calone 1951$^{®}$", *Tetrahedron Letters,* **2005**, *46*, 39.

Drevermann, B.; Lingham, A. R.; Hugel, H. M.; Marriott, P. J. "Synthesis and Qualitative Olfactory Evaluation of Benzodioxepine Analogues", *Helvetica Chimica Acta,* **2007**, *90*, 854.

Drevermann, B. Lingham, A.; Hügel, H. M.; Marriott, P. J. "Synthesis of Benzodioxepinone Analogues *via* a Novel Synthetic Route with Qualitative Olfactory Evaluation", *Helvetica Chimica Acta,* **2007**, *90*, 1006.

Calone 1951® (7-methyl-2*H*-1,5-benzodioxepin-3(4*H*)-one) is renowned in the fragrance industry for its distinct marine odour and offers an interesting molecular framework for structure-odour-relationship (SOR) research. Limited olfactory reports on 7-membered benzodioxepine analogues with modification influenced by functionality, polarity, and ring size, prompted us to construct a range of aromatic and C-3 substituted structures for olfactory evaluation. Incorporation of a diverse range of functionality contributes valuable information on the molecular aspects that determine the archetypal marine character of Calone 1951®. Here we present the preparation of Calone 1951® analogues including spectroscopic and olfactory details to contribute to the sparse marine fragrance arena. In these studies pertaining to the odour properties of benzodioxepinone systems, we considered the modification of substitution and functionality on the aromatic ring in the context of qualitative olfactory analysis.

Application of the patented Williamson and Dieckmann reaction pathways resulted in construction of the benzodioxepinone molecule. Preparation of aryl-substituted benzodioxepinones required introduction of an alternate broadly applicable synthetic pathway due to the diverse nature of the introduced substituents. Limitations of the patented approach led to incorporation of a simple but novel methodology applied to the same range of substituted catechol reagents for synthesis of the benzodioxepinone skeleton and an overview of comparable yields. Single-step mechanisms were also successfully applied to contribute to the repertoire of benzodioxepin(on)e structures prepared for olfactory analysis.

Semi-empirical models of the synthesised data set were generated and evaluated in light of previous research undertaken by Archer and Claret and related to the olfactory characteristics of each compound. Evaluation of the models with corresponding olfactory information revealed that functionality and ring size contribute significantly to the conformation adopted by the benzodioxepinone species and therefore the olfactory character of the molecule.

It is evident from our observations that aromatic ring substitution and functional alteration of the cyclic ketone modifies the perceived odour of Calone 1951®. Structural modification overall led to a decrease in odour potency. The presence of the aromatic methyl substituent in Calone 1951® reinforces, but is not critical for, the marine tonality. Modification of the ketone of Calone 1951® led to significant deviation in character from the prototypical marine odour.

Table of Contents

1D	Primary dimension
2D	Secondary dimension
ADP	Adenosine diphosphate
AEDA	Aroma Extraction Dilution Analysis
AM1	Austin Model 1
AR	Analytical reagent
ATP	Adenosine triphosphate
CAN	Ceric ammonium nitrate
Camp	Adenosine 3'5'-monophosphate
Charm	Combined Hedonic Aroma Response
CNS	Central nervous system
COSY	Correlated spectroscopy
DEPT	Distortionless enhancement by polarization transfer
DHP	Dihydropyran
DIAD	Diisopropyl azodicarboxylate
DMA	N,N-Dimethylacetamide
DMAP	4-Dimethylaminopyridine
DME	Dimethoxyethane
DMF	N,N-Dimethyl formamide
DMSO	Dimethyl sulphoxide
ED	Electron-donating
EDG	Electron-donating group
EEG	Electroencephalography
EIC	Extracted ion chromatogram
EtOH	Ethanol
EW	Electron-withdrawing
EWG	Electron-withdrawing group
FID	Flame ionization detector
FT-IR	Fourier transform infrared spectroscopy
GC	Gas chromatography
GCxGC	Comprehensive two-dimensional gas chromatography
GC-MS	Gas chromatography-mass spectrometry
GC-O	Gas chromatography-olfactometry
GDP	Guanosine diphosphate
GPCR	G-protein coupled receptor
GTP	Guanosine triphosphate
HMBC	Heteronuclear multiple bond correlation
HMQC	Heteronuclear multiple quantum coherence
HOMO	Highest occupied molecular orbital
HPLC	High performance liquid chromatography
HRESI	High resolution-electrospray ionization spectrometry
HS	Headspace
IBX	*o*-Iodoxy-benzoic acid
IETS	Inelastic electron tunneling spectroscopy
IP_3	Inositol 1,4,5-triphosphate
IR	Infrared
JND	Just noticeable difference
KOtBu	Potassium t-butoxide
LMCS	Longitudinally modulating cryogenic system
LR	Lawesson's reagent
LUMO	Lowest unoccupied molecular orbital
MDGC	Multidimensional gas chromatography
MR	Modulation ratio
NDDO	Neglect of Diatomic Differential Overlap
NMR	Nuclear magnetic resonance

OAV	Odour activity value
OB	Olfactory bulb
OBPs	Odourant-binding proteins
OE	Olfactory epithelium
OR	Olfactory receptor
ORN	Olfactory receptor neuron
PES	Potential energy surfaces
PFG	Profile functional group
PM	Modulation period
PM3	Parameterisation Method 3
POC	Primary olfactory cortex
QM	Quantum mechanical
QMS	Quadrupole mass spectrometry
RCM	Ring closing metathesis
RI	Retention index
SAR	Structure-activity-relationship
SE	Semi-empirical
SIM	Selected ion monitoring
SOR	Structure-odour-relationship
SPME	Solid-phase microextraction
TEA	Triethylamine
THF	Tetrahydrofuran
THP	Tetrahydropyran
TIC	Total ion chromatogram
TMS	Trimethylsilyl
TOFMS	Time-of-flight mass spectrometry

1 Introduction

1.1 Preamble

Monell Chemical Senses Centre in Philadelphia collected and analysed air samples from Ground Zero following reports that a "weird" odour lingered in the aftermath of the September 11 terrorist attack on the World Trade Centre [1]. It was thought that if the odour, containing acids, aldehydes, aromatic hydrocarbons (benzene and styrene), mercaptans, quaiacol and diethyl phthalate, could be re-created it could provide some therapeutic use for those psychologically attached to the events of that date [1].

Recognition of odours and appreciation of fragrances began in biblical times. At present we are both wittingly and unwittingly bombarded by olfactory stimulation on a daily basis. This olfactory prevalence means developed comprehension of odour activity would have a desirable impact on many diverse industries and applications. There exist the apparent, macro-market trades such as commercial perfumery, domestic products and personal hygiene, but also more obscure areas such as eco-friendly pest control and psychotherapy. For example, the cabbage looper moth's *Trichoplusia ni* mating was completely disrupted by the use of the sex-pheromone *cis*-7-dodecenyl acetate in evaporators in fields infested with the moth [2]. The Oriental fruit fly, *Dacus dorsalis* has been eradicated from numerous islands in the Pacific ocean by controlled distribution of a poison alongside a powerful odourous attractant (methyl eugenol) to the male species [2]. As well as mating rituals, many other natural, ecological interactions are dependent on smell; the salmon spawning ritual involves swimming to select waters that they locate by ancestral olfactory triggers [3]. To suit the magnitude of diverse sensory requirements present among species, the olfactory system has evolved to provide a huge array of olfactory adaptations; such as the frog which features both an 'aquatic nose' and an 'air nose' for its survival [4]. Reports speculate that communication between humans may also involve "subliminal" communications via odours and that "supraliminal" odour detection may be linked to schizophrenia [2]. It is now known that activation of cortical regions of a schizophrenic experiencing an odour stimulus is impaired which results in mis-recognition and sometimes inverted hedonic judgements [5].

Scientific research of olfaction encompasses many areas including physiology, genetics, biochemistry/molecular biology, chemistry and psychology (Table 1.1). Considering they all strongly overlap, one may argue that a complete understanding will never be achieved until we learn to successfully marry these broad disciplines. To understand one area, it must be placed in perspective of the broader overview of olfaction. For this reason, the research presented here is based on fragrance chemistry (shown in bold), however psychology, physiology, biochemistry and genetic principles must be considered for the properties of fragrance chemistry to be placed into context.

Table 1.1 Overview of scientific contribution to olfactory research

Information	Physiology	Discipline
Electrical	Olfactory cortex	Psychology Physiology
	Olfactory bulb	Biochemistry
Chemical	Olfactory reception	Genetics Chemistry

Studies in olfactory chemistry alone involve many different structural aspects, namely, functional groups, electron-topological investigations (polarity, hydrophobicity, dipole moments), flexibility (rotation, vibration), morphology (shape, steric bulk), dynamics (kinetics) and stereochemistry. Odour concentration is related to physicochemical parameters such as volatility, vapour pressure and partition coefficient.

Odour recognition associated with nostalgia can be extremely powerful and precise. Interestingly, in contrast, olfactory association involving specific sniff identification with apposite cues can leave a subject completely misguided by a strong placebo effect, resulting in misleading olfactory identification [6]. Higher eukaryotes are mobile evidence of the evolution and subsequent conservation of specific signalling pathways that make up the effectively functional olfactory system [7]. The discriminatory abilities of the mammalian olfactory system are vast. The overall perception of an odour can involve receptor sites interacting with different areas of the same odour molecule, analogous to a musical chord played on an instrument to create a sound [8]. A prime example of differences in odour detection within the mammalian species: at low concentrations Androstenone, a pig pheromone, has a mild pleasant odour according to reported human

detection; others specified a urinous odour and others demonstrated specific anosmia to this compound [9].

Perhaps the *Homo sapien* sense of smell has not only evolved but also devolved in some respects considering that evolution of olfaction has diverged from smell for purposes of survival, to smell motivated by attraction and satiety. In either case it has maintained itself as a highly refined uniquely designed detection system that humans have been privileged enough to maintain since the original era.

1.2   The Olfactory System

The olfactory system consists of three main structures: the olfactory epithelium (OE), the olfactory bulb (OB), and the primary olfactory (piriform) cortex (POC) outlined in Figure 1.1. Olfactory perception results in a composite response:

1. Odourants dynamically interact with receptors (ORs) of the OE, this chemical interaction activates the OR
2. Activated OR cells then transmit a signal to the glomeruli of the OB via nerve fibres
3. The OB processes these signals and relays them toward the higher cortical regions (POC) for terminal processing
4. Cortical processing results in perception of the odourant as an odour.

1.2.1   Olfactory Gene Expression and Architecture
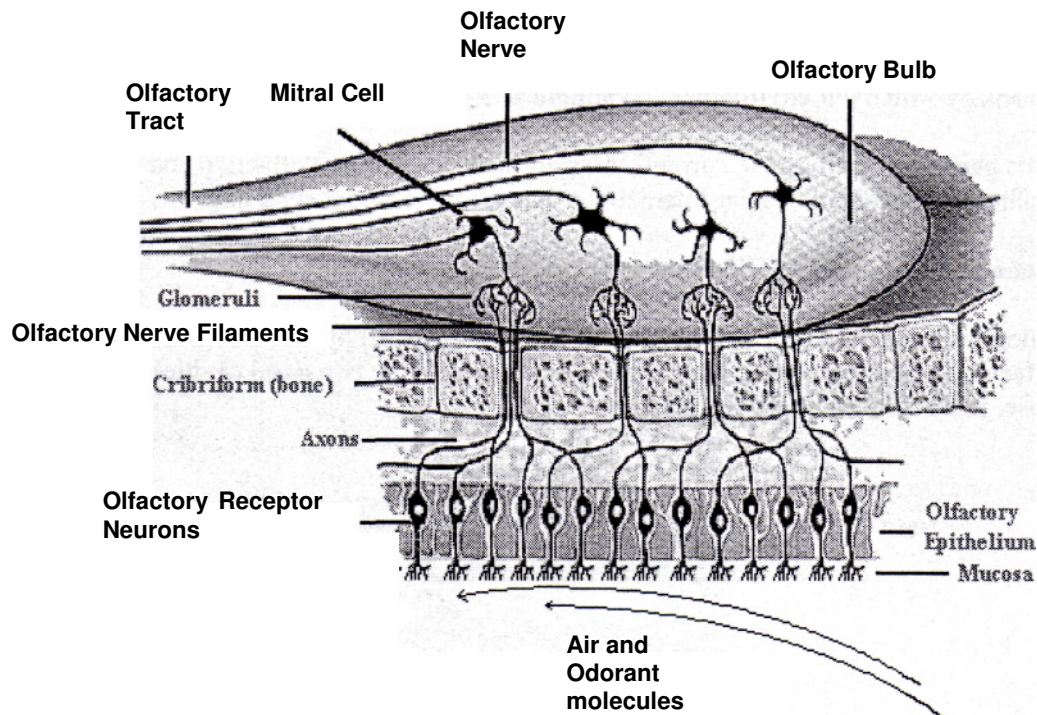
Figure 1.1 Overview of olfactory topography [8]

The human olfactory receptor gene repertoire contributes ~3% to the mammalian genome, which consists of around 1000 olfactory genes [10]. Of these 60% are non-expressed (pseudogenes) [10]. High sensitivity is maintained through the nature of gene expression, whereby one olfactory receptor neuron (ORN) expresses one olfactory receptor (OR) type per cell [11]. A mere 1% of ORs have been identified with specific odourant-binding capabilities through *in vitro* gene expression [7].

In 1950 Adrian confirmed that electrical activity was involved with the odour stimulus response pathway [12]. Binding of an odourant to the receptor cell triggers depolarisation of the membrane that involves cation/anion gradients across the axonal cell surface to produce electrical transmission down the length of the neuron. This signal carries all the information generated from the receptor-odourant complex. Depolarisation results from a change in electrochemical gradient across a cell membrane, known as an action potential. Stimulation of an action potential occurs when the voltage across the cell membrane increases to about –45mV from a normal latent voltage of about –65mV [13]. This is due to the temporal opening of ion channels along the lateral length of the neuron causing subsequent cation influx. A synapse is a co-junction of the dendritic end of one neuron onto a target area, usually a second neuron. Neurotransmitters are released at the

synapse of a neuron, which communicates the electrical signal via chemical means to the target. Feedback cycles between neuron excitation and inhibition cause oscillations in the OB. ORNs responsible for transmission of the electrical olfactory information consist of a terminal receptor site, which detects the odourant stimulus, and an unbranched neuronal stem (axon), which connects the receptor to a processing site known as the OB [14]. The olfactory bulb is an intermediate processing unit prior to emotional and psychological perception by the primary olfactory cortex in the brain [9]. Activation of defined cortices in the brain from transmission of the signal received from the OB can then be detected and visualised by electroencephalography (EEG) in milliseconds [15]. This allows frequency range traces to be analysed [16], along with latent periods, sequence and span of activations [17]. This signal carries the information that will be interpreted by explicit brain cortices as specific intensity, duration and quality of an odour stimulus [18].

In *Homo sapien* olfactory systems millions of ORNs are converging onto thousands of select glomeruli [7], in contrast with rabbits featuring 26 000 ORNs projecting onto 200 glomeruli [8].

Coordination of the bulb ensures a 1000:1 convergence of neurons to mitral cells, which means a large percentage of the signal is redundant. Signal dissipation ensures there is complete absence of one signal before the next glomerular input occurs. However cumulation and integration of many signals results in the high sensitivity exhibited by the system [7]. Relay of this condensed information to higher cortical regions occurs via the lateral olfactory tract, which suggests that odourant stimulation does involve a negative feedback system based on input to the OB [19].

1.2.1.1   The Olfactory Bulb (OB)

The human OB surface physiologically appears as two bulb halves (Figure 1.2) with medial and lateral surfaces that mirror each other [20]. This is termed "bilateral symmetry", where axons of ORNs that express the same receptor are represented similarly on both bulb surface halves [20]. Glomeruli contribute significantly to data processing of olfactory information [21]. Mammalian OBs typically possess around 2500 glomeruli, which are specialised neuropil structures, capable of independent function [20].
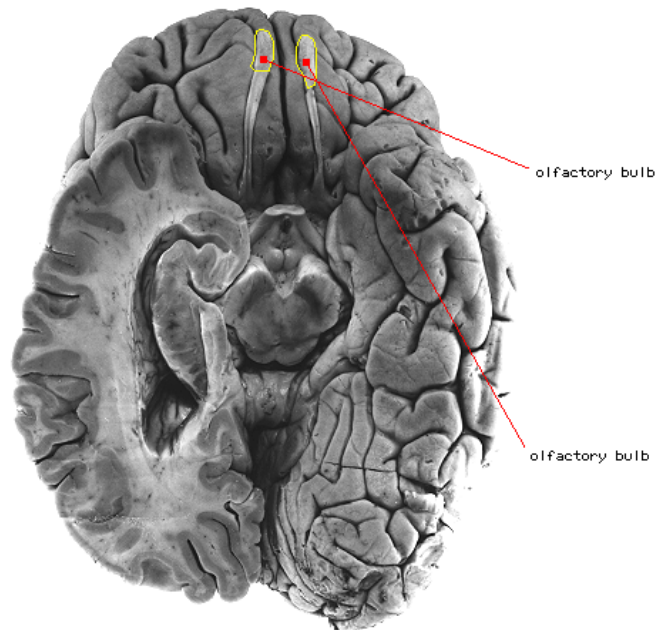
Figure 1.2 The two replica bulb halves which make up the olfactory bulb [22]

Glomeruli modules are the key structural and functional units in odour processing which refine the relayed odour information, enabling mammalian olfactory systems to detect low concentrations of odourants in the environment [23]. Schoenfeld and co-workers have shown that there are intrabulbar pathways associating the medially and laterally related regions of glomeruli on the OB surface [24]. Amplification and refinement occur at both reception and bulb processing levels [25]. Negative feedback and lateral inhibition are also programmed into the olfactory bulb circuitry, which enables modulation [26] or complete stagnation of the signal [27].

Olfaction is a detection mechanism that processes chemical data (odour stimuli) via an "odour image" on neuronal spaces [28]. The OR component of ORNs are dispersed within each of one of four dorsal-ventral [10] expression zones (quadrants) within the OE [29]. These activity patterns, also termed an odour image, odotopic map, or sensory response map, across the bulbar surface are created by distinct but overlapping individual glomerulus unit activation [30] [31]. The response of each region is highly specific: each olfactory glomerulus is dedicated to information input from one class of olfactory receptor [9]. Location of the corresponding glomerular targets involves arrangement based on "activity-dependence" or "chemoaffinity" [32], which results in spatiotemporal and medial/lateral surface distribution symmetry [33]. The synapsed distribution is highly conserved [34] and therefore the activity pattern is precisely reproducible for each odourant [35].
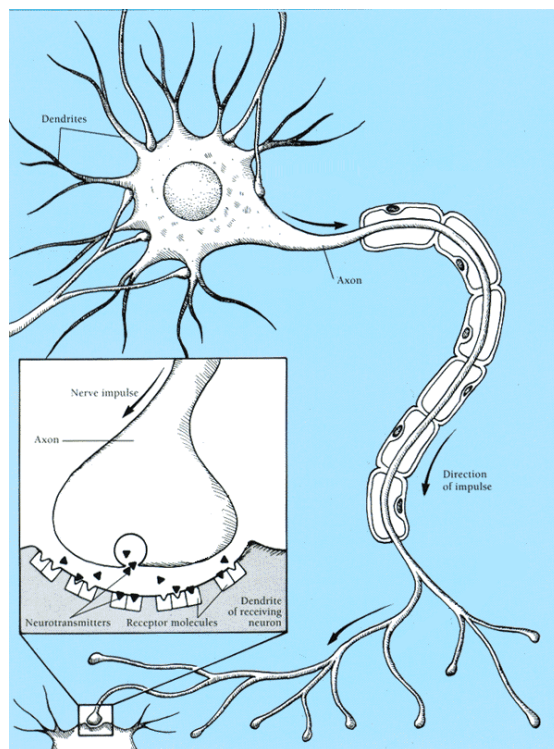
Figure 1.3 Structure of a neuron [36]

Typical structure of a neuron is shown in Figure 1.3. ORNs whose afferents (neurons that transport signal towards the central nervous system) converge to a local region of glomeruli of the intermediary OB are simultaneously activated and express the same putative OR gene [32]. The synchronisation of ORNs ensures assimilation and coherency of the axonal information conferred onto glomeruli of the OB. In addition to their primary role in olfactory transduction, ORs appear to have a role in axon targeting [37].

Data collected by Bozza and Kauer reveals a relationship between local activation on the OB and the molecular structure of odourants. Each odourant stimulated a specific spatially distributed region of the OE [14] [38]. Bozza and Kauer also found that not only does odourant detection ability vary between species but also within a mammalian species: some mice ORN activation could discriminate among molecules that varied only in carbon chain length or one functional group, whereas others could not [14]. However the structural organization of mammalian OBs and the associated response patterns are akin within the mammalian group [14]. Similar pattern recognition occurs in visual (retinotopic maps) and somatosensory/touch (somatotopic maps) systems.

Whether the ability of the mammalian olfactory system to distinguish isomers such as enantiomers is directly correlated to the discrete spatial distribution of the activation

pattern on the OB surface for individual isomers is as yet unknown [39]. Rat olfactory systems are able to differentiate some isomeric pairs beyond human olfactory capabilities [40]. Studies performed by numerous research groups have shown that glomeruli activity maps are concordant with physiochemical odour recognition in rats [7].

Odour intensity prototypes have been developed by recording glomeruli activity from incremental concentration increases of specific odours. The number of receptors activated increases with increasing concentration of odourant [15]. It was confirmed that additional glomeruli activation results in an altered activity pattern, which suggests corresponding changes in perceived odour character with an increase in odourant concentration [7], most likely from alterations in frequency and/or amplitude of the OR signal detected by the bulb surface synapses [41].

1.2.2   Odour Detection at the Olfactory Epithelium

The macroscopic level of odour reception involves protruding hair-like extensions known as cilia protected by a mucous layer spanning the OE. These cilia provide a large surface area required for odour detection. These nasal passage cilia are extensions from the apical end of ORN dendritic terminals [10]. Each dendrite contains 20-30 cilia extensions that house the ORs on the olfactory epithelium [7]. These ORNs extend to the central nervous system and synapse on olfactory cortical regions for processing [7]. The transient nature of cilia protrusion from the mucous layer means at any one time some receptors are easily accessible to odour molecule binding and others are inaccessible due to immersion [2]. This is evidently a physical barrier and not due to response specificity [2]. Odourant-binding-proteins (OBPs) are confirmed to assist in docking of the odour molecule to the binding pocket of the receptor site of the ORN. This may occur via either of two means. Active transport would involve the OBPs directly escorting the odour molecules through the mucous, which often occurs against a concentration gradient [42]. This would also mean that the solubilisation capabilities of the odourant in the mucous layer would have no influence on its transport and detection. Passive transport is a result of the concentration gradient, whereby the odourant moves by diffusion. In the latter case OBPs would indirectly assist in transport by influencing the gradient and the solubility of the odourant in the mucosa.

OBPs are also able to discriminate between odour molecules and agents that pose a toxic threat, hence establishing a protective barrier at the primal olfactory stage [43].

Consequently they also have the capacity to assist in lysing to destroy captured microbes or chemicals, which may otherwise result in infection [7].

OBPs may assist in affinity of odourant binding and directional discrimination associated with binding. Odourant binding affinity contributes to the detected potency of an odourant, whereas coordination of an odourant molecule in the receptor site determines what molecular features emanate the properties of the odour perceived. Briand and co-workers discovered that odourants exhibiting a potent sensory effect had low binding affinities to OBPs, whereas aldehydes and large fatty acids with humble odour potency had high binding affinities [44].

1.2.3   Secondary Messenger Pathways

The presence of protein molecules in olfactory receptors and their ligand-binding properties was realised around 1970 [45]. Lancet and colleagues suggested that a G-protein coupling system was involved and through odour stimulation experiments also identified G-protein activated adenylate cyclase in olfactory cilia [46]. In the early 1990s Buck and Axel officially confirmed that olfactory odour receptors were part of the G-protein coupled receptor superfamily [47]. It is now known that detection of odourants is mediated by ~1000 different G protein-coupled odourant receptors that are encoded by a multigene family [47]. ORs possess the same type of G-protein coupled neurotransmitter receptors as for a mammalian immune response, alluding to the existence of olfactory agonists and antagonists. More recently (2006) Buck, in conjunction with Liberles [48], have discovered genes in humans, mice and fish encoding receptors for 'trace-amine associated receptors' (TAARs). These receptors, as their name implies, detect volatile amines, not all of which possess an odour, however all have been shown to activate these TAAR receptors. Liberles and Buck also postulated that some receptors of the OE could be pheromone receptors based on their discovery that not all ORs possess a G-protein system.

The superfamily of G-protein coupled receptor proteins (GPCRs) includes receptors for many neurotransmitters, including dopamine, serotonin and histamine, as well as the opsins in photoreceptors [30]. Common to the GPCR class, vertebrate olfactory GPCRs also adopt a seven α-helical transmembrane conformation (Figure 1.4). The 7 α-helices featuring extracellular loops protrude to varying degrees from the cell wall membrane [10]. These loops coordinate to form the binding pocket for the odour molecule [10].
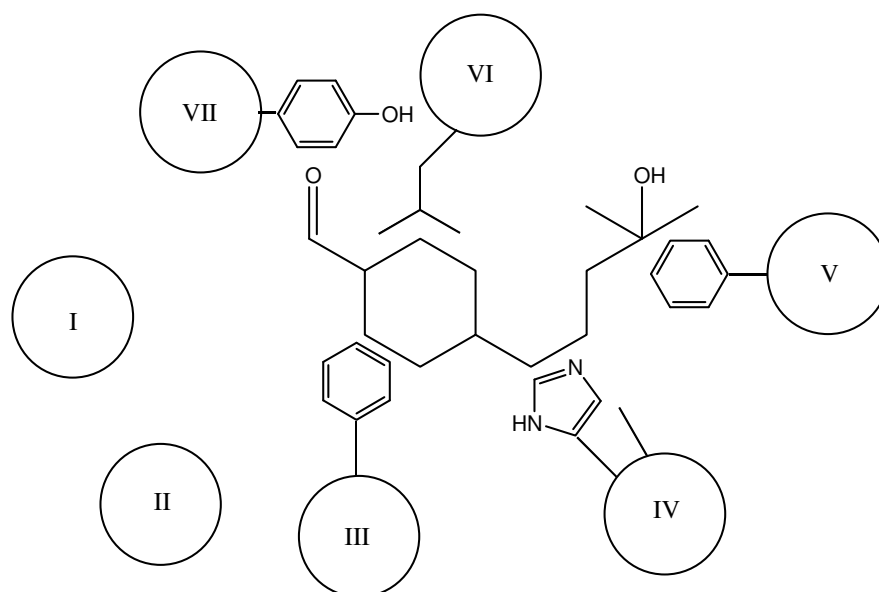
Figure 1.4 Representation of the interaction of an odour molecule with a transmembrane olfactory receptor protein. The 7 α-helices of the protein labelled I-VII, with binding functional groups shown [49]

Olfactory receptors are in the metabotropic receptor class, as opposed to the ionotropic class that are coupled directly to an ion channel. Odourant disengaging and subsequent orientation of proteins back to their original state follows a classical negative-feedback cycle. Once activated, the protein arrestin sterically hinders further interaction between the receptor and the G-protein [7]. The duration of odourant perception once the negative-feedback cycle is complete is influenced by factors such as odourant concentration, ORN axonal firing and receptor saturation levels.

The transduction mechanism in which the odour molecule activates an OR involves multiple second messenger pathways [50] and is where physiochemical neuronal signal adaptation is initiated [51]. Incorporation of a secondary messenger cascade rather than simply a secondary messenger molecule ensures augmentation and integration of olfactory information [13]. This integration occurs by a flux; a temporal response recording summation of all receptor site events over a time period [13].

From studies performed on various species it is now widely accepted that receptor activation involves stimulation of a secondary messenger system involving either cAMP and/or inositol 1,4,5-triphosphate (IP$_3$) (Figure 1.5) [52]. Amplification levels of the olfactory detection process enhance specificity, sensitivity and adaptation. The degree of receptor proteins activated by odourant docking influence the number of adenylase cyclase enzyme molecules activated by coupled G-protein α-subunits, which in turn

determine the number of cAMP molecules stimulated by adenylase cyclase. The number of axonal cation channels gated are a result of the cAMP signalling cascade, which is directly related to the amplification level of the action potential, generated [7].
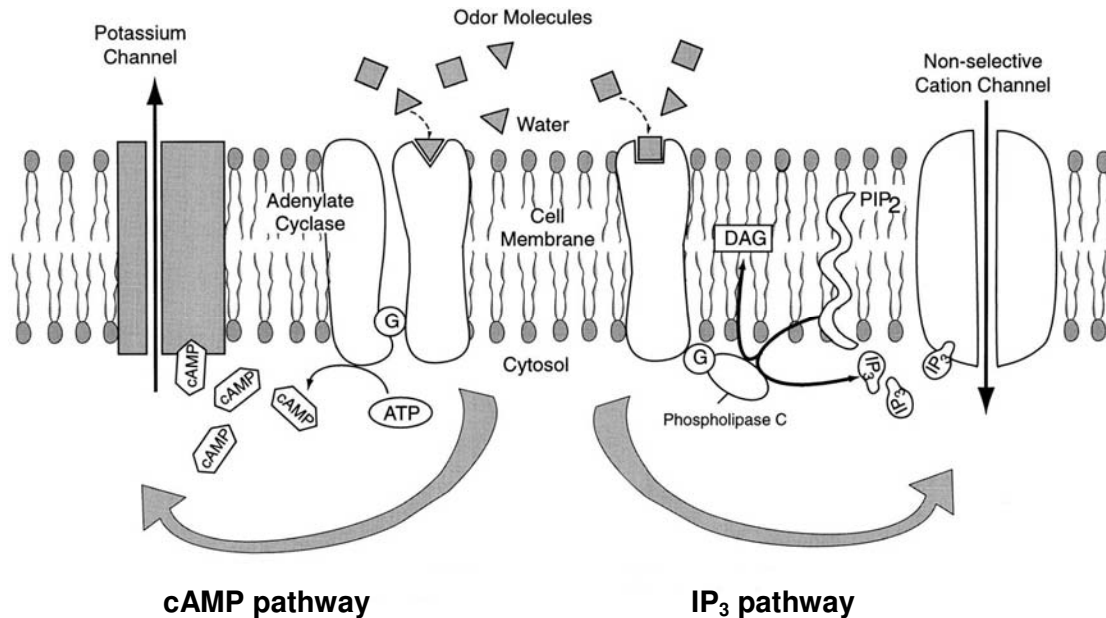
Figure 1.5 Dual olfactory transduction pathways in olfactory receptor neurons (adapted from [53])

The G protein serves as a guanine-nucleotide exchange factor, leading to dissociation and phosphorylation of inactive guanosine diphosphate (GDP) forming active guanosine triphosphate (GTP) [7]. The activation/binding/regeneration cycle of GDP/GTP is analogous to the ADP/ATP energy cycle and both often occur reciprocally in the olfactory system. The guanosine pathway assists the transfer of receptor information in olfactory processes [44]. Active GTP catalyses an enzyme cascade which triggers ion channel transport and hence an action potential along the neuron. The enzyme cascade involves activation of adenylyl cyclase, which catalyses production of adenosine 3'5'-monophosphate (cAMP). cAMP in turn activates the enzyme protein kinase that phosphorylates target proteins into action [7].

The IP$_3$ pathway usually exists as an alternative to the cAMP pathway in biosystems. The overall response is from mediation of the two messenger cascades; when one is dominant the other is subdued dependent on the odourant stimulus [54]. Studies performed by Sanhueza and colleagues on rat ORNs revealed that "bipolar" transduction exists in particular species. "Bipolar" referring to both an excitatory cAMP-mediated current and an inhibitory Ca^{2+}-mediated current observed in the one neuron [55]. Vogl and co-workers

looked specifically at rat olfactory cilia and termed the dual pathway system a demonstration of "functional antagonism" [54].

1.2.4   Odour Reception

Exteroreceptors include mechanoreceptors, chemoreceptors, electromagnetic receptors, photoreceptors, thermoreceptors and pain receptors [3].   Exteroreceptors relay information from the external environment and interoreceptors monitor the body's internal environment [3].   Chemoreceptors are an example of exteroreceptors present in visual, auditory, tactile and olfactory sense regions [3].

Numerous researchers have reported that the human olfactory system is able to detect up to 10 000 odourants [56].   Querying how many odours humans are capable of detecting is comparable to querying the number of colour hues that can be visualised, or attempting to quantify sound combinations.   The signal generated is a function of the odourant-receptor interaction.   The functionalised cavities of an OR enable a vast array of odourants to be perceived and the same ORN can respond to many odour stimuli [14], hence no OR type has been fundamentally partnered with a correspondent active molecular region (odotope) [13].   The signal generated by odour-OR activation is largely attributed to the osmophore, which is usually the polar group of the odourant molecule.   In 1999 Malnic and colleagues were the first to decipher the combinatorial receptor code for odours [9].   Malnic, Hirono, Sato and Buck performed a study using odourant species with strikingly different odours but related structures, aliphatic alcohols and carboxylic acids, which differed structurally in no way other than progressive chain length [9].   Their conclusions were derived using both calcium imaging and single-cell RT-PCR, and demonstrated that one OR recognises multiple odourants and one odourant is recognised by multiple ORs.   In conclusion, the authors have labelled odour reception as a "combinatorial receptor coding scheme" to demonstrate that an odourant will bind and activate a unique combination of receptors, hence having it's own "identity" [9].

The term odotope [57] was allocated to the interactive binding region, the profile region, of an odour molecule [30].   It is still debatable whether the odour gradations, or nuances, we perceive are a result of different odotopes of an odourant detected by ORs, rather than engulfing of the odourant by the receptor site.   In either case hydrophobic regions are more likely to alter molecular conformation to fit the dynamic nature of the receptor site with polar regions remaining more rigid [58].   Taylor and Roberts proposed that a receptor

would bind similar types of odotopes of various odour molecules [7]. This maintains high specificity and the combinatorial character of odour recognition [7].

Sánchez-Montañés and fellow researchers employed Fischer analysis for a quantitative measurement of how olfactory reception performance is affected by the "distribution" and "tunings" of partitioned receptive domains of the OE [55]. Evolution resulted in olfactory receptive fields involving non-specific tuning (each neuron responds to a chemical populous) rather than specific tuning (each neuron responds to a single chemical compound) [55]. The authors studied the advantages of high stimulus dimensionality (number of stimulus components) [55]to decipher this phenomenon. Research revealed that the non-specific tuning case provided the best performance. This ensures that the olfactory system is broadly tuned to the environment containing both unique and unfamiliar odourants [55]. Receptors that identify the same chemical features of odours form a class which could make up 0.1-0.5 % of the ORN total [59].

What Firestein terms "broadly tuned receptors" entails receptors that can detect and process a large range of odour molecule structural features [13]. Firestein states that broad tuning and high affinity capabilities are mutually exclusive. Therefore an olfactory receptor's ability to detect a broad range of odourants is partnered with a loss in detection sensitivity and signal resolution [13]. This is compensated by a longer detection period, which complements the time required for perception of an odour. As a contrast vision requires continuous immediate processing [13].

Both odour composition modification and a change in concentration [60] influence receptor activation through the specificity and affinity to which each OR binds to constituent odourants [7]. Physiological odour detection thresholds (10^{-6}-10^{-8} M) were found to be complementary to *in vitro* reconstruct procedures [61]. Calcium imaging performed by Hamma and co-researchers indicates that the detection threshold seems to be the level at which the qualitative characteristics of an odour compound are most archetypal [62]. The most focal ORs detect the primary characteristics of an odour and the non-focal odour qualities are perceived by less sensitive ORs [7]. Specificity of ORN to odourant was higher in humans indicating that the human olfactory system is more refined than other species [63].

1.2.5   Neuronal Activation

Neuronal transmission carries all the quantitative and qualitative information of an odourant stimulus to the brain via the OB. The pulses of information that encode this information are known as spikes. In 1997 Chastrette reported that modulation of spike frequency determines odour stimulus intensity, and noted that spike activation intensity remains constant [64].

Visualisation of neuronal firing on the OB surface reveals a constant resting state firing (white noise) exists that exhibits a "chaotic" nature [65].   Upon polarisation from stimulus activation a specific coordinated pattern dependant on odourant character develops [65]. Each stimulus can influence the next, a type of "conditioning" [65]. These findings are supported by the knowledge that all receptor input onto one glomeruli stems from neurons that express the same receptors [15].

1.3   Fragrance   Chemistry: Structure-Odour-Relationships (SORs)

Overall olfactory recognition is a complex multidimensional sensory system.   The structural influence of a drug on the appropriate receptor determines the pharmacological activity of that compound, termed the structure-activity-relationship (SAR). Likewise, the structure of an odourant molecule contributes to the structure-odour-relationship (SOR), which relates the molecular attributes of an odourant to the physiological sensory response it triggers. Factors that determine whether a molecule qualifies as an odourant and contributing to the dynamics of an odour molecule-receptor site interface include molecular weight, geometry, chirality, flexibility (vibrational frequencies and rotation), and biochemical (enzymatic) influence [66]. Structural features of a receptor site such as electrical charge distribution, chirality and polarity of exposed functional groups ensures remarkable selectivity and discrimination for specific binding [30].

The empirical nature of odour perception remains, however understanding of olfactory processes contributes significantly towards *de novo* design and synthesis of novel fragrant compounds.   Contributions through biophysical, genetic, psychological and synthetic methods have moved SORs beyond mere conceptualisation and enabled structural characteristics of odourants to be correlated with odour modalities. Evolving fragrance

chemistry should be based on prediction rather than chance. Predictability in qualitative and quantitative odourant dimensions enables rationalisation of synthetic design through definitive molecular structural parameters for desirable fragrant properties.

Currently SORs alone are not sufficiently reliable to set a paradigm, however they have proved useful for clarification of odour group trends. Despite the formidable challenge of SOR chemistry, it provides a suitable template approach for odourant classifications. For example ambergris fragrance can often be predicted by triaxial rules (discussed in more detail in 1.3.2 Fragrance Categories: Associative SORs), musks are commonly macrocyclic, and ester functionality has spurred an independent estery class of fragrance.

1.3.1   History of Odour Classification

Lucretius' proposal of 'smooth' and 'hooked' odour molecules was a primitive approach that initiated a chain of events resulting in our current understanding of olfaction [67].

Linnaeus (1756) was one of the first to document systematic classification of odours by apportioning existing odours into 4 categories. Aristotles followed suit and established his own 6, and later Linnaeus published 7 [68]. Lorry (1784-1785) [69]added the ethereal class, followed by a "ephreumatic" addition by von Haller (1763), which then resulted in a 9-category system [70]. Zwaardemaker decided to contribute these same 2 classes to Linnaeus' system (1895, 1925) [71]. Longstanding ambivalence resulted with the number ranging from 9 for Zwaardemaker [71] to 18 for Rimmel (1868) [72] and reaching 45 for Cerbelaud (1951) [73].

Henning (1916, 1924) [74] was the first to go beyond mere classification and integrated odour classes into a practicable model [75]. He proposed an odour classification concept in 1916 involving allocation of six odour types; flowery, fragrant, ethereal, resinous, spicy, burned and putrid at the six points of a hexagonal prism. Allocation of a point in the hexagon was representative of the quality of a fragrance in an attempt to demonstrate the degree to which an odour emanates from each of these odour types. Although a promising facilitator in the direction of qualitative odour classification this model had numerous obvious limitations, its simplicity being the most apparent.

Crocker and Henderson's (1927) 1-8 numerical odour scale ensued, which was linked to four psychological odour modalities: fragrant, acid, burnt and caprylic [76]. Ruzicka

(1920) [77] derived the concept of the profile-functional group (PFG) and Beets (1957, 1964) later extended on this with practical exemplars in which one functional group of an odour molecule determines the binding orientation of the rest of the molecule. This was also dependent to a certain extent on the hydrogen bonding capacity, with surrounding functional groups taking on a more passive role conforming to the overall shape of the molecule. The final profile of the binding transition site of the molecule therefore proves seminal for the odour quality given. Beets did concede during his investigations that the theory was quite rudimentary however he emphasised its potential for future research [78]. Ruzicka and Stoll later demonstrated that large macrocyclic compounds would convey a musk fragrance independent of the functionality present, proving that molecular size can invoke musk character [79].

In the late 1930s Dyson postulated a link between infrared absorption bands from functional groups within a molecule in the normal infrared (IR) frequency range of 1400-3500 cm^{-1}. Unfortunately in further work he struggled to find strong associations [80]. In 1954 Wright [81, 82] proposed a slightly different theory involving characteristic bands in the lower infrared frequency range (50-500 cm^{-1}) and the fingerprint region (below 1000 cm^{-1}) [83]. These bands were expected to correspond for active vibrations, resulting from the whole molecule, not its separate structural components [83]. Two decades later, previous attempts to relate the far IR region below 500 cm^{-1} to odourant properties were declared redundant [83]. Prior to this, loopholes were identified in Wright's theory challenging the validity, so in 1966 he modified his hypothesis to such an extent that verification proved difficult [84]. He exclaimed that "difference frequencies" would also exist whereby two normal infrared vibrational modes are excited in the same molecule at the same time, but these active difference frequencies may not necessarily cause bands in the far-infrared region [83]. Although Wright later iterated that the net effect of odour quality was influenced by both shape and frequency, he failed to explain the strong, distinctive odours of Lewis bases such as H_2S, NH_3 and HCN, which impart no far infrared bands [85]. These propositions remained erroneous and were also incapable of elucidating the difference in odours of some enantiomers that produce the same vibrational fingerprint [86].

Studies by Amoore conducted between 1952-1964 concluded with seven primary odour classifications; ethereal, camphoraceous, musky, floral, minty, pungent and putrid [87]. The latter two were based purely on electronic status rather than molecular size and shape. He elaborated that a narrow receptor site matched ethereal odours, and camphoraceous odours are hemispherical in shape with receptor sites to match [88].

Correspondingly musks are larger and elliptical with large receptors to accommodate [88]. He speculated that strongly electrophilic molecules exhibited a pungent odour, while strongly nucleophilic molecules exhibited a putrid odour (Figure 1.6) [87].

$$S=C=N^-$$

isothiocyanate
pungent

acrimyl isothiocyanate
pungent

α-Ambrinol
putrid
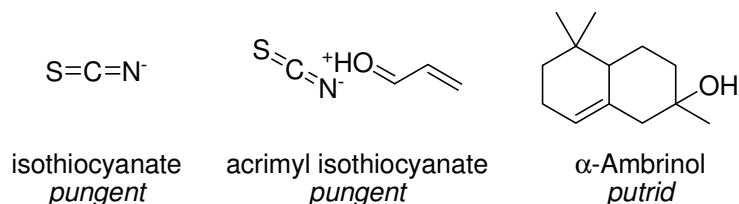
Figure 1.6 Examples of pungent and putrid odourants [89]

Molecular shape was classified as the dominant determinant for minty and floral group odourants [87]. Like others, Amoore's generalised odour group theory failed to explain many small strongly odourous compounds [87]. Amoore's quest to categorise odour becomes tangential, and pungent and putrid are terms more appropriate for taste analysis. Despite this some odourants are distinctively known as pungent such as allyl iso-thiocyanate, a component in mustard oil, and acrimyl iso-thiocyanate [89].

A more recent theory by Mori and Shepherd arose in 1994, known as the "odotope" theory, in which they proposed that select sections of an odour molecule are recognised by the receptor site and are responsible for the odour detected. Mori and Shepherd's "one receptor type fits one odour type" concept has contributed a basis for research however it falls short as a fundamental model due to the equivocal nature of the theory [90].

Turin has been the most recent to propose an olfactory reception theory [91]. His theory differs from those of his predecessors by the introduction of modern spectroscopic techniques. More specifically inelastic electron tunnelling spectroscopy (IETS) is a term for a solid-state vibrational spectroscopy method involving measurement of energy differences between electron energy levels of a compound. Under an applied voltage electron scattering is induced by the atomic partial charges of the molecule being analysed [91]. Turin conceptualised a biological equivalent by applying the theory to electron tunnelling occurring down the backbone of the protein present in the receptor site binding pocket of an olfactory receptor site [91]. The energy differences can be represented by a spectrum produced by algorithmic conversion of IR data, including the far IR region, which provides information on odour character (not intensity) [92]. The algorithm was proposed by Turin based on a linear regression model [92] and derives

vibrational mode frequencies for a pure odourant. Turin proposes each receptor is tuned to a limited range of vibrational modes (frequencies) which the work performed by Firestein and colleagues (1993) supported after patch clamp receptor stimulation tests revealed cells responded differently to application of different combinations of cineole, isoamyl acetate and acetophenone [93]. Application of Turin's algorithm to derive spectra of the three odourants revealed that each odourant has a single characteristic vibrational band [91]. Turin has applied his theory to explain a few long-standing odourant enigmas such as molecules with near-identical shapes and dissimilar odours [91].
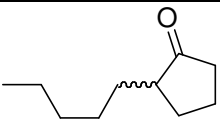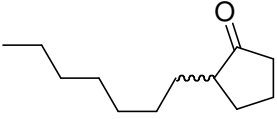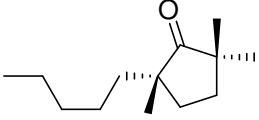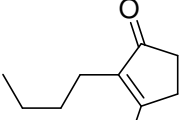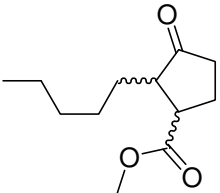
1.3.2   Fragrance Categories: Associative SORs

Coumarin was the first synthetic fragrance compound released on the market in 1866, followed by salicylaldehyde (1876) and vanillin (1876) [94]. Thus synthetic fragrance chemistry was born. In 2004 the top three flavour and fragrance companies by sales volumes, Givaudan (Geneva, Switzerland), International Flavour and Fragrance (IFF) (New York, U.S.A.) and Firmenich (Geneva, Switzerland) reported sales figures of CHF 2680 million (US $ 2171 million), US $ 2033 million and CHF 1976 million (US $ 1601 million), respectively.

Broadly established fragrance classifications of contemporary or traditional origin include floral, fruity, spicy, woody, musky, green, amber and marine.

Succinct coverage of floral odourants is difficult due to the vastness of the category. Jasmine (Table 1.2), rose and muguet (lily-of-the-valley) are the most dominant fragrance modalities. Many floral odourants incorporate terpenoid molecular structure.

Table 1.2 Various jasmines and their odour properties (adapted from [95])

Name	Molecular structure	Odour description
Delphone® (Firmenich)		complex floral, fruity, lactonic undertone
2-Heptylcyclopentanone		fruity, jasmine, slightly herbaceous
Veloutone® (Firmenich)		jasmine, lactonic, fruity
Dihydrojasmone		jasmine
Methyl dihydrojasmonate		fruity, jasmine-like

No component currently isolated from lily-of-the-valley oil from the flowers of the perennial herb (*Convallaria majalis L.*) exhibits the characteristic muguet fragrance of the blossom [96]. Perfumery applications are therefore reliant on utilisation of synthetic varieties. The alcohol/aldehyde sub-category often exhibits floral, green or spicy tonalities. Aldehyde fragrances tend to exhibit a more intense odour than their alcohol counterparts [97].

Likewise, there is also an immense array of ester variety odourants. The ester functionality is often partnered with aldehydes and alcohols to create the fragrant nuances perceived. Smaller structural esters are typically fruity, whilst with increase in molecular size the odour intensity tends to decrease. The contrast in odour character between the nona- and deca-lactone homologues is noteworthy (Figure 1.7).
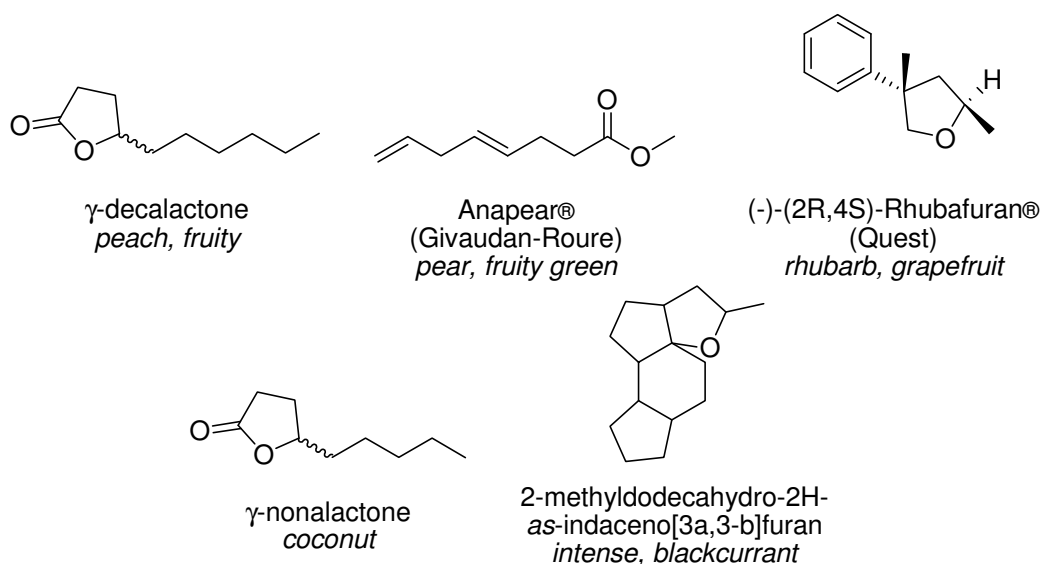
Figure 1.7 Examples of fruity odourants [96]

Structures based on an ionone skeleton often exhibit a violet or woody type character [98]. Ionones are often also typically floral. Carbonyls, olefins and acetate groups also feature commonly in molecules with a woody character (Table 1.3) [99].

Table 1.3 Common ionones and their odour properties (adapted from [95])

Name	Molecular structure	Odour description
α-Ionone		sweet-floral, reminiscent of violets
β-Ionone		reminiscent of cedarwood, violet-like upon dilution
γ-Ionone		violet-like with woody-resinous tonality
α-Irone		responsible for the fragrance of natural orris oil
β-Irone		reminiscent of β-ionone, slightly more intense

Musks are characteristically macrocyclic or polycyclic and often constitute base notes of a fragrance. Some more traditional musks feature nitro groups and benzenoid musks have become a category in their own right. In search of a novel synthetic nitro explosive, Albert Baur stumbled across 2-*tert*-butyl-4-methyl-1,3,5-trinitrobenzene in 1888, which became known as 'Musk Baur' and later developed 'Musk Ketone' in 1894 [98]. Development of musk type odours is shown in Figure 1.8.
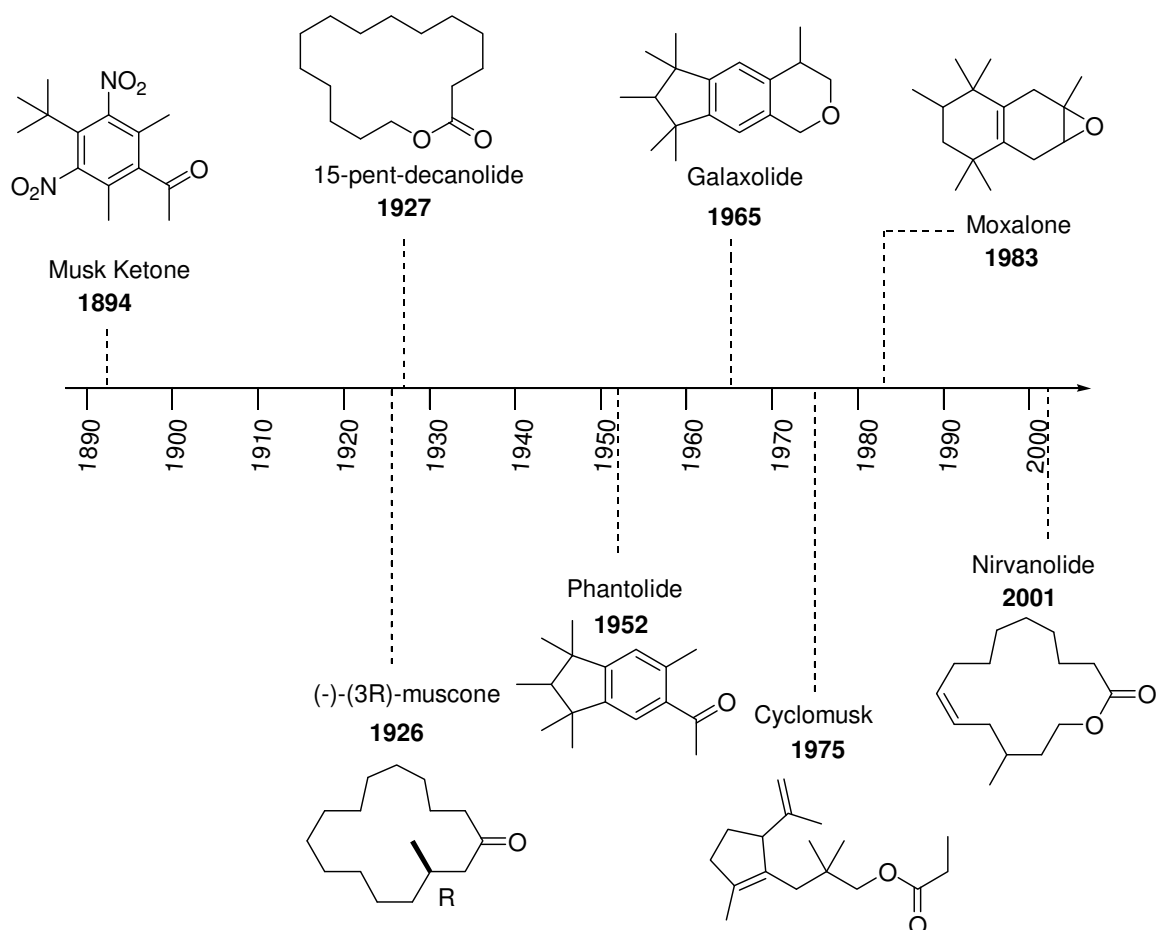
Figure 1.8 Musk odourant chronology [98]

Galbanum oil from *Ferula galbaniflua* and *Ferula rubicaulis* contains constituents that provide its characteristic green odour. Despite existing as minor constituents, (*3E,5Z*)-undeca-1,3,5-triene and 2-methoxy-3-isobutylpyrazine (Galbazine®) subdue their co-substituents due to their low odour thresholds. Green galbanum-type odours (Figure 1.9) typically feature a non-aromatic hydrophobic region, a specifically oriented hydrogen-bond acceptor, and an electron-rich moiety [96].
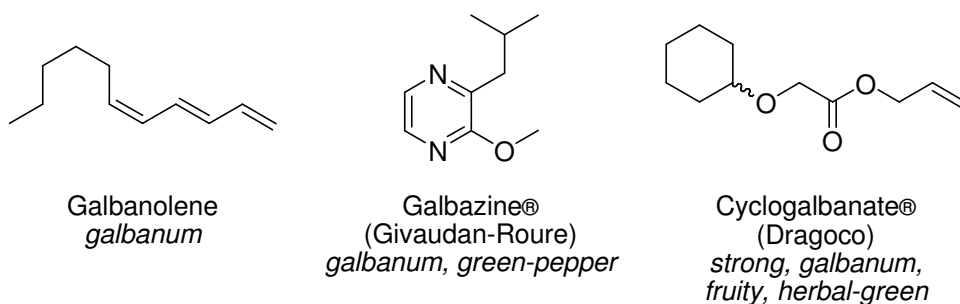
Figure 1.9 Examples of galbanum odourants [96]

The compound released from cut grass, cis-3-hexen-1-ol (leaf alcohol), began the green nascence in the 1960's [100]. Bedoukian discovered that *cis* derivatives tended to be sharper, whereas *trans* equivalents were more fatty in character [101]. Double bonds, alcohols and aldehydes feature prominently in the green category (for example see Figure 1.10).
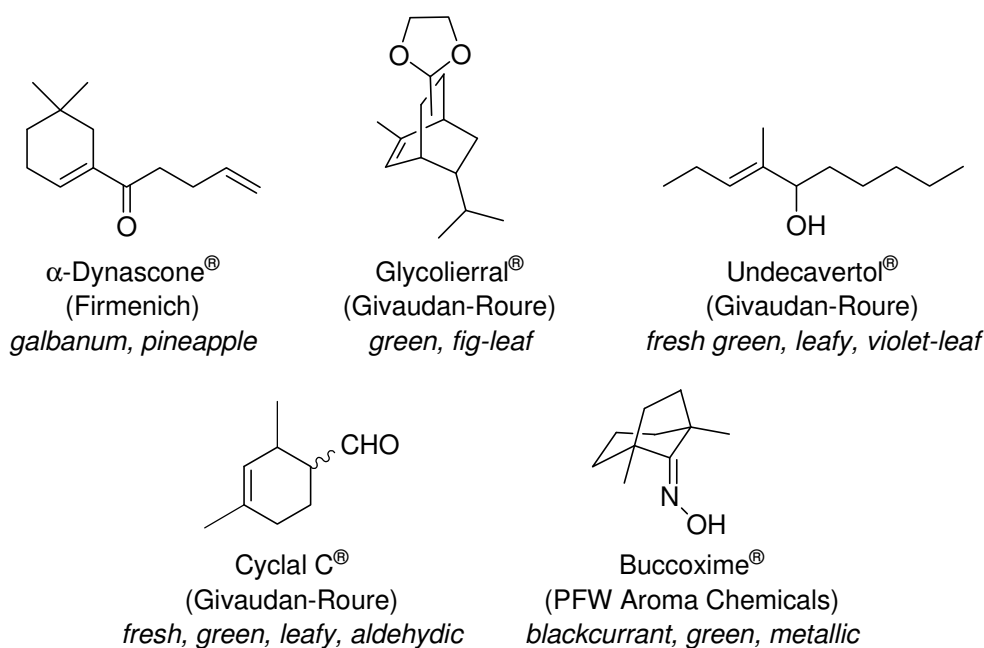
Figure 1.10 Examples of green odourants [94]

Natural ambergris is a metabolic by-product excreted by the sperm whale, *Physeter catodon* (*P. macrocephalus* L.). Photo oxidation and exposure to seawater convert freshly secreted black ambergris to a light grey [95]. This process results in components that give ambergris a discernable pleasant odour. Crude isolated ambergris includes the major components epicoprosterol and odourless triterpene alcohol, ambrein (Figure 1.11) [95].
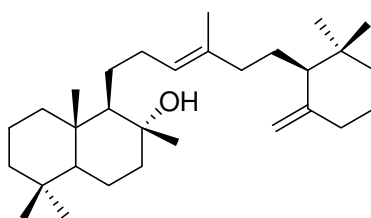
Figure 1.11 Structure of Ambrein, the precursor to ambergris odourants [95]

Further auto- and photo oxidation of the ambrein precursor result in formation of mono-, bi- and tricyclic compounds with oxygen functionality. These compounds exhibit potent ambergris based odour profiles (Figure 1.12) [95].

γ-Dihydroionone
tobacco

2-Methylene-4-(2,2-dimethyl-
6-methylenecyclohexyl)butanal
seawater

α-Ambrinol
moldy, animal, fecal

(+)-(5S, 8R, 9R, 10S)-20desmethyl
-8a, 13-desoxyambreinolide
ambergris
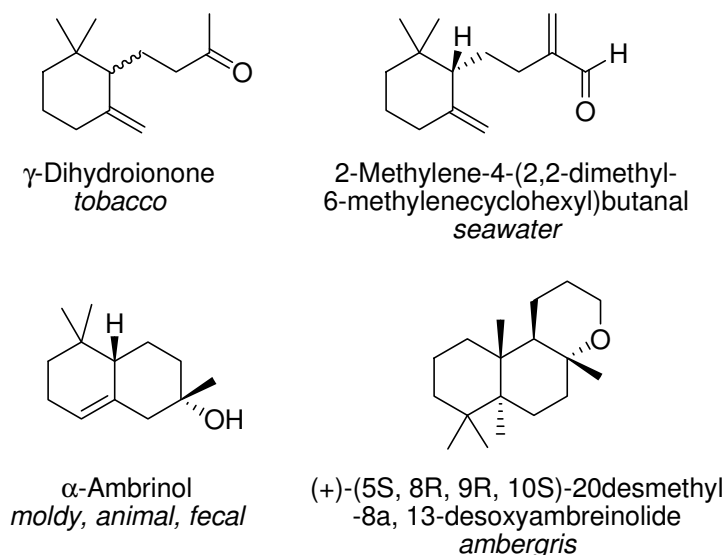
Figure 1.12 Examples of ambergris odourants [95] [8]

The triaxial rule established by Ohloff [102] denotes that molecular structures emanating ambergris fragrance will feature a *trans*-decalin ring system featuring three axial groups in the 1, 2 and 4 positions with one oxygenated functional group (Figure 1.13).

trans-decalin
ambergris

cis-decalin
odourless
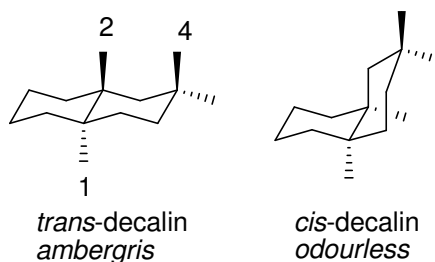
Figure 1.13 Structural representation of Ohloff's "triaxial rule" [100]

Fellow researchers have since discovered an array of SOR exceptions to the precepts discovered by Ohloff. Since the time that Ohloff's theories were prevalent, several new or extended models have been proposed, most taking orbital activity into account, such as Vlad's triangle [103] [104] [105], and Bajgrowicz' CATALYST® model [106].

Resins and resinoids often carry a spicy fragrance. The spicy category can include some herbs such as dill and oreganum alongside the full range of spice extracts such as myrrh, clove, coumarin, cinnamon and black pepper. Selected compounds in this range are illustrated in Figure 1.14.

Piperine
pepper

Lindestrene
myrrh, balsamic

Coumarin
coumarin

Eugenol
clove

Cinnamaldehyde
cinnamon
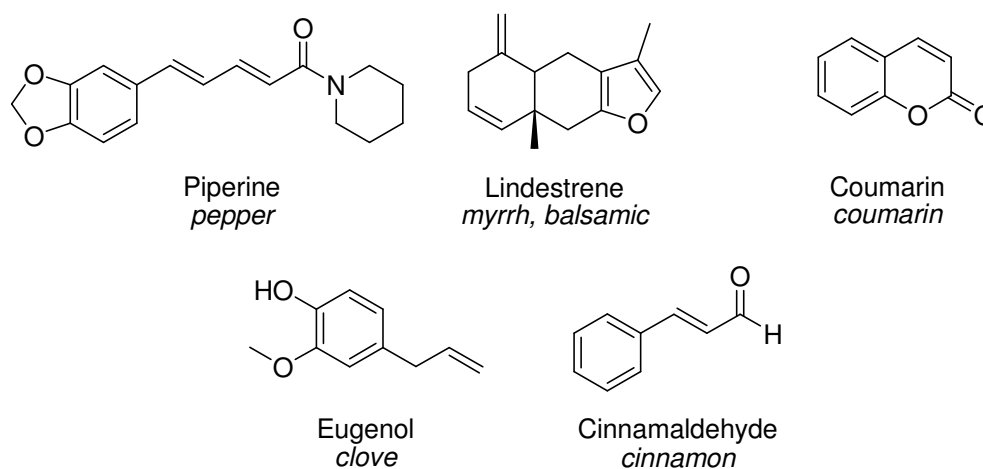
Figure 1.14 Examples of spicy odourants [95]

Conclusions made by Amoore and Beets [107], resulted in the early consensus that ellipsoidal geometry and hydrophobic character produces a camphoraceous odour. In addition to camphor, which is closely linked with safrole/sassafras, other less prominent odour categories include mint, balsamic, sweet, bitter almond, pine (as distinguished from green), cineole/eucalyptus, herby and citrus/hesperidic. Considering a significant portion of taste can be attributed to smell [3], it becomes evident some of these categories coincide with flavour allocations. The compounds reproduced in Figure 1.15 represent the range of such varieties of odour categories.
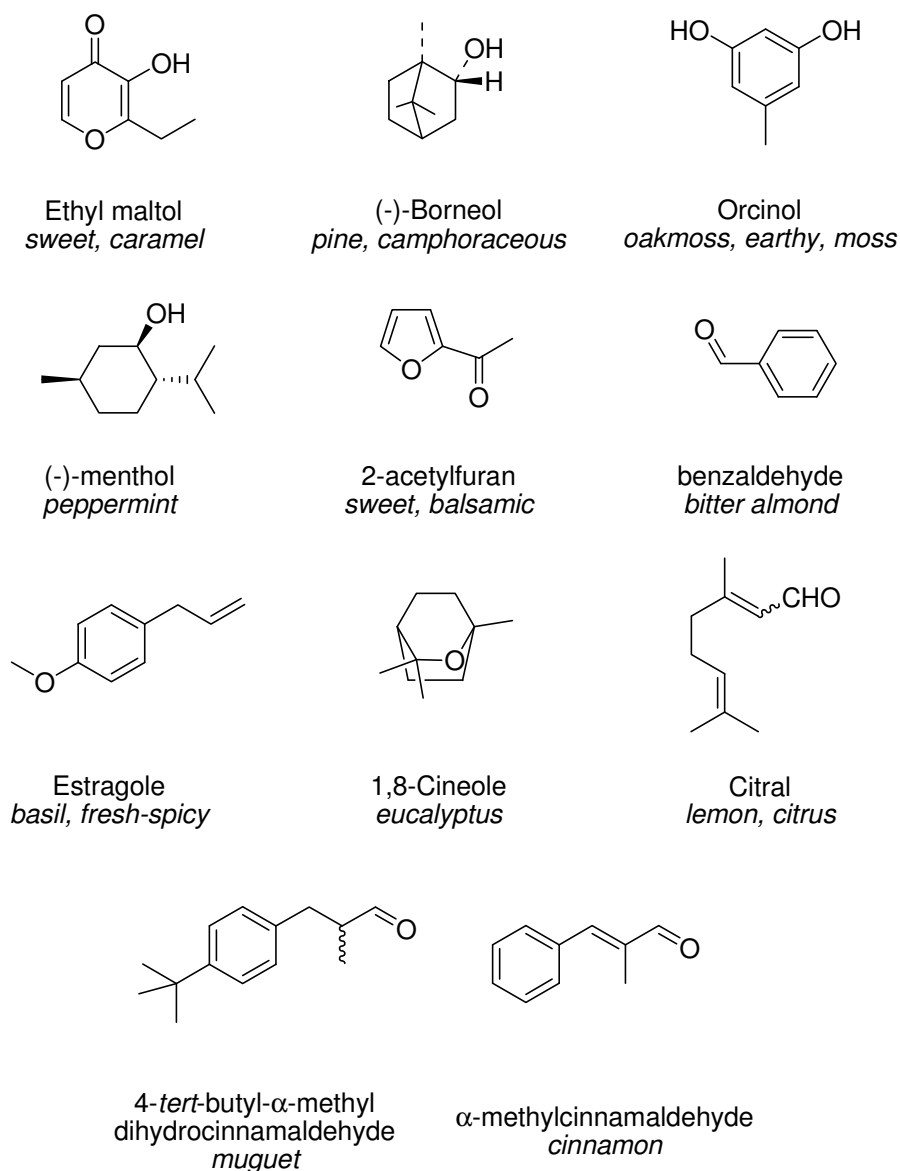
Figure 1.15 Some miscellaneous odourants [95]

The above considerations focus on qualitative odour aspects. Quantitative aspects are also structure-dependent with molecular axioms beginning to emerge. When reviewing fragrance categories varying extents of overlap exist and implementation of definitive class boundaries is limited as covered by an informative and succinct review by Sell [108]. Sell stipulates that prediction of odour will remain serendipitous and based on probable predictions rather than consistently reliable models. He suggests that to maximise accuracy odour-receptor site binding considerations should be based on dynamic rather than static models. He draws on research by his peers to illustrate that one odourant can dock on multiple binding sites and suggests that interaction may in fact be allosteric. He has also drawn the conclusion from that receptors seem selective within functional classes such as alcohols, acids, aldehydes, and lactones but not between classes. Sell

proposes that often odourant molecules can be grouped into triads where the structural outlier is different to the member of the group that exhibits an unrelated odour. An example of this is shown at the bottom Figure 1.15 where two molecules with a cinnamaldehyde structure exhibit different odours and the pyranol that is structurally unrelated also has muguet odour character.

1.3.3   Molecular Chirality

Chirality can be defined as the spatial geometry of stereochemical isomeric structures [109]. "An object is chiral if and only if it is not superposable on its mirror image; otherwise it is achiral" [110]. A racemic mixture is a 50:50 mixture of enantiomers. Enantiomeric (R and S) forms are differentiated by the arrangement of substituents around the asymmetric (stereogenic) carbon atom of the molecular structure [109]. Not related to R and S nomenclature is the (+) or (-) indicator which may also be used to differentiate enantiomers, denoting the direction the molecule rotates the plane of polarised light. In biological systems, chirality can only be recognised by chirality, therefore biological chemo-sensors such as physiological receptor sites are assumed to be chiral because they respond differently to discrete enantiomers [109]. Supportive evidence is provided by the enantio-differentiation capabilities via taste and smell. Knowledge that enantiomers exhibit the same physical and chemical properties means odour discrimination of chiral odourants (Figure 1.16) may often be dominated by chiral selectivity, as biological discrimination is commonly observed [109].

(S)-(-)-Nerol oxide
green, spicy, geranium

(R)-(+)-Nerol oxide
green, floral

(+)-Nootkatone
grapefruit

(-)-Nootkatone
woody, spicy
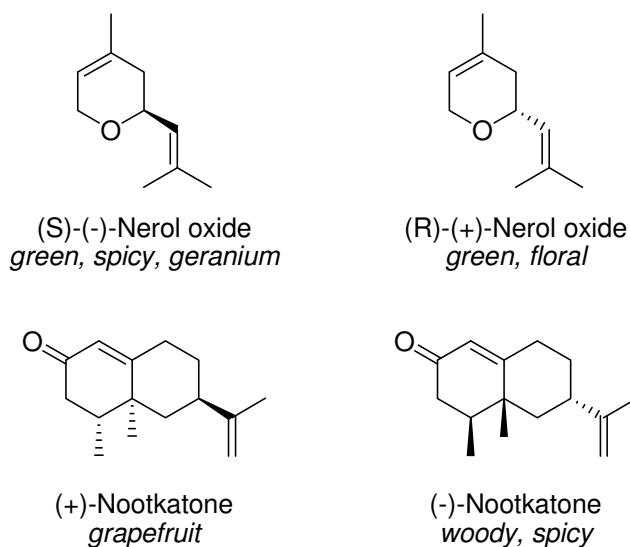
Figure 1.16 Examples of chiral odourant pairs [1]

Interaction of a chiral odourant with a stereoselective receptor site results in a diastereomeric interaction, enabling enantiomers to elicit markedly different sensory properties [111]. Enantiomeric odour studies contribute significant information to odour recognition based on molecular peripheries. In the case of antipodes the possibility exists that the odour-inactive enantiomer mimics the chemo-active enantiomer and competitively binds to ORs to varying degrees. This possibility means the olfactory properties of the chiral odourant may be nullified or distorted, and antagonistic or agonistic olfactory activity may exist. In the quest to produce stereochemical fragrance (and flavour) compounds, avenues of synthesis and purification include: diastereomeric resolution; stereoselective synthesis, both chemo-chiral and catalytic; and enzyme-mediated conversions [1]. Constant challenges for assessment of biological and physiological enantioselectivity include chemical resolution, methods of sensory analysis, and the presence of trace impurities. It is important that, for realisable odour characterisation, pure enantiomers should be employed. The same antagonistic/agonistic effects can occur in mixtures of odour compounds, where one compound may interfere with the perception of another.

1.3.4   Odour Agonist/Antagonist Activity

The possibility of antagonist or agonist action in odour detection introduces further gradations to an already complex sensory mechanism. An example of the dependence of perceived odour character on odour concentration is provided by indole (Figure 1.17), which appears putrid/fecal at high concentration however emanates a floral odour when diluted.

Indole
low dilution: fecal
high dilution: floral
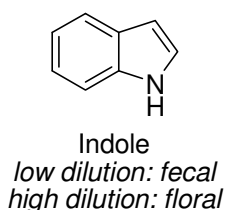
Figure 1.17 Odour properties of indole at high and low concentrations

When concentration of an odour molecule reaches OR saturation levels, it can begin to act as an antagonist or agonist, forcing itself into ORs it would not normally occupy. Both antagonist and agonist compete with the actual receptor substrate; an antagonist will merely block the cell, whereas an agonist will trigger the cell receptor and mimic the substrate [56].

Agonist activity can also introduce ancillary characteristics to the fundamental odour perceived. Over-saturation provides a unique example of agonist activity demonstrated by compounds that feature a pleasant smell at lower concentrations (optimum potency) that converts to unpleasant or indiscriminate at higher concentrations (exceeding optimum potency). At higher concentrations receptors become saturated so odours capable of agonist activity will continue to trigger sites beyond their saturation level. Calone 1951® provides a pertinent example, which has a pleasant marine fragrance at high dilution but potent/seaweed/salty odour at high concentrations.

1.3.5 Eligibility as an Odourant: Structural Requirements at the Peripheral Level

For select odourants at higher concentrations there is an increase in receptor activation that is partnered by an increase in activated glomeruli and modified qualitative characteristics of the odour [112]. This over saturation can result in a change in hedonistic character by intensified sensory unpleasantness [7]. Evaluation of whether the primary stimulus is solely responsible, or if trace contaminants have reached their detection thresholds remains elusive [7]. An odourant that has the same perceptive quality over a concentration range would predictably exhibit a constant affinity for binding receptors [7]. In contrast those odours that transform as a result of concentration variance would feature degrees of binding affinity [7].

Changes in concentration can affect the overall qualitative perception of an odour stimulus [113]. This concept is interesting when compared with volatility. A perfume accord provides a good illustration: with initial detection the top notes (the most volatile components) dominate the qualitative character as initially they are at the highest concentration, as the fragrance lingers the middle notes surpass the top notes, and finally the least volatile and most persistent components (base notes) predominate as their concentration per unit air increases. A practical example of these volatility differences is the selective absorption of volatiles onto an SPME fibre for headspace GC. During olfactory detection at the nasal epithelium surface potency of an odourant is a result of the volatility of that odourant. An odourant's availability to ORNs as a measure of its concentration in the surrounding air and its binding affinity with ORNs collectively contribute to volatility.

Olfactory receptor sites demand that for a molecule to exhibit odour it must have sufficient volatility and must be present in the air surrounding the receptor site at greater than a minimum concentration defined as the threshold concentration, which varies enormously between odorants [83]. It is now understood that a chemical conversion occurs when an odorant molecule binds. This highlights the chemical significance of the interaction, and disregards the notion that it is purely a physical process [83].

A well-defined receptor site demands the ability to exist in many structurally divergent conformations enabling binding to many different substrates [30]. Van der Waals interactions are the underlying forces responsible for formation of the bound receptor-substrate complex. Hydrogen bonding and ionic interactions offers secondary supports to van der Waals forces in the binding pocket [30]. An odorant must possess particular structural properties in order to be eligible as an odour stimulus. It must be below 300 in molecular weight, be water-soluble, exhibit a high vapour pressure, feature a degree of lipophilicity, and have surface activity [8].

In some cases it has been found that an electropositive group can replace an electronegative group without significantly altering the olfactive quality [99]. Examples of this replacement include substitution of a chlorine with a methyl in aliphatic esters, and nitro by t-butyl in benzenoid musks [99]. In this case their electronic effects may be negligible and they may only be contributing steric bulk. Boelens proposed that electronic and steric factors are the dominating components and it is possible to maintain an odour's integrity even with significant changes in structure, as long as electronic and steric factors are kept reasonably equivalent [99]. Odour molecules with a permanent ionic charge are not known since ionic species are generally not volatile. The molecular weight limit of 300 suggests that most of the molecule is engulfed by the receptor site in the process of recognition, incapable of docking an odourant exceeding the corresponding volume. Parry states that olefinic compounds exhibit greater residual binding affinity than their saturated counterparts providing crotonic aldehdye, n-butyl aldehyde and allyl alcohol, n-propyl alcohol as examples (Figure 1.18) [114].

Error! Reference source not found. also serves as a good illustration that most odourants contain one polar functional group, which facilitates anchoring to a polar site on the OR with the rest of the molecule orienting into the hydrophobic pocket of the OR.
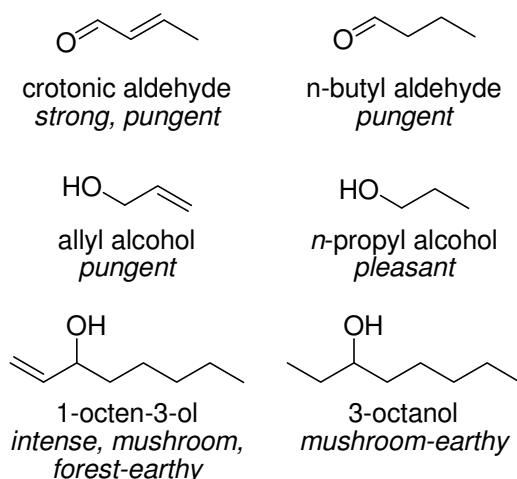
Figure 1.18 Correlation of saturation to odour intensity, related to affinity for olfactory receptors [114]

It has been demonstrated by Backman [115] that compounds with both high water and lipid solubility are strong odourants and these tend to be the middle members of existing homologous series. The examples provided included butyl alcohol, with higher alcohols having good lipid solubility and poor water solubility and lower alcohols the opposite [116]. The following n-octanol/water partition coefficients (clogP) were calculated using least squares analyses: Methanol has a logP of −0.27, ethanol 0.07 and butyl alcohol 0.97. Benzyl benzoate has a weak, sweet balsamic odour whereas the lower ester methyl propionate exhibits a strong fruity odour [95]. The former is lipophilic with a logP of 3.0, the latter more hydrophilic with a clogP of 0.86 [117].

Rossiter [100] has highlighted the relationship between shape and odour intensity. Turin presented the notion that intensity is more dependent on electronic properties than structural features [91] [92]. Functionality such as olefins and carbonyls that exhibit higher reactivity tend to also feature stronger odours, an example for which is provided in Figure 1.19 [116].

weak, woody   *woody*

strong, woody   *virtually odourless*
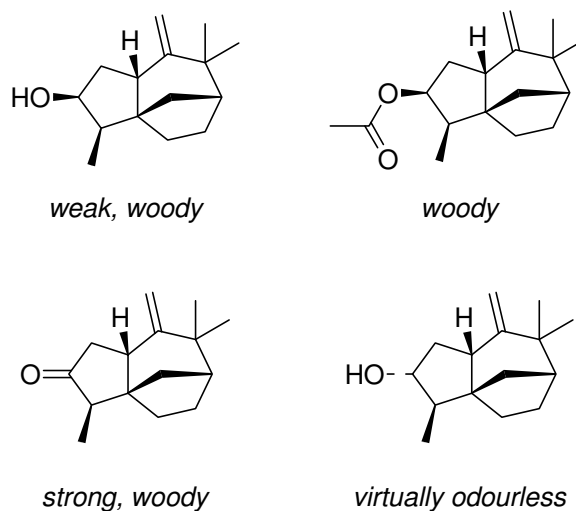
Figure 1.19 Odour intensity from functional group modifications [99]

An example provided by Moncrieff [116] involves ethane (odourless), ethylene (faint sweet smell) and acetylene (strong garlicky odour) [116]. A modification of the terminal functional group of 4-ethyloctane and the corresponding odour variation is shown in Figure 1.20 [99].

4-ethyloctanol
weak, fatty

4-ethyloctanal
rancid

4-ethyloctanoic acid
strong, animalic
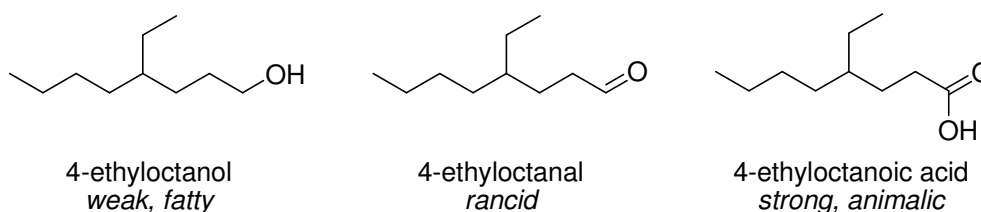
Figure 1.20 Odour properties from functional group modifications [99]

Ohloff and Giersch explored the olfactory potential of introduction of proton donor/proton acceptor combinations on a range of bi-functional cyclohexanes [118]. They discovered that the stereospecificity of the olfactory receptor required that the H-donor and H-acceptor on the molecule could be no further than 3Å apart for odour activity.

Hypotheses by Turin have led to the notion that the receptor-odourant binding interaction is a redox process [91]. He stipulates that a metal ion is present in the binding site, acting as a co-factor for an electron donor, such as a reductase enzyme or some other soluble electron carrier [91]. Turin discovered the presence of a motif in the binding protein structure with affinity to soluble electron donors alluding to the electron acceptor role of the protein and the redox environment of the receptor site [91]. Upon binding, the electron

current generated by the redox interaction would be involved in an electrochemical process: the current is converted to a chemical signal to provide a conventional signal transduction pathway [91]. The reduction should therefore be the final step in the transduction [91].

Wang and colleagues found that methyl thiol was bound to receptors around one million times stronger, and methylamine one hundred thousand times stronger than methanol [119]. It is unfeasible for these differences to be accounted for by hydrogen bonding or van der Waals interactions alone [119]. This phenomenon can only be explained by differences in Lewis basicity to metal ions [119]. Volatile molecules that act as good ligands for metal ion coordination complexes often exhibit strong odour character [119]. A trend noticed by Wang and co-workers correlates well with current metal-receptor site binding theories. With the exception of carbon monoxide (CO) and nitrogen oxide (NO), ligands such as amines and thiols that exhibit high affinity constants (degree of binding) with binding metals possess potent odours (low odour thresholds), and those with low binding affinity such as alcohols and acids expectantly have high odour thresholds [120]. The carbon monoxide and nitrogen oxide irregularity can be understood in light of their functional roles as neural messengers [120].

1.4   Benzodioxepin(on)e Syntheses

The distinct marine odour character and substantivity of Calone 1951® (7-methyl-2*H*-1,5-benzodioxepin-3(4*H*)-one), first synthesised by Beereboom, Cameron and Stephens (Pfizer) [121] contributed to its incorporation in the fragrance industry. Calone 1951® is used for seabreeze accords in fragrances such as "Escape" (C. Klein, 1991), "Polo Sport Woman" (R. Lauren, 1996) and "Cool Water Woman" (Davidoff, 1997) [96]. Amongst traditional perpetual fragrance groups such as woody and floral, Calone 1951® has become an eminent compound in an atypical, formerly unestablished marine fragrance category. The single synthetic compound used in commercial perfumery known to exhibit a typical marine odour is **1**. Sea material such as algae is a natural resource for organic structures that exhibit a prototypical marine odour (Figure 1.21).

1
Calone 1951®
marine

2
giffordene
sea-algae

3
ectocarpene dictyopterene D
green, tomato-leaf

4
(+)-dictyopterene A
seawater
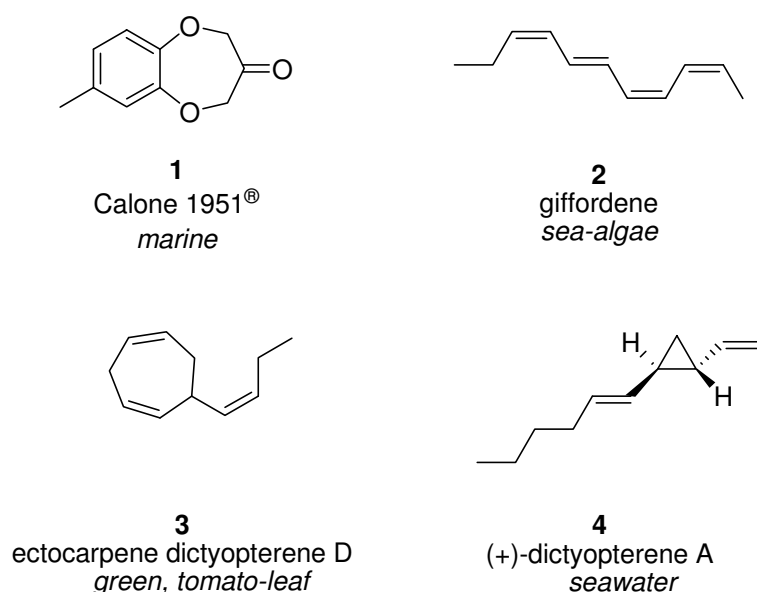
Figure 1.21 Calone 1951® (**1**) and some marine compounds naturally derived from algae (**2**-**5**) [96]

Isolated fragrant compounds obtained from marine algae have included the conjugated acyclic hydrocarbon giffordene (**2**) and carbocycle-containing species of various size and saturation (**3**-**5**) [96]. Unlike the hydrocarbon-derived marine odourants, the benzodioxepinone structure of **1** consists of an oxygenated bicyclic system. A potentially generic feature of marine odourants is two or more olefinic groups in, or in close proximity to a carbon ring system exemplified by (+)-dictyopterene A (**4**), and present as an aromatic ring in **1**. The presence of an olefin in both the naturally acquired and synthetic marine assembly may serve as marine odour indicators.

The novel properties of Calone 1951® render it suitable as a template for structure-odour-relationships (SOR) applications. The Calone 1951® molecule was selected for the current study due to the constructive segregation of polarity and the presence of binding centres such as the carbonyl, the methylene groups and the aromatic ring. Calone's odour persistence (interchangeable with tenacity) and potency can in part be explained by the polar gradation of the molecule. The polar attributes are probably those most relevant to affinity for the receptor site, whereas it's non-polar component allows easy transport through the mucous layer, increasing the concentration of molecules available for receptor binding. Altering the chemical characteristic of each identified region of Calone may permit the function of each to be probed systematically.

The significant olfactory influence of the heterocycle oxygens is evident in the contrast of odour character between the annulenone structures (**7**-**9**) and the benzoxepine (**6**) or benzodioxepines (**1** and **10**). Some olfactory data for analogues of **1** are presented in Table 1.4.

Table 1.4 Molecular features of some benzodioxepinone odourants
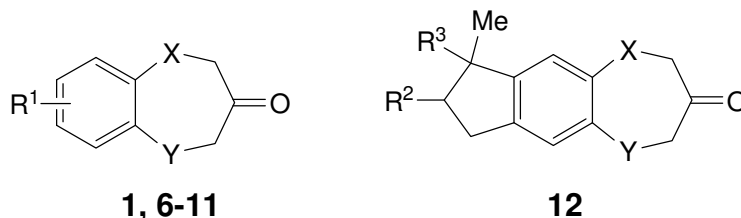
Compound	X	Y	R^1	R^2, R^3	Odour character
1	O	O	CH_3		marine, floral nuance
6	O	CH_2	H		watermelon, green
7	CH_2	CH_2	H		bitter almond, peppermint
8	CH_2	CH_2	^tBu		lily-of-the-valley
9	CH_2	CH_2	CH_3		lily-of-the-valley, marine
10	O	O	^nPr		aldehydic
11	O	O	straight-chain and branched alkyl		marine, floral, aldehydic, fruity, with ozone, animalic, and ink-like appearances
12	O	O	indenone	H, Me	marine, aldehydic, floral, with citrus, nutty, and lichen facets

Olfactory analysis of the benzoxepinone (**6**), also prepared by Beereboom and colleagues [121], was restricted to the term "watermelon ketone" and β-keto substituted derivatives of both **1** and **6** were assigned the same odour description. The annulenone analogue (**7**) was prepared by Kubota and Isemura in 1931 and described as exhibiting a bitter almond/peppermint odour [122]. More recently benzocycloheptanones **8** and **9** were developed by Yoshii and co-workers [123] defining the fragrance as lily-of-the-valley with addition of a marine accord in **9**, the carbocyclic equivalent of **1**. 7-Propyl-2H,4H-1,5-benzodioxepin-3-one (**10**) was prepared by Gaudin and Blanc [124] and a range of other *meta*-substituted varieties (**11**) have been designed by Kraft [125] for which olfactory accords are dominated by marine, floral, aldehydic and fruity notes. Tricyclic indenone structures (**12**), also by Kraft, provided novel and reasonably intense marine analogues

with the occasional citrus inflection, and singular nutty, moss, and animalic/civet appearances.

A publication released by Kraft and Eichenberger in 2003 replicated the previously patented compounds [126] and included olfactory analysis of the open chain dioxepinone compounds alongside a range of fused ring indenone analogues. A large change in intensity can be observed when comparisons are drawn between open chain and fused ring systems. For example a 40-fold decrease in threshold intensity was seen in the indenone analogue **12b** in comparison to the open chain compound **11c**. A 14.5 fold decrease in threshold intensity was also experienced in the indenone **12c** in comparison to the open chain **11b**. This decrease in threshold intensity may be responsible for the lack of strong salty-marine character in recently developed indenone fragrant compounds, indicating that receptor saturation is not an issue when fragrant compounds are of lesser potency. A general trend of a decrease in fragrant intensity upon increases in alkyl chain length is evident, yet expected due to decreases in volatility with increasing molecular weight. Outliers of this trend may possess structures that present specific hindrance or affinity to the receptor system. The range of benzodioxepinone and indenone compounds prepared and corresponding olfactory descriptions and odour thresholds (ng/L) are presented in Table 1.5 [126].

Table 1.5 Substituted benzodioxepinones and cycloheptaindenones prepared by Kraft and Eichenberger [126]
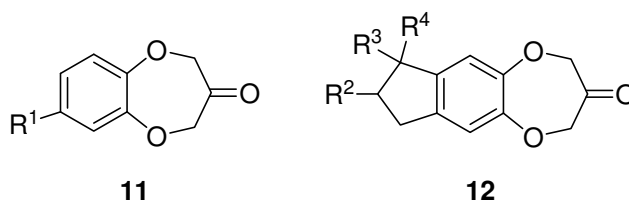
	R^1	R^2	R^3	R^4	odour descriptors	threshold (ng/L)
11a	^{i}Bu				marine, ozone, aldehydic	1.65
b	CH$_2$CHMeCH$_2$CH$_3$				intense, marine, floral	0.08
c	(CH$_2$)$_2$CHMe$_2$				very intense, diffusive, marine	0.014
d	(CH$_2$)$_4$CH$_3$				intense, marine, floral-aldehydic	0.013
e	(CH$_2$)$_3$CHMe$_2$				marine, floral-aldehydic	0.038
f	(CH$_2$)$_2$CHMeCH$_2$CH$_3$				marine, animalic, civet	0.043
g	CH$_2$CHMe(CH$_2$)$_2$CH$_3$				marine, floral-aldehydic	0.38
h	(CH$_2$)$_5$CH$_3$				marine, aquatic	0.019
i	CH$_2$CHEtCH$_2$CH$_3$				very weak, marine, fruity	4.70
j	(CH$_2$)$_6$CH$_3$				weak marine, slight ink-like	0.64
k	(CH$_2$)$_7$CH$_3$				very weak, slight mandarin	4.05
l	CH$_2$Ph				very weak, leathery, slight marine	6.80
m	CH$_2$CH=CH$_2$				marine, watermelon, ozone	0.051
12a		H	Me	H	marine, floral	0.26
b		H	Me	Me	marine-aldehydic, floral-rosy	0.55
c		Me	Me	H	walnut, fenugreek, seawater	1.16

Diacetate precursors were reliably prepared according to the procedure outlined by Carter and Lawrence in 1900 [127] (Table 1.6). Base-mediated Dieckmann cyclisation followed by decarboxylation in mineral acid gave **13** and **14** in gram quantities for chemical and odour characterisation. Research successors have adopted synthetic methods for the synthesis of Calone 1951® derivatives from the general outline provided in the patent [121]. General comments on the fresh, leafy, green, watermelon odour characteristics have made mention in both patent [121] and literature.

Table 1.6 Substituted benzodioxepinones prepared by Carter and Lawrence [127]

| **13** | | **14** | |
R^1	R^2	R^1	R^2
H	H	(**6**) H	H
H	CH$_3$	H	CH$_3$
H	C$_2$H$_5$	H	C$_2$H$_5$
H	n-C$_3$H$_7$	H	n-C$_3$H$_7$
H	n-C$_4$H$_9$	H	n-C$_4$H$_9$
H	iso-C$_3$H$_7$	H	iso-C$_3$H$_7$
H	iso-C$_4$H$_9$	H	iso-C$_4$H$_9$
H	*tert*-C$_4$H$_9$	H	*tert*-C$_4$H$_9$
(**1**) 7-CH$_3$	H	7-CH$_3$	H
7-CH$_3$	n-C$_4$H$_9$	6-C$_2$H$_5$	n-C$_4$H$_9$
7-,8-CH$_2$	iso-C$_3$H$_7$	7-n-C$_2$H$_7$	iso-C$_3$H$_7$
7-,8-C$_2$H$_5$	CH$_3$	7-iso-C$_3$H$_8$	H
7-,8-n-C$_4$H$_9$	CH$_3$	7-*tert*-C$_4$H$_9$	H
6-,9-CH$_3$	CH$_3$	9-CH$_3$	n-C$_4$H$_9$
6-,9-iso-C$_3$H$_7$	iso-C$_3$H$_7$	8-C$_2$H$_5$	iso-C$_3$H$_7$
6-,9-CH$_3$	H	6-CH$_3$	CH$_3$

Studies performed by Dallacker and Coerver experimented with cyclic catechol ethers of various ring size possessing a minor range of aromatic substitutions, of which the most explorative were hydroxy, formyl and bromine moieties [128] (Scheme 1.1).

R_1 OH a R_1 O b OHC R_1 O c HO R_1 O
OH $(CH_2)n$ $(CH_2)n$ $(CH_2)n$
R^2 R^2 O R^2 O R^2 O

15   **16**   **17**   **18**
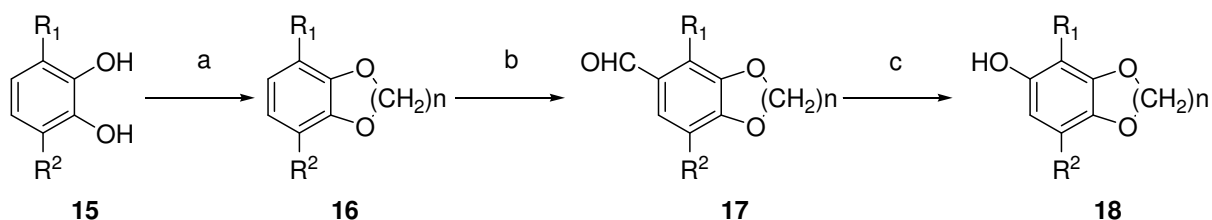
Scheme 1.1 a) **15a→16a** K_2CO_3, halogenated alkylating agent, DMF; **16a→17b**-**17d** K_2CO_3, halogenated alkylating agent, DMF; **16b→17e** NaOH, DMSO, CH_2Cl_2; b) **16a-e→17a-e** $POCl_3$, DMF; c) **17a-e→18a-e** aq folic acid, aq H_2O_2

The ring size ranged from benzodioxoles to benzodioxecines [128] (Table 1.7).

Table 1.7 Substitution of benzodioxepines prepared by Dallacker and Coerver [128]

	R^1	R^2	n
15a	CH_3	CH_3	
b	CH_3	$(CH_3)_2CH$	
16, 17, 18a	CH_3	CH_3	1
b	CH_3	CH_3	2
c	CH_3	CH_3	3
d	CH_3	CH_3	4
e	CH_3	$(CH_3)_2CH$	1

The catechols were alkylated by Williamson etherification methods. The carbaldehydes were obtained *via* Vilsmeyer formylation, which were then subjected to Baeyer-Villiger oxidation to derive the benzodioxol analogues (Scheme 1.2). The target dioxepinochromenes (**19**) (Table 1.8) were obtained by cyclisation with prenyl and phytyl bromide to form the dioxane ring. Optimal yields were obtained with catalytic addition of zinc chloride ($ZnCl_2$) [128]. No attempt was made to introduce functionality to the dioxole ether chain.
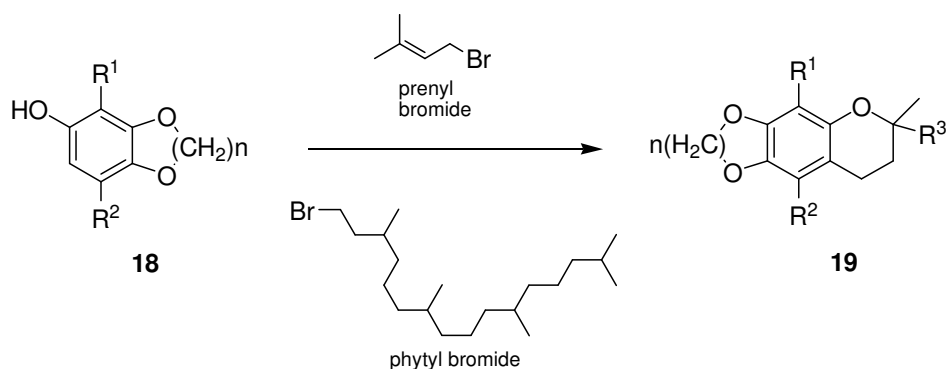
Scheme 1.2 19a, f ZnCl$_2$, prenyl bromide, anhydrous benzene; **19b-e, 19g, h, j** ZnCl$_2$, prenyl bromide, phytyl bromide, anhydrous benzene; **19i** ZnCl$_2$, prenyl bromide, phytyl bromide, anhydrous benzene, followed by Br$_2$, CHCl$_3$

Table 1.8 Substitution of the tricyclic dioxyl compounds **19** prepared by Dallacker and Coerver [128]

	R^1	R^2	R^3	n
19a	CH$_3$	CH$_3$	CH$_3$	1
b	CH$_3$	CH$_3$	C$_{16}$H$_{33}$	1
c	CH$_3$	CH$_3$	C$_{16}$H$_{33}$	2
d	CH$_3$	CH$_3$	C$_{16}$H$_{33}$	3
e	CH$_3$	CH$_3$	C$_{16}$H$_{33}$	4
f	CH$_3$	(CH$_3$)$_2$CH	CH$_3$	1
g	CH$_3$	(CH$_3$)$_2$CH	C$_{16}$H$_{33}$	1
h	CH$_3$O	H	C$_{16}$H$_{33}$	1
i	CH$_3$O	Br	C$_{16}$H$_{33}$	1
j	H	H	C$_{16}$H$_{33}$	1

A patent released by Gaudin and Blanc in 1998 covered extensive application of the *m*-propyl benzodioxepinone in fragrant formulations [124]. According to the authors the propyl derivative emanates strong aldehyde-type, clean linen fragrance with spicy connotations with commercial fragrance applications as a chemically stable odourant [124]. The authors comprehensively tested the stability of the key propyl derivative in an exhaustive range of fragrance-based domestic products covering perfumes, deodorants, hair-care, talc, skin creams, soap, detergent, fabric treatment and acidic solutions at

temperatures up to 40°C. Odour modification only occurred at temperatures above 40°C for the fabric softener and Eau de Javel, however the compound maintained key odour properties under oxidising conditions such as those found in hypochlorite and peroxy-derived bleaching agents. This is significant in fragrance application as traditional aldehyde containing additives are unstable under redox conditions such as those found in commercial detergents and bleaches. This compound demonstrated high substantivity particularly when tested for detergent and fabric applications.

Gaudin et al. (2007) [129] explored syntheses, olfactory evaluation and molecular modelling of Calone analogues in order to more thoroughly evaluate the structure-odour-relationship trends of marine-type odourants and contribute to syntheses already achieved by previous research such as that in the Pfizer patent [121] or by Yoshii [123].

Their general conclusions began with their discovery that the dicarba analogues exhibit weaker odours than their dioxy counterparts, which they attributed in part to differing conformations adopted by the two. Also substitution at the α-carbonyl position dramatically changes the odour and decreases the intensity, most likely due to hindered H-bonding with the carbonyl group upon binding. They also concluded that optimum carbon chain size for marine odour and intensity is C_3-C_6 and dialkylation of the aromatic ring destroys the marine characteristic. Absence of aromatic substitution decreases the odour intensity and alternative odour notes begin to take over from marine. Also substitution at the α-carbonyl position dramatically changes the odour and decreases the intensity, most likely due to hindered H-bonding with the carbonyl group upon binding.

1.5 Methods for Assessment of Odour Activity

1.5.1 Gas Chromatography-Olfactometry

1.5.1.1 History

The inception of sniff methods as a component of gas chromatography analysis occurred in the 1960s. Prior to implementation of an individual sniffer port, the technique originally coined 'olfactometry' involved sniffing the effluent escaping a non-destructive GC detector, such as thermal conductivity [130]. As the design was very primitive, problems arose including the interfering burnt odour associated with hot exhaust gases in conjunction with dehydration of the nasal passage which deteriorates smelling ability [130]. Health and

safety concerns such as co-elution of hydrogen gas provided the impetus for design evolution [130]. Continual design modifications led to what is presently regarded as Gas Chromatography-Olfactometry (GC-O) [130].

This relatively new technique supercedes other historical procedures for odour detection and threshold values including the draw tube olfactometer by Zwaardemaker (1927) [131], glass sniff bottles (1950s) [132], air dilution olfactometers (1960s) [133], glass rods, wooden sticks, or strips of blotter paper dipped in odourant (1960s) [134], and plastic squeeze bottles (1980s) [135].

The birth of perpetual vapour phase chromatography by James and Martin in 1951 preceded the release of a manuscript by Fuller and colleagues at the Colgate-Palmolive Co. in 1964 complete with photographs that described a system for sniffing GC effluents [136]. An evolved GCO design was essentially devised in 1971 by Dravnieks and O'Donnell [137]. Their main addition involved mixing the hot GC gases eluting from the capillary outlet with humidified air, which introduced a dynamic element by providing an odour concentration gradient of Gaussian distribution to partner that from the column. In addition, the bandwidth of the odour escaping the sniffer port replicated the odourant retained on the column and laminar flow was preserved for optimal column output [137].

Current olfactometers come in two forms: static and dynamic [130]. Static olfactometers can be as simple as a plastic squeeze bottle or plastic bag with an odourless carrier; usually humidified air [130]. This method is simple and portable and it can be volumetrically standardised [130]. Dynamic olfactometers provide a constant, humidified stimulant dosage from the sniffer port [130] that incorporates an effluent splitter between the detector and the sniffer outlet [138]. In an attempt to overcome nasal fatigue, dynamic systems are pulsed with square-wave odorant profiles with constant relative humidity (RH) ~50% [130]. In both systems volatility of constituents and flow rates can influence olfactory measurements [130].

1.5.1.2   Theoretical Considerations

The human nose acts as the fundamental detector component when GC is coupled with olfactometry [139]. Analysis is performed by the human olfactory system, which with a detection limit of 10^{-19} moles [140] is principally more sensitive than any current analytical device such as a chromatographic detector or E-nose [130].

GCO attempts to synchronise a mostly continuous stimulus emission response (GC output), with an antiparallel, discontinuous detection mechanism (the human nose) [139]. Inhalation cycles become progressively sporadic as self-awareness of breathing increases [139]. Some researchers are coupling a breathing recorder to GCO systems spurred by data suggesting a faster breathing rate detects an increased number of odourants. Sniffer panellists are often selected according to this breathing criterion [139].

A major limitation of GCO evaluation is analysis time constraints due to odourant anaesthesia from exceeding olfactory receptor saturation levels. An unavoidable tedium associated with continuous odourant inhalation is sensory fatigue mainly due to low oxygen levels required by the nose for oxidation of protein structures that enable odourant detection [141]. Detection periods are therefore limited to short spans of time. Other sensory experiments, such as taste or tactile allow prolonged assessment which maximises evaluation accuracy. Many factors influence odour assessment outcome: vigilance, odour adaptation (also known as odour "compression") [142], breathing [139], expertise, specific anosmia, odour threshold sensitivity, as well as implicit parameters such as emotional state, ingested substances, and sensory saturation, hence reproducibility becomes a formidable task [139]. Specific anosmia is the term used when a member of the sensory panel proves impervious to a particular odour or class of compound, or exhibits a period of laxity [143]. In a normal breathing cycle the exhalation period is an example of specific anosmia due to the inability to detect odours in these periods between inhalation [143]. Gas flow fluctuations between the column outlet and the sniffer port and also the conic shape of the port outlet can alter the theoretical Gaussian shape expected in odour compound elution [139]. Often, reproducibility in odour characterisation is maximised by training the sensory panel, use of odour standards, and eradication of anecdotal influences related to odour analysis [143]. Minimal interaction between eluting odourants and the sniffer port material must be ensured, with fluent elution at the interface to the detector and the port, and hence synchronicity between the two.

Proximal eluting compounds can impart quantitative and qualitative influential effects on each other [141]. This is known as the contrast effect [140], or cross adaptation, and can be monitored to provide beneficial results by column selection and manipulation of chromatographic dynamics to influence elution time and sequence. Discrepant results can be avoided by utilising at least two varying column phases in preliminary GC studies

on odourants of interest [141]. For example, use of a chiral column ensures identification of enantiomers or verification of diastereomers.

1.5.2   Quantitative GCO

1.5.2.1   Odour Intensity Parameters

Odour persistence is exploited in commercial perfumery where the term 'accord' defines the unique blend of top, middle and base notes. Top notes are perceived initially, so have the highest vapour pressures, middle notes are detectable next, followed by base notes, which elicit the highest odour persistence, effectively due to strongest binding affinities and lowest adaptation.

Odour intensity is an implicit parameter, more definitively it is the perception of odour at a given concentration [130]. The absolute odour intensity value is the minimum concentration (dilution level) at which the nose is capable of detection of the odourant. Odour potency is a relative parameter: the dose level of an odourant in relation to all others in the accord when intensity of the component mixture is kept constant [130]. The highest potency for a particular odourant is the dilution level at which it is most prominently perceptible. The choice of solvent for delivery of an odourant to the nose can modify its perceived intensity threshold level which can be affected by the solvent's volatility and vapour pressure [130]. This problem is removed by the use of GC as the separation process removes the solvent. Thermodynamic considerations can indirectly increase potency of an odourant by increasing the volatility (gas phase concentration per unit air), however there are no reports on whether an increase in temperature of an odourant, avoiding decomposition, can also directly influence saturation capacity of olfactory receptors. Separation by gas chromatography when based on boiling point can be directly related to volatility and vapour pressure, a property relevant to olfactory delivery [130].

Acree states that our perception of odour intensity in relation to odour concentration is a psychophysical detection [130]. There is no simple relationship for odour intensity; some odourants can be perceived as weak at high concentrations yet become clearly detectable at low concentrations [144]. The pineapple odourant, allyl hexanoate is an apt example of a compound which is detected by nose at a concentration much lower than that required for visualisation in the GC trace [141]. The physical intensity threshold (O_x) of an

odourant in ng/litre of air can be calculated relative to an internal standard using the following formula:

$$O_x = (O_i.D_i/C_i).(C_x/D_x)$$

where C_i = concentration of the internal standard

C_x = concentration of odourant

D_i = dilution value of the internal standard

D_x = dilution value of the odourant

O_i = physical intensity threshold of the internal standard

The term odour activity value (OAV); interchangeable with 'unit flavour base', 'odour unit', 'odour value', or 'aroma value', was conceptualised by Patton for the purpose of a generalised value which denotes the ratio of concentration to intensity threshold [145]. Critics of the use of OAVs such as Frijters [146] claim it is arbitrary and therefore not reliable. Frijters also states that two audacious assumptions arise due to OAV derivation based on psychophysical observations: a) the same OAV between compounds means an equal perceived intensity; b) the concentration of a compound and its perceived intensity form a linear relationship [141]. OAV's for a range of odourants extracted from beef are presented in Table 1.9.

Table 1.9 Concentrations and OAVs of six key odour active compounds in roasted beef [141]

Compound	Concentration (µg/kg)	OAV*
4-Hydroxy-2,5-dimethyl-3(2H)-furanone	928	9
2-Acetyl-2-thiazoline	28	28
2-Ethyl-3,5-dimethylpyrazine	5.4	3
2,3-Diethyl-5-methylpyrazine	27	27
Guaiacol	2.1	1
Methional	12.5	7

* For OAV, a nasally estimated odour threshold in water was determined.

1.5.2.2 Sensory Power Laws

Due to the multi-modal nature of odour perception a number of laws have been proposed in an attempt to elucidate the quantitative aspect of odour [7]. All laws are in some form deficient and too simplistic in their approach, failing to take factors such as perception fatigue, or cross-modal influences into account [7]. For example, taste sensation is influenced by aroma, texture and taste modes and likewise odour is a construct of modal influences such as character, potency, persistence and adaptation for the overall sensory experience.

The odour intensity-concentration relationship is not linear [147]. A standard plot of intensity vs concentration shows a logarithmic decay as physical concentration approaches a stimuli saturation level [148]. Weber's fraction (1834) denotes that 75% of research performed proved that the increase in odourant concentration (ΔI) required to produce a just noticeable difference (JND) of intensity represents a constant (k) relative to the concentration of the standard stimulus (I).
Weber's law [149] is given by the formula [150]:

$$\Delta I/I = k$$

Weber's law indicates that thresholds and therefore JNDs concomitantly increase with background intensity [149]. A smaller Weber fraction indicates a greater distinction within a sensory system upon change in concentration [144]. Although Weber's fraction is based on a large approximation it can be applied when odourant concentrations are reasonably constant, and therefore the odour threshold is constant [144]. Weber's law denotes that increasing intensity results in decreasing perception to stimulus change [149].

The most commonly utilised and prominent law is that of Stevens (1969) [150]which models how the perceived stimulus magnitude (φ [144], S [150], I [144]) grows as a power function of perceived concentration (φ [144], P [150]). In general, perceived magnitude (ψ) grows as a power function of concentration (φ) thus the exponential form is:

$$\psi = k\varphi^{\beta}$$

where ψ = perceived intensity

k = the Y intercept, constant

φ = stimulus concentration

β = the slope

This can be plotted as a straight line according to an older sensory law developed by Fechner (1860) [151]. The log plot is formed by stimulus magnitude against concentration of which the data can be represented as:

$$\log \psi = \beta \log \varphi + \log k$$

Fechner's paradigm is based on the premise that mental recognition must surpass a threshold before there is conscious perception [152]. A limitation inherent to Fechner's law is that the model is only accurate in cases where $\beta > 1$ and assumes all JNDs are alike [152]. The exponential Stevens law expression is a general algorithm applicable to many physiological responses since the exponent (β) which represents the slope of the curve describes the variable involved in the response of the sensory system to the stimulant [152]. Practically in the case of an odourant, upon serial dilution 1:2 (a dilution factor of 3), if an odourant can still be detected in the fourth dilution, the dilution factor at this stage is 3^4=81 [141]. The Steven's relationship of between two arbitrary odourants is compared in Figure 1.22.
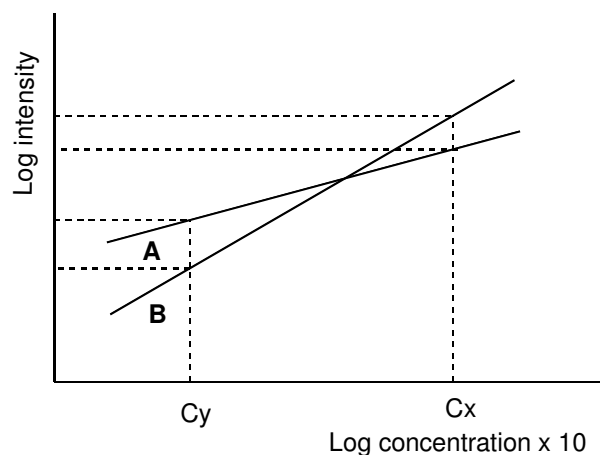
Figure 1.22 Logarithmic relationship between odourants A and B demonstrating differences in perceived intensity threshold gradients. Origins of the lines indicate the just perceived intensity thresholds. Slope indicates the rise in perceived odour intensity with increasing concentration. At Cy, A is more intense than B, at Cx B is more intense than A. Stevens' law relates log intensity to log concentration [153]

For Stevens' law the exponent can be greater than one or less than one representing an intensifying function or a moderating compressive function, respectively. Fechner's law is restricted to compressive parameters [152]. Stevens' law has been used to model loudness, vibration, brightness, taste, warmth, thermal, pain, tactile pressure, muscle force, viscosity, and vocal sound pressure.

Borg and colleagues [154] [155] noted that "the summated electrical response satisfies a Stevens' power function or a Fechnerian log function, it is apparent that there is a fundamental congruity between neural activity and perceptual intensity." Stevens' power function applied by Borg and colleagues resulted in:

$$\log \psi = 1.3 \log \varphi + \log k$$

$\psi = k \, \varphi^{1.3}$

ψ is a character i.e. fruitiness

φ is stimulus concentration

k is a constant and depends on the units used

Borg concluded "subjective intensity grows as a power function of stimulus concentration."

1.5.3   Headspace Gas Chromatography (HS-GC)

Both dynamic and static headspace techniques provide a perfectly suitable solvent-free partner to AEDA, Charm or Osme data [141]. Headspace GC (Figure 1.23) can be coupled to GC-O to exploit the volatile nature of odourants [138].
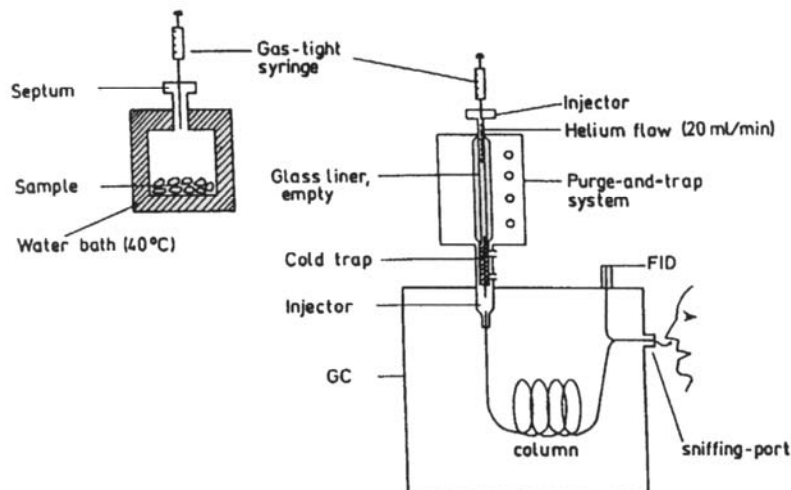
Figure 1.23 Schematic representation for headspace GC-O analysis with dual FID + O detection [156]

Even in HS-GC-O it is not uncommon for the human nose to detect an odour corresponding to a time where no odour is detected as retained in headspace techniques [100]. This demonstrates the superiority of the mammalian nose over even the most sensitive of instruments for low odour threshold compounds.

Static headspace GC involves an aliquot injection of headspace gas onto a GC column [157]. Trapping or cryotrapping a sample component from a continuous stream of volatiles within a carrier gas followed by introduction onto the GC column is the dynamic variation of headspace GC analysis [158]. Solid-phase microextraction (SPME) is a headspace extraction technique that can be used in conjunction with GC or GC-MS for sensory analysis [159]. SPME involves the adsorption of volatiles in the headspace onto a polymer-coated fiber; upon heating in the GC injector port, the analytes are desorbed from the fiber and are subjected to GC analysis. The fibre is exposed to the headspace for a period that ensures equilibrium between the solid phase (fibre) and the gas phase (headspace) is established. Volatiles of the highest concentration will theoretically adsorb to the highest degree, although other factors that need to be considered include the fibre coating polarity, the fibre film thickness and temperature. Relative volatility of an odourant in a mixture can be effectively measured by utilisation of headspace methods or by use of a standard. HS-GC can be combined with AEDA for identification of volatiles via their RI values [138].

1.5.4   Qualitative GCO

Olfactory acuity is as much an individual as a relatable experience. Replication of another's appreciation of an odour through verbal description can be as much a fallacy as attempting to relate to another's emotional profile. In contrast, the power of odour perception evocation can also prove as potent as a placebo drug.

Odour mnemonics are based on association with reference material, which contributes to the subjective nature of odour character. A universal language for odour linguistics should be created and refined for progression towards an "olfactory alphabet" in the form of basic olfactory codons [147].   The problem of semantics exists in attempts to verbalise psychological odour reference material. This can result in ambiguity where odour analysis comparisons between research groups are relied upon. The overall perceptual profile of an odourant is the organoleptic factor of that odourant. Comparisons of GC effluent and the crude odour compound can provide very distinct odour profiles introducing discrepancies to olfactory assessment as demonstrated in Figure 1.24. Fortunately in both methods dominant odour notes are discernible *per se* and prove inter-relatable and reproducible. So in light of these points on GC-O, rudimentary blotter analysis in many respects proves superior for qualitative olfactory determination.
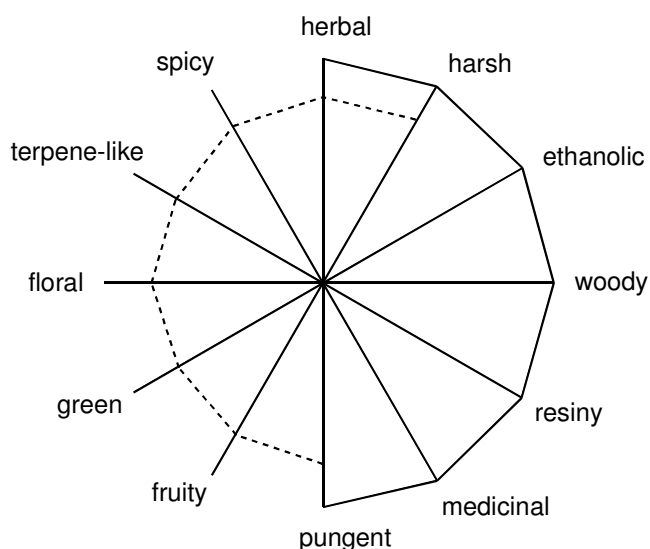
Figure 1.24 An odour wheel of davana oil (— sensory analysis, ----- GC-O analysis) [160]

The synergistic effect (hyperadditivity) can cause a change in odour characteristics from the influence of co-odours present in an odourant profile.   The masking effect

(hypoadditivity) results in lack of detection of odours from masking caused by a particular co-odourant. Ideally comparisons between mixture analyses and individual odour component data need to be compiled [161]. Omission tests that utilise GC-O have been performed on volatile food blends and it would prove useful if these methods were extended to analysis of perfume blends. The tests involve assessment of the odour character of a blend and then subsequent omission of individual components to determine how this affects the overall character [161].

1.5.5   Comprehensive Two-dimensional Gas Chromatography (GC×GC)

Gas chromatography is a technique that demands a balance between efficiency and separation speed, the former for achieving adequate separation, the latter reducing analysis time. Sample separation space is evidently restricted in a conventional one-dimensional chromatogram and for very complex samples resolving sufficient peaks demands GC runtimes in the order of hours. Comprehensive two-dimensional gas chromatography (GC×GC) offers high separation capacity, improved detectability, and unique selectivity possibilities [130]. Introduction of a second dimension introduces additional separation and retention information based on chemical nature providing true comprehensive analysis. GC×GC apportions the entire sample to two simultaneous independent separation dimensions (^{1}D and ^{2}D) by a dual column system. In comprehensive GC×GC the peak capacity of the primary column is multiplied by that of the secondary column for increased net peak capacity.

Multi-dimensional gas chromatography (MDGC) involves retention on two orthogonal columns, and this feature is also the key to GC×GC separation [162], however the latter exhibits an evident increase in total peak capacity (Figure 1.25, Figure 1.26).
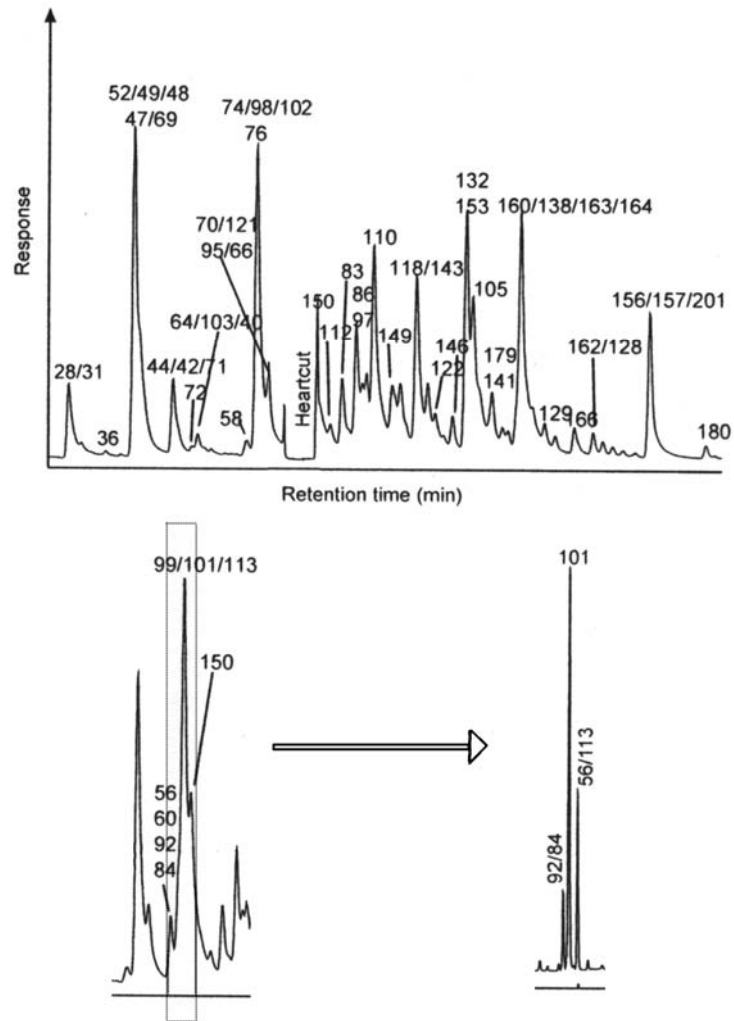
Figure 1.25 Modulation applied to a single heart cut from a one-dimensional chromatogram highlighting separation capabilities prior to application to two-dimensional space (adapted from [162])

The entire sample is subjected to analysis in both separation dimensions, so for specific applications where high sensitivity and resolution are essential, the advantage over MDGC techniques is evident [162].
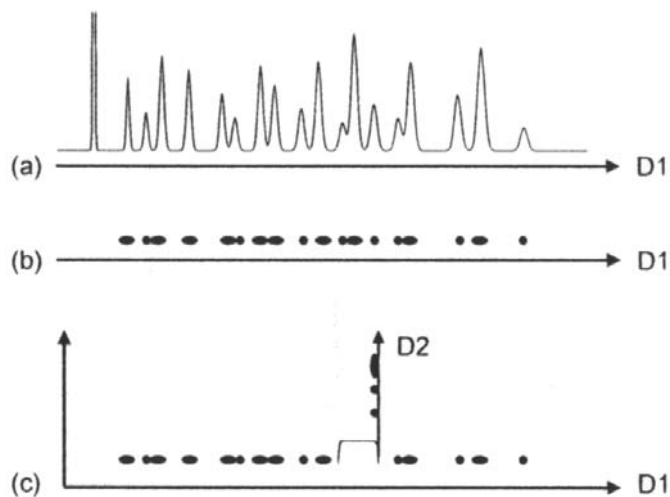
Figure 1.26 Layout of comprehensive information onto a two-dimensional space from a heart cut zone (D2) (c) derived from chromatographic analysis from the first dimension (D1) (a) also represented as peak zones (b) [162]

Where MDGC involves discrete heart cut events to provide enhanced separation, GC×GC provides a continuous second dimensional analysis of the effluent from the first column [162] (Figure 1.27).
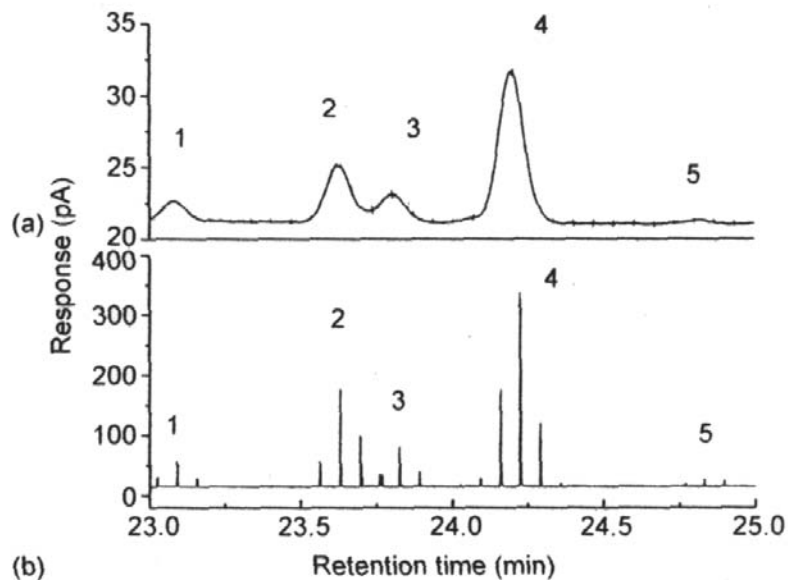
Figure 1.27 One-dimensional GC-FID (a), with modulation from cryotrapping of the same peaks 1-5 (b) resulting in increased response and corresponding sensitivity. Total peak area is contained within the summed pulses [162]

The rapid purge-and-trap cryogenic process focuses small fractions of analytes onto the second column, typically a fast GC column, at the prevailing oven temperature [162]. Coupling GC×GC with a mass spectral detector creates a third dimension of analysis. The most desirable mass-selective response is provided by mass spectral acquisition of spectra on a time frame compatible with the fast GC elution on the second dimension, which the time-of-flight instrument (TOFMS) provides. In the present study GC-qMS and GC×GC-TOFMS were utilised for analysis of a commercial perfume sample for positive identification of the fragrant compound Calone 1951®. Combining GC×GC technology with GCO analysis creates innovative system combinations that can assist in olfactory identification of complex odour-active samples. Orthogonality predicts that retention on two dimensions of different resolving capacity can provide independent separation mechanisms enabling resolution in two dimensions. Separation achieved on the first column is preserved, resulting in orthogonal analysis [162].

1.6   References

[1]   E. Brenna, C. Fuganti, S. Serra, Enantioselective perception of chiral odorants. Tetrahedron: Asymmetry 14(1) (2003) 1-42.

[2]   R.H.B. Wright, R. E., The Physical Chemistry of Smell. Method. Chim. 11(2) (1977) 268-273.

[3]   P. Churchland, in: N. A. Campbell (Ed.), Biology, (Ed.), The Benjamin/Cummings Publishing Company, California, U.S.A., 1996, pp. 1028-1029.

[4]   P. Mombaerts, Introduction: Development of the Olfactory System. Semin. Cell Dev. Biol. 8(2) (1997) 151-152.

[5]   J.d.A. Plailly, T.; Saoud, M.; Royet Jean, P., Left Temporo-limbic and Orbital Dysfunction in Schizophrenia During Odor Familiarity and Hedonicity Judgments. Neuroimage 29(1) (2006) 302-313.

[6]   T. Engen, The Perception of Odors, Academic Press, New York, U.S.A, 1982.

[7]   A.J.R. Taylor, D. D. (Eds.), Flavor Perception, Blackwell Publishing, England, U.K., 2004.

[8]   J.C. Leffingwell, Olfaction-Update No. 5. Leffingwell Reports 2(1) (2002) 1-33.

[9]   B.H. Malnic, J.; Sato, T.; Buck, L. B., Combinatorial Receptor Codes for Odors. Cell (Cambridge, MA, U. S.) 96(5) (1999) 713-723.

[10]   P. Mombaerts, Seven-transmembrane Proteins as Odorant and Chemosensory Receptors. Science (Washington, DC, U. S.) 286(5440) (1999) 707-711.

[11]   H.F. Zhao, S., Vertebrate Odorant Receptors. Cell Mol. Life Sci. 56(7-8) (1999) 647-659.

[12]   E.D. Adrian, The Electrical Activity of the Mammalian Olfactory Bulb. Electroencephalogr. Clin. Neurophysiol. 2(4) (1950) 377-388.

[13] S. Firestein, How the Olfactory System Makes Sense of Scents. Nature (London, U.K.) 413(6852) (2001) 211-218.

[14] T.C.K. Bozza, J. S., Odorant Response Properties of Convergent Olfactory Receptor Neurons. J. Neurosci. 18(12) (1998) 4560-4569.

[15] W.J. Freeman, Olfactory System: Odorant detection and Classification, Academic Press, New York, U.S.A, 1997.

[16] W. Singer, Neurobiology: Striving for Coherence. Nature (London, U. K.) 397(6718) (1999) 391-393.

[17] J.H. Jung, J.; Ryvlin, P.; Royet, J.-P.; Bertrand, O.; Lachaux, J.-P., Functional Significance of Olfactory-induced Oscillations in the Human Amygdala. Cereb. Cortex 16(1) (2006) 1-8.

[18] E.T. Theimer, Fragrance Chemistry. The Science of the Sense of Smell, Academic Press, London, U.K., 1982.

[19] T.E.S. Finger, W. L. (Eds.), Neurobiology of Taste and Smell, Wiley-Interscience, New York, U.S.A., 1987.

[20] P. Mombaerts, Targeting Olfaction. Curr. Opin. Neurobiol. 6(4) (1996) 481-486.

[21] J.S.C. Kauer, A. R., Are There Structural and Functional Modules in the Vertebrate Olfactory Bulb? Microsc. Res. Tech. 24(2) (1993) 157-167.

[22] S.D. Chu, J. J., Odour-evoked Autobiographical Memories: Psychological Investigations of Proustian Phenomena. Chem. Senses 25(1) (2000) 111-116.

[23] G. Salvadori, Olfaction and Taste: A Century for the Senses. Proceedings of the Firmenich Jubilee Symposium 1895-1995, Geneva, 1997, p. 248 pp.

[24] T.A.M. Schoenfeld, J. E.; Macrides, F., Topographic Organization of Tufted Cell Axonal Projections in the Hamster Main Olfactory Bulb: An Intrabulbar Associational System. J. Comp. Neurol. 235(4) (1985) 503-518.

[25] G. Lowe, Electrical Signaling in the Olfactory Bulb. Curr. Opin. Neurobiol. 13(4) (2003) 476-481.

[26] G. Lowe, Inhibition of Backpropagating Action Potentials in Mitral Cell Secondary Dendrites. J. Neurophysiol. 88(1) (2002) 64-85.

[27] W.C. Xiong, W. R., Dynamic Gating of Spike Propagation in the Mitral Cell Lateral Dendrites. Neuron 34(1) (2002) 115-126.

[28] T.F. Bozza, P.; Zheng, C.; Mombaerts, P., Odorant Receptor Expression Defines Functional Units in the Mouse Olfactory System. J. Neurosci. 22(8) (2002) 3033-3043.

[29] K.J.S. Ressler, S. L.; Buck, L. B., A Zonal Organization of Odorant Receptor Gene Expression in the Olfactory Epithelium. Cell (Cambridge, MA, U. S.) 73(3) (1993) 597-609.

[30] W.C. Still, Modeling biological receptors. Olfaction and Taste: A Century for the Senses, Firmenich Jubilee Symposium 1895-1995, Geneva, Sept. 3-5, 1995 (1997) 223-229.

[31] Z.B. Zou, L. B., Combinatorial Effects of Odorant Mixes in Olfactory Cortex. Science 311 (2006) 1477-1481.

[32] P.W. Mombaerts, F.; Dulac, C.; Chao, S.; Nemes, A.; Mendelsohn, M.; Edmondson, J.; Axel, R., Visualizing an Olfactory Sensory Map. Cell (Cambridge, MA, U. S.) 87(4) (1996) 675-686.

[33] W.B.K. Stewart, J. S.; Shepherd, G. M., Functional Organization of Rat Olfactory Bulb Analyzed by the 2-Deoxyglucose Method. J. Comp. Neurol. 185(4) (1979) 715-734.

[34] J.S. Kauer, Contributions of Topography and Parallel Processing to Odor Coding in the Vertebrate Olfactory Pathway. Trends Neurosci. 14(2) (1991) 79-85.

[35] B.D.K. Rubin, L. C., Optical Imaging of Odorant Representations in the Mammalian Olfactory Bulb. Neuron 23(3) (1999) 499-511.

[36] Pfizer, Pfizer Inc.

[37] H.B.F. Treloar, P.; Mombaerts, P.; Greer, C. A., Specificity of Glomerular Targeting by Olfactory Sensory Axons. J. Neurosci. 22(7) (2002) 2469-2477.

[38] A.T.M. Schaefer, T. W., Spatiotemporal Representations in the Olfactory System. Trends in Neurosciences 30(3) (2007) 92-100.

[39] T.C.M. Bozza, P., Olfactory Coding: Revealing Intrinsic Representations of Odors. Curr. Biol. 11(17) (2001) R687-R690.

[40] B.D. Rubin, L.C. Katz, Spatial coding of enantiomers in the rat olfactory bulb. Nature Neuroscience 4(4) (2001) 355-356.

[41] P.D. Duchamp-Viret, A.; Chaput, M. A., Peripheral Odor Coding in the Rat and Frog: Quality and Intensity Specification. J. Neurosci. 20(6) (2000) 2383-2390.

[42] E.P. Hajjar, D.; Debat, H.; Nespoulous, C.; Robert, C. H., Odorant Binding and Conformational Dynamics in the Odorant-binding Protein. J. Biol. Chem. 281 (2006) 29929-29937.

[43] J. Pevsner, V. Hou, A.M. Snowman, S.H. Snyder, Odorant-binding Protein. Characterization of Ligand Binding. J. Biol. Chem. 265(11) (1990) 6118-6125.

[44] L.N. Briand, C.; Perez, V.; Remy, J.-J.; Huet, J.-C.; Pernollet, J.-C., Ligand-Binding Properties and Structural Characterization of a Novel Rat Odorant-binding Protein Variant. Eur. J. Biochem. 267(10) (2000) 3079-3089.

[45] M.L.G. Getchell, R. C., The Chemistry of Olfactory Reception: Stimulus-specific Protection from Sulfhydryl Reagent Inhibition. Proc. Natl. Acad. Sci. U.S.A. 69(6) (1972) 1494-1498.

[46] U.H. Pace, E.; Salomon, Y.; Lancet, D., Odorant-sensitive Adenylate Cyclase May Mediate Olfactory Reception. Nature (London, U. K.) 316(6025) (1985) 255-258.

[47] L.A. Buck, R., A Novel Multigene Family May Encode Odorant Receptors: A Molecular Basis for Odor Recognition. Cell (Cambridge, MA, U. S.) 65(1) (1991) 175-187.

[48] S.D.B. Liberles, L. B., A Second Class of Chemosensory Receptors in the Olfactory Epithelium. Nature 442 (2006) 645-650.

[49] M.S.S. Singer, G. M., Molecular Modeling of Ligand-receptor Interactions in the OR5 Olfactory Receptor. Neuroreport 5(10) (1994) 1297-1300.

[50] G.M. Shepherd, From Odor Molecules to Odor Images: Toward a Molecular Psychology of Smell. Olfaction and Taste: A Century for the Senses, Firmenich Jubilee Symposium 1895-1995, Geneva, Sept. 3-5, 1995, 1997, pp. 204-222.

[51] B.W.Z. Ache, A., Dual Second-messenger Pathways in Olfactory Transduction. Curr. Opin. Neurobiol. 5(4) (1995) 461-466.

[52] G.M. Shepherd, Discrimination of Molecular Signals by the Olfactory Receptor Neuron. Neuron 13(4) (1994) 771-790.

[53] B.W. Ache, Towards a Common Strategy for Transducing Olfactory Information. Semin. Cell Biol. 5(1) (1994) 55-63.

[54] A.N. Vogl, J.; Breer, H.; Boekhoff, I., Cross-talk Between Olfactory Second Messenger Pathways. Eur. J. Biochem. 267(14) (2000) 4529-4535.

[55] M.A.P. Sanchez-Montanes, T. C., Why do olfactory neurons have unspecific receptive fields? Biosystems 67(1-3) (2002) 229-238.

[56] A.S. Vander, J.; Luciano, D. (Eds.), Human Physiology, McGraw-Hill, U.S.A., 1998.

[57] G.M. Shepherd, A Molecular Vocabulary for Olfaction. Ann. N. Y. Acad. Sci. 510 (1987) 98-103.

[58] M.G. Beets, The Molecular Parameters of Olfactory Response. Pharmacol. Rev. 22(1) (1970) 1-34.

[59] R.R. Randall, in: G. E. Salvadori (Ed.), Olfaction and Taste. A Century of the Senses, Allured Publishing Corporation, Carol Stream, U.S.A., 1997, pp. 137-146.

[60] K.I. Kajiya, K.; Tanaka, M.; Haga, T.; Kataoka, H.; Touhara, K., Molecular Bases of Odor Discrimination: Reconstitution of Olfactory Receptors that Recognize Overlapping Sets of Odorants. J. Neurosci. 21(16) (2001) 6018-6025.

[61] D.Y. Krautwurst, K. W.; Reed, R. R., Identification of Ligands for Olfactory Receptors by Functional Expression of a Receptor Library. Cell (Cambridge, MA, U. S.) 95(7) (1998) 917-926.

[62] H.H. Hamana, J.; Kizumi, M.; Sato, T., Sensitivity-dependent Hierarchical Receptor Codes for Odors. Chem. Senses 28(2) (2003) 87-104.

[63] N.E.G. Rawson, G.; Cowart, B.; Brand, J. G.; Lowry, L. D.; Pribitkin, E. A.; Restrepo, D., Selectivity and Response Characteristics of Human Olfactory Neurons. J. Neurophysiol. 77(3) (1997) 1606-1613.

[64] M. Chastrette, Trends in Structure-odor Relationships. SAR QSAR Environ. Res. 6(3-4) (1997) 215-254.

[65] W.J. Freeman, The Physiology of Perception. Sci. Am. 264(2) (1991) 78-85.

[66] H. Eichenbaum, in: R. C. Llinas, P. S. (Eds.) (Ed.), The Mind-Brain Continuum. Sensory Processes, MIT Press, Cambridge, U.K., 1998, pp. 173-199.

[67] D.A. Leopold, in: R. L. Doty (Ed.), Handbook of Olfaction and Gustation, (Ed.), Marcel Dekker, New York, U.S.A., 1995, pp. 441-454.

[68] C. Linnaeus, Odores Medicamentorum. Amoenitates Academicae 3 (1756) 183-201.

[69] M. Lorry, Sur les Parties Volatiles et Odorants des Médicaments Tirés des Substances Végétales et Animals. Hist. Soc. Roy. Med. Paris: Librairie de la Société royale dé médecine, Barrois (1788) 306-318.

[70] A.v. Haller, Elementa Physiologiae Corporis Humani, 1763.

[71] H. Zwaardemaker, Die Physiologie des Geruchs, Leipzig, 1895.

[72] E. Rimmel, Le Livre des Parfums, Paris, France, 1868.

[73] R. Cerbelaud, Formulaire de Parfumerie. T I, II, and III, 1951.

[74] K.H. Plattig, Electrophysiology of Taste and Smell. Clin. Phys. Physiol. Meas. 10(2) (1989) 91-125.

[75] E. Sagarin, On the Inherent Invalidity of all Current Systems of Odor Classification. J. Soc. Cosmet. Chem. 2(1) (1950) 25-35.

[76]   E.C.H. Crocker, L. F., American Perfume Essential Oil Review 22 (1927) 325-327.

[77]   L. Ruzicka, Chem. Ztg 44 (1920) 129.

[78]   M.G.J. Beets, Structure and Odor. SCI Monograph No. 1 (1957) 54-90.

[79]   M. Stoll, Musk Odor. The Significance of the Constitution of Polyatomic Rings for its Development. Mfg. Perfumer 1 (1937) 107-108.

[80]   G.M. Dyson, The Scientific Basis of Odor. Chem. Ind.(London, U. K.) (1938) 647-651.

[81]   R.H. Wright, Odor and Molecular Vibration. I. Quantum and Thermodynamic Considerations. J. Appl. Chem. 4 (1954) 611-615.

[82]   R.H.S. Wright, R. S. E., Odor and Molecular Vibration. II. Raman Spectra of Substances with the Nitrobenzene Odor. J. App. Chem. 4 (1954) 615-621.

[83]   H.L. Klopping, Olfactory Theories and the Odors of Small Molecules. J. Agric. Food Chem. 19(5) (1971) 999-1004.

[84]   R.H. Wright, Why is an Odour? Nature (London, U. K.) 209(5023) (1966) 551-554.

[85]   R.H. Wright, Odor and Molecular Vibration. SCI Monograph No. 1 (1957) 91-102.

[86]   M. Stoll, Ivme Symposium Mediterraneen sur l'Odorat. Cannes, 1965.

[87]   J.E. Amoore, The Stereochemical Theory of Olfaction. I. Identification of the Seven Primary Odors. Proc. Sci. Sect. Toilet Goods Assoc. Suppl. 37 (1962) 2-12.

[88]   R.W. Moncrieff, Molecular Configuration and Odour. Symposium on Drugs and Sensory Functions, Churchill, London, U.K., 1968, pp. 22-38.

[89]   E.J. Parry, The Chemistry of Essential Oils and Artificial Perfumes. 2 Vols. Vol. I.

[90]   L. Turin, Rational Odorant Design, 2005.

[91]   L. Turin, A Spectroscopic Mechanism for Primary Olfactory Reception. Chem. Senses 21(6) (1996) 773-791.

[92]   L. Turin, A Method for the Calculation of Odor Character from Molecular Structure. J. Theor. Biol. 216(3) (2002) 367-385.

[93]   S.P. Firestein, C.; Menini, A., The Relation Between Stimulus and Response in Olfactory Receptor Cells of the Tiger Salamander. J. Physiol. (Oxford, U.K.) 468 (1993) 1-10.

[94]   G.B. Frater, J. A.; Kraft, P., Fragrance Chemistry. Tetrahedron 54(27) (1998) 7633-7703.

[95]   K.G. Bauer, D.; Surburg, H., Common Fragrance and Flavor Materials: Preparation, Properties and Uses, Wiley-VCH, Weinheim, Germany, 2001.

[96]   P.B. Kraft, J. A.; Denis, C.; Frater, G., Odds and Trends: Recent Developments in the Chemistry of Odorants. Angew. Chem., Int. Ed. 39(17) (2000) 2980-3010.

[97]   R.J. Calkin, J. S., Perfumery. Practice and Principles, Wiley-Interscience, New York, U.S.A., 1994.

[98]   M.B. Gautschi, J. A.; Kraft, P., Fragrance Chemistry - Milestones and Perspectives. Chimia 55(5) (2001) 379-387.

[99]   H. Boelens, Structure-activity Relationships in Chemoreception by Human Olfaction. Trends in Pharmacol. Sci. 4(10) (1983) 421-426.

[100]   K.J. Rossiter, Structure-Odor Relationships. Chemical Reviews (Washington, D. C.) 96(8) (1996) 3201-3240.

[101] P.Z. Bedoukian, Progress in Perfumery Materials. American Perfumer and Cosmetics 86(4) (1971) 25-36.

[102] G.T. Ohloff, A. F., Gustation and Olfaction, Academic Press, New York, U.S.A., 1971.

[103] P.F.M. Vlad, A. F.; Koltsa, M. N., 2-Methyl-3-(1*S*,2*S*)-1,3,3-trimethyl-2-ethylcyclohexyltetrahydrofuran as a Fragrant Component in a Perfume Composition, SU Patent 83-3672355

1169971, 19831208., 1985.

[104] I.B.D. Bersuker, A. S.; Gorbachov, M. Y.; Koltsa, M. N.; Vlad, P. F., Structural and Electronic Origin of Ambergris Odor of Cyclic Compounds. Nouv. J. Chim. 9(3) (1985) 211-218.

[105] I.B.D. Bersuker, A. S.; Gorbachov, M. Y.; Vlad, P. F.; Koltsa, M. N., Structural and Electronic Origin of Odor Properties of Organic Compounds as Revealed by the Electron-topological Approach to the QSAR Problem. Pharmacochemistry Library 10(QSAR Drug Des. Toxicol.) (1987) 340-342.

[106] J.A.B. Bajgrowicz, C., Flavours, Fragrances and Essential Oils. in: K. H. C. Baser (Ed.), Vol. 3, AREP Publishers, Istanbul, Turkey, 1995, pp. 1-15.

[107] J.E. Amoore, Current Status of the Steric Theory of Odor. Ann. N. Y. Acad. Sci. 116(2) (1964) 457-476.

[108] C.S. Sell, On the Unpredictability of Odor. Angew. Chem. Int. Ed. 45 (2006) 6254-6261.

[109] J. McMurry, Organic Chemistry, Thomson Learning, CA, U.S.A., 2000.

[110] K. Mislow, Stereochemical Terminology and Its Discontents. Chirality 14 (2002) 126-134.

[111] P.F. Kraft, G., Enantioselectivity of the Musk Odor Sensation. Chirality 13(8) (2001) 388-394.

[112] B.A.L. Johnson, M., Modular Representations of Odorants in the Glomerular Layer of the Rat Olfactory Bulb and the Effects of Stimulus Concentration. J. Comp. Neurol. 422(4) (2000) 496-509.

[113] A.L. Jinks, D. G., The Analysis of Odor Mixtures by Humans: Evidence for a Configurational Process. Physiol. Behav. 72(1-2) (2001) 51-63.

[114] E.J. Parry, The Chemistry of Essential Oils and Artificial Perfumes. 2 Vols. Vol. II.

[115] E.L. Backman, The Strength of Odorous Substances and their Solubility in Water and in Oil. Journal de Physiologie et de Pathologie Generale 17 (1917) 1-4.

[116] R.W. Moncrieff, The Odorants. Ann. N. Y. Acad. Sci. 58(2) (1954) 73-82.

[117] Y.K. Ishikawa, K., Molecular Orbital Approach to Possible Discrimination of Musk Odor Intensity. Int. J. Quantum Chem. 79(2) (2000) 109-119.

[118] G.G. Ohloff, W., Stereochemistry-activity Relationships in Olfaction. Odorants Containing a Proton Donor/Proton Acceptor Unit. Helv. Chim. Acta 63(1) (1980) 76-94.

[119] J.L.-S. Wang, Z. A.; Suslick, K. S., Is the Olfactory Receptor a Metalloprotein? , Proceedings of the National Academy of Sciences of the United States of America, Vol. 100, 2003, pp. 3035-3039.

[120] S.H.J. Snyder, S. R.; Zakhary, R., Nitric Oxide and Carbon Monoxide: Parallel Roles as Neural Messengers. Brain. Res. Brain Res. Rev. 26(2-3) (1998) 167-175.

[121] J.J.C. Beereboom, D. P.; Stephens, C. R., Flavoring Foods with Benzoxepin-3-ones and Benzodioxepin-3-ones, U.S. Patent 3,517,031, October 28, 1969, 1972.

[122] B.I. Kubota, T., 1,2-Benzene(pentanon-3-ylene). Bull. Chem. Soc. Jpn 6 (1931) 103-106.

[123] F.N. Yoshii, T.; Hirono, S.; Shimizu, Y.; Hoshi, T.; Ando, M.; Hagiwara, H., Conformational Analysis and Selection of Odor-active Conformers: Synthesis of Molecules Designed for the Lily-of-the-Valley(Muguet)-type Odor. Helv. Chim. Acta 84(7) (2001) 2051-2063.

[124] J.-M.B. Gaudin, P.-A., Use of 7-Propyl-benzodioxepin-3-one in Perfumery, E.P. Patent 5, 990, 076, August 17, 1998, 1999.

[125] P. Kraft, Preparation of 1,2-Substituted 2,3-Dihydro-1*H*-5,9-dioxacyclohepta[*f*]inden-7-ones and 7-Substituted Benzo[*b*][1,4]dioxepin-3-ones for Perfumes, E.P. Patent 1, 136, 481, October 3, 2001, 2001.

[126] P.E. Kraft, W., Conception, Characterization and Correlation of New Marine Odorants. Eur. J. Org. Chem.(19) (2003) 3735-3743.

[127] W.L. Carter, W. T., The Hydroxyphenoxy- and Phenylenedioxy-acetic acids. J. Chem. Soc. Trans. 77 (1900) 1222-1227.

[128] F.C. Dallacker, W., Derivatives of 1,3-Benzodioxoles. 50. Preparation of 6,7-Dihydroxychromans Fused to Cyclic Diethers. Z. Naturforsch., B: Anorg. Chem. Org. Chem. 38B(10) (1983) 1243-1248.

[129] J.-M.N. Gaudin, O.; de Saint Laumer, J.-Y.; Winter, B.; Blanc, P.-A., Structure-Activity Relationship in the Domain of Odorants Having Marine Notes. Helvetica Chimica Acta 90 (2007) 1245-1265.

[130] T.E. Acree, GC/Olfactometry. Anal. Chem. 69(5) (1997) 170A-175A.

[131] H. Zwaardemaker, Acta Oto.-Laryngol. 11 (1927) 3-15.

[132] G.H.T. Cheeseman, M. J., Further Experiments on the Olfactory Thresholds of Pure Chemical Substances using the "Sniff-Bottle Method". Quart. J. Exp. Psychol. 8 (1956) 8-14.

[133] H.B. Stone, J. J., Olfactory Discrimination and Weber's Law. Percept. Mot. Skills 20 (1965) 657-665.

[134] G. Semb, The Detectability of the Odor of Butanol. Percept. Psychophys. 4 (1968) 335-340.

[135] J.E.O. Amoore, B. G., Practical Test Kits for Quantitatively Evaluating the Sense of Smell. Rhinology 21(1) (1983) 49-54.

[136] G.H.S. Fuller, R.; Tisserand, G. A., The Gas Chromatograph with Human Sensor: Perfumer Model. Ann. N. Y. Acad. Sci. 116 (1964) 711-724.

[137] A.O.D. Dravnieks, A., Principles and Some Techniques of High-resolution Headspace Analysis. J. Agric. Food Chem. 19(6) (1971) 1049-1056.

[138] B. Imre, Techniques for Analyzing Food Aroma, Vol. 79,, 1997, pp. 293-329.

[139] K.V. Hanaoka, N.; Giampaoli, P.; Heyd, B.; MacLeod, P., Possible Influence of Breathing on Detection Frequency and Intensity Rating in Gas Chromatography-olfactometry. Food Chem. 72(1) (2000) 97-103.

[140] M. Gillette, Source Book of Flavors, Chapman and Hall, New York, U.S.A., 1994.

[141] B.S.R. Mistry, T.; Olson, L. K., Techniques for Analyzing Food Aroma, Vol. 79,, 1997, pp. 265-292.

[142] R.W.G.S. Kleykers, H. N. J., Voedingsmiddelentechnologie 21 (1995) 26-29.

[143] P.M.G.B. Curioni, J. O., Key Odorants in Various Cheese Types as Determined by Gas Chromatography-olfactometry. Int. Dairy J. 12(12) (2002) 959-984.

[144] R.L. Doty, in: D. G. D. Laing, R. L.; Breipohl, W. (Eds.) (Ed.), The Human Sense of Smell, Springer-Verlag, Berlin, Germany, 1992, pp. 96-127.

[145] S. Patton, Flavor of Milk and Milk Products. Flavor Research and Food Acceptance (1958) 315-323.

[146] J. Frijters, Progress in Flavor Research, Applied Science Publishers, London, U.K., 1978.

[147] C. Sell, Structure/Odor Correlations: The Mechanism of Olfaction and the Design of Novel Fragrance Ingredients. Perfumer & Flavorist 25(1) (2000) 67-73.

[148] B.B. Berglund, U.; Ekman, G.; Engen, T., Individual Psychophysical Functions for Twenty-eight Odourants. Percept. Psychophys. 9 (1971) 379-384.

[149] E.H. Weber, De pulsu, resorptione, auditu et tactu: Annotationes anatomicae et physiologicae, Koehler, Leipzig, Germany, 1834.

[150] S.S. Stevens, Sensory Scales of Taste Intensity. Percept. Psychophys. 6 (1969) 302-308.

[151] W.S.J. Cain, F. Jr., Lability of Odor Pleasantness: Influence of Mere Exposure. Perception 7(4) (1978) 459-465.

[152] G.T. Fechner, Elemente der psychophysik, Breitkopf and Harterl, Leipzig, Germany, 1860.

[153] K. Rossiter, in: D. H. S. Pybus, C. S. (Ed.), The Chemistry of Fragrances, (Eds.), The Royal Society of Chemistry, Cambridge, UK, 1999, pp. 233-253.

[154] G.D. Borg, H.; Strom, L.; Zotterman, Y., The Relation Between Neural and Perceptual Intensity: A Comparative Study on the Neural and Psychophysical Response to Taste Stimuli. J. Physiol. (Oxford, U.K.) 192(1) (1967) 13-20.

[155] G.D. Borg, H.; Strom, L.; Zotterman, Y., Neural and Perceptual Intensity. J. Physiol. (Oxford, U.K.) 191(2) (1967) 118P-119P.

[156] H.G. Guth, W., Odorants of Extrusion Products of Oat Meal - Changes During Storage. Z. Lebensm.-Unters. -Forsch. A 196(1) (1993) 22-28.

[157] H.G. Guth, W., Identification of Potent Odorants in Static Headspace Samples of Green and Black Tea Powders on the Basis of Aroma Extract Dilution Analysis (AEDA). Flavour Frag. J. 8(4) (1993) 173-178.

[158] P.G. Schieberle, W., Changes in the Concentrations of Potent Crust Odorants During Storage of White Bread. Flavour Frag. J. 7(4) (1992) 213-218.

[159] C.L. Garcia-Jares, M.; Polo, M.; Salgado, C.; Macias, S.; Cela, R., Optimization of a Solid-phase Microextraction Method for Synthetic Musk Compounds in Water. J. Chromatogr., A 963(1-2) (2002) 277-285.

[160] A.A. Kamath, M. R.; Ravi, R.; Narasimhan, S.; Rajalakshmi, D., Comparative Study of Odor and GC-olfactometric Profiles of Selected Essential Oils. Flavour Frag. J. 16(6) (2001) 401-407.

[161] A.C. Hallier, P.; Serot, T.; Prost, C., New Gas Chromatography-olfactometric Investigative Method, and its Application to Cooked *Silurus Glanis* (European catfish) Odor Characterization. J. Chromatogr. A 1056(1-2) (2004) 201-208.

[162] P.J.K. Marriott, R. M., in: E. R. H. Adlard, A. J. (Ed.), Gas Chromatographic Techniques and Applications, (Eds.), Sheffield Academic Press, Sheffield, U.K., 2001, pp. 260-297.

2 Synthesis of Benzodioxepinones: Calone 1951[®] Analogues by Procedure A

2.1 Introduction

The methodology for Procedure A (Scheme 2.1) involves a Williamson reaction with a 2 mole excess of methyl bromoacetate to afford a di-etherified product (**21** derivatives) from a substituted catechol. Subsequent Dieckmann condensation on the symmetrical hetero-ester chains resulted in a racemic mixture of regioisomers (isomer 1 and isomer 2). For liberation of the target benzodioxepinone a single-step acidic decarboxylation afforded results faster than a two-step procedure involving saponification and consequent decarboxylation.
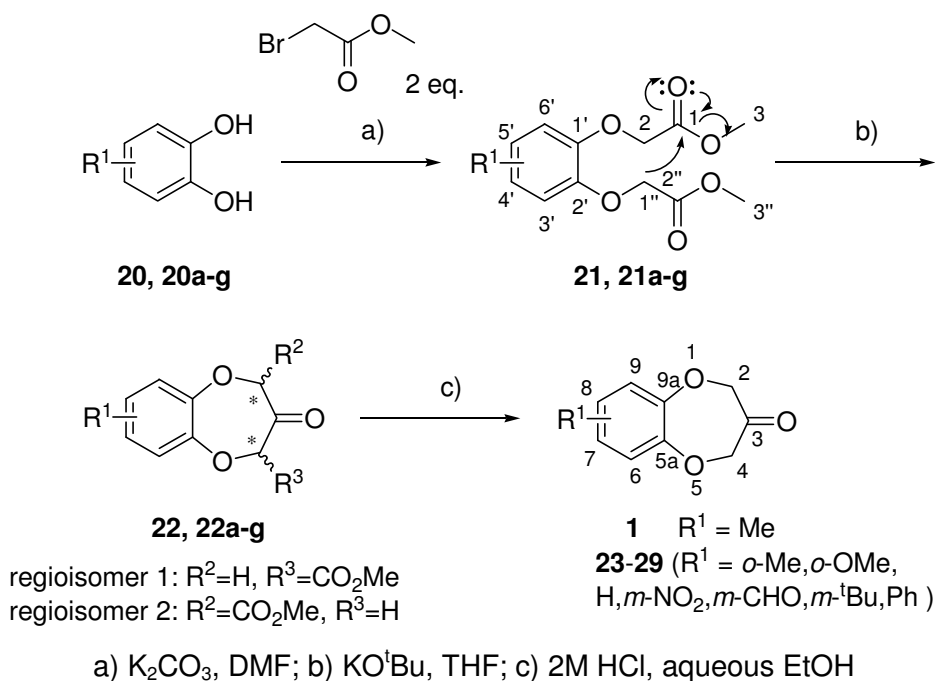
Scheme 2.1 Preparation of **1** and derivatives **23**-**29** by Procedure A

The synthetic methodology presented in Scheme 2.1 was employed to form the intermediates **21a**-**g**, leading to a range of benzodioxepinone analogues (compounds **23**-**29**) involving the use of *o*-dihydroxy substituted aromatics (**20a**-**g**) utilising both microwave and conventional methods.

Table 2.1 Overview of yields derived for benzodioxepinone analogues **23**-**29**
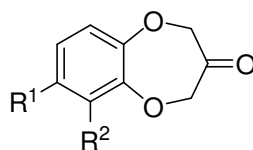
Compound	R^1	R^2	Yield (%)	Purity (%)*
1	Me	H	78	95
23	H	Me	14	97
24	H	OMe	95	99
25	H	H	10	100
26	NO$_2$	H	2	87
27	CHO	H	11	75
28	^{t}Bu	H	84	95
29	Ph (naphthyl)	H	7	88

* Purity values were derived from GC-MS

As shown in Table 2.1, the nature of the aromatic ring substituents, R^1 and R^2, strongly influenced the yield and the degree of product purity. Analogues with electron-donating aromatic substituents akin to **1** (R^1 = Me) (**23**, **24**, **28**) could effectively be purified by vacuum distillation, whereas those with an EWG (**26**-**27**) or no electron-donating contributor (**25**, **29**) demanded separation by semi-preparative HPLC. Compounds **23** and **25** have been synthesised previously by Beereboom et al. and Rosnati and De Marchi respectively. Their procedures and discoveries are discussed in more detail in Section 3.1.

In pursuit of odour-active benzodioxepinones, experimentation with substituted catechols demonstrated distinct differences in the physico-chemical properties involved in catechol chemistry in comparison with phenol derivatives. For this reason a brief overview of the physical and chemical properties of catechol forms will be discussed in the context of preparation of catechol di-ether derivatives.

Dihydroxybenzene can exist as three possible isomers: *ortho*-dihydroxy benzene (catechol), *meta*-dihydroxy benzene (resorcinol) and *para*-dihydroxy benzene (quinol) (Figure 2.1).
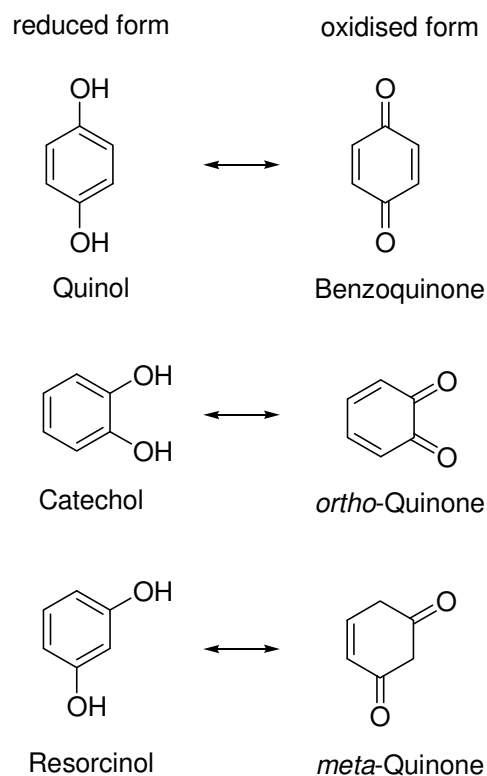
Figure 2.1 *Ortho-*, *meta-* and *para*-dihydroxy benzenes [1]

The aromaticity of these compounds provides a strong stabilising influence for the easily derivatised diols. All three catechols exhibit diverse chemical properties providing versatile building blocks for synthesis such as pigments and pharmaceuticals [2]. Similar to phenols, the hydrogen-bonding capabilities and lipophilic aromatic ring of catechol, resorcinol and quinol render them volatile and potently odourous compounds.

The redox properties of catechol and quinol determine their application as general antioxidants, and as strong reducing agents in photographic developers [2]. Quinol will readily inter-convert between oxidised and reduced counterparts and is synthetically utilised as a polymerisation inhibitor, whereas catechol will itself undergo oxidative polymerisation [3]. Resorcinol's tendency to polymerise leads to its incorporation into plasticiser, resin and adhesive manufacture [2].

For construction of the benzodioxepinone ring of **1**, *ortho*-catechol is required. Selective de-protonation of *ortho*-catechol hydroxy groups demonstrates the variable acidity of the compound, represented in Figure 2.2 by pKa values and corresponding melting points. Experimentally, a simple procedure for the isolation of the exposed *ortho*-phenolate is via the mono-substituted salts, these however remain difficult to isolate prior to derivatisation.
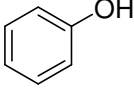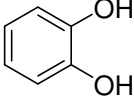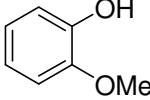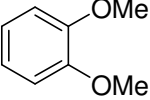
pKa (at 25°C):	9.86	9.50	9.97	-
m.p.(°C):	40-42	103-105	27-32	19-21

Figure 2.2 Comparison of some chemical properties of phenol, catechol and catechol ethers [1]

A moderate decrease in pKa is noticeable when comparing catechol and the mono-alkylated derivative. Application of the Williamson reaction proved catechol is sufficiently acidic for K_2CO_3 to de-protonate the aromatic hydroxy groups in dipolar aprotic solvents, dimethyl formamide (DMF) and dimethyl sulphoxide (DMSO), also reported by Beereboom et al. [4]. Catechol is easily oxidised in EtOH yet can be recrystallised from water. Aromatic substitution of a catechol can significantly alter the physical and chemical properties of the molecule, for example methyl catechol oxidises over time in air and can be recrystallised from a non-polar hydrocarbon solvent. As functionalised chain length of mono-substituted *ortho*-catechol increases dimerisation becomes more favourable over intramolecular cyclisation. In order to arrive at the benzodioxepinone ring, formation of the di-ether bridge can be conveniently derived from dialkyl-substituted catechol with subsequent cyclisation, rather than aromatic functional group interconversion.

Resistance of **20g**, and to a lesser extent **20c** (Figure 2.3) to cyclise under the Dieckmann conditions employed was also detected. This may be explained by the polar surface area (predicted using ACD Labs V8.14 for Solaris), and hence electronegative distribution. The presence of an electron-donating group (EDG) decreases stabilization by donating charge into the ring, and an electron-withdrawing group (EWG) contributes π-resonance stabilization depicted in Figure 2.4. Etherification of the hydroxyl groups can potentially hinder intra-molecular nucleophilic attack and cyclisation of the ether chains through steric hindrance. This discussion is covered more thoroughly in 2.3.2 *Ab initio* Models - Inductive and Resonance Effects of Aromatic Substitution Relevant to Success of Procedure A.
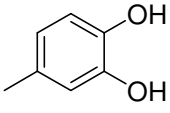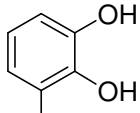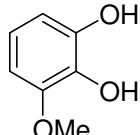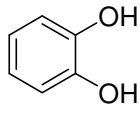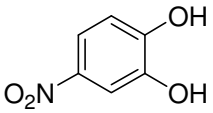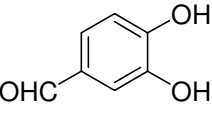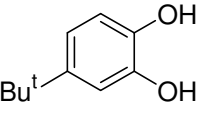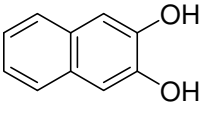
	20	**20a**	**20b**	**20c**
pKa (at 25°C):	9.69	9.71	9.27	9.50
m.p.(°C):	67-69	65-68	40-43	103-105
polar surface area (A2):	40.5	40.5	49.7	40.5

	20d	**20e**	**20f**	**20g**
pKa (at 25°C):	6.84	7.59	9.66	9.10
m.p.(°C):	174-176	153-155	52-55	162-164
polar surface area (A2):	86.3	57.5	40.5	40.5

Figure 2.3 Chemical properties of substituted catechols [1] [5]
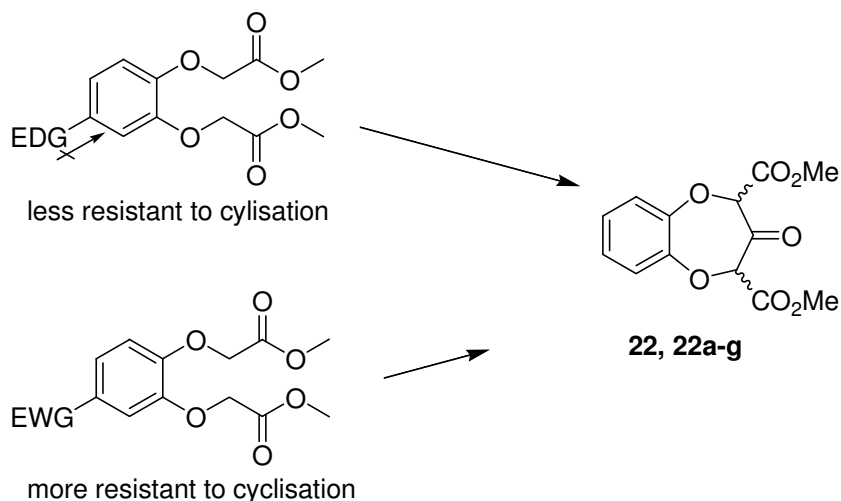
Figure 2.4 An EDG donates charge into the aromatic ring, destabilising the electronegative distribution throughout the structure causing it to be more susceptible to S_N2 cyclisation. With an EWG the molecule is stabilised through enhanced pi-resonance with the aromatic ring, resulting in hindered cyclisation. This is discussed in more detail in 2.3.2.

2.2 Preparation of Benzodioxepinone Analogues by Procedure A: Williamson Etherification

R^1 = Me, *o*-Me,*o*-OMe,
H,*m*-NO$_2$,*m*-CHO,*m*-^{t}Bu,Ph
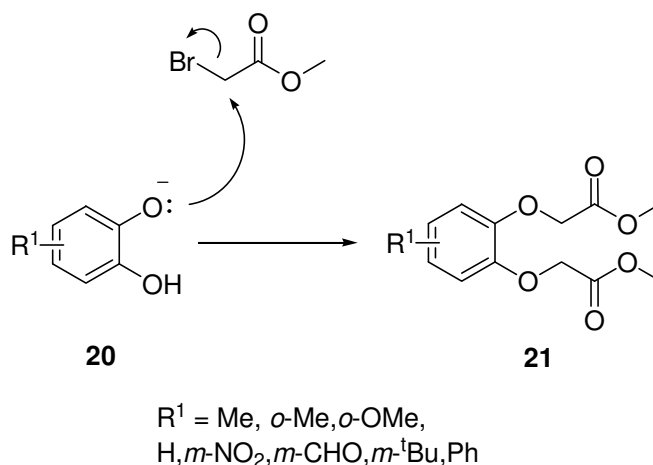
conventional: K$_2$CO$_3$, DMF, 120°C, 2 hr
microwave: K$_2$CO$_3$, DMF, 4 min, 200W

Scheme 2.2 Williamson etherification

The Williamson etherification (Scheme 2.2) occurs in two intrinsic steps; the acid-base de-protonation of the catechol hydroxyl groups with carbonate, and attack at the halogenated methylene of methyl bromoacetate by the de-protonated catechol oxy-anions. Other factors such as solvation and bond strength should also be considered when reviewing the ability for catechols to undergo S$_N$2 reaction with an alkylating agent such as methyl bromoacetate. Problems encountered with nucleophilic cyclisation will be discussed in more detail in Sections *2.3.1* and *2.3.2*. It is worthwhile highlighting here factors contributing to nucleophilicity in light of the flexibility of the di-acetate chains of **21** and its derivatives. Molecular size and corresponding solvolysis (the degree of clustering of solvent molecules) will come into play. As molecules increase in complexity and size, molecular conformation plays a significant role in the degree to which a molecule becomes solvated. The higher the degree of solvation, the more the nucleophilic ability of the molecule is suppressed (or any property requiring access by another molecule).

Nucleophilicity and Brønsted-Lowry acidity trends do not necessarily always coincide, however when generalized one can be used as a guide for the other. For neutral organic molecules increased basicity corresponds to increased nucleophilicity. Nucleophilicity is

also related to polarisability; the ease of distortion of the molecular electron cloud, whereby increased polarisability equates to increased nucleophilicity. Nucleophilicity in general is influenced by a combination of electrostatic attractions and orbital (HOMO-LUMO) interactions. Electrostatic attractions, including polarisability, do not influence the transition state and reactivity of S_N2 reactions, demonstrated by the lack of dipole of the carbon-halogen bond (as in methyl bromoacetate) and its contrasting high electrophilic activity in S_N2 reactions. The directional effect of the substituent is demonstrated in the variation in pKa_1 values (**20d** (nitro): 7.73 and **20** (methyl): 9.33) (Figure 2.5 and Figure 2.6), in conjunction with those featuring the substituent (nitro or methyl) *ortho* to the hydroxyl group. The *meta*-directing effect of the nitro group reinforces the de-activating character of the ring.
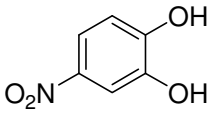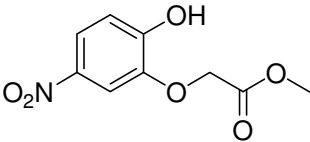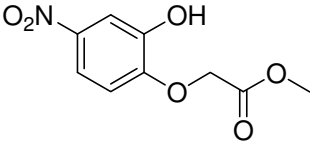
	20d		
pKa_1:	6.87 ± 0.22	5.96 ± 0.16	7.73 ± 0.10
pKa_2:	11.09 ± 0.19	-	-

Figure 2.5 pKa values for **20d** derivatives [6]
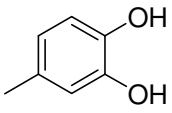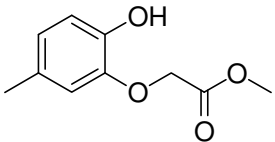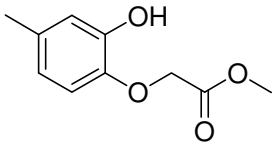
	20		
pKa_1:	9.91 ± 0.10	9.52 ± 0.43	9.33 ± 0.35
pKa_2:	12.84 ± 0.18	-	-

Figure 2.6 pKa values for **20** derivatives [6]

In general EWGs delocalise charge and therefore stabilize the molecule, which coincides with increased acidity (pKa), resulting in a weaker (more stable) conjugate base. EDGs have the opposite effect through donating more charge into a structure. The pKa2 predictions for both **20d** and **20** concur with the mono-alkylated values as expected. The calculated pKa values for *meta*-methyl catechol and the mono-alkylated derivative (Figure

2.5) are relatively close, indicating that the weakly acidic catechol (higher pKa) contains similar reactivity at the second hydroxyl position.

2.2.1   Microwave Synthesis Comparisons

Our previous studies [7] suggested that Williamson ether synthesis conducted under microwave irradiation can lead to improvements in yield or purity of di-etherified intermediates.   This is advantageous in the preparation of fragrance chemicals, as structurally related impurities noticeably persistent in benzodioxepinone products, are difficult to eradicate, and lead to erroneous olfactory evaluation.   Comparison of results from di-etherification (Scheme 2.1: step a) of various catechol reagents via conventional methods and, as an experimental alternative, exposure to microwave irradiation is provided (Table 2.2).

Table 2.2 Microwave vs conventional methods for Williamson etherification of various substituted catechols to form aromatic di-ethers

Compound		Conventional method[^]		Microwave method[#]	
		Yield (%)	Purity(%)[+]	Yield (%)	Purity (%)[+]
1	*meta*-Me	78[a]	98	83	98
21a	*ortho*-Me	92[a]	95	36[b]	100
b	*ortho*-OMe	66[a]	98	45[b]	100
c	-	88[a]	98	48[b]	85
d	*meta*-NO$_2$	53[c]	98	74[b]	>99
e	*meta*-CHO	55[a]	98	79[a]	91
f	*meta*-*t*Bu	75[a]	98	65[a]	76
g	*face*-benzo	96[*]	97	75[*]	94

[^] Reaction time: 2 hr

[#] Reaction time: 4 min

[+] Purity determined by GC-MS

[*] Purification via vacuum only

[a] Following bulb distillation

[b] Following purification via flash chromatography and bulb distillation

[c] Bulb distillation solely used to remove solvent and alkylating agent

Improved yields for catechols containing electron-withdrawing substituents (**20d-e**) were obtained with microwave-assisted synthesis and can be attributed to the increase in

heating efficiency of the reaction mixture to overcome differences in acidity of the intermediate mono-alkylated phenol. Despite superior yields for *steps b* and *c* (Scheme 2.1) by conventional means, the success of irradiation from *step a* contributes enhanced overall efficiency to the total reaction scheme.

A summary of methylene shifts is presented in Table 2.3 for all structures **21**, **21a-g** as an overview of the influence of the various aromatic substituents.

Table 2.3 Methylene ^{1}H and ^{13}C NMR shifts for structures **21**, **21a-g**

21
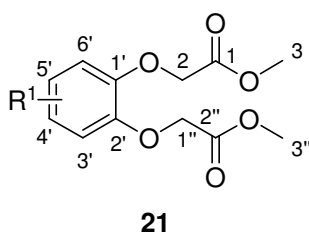
	R^1	^{1}H δ		^{13}C δ	
		(s, 1"-CH$_2$)	(s, 2-CH$_2$)	1"-CH$_2$	2-CH$_2$
21	4'-Me	4.71	4.69	66.6	66.2
a	3'-Me	4.69	4.60	69.0	65.6
b	3'-OMe	4.65	4.64	66.6	69.5
c	H	4.71		66.5	
d	4'-NO$_2$	4.80	4.83	66.0	66.1
e	4'-CHO	4.78	4.81		65.9
f	4'-^{t}Bu	4.68	4.72	66.7	67.2
g	Ph	4.83			66.2

Products were confirmed by molecular ion in GC-MS analysis represented by the *meta*-nitro derivative (**21d**) (299.50 *m/z*) to define the molar mass and empirical formula, in conjunction with ^{1}H, ^{13}C NMR (Figure 2.7) and HMBC. Rationalisation of mass spectral fragmentation of the base structure of **21** is provided in Appendix 1. Full characterisation was carried out for all intermediates **21a-g** and structures were assigned using 2D COSY, HMQC and HMBC analysis.

ABUNDANCE

45.10

79.15

120.20 135.20 151.30

166.25 180.35

207.30

240.40

267.45

299.50

90
80
70
60
50
40
30
20
10
0

13   63   113   163   213   263   313

7.934
7.743
7.735
7.925
7.903
6.897
6.867
7.895

4.828
4.798

3.822
3.809

O₂N

21d

1.8   0.8   3.9   5.5

8   7   6   5   4   3

168.31

153.08
147.48
142.27

118.72
113.17
110.03

66.25
66.11

52.47
52.43

175   150   125   100   75   50   25
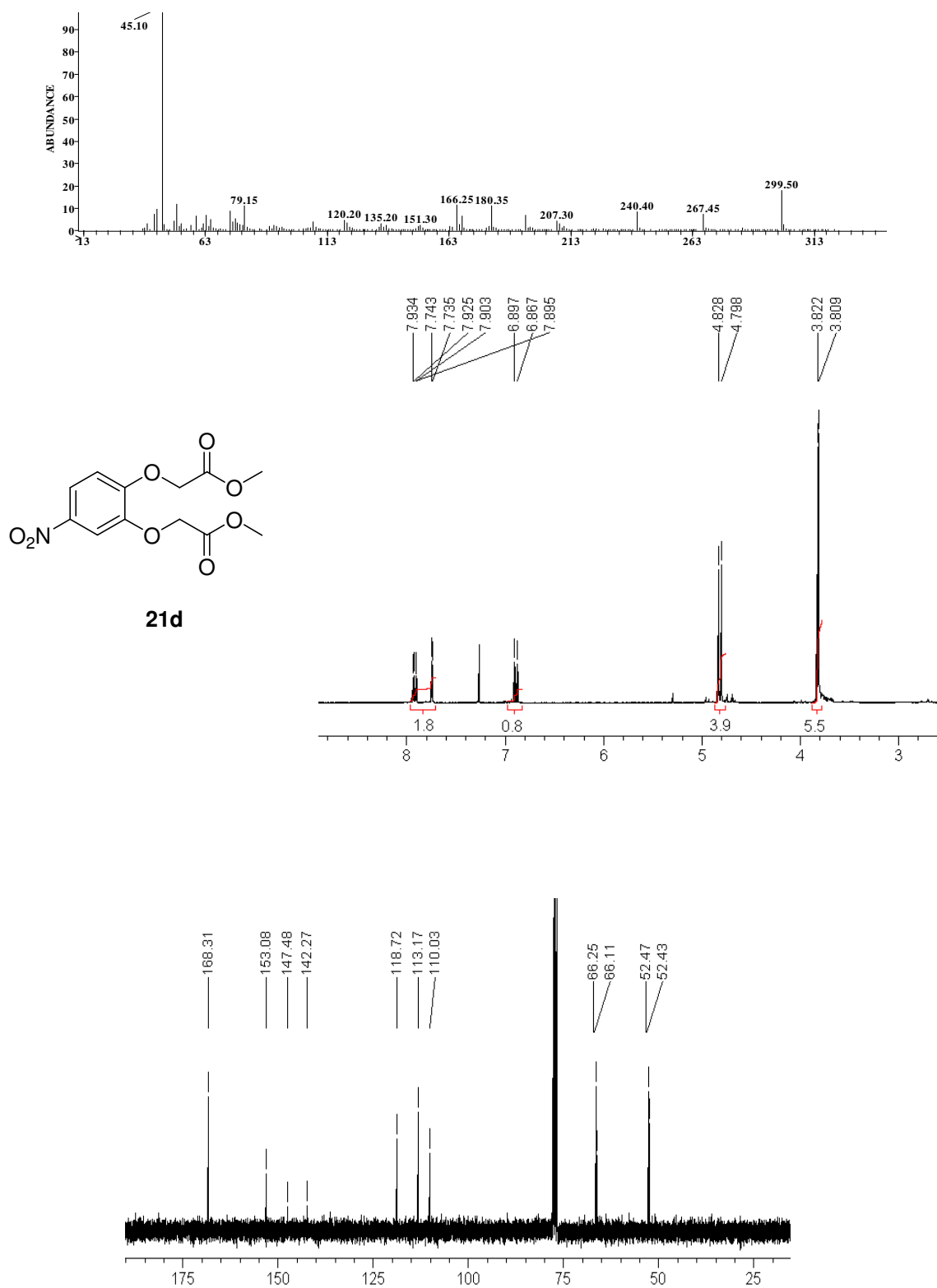
Figure 2.7 EI mass spectrum, ¹H and ¹³C NMR spectra of **21d**

Separate ^{1}H and ^{13}C shifts for the acetate chains demonstrates that the inductive influence of aromatic substituents spans the entire molecular structure through to the methylene and terminal methyl ester regions, perceptible for *o*-substituted **21a** (Appendix 2) and **21b** (Appendix 3) by slight shift differences in 1D NMR data for the terminal methyl groups C-3 and C-3''.

Methylene signals, C-1'' and C-2 of **21a** with an *o*-methyl aromatic substituent in HMQC spectra demonstrates the carbon signal further upfield coupled to the corresponding upfield proton signal, likewise **21f** reveals low carbon signal, low proton signal coupling. HMBC data of **21a** is presented Figure 2.8, the proton/carbon CH_2 coupling is highlighted with the upper square. Compounds **21**, **21d**, **21e** and **21b** all lacked a proton-carbon methylene coupling 'skew', in HMQC or HMBC.

Long-range heteronuclear HMBC data for compound **21d** (Figure 2.9) reveals the low carbon shift carbons 1' and 2' coupled to the lower proton shift methylenes, as indicated by the square. Methylene groups 1''-CH_2 (66.0 ppm) and 2-CH_2 (66.1 ppm) were coupled to carbons C-2' (147.4 ppm) and C-1' (153.0 ppm) respectively. In contrast, **21a** reveals the low signal (further upfield) (C-2') coupled to the higher CH_2 shift (further downfield) (1''-CH_2), and correspondingly C-1' is coupled to 2-CH_2, as indicated by the lower square in Figure 2.8. Compound **21** reveals no trend. Quaternary carbons of compounds with an alkyl aromatic substituent were verified by HMBC coupling to the aromatic substituent.

Some of the compounds mentioned here clearly deviate from expected trends, such as the common CH_2-aromatic coupling order demonstrated in **21d**, with an EWG, and contrasting **21a**, with an ED aromatic substituent. Evidently the delineation of aromatic substituent character into the EW or ED classification is not a direct indicator of NMR splitting patterns.
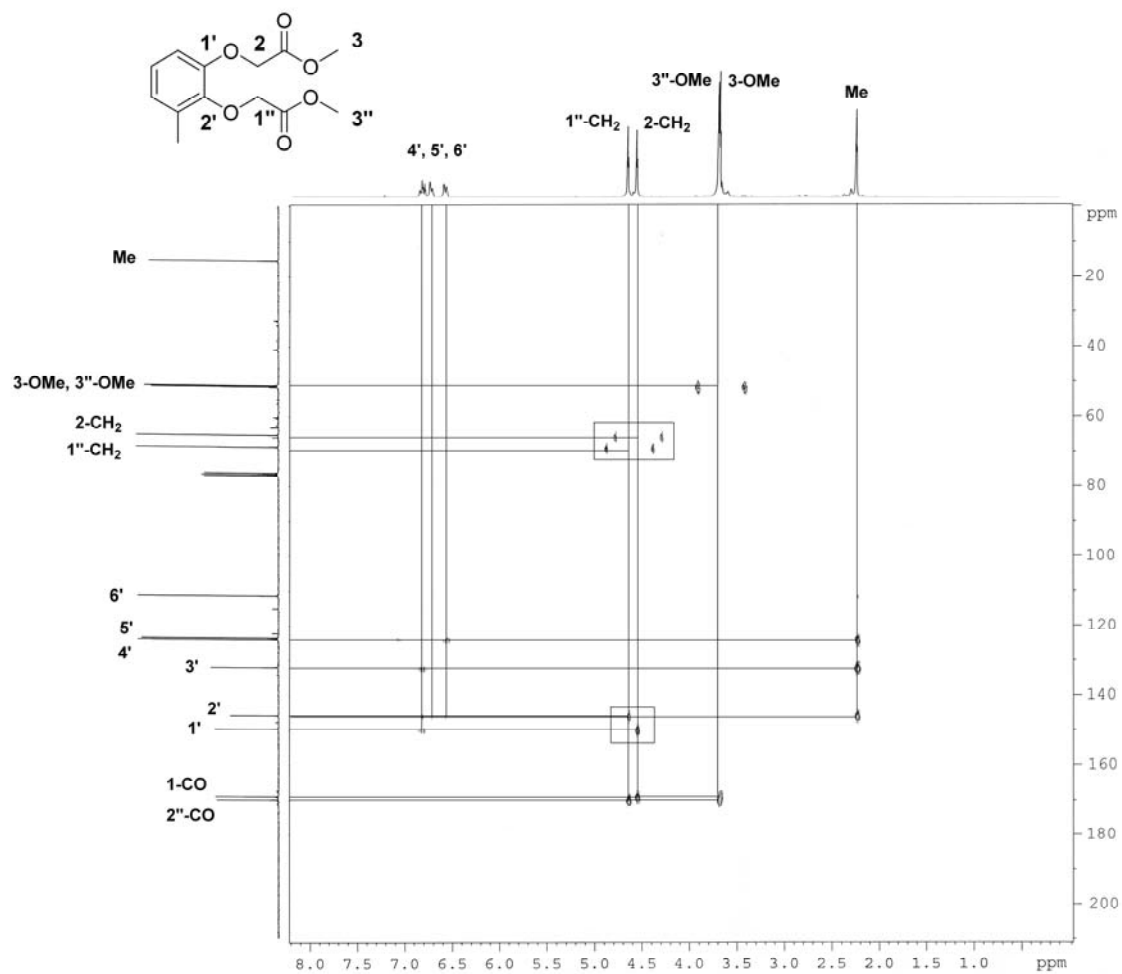
Figure 2.8 ^{1}H,^{13}C HMBC of **21a**
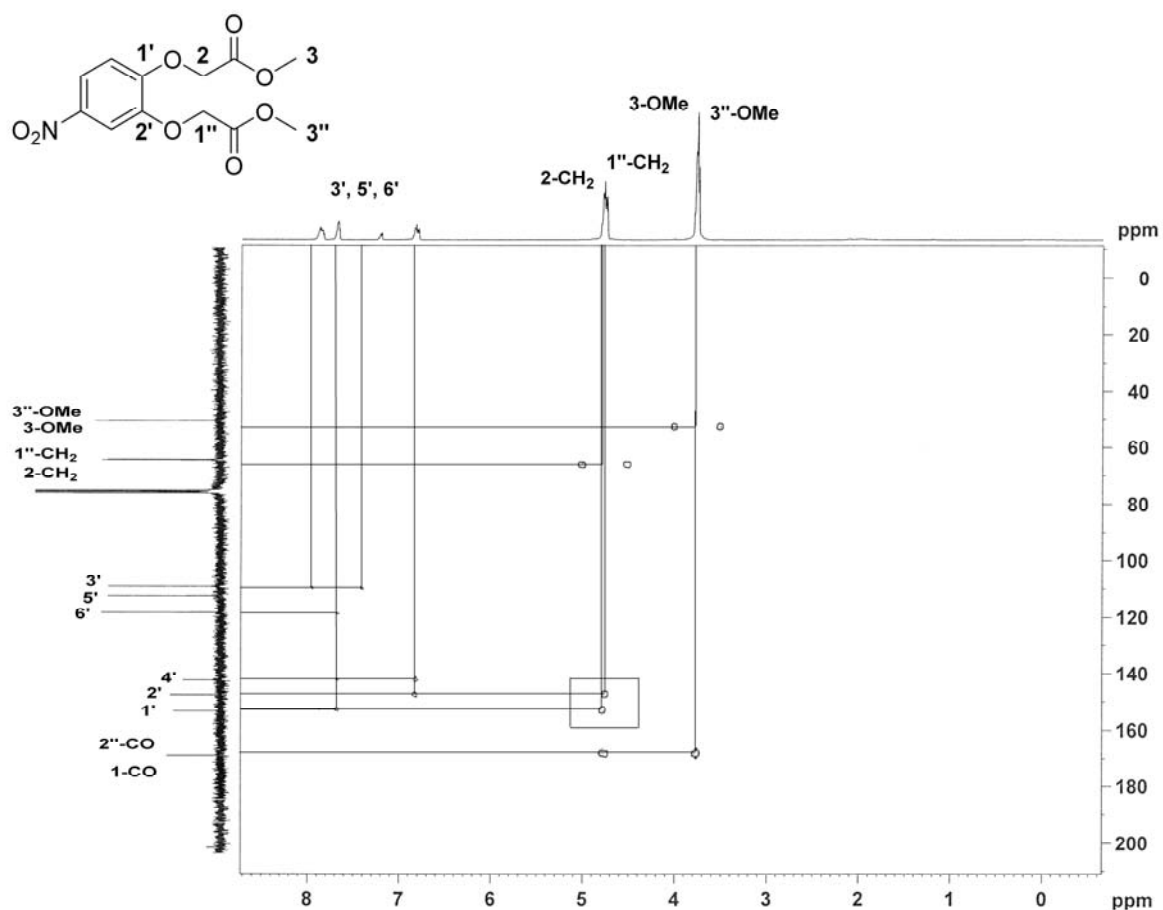
Figure 2.9 ^{1}H,^{13}C HMBC of **21d**

2.3 Preparation of Benzodioxepinone Analogues by Procedure A: Dieckmann Cyclisation

Preliminary experiments for *step b* (Scheme 2.1) involved, among other bases, sodium amide (NaNH$_2$) and sodium hydride (NaH), according to the protocol proposed for Calone 1951® in the patent literature, with limited success and no detection of the cyclic product. Our trials to form the β-keto ester, **22**, were successful with potassium *tert*-butoxide (KO^{t}Bu). The use of NaH for the attempted cyclisation of derivatives of **21**, refluxed for 48 hr, generated no product at 2 hr, 12 hr, 24 hr and 48 hr. Employing a similar protocol to Funk et al. [8], trials were performed on **21c** and **21g** mediated by the presence of a Lewis acid; TiCl$_4$ (Scheme 2.3).
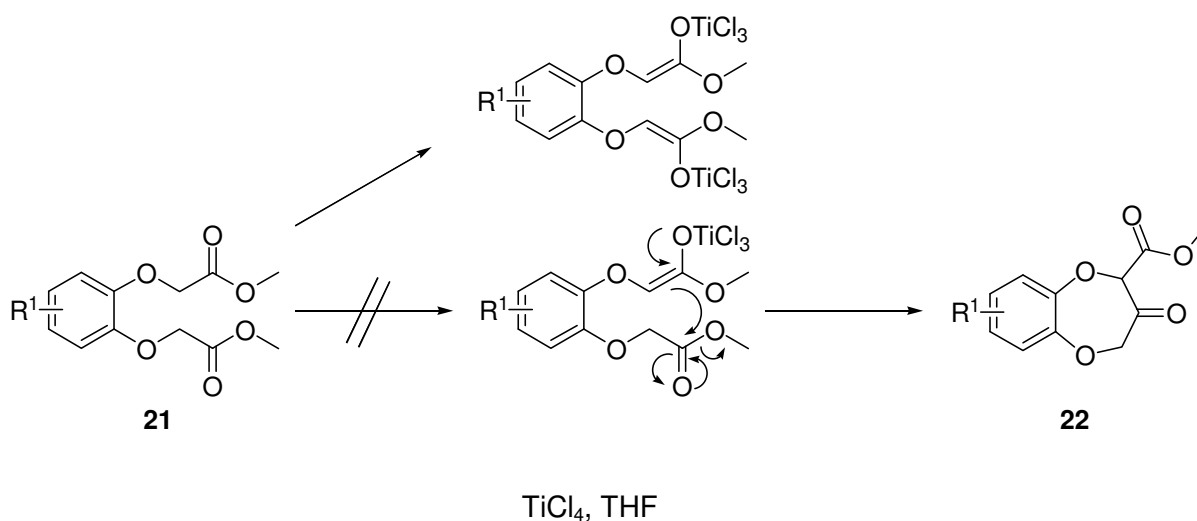
Scheme 2.3 Attempted preparation of **22**

The symmetrical side chains prevented cyclisation despite the use of 0.5 equivalents of TiCl$_4$ to encourage formation of mono- rather than di-titanium enolate. The pale yellow TiCl$_4$ complex proceeded to darken upon heating and led to a complex mixture. GC-MS analysis verified that no cyclisation had occurred.

2.3.1   Identification of Impurities Formed During Dieckmann Cyclisation

In 1962, prior to release of the Pfizer patent, Rosnati and De Marchi derived no success with a Dieckmann condensation for cyclisation to the benzodioxepinone structure [9]. Our experimental procedures revealed that KO^{t}Bu/THF provided the most promising results. However, success of the Dieckmann cyclisation on the substrates used (refer back to Figure 2.3) demanded reagent purity ≥98%, otherwise a 5-10% impurity would render only 30-50% product yield. The results for each analogue are presented in Table 2.4.

Table 2.4 Conventional yields for cyclized products, **22**, from Dieckmann cyclisation using KO^{t}Bu

Compound	R^1	Isomeric ratios (GC-MS)	Yield-isomeric mixture (%)	Purity-isomeric mixture (%)[+]
22	*m*-Me	50:50	92	95
a	*o*-Me	30:70	82	96
b	*o*-OMe	81:19	85	93
c	H	-	87	93
d	*m*-NO$_2$	57:43	Not isolated from HPLC fractions	78[*]
e	*m*-CHO	100	Not isolated from HPLC fractions	74[^]
f	*m*-^{t}Bu	51:49	87	86
g	Ph (*face*)	-	2	80[#]

[+] Purity determined by GC-MS

[*] molecular ion found: 233 m/z

[^] molecular ion found: 178 m/z

[#] molecular ion found: 200 m/z

Dieckmann condensation (Scheme 2.4) on the symmetrical acetate chains resulted in a 50:50 mixture of regioisomeric forms (compound **22**). Separation of the regioisomeric mixture (**22**) was unnecessary since subsequent decarboxylation of both isomers led to the desired benzodioxepinone targets. Despite superior yields obtained by conventional methods in comparison to microwave irradiation for products **22a-g**, irradiation is a viable alternative to obtain pure compounds in shorter reaction times. However in this case conventional heating or microwave irradiation produced similar outcomes.

isomer 1: R^2=H, R^3=CO$_2$Me
isomer 2: R^2=CO$_2$Me, R^3=H
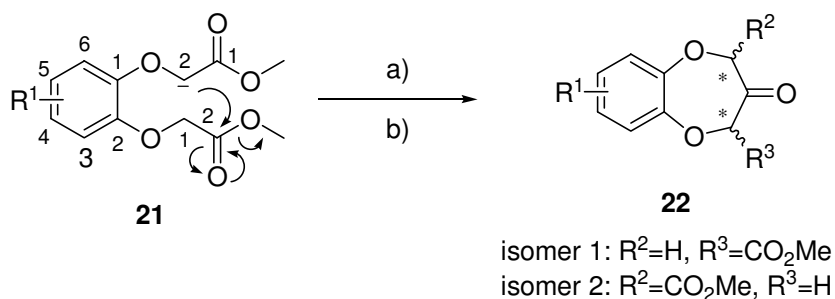
a) KO^{t}Bu (2 mole), THF, 0.5 hr, 70°C; b) aq. HCl

Scheme 2.4 Dieckmann condensation

Initially, no molecular ions were detectable for **22e** and **22g** in quadrupole MS analysis. The highest detectable masses were 178 m/z and 200 m/z, respectively. The fragments appearing from ionisation corresponded to a loss of 72 m/z; similarly an initial cleavage of 34 m/z was evident for **22d** (233 m/z). Nevertheless, the efficiency of the decarboxylation ensured formation of the desired analogue products, albeit in low yields requiring HPLC separation (2% (**22d**), 11% (**22e**) and 7% (**22g**)). Evidently, EDGs present on compounds **21a**, **21b** and **21f** assist in localising the charge of the hetero-oxygens leading to de-stabilisation of the aromatic ring. Conversely the EWGs of **21d** and **21e** and the conjugated naphthalene system of **21g** contribute to resonance stabilisation of the aromatic ring, resulting in hindered cyclisation. In light of the irreproducible and impure yields obtained for intramolecular cyclisation of **21d**, **21e** and **21g** initially it was suspected that the major by-product appearing in the production of all analogues of **22** was the substituted benzodioxane impurity shown in Figure 2.10. The molecular ion of 164.00 *m/z* in GC-MS was concordant with the proposed structures **30a** and **30b**.
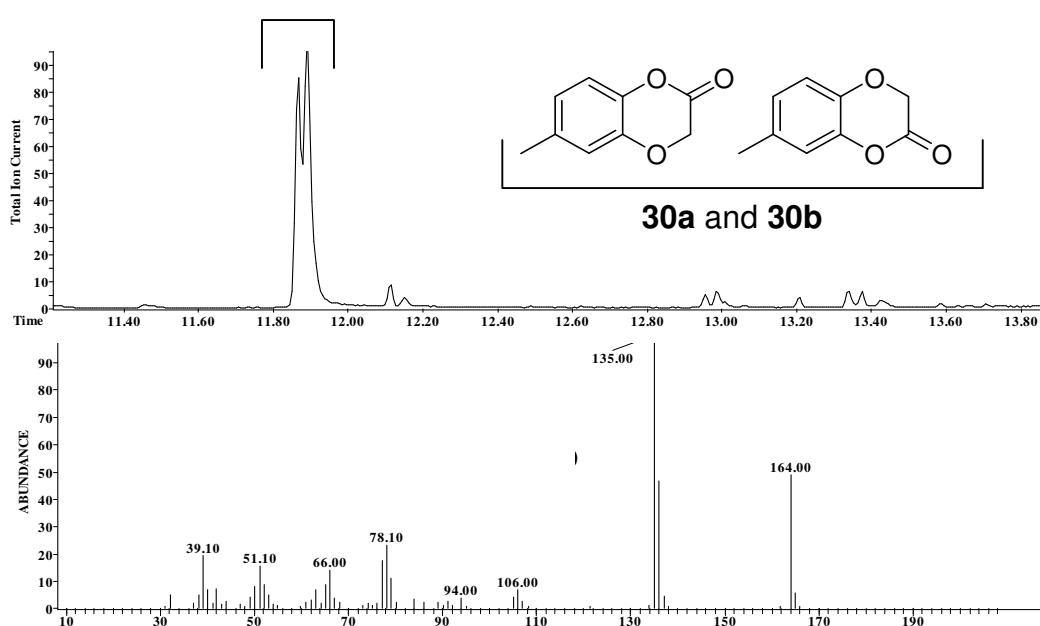
Figure 2.10 GC-MS of proposed regio-isomeric impurity 6/7-Methyl-1,4-benzodioxin-2(3*H*)-one (**30a** and **30b**)

Isolation of the impurity (164 *m/z* molecular ion) from the complex reaction mixtures via semi-preparative HPLC revealed inconsistent results when NMR data of the isolated fraction were compared with the mass spectrum. Isomers **30a** and **30b** eluted from the

GC column with very similar retention times (as shown in Figure 2.10) and identical mass spectrum fragmentation.

Potential hydrolysis of the methyl ester to an acid was ruled out by the absence of a broad hydroxy band in the 2000-3000 cm^{-1} range from FT-IR analysis. The possibility of a Favorskii-type rearrangement (Scheme 2.5) was considered, as complex inconclusive ^{1}H and ^{13}C NMR spectra alluded to the formation of polymerised material.
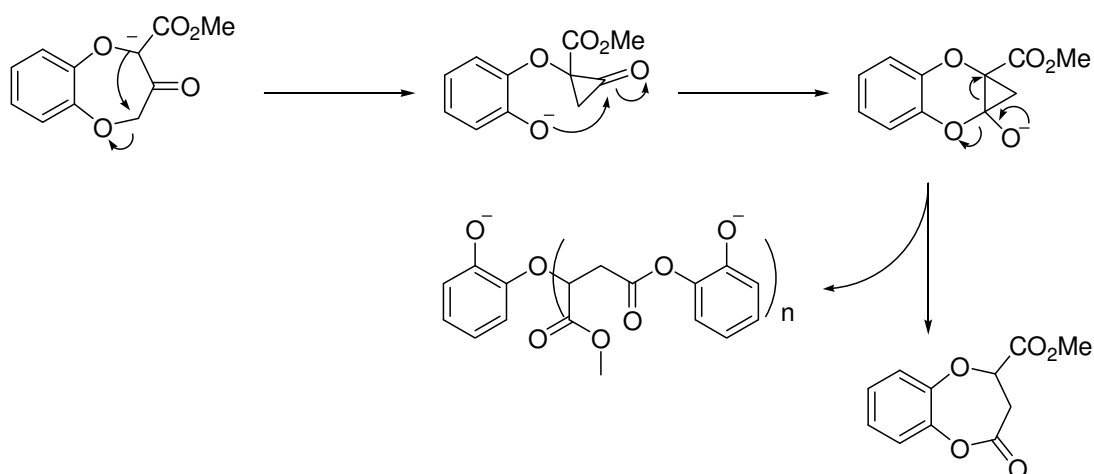
Scheme 2.5 Proposed Favorskii-type rearrangement of **22**

No 1D NMR signals characteristic of cyclized material from Favorskii-type rearrangements of isolated compounds from HPLC fractions, were detected.

NMR data was most concordant with the precursor structure shown in Scheme 2.6 and so it was proposed from GC-MS analysis that **30** was formed within the crude mixture of **22d**.

$R^1 = m\text{-NO}_2, m\text{-CHO}$
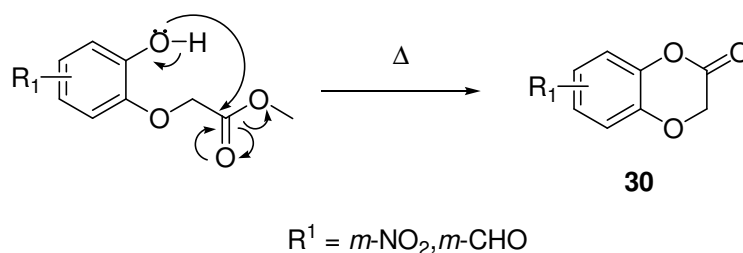
Scheme 2.6 Proposed mechanism for thermally-catalysed formation of **30** on the GC column, concordant with both NMR data and GC-MS data of the same isolated fraction by HPLC

Those variants with an electron-withdrawing substituent present on the aromatic region were more susceptible to basic KO^{t}Bu. The mono-etherified catechol resulting from this

cleavage formed the sterically favoured 6-membered heterocyclic ring thermally catalysed on the GC port. These results were concordant with both NMR (Figure 2.11) and GC-MS data. Rudimentary isolation of the cyclized impurity revealed a red-coloured resin, devoid of olfactory character, that forms a brittle solid on prolonged exposure to the atmosphere.

The difficult isolation of viscous resins of **22** and **22a-g** was also documented by Carter and Lawrence [10] in their quest to synthesise acetic acid derivatives of catechol, resorcinol and quinol. In the presence of aromatic EWG influence, mono-alkylated intermediates **21d** and **21e** (Figure 2.11) were resistant to cyclisation under Dieckmann cyclisation conditions.
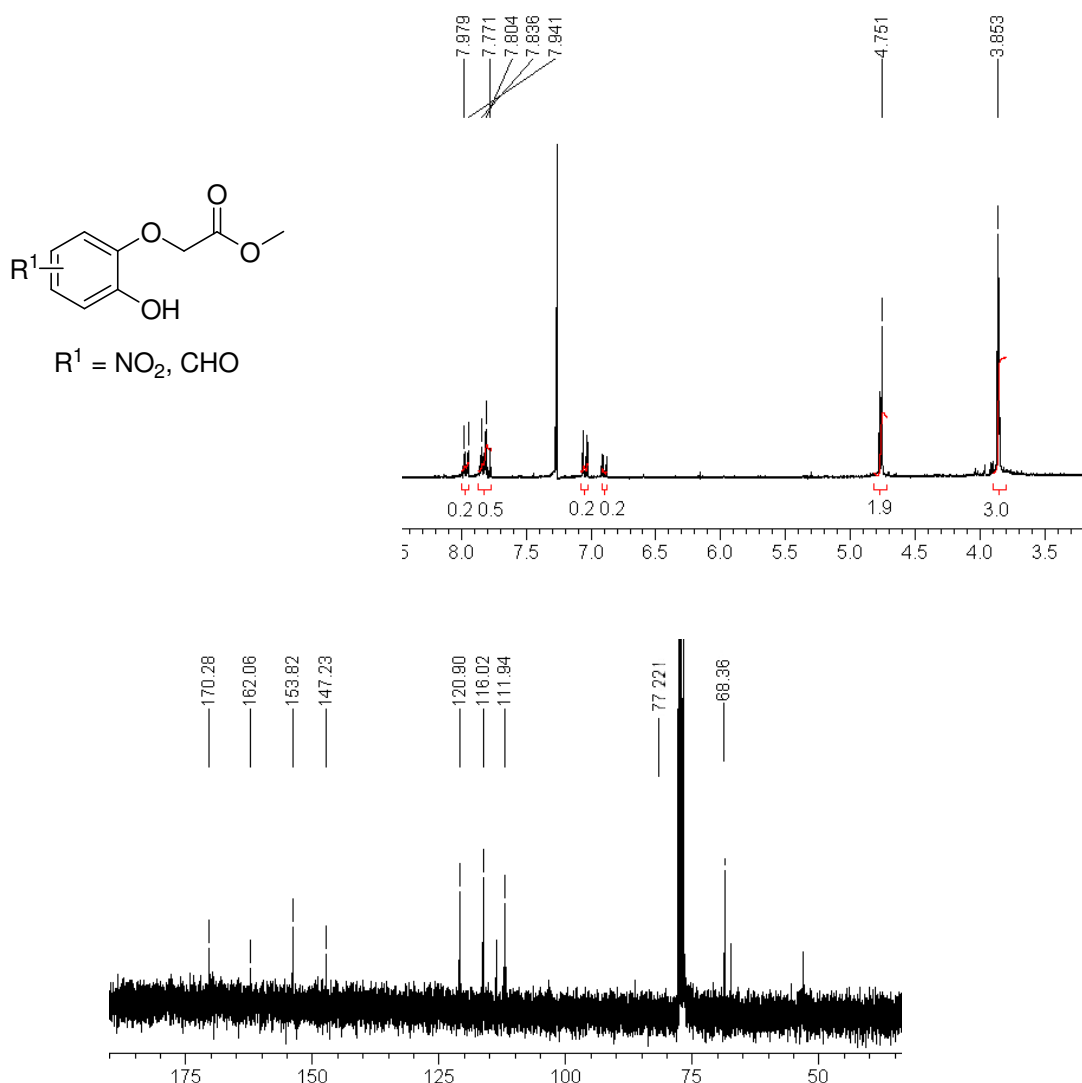
Figure 2.11 Mono-alkylated impurities formed in the Dieckmann cyclisation in **22d** and **22e** product mixtures (NMR shown; R^1 = NO$_2$)

Isolatable fractions from **22g** (R[1] = naphthalene) provided crude material that NMR data confirmed as purified **22g** and **29** (Table 2.1), the corresponding target benzodioxepinone.

2.3.2 *Ab initio* Models - Inductive and Resonance Effects of Aromatic Substitution Relevant to Success of Procedure A

Generation of HOMO/LUMO predictions with semi-empirical calculation systems (MOPAC; AM1 followed by PM3) and *ab initio* modelling confirmed the differences in reactivity demonstrated by derivatives of **21** (Figure 2.12 and Figure 2.13).

21
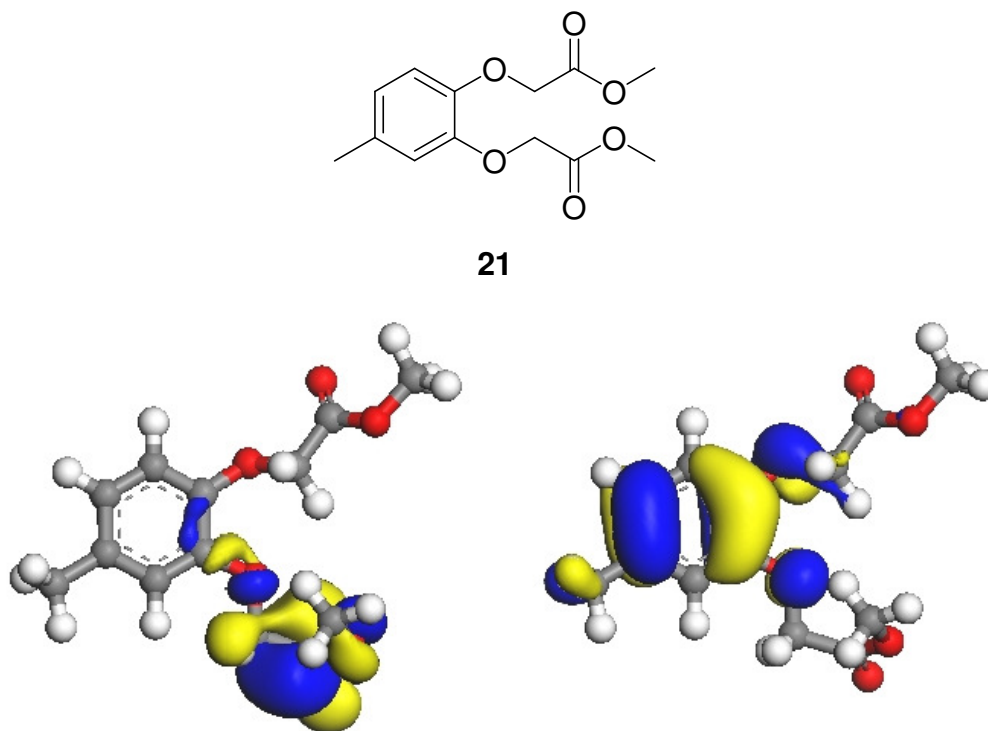
Figure 2.12 LUMO (left) and HOMO (right) representations of compound **21**
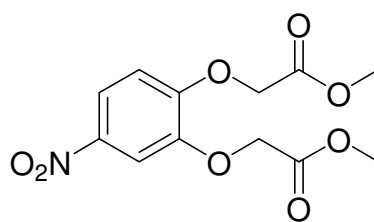
21d
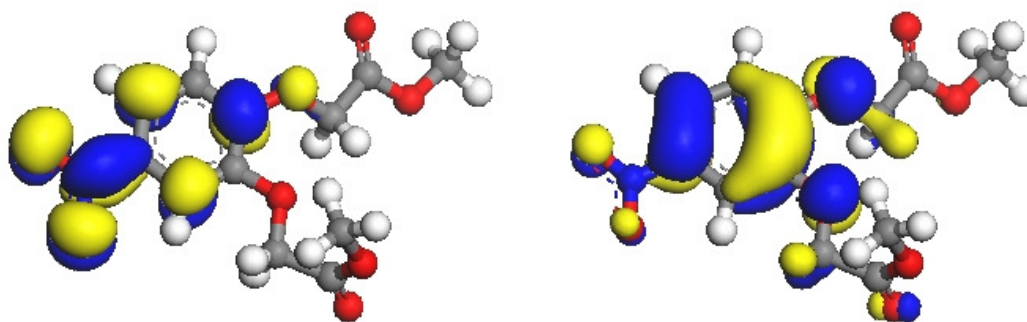
Figure 2.13 LUMO (left) and HOMO (right) representations of compound **21d**

Presenting compound **21d** as a representative model as shown in Figure 2.13, the cause of impeded cyclisation of compounds **21d**, **21e,** and to an extent **21c** and **21g** became evident. LUMO hybridisation is drawn away from the alicyclic portion and concentrated around the aromatic ring, unlike those with EDGs as demonstrated by the 4-methyl derivative, **21** (Figure 2.12). A uniform trend was evident for collective **21** derivatives with EWGs (nitro, formyl, naphthalene) revealing deprivation of LUMO energy around the acetate chains.

Based on these models, intramolecular cyclisation is inhibited as new σ bonds are hindered from forming due to lack of available LUMO for acceptance of electrons. For decarboxylation to proceed (Scheme 2.1*: step c*), with absence of LUMO around the regiocentre, energy demands for bond breaking and forming for the saponified side chain is much greater than that offered by external HOMO. Other factors such as polarisation and potential tautomerism may also contribute.

21
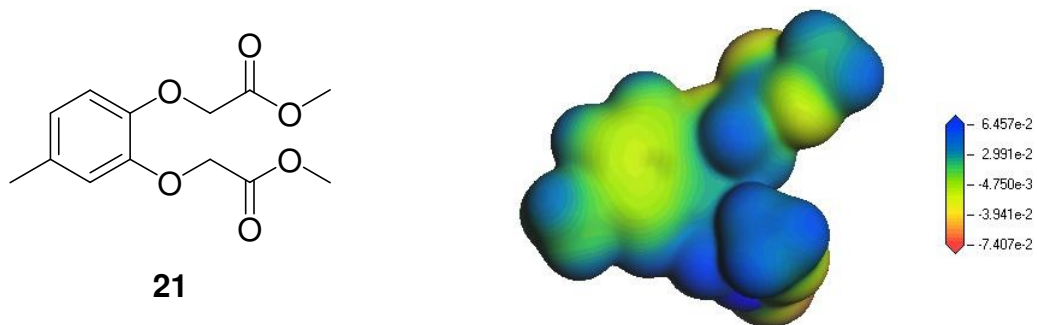
Figure 2.14 Graphical depiction of electron density for *m*-Me substituted **21**; blue-highest electron density, red-lowest electron density

21d
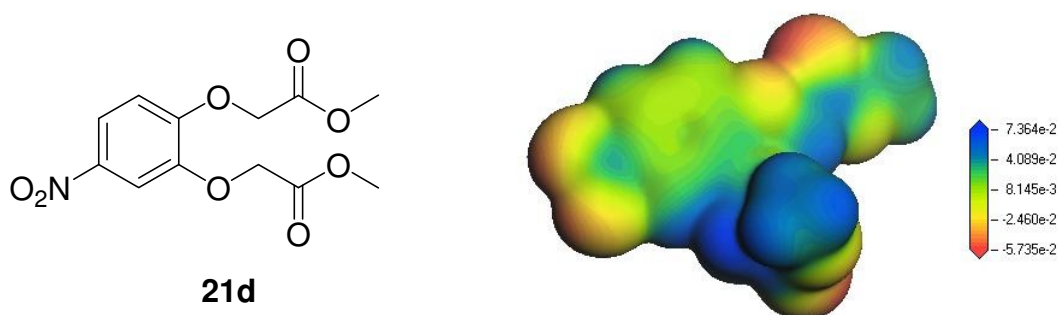
Figure 2.15 Graphical depiction of electron density for *m*-NO₂ substituted **21d**; blue-highest electron density, red-lowest electron density

These graphical representations highlight the distribution of electron density. Consideration of electron density distribution in light of reactivity supports the contrast in activity demonstrated by reagents featuring both aromatic EDGs (Figure 2.14) and EWGs (Figure 2.15). An EDG causes electron density to concentrate around the aromatic ring (**21**). Nitro substitution results in distribution of electron density, as a result the molecule possesses an increase in electrophilic character, and is hence more susceptible to attack from de-protonated carbon in the presence of basic ⁻OtBu. It is also worth noting that due to the flexibility of the side chains molecular orientation and electronegative field effects through space may also contribute significantly to reactivity outcome.

2.3.3   Structural Characterisation

Table 2.5 Methine ^{1}H and ^{13}C NMR shifts for structures **22**, **22a-g**

22

| Regioisomer: | | ^{1}H δ (d, J = 16-17 Hz) | | | | ^{13}C δ | | | |
| | | 1 | | 2 | | 1 | | 2 | |
	R^1	H-4$_A$	H-4$_B$	H-2$_A$	H-2$_B$	C-2	C-4	C-2	C-4
22	7-Me	4.74	4.51	4.71	4.49	81.8	76.6	82.1	77.0
a	6-Me	4.81	4.62	4.87	4.56	81.8	76.4	81.8	76.4
b	6-OMe	4.75	4.54			82.4	76.9		
c	H	4.82	4.60			81.8	76.8		
d	7-NO$_2$			Not isolated					
e	7-CHO			Not isolated					
f	7-^{t}Bu	4.82	4.60	4.81	4.58	81.7	76.7	81.9	76.8
g	Ph	4.96	4.81			81.7	76.5		

Referring to Table 2.5 above, the *o*-methoxy derivative (**22b**) is the only product from compounds **22**, **22a**-**g** obtained as a solid and the only intermediate for which NMR data has no distinguishable regioisomers, although GC-MS data reveals an 81:19 isomeric ratio. The isomeric ratio for **22a**, **22d, 22e** and **22f** are 30:70, 57:43, 100 and 51:49 respectively. Compound **22**, the precursor to **1**, features a single peak in the GC trace while ^{1}H and ^{13}C NMR data reveals an approximate 50:50 isomeric ratio. Signals due to an enol-form of compounds **22a**-**g** or the targets **23**-**29** were not observed in ^{1}H NMR or FT-IR analysis. Enolisation was also refuted by confirmation of ^{1}H methylene double doublets. Two overlapping AB quartet signals for isoform 1 and isoform 2 are apparent in ^{1}H NMR analysis of **22a**, **22c-g** as exemplified by COSY NMR analysis of **22** (Figure 1.26). Methine and methylene signals of the chiral and prochiral carbons for **22a-g** analogues were confirmed by DEPT 135, COSY and HMQC.
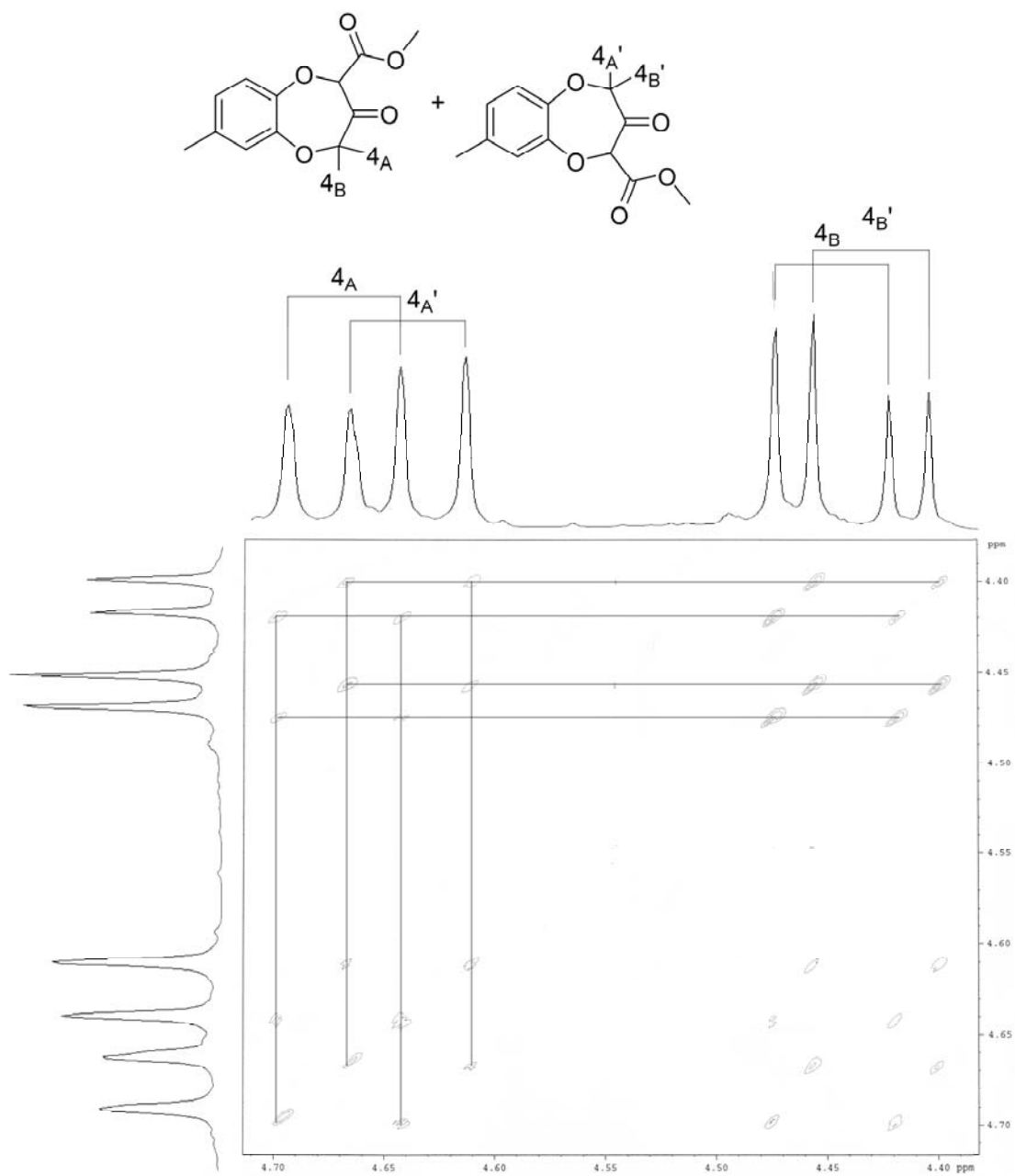
Figure 2.16 Magnified COSY region of **22,** highlighting the AB quartet relationship of C-4 protons for isoforms 1 and 2
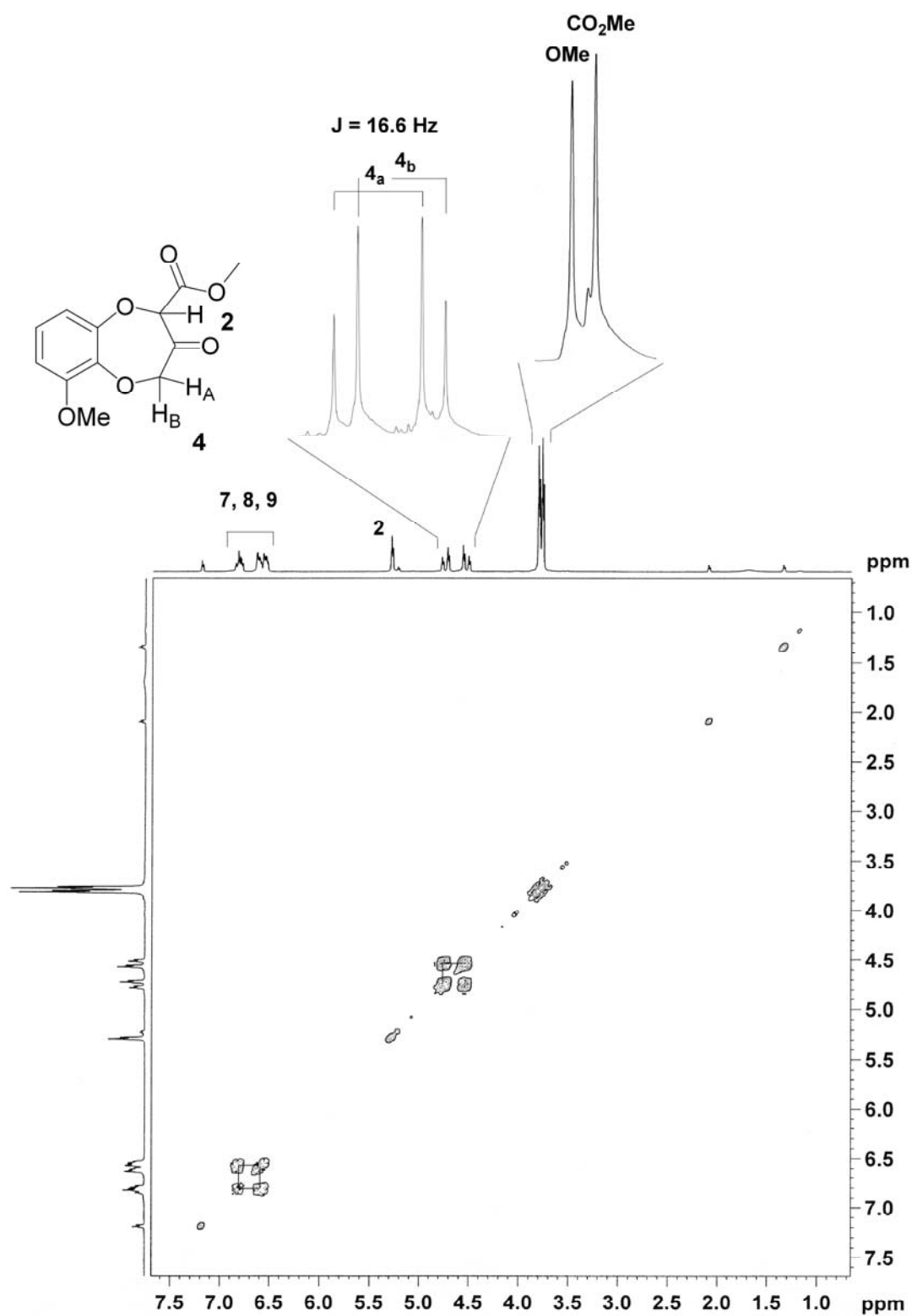
Figure 2.17 ^{1}H,^{1}H COSY of **22b**

HMQC signals for all **22** analogues revealed vaguely detectable low/high carbon, high/low proton methylene coupling (see Appendix 4). C-4 and C-2 carbon signals from **22** derivatives were confirmed by correlations to HMBC quaternary resonances (Figure 2.17).
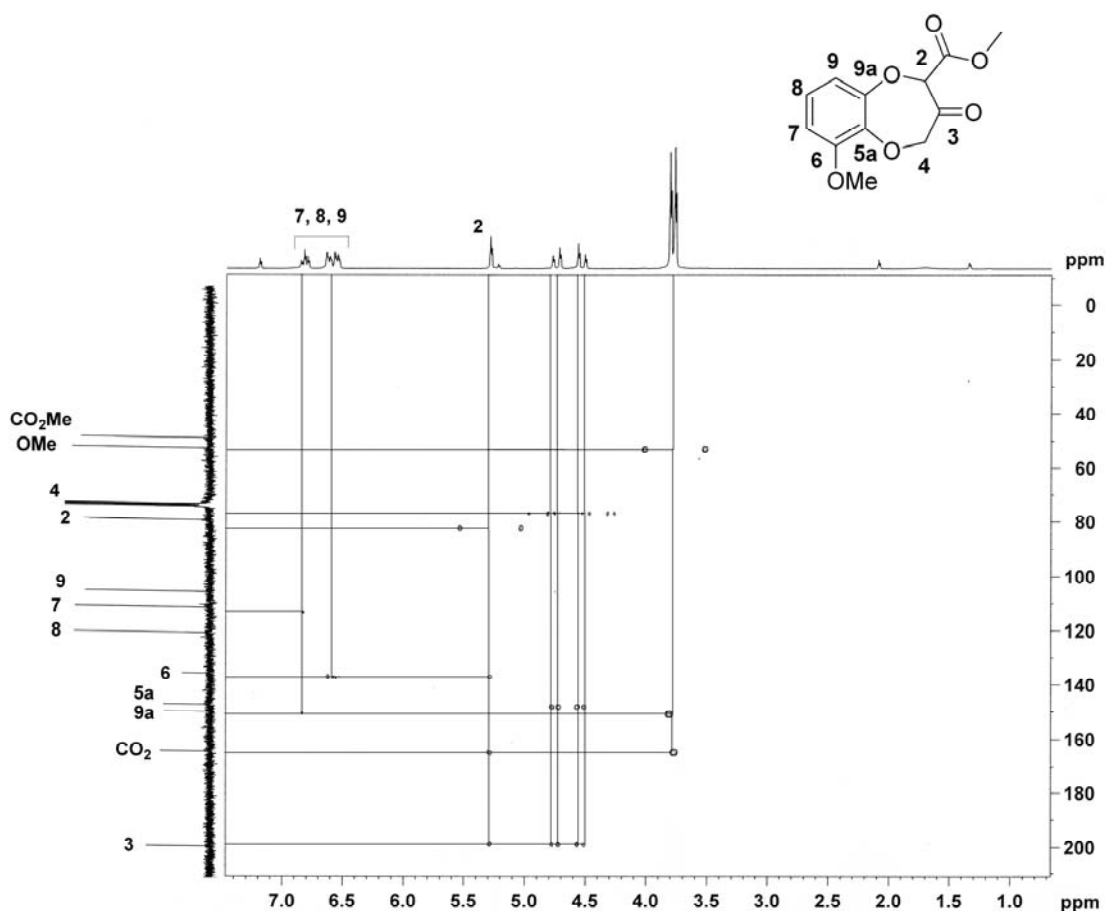
Figure 2.18 ^{1}H,^{13}C HMBC of **22b**

No proton/carbon coupling skew was evident upon long-range HMBC (Figure 2.18) analysis of quaternary carbons C9a, C-5a coupling with C-4, C-2 methylene groups of all analogues of **22**.

2.4 Preparation of Benzodioxepinone Analogues by Procedure A: Decarboxylation

For liberation of the target benzodioxepinones a single-step acid-catalysed hydrolysis afforded more favourable results than base-mediated saponification with subsequent acidic decarboxylation. Trials performed using the two-step saponification under basic conditions alone provided a poor recovery of product material, possibly due to adverse cleavage of the α-carbonyl. Heating under acidic conditions gave the intermediate carboxylic acid as the hydrolysis product, followed by thermal decarboxylation via a six-

membered hydrogen-bonded transition state. The mechanism for this process is presented in Scheme 2.7.
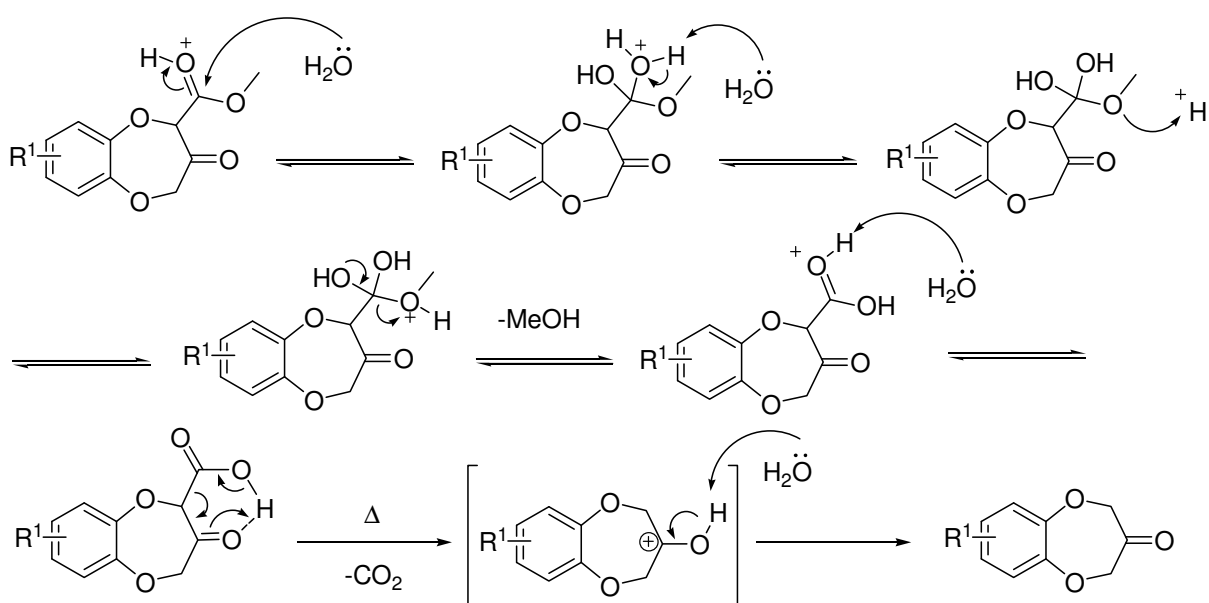
Scheme 2.7 Synthetic mechanism for acid-catalysed hydrolysis to form **23**-**29**

Analogue products **23**-**29** were confirmed as the desired 7-membered heterocyclic structures and not their benzodioxane counterparts by the presence of a single peak in GC-MS rather than a pair of regioisomeric peaks, in conjunction with the expected mass difference of a methylene. Carbon ^{13}C peak(s) for methylene signals of the 7-membered products appear further downfield as two signals rather than one, as would be expected of the benzodioxane cyclic ester. A proposed rationalisation for the fragmentation pattern of the structure of **1** and corresponding analogues is provided in Appendix 5.

Decarboxylated products were identified by molecular ions in GC-MS analysis and the purified products, characterised by ^{1}H and ^{13}C NMR analysis exemplified by compound **24** (Figure 2.19). Full characterisation (FT-IR, GC-MS, 1D and 2D NMR) verified the target benzodioxepinones **23-29**.

Table 2.6 Methylene ^1H and ^{13}C NMR shifts for structures **1**, **23-29**

1, 23-29
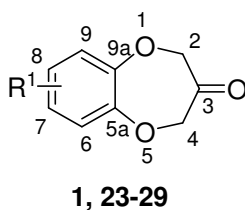
	R^1	$^1H\ \delta$ (s, H-2)	$^1H\ \delta$ (s, H-4)	$^{13}C\ \delta$ C-2	$^{13}C\ \delta$ C-4
1	7-Me	4.67	4.72	75.4	75.7
23	6-Me	4.70	4.74	75.5	75.6
24	6-OMe	4.73	4.87	76.2	75.6
25	H	4.08		79.4	
26	7-NO$_2$	4.98	4.91	75.3	76.3
27	7-CHO	4.79	4.71	75.2	76.1
28	7-^{t}Bu	4.72	4.69	75.7	75.6
29	Ph	4.60		75.4	

A summary of methylene shifts for the benzodioxepinone targets is presented above in Table 2.6. The appearance of two non-equivalent singlets from each methylene of the benzodioxepinone targets reveals the strong inductive and resonance influence throughout the molecule, just as intermediates **21** and **22** had demonstrated. The 1D shifts were confirmed with HMQC and COSY analysis. The extent of influence of aromatic substitution on the remainder of the molecule was concordant with previously evident trends in the NMR data of **21** and **22** derivatives.
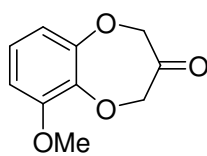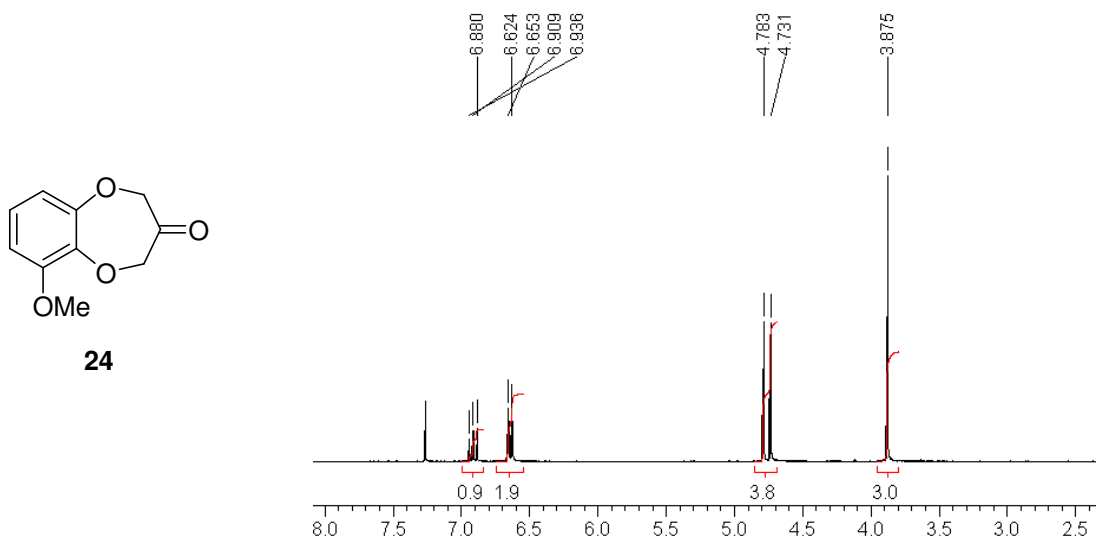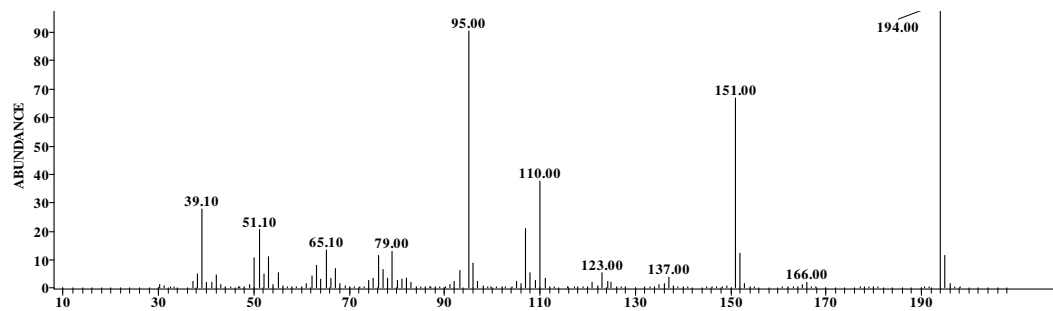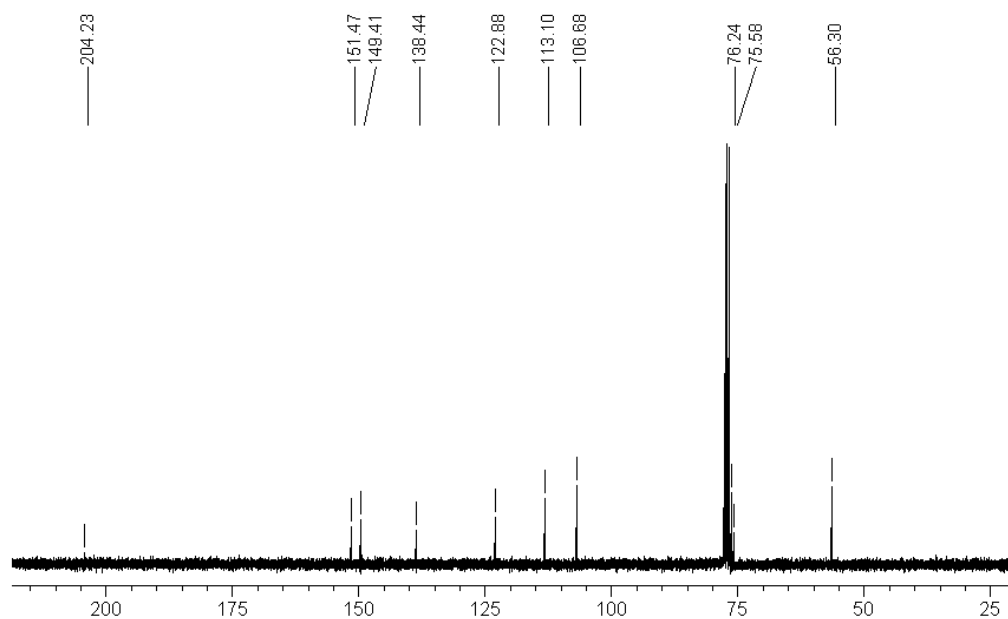
Figure 2.19 EI mass spectrum, ^{1}H and ^{13}C NMR spectra of **24**

2.5   References

[1]   Advanced Chemistry Development (ACD) Labs. Solaris, V8.14.

[2]   D.W.A. Sharp, The Penguin Dictionary of Chemistry, Penguin Group, England, 1990.

[3]   M.B. Smith, J. March, March's Advanced Organic Chemistry, Wiley-Interscience, New York, U.S.A, 2001.

[4]   J.J. Beereboom, D.P. Cameron, C.R. Stephens, Flavoring Foods with Benzoxepin-3-ones and Benzodioxepin-3-ones, U.S. Patent 3,517,031, October 28, 1969, 1972.

[5]   Sigma-Aldrich, Aldrich Handbook of Fine Chemicals and Laboratory Equipment. 2003-2004.

[6]   Advanced Chemistry Development. ACD/I-Lab, V8.02.

[7]   B. Drevermann, A. Lingham, H. Huegel, P. Marriott, Microwave Assisted Synthesis of the Fragrant Compound Calone 1951®. Tetrahedron Lett. 46(1) (2004) 39-41.

[8]   R.L.F. Funk, J. F.; Olmstead, T. A.; Para, K. S.; Wos, J. A., Titanium-mediated Cyclizations of β-Keto Esters with Acetals: A Convenient Route to 2-Carbalkoxycycloalkenones. J. Am. Chem. Soc. 115(19) (1993) 8849-8850.

[9]   V. Rosnati, F.D. Marchi, Chemical and Spectroscopic Properties of 2-Formyl-1,4-benzodioxane and 3-Oxo-3,4-dihydro-2*H*-1,5-benzodioxepin. Tetrahedron 18 (1962) 289-298.

[10]   W. Carter, W.T. Lawrence, The Hydroxyphenoxy- and Phenylenedioxy-acetic acids. J. Chem. Soc. Trans. 77 (1900) 1222-1227.

3 Synthesis of Benzodioxepinones: Calone 1951® Analogues by Procedure B

3.1 Introduction

As a contribution to the benzodioxepinone system, synthetic analogues prepared focused on diverse position and class of aromatic substitution. The low yields and inherent instability of compounds **22d** and **22e** required an alternative approach to Procedure A for the preparation of analogues containing reactive or strongly electron-withdrawing substituents. Literature searches revealed a number of alternate methodologies to prepare fused benzocyclo ketones. Yoshii and colleagues [1] used alkyl addition of 3-oxopentanedioate to the di-bromide to derive the benzocycloheptanone (**35**) following decarboxylation (Scheme 3.1).
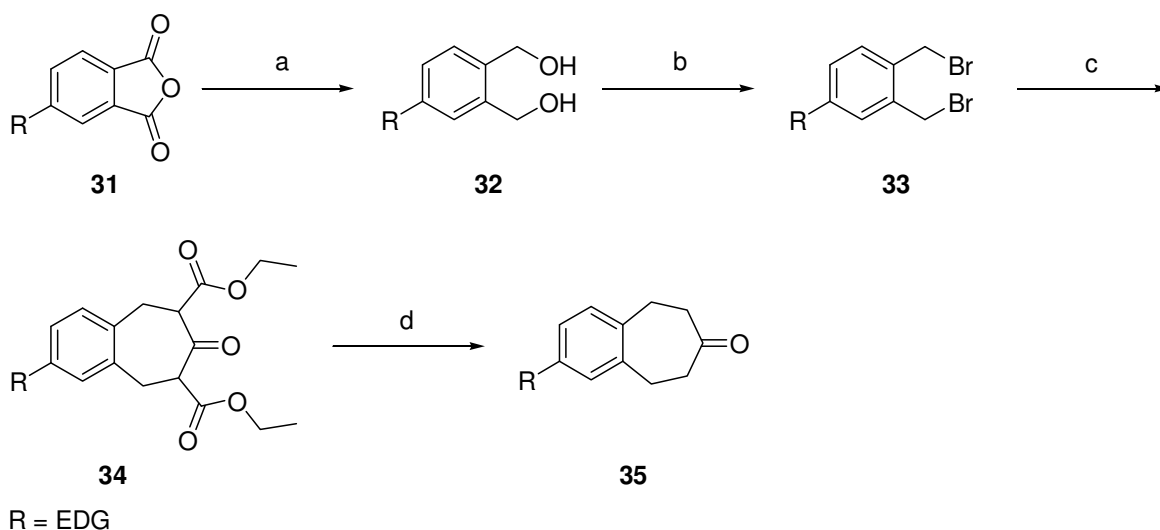
Scheme 3.1 Synthetic approach by Yoshii et al. [1] based on synthetic methodology proposed by Mataka et al. [2], a) LiAlH$_4$, Et$_2$O; b) CBr$_4$, PPh$_3$, CCl$_4$; c) Bu$_4$NI, 5% aq. NaHCO$_3$, (EtO$_2$CCH$_2$)$_2$CO, DCM; d) KOH, H$_2$O/EtOH

Rooney and colleagues have explored syntheses of various substituted benzodioxepines in the interest of discovering novel β-adrenergic stimulants [3]. Di-etherification of reagent catechols using chloroacetonitrile followed by Thorpe cyclisation to afford an enamino nitrile (**38**) provided the fused 7-membered heterocycle (**39**) in an analogous manner to the synthesis devised by Beereboom et al. [4]. Subsequent hydrolysis and

decarboxylation in a mixture of concentrated orthophosphoric acid (H_3PO_4) and AcOH provided the ketone product (**25**) in moderate yield [5] (Scheme 3.2).
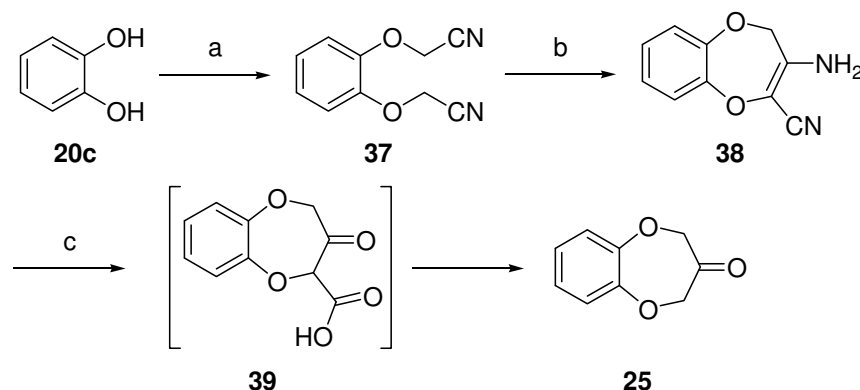
Scheme 3.2 a) K_2CO_3, $CNCH_2Cl$, Ac_2O; b) KO^{t}Bu, DMSO; c) H_3PO_4, AcOH

The benzodioxepines constructed allow access to a range of nitrile and methylamine addition products (Figure 3.1) [5]. Chloro (**40**-**44b**), methyl (**40**-**44c**) and methoxy (**40**-**44d**) compounds were prepared from the corresponding substituted catechols, alternatively the nitro (**42**-**44e**), amine (**42**-**44f**) and bromo (**42**-**44g**) compounds were synthesised by nitration or bromination of the benzodioxepine (R^1=R^2=H). Over 30 various N-alkyl amine compounds were prepared, and in most cases the effect of amine substitution on compound activity was negligible. Incorporation of R^1 and R^2 substituents generally decreased stimulant activity [5], however the aryl amino-substituted (**44f**) compound retained strong activity. The route devised by Rooney and co-workers is not ideal for the exploration of novel fragrance compounds in light of the involvement of cyano groups [5] and no mention of olfactory character of the benzodioxepinones was included.

40, 41	R^1	R^2
a	H	H
b	Cl	H
c	CH$_3$	H
d	H	CH$_3$O

	42, 43, 44	R^1	R^2
(25)	a	H	H
	b	Cl	H
(1)	c	CH$_3$	H
(24)	d	H	CH$_3$O
(26)	e	NO$_2$	H
	f	NH$_2$	H
	g	Br	H
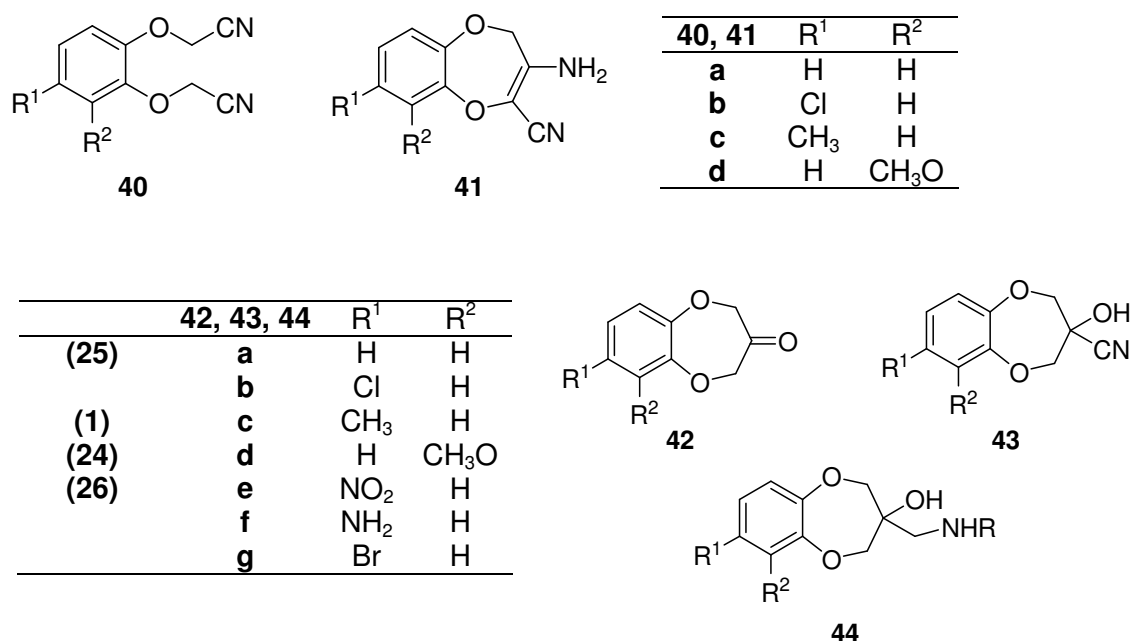
Figure 3.1 Substituted enamino nitriles (**40**, **41**), hydroxy nitrile and hydroxy amine benzodioxepines (**42**, **43**, **44**) prepared by Rooney et al. [5]

Jamrozik and colleagues reported the synthesis of symmetrical tetraoxaspirans (**46**) and corresponding dimeric benzodioxepine adducts as presented in Scheme 3.3. Williamson ether synthesis with *m*-substituted catechols and brominated alkylating agents resulted in a small range of analogues with no olfactory evaluation provided [6].

R^1, R^2 = H, CH$_3$, C(CH$_3$)$_3$
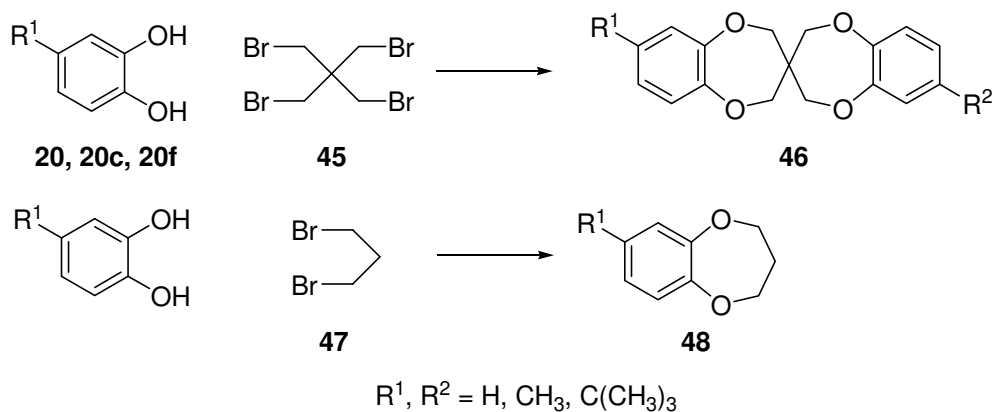
Scheme 3.3 Dimeric benzodioxepines prepared by Jamrozik et al.; sodium metal, ethylene glycol monoethyl ether [7]

Kraft released a patent on synthesis of dioxacyclohepta-indenone systems and *meta*-substituted benzo[*b*][1,4]dioxepin-3-ones [8] provided by a synthetic pathway as presented in Scheme 3.4, olfactory evaluation inclusive [8]. The benzodioxepine was constructed by Williamson ether synthesis of the catechol with 3-chloro-2-

(chloromethyl)prop-1-ene (**49**), by method of Schirmann et al. [9]. The terminal olefinic bond (structure **50**) was oxidatively cleaved using ruthenium tetroxide (RuO_4), pre-formed from $RuCl_3$ in sodium periodate ($NaIO_4$) to provide the benzodioxepinones in low yields [10]. RuO_4 cleavage investigated by Carlsen et al. [11] involved the generation of a mixture of *cis* and *trans* diols from unactivated olefins and subsequent diol cleavage in the presence of $NaIO_4$, provided the ketone product.
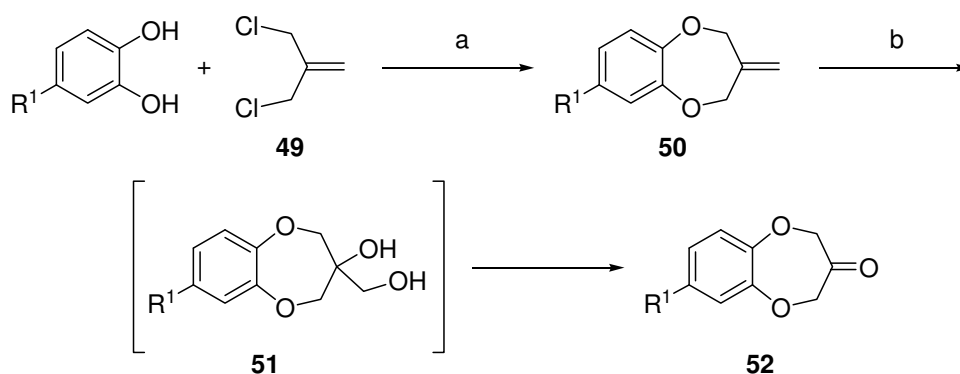
R^1 = refer to *Table 1.6*

Scheme 3.4 Synthetic approach by Kraft and Eichenberger [12] incorporating a synthetic method previously published by Carlsen et al. [10]: a) K_2CO_3, dioxane; b) $RuCl_3$, $NaIO_4$, $CCl_4/MeCN/H_2O$

In situ cleavage of the resulting diol (**51**) liberated the corresponding carbonyl compound (**52**) in a single-step procedure, although the diol products are often reliably obtained in higher yield than the carbonyl compound. This pathway is more direct than Dieckmann and Thorpe cyclisation methodologies, with reported yields for the olefin cleavage of aralkyl-substituted products within a range of 7-50%.

Rosnati and De Marchi [13] reported the characterisation of 3-oxobenzodioxepin (**25**) as a minor constituent in the preparation of 1,4-benzodioxanes (**54**, **56**) using 1,3-dichloro-2-propanol. Their synthetic investigations are presented in Scheme 3.5. Despite minor formation of the 7-membered ring by intramolecular halide displacement, the alcohol was oxidised by permanganate and characterised as the ketone product, despite favoured formation of a carboxylic acid.
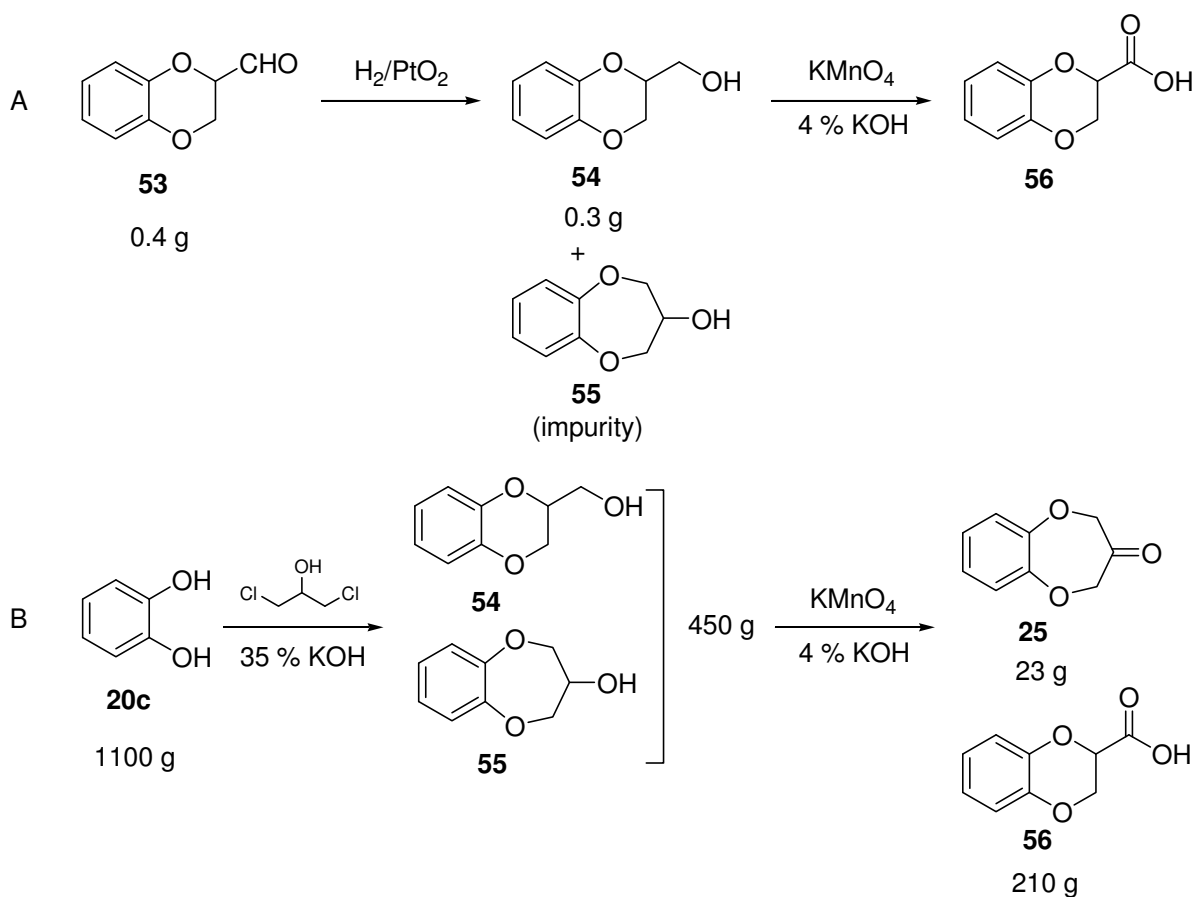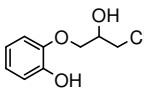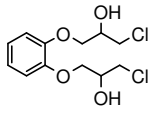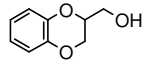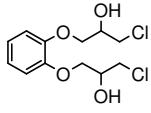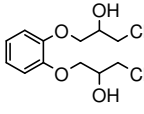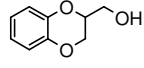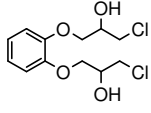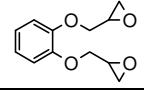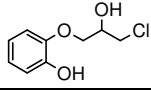
Scheme 3.5 Synthetic steps to benzodioxanes and benzodioxepinones by Rosnati and
DeMarchi [13]

The benzodioxane ring closure in this instance proceeds via the epoxide (**57**) as
described by Stephenson (1954, 1971) [14] [15]. Scheme 3.6 shows the synthetic
pathway to a benzodioxane (**54**) explored by Stephenson, and Table 3.1 presents a
summary of the major and minor products encountered.
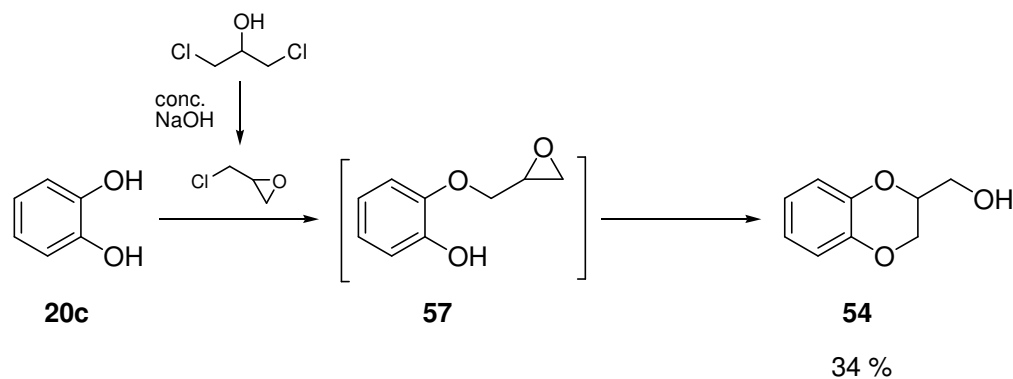
Scheme 3.6 Synthetic approach by Stephenson [14]

Table 3.1 Products prepared by Stephenson [14]

	Cat. (g)	Ep. (g)	Reagent	Time	Temp. (°C)	Major Product	Yield %	Minor Product	Yield %
a	110	92.5	pyridine	2 hr	100	*(structure)*	48	*(structure)*	11
b	33	55.5	pyridine	4 hr	100	*(structure)*	50	*(structure)*	23
c	55	185	piperidine HCl	3 days	r.t.	*(structure)*	74		
d	55	185	piperidine HCl	20 hr	100	*(structure)*	52	*(structure)*	11
e	55	102	NaOH	12 days	r.t.	*(structure)*	49	*(structure)*	34

Cat. = catechol

Ep. = epichlorohydrin

Modification of this generally unutilised approach was applied to our current studies with the incorporation of a protected 1,3-dihaloalcohol. As far as the author of this thesis is aware no literature precedent exists for a mechanistic pathway to benzodioxepinones involving ring closure with a protected halohydrin. A variation of this novel synthetic route has successfully been applied to derive analogues **23**-**29** (Section *3.2*).

3.2 Preparation of Benzodioxepinone Analogues by Procedure B

Following the success of the intramolecular etherification to form **70** using di-bromo alkanes (Section 4.2.5), and in contrast with the poor results from 1,3-dichloroacetone, it was observed that facile cyclisation was facilitated by free rotation at the sp^3 C-2 carbon of structure **58**. Continued studies focused on the application of 1,3-dihalo-2-hydroxy-propane derivatives toward the preparation of cyclic catechol ethers as a precursor to the ketone by means of oxidation at C-2. The synthetic methodology implemented to synthesise the analogues of **1** via this novel approach is presented in Scheme 3.7.
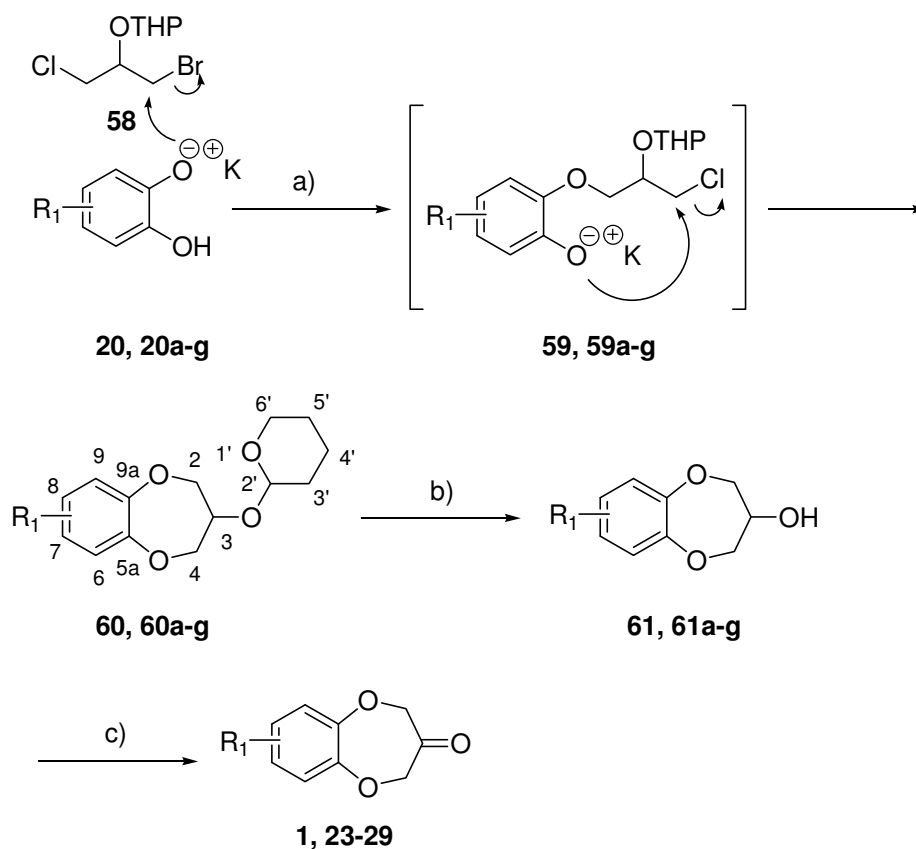
a) K_2CO_3, 1 equiv. **58**, DMF, reflux, 24 hr; b) V_2O_5, H_2O_2, 70°C, 15 min; c) $KMnO_4$, 4% KOH, r.t., 1-4 hr (**61a**-**c**, **f**-**g**), or oxalyl chloride, DMSO, TEA, -78°C, 4 hr (**61d**-**e**)

Scheme 3.7 Preparation of **1** and derivatives **23-29** by Procedure B

3.2.1   Comparison of Experimental Yields from Procedures A and B

Table 3.2 reflects the general increase in isolated yield and purity of the range of analogues synthesised via Procedure B.

Table 3.2 Comparison of yields from Procedures A and B for analogues **23**-**29**
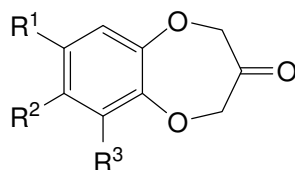
Compound	R^1	R^2	R^3	Procedure A		Procedure B	
				Yield[a] %	Purity[b] %	Yield[a] %	Purity[b] %
1	H	Me	H	78	95	87	99
23	H	H	CH$_3$	14	97	56	78
24	H	H	OCH$_3$	95	99	87	86
25	H	H	H	10	87	60	98
26	H	NO$_2$	H	2	53	84	99
27	H	CHO	H	11	69	52	93
28	H	^{t}Bu	H	84	95	73	94
29	Ph (*face*)		H	7	81	61	58

[a] Values following purification.

[b] Purity values were derived from GC-MS prior to purification by column chromatography or HPLC.

As the synthesis of Procedure B was undertaken, it seemed initially that Procedure A was more applicable to catechol reagents with EDGs and Procedure B derived more favourable yields for those with EWGs, however on overall inspection the yields seemed variable. For commercial, **1**, and compound **25**, improved overall yield was obtained from Procedure B. Compounds **23** and **24** were derived in enhanced purity with Procedure A and improved yield in the case of **24**. Comparable purities from both procedures were obtained in relation to compound **28**, with increased yield from Procedure A. Following HPLC purification **29** was obtained in considerably improved purity using Procedure A. Without the need for purification **29** can be obtained using Procedure B in moderate yield and purity. Similarly, compounds **26** and **27** required HPLC purification following application of Procedure A, however can be derived in significantly enhanced yield and purity with Procedure B, without the need for purification methods.

3.2.2   Epichlorohydrin Ring Opening and Protective Group Considerations

Formation of the halohydrin, 1-bromo-3-chloropropan-2-ol, was achieved by acid-catalysed epoxide opening of epichlorohydrin with hydrogen bromide (HBr) as hydrohalic acid (Scheme 3.8) to give the secondary alcohol exclusively (**62**), as indicated by ^{1}H NMR. Formation of this molecule was traced back to syntheses of 3-arylpropane-1,2-diols published by Beasley [16].
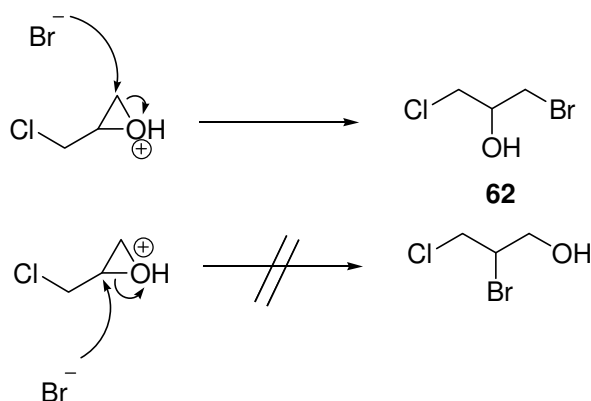
HBr (48%), r.t., 2 hr, KOH, distil, 71%

Scheme 3.8 Halogenative cleavage for formation of **62**; 2 hr dropwise addition of HBr to epichlorohydrin with additional stirring for 45 min provided the secondary alcohol in 71% yield

The ambident nature of halogenative cleavage means that a secondary or a primary alcohol may result. Epoxide cleavage can be performed under basic or neutral conditions via an S_N2 mechanism, or in acidic conditions via the same type of backside attack once the ether oxygen is protonated. A basic or neutral environment encourage regiospecific attack by the nucleophilic halide reacting at the primary epoxide carbon with retention of configuration of the secondary epoxide carbon, forming the desired secondary alcohol product.   Epoxide cleavage under acidic conditions shows both S_N1 and S_N2 characteristics. For this reason epoxide cleavage in the presence of acid encourages a mixture of regiosisomers more so than basic or neutral conditions. Less steric hindrance at the non-substituted carbon favours formation of compound **62**. Addition of a catalyst also enables regiospecific control as reported by Sharghi and colleagues [17]. Dropwise addition of the hydrogen halide ensured 71% selective formation of the secondary alcohol regioisomer **62**. GC-MS monitoring identified Br and Cl by isotope patterns in the fragment ions, as shown in Figure 3.2. The expected molecular ion (M_r = 172) was

absent, however major fragments (M-CH$_2$Cl, M-Br and M-CH$_2$Br) (Appendix 6) were observed.
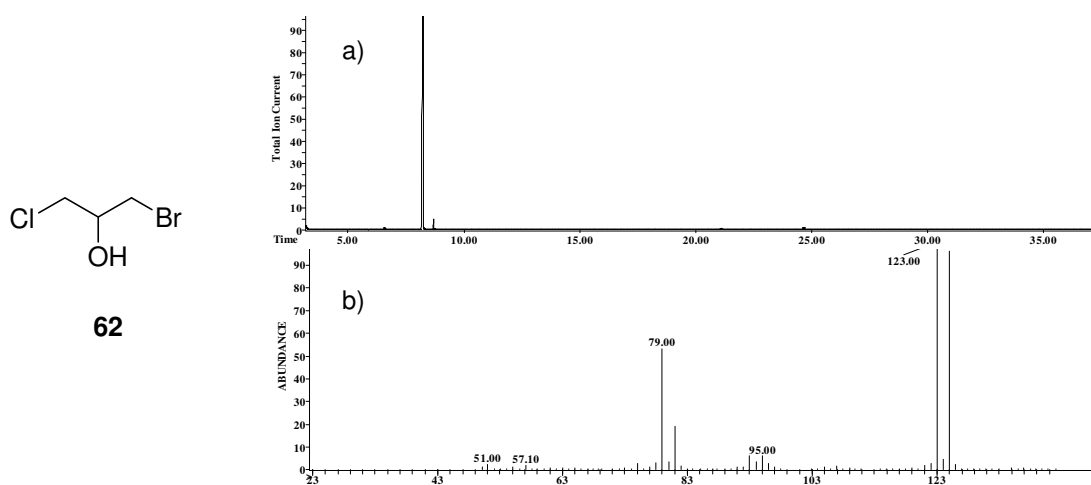
Figure 3.2 a) GC-MS of **62** (Mr = 172); b) mass spectrum of main product peak at 8.22 min

Trimethylsilylation (TMS) was initially implemented as a protecting group as shown in Scheme 3.9. Protection of the dihalo alcohol was successful using TMSCl in 73% isolated yield following vacuum distillation (49-50°C/0.5 mmHg). Compound **63** was confirmed with 1D NMR data as presented in Appendix 7.
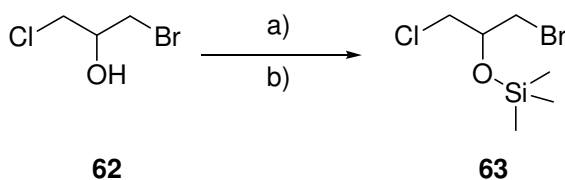
a) TMSCl, Et$_2$O, TEA (0.9 eq.), r.t., 2 hr; b) distil, 73%

Scheme 3.9 Preparation of **63** by TMS protection

No migration of the silyl group was observed in the GC-MS analysis, which was favourable. The TMS group however proved too labile in the basic conditions required for the etherification step, despite use of milder temperatures (70°C), and so therefore was abandoned as the protecting group for this synthesis. As silyl groups are commonly labile under basic conditions silylation of the alcohol in general was abandoned for an alternative protecting group approach.

As a robust protecting group under basic conditions tetrahydropyranyl ether (THP) was selected for the alcohol, **62**, which proved stable under the Williamson conditions employed for di-alkylation. Tetrahydropyranylation of the alcohol [18] was carried out under solvent-free conditions in 3,4-dihydropyran (DHP), with P_2O_5 as catalyst as shown in Scheme 3.10.

a) P_2O_5, r.t.; b) KOH, distil, 91%
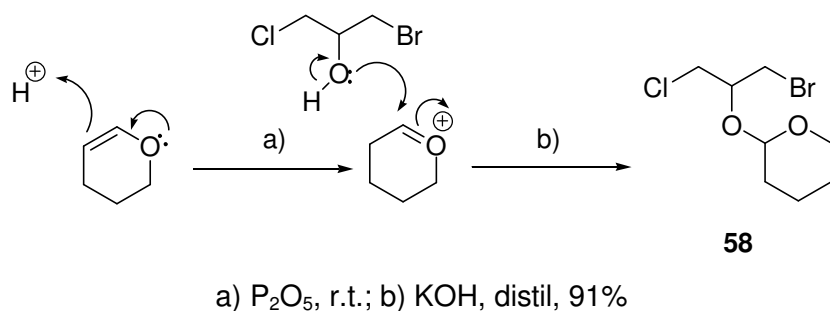
Scheme 3.10 Formation of **58** by THP protection

Neutralisation with $NaHCO_3$ and distillation (101-102°C/50 mmHg) provided the pure THP derivative in 91% yield. GC-MS monitoring revealed complete addition of the THP group by a characteristic ion at 85 *m/z* at 2 hours. Both compounds **62** (Appendix 6) and **58** (Figure 3.3) were detected by GC-MS and characterised with NMR and IR analysis. Strong bands present in the 1000-1100 cm^{-1} region in FT-IR, indicative of C-Cl and C-Br stretching were present for both compounds **62** and **58**. In addition disappearance of the broad band at 3380 cm^{-1} was indicative of pyranylation of the hydroxyl group of **62** in forming compound **58**.
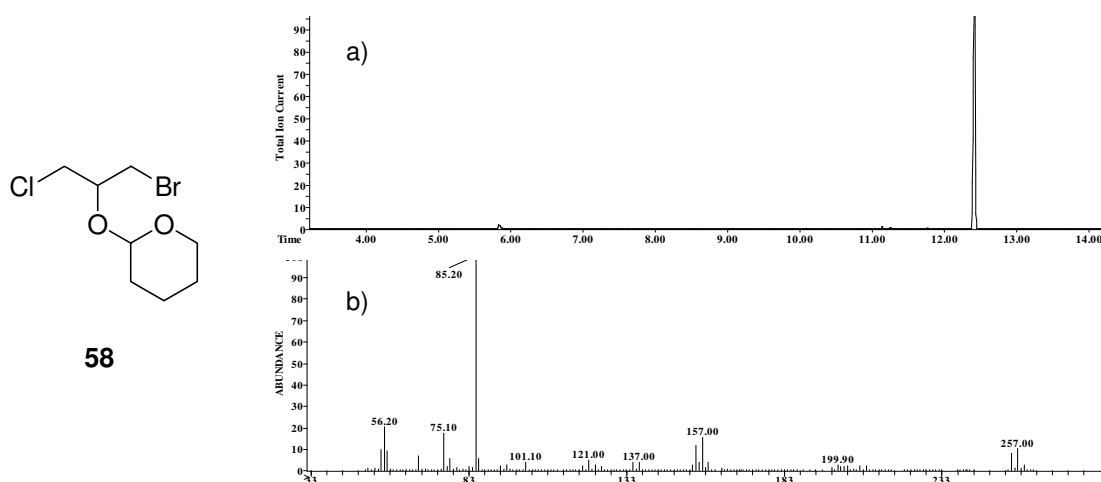
Figure 3.3 a) GC-MS of **58**; b) mass spectrum of the major peak in a) at t_R = 12.41 min

The molecular ion derived empirically (257 m/z) from **58** exhibited ^{1}H NMR signals for acetal H-2' H-6' of the THP ring overlapped with those of the cyclic region C-2, C-4 and diastereomeric C-3, forming a complex multiplet distinguishable only by COSY (Appendix 8) and HMQC (Figure 3.4).
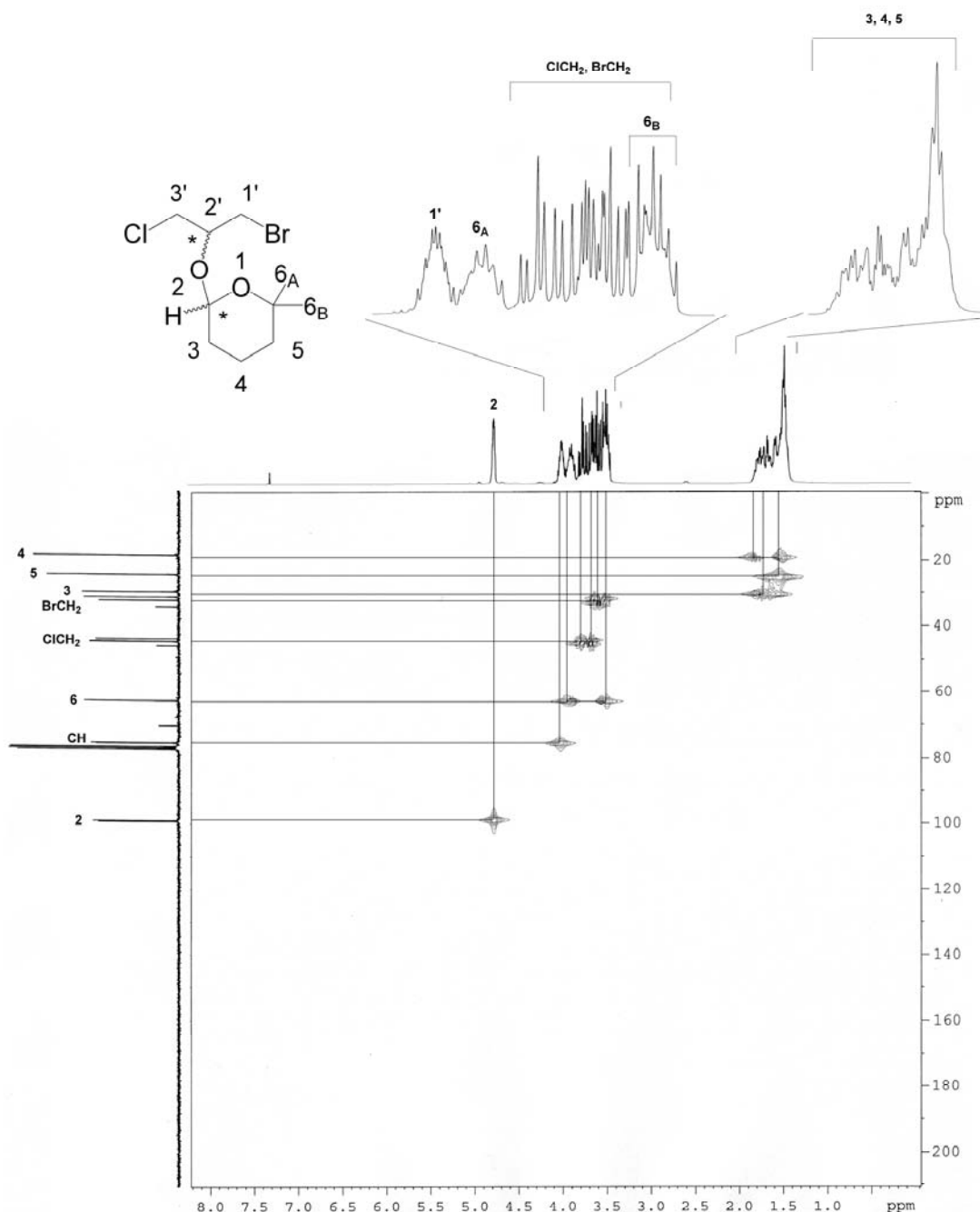
Figure 3.4 ^{1}H,[13]C HMQC of **58**

3.2.3 Alkylation and Ring Closure with 2-[2-Bromo-1-(chloromethyl) ethoxy]tetrahydro-2*H*-pyran for Formation of the Benzodioxepine Ring

o-Dihydroxyaromatics **20a**-**g** were reacted with the freshly distilled alkylating agent, **58**, to expediently form the mono-alkylated intermediate (**59**) (refer to Scheme 3.7, Figure 3.5 and Figure 3.6) by displacement of the bromine as shown by GC-MS.
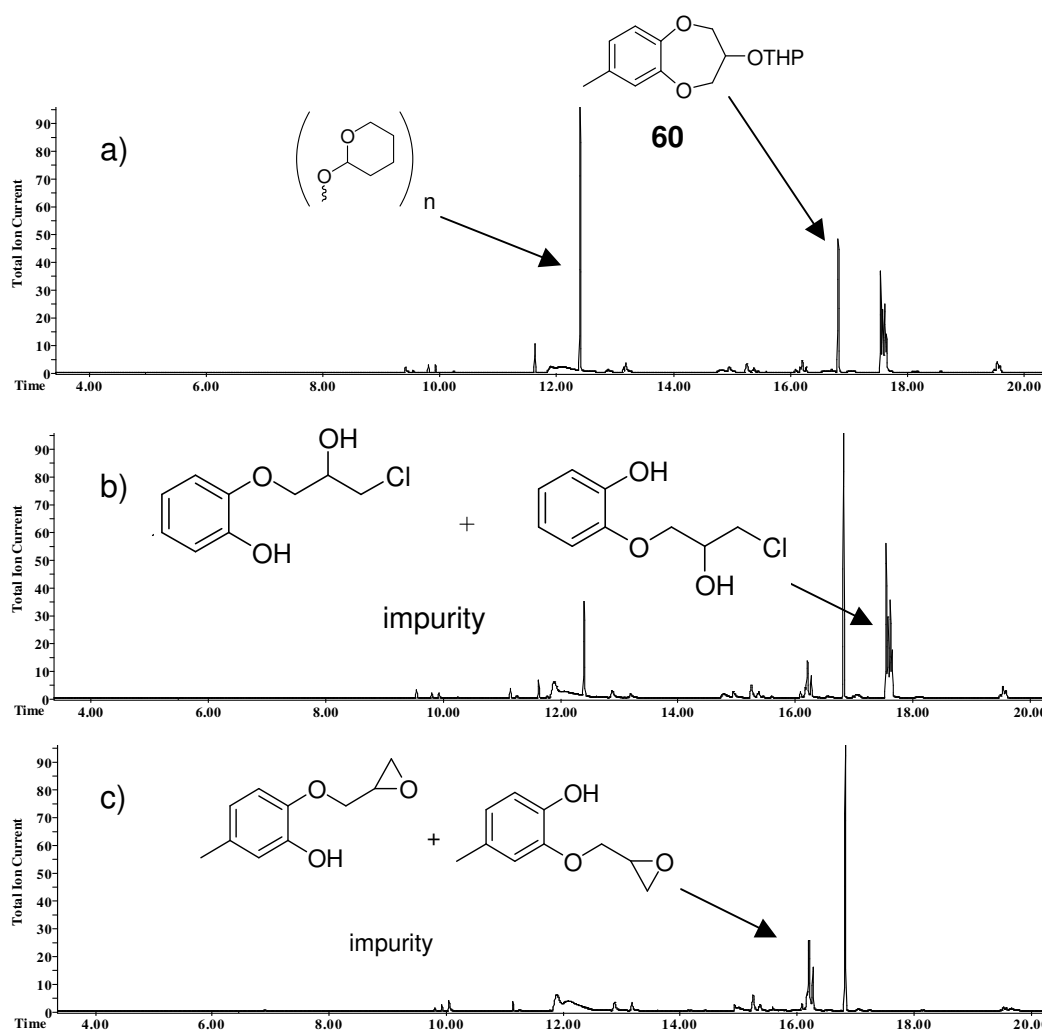
Figure 3.5 GC TIC of etherification trials of 4-methyl catechol (**20**): a) NaH; b) NaH and K_2CO_3; c) K_2CO_3
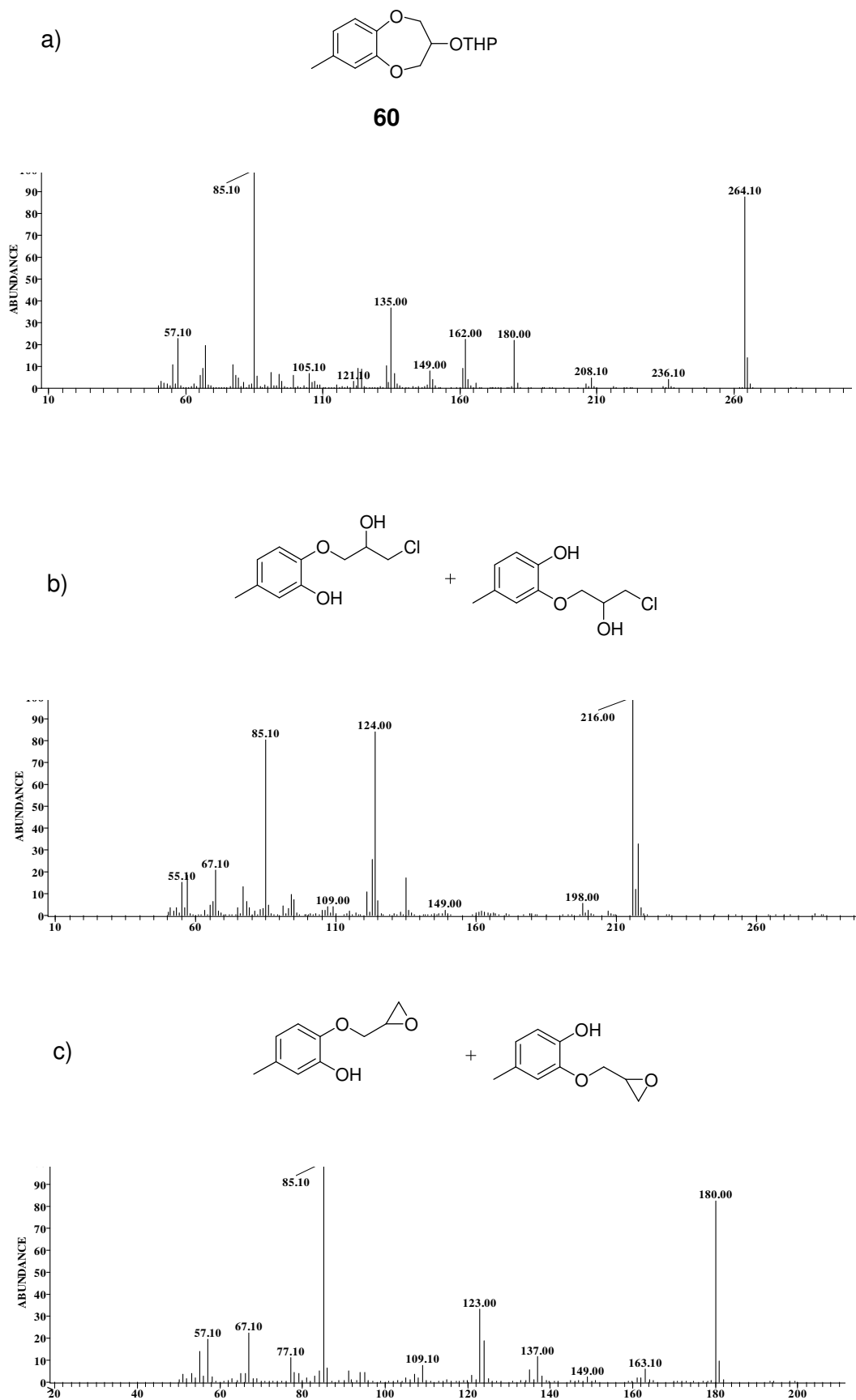
Figure 3.6 Mass spectrums corresponding to compounds presented in the GC traces in Figure 3.5: a) mass spectrum of **60**, m/z 264.10; b) mass spectrum of alcohol impurity, m/z 216.00; c) mass spectrum of the epoxidised impurity, m/z 180.00

Ring closure with etherification of the second hydroxyl group by chloride displacement provided the cyclized 7-membered ring upon prolonged heating in DMF (Scheme 3.7, *step a*). NaH, both as an alternative base and used in conjunction with K_2CO_3 was also successful in the formation of **60a**-**g** however improved yields were obtained with K_2CO_3 alone, as revealed in Table 3.3 and Figure 3.5. GC-MS monitoring revealed that ring closure was complete in 24 hours at 100°C-140°C providing more favourable results than a milder 70°C-100°C. Unless absolute anhydrous conditions were maintained variants of the mono-alkylated intermediate were preserved in the reaction medium up to 24 hr. Although the chloride displacement required 24 hr, no dimeric compounds or polymeric material was encountered, since the alkylating agent was the limiting reagent (0.95 eq.). A small degree of epoxy by-products were also formed as illustrated in Figure 3.5 (*trace c*).

Table 3.3 Yields for THP-protected intermediates **60** and **60a**-**g**
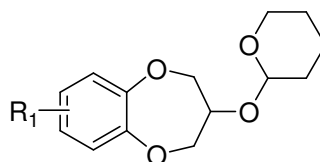
Compound	R^1	Yield (%)	Purity (%)
60	*m*-Me	92	49
a	*o*-Me	90	83
b	*o*-OMe	91	61
c	H	87	47
d	*m*-NO$_2$	85	97
e	*m*-CHO	74	95
f	*m*-^{t}Bu	98	53
g	Ph(*face*)	82	84

GC-MS (Figure 3.7), ^{1}H NMR and ^{13}C NMR (Figure 3.8) data for **60d** is provided here as an illustration of characterisation of the THP-protected benzodioxepinone structure. Characterisation data of **60a** and supplementary data for **60d** are provided in Appendices 9 and 10.
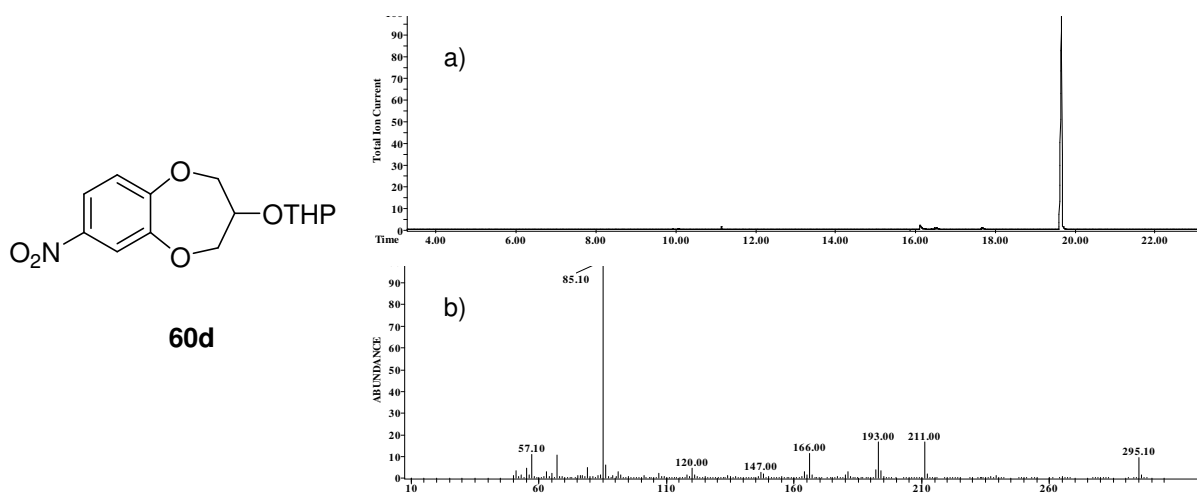
Figure 3.7 a) GC-MS of **60d**; b) mass spectrum of main peak
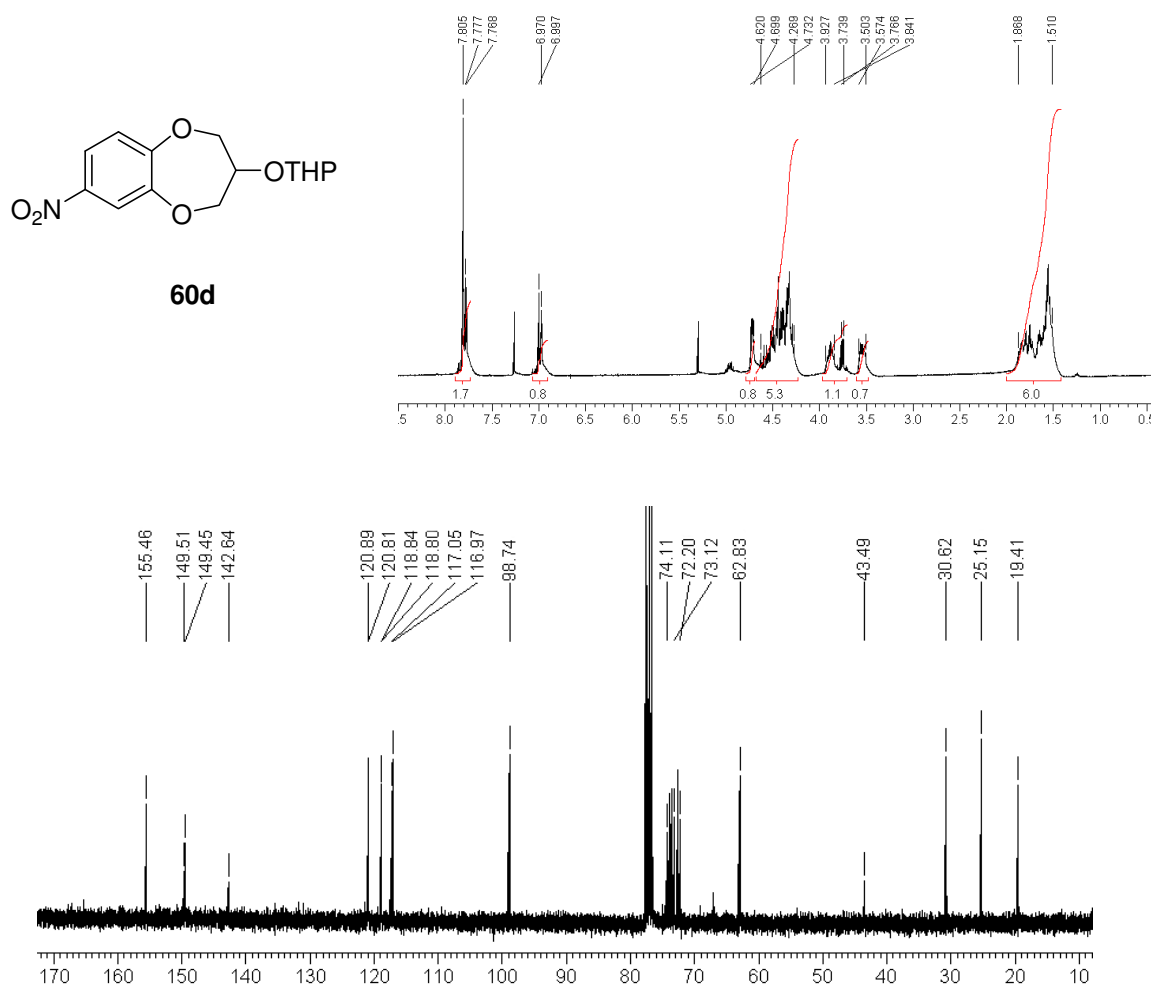
Figure 3.8 ^{1}H and ^{13}C NMR spectra of **60d**

The ^{1}H signal for the asymmetric C-3 proton of compounds **60a-g** characteristically overlapped with the diastereotopic C-2 and C-4 methylene protons. The ambiguous signals of ^{1}H data were clarified by COSY (Figure 3.9) and HMQC (Figure 3.10) (refer also Appendix 10) as exemplified by **60d** data.
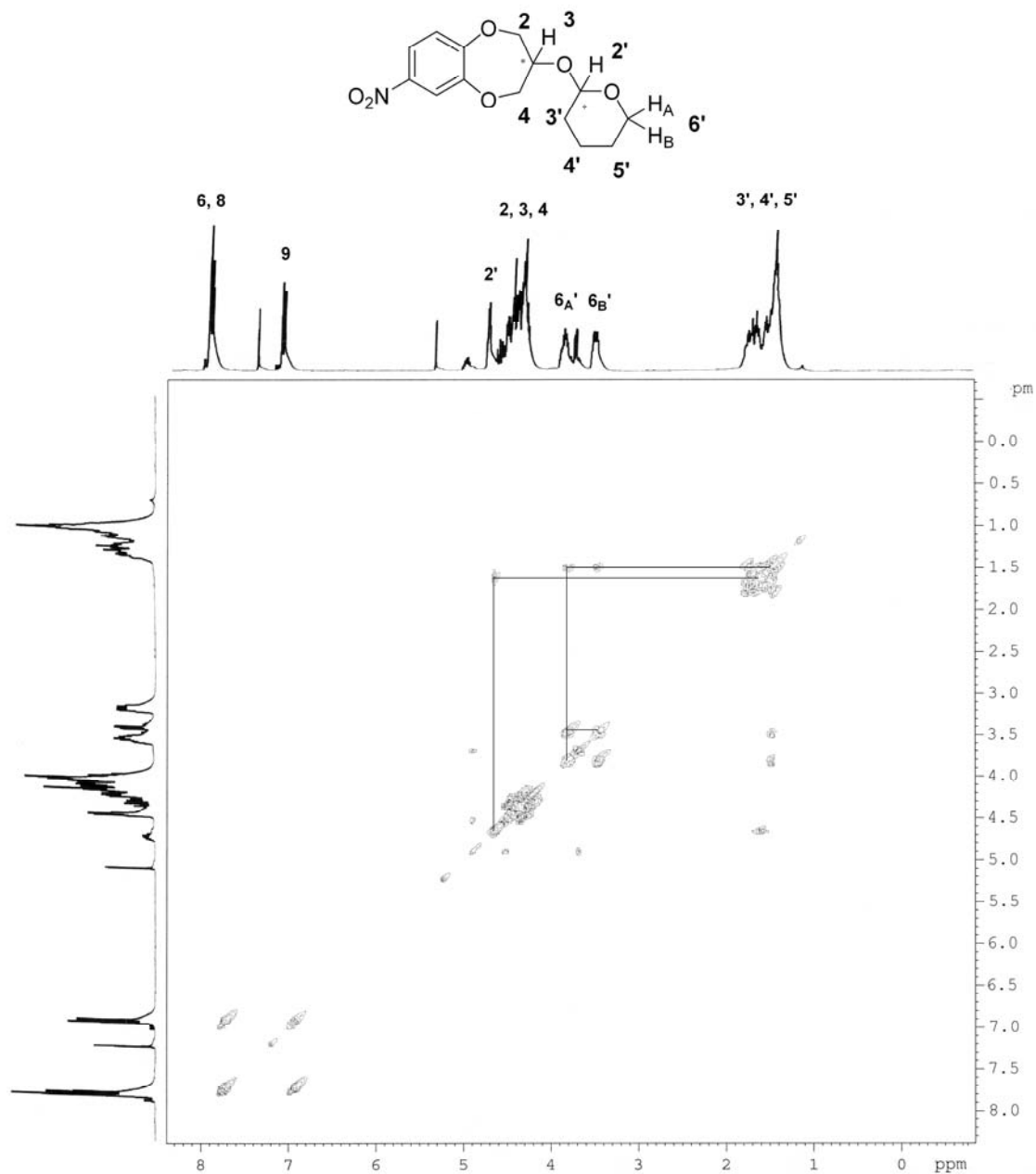
Figure 3.9 ^{1}H,^{1}H COSY NMR of **60d**
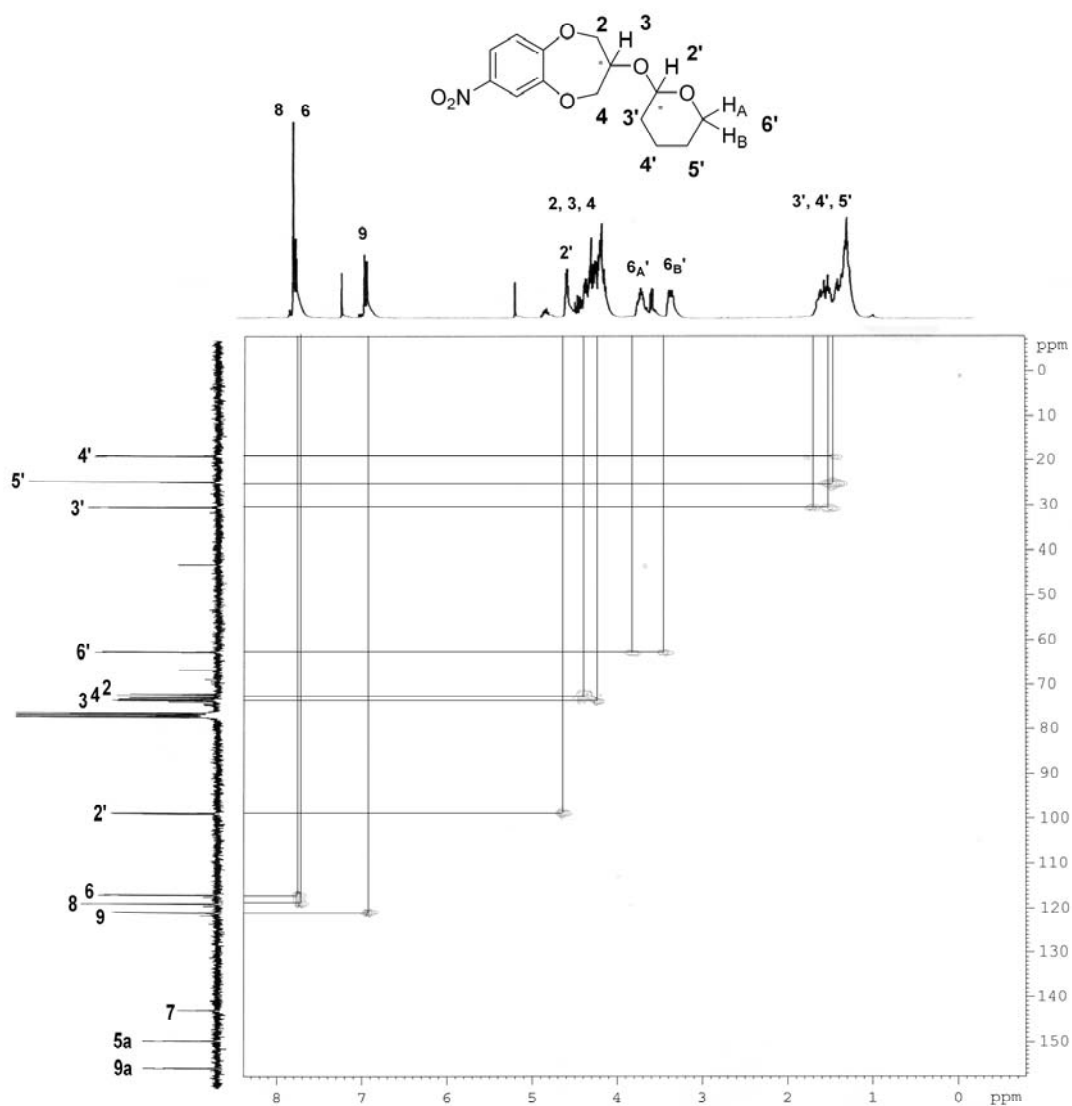
Figure 3.10 ^{1}H,^{13}C HMQC of **60d**

Resonance overlap of C-2, C-3 and C-4 signals prevents any discrimination of C-2, C-4 signals, even in 2D heteronuclear spectra.

3.2.4 Liberation of Benzodioxepine Secondary Alcohols via Deprotection of the THP Group with Exploration of One-pot Oxidative Deprotection

Firouzabadi et al. reported the use of activated silica chloride with KMnO$_4$ [19] as effective for oxidative de-protection when applied to primary and secondary aryl and alkyl alcohols with TMS, TBDMS and THP groups. Firouzabadi and colleagues discovered that in the absence of silica chloride, KMnO$_4$ was ineffective at oxidation of thioacetals to their

corresponding carbonyls and at the time of writing were unsure as to the mechanism by which this system proves effective. However they do comment that order of addition is crucial to success, where silica chloride should be prior to KMnO$_4$. For this reason despite KMnO$_4$ previously proving unsuccessful as oxidant for benxodioxepinols this methodology was applied.
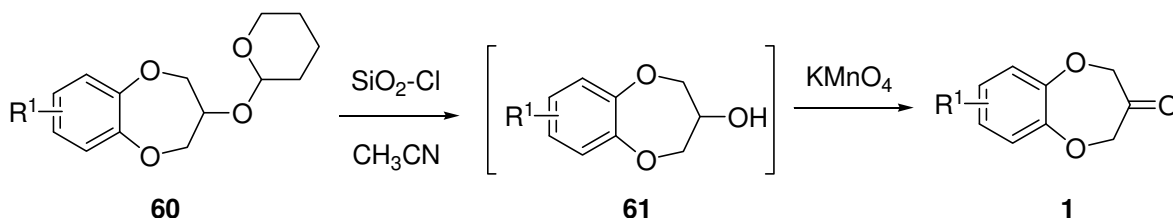
Scheme 3.11 Oxidative deprotection trial for removal of THP and oxidation of the benzodioxepinol, 3hr, r.t.

Following the protocol represented by Scheme 3.11, reaction of **60** with silica chloride [20] was successful in removal of THP alongside introduction of by-products, without oxidation of the C-2 alcohol as shown in the GC of Figure 3.11.
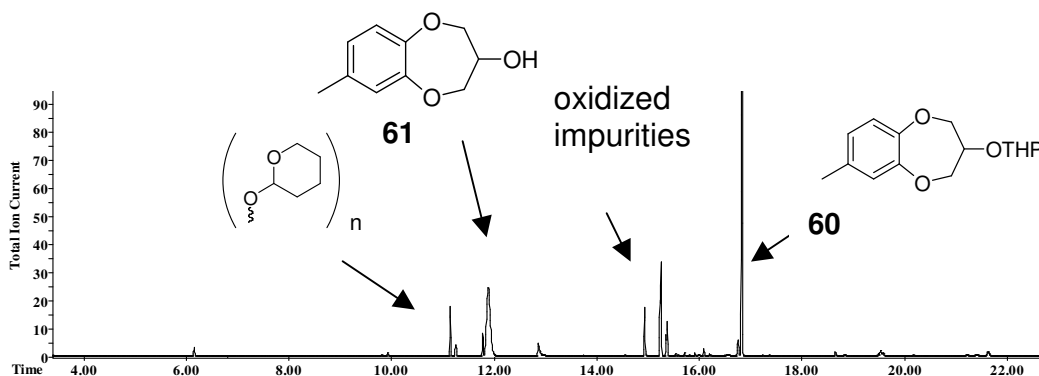
Figure 3.11 GC TIC of one-pot oxidative de-protection trial on structure **60** with silica chloride/KMnO$_4$, MeCN, r.t, 3 hr

In pursuit of a one-step procedure for formation of the carbonyl with removal of the THP group oxidative deprotection trials were continued. Deprotection of the THP group is reported to be facile under acidic conditions [21], therefore continued attempts at oxidative deprotection involved implementation of acidic conditions. Further trials included ceric ammonium nitrate (CAN) in AcOH and MeCN (Figure 3.12), Jones reagent (CrO$_3$/H$_2$SO$_4$/acetone) (Figure 3.13), NaOCl/AcOH [22], acetic anhydride (Ac$_2$O)/DMSO [23], and a NaBrO$_3$-NH$_4$Cl oxidative complex (Figure 3.14), returning only a small yield of the alcohol. Reaction of Jones reagent with compound **60g** also successfully de-protected the alcohol to a small degree, with no detectable yield of the ketone. The

NaBrO$_3$-NH$_4$Cl reagent [24] in aqueous MeCN, recommended for oxidative de-protection of silyl ethers resulted in attack of the quaternary aromatic carbons forming over oxidised catechol derivatives.
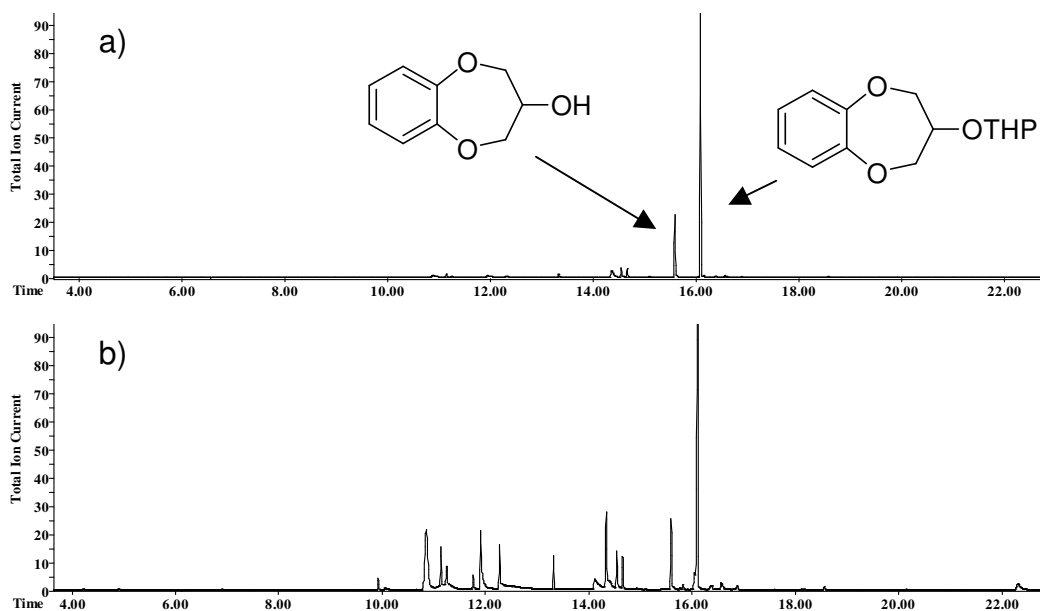
Figure 3.12 GC TIC of oxidation trials on the unsubstituted analogue, **60c**, a) CAN, r.t., AcOH, 5 hr; b) CAN, MeCN, r.t., 5 hr
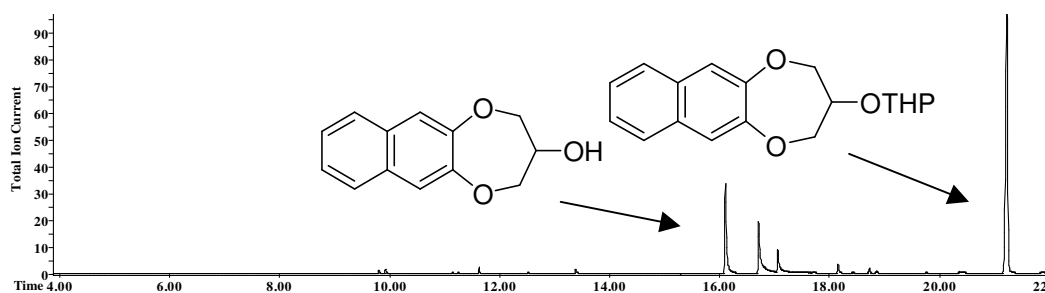
Figure 3.13 GC TIC of oxidative deprotection trial with Jones reagent (Na$_2$Cr$_2$O$_7$) on the naphthalene analogue, **60g**; aq. Na$_2$Cr$_2$O$_7$, Et$_2$O, r.t., 10 min
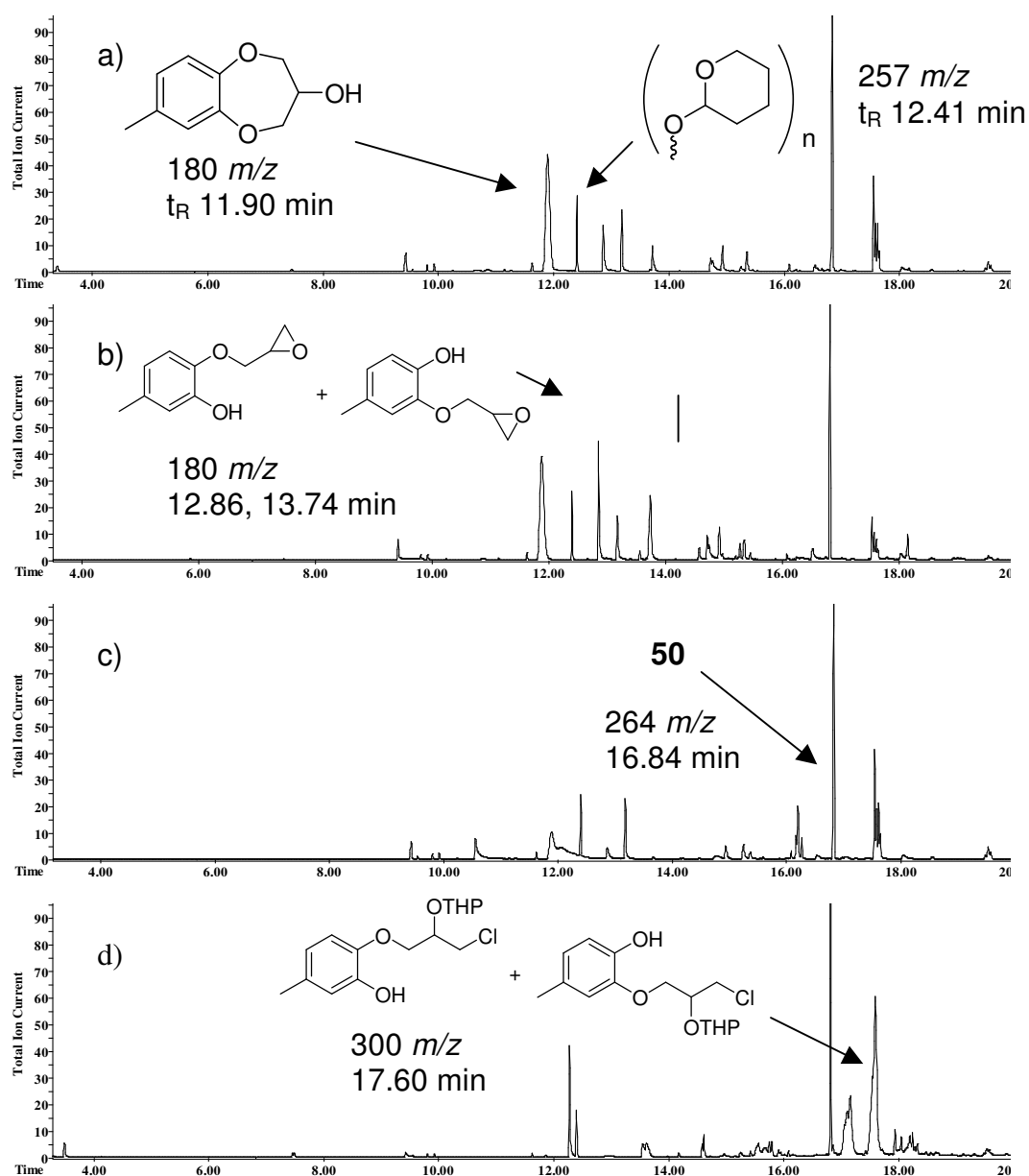
Figure 3.14 GC TIC of oxidative deprotection trials on the *meta*-methyl analogue (original GC of **60**): a) NaOCl, AcOH, r.t. 3 hr; b) NaOCl, PTC (tetra butyl ammonium iodide), AcOH, 50°C, 12 hr; c) NaBrO$_3$-NH$_4$Cl, MeCN:H$_2$O (7:3), 80°C, 3 hr; d) Ac$_2$O, DMSO, 120°C, 24 hr

The THP group proved stable to many hydrolysis conditions. Aqueous acid (0.5M HCl) reaction conditions with heating in EtOH and a catalytic portion of pTsOH failed to provide clean deprotection to the alcohol. De-protection of the THP group using V$_2$O$_5$ catalyst under conditions developed by Gopinath and colleagues [25] produced the alcohol in quantitative yield under mild conditions. The aldehyde derivative (**60e**) was also successfully de-protected with V$_2$O$_5$ with no evidence of over-oxidation or polymerisation.

Use of MeCN rather than MeOH as solvent avoided esterification of the aldehyde as suggested by Gopinath et al.

GC-MS fragmentation of the alcohol showed the molecular ion as the base peak, exemplified by the *m*-nitro derivative (**61d**) in Figure 3.15, and identical fragmentation to the reduced analogue of **1**, **23**. Analogues **61c**-**d** and **61g** required purification by recrystallisation. The alcohol products were confirmed by the absence of THP signals in ^{1}H NMR at 1.5 ppm and the presence of an OH peak at approximately 3 ppm as shown in Figure 3.16. 2D COSY spectra of all **61a-g** analogues resembled compound **61** (see Appendices 11 and 12 for examples).
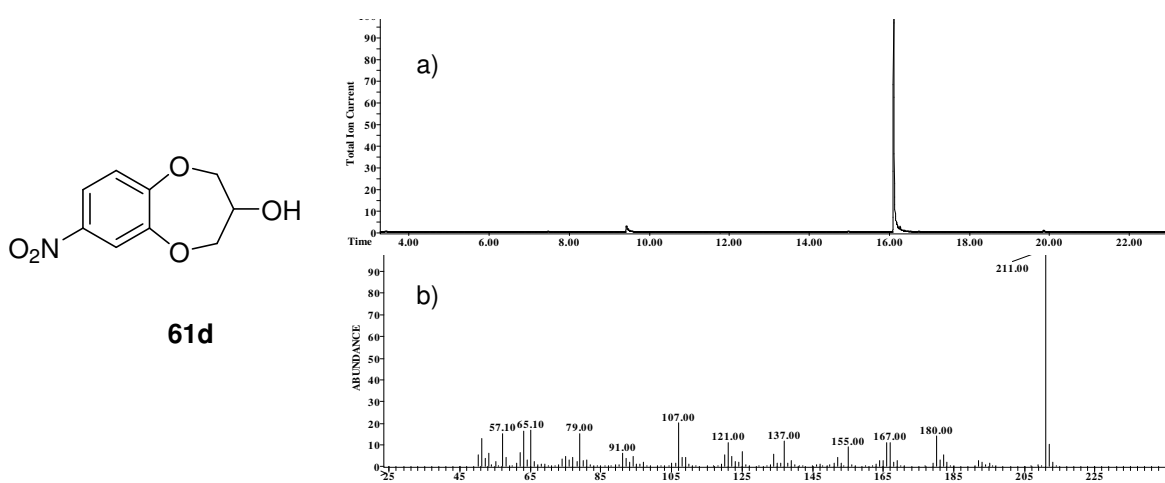
Figure 3.15 a) GC-MS of **61d**; b) mass spectrum of **61d** at t_R = 16.13 min
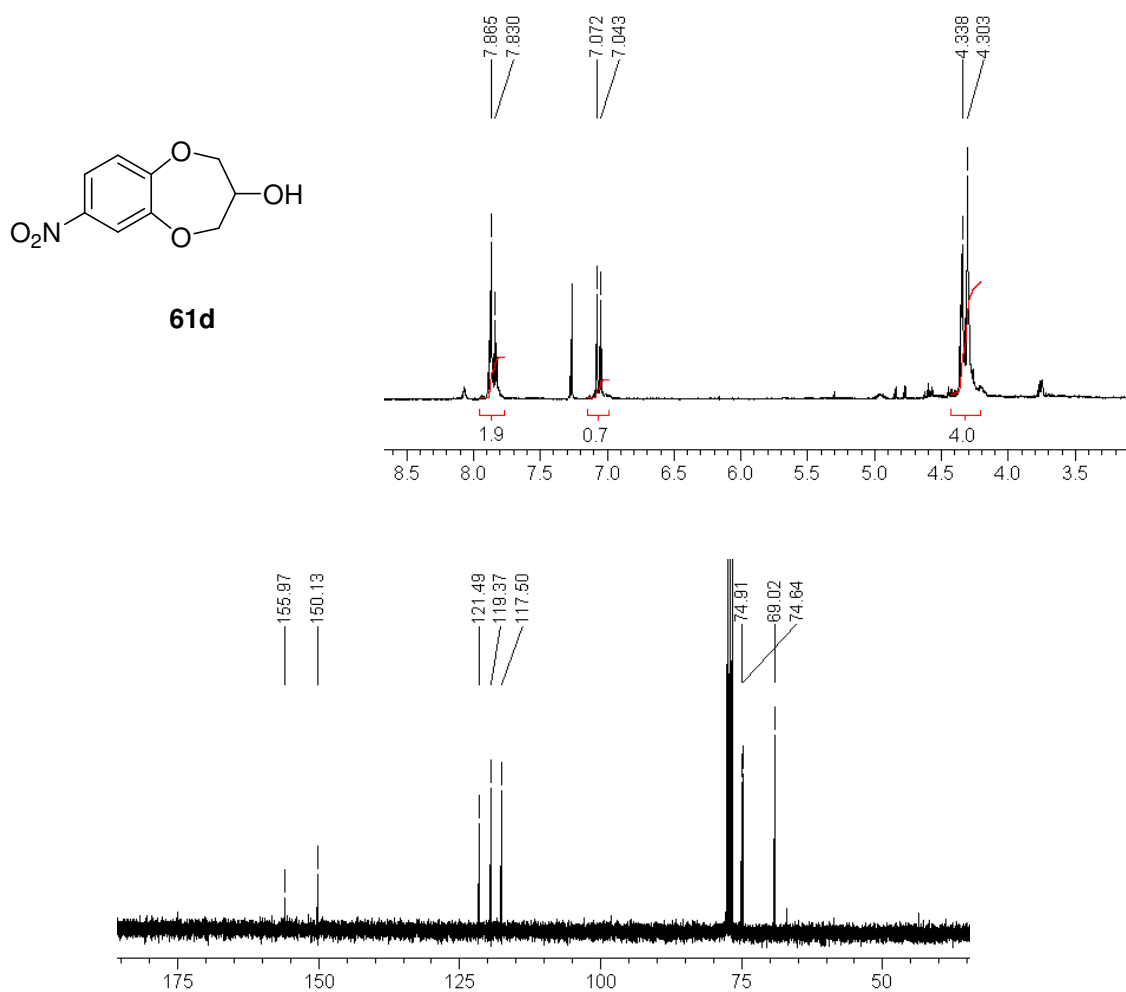
Figure 3.16 ^{1}H and ^{13}C NMR spectra of **61d**

3.2.5 Formation of the Target Benzodioxepines by Oxidation of the Secondary Alcohol

Potassium permanganate (KMnO$_4$) in benzene and DCM failed to provide conditions sufficiently reactive for oxidation of the alcohol presented in Figure 3.17. A KMnO$_4$/copper (II) sulphate (CuSO$_4$) hydrate in H$_2$O/DCM with *tert*-butyl alcohol (tBuOH) [26] also failed to provide appropriate oxidative conditions. The addition of a phase transfer catalyst tetrabutylammonium bromide (TBAB) was used to increase the reactivity of MnO$_4^-$ in organic solvent however product mixtures were still poor and heating had minimal effect on oxidation rate, but rather led to decomposition products, also presented in Figure 3.17.
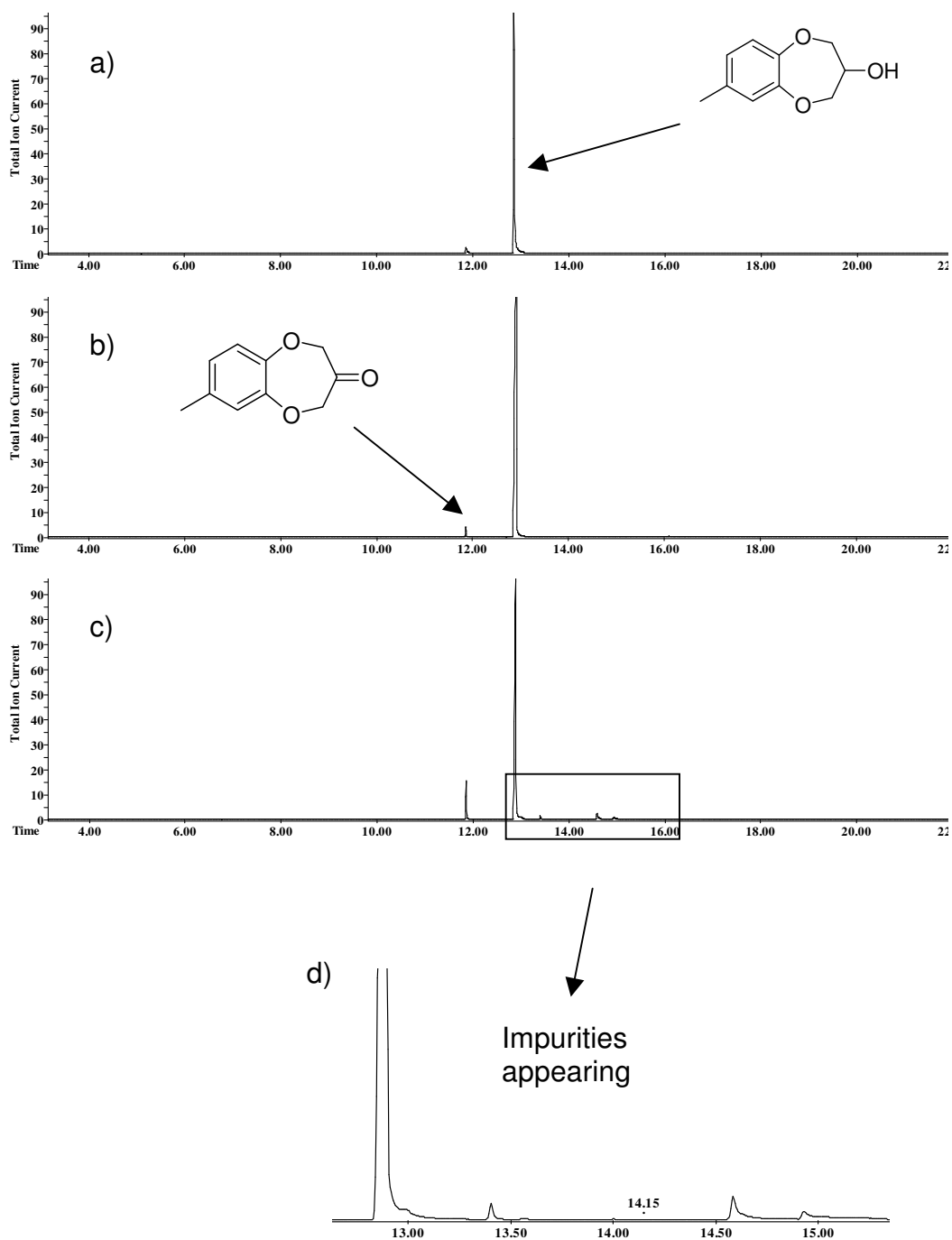
Figure 3.17 GC TIC of oxidation trials on **61** a) KMnO$_4$ in benzene, r.t., 24 hr; b) KMnO$_4$/DCM/TBAB, 24 hr, r.t.; c) KMnO$_4$/TBAB/DCM, 50°C, 3 hr; d) expanded region of c)

The most efficient general oxidation of the secondary alcohol was also the simplest, based on that proposed by Rosnati and De Marchi. Et$_2$O was implemented as extraction solvent in the work-up procedure as the action of HCl on MnO$_4^-$ in the presence of DCM resulted in chlorinated by-products, likely due to the production of Cl$_2$ upon quenching. The GC-MS result of oxidation to analogue **24** is presented in Figure 3.18 as an example,

additional spectroscopic data is provided in Appendix 13. The reaction times and purity of the KMnO$_4$ oxidations varied considerably between species.
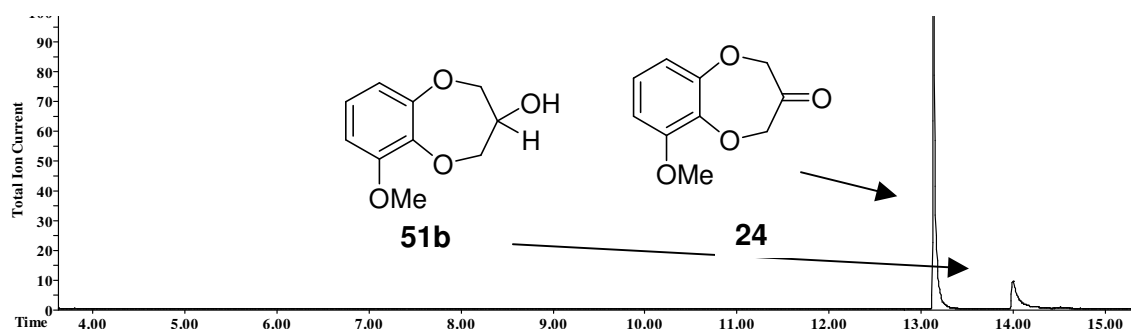
Figure 3.18 GC TIC of **61b** (minor) and **24** (major); oxidation with KMnO$_4$/KOH/H$_2$O, 3 hr, Et$_2$O work up

Permanganate was not a suitable oxidising agent for the formation of benzodioxepinones analogues with electron-withdrawing aromatic substitution. Analogues **61d** (*m*-nitro) and **61e** (*m*-formyl) required a more selective and mild approach.

Application of Swern methodology [27] [28] (Scheme 3.12) provided analogues **26** (also refer to Appendix 14) and **27** in good yields (85% and 53% respectively) (Figure 3.19) and favourable purity (>98% and 93% respectively) with high reproducibility.
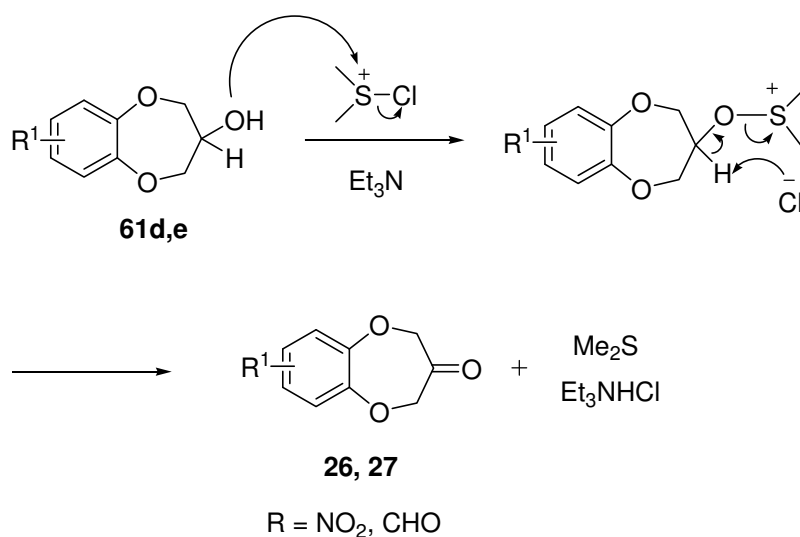
(COCl)$_2$, DMSO, TEA, -78°C, 4 hr

Scheme 3.12 Application of Swern methodology to oxidative generation of **26** and **27**

Dimethyl sulphide (Me$_2$S) is a labile leaving group from the intermediate for generation of the ketone under the basic conditions supplied by addition of TEA. The olfactory properties of **26** were weak and lacked commercial potential however the auxochrome properties of the nitro group highlight the potential of **26** as a pigment, maintaining the characteristic orange colour through to the target product. Analogue **27** provided the most interesting olfactory profile of the series presented in this chapter for potential fragrance application as detailed in Chapter 6. Oxidation products were confirmed by comparative mass spectrum fragmentation with the identical structures previously synthesised by Procedure A (Chapter 2). Further purification was performed by semi-preparative HPLC prior to olfactory analysis ensuring an optimum purity level.
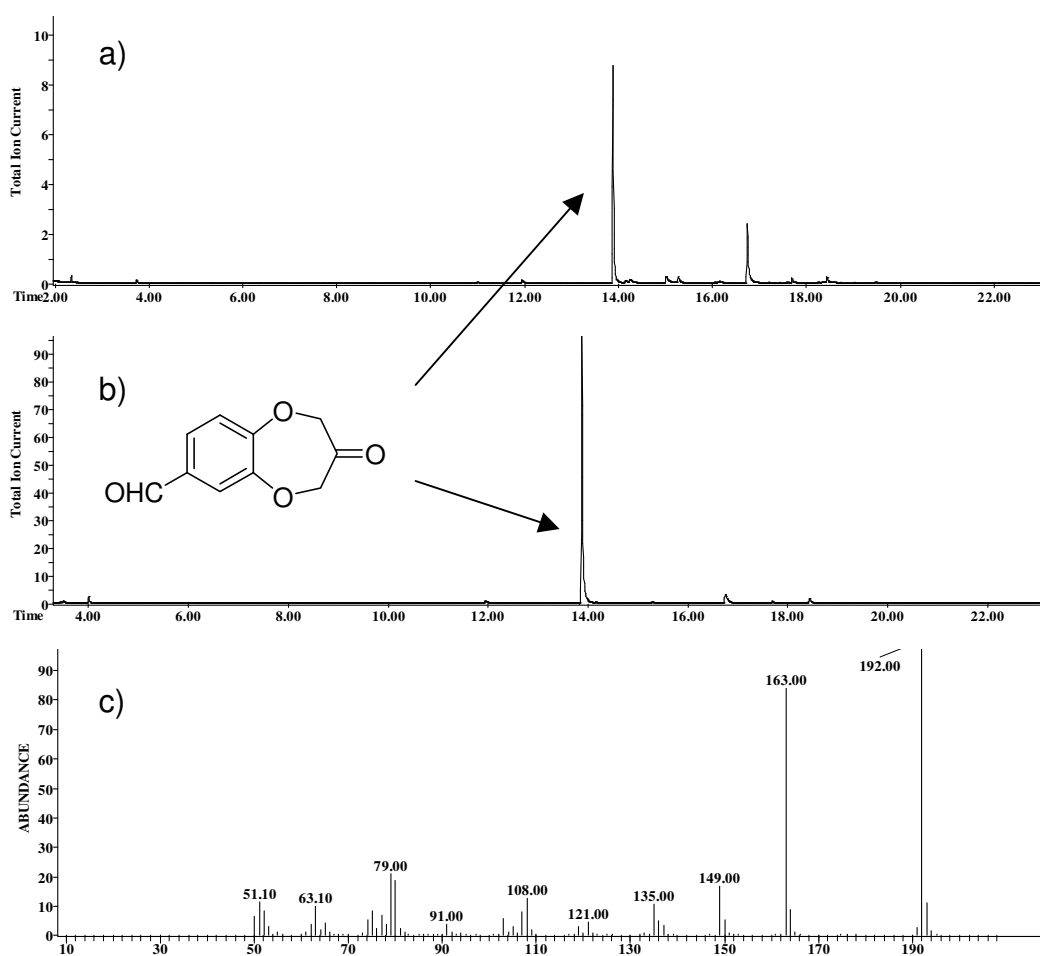
Figure 3.19 GC-MS of oxidation methods to form **27**: a) KMnO$_4$; b) Swern; c) mass spectrum of major peak at t$_R$ = 13.91 min

3.3   References

[1]   F. Yoshii, T. Nakamura, S. Hirono, Y. Shimizu, T. Hoshi, M. Ando, H. Hagiwara, Conformational Analysis and Selection of Odor-active Conformers: Synthesis of Molecules Designed for the Lily-of-the-Valley(Muguet)-type Odor. Helv. Chim. Acta 84(7) (2001) 2051-2063.

[2]   S. Mataka, Y. Mitoma, T. Thiemann, T. Sawada, M. Taniguchi, M. Kobuchi, M. Tashiro, Bisacetals of Aromatic Ring-annelated Benzo[a,d]bis{bicyclo[4.4.1]undeca-3,8-diene-11-one}. [3.3][3.3]Orthocyclophanes with Triple-layered Benzo/Benzo/Benzo and Naphtho/Benzo/Naphtho System. Tetrahedron 53(9) (1997) 3015-3026.

[3]   C.S. Rooney, R.S. Stuart, B.K. Wasson, H.W.R. Williams, 3,4-Dihydro-2*H*-1,5-benzodioxepins. Novel Class of β-Adrenergic Stimulants. Can. J. Chem. 53(15) (1975) 2279-2292.

[4]   J.J. Beereboom, D.P. Cameron, C.R. Stephens, Flavoring Foods with Benzoxepin-3-ones and Benzodioxepin-3-ones, U.S. Patent 3,517,031, October 28, 1969, 1972.

[5]   C.S.S. Rooney, R. S.; Wasson, B. K.; Williams, H. W. R., 3,4-Dihydro-2*H*-1,5-benzodioxepins. Novel Class of β-Adrenergic Stimulants. Can. J. Chem. 53(15) (1975) 2279-2292.

[6]   J. Jamrozik, S. Schab, K. Nagraba, Synthesis and Conformation of Some Tetraoxaspiranes. Monatsh. Chem. 125(4) (1994) 451-456.

[7]   J.S. Jamrozik, S.; Nagraba, K., Synthesis and Conformation of Some Tetraoxaspiranes. Monatsh. Chem. 125(4) (1994) 451-456.

[8]   P. Kraft, Preparation of 1,2-Substituted 2,3-Dihydro-1*H*-5,9-dioxacyclohepta[*f*]inden-7-ones and 7-Substituted Benzo[*b*][1,4]dioxepin-3-ones for Perfumes, E.P. Patent 1, 136, 481, October 3, 2001, 2001.

[9]   J.P. Schirmann, A. Isard, F. Weiss, Rearrangement of Diallylic-type Structures. IV. α,α'-Disubstituted Isobutenes: Thermal Rearrangements of 3-Methylene-1,5-benzodioxepane. Tetrahedron 24(22) (1968) 6475-6483.

[10] P.H.J. Carlsen, T. Katsuki, V.S. Martin, K.B. Sharpless, A Greatly Improved Procedure for Ruthenium Tetroxide Catalyzed Oxidations of Organic Compounds. J. Org. Chem. 46(19) (1981) 3936-3938.

[11] P.H.J.K. Carlsen, T.; Martin, V. S.; Sharpless, K. B., A Greatly Improved Procedure for Ruthenium Tetroxide Catalyzed Oxidations of Organic Compounds. J. Org. Chem. 46(19) (1981) 3936-3938.

[12] P.E. Kraft, W., Conception, Characterization and Correlation of New Marine Odorants. Eur. J. Org. Chem.(19) (2003) 3735-3743.

[13] V. Rosnati, F.D. Marchi, Chemical and Spectroscopic Properties of 2-Formyl-1,4-benzodioxane and 3-Oxo-3,4-dihydro-2*H*-1,5-benzodioxepin. Tetrahedron 18 (1962) 289-298.

[14] O. Stephenson, The Condensation of Epichlorohydrin with Monohydric Phenols and with Catechol. J. Chem. Soc. B: Phys. Org. (1954) 1571-1577.

[15] O. Stephenson, A.M. Wild, D.F. Hayman, Antiinflammatory Esters of *p*-Biphenylylacetic acid with Polyhydric Alcohols, DE Patent 70-2034179, 19700709, 1971.

[16] Y.M. Beasley, Some 3-Arylpropane-1,2-diols. Journal of Pharmacy and Pharmacology VII (1959) 36-42.

[17] H. Sharghi, Z. Paziraee, K. Niknam, Halogenated Cleavage of Epoxides into Halohydrins in the Presence of a Series of Diamine Podands as Catalyst with Elemental Iodine and Bromine. Bull. Korean Chem. Soc. 23(11) (2002) 1611-1615.

[18] H.S. Eshghi, P., Phosphorus Pentoxide as an Efficient Catalyst for the Tetrahydropyranylation of Alcohols under Solvent-free Conditions. Phosphorus, Sulfur Silicon Relat. Elem. 179(10) (2004) 2149-2152.

[19] H. Firouzabadi, H. Hazarkhani, H. Hassani, New Applications of Solid Silica Chloride (-SiO$_2$Cl). Efficient Oxidation of Cyclic Thioacetals, TMS, TBDMS, and THP Ethers to their Carbonyl Compounds by Solid Silica Chloride/KMnO$_4$ System. Phosphorus, Sulfur Silicon Relat. Elem. 179(2) (2004) 403-409.

[20] M.A. Zolfigol, T. Madrakian, E. Ghaemi, A. Afkhami, S. Azizian, S. Afshar, Synthesis of Morpholinated and 8-Hydroxyquinolinated Silica Gel and their Application to Water Softening. Green Chem. 4(6) (2002) 611-614.

[21] T.W. Greene, P.G.M. Wuts, Protective Groups in Organic Synthesis. 2nd Ed, 1991.

[22] R.V.C. Stevens, K. T.; Weller, H. N., Convenient and Inexpensive Procedure for Oxidation of Secondary Alcohols to Ketones. J. Org. Chem. 45(10) (1980) 2030-2032.

[23] J.D.G. Albright, L., Dimethyl Sulfoxide-acid Anhydride Mixtures for the Oxidation of Alcohols. J. Am. Chem. Soc. 89(10) (1967) 2416-2423.

[24] A.K. Shaabani, A.-R., Oxidation Deprotection of Trimethylsilyl Ethers to Carbonyl Compounds by NaBrO$_3$-NH$_4$Cl Reagent in Aqueous Acetonitrile. Synth. Commun. 31(5) (2001) 759-765.

[25] R.P. Gopinath, A. R.; Patel, B. K., V$_2$O$_5$-H$_2$O$_2$: A Convenient Reagent for the Direct Oxidation of Acetals to Esters. Tetrahedron Lett. 43(29) (2002) 5123-5126.

[26] S.D. Baskaran, J.; Chandrasekaran, S., Heterogeneous Permanganate Oxidations: An Improved Procedure for the Direct Conversion of Olefins to α-Diketones/α-Hydroxy ketones. J. Org. Chem. 54(21) (1989) 5182-5184.

[27] K.S. Omura, D., Oxidation of Alcohols by "Activated" Dimethyl Sulfoxide. A Preparative Steric and Mechanistic Study. Tetrahedron 34(11) (1978) 1651-1660.

[28] X.B. Fang, U. K.; Wang, T.; Schroeder, J. D.; Garvey, D. S., First Examples of Oxidizing Secondary Alcohols to Ketones in the Presence of the Disulfide Functional Group: Synthesis of Novel Diketone Disulfides. J. Org. Chem. 66(11) (2001) 4019-4021.

4 Synthesis of Benzodioxepines: Calone 1951® Analogues

4.1 Introduction

The polar region of Calone 1951® (**1**), more specifically the cyclic ketone, has been hypothesised as fundamental to the olfactory character of the molecule. Dramatic olfactory changes from tailored synthetic modifications of this moiety support this premise. In addition heterocyclic ring size variation was explored. Synthesis of ten analogues based on the structures shown in Figure 4.1 provided a useful synthetic data set with suitable purity for olfactory evaluation.

65 R^1 = NOH;
66 R^1 = OH, R^2 = H;
67 R^1 = OMe, R^2 = OMe;
68 R^1, R^2 = C=O, R^3 = Br

69 n = 1
70 n = 2

71 R^1 = OCOMe, R^2 = H;
72 R^1 = OCOPh, R^2 = H;
73 R^1 = OCOCH=CH$_2$, R^2 = H

74 R^1 = NH$_2$, R^2 = H
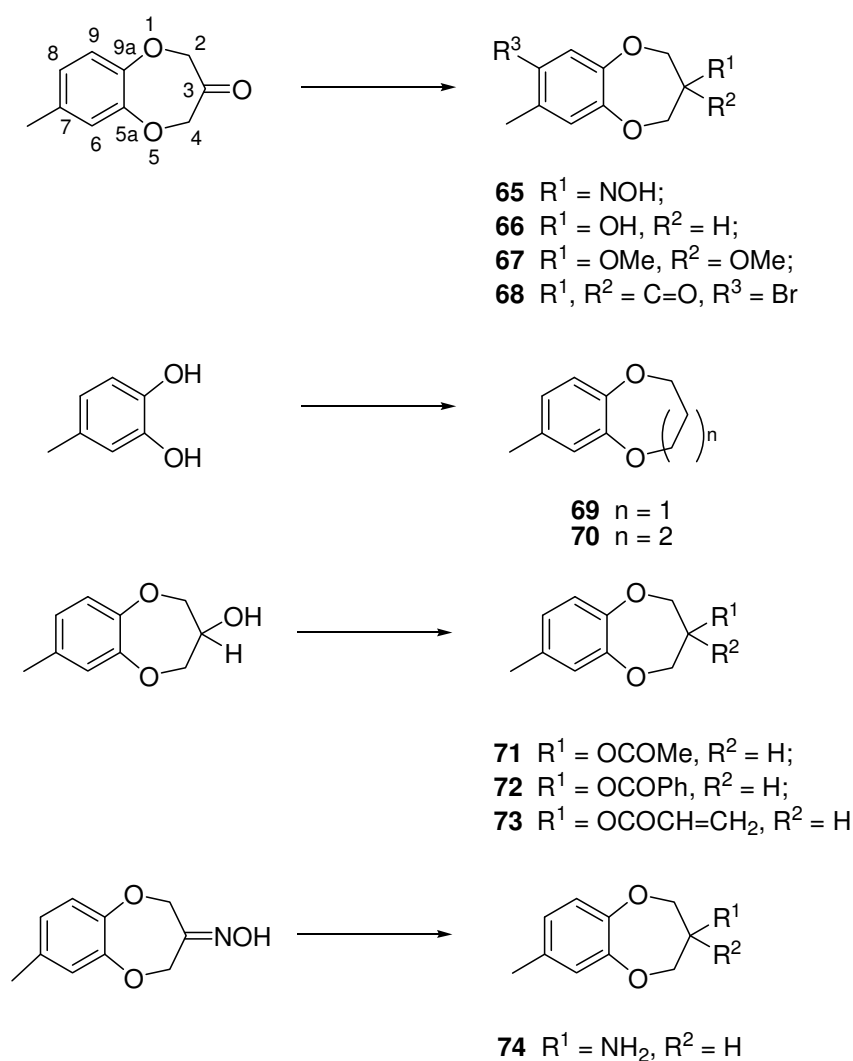
Figure 4.1 Benzodioxepine analogues **65-74**

4.1.1　Overview of Analogues 65-74

Overall purity values achieved for the benzodioxepinone compounds in this data set were high as shown in Table 4.1. Compounds **65**, **66** and **68** were ideally extracted in high isolated yields and demanded no further purification once isolated, washed and solidified. Due to the extensive purification required for **69** and **70**, the isolated yields were evidently lower. Lower isolated yields were also obtained for **72** and **73**, the latter from potential polymerisation. The returned purity for **74** following semi-preparative HPLC purification was favourable.

Table 4.1 Yield and purity values obtained for compounds **65-74**
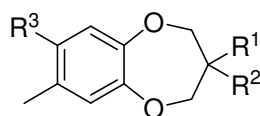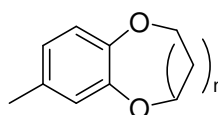
65-68, 71-74　　　　**69, 70**

Compound	R^1	R^2	R^3	n =	Yield (%)	Purity (%)
65	NOH	-		-	94	>99
66	OH	H		-	89	>99
67	OMe	OMe		-	72	>99
68	CO	-	Br		85	95
69	-	-		1	78	97
70	-	-		2	65	96
71	O$_2$CMe	H		-	88	100
72	O$_2$CPh	H		-	44	99
73	O$_2$CCH=CH$_2$	H		-	22	97
74	NH$_2$	H		-	54	98

Table 4.2 is presented on the next page as a summary for comparison of methylene and methine shifts for C-2, C-3 and C-4 protons and carbons. It is also interesting to compare these back to corresponding assignments for the benzodioxepinones presented in Chapter 2 (Table 2.6).

Table 4.2 Relevant methylene and methine shifts for structures **65-74**

	R¹	¹H δ*								¹³C δ			
		H-2	*J* (Hz)	H-3	*J* (Hz)	H-4	*J* (Hz)	H-5	*J* (Hz)	C-2	C-3	C-4	C-5
65		4.91(α) 4.88(β)				5.05(α) 5.03(β)				68.7(α) 68.4(β)		68.3(α) 68.1(β)	
66	4-Me	4.25(2ₐ), 4.04(2ᵦ)		4.04		4.25 (4ₐ) 4.04 (4ᵦ)				74.6		74.4	
67		4.20				4.19				71.7		71.5	
68	5-Br	4.67				4.66				75.7		75.5	
69		4.10	5.3	2.11	5.5	4.08	5.1			72.4	34.1	72.3	
70		4.29	5.5	1.88		1.88		4.21	5.5	73.1	26.4	27.3	72.2
71		4.37(2ₐ), 4.35(2ᵦ)	12.8, 4.3	5.26	5.1, 4.3	4.28(4ₐ) 4.26(4ᵦ)	12.8, 5.1			71.4	71.5	71.2	
72	4-Me	4.51(2ₐ), 4.50(2ᵦ)	12.8, 4.3	5.53	5.1, 4.3	4.43(4ₐ) 4.42(4ᵦ)	12.8, 5.1			71.6	71.9	71.3	
73		4.34(2ₐ), 4.33(2ᵦ)	12.8, 4.3	5.35	5.1, 4.3	4.25(4ₐ) 4.23(4ᵦ)	12.8, 5.1			71.4	71.5	71.2	
74		4.32- 3.97		4.32- 3.97		4.32- 3.97				74.1	50.7	74.0	

* For multiplicities refer to individual experimental sections

4.2   Preparation of Benzodioxepine Analogues

4.2.1   7-Methyl-2H-1,5-benzodioxepin-3(4H)-one oxime (65)

Introduction of alternative sp^2 chemistry to the C-3 of **1** provided useful olfactory information (discussed in Chapter 6). This was achieved by conversion of the carbonyl of **1** by oximation as shown in Scheme 4.1. Whilst the oxime group exhibits the known structural requirements for odour character oximes are seldom explored in literature for their potential as odour-active compounds.

NH$_2$OH.HCl, NaOAc, H$_2$O:MeCN, 94%
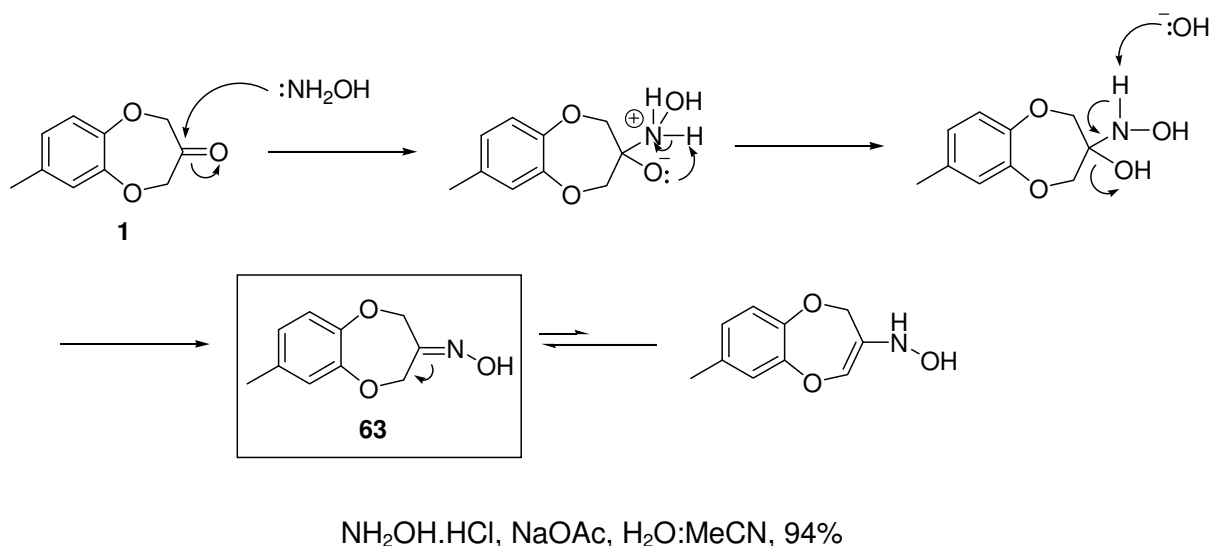
Scheme 4.1 Preparation of **65**

Gentle heating (50°C) for 12 hours enabled the formation of **65**, isolated as pure crystalline material upon quenching in ice/H$_2$O. Formation of the ketoxime (Figure 4.2) was loosely based on the conditions of Dondas et al. [1] whose method exhibited higher efficiency, in relation to both time and yield (94%), to that proposed by Guziec and Russo [2] (73%). The latter method is recommended for oximation of sterically hindered ketones and carried out in ethanol (EtOH)/H$_2$O. The method proposed by Dondas and colleagues maintains a balance between the hydroxyl-amination and hydroxy cleavage/oximation rate-determining steps, assisted by the buffering capacity of sodium acetate in acetonitrile (MeCN)/H$_2$O.
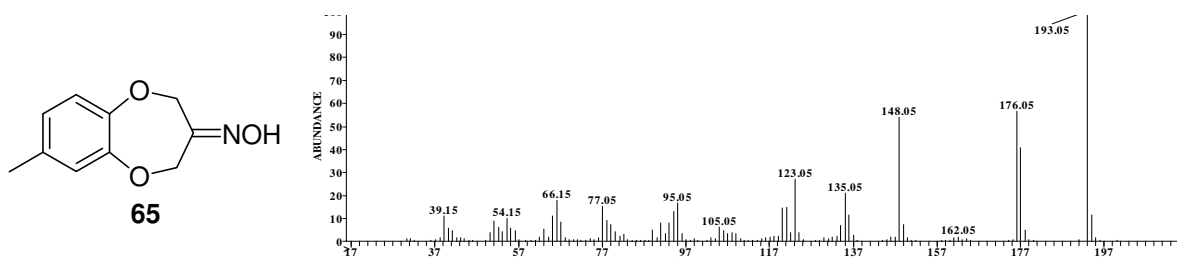
Figure 4.2 EI mass spectrum of **65**

Excellent yields of the oxime target were dictated by thermodynamic control: the three-hour reaction time suggested by the authors was insufficient and gave a residue that required purification by column chromatography. Reaction monitoring by GC-MS revealed the appearance of impurities in the reaction mixture at 12 hours. High Resolution-Electrospray Ionisation spectrometry (HRESI) verified the molecular ion of the oxime benzodioxepine structure, **65**, ([M + H]$^{+\bullet}$; calculated: 194.0817, found: 194.0812). Quadrupole EI MS fragments from the molecular ion are representative of cleavage of the hydroxyl group and the oxime nitrogen [M-17-14]$^{+}$. FT-IR analysis confirmed a strong band at 1509 cm^{-1}, in the overlapping range of imines and ketones, medium-broad bands at 3289 and 2921 cm^{-1} verified the hydroxyl group attached. ^{1}H NMR analysis of **65** indicated that C-2 and C-4 of the oxime are locked into two alternate geometrical conformations in equivalent amounts (α and β isoforms). More commonly the isomeric arrangement will favour one of the E/Z forms both in aliphatic [3] and alicyclic [4] oximes, in addition no enolised product was detected in the NMR data. Long-range heteronuclear HMBC experiments confirmed the formation of α (syn-), β (anti-) isoforms showing distinguishable isomeric signals for C-9a and C-5a coupling with the α isomer (146.9 ppm, 145.0 ppm respectively) and the β isomer (148.3 ppm, 146.5 ppm respectively) (Figure 4.3).
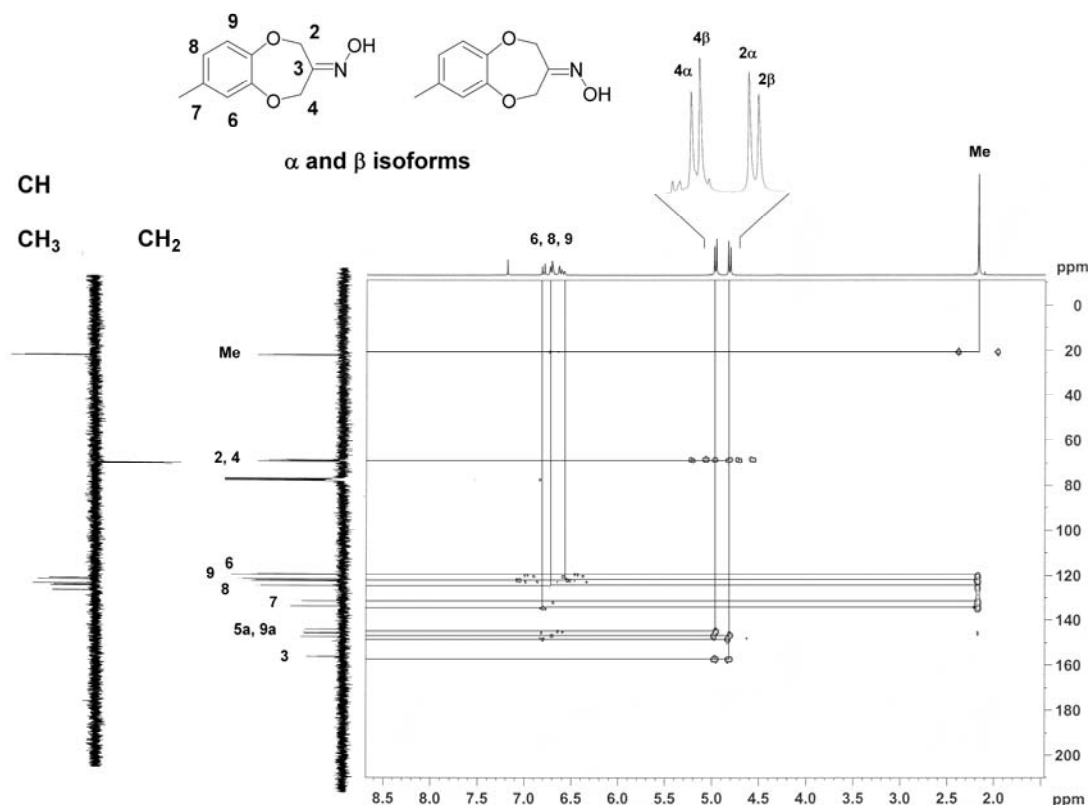
Figure 4.3 ^{1}H,^{13}C HMBC and DEPT135 NMR spectra of **65**

Intensity difference in the ^{13}C spectrum allowed allocation of isomeric signals, the nature of which was confirmed by DEPT135. The carbon-proton resonance of both isomers of **65** corroborates with heteronuclear HMBC. The α isomer reveals C-4 (68.3 ppm) coupled with H-4$_A$ and H-4$_B$ (5.05 ppm), and C-2 (68.7 ppm) coupled with H-2$_A$ and H-2$_B$ (4.91 ppm). Conversely C-4 (68.1 ppm) of the β-isomer couples to H-4$_A$ and H-4$_B$ (5.03 ppm), and C-2 (68.4 ppm) is coupled to H-2$_A$ and H-2$_B$ (4.88 ppm). For ^{1}H,^{13}C and COSY NMR data refer to Appendix 15.

4.2.2   3,4-Dihydro-7-methyl-2H-1,5-benzodioxepin-3-ol (rac-66) and 3,4-Dihydro-(R/S)-7-Methyl-2H-1,5-benzodioxepin-3-ol (ent-66)

Similar to oximes, alcohols provide hydrogen-bonding capabilities perfectly suited for a protein-structured biological receptor. The benzodioxol, **66**, was prepared by simple

reduction using sodium borohydride (NaBH$_4$) providing **rac**-**66** in 90% isolated yield (Scheme 4.2).

1 → **rac-66** / **ent-66**
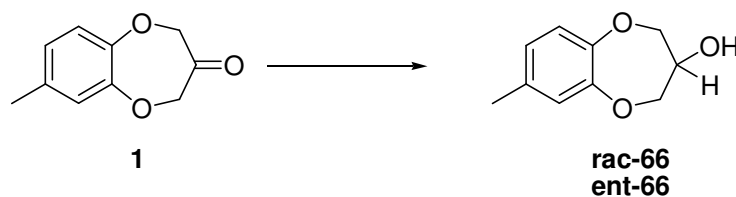
rac-**66**: NaBH$_4$, H$_2$O:MeOH, 90%

ent-**66**: baker's yeast, glucose, phosphate buffer, H$_2$O/EtOH/DMSO, 70%

Scheme 4.2 Preparation of **66**

Reaction monitoring by GC-MS revealed that reduction of the ketone was complete in 4 hours. Implementation of a procedure recommended by Caycho and colleagues [5] involving a reductive borohydride-proton donor (Amberlyst-15) complex [6] failed to improve formation of the reduced benzodioxepinone. Experimentation with solvents demonstrated that reduction attempts in an EtOH/dichloromethane (DCM) or H$_2$O/EtOH solvent mix returned lower, and more irreproducible yields than H$_2$O/methanol (MeOH). The mass spectrum of structure **66** is presented in Figure 4.4.
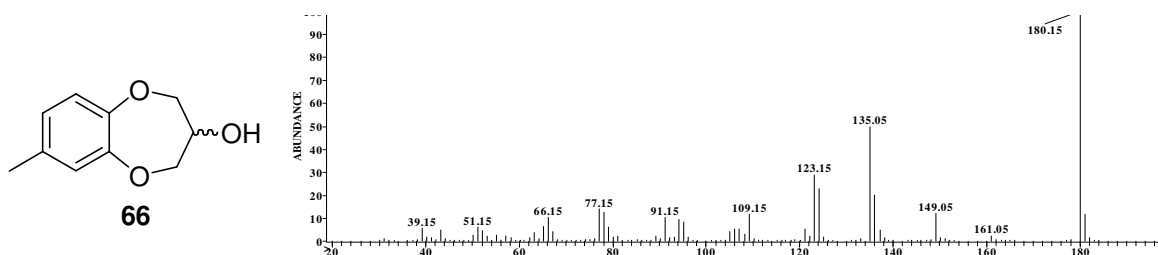
Figure 4.4 EI mass spectrum of **rac-66**

A non-racemic mixture of **66** was prepared using a stereoselective bio-reduction based on that proposed by Aragozzini and co-workers [7] to provide **ent**-**66**, an asymmetric molecular replica. Intrinsic reducing power of the yeast is mediated by addition of a buffer and glucose to induce a fermenting environment. GC-MS monitoring indicated that a 24-hour reaction period returned similar isolated yields (~40%) as a 6 hour time period, with maximum enzymatic hydrolysis in 4 hours. The reduced structure was confirmed by HRESI ([M + Na]$^{+•}$]; calculated: 203.0684, found 203.0682). The connectivity of **66** was verified by HMBC NMR analysis. Homonuclear J-resolved ^{1}H spectra revealed the C-3 methine signal, at 4.00-4.07 ppm consisted of a complex splitting pattern. The larger

diastereotopic methylene signals from C-2/C-4 at 4.00-4.07 ppm (H-2$_B$, H-4$_B$) and 4.22-4.30 ppm (H-2$_A$, H-4$_A$) were confirmed as second order signals substantiated by the collapse of apparent double doublets in the 300 MHz NMR, to an AB quartet in 500 MHz ^{1}H NMR experiments. For NMR characterisation refer to Appendix 16. Asymmetric **ent-66** was confirmed to exhibit optical rotation at α = -4.8°, $[\alpha]_D$ = -120°. The optical rotation of the racemate, **rac-66** was found to be α = -0.7°, $[\alpha]_D$ = -8.3°. Resolution of enantiomers of **ent-66** was not pursued due to the weak and lacklustre olfactory characteristics of this structure.

Interconversions of **66** involved attempts at displacement of the sp^3 hydroxy group for a C-3 halogenated derivative. Reaction of **66** with thionyl chloride (SOCl$_2$) failed to provide a detectable yield of chlorinated material. Bromination based on a procedure reported by Umemura et al. [8] incorporated the inorganic acid halide, phosphorus tribromide (PBr$_3$) for the interconversion of secondary alcohols (Scheme 4.3). Despite trials involving long reaction times (5 days) and elevated temperatures (70°C) the alicyclic alcohol failed to brominate and returned only the unreacted alcohol **66**.

66
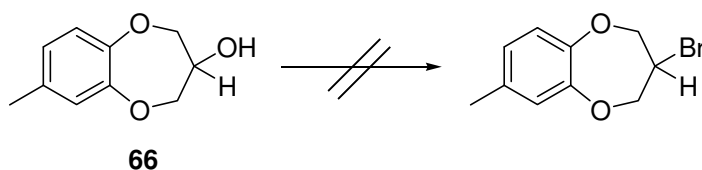
PBr$_3$, pyridine, DCM

Scheme 4.3 Attempted halogenation of **66**

4.2.3   3,4-Dihydro-3,3-dimethoxy-7-methyl-2H-1,5-benzodioxepine (67)

Further reactions of the core skeleton of **1** to introduce sp^3 connectivity at C-3 involved derivatisation of the carbonyl to acetal functionality. Conversion of the carbonyl to a diethyl-acetal was attempted with methodology proposed by Vogel [9] as presented in Scheme 4.4*, step a*. HCl gas generated using a Kipps apparatus from sulphuric acid and concentrated aqueous HCl (35%; 10.5M) was bubbled through a solution of **1** solubilised in EtOH.
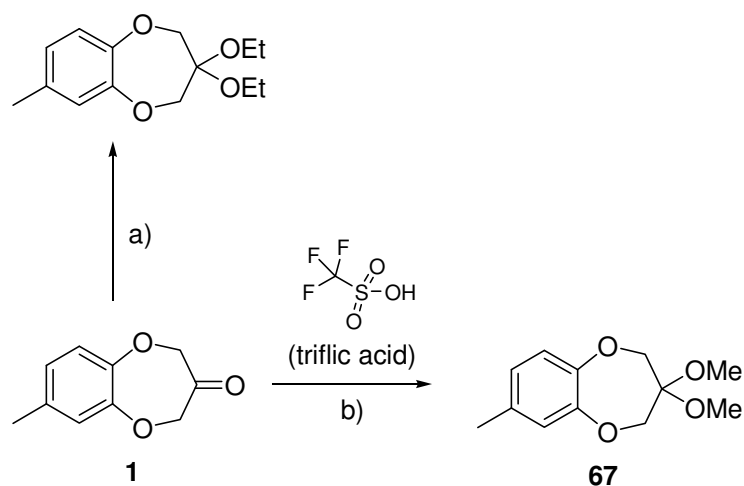
a) HCl (*g*), MeOH or EtOH; b) CH(OCH₃)₃, MeOH (4.5%), CF₃SO₃H, MeNO₂, 72%

Scheme 4.4 Acetalation of **1**

Although the ethoxylation generated good yields (81%) (Figure 4.5) the sensitivity of **1** to strong acidic conditions led to the appearance of decomposition products in GC-MS analysis that proved difficult to separate by distillation and column chromatography.
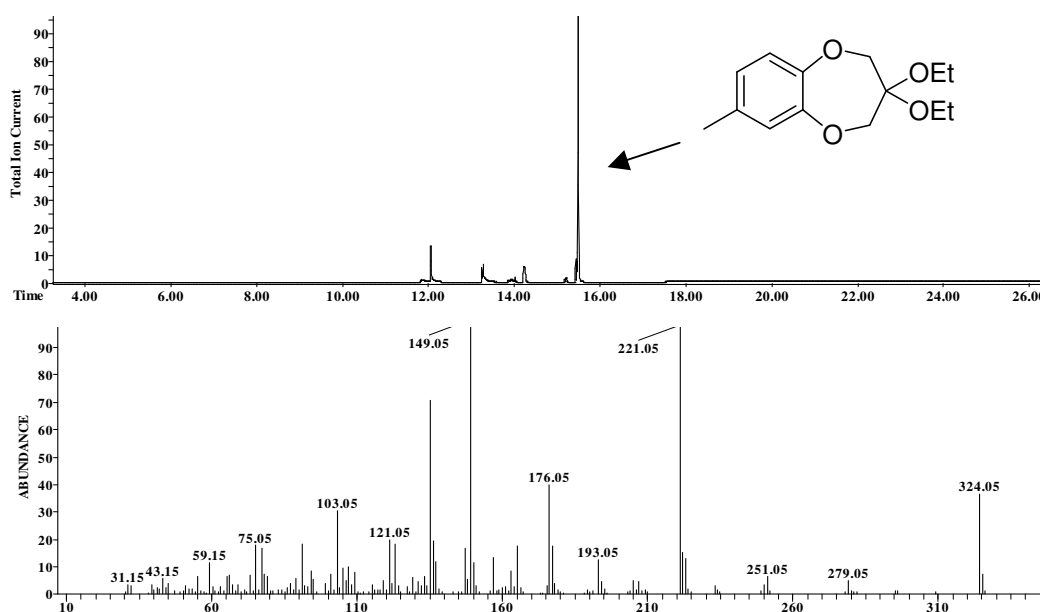
Figure 4.5 GC-MS of 3,4-dihydro-3,3-diethoxy-7-methyl-2*H*-1,5-benzodioxepine formed by HCl/EtOH

An alternative procedure reported by Thurkauf, Jacobson and Rice [10] was pursued involving a single-step, acid-catalysed trans-acetalation using triflic acid

(trifluoromethanesulphonic acid) (TfOH) with trimethylformate and catalytic MeOH to provide a clean mixture of the dimethyl acetal without the formation of decomposition products (Scheme 4.4). The acetal **65** was easily purified by bulb distillation to provide 72% yield in >99% purity as indicated by HRESI analysis ([M + Na]$^{+\bullet}$: calculated: 247.0946, found: 247.0946). Characteristic acetal fragments depicted fragmentation of **65** ([M-15-16-15]$^{+}$) from the molecular ion of m/z 224.05, in this case also the base peak. Decarbonylation (-CO) then occurs, as homolysis (cleavage of the C-C bond) is favoured.

Generally aryl groups attached to the acetal carbon promote stabilisation of the rate-determining intermediate cation formed. Despite the lack of aryl stabilisation the absence of steric hindrance allowed good yields to be obtained. The authors report that substitution of TfOH with p-toluenesulphonic acid (*p*-TsOH) or sulphuric acid (H$_2$SO$_4$) results in low yields or complete absence of reactivity for their halogenated and nitrated alkyl and aryl series. This suggests that a co-complexation/protonation could be occurring when TfOH is used, which would further encourage stabilisation of the protonated acetal intermediate. However according to Kametani and colleagues [11] trimethyl orthoformate will also form the acetal in good yield (70-90%) with a catalytic amount of *p*-TsOH, which they applied to phenylcyclohexenones. The structure of **65** was verified by ^{1}H NMR analysis (Figure 4.6), showing a large methoxy singlet at 3.33 ppm with an integral area equivalent to 6 protons.
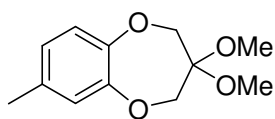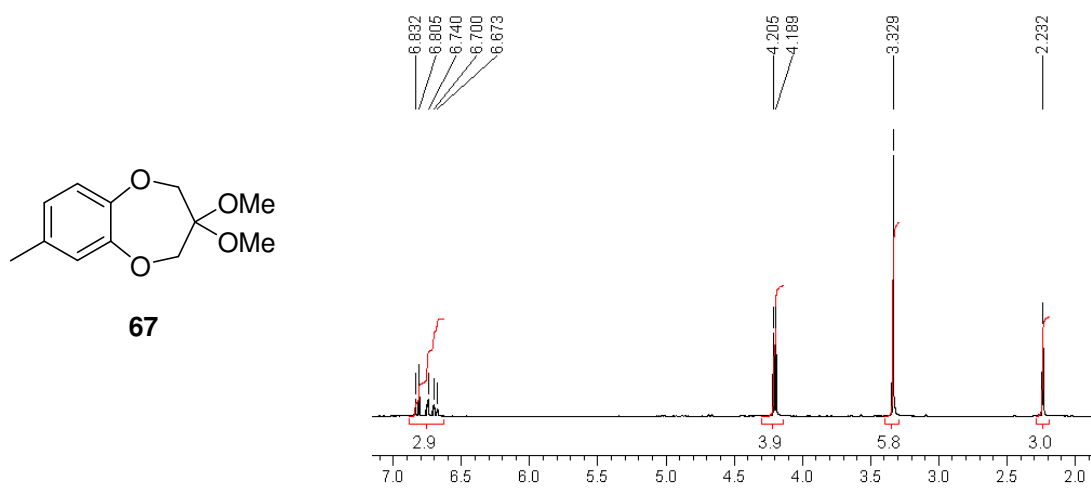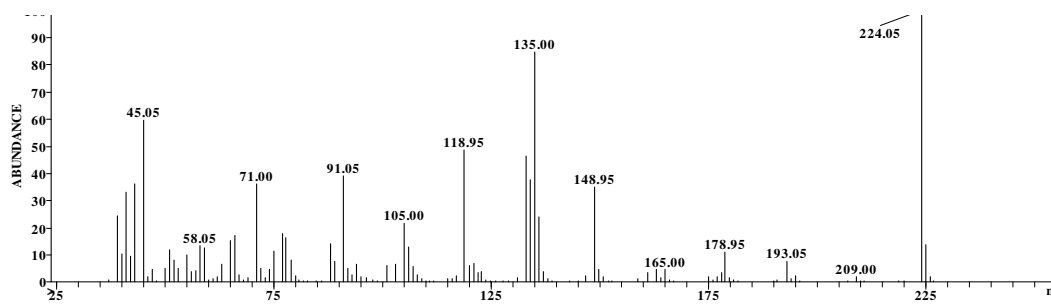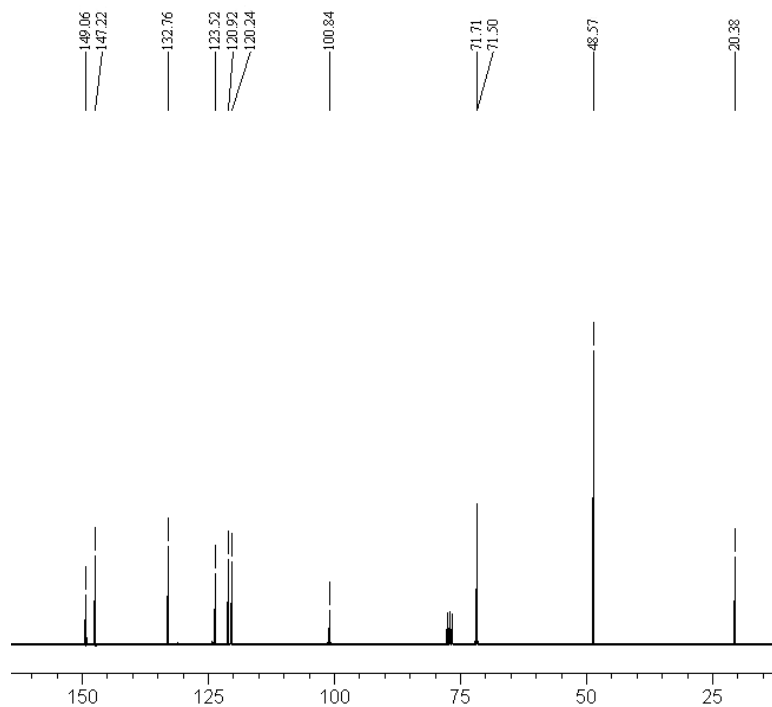
Figure 4.6 EI mass spectrum, ^{1}H and ^{13}C NMR spectra of **67**

The methoxy carbon signals were confirmed with DEPT analysis appearing at 71.6 and 71.8 ppm, the presence of two signals verifying the influence of the aromatic methyl on resonance of the alternative terminal end of the structure. The alicyclic ring signals were confirmed with HMQC data: C-2 (71.7 ppm) is coupled to 4.20 ppm and C-4 (71.5 ppm) is coupled to 4.19 ppm (for HMQC and DEPT135 refer to Appendix 17).

4.2.4   7-Bromo-8-methyl-2H-1,5-benzodioxepin-3(4H)-one (68)

The experimental protocol for the synthesis of **68** was based on a system described by Kikuchi, Sakaguchi, and Ishii [12], in which bromination involves sodium bromate (NaBrO$_3$)/sodium hydrogen sulphite (NaHSO$_3$) pairing as shown in Scheme 4.5.
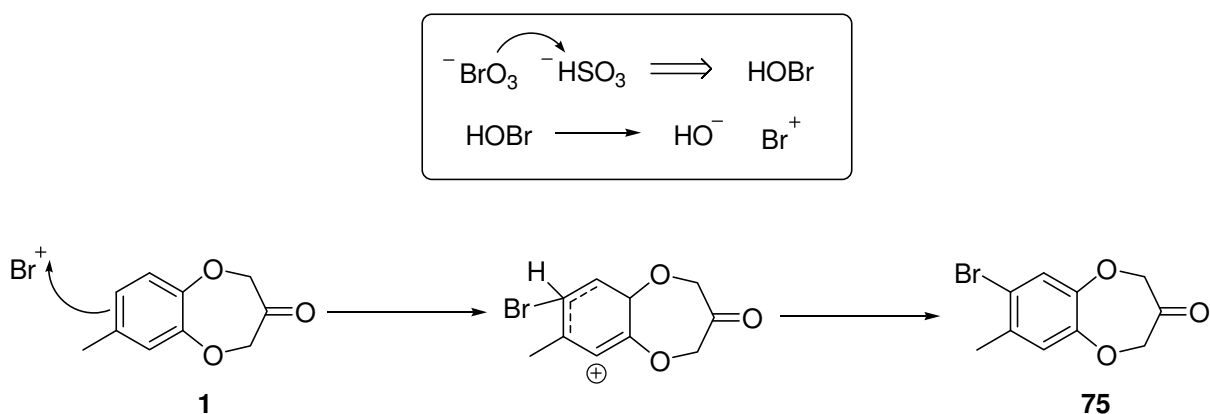
NaBrO$_3$, NaHSO$_3$, H$_2$O:cyclohexane, 85%

Scheme 4.5 Preparation of **68**

The two-phase system was employed for *in situ* generation of hypobromous acid (BrOH) in the aqueous phase and is suspected to act as a source for a cationic bromine species. This results in selective bromination on the aromatic ring, taking advantage of susceptibility to electrophilic substitution dependant on the dominant canonical form of the substituted aromatic ring. Bromination of **1** occurred entirely selectively at the less hindered *ortho*-position predicted by the activating methyl group present to provide **68** in 85%, without the need for further purification. EI mass analysis affirmed formation of the bromo derivative with a molecular ion of 255.95/257.90 *m/z* (Figure 4.7) and an isotope pattern typical of mono-bromination.
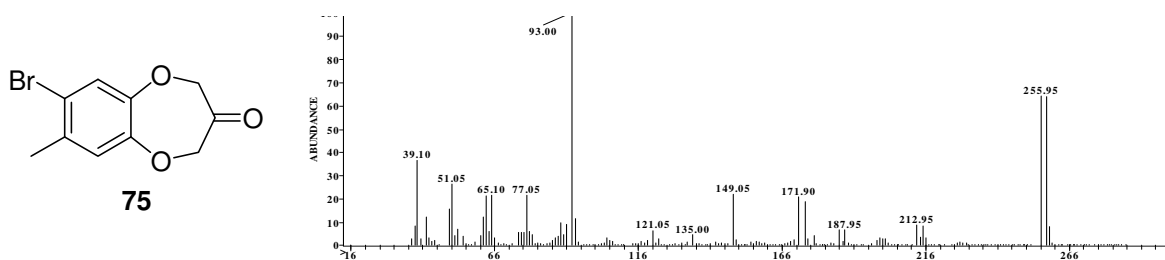
Figure 4.7 EI mass spectrum of **68**

The structure was verified by ^{1}H and ^{13}C NMR included in Appendix 18, and the high-resolution mass spectrum confirmed the structure of **68** ([M]${}^{+\bullet}$; calculated: 256.9813, found: 256.9812).

4.2.5   3,4-Dihydro-7-methyl-2*H*-1,5-benzodioxepine   (69)   and   2,3,4,5-Tetrahydro-8-methyl-1,6-benzodioxocine (70)

As the ketone was suspected as a primary requisite for the benzodioxepinone marine odour, the effect of removal of this functionality contributes a valuable analogue to the group. Both 7- and 8-membered saturated bicyclic ethers were found to be accessible via di-etherification involving intramolecular cyclisation by reacting the catechol **20** with the appropriate dihaloalkane under Williamson etherification conditions (

Scheme 4.6). Both 7- and 8-membered bicyclics were synthesised using this method. A limiting amount of dibromide reagent resulted in higher returns of unreacted 4-methyl catechol. The same reaction trials that were applied previously to find optimal reaction conditions for forming Calone 1951${}^{\circledR}$ [13] using the Williamson etherification method were applied here. The aim was to see what yields were achievable and the highest yields were achieved with the experimental details provided despite a degree of bis-alkylation occurring. The 6-membered cyclic ether ring appears as an impurity in the cyclisation mentioned in Chapter 2, Section 2.3. Even featuring a reactive carbonyl, the compound is devoid of olfactory character, and so formation of an aliphatic dioxane analogue was not pursued. In conjunction, increases in ring strain with cyclic ethers larger than 8-members lead to unfavourable conditions for intramolecular cyclisation and formation of a 9-membered analogue was abated.
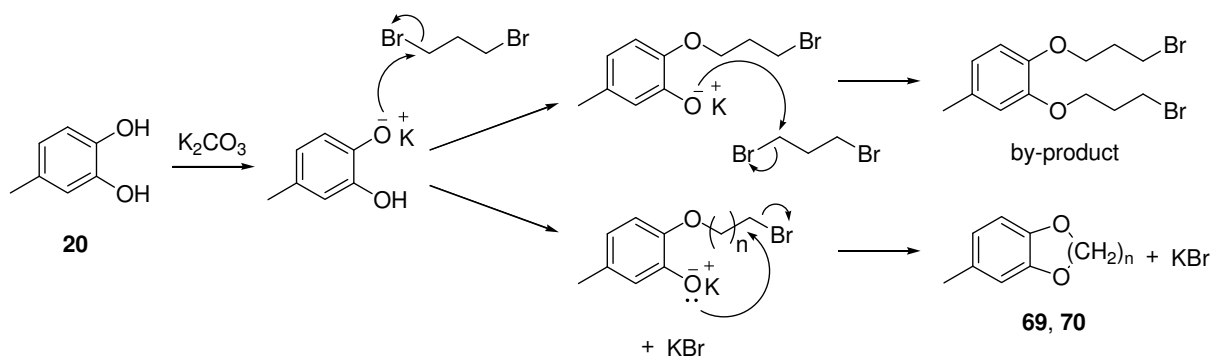
A. K$_2$CO$_3$, DMF, **69**: n = 3: 1,3-dibromopropane, 30%

    70: n = 4: 1,4-dibromobutane, 65%

B. Na (2 eq.), ethylene glycol monobutyl ether, 38%

Scheme 4.6 Preparation of **69** and **70**

Due to steric considerations the attachment of alkyl chains longer than 4 carbons could be expected to provide the di-alkylated product predominately as the material was formed in significant quantity during the formation of **69** and **70**, as identified by the molecular ion and di-bromo isotope pattern in GC-MS analysis. Products **69** and **70** were confirmed by their molecular ions from quadrupole GC-MS (164.05 and 178.10 *m/z* respectively) as shown in Figure 4.8 and Figure 4.9.
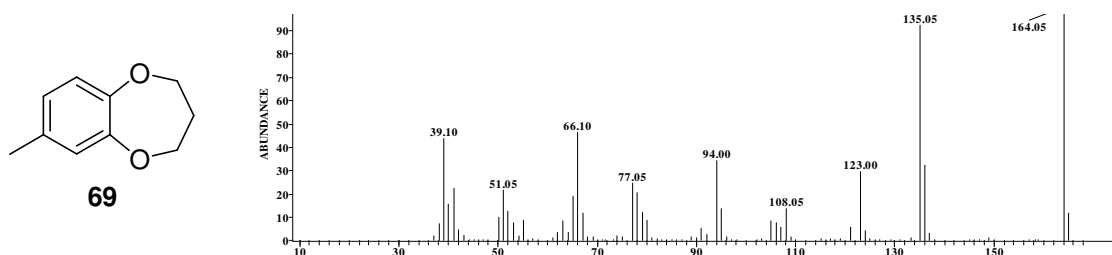
Figure 4.8 EI mass spectrum of **69**

The alkyl chain in **69** confirmed by ^{1}H COSY and HMQC NMR and showed overlapping triplets for C-2 and C-4 protons at 4.10 ppm and 4.08 ppm with respective coupling constants 5.3 Hz and 5.1 Hz, coupled to the C-3 multiplet at 2.11 ppm (*J* = 5.5 Hz) (refer to Appendix 19).
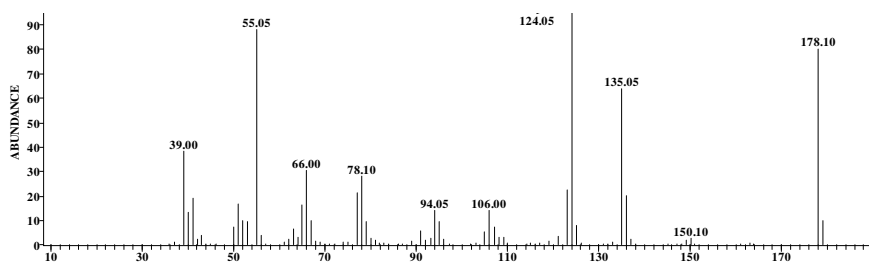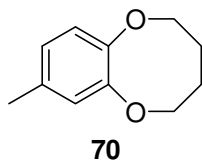
Figure 4.9 EI mass spectrum of **70**

^{1}H COSY data for **70** revealed distinct triplets (J = 5.5 Hz) for C-2 and C-5 protons at 4.29 ppm and 4.21 ppm respectively coupled to C-3 and C-4 protons (1.88 ppm) (Figure 4.10). HMQC data (Appendix 20) for **70** revealed an inverse carbon/proton coupling skew where the two heterocyclic methylenes, C-2 (73.2 ppm) and C-5 (74.5 ppm) couple with 4.18 ppm and 4.09 ppm proton shifts respectively, and alicyclic methylenes C-3 (26.6 ppm) and C-4 (28.0 ppm) were coupled to 1.72 ppm and 1.73 ppm proton shifts respectively.
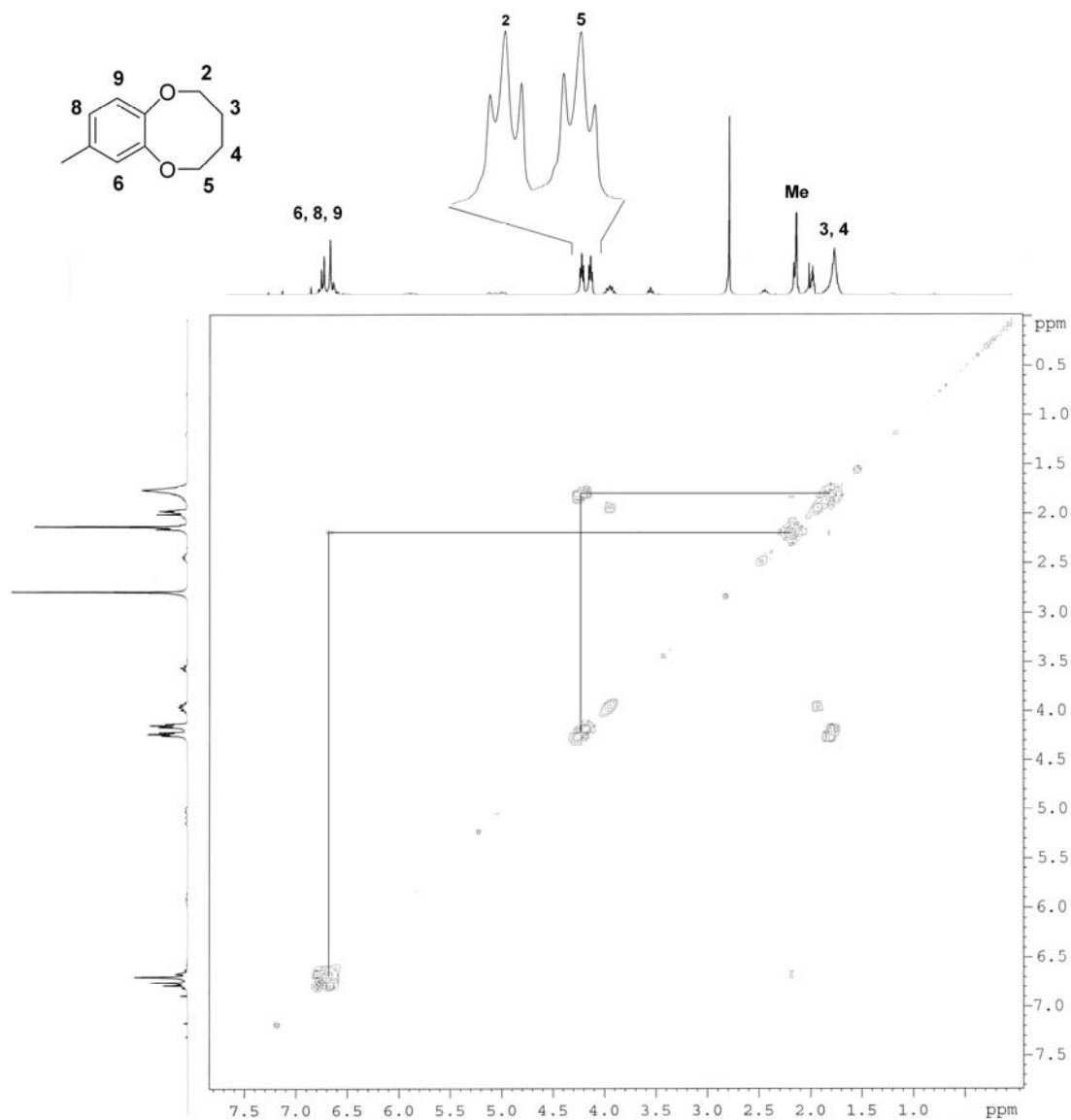
Figure 4.10 $^{1}H,^{1}H$ COSY spectrum of **70**

4.2.5.1   Microwave Synthesis Comparisons

Microwave heating in organic synthesis is suitable for polar solvents or reagents that possess a high dielectric value to allow effective interaction of the microwaves with the reaction media [14]. The Williamson etherification conditions employed for formation of the cyclic di-ethers **69** and **70** from 4-methyl catechol (**20**) are conducted in DMF, which exhibits a reasonably high dielectric constant, conducive for microwave heating [15]. Table 4.3 provides a general comparison of dielectric values for polar and nonpolar solvents; water the most microwave-absorbent, and contrastingly the microwave

transparency of benzene rendering this a non-effective solvent for irradiation-assisted synthesis. Yields obtained using conventional heating methods (oil bath) were comparable to microwave heating experiments apart from a reasonable increase in formation of the di-alkylated by-product formed in the conventional method for **69**, as compared to the favoured intramolecular cyclisation using the microwave method (Table 4.4).

Table 4.3 Dielectric constants of common solvents [16]

	Dielectric constant (ε)
Water	80[a]
DMF	37[b]
Benzene	2.3[a]

[a] literature value at 20°C

[b] literature value at 25°C

Table 4.4 Conventional vs microwave procedure for synthesis of **69** and **70**

Compound	Conventional		Microwave	
	Yield[a]	Purity[b]	Yield[a]	Purity[b]
	(%)	(%)	(%)	(%)
69	78	54	55	98
70	65	41	24	33

[a] Yields are calculated from GC-MS purity with weight of crude compound prior to purification

[b] Purity determined by GC-MS prior to purification

An alternative procedure based on the protocol of Jamrozik and colleagues [17] with sodium (Na) and ethylene glycol dimethyl ether as solvent provided similar yields (Scheme 4.6). Complete removal of the brominated alkylating material from products **69** and **70** could not be achieved by column chromatography on silica (SiO_2) or distillation under reduced pressure. Reaction of the crude mixture with Reike zinc (active Zn suspension in THF) in THF at 85°C was used to react the alkyl bromide via Zn insertion. The high temperatures required for Zn-halogen complexation also proved optimum for polymerisation of the alkylating agent. Nevertheless, this is an alternative purification, prior to elution through SiO_2 with a 9:1 non-polar:relatively polar solvent mix. Removal of brominated impurities was most effectively achieved by precipitation as the quaternary ammonium salts with TEA. Splitting, coupling constants and connectivity of C-2, C-3, C-4

and C-5 protons for compounds **69** and **70** were confirmed by COSY and HMQC data and are in agreement with data reported by Archer and Claret [18].

4.2.6 3,4-Dihydro-7-methyl-2H-1,5-benzodioxepin-3-yl acetate (71), 3,4-Dihydro-7-methyl-2H-1,5-benzodioxepin-3-yl benzoate (72) and 3,4-Dihydro-7-methyl-2H-1,5-benzodioxepin-3-yl acrylate (73)

Acylation to form carboxylic esters **71**, **72** and **73** was achieved using **66** and the appropriate acid chloride in the presence of TEA (Scheme 4.7).

66

71 R^1 = CH$_3$
72 R^1 = Ph
73 R^1 = CH=CH$_2$
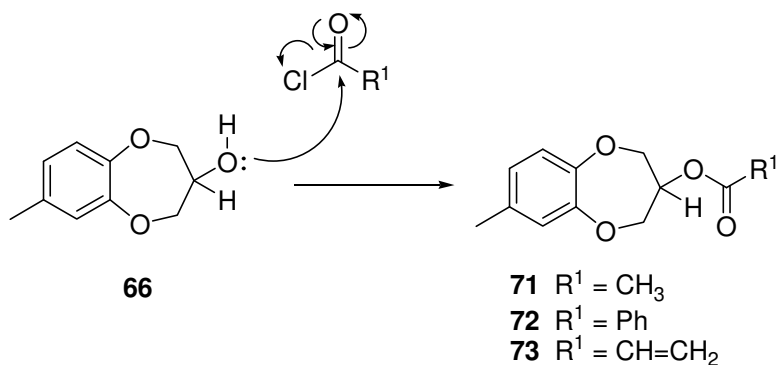
NEt$_3$, Et$_2$O, acetyl chloride (R^1 = OCOCH$_3$), 88%; benzoyl chloride (R^1 = OCOPh), 45%; acryloyl chloride (R^1 = OCOCH=CH$_2$), 22%

Scheme 4.7 Preparation of acryl benzodioxepines **71**-**73**

Removal of the quaternary ammonium salts by filtration and further washing with 2M HCl furnished the acetylated products in high purity (>95%) as indicated by GC-MS (Figure 4.11 and Figure 4.12). Mass analysis revealed molecular ions 222.35, 284.10, 234.10 m/z for **71**, **72** and **73** respectively. Respective losses from the molecular ions of [M-29]$^+$, [M-122]$^+$ and [M-72]$^+$ confirmed the corresponding acyl groups (CH$_3$CO$_2{}^+$, C$_6$H$_5$CO$_2{}^+$, CH$_2$CHCO$_2{}^+$) for each compound. Full characterisation (FT-IR, GC-MS, 1D and 2D NMR) verified the structure and purity of **71**-**73**.
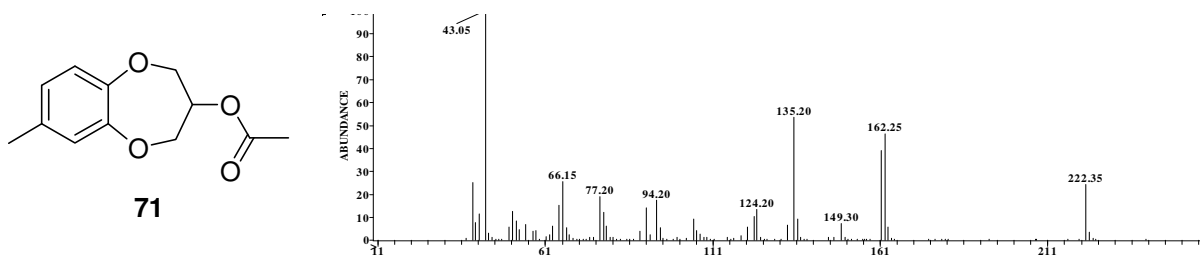
Figure 4.11 EI mass spectrum of **71**
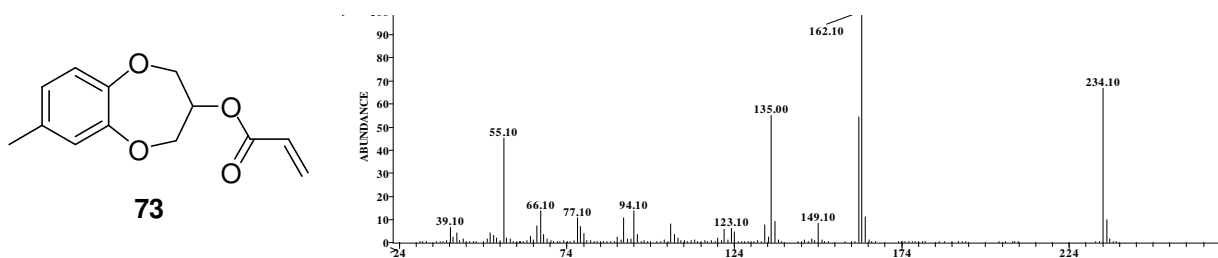
Figure 4.12 EI mass spectrum of **73**

^{1}H NMR splitting on the C-2-C-4 ether chain produced identical first order coupling patterns for all ester derivatives. The methine proton on chiral C-3 forms a triple triplet from isochronous H-2a, H-4a protons and H-2b, H-4b protons (Figure 4.13 and Figure 4.14). Homonuclear J-resolved data confirmed C-2 and C-4 protons as four overlapping sets of double doublets (C-2; 4.3, 12.8 Hz, C-4; 5.1, 12.8 Hz), and their relationship to the acyloxy-substituted carbon (C-3) was confirmed through HMQC and COSY data.
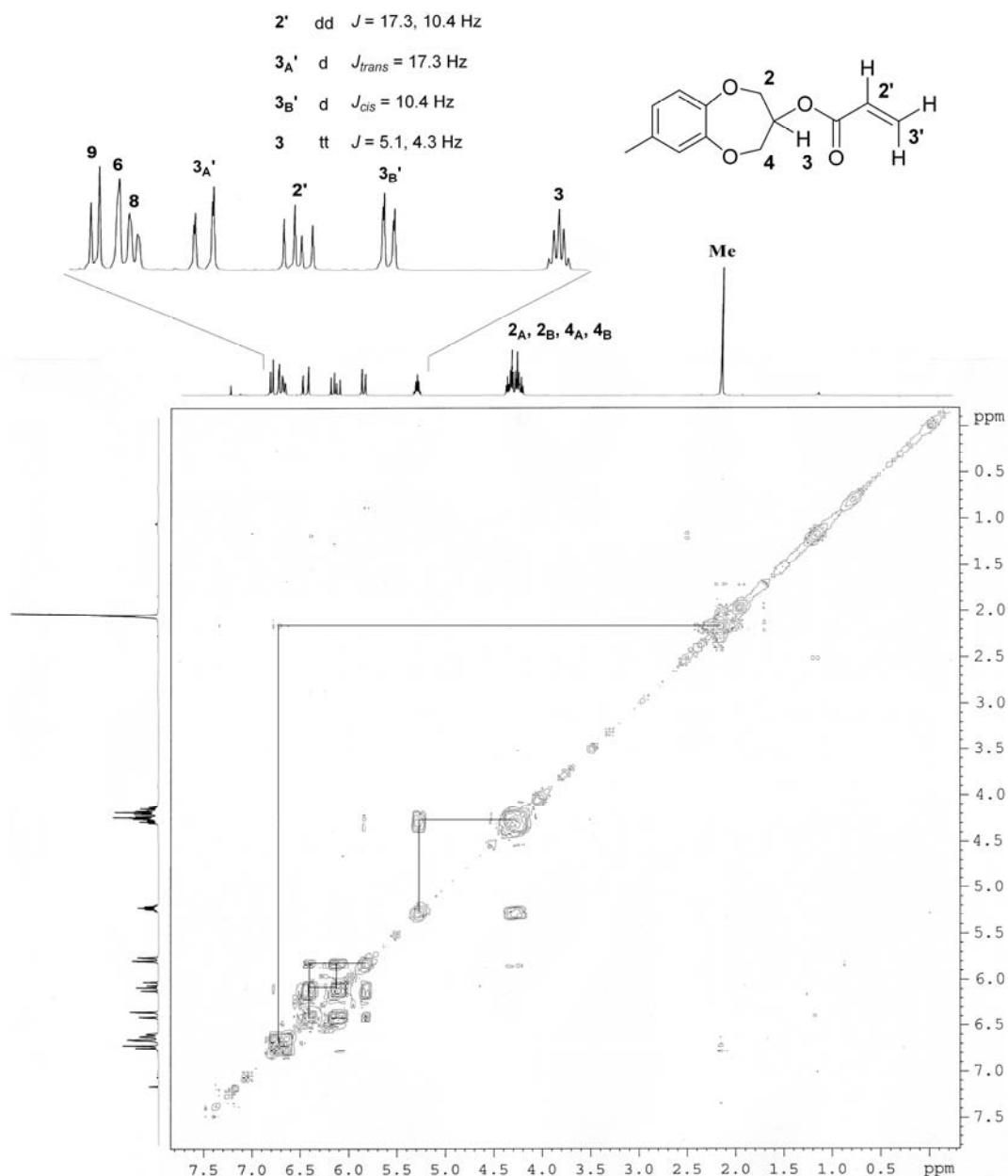
Figure 4.13 ^{1}H,^{1}H COSY spectrum of **73**

Coupling to the C-5a and C-9a quaternary aromatic carbons in HMBC data verified C-2, C-3 and C–4 proton shifts for **23-29** (Figure 4.15). The C-2' and C-3' [13]C shifts for compound **73** were confirmed by DEPT 135 at 127.8 ppm and 133.2 ppm respectively. These signals correlate to the olefinic (C-2') double doublet (10.4 Hz *cis*, 17.3 Hz *trans*) at 6.18 ppm and C-3a' (17.3 Hz *trans*/C-3b' (10.4 Hz *cis*) doublets at 6.49 and 5.90 ppm in ^{1}H analysis with confirmed COSY coupling at 5.85/6.14 ppm and 6.11/6.43 ppm. See Appendices 21, 22 and 23 for supplementary NMR data of **73** and corresponding spectral data for **71** and **72**.
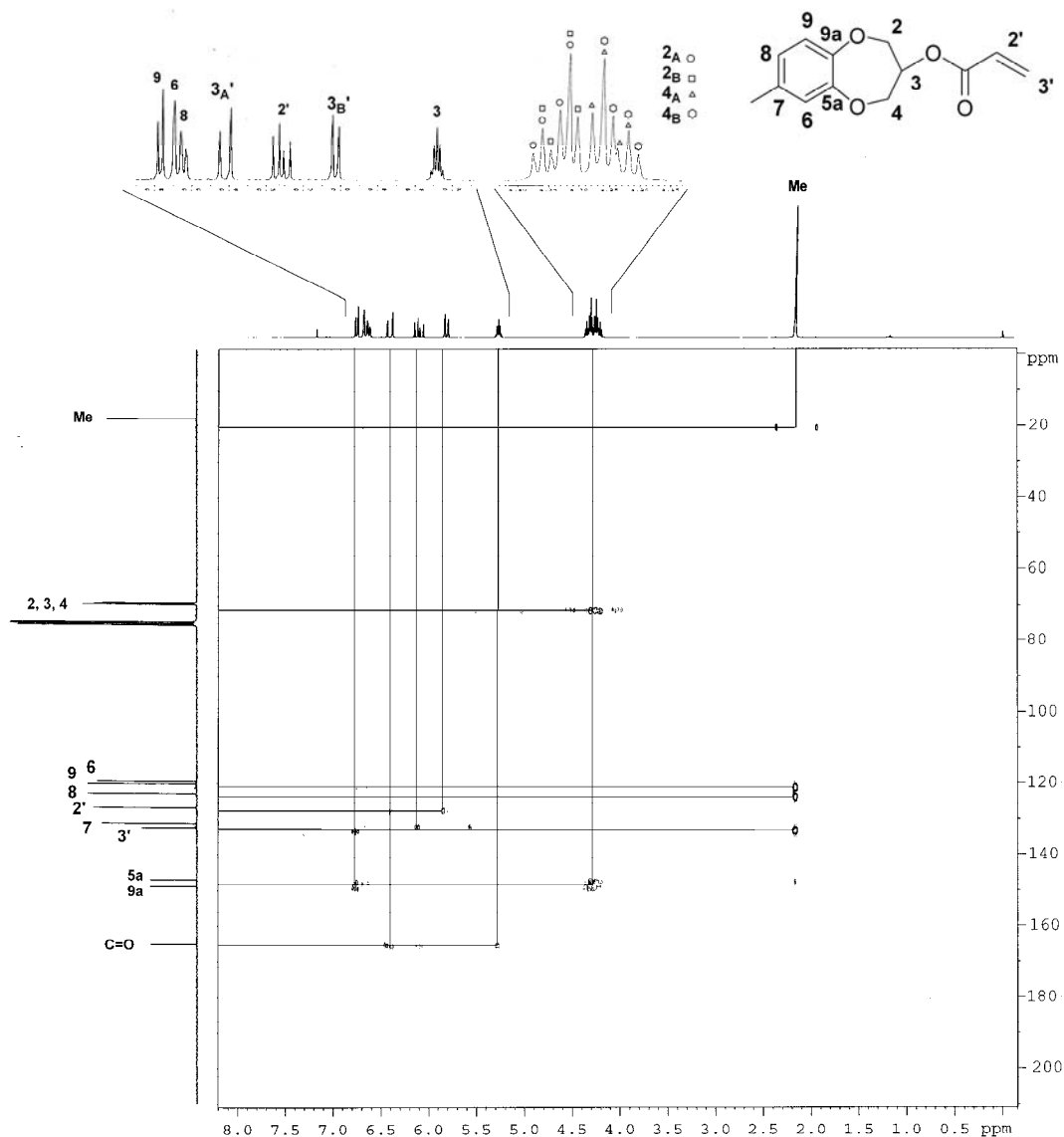
Figure 4.14 ^{1}H,^{13}C HMBC of **73**

Introduction of substitution at C-3, exemplified by compound **73**, mirrors the observations by Archer and Claret where the adjacent protons collapse to an indistinguishable multiplet. Our NMR data complies with that of Archer and Claret [18] whereby in solution at ambient temperature the benzodioxepinone exhibits clean ^{1}H splitting, eluding to a fixed chair conformation of the cycloheptyl region.

4.2.7   3,4-Dihydro-7-methyl-2H-1,5-benzodioxepin-3-amine (74)

Amines are typically potently odourous however odour becomes increasingly weak and indiscriminate as molecular size increases. Formation of a secondary amine would have

provided additional valuable olfactory information. Reductive amination of **65** using 2.0M methylamine in MeOH was attempted at room temperature with NaBH$_4$ and sodium cyanoborohydride as reducing agent, however did not provide any aminated product, and the intermediate imine is usually too unstable to be seen. The Leuckart reaction with formamide, formic acid as reductant and ammonium formate at high temperatures (180°C) also failed to aminate **1** to any significant degree [9].

Efforts to synthesise the primary amine, **74**, were attempted by reduction of **65** included Zn in AcOH [19], NaBH$_4$ in organic and aqueous media including acetic acid (AcOH) [20], lithium aluminium hydride (LiAlH$_4$) [21], Na in EtOH [22], and enantioselective reduction with Baker's yeast [23]; the oxime proving unreactive to all. Addition of lithium chloride (LiCl) to NaBH$_4$/Amberlyst-15(H$^+$) as a hydrophilic scavenger led to hydrolysis of the oxime to regenerate the ketone, **1**. The NaBH$_4$/titanium (IV) chloride (TiCl$_4$) system, proposed by Kano and colleagues [24] presented the most proficient results with dimethoxyethane (DME) as solvent (Scheme 4.8).
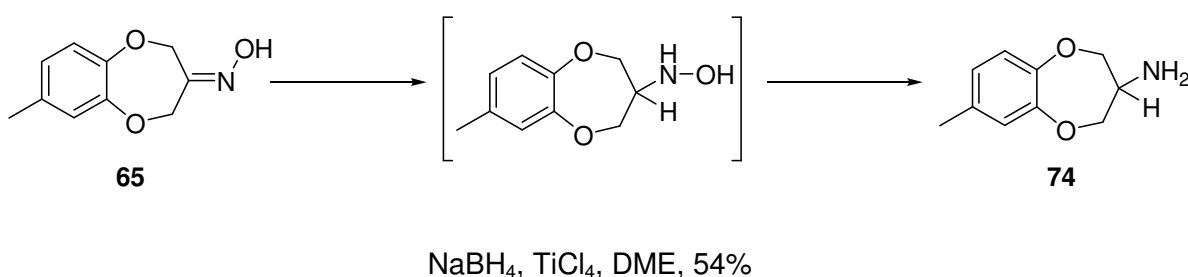
NaBH$_4$, TiCl$_4$, DME, 54%
Scheme 4.8 Preparation of **74**

Borohydride activated TiCl$_4$ through chloride displacement exhibited a characteristic blue-violet colour indicative of formation of the reducing agent complex. Subsequent exposure to **65** affected clean reduction to the amine product **74** as indicated by molecular ion (179.10 m/z) in GC-MS analysis (Figure 4.15) and required HPLC separation for olfactory purity and characterisation.
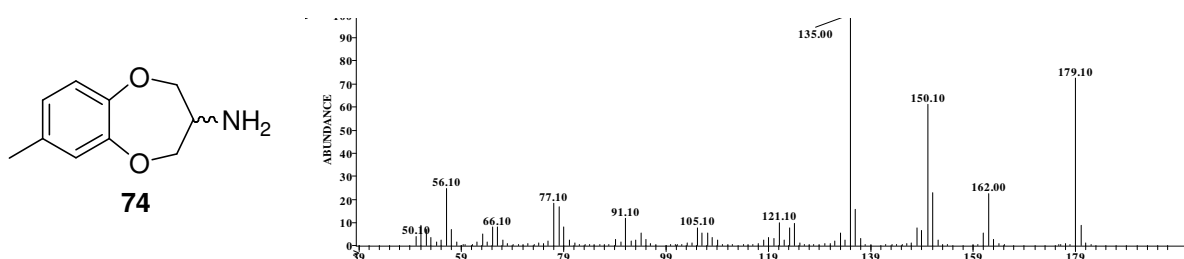
Figure 4.15 EI mass spectrum of **74**

140

Trials in 1,4-dioxane were completely unsuccessful and the reducing complex mixture produced a non-homogenous yellow solid that was inert to reaction with **65**. Reduction of the oxime proceeded via the N-hydroxyl intermediate, as suggested by the appearance of a molecular ion (194.15 m/z) in GC-MS analysis as ^{1}H shift differences between **74** and the N-hydroxyl intermediate were indistinguishable. The quadrupole mass spectrum revealed a base peak of 135.00 m/z (Δm 43), characteristic from ring opening of alicyclic amines, representing a $[M-CH_2NH=CH_2]^+$ fragment ion.

^{13}C spectral analysis supported the GC-MS results, as conversion of the oxime to the amine was confirmed by downfield shifts of the C-2, C-4 signals at 74.1 ppm and 74.0 ppm, exemplified by the conversion of the quaternary C-3 (157.3 ppm) of the oxime to a methine (50.7 ppm), indicative of reduction of the C=N component. Confirmation of complete reduction to the amine was confirmed by the slightly higher frequencies obtained for C-2 and C-4 than those expected for the intermediate and the lower resonance from the C-3 of the amine, as presence of the electronegative hydroxyl group shifts the C-3 signal more downfield. As the broad singlet from the amine protons at 4.1 ppm exhibits overlapping resonance with C-2, C-3 and C-4 proton signals, a COSY and HMQC (Figure 4.16) were required to verify the coupling, which resembled that of **64**. An integral of 3.8 denotes the 4 protons of C-2 and C-4 methylene groups. Despite no recognition of the C-3 proton in the ^{1}H spectrum, HMQC analysis verified the C-3 carbon at 50.7 ppm and proton at 4.1ppm, disproving any de-protonation or conversion to an imine. The broadness of the peak, typical for amines, evidently prevents accurate integration to reveal inclusion of the amine protons. The slightly low C-2, -3 and-4 carbon shifts indicate the amine may have protonated to the ammonium ion in the slightly acidic deuterated solvent (CDCl$_3$). HRESI analysis verified full conversion to the primary amine ($[M + H]^{+\bullet}$; calculated: 180.1024, found: 180.1017). Additional NMR data is supplied in Appendix 24.
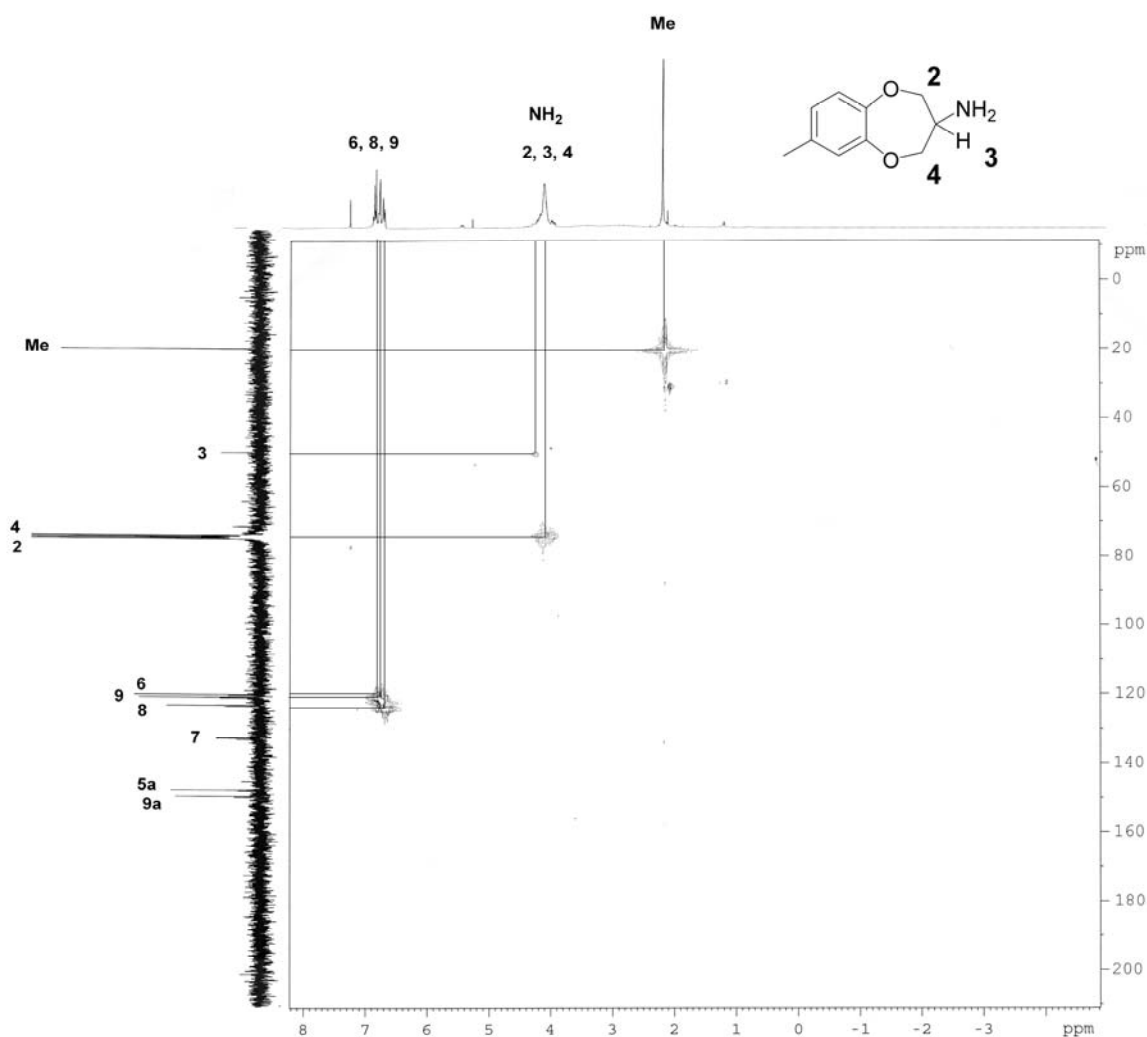
Figure 4.16 ^{1}H,^{13}C HMQC of **74**

4.3 Synthetic Attempts Towards Various Benzodioxepines

4.3.1 Synthetic Approach to 2,5-Dihydro-8-methyl-1,6-benzodioxocine (77)

One of our primary synthetic aims for contribution to the olfactory data set was the alteration of the aliphatic ring portion. Bearing in mind that reactivity and affinity of an odourant can be increased by introduction of an olefinic moiety, our initial trials aimed for the unsaturated 8-membered ring, accessible via ring closing olefin metathesis (RCM) using the ruthenium based "1,3-bis-(2,4,6-trimethylphenyl)-2-imidazolidinylidene) dichloro(phenylmethylene)-tricyclohexylphosphine)ruthenium" ($RuCl_2$(=CHPh)$(PCy_3)_2$) developed by Fu et al. [25] as shown in Scheme 4.9.
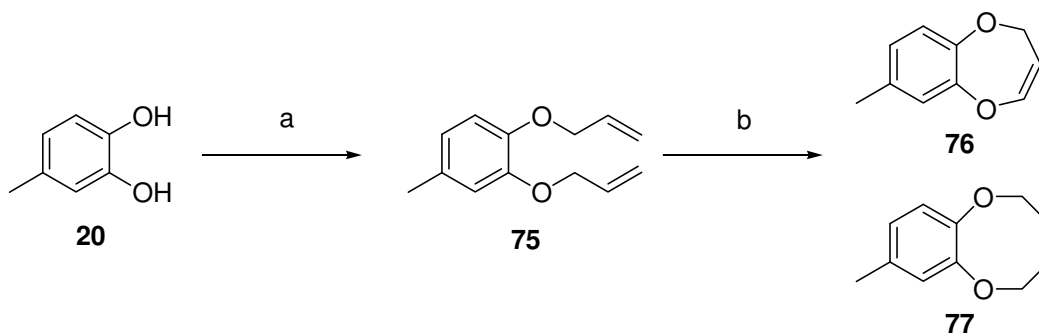
a) BrCH2CH=CH2, K2CO3, DMF, 80°C, 2 hr, 99%; b) RuCl2(=CHPh)(PCy3)2, benzene, 50°C, 2 hr, 83%

Scheme 4.9 Allylation and ring closing metathesis for the preparation of **77**

Preparation of the diallyl ether (**75**) was achieved under Williamson etherification conditions using a 3 mole excess of allyl bromide in the dipolar aprotic solvent N,N-dimethylformamide (DMF) in the presence of potassium carbonate (K_2CO_3). 1,2-Bis(allyloxy)-4-methylbenzene (**75**) was obtained in 99% purity and 87% isolated yield as confirmed by a molecular ion in GC-MS analysis (Figure 4.17). Excess allyl bromide was removed by stirring with triethylamine (TEA) encouraging formation of the insoluble quaternary ammonium bromide salt followed by filtration. The structure of **75** was verified by ^{1}H and ^{13}C NMR (see Appendix 25).
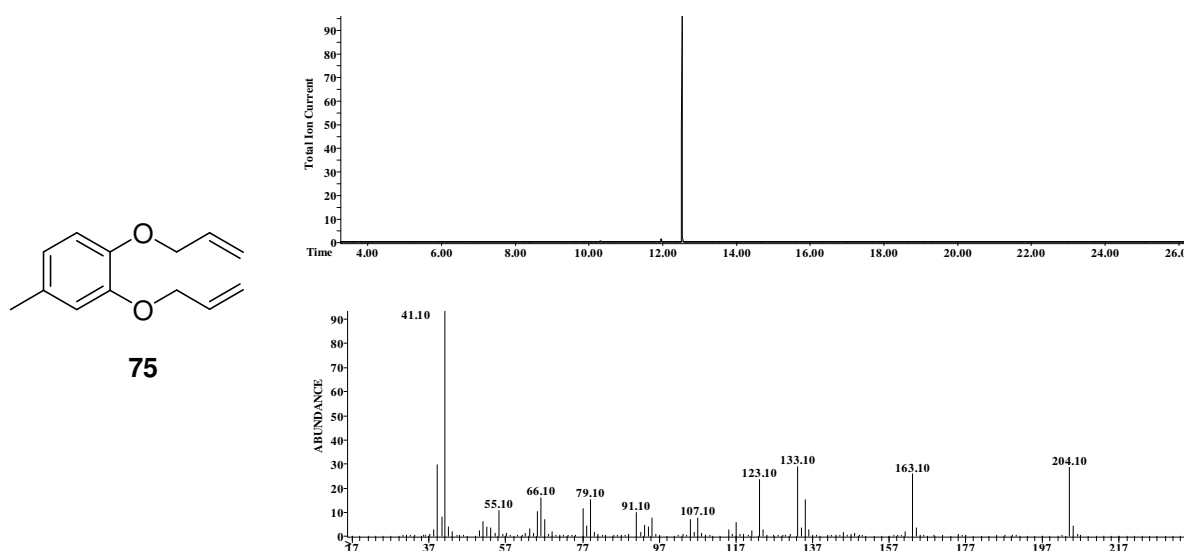
Figure 4.17 GC-MS of 1,2-Bis(allyloxy)-4-methylbenzene (**75**)

A mixture of olefinic cyclic structures was invariably obtained as presented in Scheme 4.9. Subsequent RCM [26] produced the 2,5-dihydro-8-methyl-1,6-benzodioxocine (**77**) in 83% purity (t_R = 176.10 min), with return of 18% **20** (t_R = 204.10 min) (Figure 4.18).
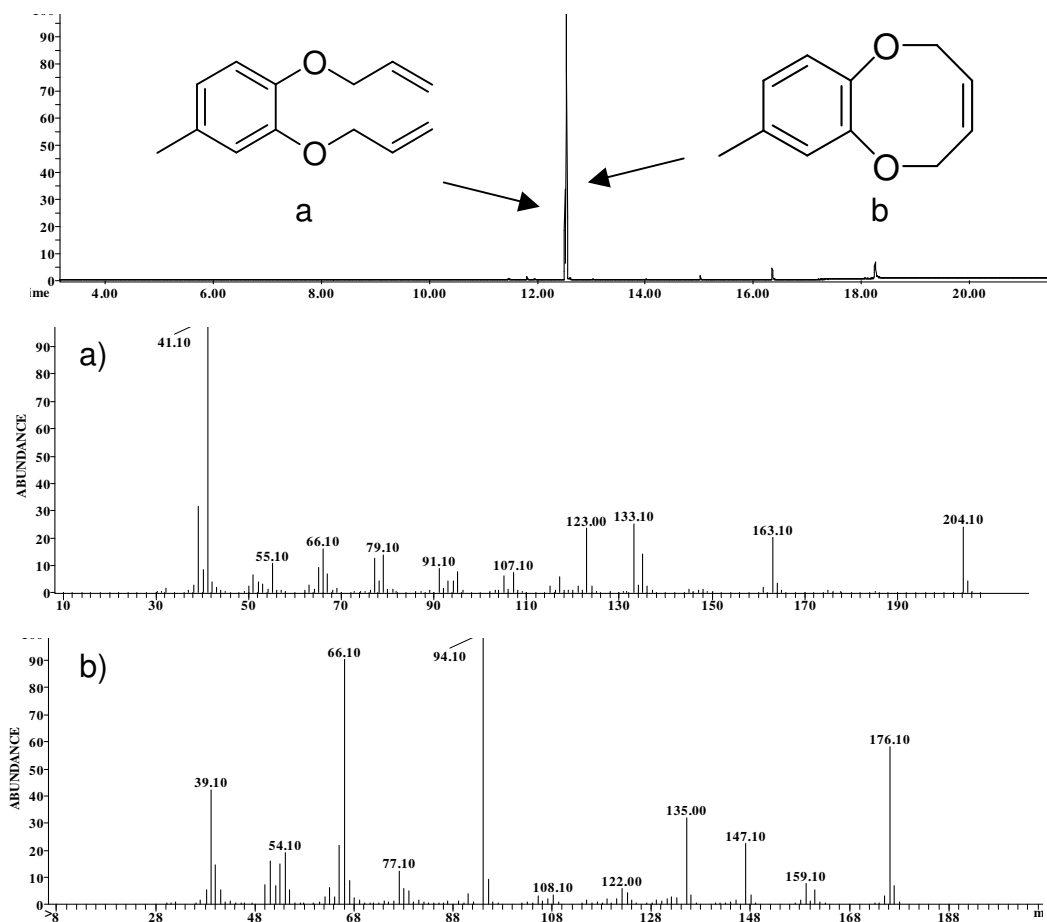
Figure 4.18 GC-MS of **77** co-eluting with **75**

Removal of residual ruthenium catalyst using tris(hydroxymethyl) phosphine with TEA in DCM reported by Maynard and Grubbs [27] did not prove as effective as elution with pentane through a short silica column. Neither dioxepine nor dioxecine were able to be isolated at purity suitable for olfactory analysis. Detectable odour from the crude product mixture was surprisingly weak.

4.3.2 Experimental Approach Towards 2*H*-[1,4]Dioxepino[2,3-*b*] pyridin-3(4*H*)-one

Synthesis of 2*H*-[1,4]dioxepin[2,3-b]pyridin-3(4*H*)-one **81**, with a pyridine ring in place of the aromatic benzene seemed innovative (Scheme 4.10). The benzodioxepinone synthesis procedure was applied to prepare the heterocyclic pyridinone **81**. As with analogues **23**-**29**, the conditions employed by Beereboom [28] offered the most direct route. Serendipitous success with di-allylation of dihydroxy pyridine with allyl bromide provided additional support for application of the patented literature methods.
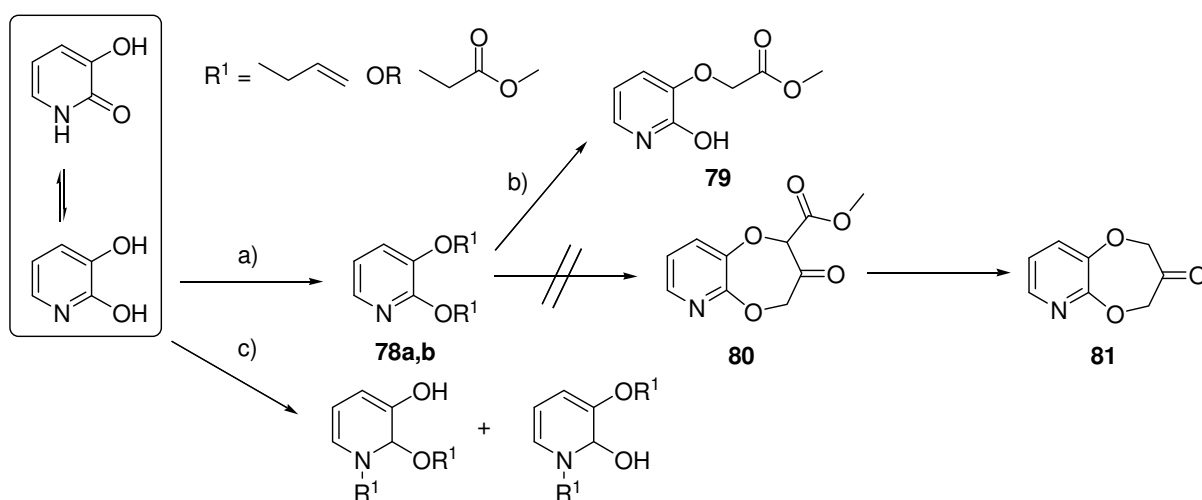
a) BrCH$_2$CH=CH$_2$ or BrCH$_2$CO$_2$Me, NaH, DMF, 0-25°C, 2 hr; b) NaH, DMF; c) BrCH$_2$CH=CH$_2$ or BrCH$_2$CO$_2$Me, K$_2$CO$_3$, DMF, 90°C, 2 hr

Scheme 4.10 Synthetic proposal for formation of 2*H*-[1,4]Dioxepin[2,3-b]pyridin-3(4*H*)-one, **81**

Initial Williamson reaction conditions applied to 2,3-dihydroxy pyridine resulted in a high degree of pyridine-nitrogen alkylation, as identified by the molecular ion in GC-MS (255 *m/z*) corresponding to a broad peak at t$_R$ = 19.10 min. Two peaks were detectable in the GC trace from K$_2$CO$_3$ de-protonation (step c), both with a molecular ion of 255.00 *m/z* (14.17 min and 15.28 min) in a ratio of 8% and 92%. This was strongly representative of regioisomers formed from mono-etherification of one aromatic hydroxy with N-alkylation of the pyridine nitrogen (Scheme 4.10; pathway *c*) rather than di-hydroxy etherification (pathway *a*), as the latter would appear as a single peak. An ideal success rate was achieved by di-allylation with allyl bromide in the presence of NaH formed 2,3-bis(allyloxy)

pyridine (**78a**) in 98% purity (t_R = 14.37 min). Chemo selectivity for alkylation of the pyridine hydroxyl groups using NaH was supported by the presence of a single peak in the GC TIC (t_R = 19.12 min). A follow on attempt with methyl bromoacetate resulted in the di-etherified target (**78b**) (Figure 4.19) in good yield (79%), confirmed by a single corresponding peak in the GC TIC with the correct molecular ion (255.00 *m/z*).
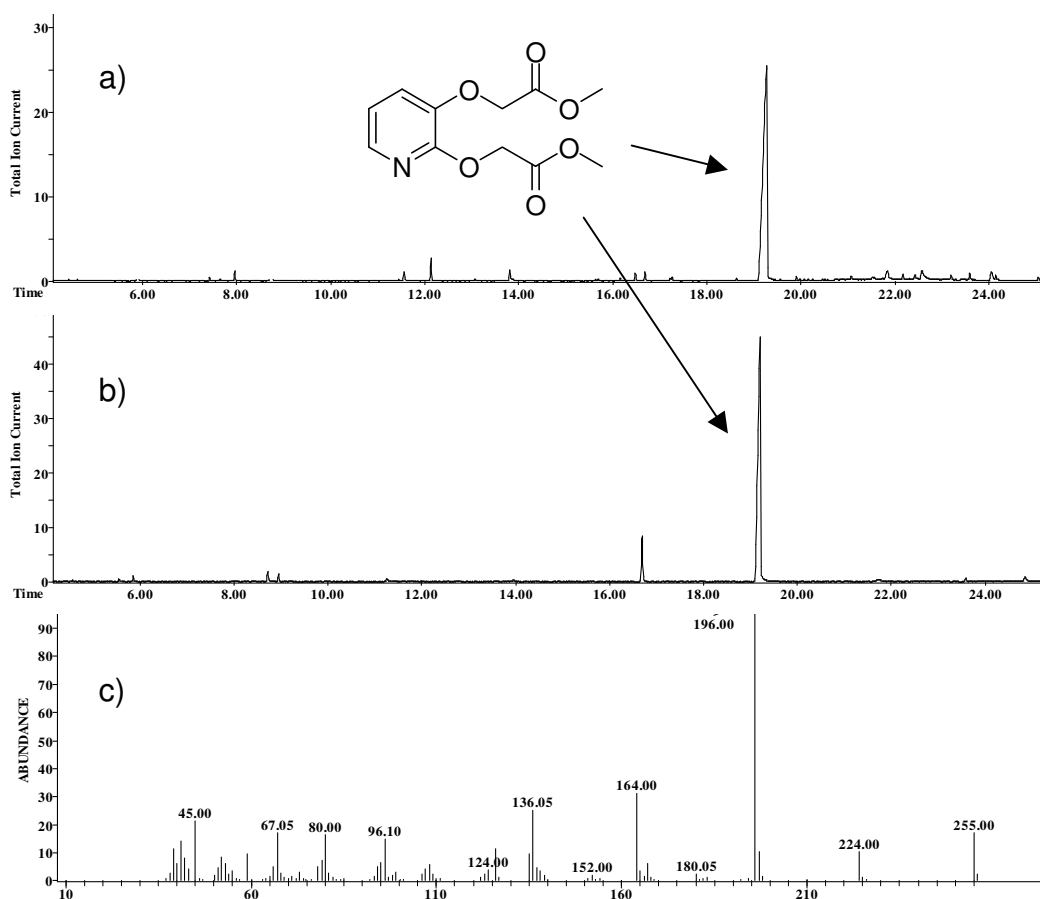
Figure 4.19 GC-MS from di-etherification of *ortho*-dihydroxy pyridine; $BrCH_2CO_2Me$, DMF, 90°C, 2 hr: a) NaH; b) K_2CO_3; c) mass spectrum of peak at 19.17 min

Cyclisation led to cleavage of the acetate chains resulting in mono-ether products shown in Figure 4.20 at t_R = 11.24 and 11.46 min, replicating the results obtained from the same synthetic strategy with EWG catechols. The pyridine ring leads to stabilisation by de-localisation of charge identical to the nature of an EWG. As this synthesis was undertaken prior to evaluation of the results presented in Section 2.3 the cleavage in the presence of KO^tBu was unexpected.
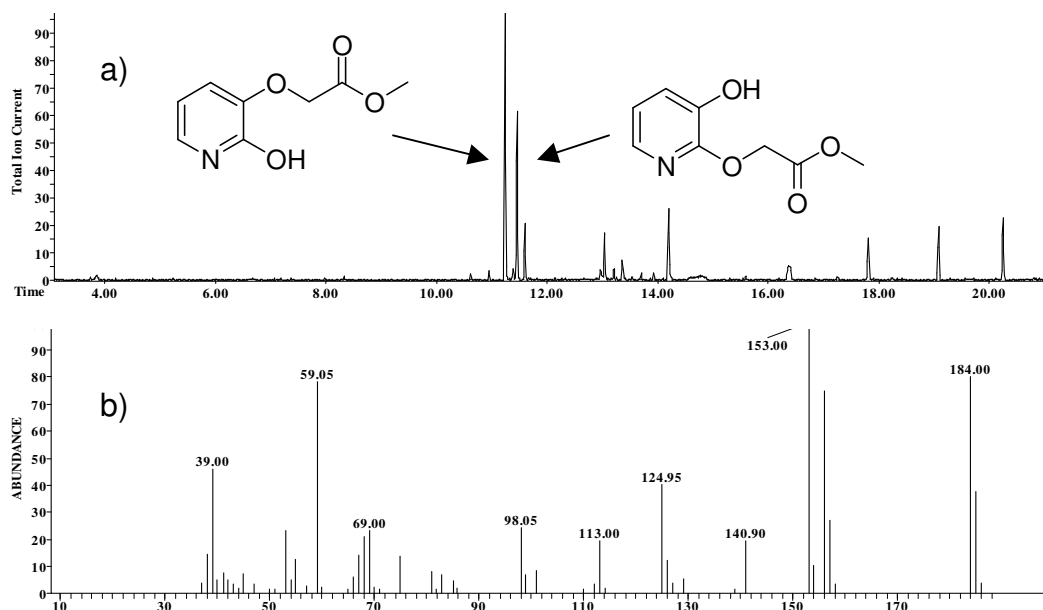
Figure 4.20 a) GC of cleavage by-products, Methyl 2-[(2/3-hydroxy-2/3-pyridinyl)oxy] acetate (**79**), formed in the presence of KO^{t}Bu/THF; b) mass spectrum of the peaks at t_R = 11.24, 11.46 min

4.3.3   Experimental Approach Towards Preparation of 7-Methyl-2*H*-1,5-benzodithiepin-3(4*H*)-one

Additional studies focused on the semi-polar heterocyclic region of the benzodioxepinone structure.   The prevalent odour-activity of sulphur-containing compounds in general prompted a trial derivatisation of the ketone by oxygen displacement with sulphur using Lawesson's reagent [29].   Lawesson's reagent, [2,4-bis(4-methoxyphenyl)-1,3-dithia-2,4-diphosphetane-2,4-disulphide], readily converted the carbonyl of **1** to a thione upon heating (120°C) in toluene. Isolation of the monomeric thioketone prior to oligomerisation proved challenging; at higher temperatures (90°C) conversion and trimerisation occurred simultaneously and lower temperatures (50°C) were not conducive for product formation (Scheme 4.11). GC-MS monitoring at 15 min intervals indicated the major product upon standing had a molecular ion corresponding to a thioacetal trimer, trithiane.

49 %

40 %   11 %

LR, toluene, 50-120°C, 2-12 hr
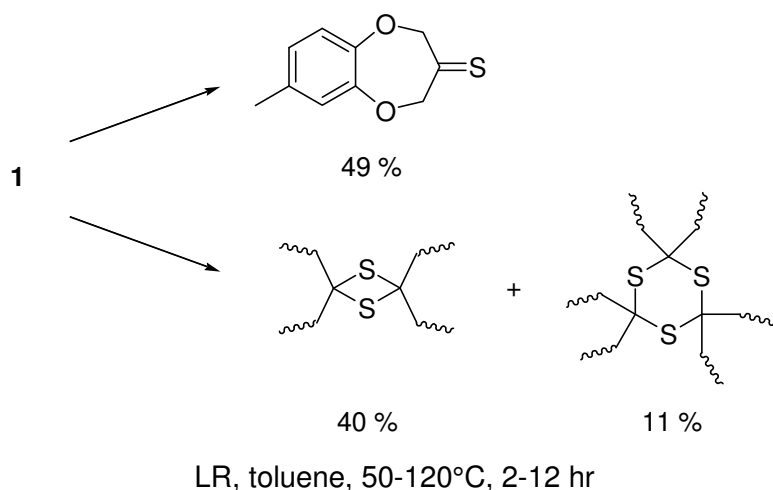
Scheme 4.11 Application of Lawesson's reagent (LR) to **1**

Thiophenol and 1,2-dithiophenol can be expected to behave similarly to their oxygen counterparts (refer to Section 2.1, Figure 2.2) as reflected by pKa values (Figure 4.21), and were intended for direct substitution into the Dieckmann cyclisation pathway. Considering the unique properties of catechols, the same chemistry could evidently not be applied to a catechol as is effective on a phenol. For this reason trials for formation of 1,2-dithiophenol did not replicate the promising results obtained for thiophenol.

pKa (at 25°C):	6.61	9.50	9.97
m.p.(°C):	40-42	103-105	27-32
polar surface area (Å^2):	38.8	77.6	77.6

Figure 4.21 Chemical properties of thiol, dithiol and *meta*-methyl dithiol benzene; note comparison with Figure 2.2

Initial attempts at oxygen-to-sulphur heteroatom interconversion were modelled by the formation of ethyl phenyl sulphide (EtSPh) with sodium ethanethiol (NaEtSH) as shown in Scheme 4.12 below.
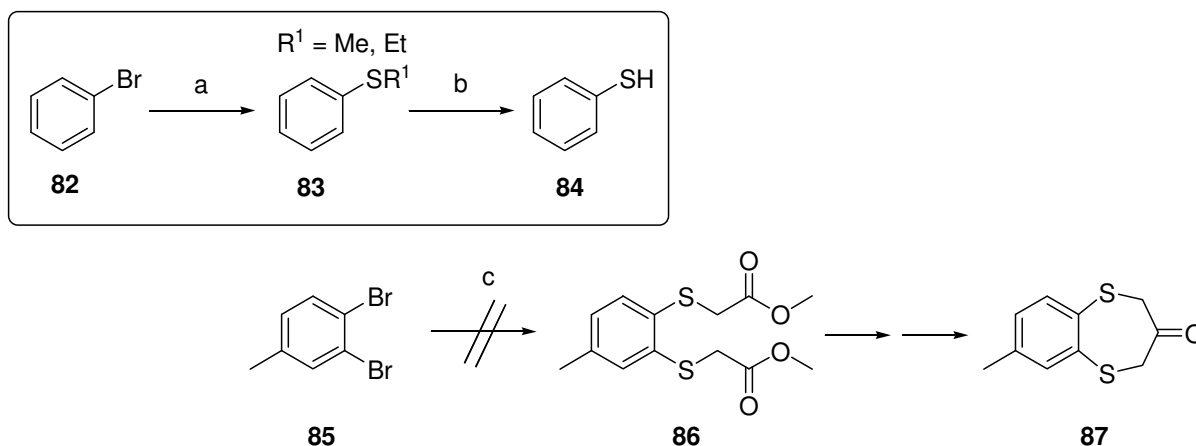
Scheme 4.12 a) Me$_2$S$_2$, Cu, DMA; NaSEt, DMF or DMA; b) Na, NH$_3$, -70°C, 1 hr; c) n-BuLi, S$_8$, BrCH$_2$CO$_2$Me, THF, -78°C-r.t., 4 hr

In situ generation of sodium ethanethiolate from EtSH and NaH was achieved in both DMF and N,N-dimethylacetamide (DMA) [30], which successfully converted bromobenzene to ethyl phenyl sulphide (Figure 4.22) in favourable yield (84%), with a small amount of thiol (3%) in agreement with Testaferri et al. [31].
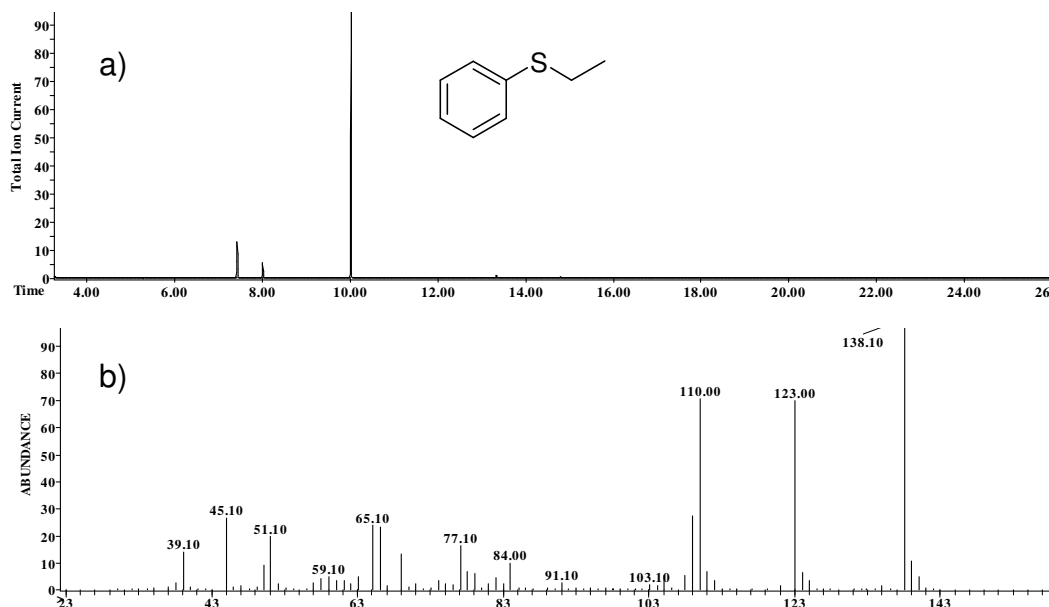
Figure 4.22 a) Preparation of ethyl phenyl sulphide (**83**) with sodium ethanethiolate; b) mass spectrum of peak at 10.01 min

Formation of impurities was encouraged in DMA where only a small degree of reduction to the thiol occurred which was not found to be reproducible. In the GC-MS shown in Figure 4.23 a 55% yield of thiol was obtained at t_R 7.59 min.
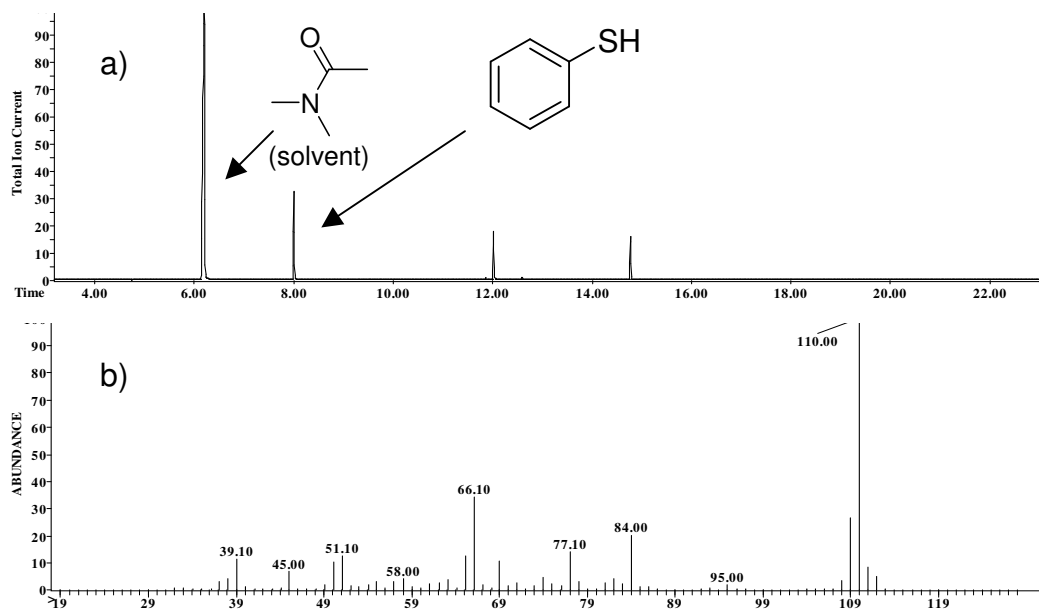
Figure 4.23 a) *In situ* reduction to thiophenol (84) in the presence of sodium ethanethiolate; b) mass spectrum of peak at 8.00 min

Reduction of ethyl phenyl sulphide to thiophenol using Na in liquid ammonia (NH_3) gave a complex product mixture with only moderate conversion to the reduced product [32].

A thiomethylation reaction on bromobenzene using copper metal and dimethyl disulphide (Me_2S_2) as proposed by Campbell [33] failed to provide a reactive environment despite long reaction times. A similarly unsuccessful trial involved conversion of bromobenzene to thiophenol using thiourea in both H_2O and DMSO as used by Pan and Fletcher [34].

A one-pot S_N2 sulphonation based on methodology by Ham et al. [35] was investigated, involving the addition of sulphur powder to a lithiated benzene species. Di-alkylation of the lithiated intermediate of 1,2-dibromo-4-methyl benzene is followed by addition of sulphur powder and methyl bromoacetate. No benzo sulphanyl acetate was detected in GC-MS analysis with EIC detection (300 m/z)(Figure 4.24). The major compounds invariably formed isomers at 340 m/z and 430 m/z, both with isotopic patterns typical of the presence of two bromines.
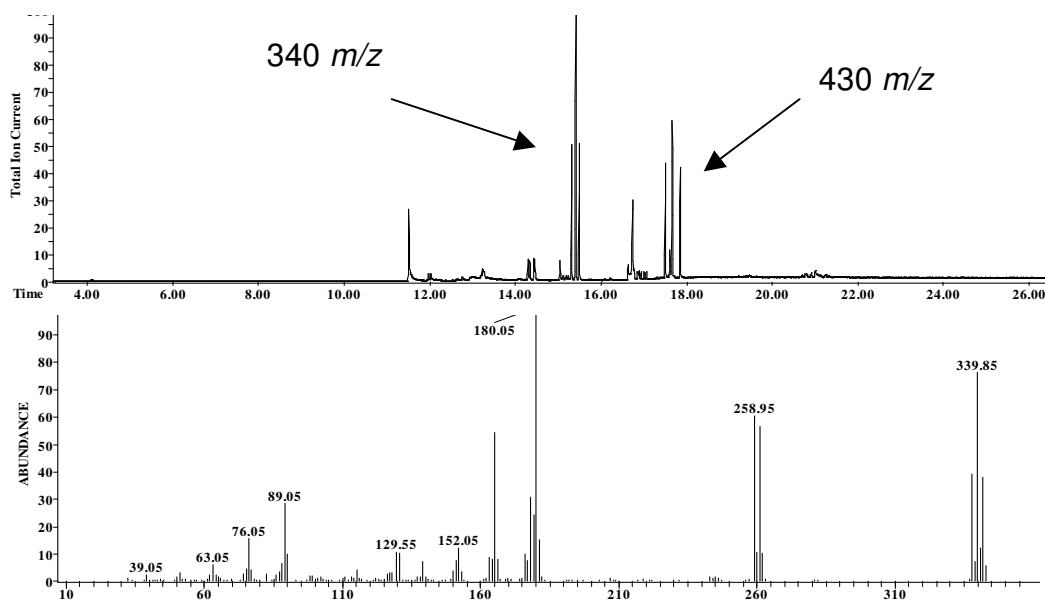
Figure 4.24 Di-thioetherification attempt to form **86** with n-BuLi, S_8 and $BrCH_2CO_2Me$

4.3.4   Experimental Approach Towards Preparation of 7-Methylhexahydro-2*H*-1,5-benzodioxepin-3(4*H*)-one

Preliminary steps towards the preparation of a dioxepinone analogue with a saturated analogue were achieved. Rather than de-aromatisation of **1**, which may readily result in a mixture of isomeric olefins, a synthesis was devised that applies the methodology illustrated in Section 3.2 to a cyclohexanediol as shown in Scheme 4.13. It was thought that an asymmetric analogue would be interesting for conformational comparisons to Calone 1951®. This methodology was not pursued with the intent to create an analogous range to that achieved with various substituted catechols in Chapters 2 and 3. Time constraints led to abandonment of this synthetic protocol.
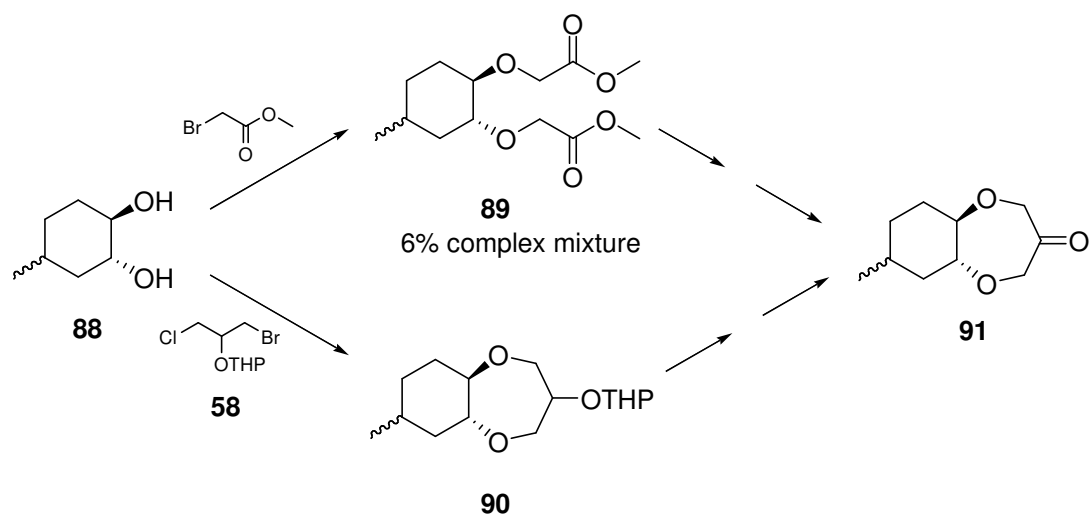
Scheme 4.13 Synthetic proposal for preparation of a cyclohexane dioxepinone analogue, 7-Methylhexahydro-2*H*-1,5-benzodioxepin-3(4*H*)-one, **91**

Synthesis of disuccinoyl peroxide (see Appendix 26 for the GC-MS) was based on a procedure proposed by Wilkins [36]. This procedure was chosen for its selectivity for *trans*-dihydroxy diols, in conjunction, availability of reagents and time constraints motivated selection of this synthesis over others in literature that may have been applied. The formation of an intermediate epoxide with subsequent asymmetric ring opening to form the diol was also drawn from this procedure (Scheme 4.14).
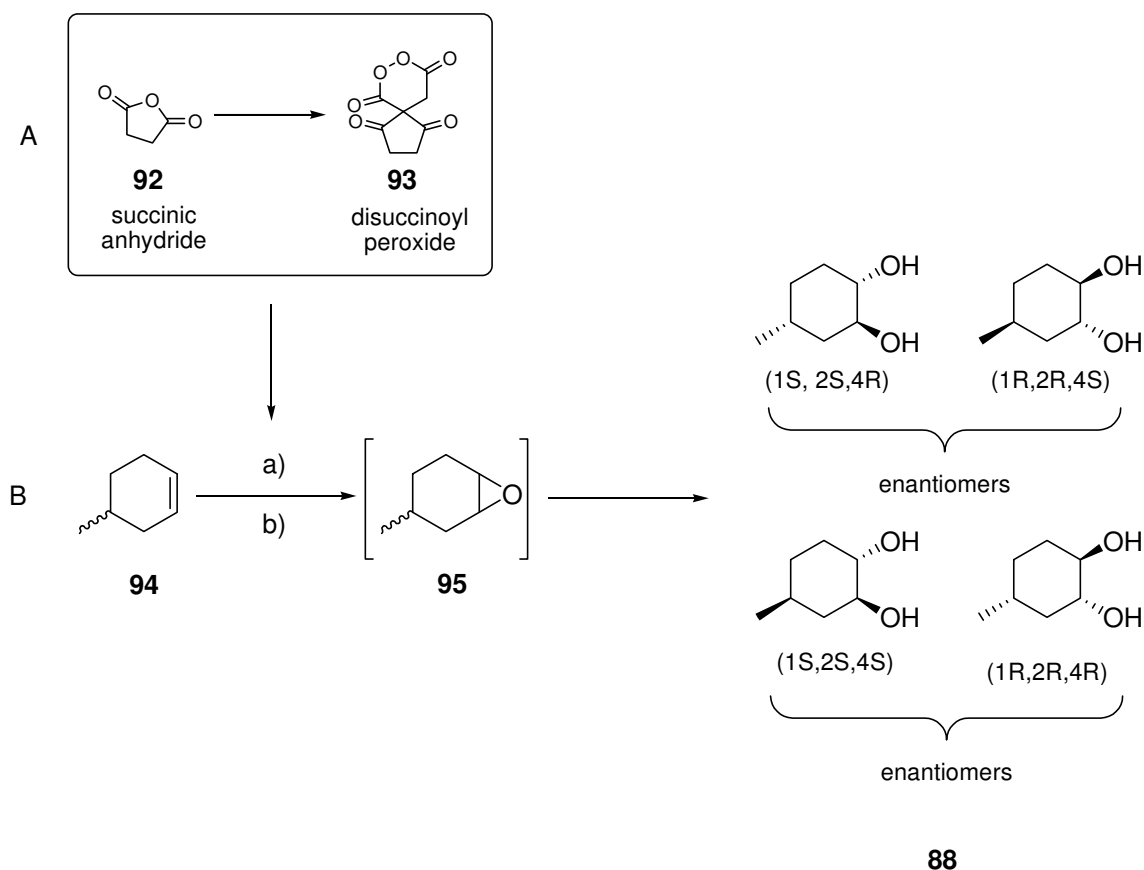
A: H₂O₂; B: a) 93, non-ionic surfactant, H₂O, temp, 22-24 hr, 50°C OR m-CPBA, KOH, DCM, 5 day, r.t.

Scheme 4.14 A: Preparation of disuccinoyl peroxide from succinic anhydride; B: Synthesis of 4-Methyl-1,2-cyclohexanediol (**88**)

The hydrolysis of methyl cyclohexene required 12-24 hr in H_2O. GC-MS monitoring revealed that the 2 hr reaction time suggested by Wilkins allowed only minor conversion to 4-methyl-1,2-cyclohexanediol, **88**. Formation of the diol, **88**, from the cyclohexene was also achieved with *m*-chloroperbenzoic acid [37] as shown in Scheme 4.14.

Trials for ring opening included H_2O, base and acid hydrolysis, the last resulting in ring opening by the halide counter-ion. The epoxide ring opening is selective for the *trans* diastereomer, however a diastereomeric excess measurement of **88** was not obtained. The epoxide intermediate and diol product were confirmed by GC-MS molecular ion (Figure 4.25), and the diol was characterized by ¹H and ¹³C NMR (Figure 4.26).
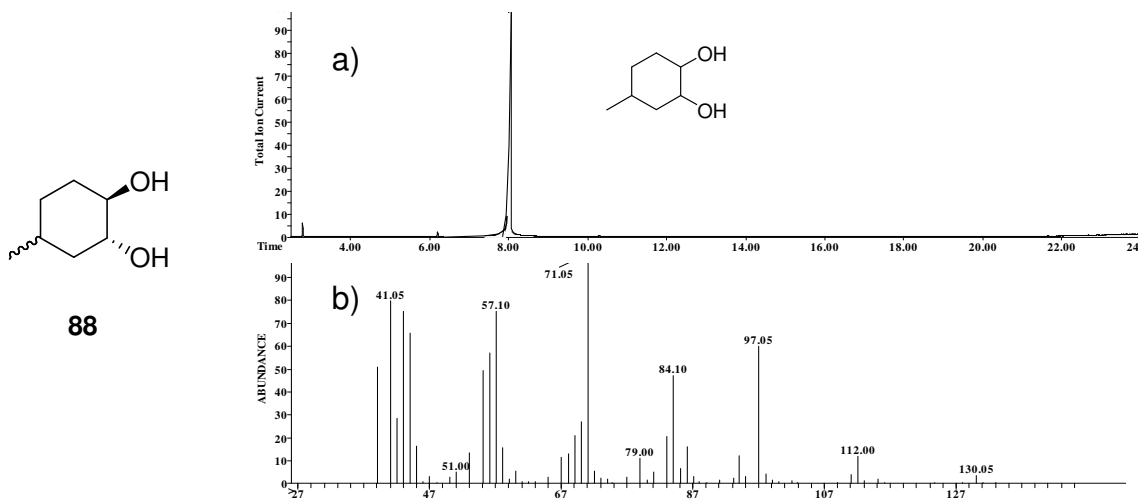
Figure 4.25 a) GC of **88**; b) mass spectrum of **88** at t_R = 7.97 min

The ^{1}H NMR spectrum presented in Figure 4.26 is representative of the cyclohexane diol with its three asymmetric centres. Allocation of splitting patterns with coupling constants was not possible from the ^{1}H due to the extent of splitting from the overlapping diastereomeric signals.
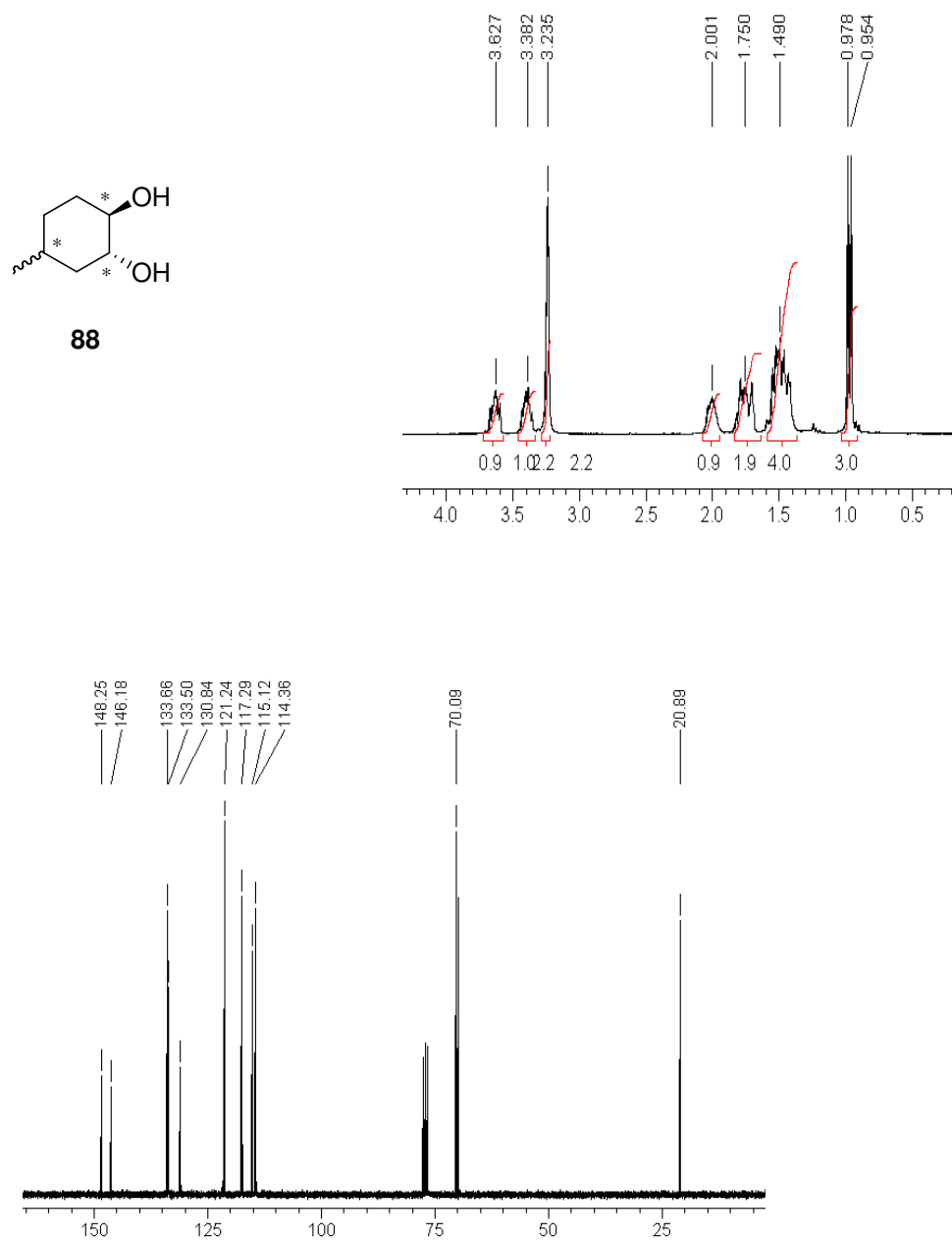
Figure 4.26 [superscript]1H and [superscript]13C NMR spectra of **88**

Alkylation with methyl bromoacetate under the same reaction conditions as that utilised for Scheme 2.1, *step a*, encouraged decomposition of the reagents and formation of by-products. Extracted ion monitoring of the GC TIC confirmed presence of a molecular ion that matched the molecular weight of the di-etherified target (273 *m/z*) (Figure 4.27). The small degree of conversion may be explained by the lack of acidity of the aliphatic diol, particularly in comparison with the acidic character of corresponding phenol or catechol hydroxyl groups.

155
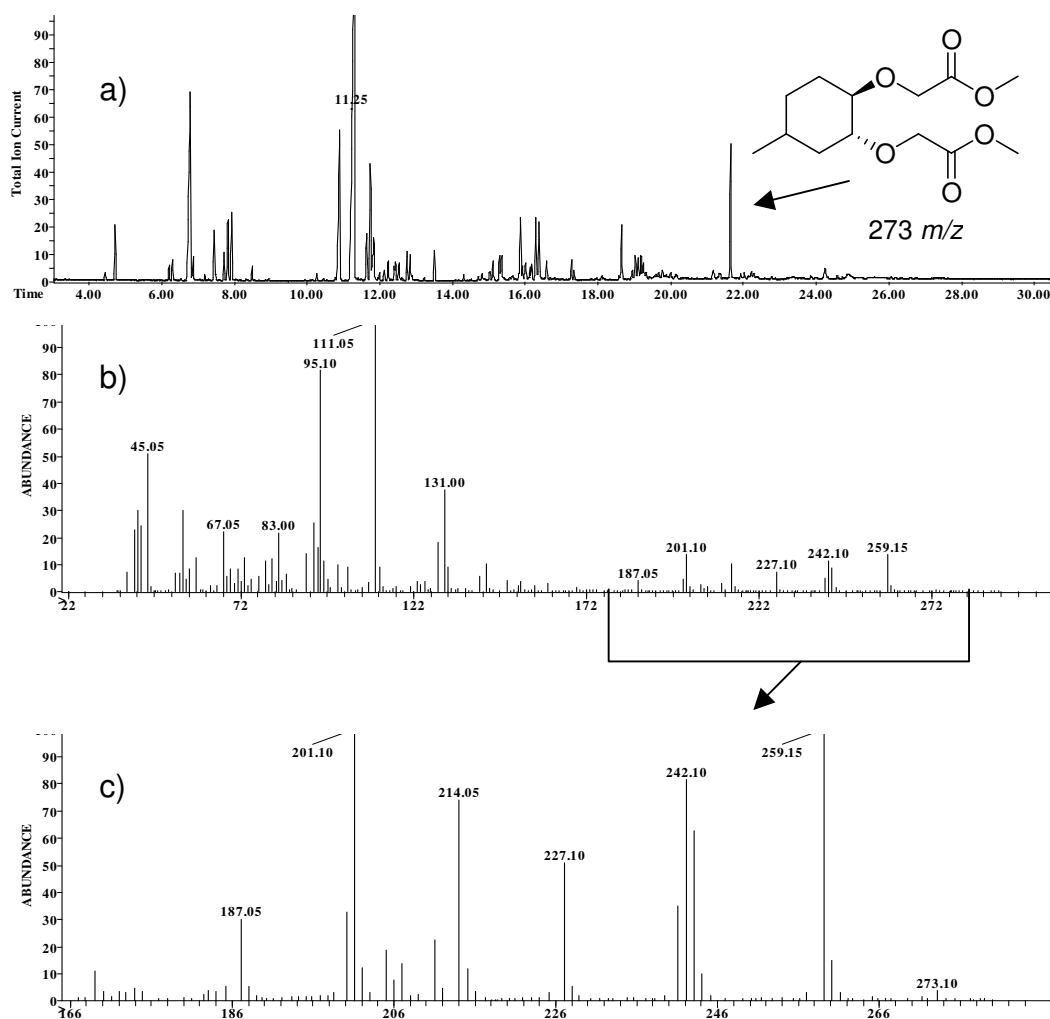
Figure 4.27 a) GC TIC of the product mixture from di-etherification of **88**; b) mass spectrum of peak at 21.66 min; c) expanded mass spectral region

4.3.5 Experimental Approach Towards 8-Methyl-5*H*-1,4-benzodioxepin-3(2*H*)-one: Preparation of Crude Material

Formation of a lactone using the synthetic protocol presented in Scheme 4.15 was successful, however purification of the target to comply with olfactory analysis standards was not achieved.
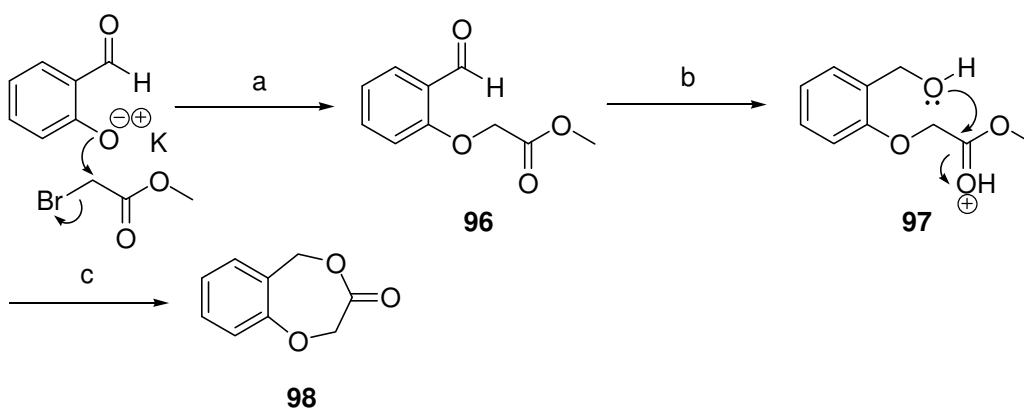
Scheme 4.15 a) BrCH$_2$CO$_2$Me, K$_2$CO$_3$, DMF, 80°C, 2 hr; b) NaBH$_4$, 1:4 MeOH/H$_2$O, 0°C-r.t., 3 hr; c) 2M HCl, 90°C, 2 hr

Mono-etherification of salicylaldehyde with Williamson conditions favourably formed methyl 2-(2-formylphenoxy)acetate (**96**) as a beige solid (m.p. 48-50°C) in 86% yield. Positive identification of the molecular ion was achieved with GC-MS (194.00 m/z) (Figure 4.28), and the structure was verified by ^{1}H and ^{13}C NMR (Figure 4.29). Preservation of the formyl group was evident from the proton signal at 10.48 ppm and a carbon signal at 180.43 ppm.
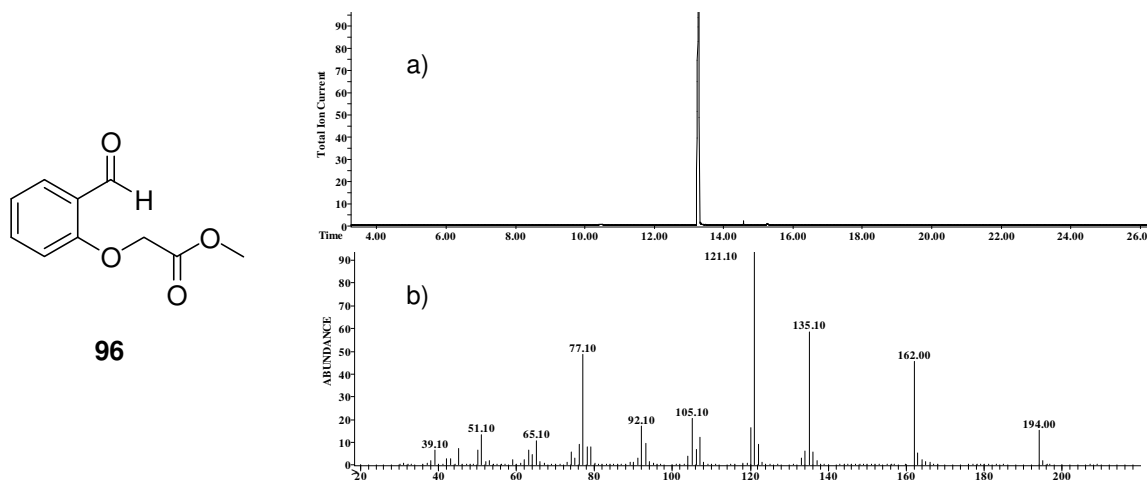
Figure 4.28 a) GC-MS of **96**; b) mass spectrum of major peak at t$_R$ = 13.26 min

157
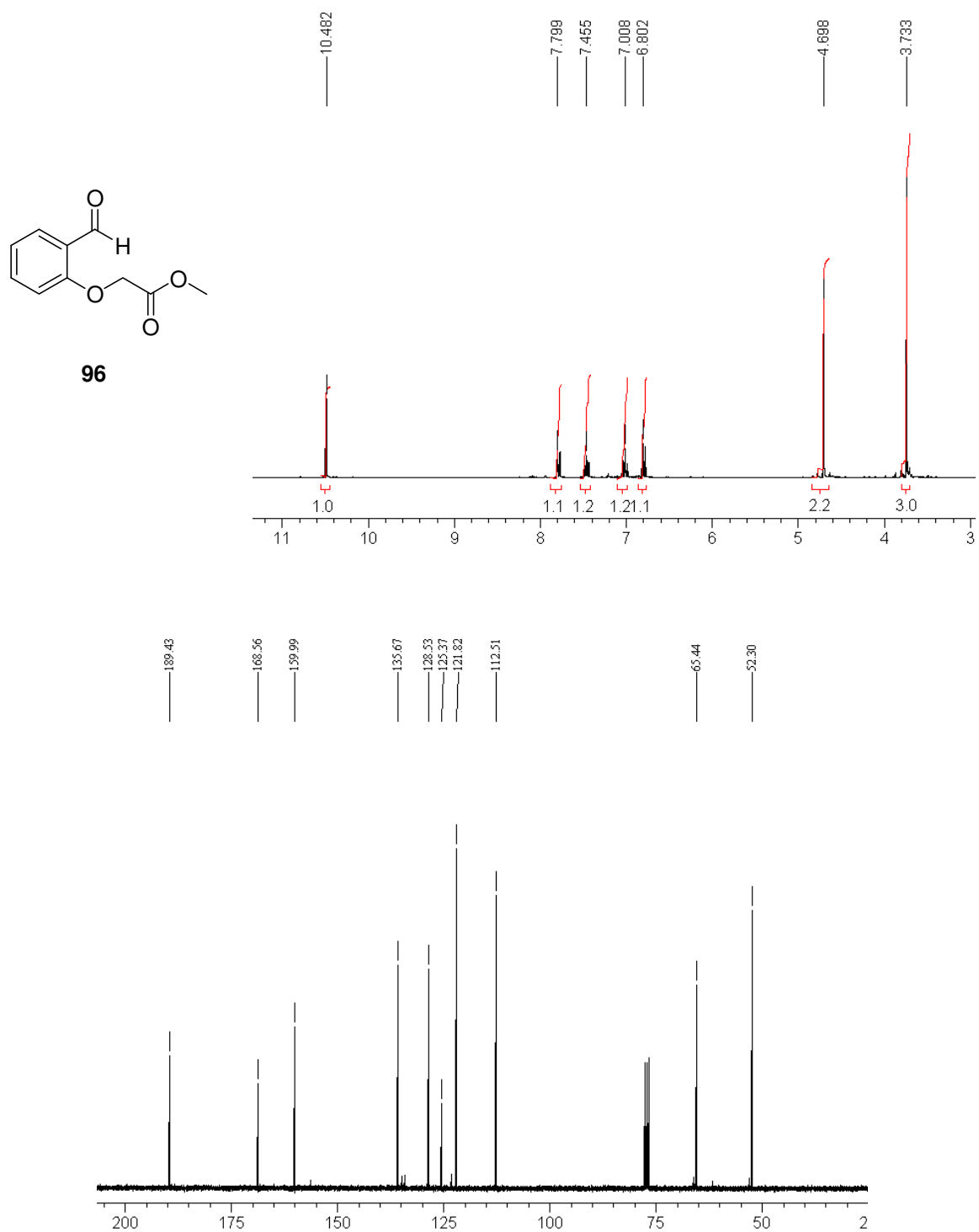
Figure 4.29 ^{1}H and ^{13}C NMR spectra of **96**

The crude yellow oil from NaBH$_4$ reduction was a variable mixture of products sensitively dependent on the reaction conditions employed. Performing the cyclisation in EtOH (refer to Scheme 4.15, *step c*) invariably formed ethyl 2-[2-(hydroxymethyl)phenoxy]acetate, **99** (81%) shown in the GC trace in Figure 4.30. Likewise, introduction of EtOH in the cyclisation *(*Scheme 4.15*,* step c*)* resulted in trans-esterification of the methyl ester, which

hindered cyclisation (see Appendix 27). Acid-induced cyclisation in MeOH increased formation of the cyclised lactone target (35%). GC-MS monitoring indicated over-reduction of both the aldehyde and ester functionalities producing the intermediate alcohol (**100**) and the di-alcohol (**101**) at elevated temperature. Formation of the latter is shown in Figure 4.31.
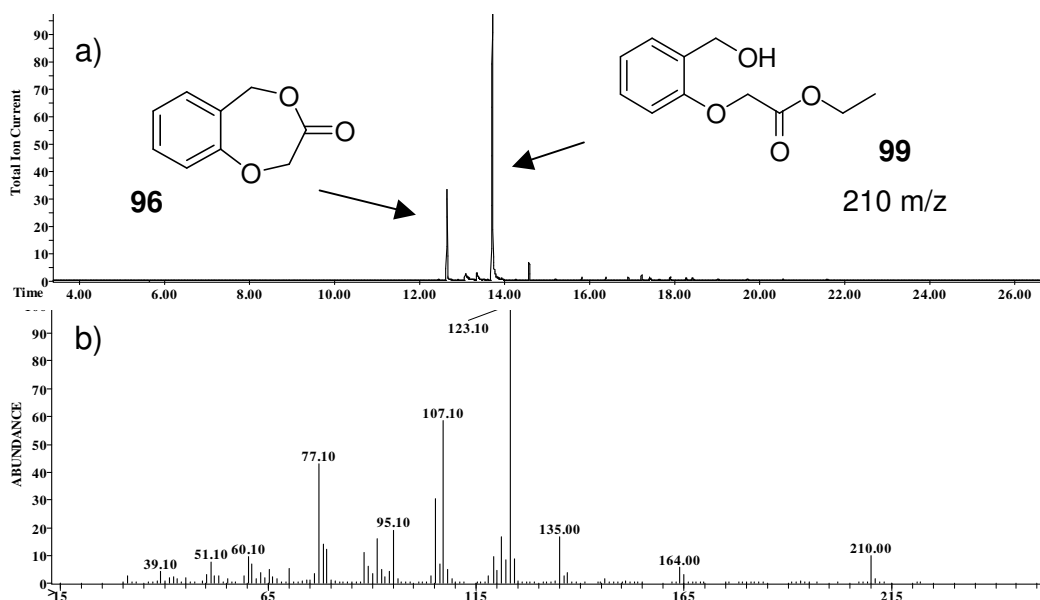
Figure 4.30 a) GC trace of transesterification impurity in EtOH (right); b) mass spectrum of peak at t_R = 13.72 min representing **99** (210 m/z)
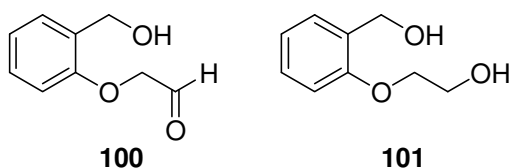
Figure 4.31 Reduced impurities, 2-[2-(hydroxymethyl)phenoxy] acetaldehyde, **100** and 2-[2-(hydroxymethyl)phenoxy]-1-ethanol, **101**, appearing in Scheme 4.15, *step b*

Application of KO^{t}Bu for cyclisation of the *o*-alcohol ester favoured the formation of by-products, mostly lower molecular weight cleavage products, rather than the cyclised target, **98**. The most favourable yields of the target, 5*H*-1,4-benzodioxepin-3(2*H*)-one (**98**), (84% by weight, 35% purity by GC-MS analysis) were obtained at 0°C-r.t. with limiting NaBH$_4$ reagent for the reduction step (Scheme 4.15, step b), represented by the GC-MS in Figure 4.32, prior to acid-catalysed formation of the lactone. Fractions

collected from chromatography on SiO$_2$ using pentane:DCM containing benzodioxepinone as the major component exhibited an odour strongly reminiscent of the acetyl benzodioxepinone, **71** (Scheme 4.7).
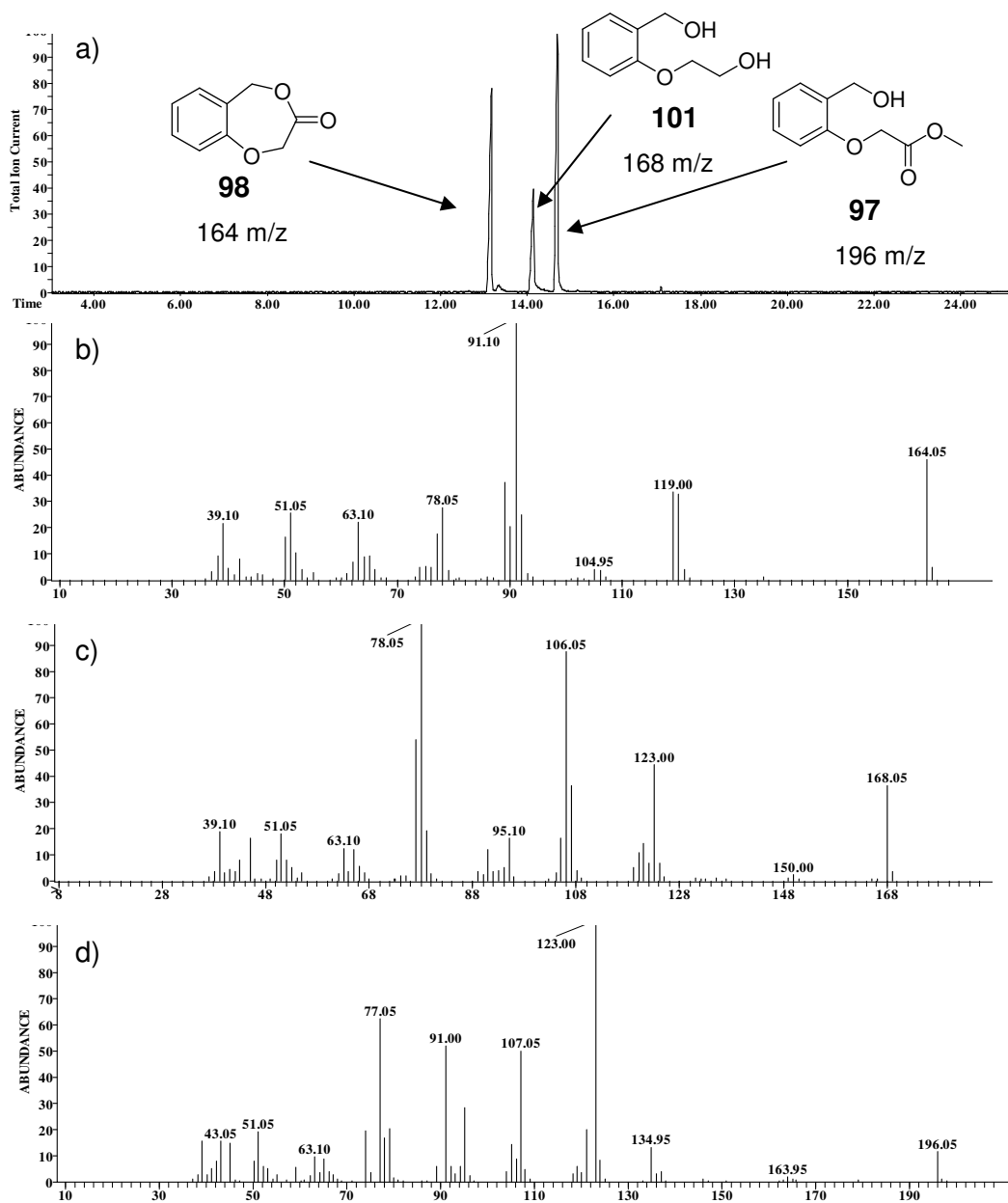
Figure 4.32 Final product mixture from synthetic procedure shown in Scheme 4.15; a) GC-MS of **98** (164 *m/z*), **101** (168 *m/z*) and **97** (196 *m/z*); b) mass spectrum of peak at t$_R$ = 13.15 min representing **98**; c) mass spectrum of peak at t$_R$ = 14.13 min representing **101**; d) mass spectrum of peak at t$_R$ = 14.68 min representing **97**

4.4   References

[1]   H.A. Dondas, R. Grigg, M. Hadjisoteriou, J. Markandu, W.A. Thomas, P. Kennewell, X:Y-ZH Systems as Potential 1,3-Dipoles. Part 50. Phenylselenyl Halide Induced Formation of Cyclic Nitrones from Alkenyl Oximes. Tetrahedron 56(51) (2000) 10087-10096.

[2]   F.S. Guziec Jr., J.M. Russo, A Convenient Conversion of Sterically Hindered Ketones into Imines. Synthesis(6) (1984) 479-481.

[3]   T.-C. Wang, I.L. Chen, D.-H. Kuo, C.-H. Liao, Synthesis and cytotoxic and antiplatelet activities of dibenzofuran- and carbazole-substituted oximes. Helv. Chim. Acta 87 (2004) 983-990.

[4]   E.J. Corey, M. Petrzilka, Y. Ueda, A New Synthetic Route to (+/-)-Perhydrohistrionicotoxin. Helv. Chim. Acta 60(7) (1977) 2294-2302.

[5]   J.R. Caycho, F. Garcia Tellado, P. de Armas, J.J. Marrero Tellado, Sodium Borohydride-Amberlyst-15 (H$^+$): An Effective Reductor for Hindered and Unreactive Ketones in Aprotic Solvent. Tetrahedron Lett. 38(2) (1997) 277-280.

[6]   B. Baruah, M.P. Dutta, A. Boruah, D. Prajapati, J.S. Sandhu, Amberlyst-15(H$^+$)-NaBH$_4$-LiCl. An Effective Reductor for Oximes and Hydrazones. Synlett. 4 (1999) 409-410.

[7]   F. Aragozzini, E. Maconi, D. Potenza, C. Scolastico, Enantioselective Microbial Reduction of Monoesters of 1,3-Dihydroxypropanone: Synthesis of (*S*)- and (*R*)-1,2-*o*-Isopropylideneglycerol. Synthesis(3) (1989) 225-227.

[8]   K. Umemura, H. Matsuyama, N. Watanabe, M. Kobayashi, N. Kamigata, Asymmetric Alkylation of β-Keto Esters with Optically Active Sulfonium Salts. J. Org. Chem. 54(10) (1989) 2374-2383.

[9]   A.I. Vogel, Vogel's Textbook of Practical Organic Chemistry, Pearson Education Limited, England, U. K., 1989.

[10]   A. Thurkauf, A.E. Jacobson, K.C. Rice, An Improved Procedure for the Preparation of Acetals from Diaryl Ketones. Synthesis(3) (1988) 233-234.

[11]   T. Kametani, M. Nishimura, K. Higurashi, Y. Suzuki, M. Tsubuki, T. Honda, Studies on the Synthesis of Morphinan and its Related Compounds: Construction of Morphinan Skeleton. J. Org. Chem. 52(23) (1987) 5233-5239.

[12]   D. Kikuchi, S. Sakaguchi, Y. Ishii, An Alternative Method for the Selective Bromination of Alkylbenzenes Using NaBrO$_3$/NaHSO$_3$ Reagent. J. Org. Chem. 63(17) (1998) 6023-6026.

[13]   B. Drevermann, A. Lingham, H. Huegel, P. Marriott, Microwave Assisted Synthesis of the Fragrant Compound Calone 1951®. Tetrahedron Lett. 46(1) (2004) 39-41.

[14]   C. Gabriel, S. Gabriel, E.H. Grant, B.S.J. Halstead, D. Mingos, M. P., Dielectric Parameters Relevant to Microwave Dielectric Heating. Chem. Soc. Rev. 27(3) (1998) 213-224.

[15]   C.G. Gabriel, S.; Grant, E. H.; Halstead, B. S. J.; Mingos, D.; Michael P., Dielectric Parameters Relevant to Microwave Dielectric Heating. Chem. Soc. Rev. 27(3) (1998) 213-224.

[16]   J.A. Dean, Lange's Handbook of Chemistry, McGraw-Hill, New York, U.S.A., 1985.

[17]   J. Jamrozik, S. Schab, K. Nagraba, Synthesis and Conformation of Some Tetraoxaspiranes. Monatsh. Chem. 125(4) (1994) 451-456.

[18] A.W. Archer, P.A. Claret, D.F. Hayman, The Conformation of 3,4-Dihydro-2*H*-1,5-benzodioxepin, and its Derivatives as Determined from their Ultraviolet Absorption Spectra. J. Chem. Soc. B: Phys. Org. 6 (1971) 1231-1240.

[19] M.B. Smith, J. March, March's Advanced Organic Chemistry, Wiley-Interscience, New York, U.S.A, 2001.

[20] M. Periasamy, M. Thirumalaikumar, Methods of Enhancement of Reactivity and Selectivity of Sodium Borohydride for Applications in Organic Synthesis. J. Organomet. Chem. 609(1-2) (2000) 137-151.

[21] H. Spreitzer, G. Buchbauer, C. Pueringer, A Study of Selective Oxime Reduction Methods. Tetrahedron 45(22) (1989) 6999-7002.

[22] M.B.M. Smith, J., March's Advanced Organic Chemistry, Wiley-Interscience, New York, U.S.A, 2001.

[23] D.E. Gibbs, D. Barnes, Asymmetric Synthesis of Amines by Action of Baker's Yeast on Oximes. Tetrahedron Lett. 31(39) (1990) 5555-5558.

[24] S. Kano, Y. Tanaka, E. Sugino, S. Hibino, Reduction of Some Functional Groups with Titanium(IV) Chloride/Sodium Borohydride. Synthesis(9) (1980) 695-697.

[25] G.C. Fu, S.T. Nguyen, R.H. Grubbs, Catalytic Ring-closing Metathesis of Functionalized Dienes by a Ruthenium Carbene Complex. J. Am. Chem. Soc. 115(21) (1993) 9856-9857.

[26] S.B. Garber, J.S. Kingsbury, B.L. Gray, A.H. Hoveyda, Efficient and Recyclable Monomeric and Dendritic Ru-Based Metathesis Catalysts. J. Am. Chem. Soc. 122(34) (2000) 8168-8179.

[27] H.D. Maynard, R.H. Grubbs, Purification Technique for the Removal of Ruthenium from Olefin Metathesis Reaction Products. Tetrahedron Lett. 40(22) (1999) 4137-4140.

[28] J.J. Beereboom, D.P. Cameron, C.R. Stephens, Flavoring Foods with Benzoxepin-3-ones and Benzodioxepin-3-ones, U.S. Patent 3,517,031, October 28, 1969, 1972.

[29] A.B. Ghattas, E.E. El-Khrisy, S.O. Lawesson, Studies on Organophosphorus Compounds. XLIII. A Convenient and Fast Carbonyl -> Thiocarbonyl Transformation of Some Esters, Thio Esters and Lactones by use of 2,4-*bis*(4-Methoxyphenyl)-1,3,2,4-dithiadiphosphetane 2,4-disulfide (Lawesson's reagent; LR). Reduction of Mono- and Dithio esters by Sodium Tetrahydroborate. Sulfur Lett. 1(3) (1982) 69-78.

[30] M. Tiecco, Selective Dealkylations of Aryl Alkyl Ethers, Thioethers, and Selenoethers. Synthesis(10) (1988) 749-759.

[31] L. Testaferri, M. Tiecco, M. Tingoli, D. Chianelli, M. Montanucci, Simple Syntheses of Aryl Alkyl Thioethers and of Aromatic Thiols from Unactivated Aryl Halides and Efficient Methods for Selective Dealkylation of Aryl Alkyl Ethers and Thioethers. Synthesis(9) (1983) 751-755.

[32] M. Rule, J.T.I. Tanner, Process for Preparation of Aromatic Thiols from Aromatic Halides and Thiourea, U.S. Patent 9323369, May 17, 1993, 1993.

[33] J.R. Campbell, Reduction of Disulfides with Copper. Preparation of Some Thioethers. J. Org. Chem. 27 (1962) 2207-2209.

[34] H.-L. Pan, T.L. Fletcher, A Facile Preparation of Sulfhydryl Compounds in Dimethyl Sulfoxide. Chem. Ind.(London, U. K.)(17) (1968) 546.

[35] J. Ham, I. Yang, H. Kang, A Facile one-pot Synthesis of Alkyl Aryl Sulfides from Aryl Bromides. J. Org. Chem. 69(9) (2004) 3236-3239.

[36] C. Wilkins, Hydroxylation and Epoxidation of Double Bonds with Disuccinoyl Peroxide. Synthesis(3) (1973) 156.

[37] J.L. Garcia Ruano, C. Fajardo, A. Fraile, M.R. Martin, *m*-CPBA/KOH: An Efficient Reagent for Nucleophilic Epoxidation of *gem*-Deactivated Olefins. J. Org. Chem. 70(11) (2005) 4300-4306.

5　Identification of Calone 1951® in a Commercial Fragrance with GC-qMS and GC×GC-TOFMS

5.1　Introduction

Calone 1951® is a highly potent synthetic fragrance (threshold: 0.031 ng/L) [1] and hence typically present at levels below 1% in commercial fragrances. As part of the research undertaken it was desirable to identify Calone 1951® in a commercial fragrance accord.

Cool Water for Women was selected as the sample for analysis based on literature reporting Calone 1951® at a level of 0.4%. Identification of Calone 1951® (Table 5.1) was predictably complicated due to co-elution of fragrance components in the GC analysis.

Table 5.1 Evolution of Calone 1951® in perfumery (adapted from [2])

	"New West for her" (1990)	"Escape for her" (1991)	"L'Eau d'Issey" (1993)	"L'Eau d'Eden" (1996)	"Cool Water fem" (1996)	"Polo sport W" (1996)
Calone 1951® (%)	1.2	0.8	0.6	0.17	0.4	0.45

Trials proved that conventional one-dimensional chromatographic methods lacked the high resolution and sensitivity necessary for separation of Calone 1951®. Positive identification was achieved with the application of two-dimensional GC×GC. In light of the high resolution and separation capabilities offered by GC×GC it proved to be ideal in identification of Calone 1951® in the "Cool Water" fragrance.

5.2　Comprehensive Two-dimensional Gas Chromatography (GC×GC)

The GC×GC separation mechanism is ideally based on orthogonal principles. Orthogonal separation demands that retention on the primary (^{1}D) and secondary (^{2}D) dimensions are statistically independent. Two-dimensional separation that is non-orthogonal can result in diagonal overlap on the retention plane (minimal peak separation) when there is

correlation between the tandem separation mechanisms due to compound similarity and phase similarity in the two dimensions.
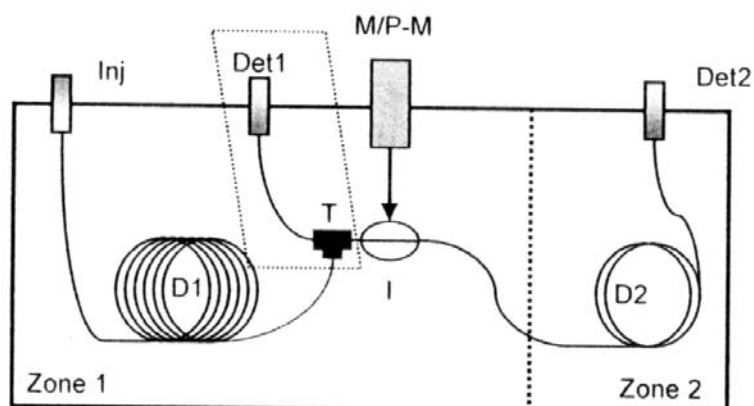
Figure 5.1 Instrumental schematic for comprehensive gas chromatography, T, T-union for splitting of effluent to first detector; I, interface device; M/P-M, modulation/pulsing mechanism [3]

The effluent collected from the primary column is concentrated by a modulator at the column interface and is periodically introduced to the second column preserving the separation achieved from ^{1}D (Figure 5.1). The result from the detector following ^{1}D and ^{2}D separation is processed as a composite of fast chromatograms to form the two-dimensional construct. It is essentially a consistent collection of heart-cut fractions over the span of the first dimension subjected to a fast sequential second dimension. The modulator allows release of one analyte band on to the secondary column while collecting the next analyte band at the interface.

Like with all forms of analyses, sensitivity (signal-to-noise ratio) is of primary concern. The relationship of the noise level to column sample capacity in GC systems provides information on the linear range of the system. Vacuum outlet conditions like those at a mass spectral interface require increased column internal diameter to ensure column efficiency and minimal fluctuation in average gas linear velocity. Sensitivity improvement is dependent on minimising band broadening which increases mass flux into the detector that can result in increased signal noise (higher signal/noise). The data acquisition rate of the detector should be low enough to maximize signal-to-noise and high enough to produce an accurate peak profile, which usually requires a minimum of ten data points per peak [4]. The flame ionisation detector (FID) has a sufficiently fast acquisition rate range for GC×GC of 50-200 Hz. The Method Translation software used in the current study for

the GC×GC-TOFMS analysis preserves the original chromatogram data and enables straightforward development of a two-dimensional GC equivalent method to the comparative 1D result.

5.3   Column Set Considerations

GC×GC aims for an optimal combination of phases to achieve maximum peak separation over the two retention axes of the 2D separation plane. The ^{1}D separation is usually a low polarity or non-polar capillary column phase, which predominately leads to a mechanism based on dispersion forces, essentially providing a boiling point separation. The ^{2}D separation is primarily specific interaction of the solute with the stationary phase e.g. hydrogen bonding, dipole-dipole interactions. Thus the secondary column should be selected to represent the chemical classes of the sample mixture to be separated, and for a phase-solute interaction that is mutually exclusive from the primary column to ensure orthogonality and maximum 2D separation. Since separation has already been achieved on the primary column, the ^{2}D analysis can afford to be fast. To correct for the difference in speed, the second column may have a smaller internal diameter, a shorter length and/or a higher phase ratio (β), although in practice often $^1\beta$ and $^2\beta$ are found to be similar [5].

Separation purely based on volatility provides limited capacity for separation of a complex sample. Constituents of perfume compositions commonly feature polar molecular attributes, which in the absence of a polar secondary separation leaves unutilised separation potential. The structure of Calone 1951$^®$ provides molecular features of polarity (carbonyl region) and low-polarity (aromatic region) so one would expect a mid-range retention factor (k) around 0.5-5 on a second dimension polar column.

5.4   The GC×GC Interface-Modulation

The key to GC×GC is the modulation process. Modulation restricts band broadening thereby improving resolution. A range of modulators now exists with varying innovations: jet-cooling [6], longitudinally modulating cryogenic trapping [7], thermal sweeping [8], non-moving dual stage modulation [9], diaphragm valve modulation [10], and differential flow modulation [11]. The diverse applicability of all modulation processes has been demonstrated thoroughly in literature methodology, with some analysts opting for the 'self-

constructed' model. Covering the theory of these modulation systems in entirety is beyond the scope of this thesis.

Those that involve temperature differentiation are known generally as thermal modulators. An elevated temperature thermal modulator is essentially a section of column acting as an interface with a very thick stationary phase coating and hence smaller phase ratio [12]. The longitudinally modulating cryogenic system (LMCS) is a reduced temperature thermal modulator. The LMCS involves cryogenic zone compression followed by rapid re-mobilization of the focused band. The latter occurs from exposure to the heat of the GC oven once the trap has moved longitudinally to 'release' mode. Separation is now possible by rapid periodic pulses with a total runtime in seconds rather than slow elution in minutes.

Beens found that the detectability limit of GC×GC was 18 times better than 'normal' capillary gas chromatography due to augmentation of signal intensity from concentration of the sample analytes in the modulation process [13]. This allows detection of trace analytes not normally visible in one-dimensional GC, as in the current study where detection of Calone 1951® at below 1% is desired.

In GC×GC phasing denotes the relation between the pulse time of the modulator and the elution time of peaks from the primary column. A modulation period that is too high can result in loss of resolution from the first column; however there will also be a gain in sensitivity due to compression of larger peak area. The maximum ^{2}D retention time must correspond to the modulation period (P_M) (or may be less) otherwise co-elution will occur. Thus, each individual component in the GC×GC chromatogram will appear as a series of pulsed peaks. In order to get maximum separation performance in the GC×GC system, each individual ^{1}D peak should be modulated into several fractions, according to the modulation ratio, M_R. The modulation ratio was defined by Khummueng and colleagues [14] as the standard deviation of the first column peak multiplied by 4 divided by the modulation period (P_M) [12].

The elution temperature of a compound from the first column is also the (isothermal) temperature at which it is analysed on the second column. The fast analysis on the second column produces sharp narrow peaks (~0.1s) with greatly enhanced intensity (hence accurate peak area is preserved). Potential introduction of phase bleed only occurs at temperatures of 220°C and above for GC×GC [15].

5.5   The 2D GC×GC Chromatogram

Separation of co-eluting peaks is not necessarily apparent in the one-dimensional representation of the pulsed peaks from GC×GC modulation. Retention overlap in a 2D separation leads to diagonal co-elution (distribution along the diagonal) rather than utilization of the full 2D separation space available. If the separation space is not utilized to maximum capacity then redundant space exists.   GC×GC offers enhanced reproducibility of peak positioning provided conditions are kept consistent. A peak on the 2D separation plane can be identified by retention times of both the 1st and 2nd dimension (retention coordinates). A broad range of molecular composition within a sample is suited to GC×GC due to an increased capability for compound class separation.   Similar retention times are visible as elution groupings in the 2D contour plot.   Compound classes, such as alkanes or aromatics can be identified at a glance in representative regions on the 2D chromatogram. 'Wrap-around' peaks are repeated peaks that appear as artefacts on the 2D plane, a phenomenon of 2D representation caused by excessive retention on the second column.

5.6   Gas Chromatography-quadrupole Mass Spectrometry (GC-qMS)

A straightforward, consistent and accessible method for thorough sample analysis is provided by gas chromatography-quadrupole mass spectrometry (GC-qMS). With the aim of identifying Calone 1951® in a 'Cool Water Woman' sample, the sample was subjected to one-dimensional GC with quadrupole mass detection.

Observed variable MS fragmentation across the breadth of a given peak is due to a mass spectral skewing effect. Even with increased sensitivity (increased scanning time and decreased scanning range), or faster mass flux MS often reveals some degree of skewing [16]. With 1D separation the mass spectrum at any arbitrary scan will be a fusion of the unresolved components at that point, for which background subtraction may not prove reliable due to peak saturation of the separation space. However the wide acceptance and application of GC-qMS testifies to the value inherent in the method. Higher data acquisition minimizes mass spectral skewing by keeping sample concentration in the ion source relatively constant during the mass measurement scanning cycle.

5.6.1   Analysis of 'Cool Water Woman' with GC-qMS
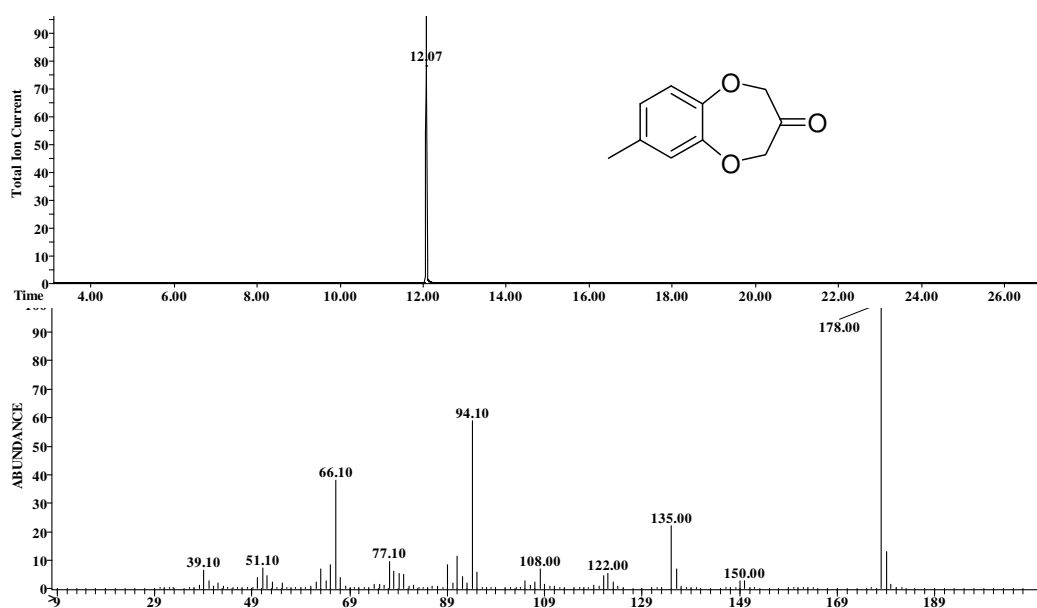
Figure 5.2 Calone 1951® standard (a) GCMS chromatogram (b) mass spectrum at 12.1 min
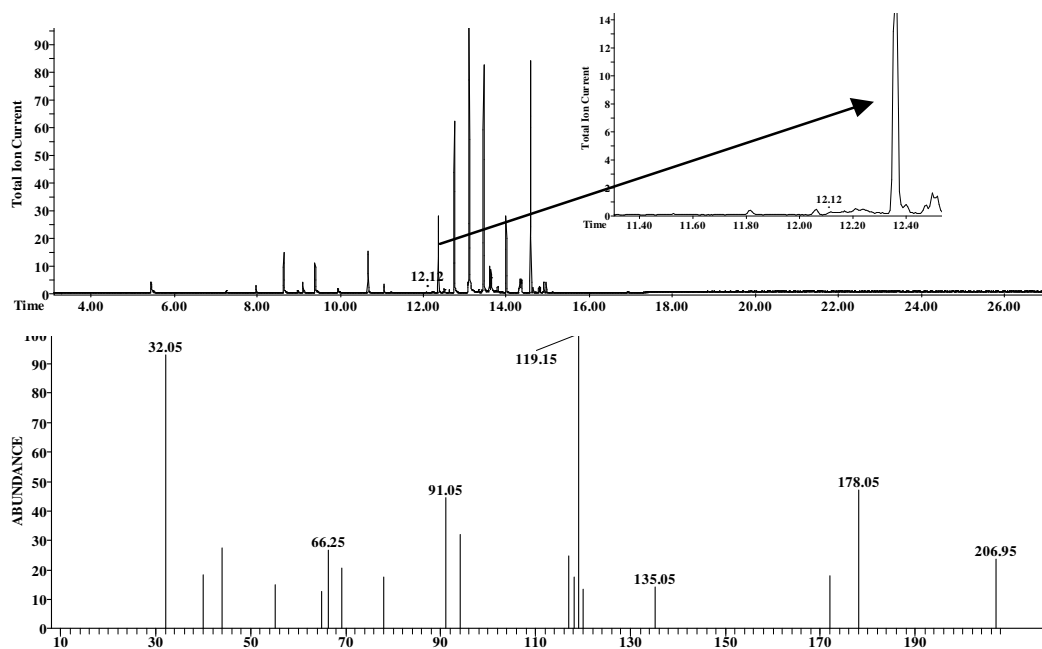
Figure 5.3 Cool Water Woman sample (a) GC-MS chromatogram (b) mass spectrum at 12.1 min

In comparison with the Calone 1951® standard (Figure 5.2) it is evident from the GC-qMS total ion current (TIC) chromatogram (Figure 5.3) that many peaks are only partially resolved.

Here, the suspected peak of Calone 1951® at 12.1 min overlaps with other components to produce a mass spectrum array from all components at that point in the GC trace.

The mass scan range and data acquisition rate of the GC-qMS run were m/z 30-550 and 20 Hz respectively. Extracted ion (EI) monitoring of the TIC (EIC; 178, 149, 135, 122, 74 m/z ions extracted) failed to provide absolute identification of Calone 1951®.
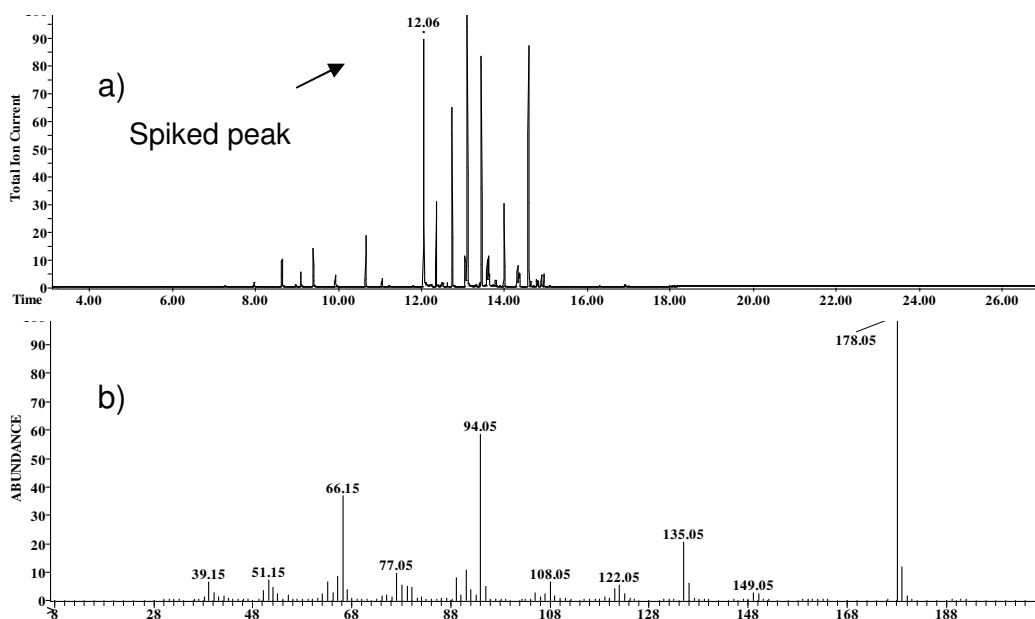
Figure 5.4 Calone-spiked Cool Water Woman perfume a) GC-MS chromatogram b) mass spectrum at 12.1 min

Identification of the correct retention time for Calone 1951® in the perfume sample was achieved *via* a standard-spiked TIC and SIM. Spiking of the perfume sample with standard Calone 1951® allowed an accurate baseline location to be attributed to the compound, and hence mass spectral analysis of this baseline region (12.1 min) provided more accurate identification (Figure 5.4).
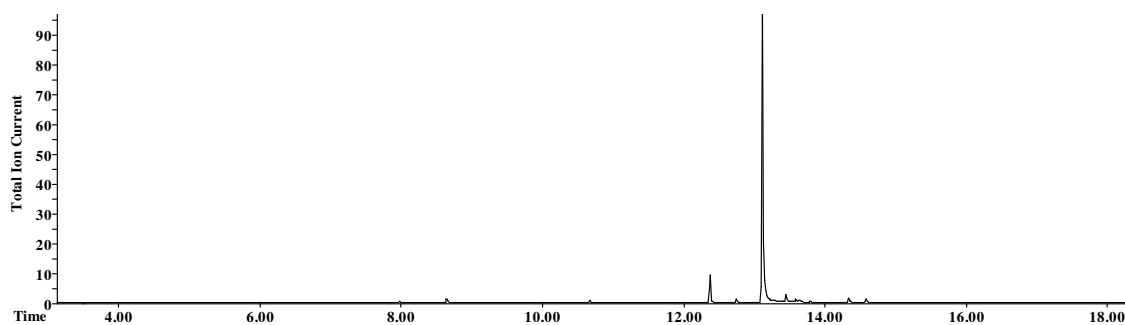
Figure 5.5 Selected Ion Monitoring (SIM) for Calone 1951® fragments in Cool Water Woman sample; 178, 149, 135, 122, 94, 77 *m/z*

Selected ion monitoring (SIM; 178 m/z ion selected) mode identified a range of peaks. Scanning for multiple fragments (SIM; 178, 149, 135, 122, 94, 77 *m/z* ions selected) identified false positive results (Figure 5.5). FID quantification is evidently erroneous when the peaks of interest are co-eluting with matrix components.

5.7 GC×GC-qMS vs GC×GC time-of-flight (TOF)MS

Unlike mass-scanning quadrupoles, TOF generates instant mass spectra, avoiding the mass spectral skewing problems often experienced with qMS due to mismatch between scan rate (duty cycle) and peak abundance changes. The fast acquisition capabilities of TOFMS are compatible with fast GC techniques, such as that employed in GC×GC [17]. A high acquisition frequency means more data points per peak resulting in a more definitive chromatographic profile. The detection capabilities of TOFMS have now surpassed many of its scanning mass spectral counterparts. Quadrupole MS analysers previously exceeded TOF in sensitivity, however technological advances in TOF design have led to high transmission efficiency, leading to high sensitivity and accurate mass detection. The poorer mass resolution previously exhibited by TOFMS was a result of temporal distribution of ions with the same m/z ratio. This problem was solved by the introduction of a reflectron, which corrects for changes in kinetic energy of ions with the same mass resulting in simultaneous detection. TOFMS stands out from its mass spectrometry counterparts as it can acquire 100 or more mass spectra per second, ideal for monitoring GC×GC chromatograms, for quantification and deconvolution [18]. Modern quadrupole instruments can also meet the 50 Hz requirement, provided proper mass range settings are selected (reduced scan range) [19].

5.7.1   Analysis of 'Cool Water Woman' with GC×GC-TOFMS
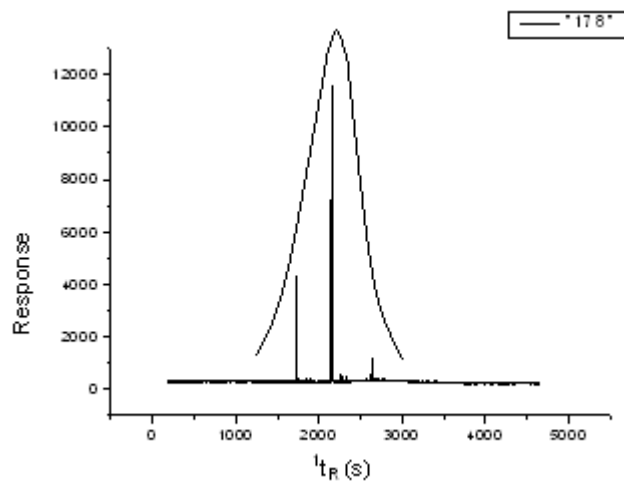
Figure 5.6 Modulated chromatogram of Calone 1951® standard, using GC×GC-TOFMS extracted ion m/z 178

The modulated chromatogram traces of both standard Calone 1951® (Figure 5.6) and the 'Cool Water Woman' sample (Figure 5.7) highlight the increased signal intensity resulting in the high sensitivity capabilities of GC×GC.
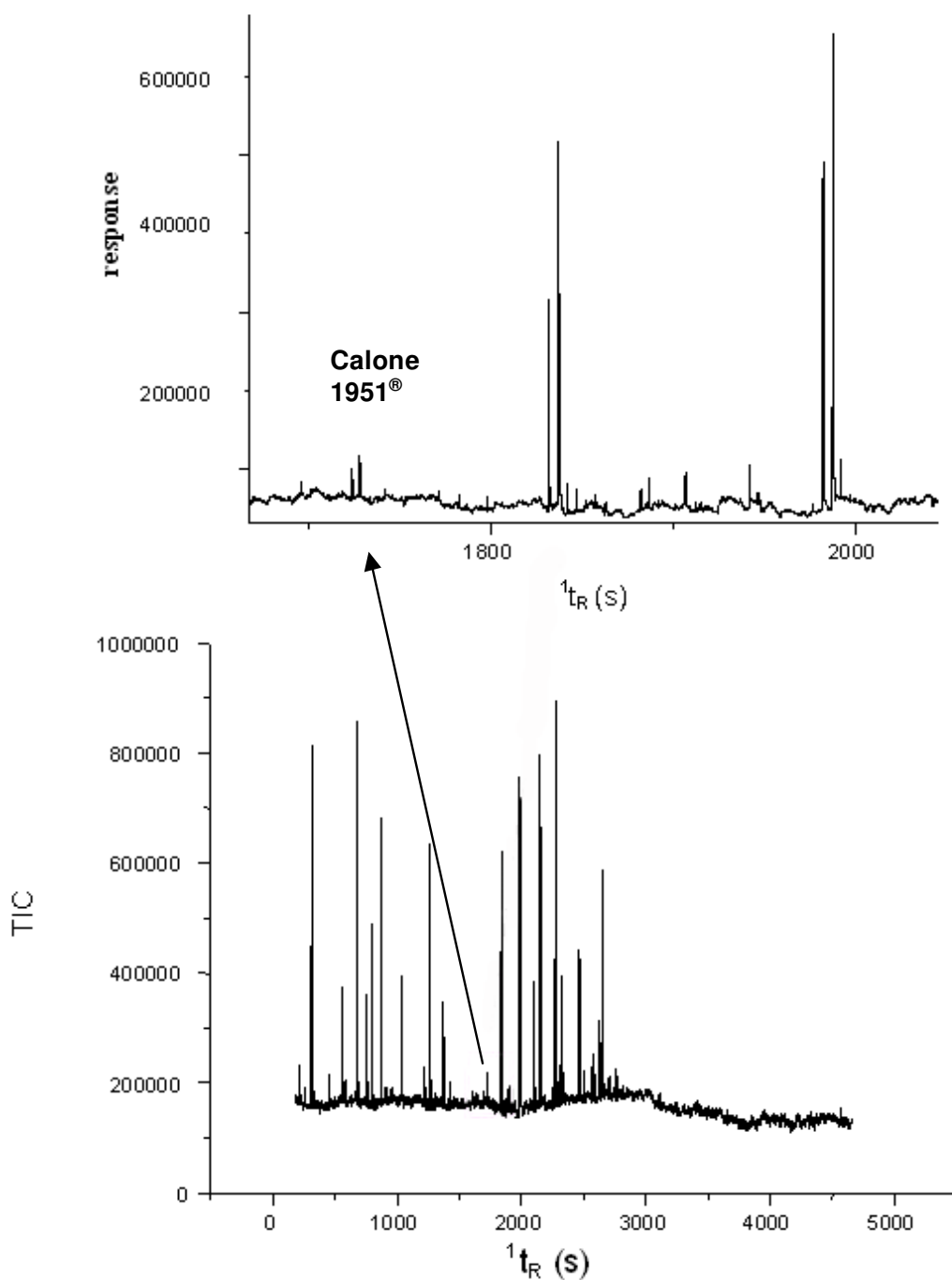
Figure 5.7 Modulated chromatogram of Cool Water Woman perfume sample

As in the GC-qMS run, the ^{1}D separation with TOFMS detection revealed multiple co-elution of the components within the perfume sample. The ^{2}D GC separation based on polarity enabled visualisation and subsequent identification once the 2D contour plot had been generated. Quantitative data from integration of the 1D chromatogram revealed Calone 1951® present in Cool Water Woman at a comparable value (0.47 %) with literature (0.4 %). As the MS specifications for derivation of the former value (from Table

5.1) are not provided, these values need to be considered in light of potential response factor discrepancies for Calone 1951® and the appointed internal standard for the interlaboratory results.
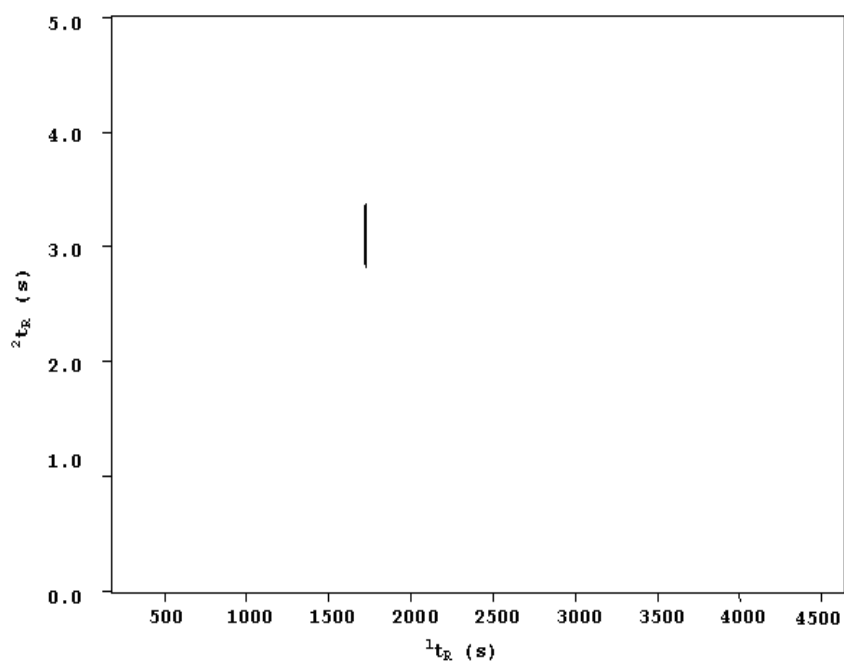
Figure 5.8 GC×GC 2D contour plot of Calone 1951® standard

Applying GC×GC to the Calone 1951® standard (Figure 5.8) enabled positive identification of the exact retention position for location of the minor component in the perfume sample.
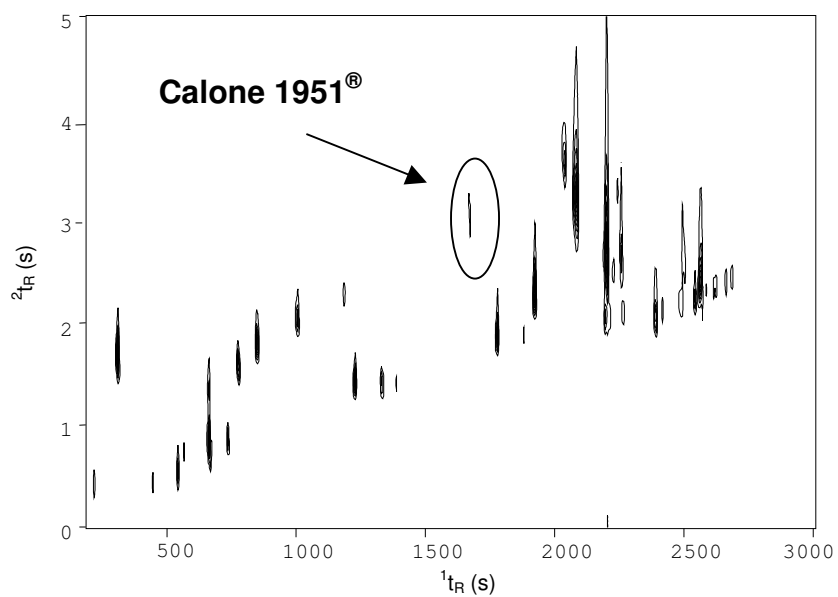
Figure 5.9 GC×GC 2D contour plot of Cool Water Woman perfume

Calone 1951® can clearly be identified in the perfume sample in Figure 5.9 (peak apex; 1D: 1735 s, 2D: 3.00 s) even at its extremely low relative concentration, matching the coordinates with those of the standard inFigure 5.8; the retention coordinates match exactly with the standard run. Note differences in retention times of the ^{1}D axis between standard and perfume sample.

In order for Calone 1951® to be visualised higher concentrations were analysed which has resulted in a small degree of tailing. The tailing may also be due to higher overall retention on the polar ^{2}D column. By resolving co-eluting peaks from the first dimension, GC×GC ultimately introduced a form of deconvolution to the sample where correspondence of a component and accurate mass spectral fragmentation were straightforward. Without the need for spiking, accurate TOF mass spectral identification was achieved with the appearance of all major fragments expected for Calone 1951® as shown in Figure 5.10.
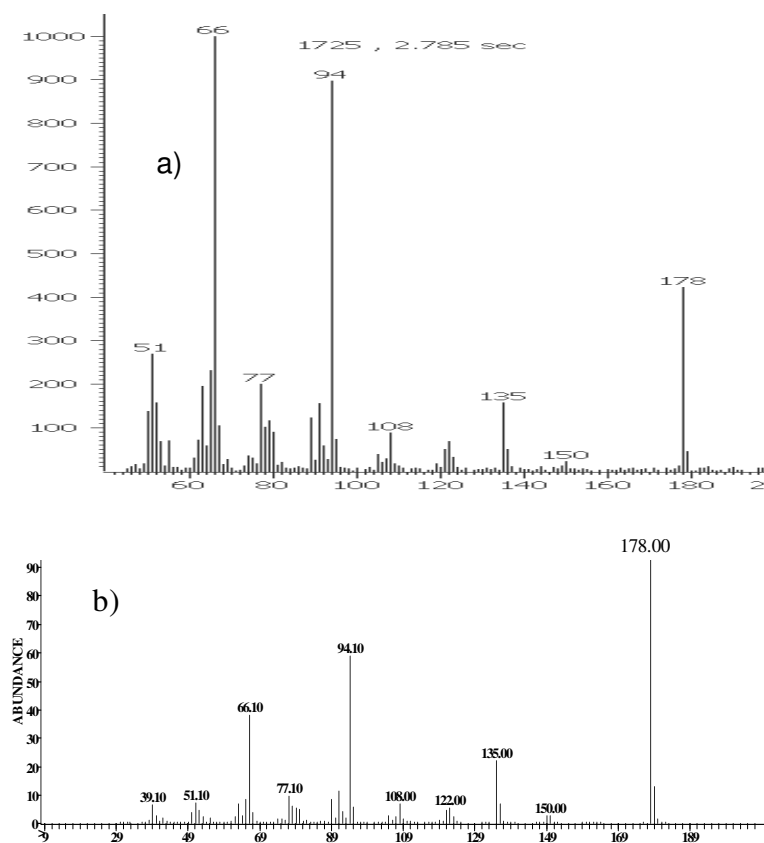
Figure 5.10 (a) TOF mass spectrum for Calone 1951® from EIC of modulated TIC of Cool Water Woman perfume (b) mass spectrum of Calone standard from qGC-MS

In the absence of a standard or for further confirmation, selective heart-cut of the sample to isolate the retention time region of Calone 1951® and subsequent olfactory analysis with GC-O may be performed.

5.8   Analysis Specifications

5.8.1   Sample Preparation

The Cool Water Woman perfume was purchased and stored at room temperature. Calone 1951® is a solid compound and was stored at 4°C. The Calone 1951® standard was analysed at 10% dilution in analytical (AR) grade hexane. The perfume sample was analysed at 10% dilution in analytical (AR) grade hexane, and with a 10% Calone 1951® spike addition.

5.8.2   Instrument Conditions for GC-qMS

GC-qMS was performed on an Agilent HP6890 system equipped with a HP5973 mass selective detector (Agilent Technologies, Burwood, Australia) with an Agilent 7683 Series autosampler (Agilent Technologies, Palo Alto, CA, USA). The sample was run on a BPX5 (5% phenyl polysilphenylene-siloxane) capillary column with dimensions of 30 m $\times$ 0.25 mm I.D. $\times$ 0.25 μm d_f. The oven was held at 50°C for 5 min then increased to 300°C at 20°C/min and held for 10 min. The injected sample volume was 1 μL with a split ratio of 50:1. Helium was used as carrier gas at a flow rate of 1.0 mL/min. For all analyses the transfer line temperature was 260°C. The source temperature was 230°C with a mass scan range of m/z 30-550 at a data acquisition rate of 20 cycles/sec (Hz). The detector (electron multiplier) voltage was 2 kV with ionisation energy of 70 eV. Selected ion monitoring (SIM; 178, 149, 135, 122, 94, 77 m/z ions selected) mode was run at a data acquisition rate of 8.33 Hz.

5.8.3   Instrument Conditions for GC$\times$GC-TOFMS

An Agilent HP6890 GC (Agilent Technologies, Burwood, Australia) with Chemstation data system to program modulation was interfaced to the Pegasus III time-of-flight mass spectrometer (TOFMS) (LECO, ST Joseph, MI, USA) for mass spectral data. Injection

methods employed an Agilent 7683 Series autosampler (Agilent Technologies, Palo Alto, CA, USA). The primary column was a 30 m x 0.25 mm I.D. x 0.25 μm d_f BPX5 (5% phenyl polysilphenylene-siloxane) capillary directly coupled to a secondary BP20 column 1 m x 0.1 mm I.D. x 0.1 mm d_f (polyethylene glycol) capillary, both from SGE International, Ringwood, Australia. The GC oven temperature was programmed from 50°C (held for 5 min) to 250°C at a rate of 20°C/min, which was held for 10 min. The detector voltage for electron impact ionisation was set at 70 eV. The ion source temperature was set at 200°C to acquire ions in the mass range 45-5000 m/z at 50 spectra/s. Samples (1 μL) were injected at 250°C using split conditions (10:1) with helium as carrier gas and a flow rate of 1 mL/min.

The primary and secondary columns were connected via a transfer line with zero dead volume (SGE International, Ringwood, Australia) operated at 260°C. The 6890GC was retrofitted with an Everest model Longitudinally Modulated Cryogenic System (LMCS) (Chromatography Concepts, Doncaster, Australia). Modulation period (P_M) was set at 5 seconds.

5.8.3.1   Software

Importation of the raw data matrix was achieved using the ASCII (.csv) format. Origin (Microcal Software, Northampton, MA) was used to convert the original ASCII file to a conventional chromatogram trace. 2D-GC converter (Chromatography Concepts) software enabled importation into Transform (Fortner Research, Boulder, USA) to generate the 2D contour plot. ChromaTOF™ software (LECO) was used for peak integration and identification of peaks and referenced to the mass spectra from NIST (1998) and Wiley (7th Edition, 2000) libraries.

5.9   References

[1] P. Kraft, W. Eichenberger, Conception, Characterization and Correlation of New Marine Odorants. Eur. J. Org. Chem.(19) (2003) 3735-3743.

[2] P. Kraft, J.A. Bajgrowicz, C. Denis, G. Frater, Odds and Trends: Recent Developments in the Chemistry of Odorants. Angew. Chem., Int. Ed. 39(17) (2000) 2980-3010.

[3] P.J. Marriott, R.M. Kinghorn, in: E. R. H. Adlard, A. J. (Ed.), Gas Chromatographic Techniques and Applications, (Eds.), Sheffield Academic Press, Sheffield, U.K., 2001, pp. 260-297.

[4] H. Boelens, Structure-activity Relationships in Chemoreception by Human Olfaction. Trends in Pharmacol. Sci. 4(10) (1983) 421-426.

[5] J. Beens, R. Tijssen, J. Blomberg, Prediction of Comprehensive Two-dimensional Gas Chromatographic Separations. A Theoretical and Practical Exercise. J. Chromatogr., A 822(2) (1998) 233-251.

[6] M. Adahchour, J. Beens, U.A.T. Brinkman, Single-jet, Single-stage Cryogenic Modulator for Comprehensive Two-dimensional Gas Chromatography (GC x GC). Analyst (Cambridge, U. K.) 128(3) (2003) 213-216.

[7] P.J. Marriott, R.M. Kinghorn, R. Ong, P. Morrison, P. Haglund, M. Harju, Comparison of Thermal Sweeper and Cryogenic Modulator Technology for Comprehensive Gas Chromatography. J. High Resol. Chromatogr. 23(3) (2000) 253-258.

[8] P.J.K. Marriott, R. M.; Ong, R.; Morrison, P.; Haglund, P.; Harju, M., Comparison of Thermal Sweeper and Cryogenic Modulator Technology for Comprehensive Gas Chromatography. J. High Resol. Chromatogr. 23(3) (2000) 253-258.

[9] J. Beens, M. Adahchour, R.J.J. Vreuls, K. van Altena, U.A.T. Brinkman, Simple, Non-moving Modulation Interface for Comprehensive Two-dimensional Gas Chromatography. J. Chromatogr., A 919(1) (2001) 127-132.

[10] R.W. LaClair, P.A. Bueno, Jr., J.V. Seeley, A Systematic Analysis of a Flow-switching Modulator for Comprehensive Two-dimensional Gas Chromatography. J. Sep. Sci. 27(5-6) (2004) 389-396.

[11] J.V. Seeley, F. Kramp, C.J. Hicks, Comprehensive Two-dimensional Gas Chromatography *via* Differential Flow Modulation. Anal. Chem. 72(18) (2000) 4346-4352.

[12] J.T. Beens, R.; Blomberg, J., Prediction of Comprehensive Two-dimensional Gas Chromatographic Separations. A Theoretical and Practical Exercise. J. Chromatogr., A 822(2) (1998) 233-251.

[13] J. Beens, H. Boelens, R. Tijssen, J. Blomberg, Quantitative Aspects of Comprehensive Two-dimensional Gas Chromatography (GC x GC). J. High Resol. Chromatogr. 21(1) (1998) 47-54.

[14] W.H. Khummueng, J.; Marriott, P. J., Modulation Ratio in Comprehensive Two-dimensional Gas Chromatography. Anal. Chem. 78 (2006) 4578-4587.

[15] P.J.O. Marriott, Ruby C. Y.; Kinghorn, R. M.; Morrison, P. D., Time-resolved Cryogenic Modulation for Targeted Multidimensional Capillary Gas Chromatography Analysis. J. Chromatogr., A 892(1+2) (2000) 15-28.

[16] L. Mondello, A. Casilli, P.Q. Tranchida, G. Dugo, P. Dugo, Comprehensive Two-dimensional Gas Chromatography in Combination with Rapid Scanning Quadrupole Mass Spectrometry in Perfume Analysis. J. Chromatogr., A 1067(1-2) (2005) 235-243.

[17] P.J. Marriott, R. Shellie, C. Cornwell, Gas Chromatographic Technologies for the Analysis of Essential Oils. J. Chromatogr., A 936(1-2) (2001) 1-22.

[18] M. Adahchour, J. Beens, R.J.J. Vreuls, A.M. Batenburg, U.A.T. Brinkman, Comprehensive Two-dimensional Gas Chromatography of Complex Samples by Using a 'Reversed-type' Column Combination: Application to Food Analysis. J. Chromatogr., A 1054(1-2) (2004) 47-55.

[19] M.B. Adahchour, J.; Vreuls, Rene J. J.; Batenburg, A. M.; Brinkman, U. A. Th, Comprehensive Two-dimensional Gas Chromatography of Complex Samples by Using a 'Reversed-type' Column Combination: Application to Food Analysis. J. Chromatogr., A 1054(1-2) (2004) 47-55.

6 Structure-Odour-Relationships (SOR): Qualitative Analysis with Gas Chromatography-Olfactometry (GC-O) vs Blotter Analysis, and Conformational Modelling

6.1 Introduction

Physiological analysis of odourants and correspondence with molecular structure enables structure-odour relationships to be explored, however research in this field remains underdeveloped. Qualitative olfactory evaluation was performed using Gas-Chromatography-Olfactometry (GC-O) and blotter analysis. GC-O (Figure 6.1) methods were used to assess the odour modalities of the analogues synthesised in Chapters 2, 3 and 4. Four subjects were employed to establish frequency detection and minimise subjectivity. Odour descriptor tables were derived providing a summary of the qualitative olfactory perception collected from all four subjects. Professional olfactory assessment by Philip Kraft and Alain Alchenberger is provided for comparison. An overview of olfactophore models generated with CATALYST™ and inclusion of select quantitative odour intensity values reflects the capabilities of CATALYST™ as a powerful tool for SOR.
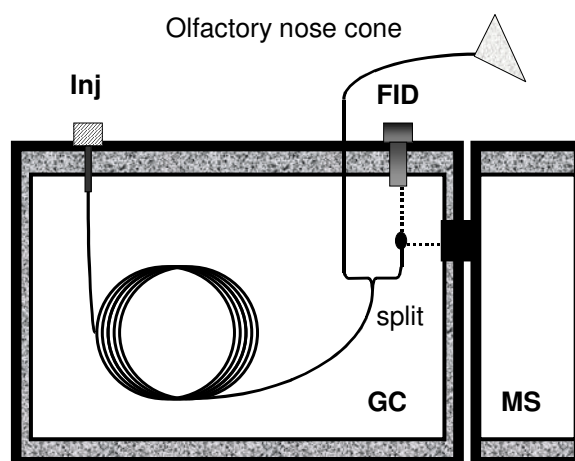
Figure 6.1 Gas Chromatography-Olfactometry (GC-O)

6.2 An Introduction to Quantitative and Qualitative Olfactory Perception

6.2.1 Theoretical Muse

Through experimentation Boeckh came to define the electro-physiological threshold of an odour as the lowest concentration at which a nerve impulse distinguishable from the control is generated [1]. An earlier assumption by Beets postulated that odour intensity incorporates both an "intrinsic" and a "nonintrinsic" component. Molecular features are precepts for the intrinsic element, and the nonintrinsic term is determined by the ability of the odourant to absorb into the mucous carrier layer - the lipophilicity character [2].

Beets proposed in 1970 that odour intensity was encoded by electro-physiological amplitude and frequency, and odour quality was based on molecular dimensions [2]. Beets recorded trends in amplitude response, which is indirectly related to volatility and functional features such as steric bulk and conjugation [2]. He discovered that the amplitude order for a series of butyl alcohols decreases from secondary > normal > iso- > tertiary butanol [2], whereas the trend for decreasing vapour pressure is tertiary > secondary > iso- > normal (n-) butanol. A later theory demonstrated that a change in odourant concentration will alter the information pattern, and a threshold value can be reached.

Compound **1** is a suitable exemplar of an odourant that features qualitative odour characteristics that alter with odourant concentration. At increased concentrations the marine character is pronounced - more reminiscent of seaweed. At low potency, the floral nuances become evident.

Turin proposed that each receptor is tuned to a limited range of vibrational modes (frequencies) that Firestein's (1993) [3] work supported after patch clamp receptor stimulation tests revealed cells responded differently to application of different odourants. Isolated olfactory neurons were exposed to three odorants: cineole, isoamyl acetate and acetophenone. Cells were found that responded to one odourant, to two odourants, and to all three. The response pattern of all three cells is as follows: one cell responded to all three odorants, one cell to acetophenone and isoamyl acetate but not to cineole, and one responded to cineole alone. When the spectra of the three odourants are calculated using an algorithm that stimulates tunnelling spectra, the results are consistent with their

sensing three different vibrational bands [4] (see Chapter 1, Section 1.3.1). Turin also adds that differing sections of an odorant molecule are recognised by different receptor types, which contributes to the gradations in odour quality [5]. So odour molecules contribute segregated information to the brain for processing. Turin's algorithm is heavily reliant on the partial charges of the molecule as they cause the e- scattering [5].

In contrast the hologram theory would predict that olfaction is a binary system: select cells detect the entire vibrational information from the odourant and some cells are not stimulated at all. This information is then integrated to form a holographic 3D odour profile when processed by the brain. Other sense modalities such as sight have been linked to a holographic form of stimulus detection in conjunction with brain processing methods [6]. The mathematical language of a hologram is Fourier transform. If Fourier transform mathematics were applied to olfaction this would most likely entail that a) information processing is based on frequency, as Turin has detailed; b) select receptors bind with select odourants; c) each receptor that binds with the odour molecule detects the absolute molecular information offered by that odourant, as each portion of a hologram encompasses the composite of the hologram.

6.2.2 CATALYST™ models for SOR

A CATALYST™ model is presented here to illustrate the compatibility of partnering an olfactophore model with olfactory perception data to provide powerful SORs, just as pharmacophore models are integrated into drug analysis. Most olfactophore models generated in this manner are optimised within a conformational energy limit of 3 kcal mol^{-1}. A model generated through CATALYST aims to predict the geometry and molecular affinity of the olfactory receptor binding site.

The CATALYST™-derived olfactophore model of **66** is presented in Figure 6.2. The terminal hydroxy group of **66** is depicted in green, as the primary hydrogen-bond acceptor. Potential hydrophobic pockets of the receptor site are depicted in cyan, logically with proximity to the alkyl aromatic substituents. Excluded volumes (represented by the white spheres) are oriented in light of putative receptor site constraints enforced by limitations such as steric bulk or configurational antagonism.
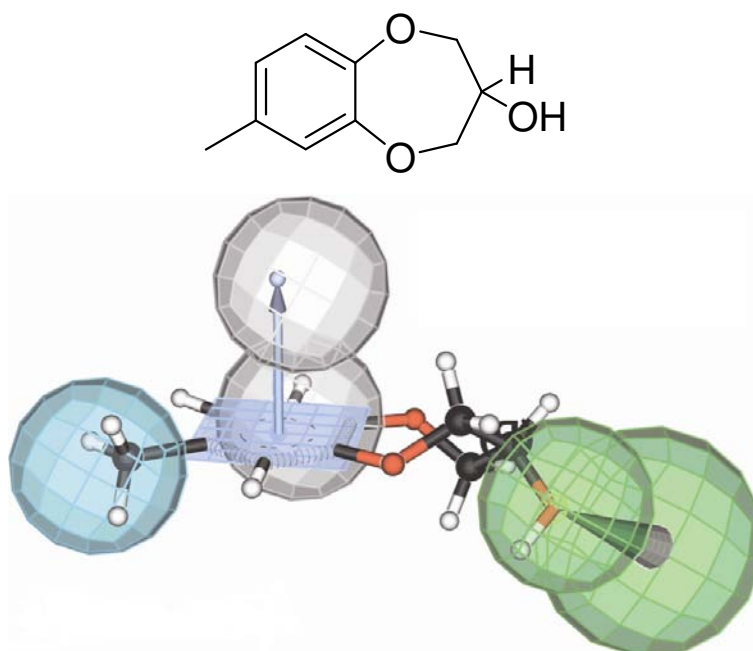
Figure 6.2 Putative CATALYST™ model of **rac-66**: green represents hydrogen bond acceptors; cyan represents hydrophobic pockets; white represents excluded volumes

Inclusion of 'trial-and-error' excluded volumes allows hypotheses that can save valuable time in synthesis of potential new odourants, which has been demonstrated by Kraft and his team at Givaudan [7]. The energy considerations in deriving the most favourable conformer in combination with predicted intensity thresholds allow foresight into pursuit of valuable synthetic odourants. The odour intensity and concentration of an odourant share a linear relationship as predicted by Steven's law (Chapter 1, Section 1.5.2.2), however the magnitude of increase in intensity is determined by the odourant and hence, the rank order of two odourants can switch at a given concentration (refer to Figure 1.22, Section 1.5.2.2). This must be considered when assessing a novel odourant for commercial potential.

The deficiency of an established data set of benzodioxepin(on)es results in limitations for relative CATALYST™ models to be generated. For this reason it is beneficial to expand the marine and benzodioxepinone fragrance arena through synthesis and SOR analysis.

6.2.3   Select intensity thresholds

Intensity thresholds derived using GC-O for select compounds from the analogue data set are presented in Table 6.1. The intensity threshold of an odourant *per se* becomes

questionable around $\geq$ 2ng/L. An odourant with promising olfactory character and slightly higher intensity threshold would still quite likely be considered for its commercial applicability. Compound **28**, featuring an aromatic *m-tert*-butyl substituent and potentially compound **24** with an *o*-methoxy aromatic substituent, provide the most favourable odour intensities for use as fragrance materials.

Table 6.1 Measured intensity thresholds of select benzodioxepinones

Compound	Quantitative data: intensity thresholds (ng/L)*
24	6.0
28	1.28
65	16
***rac*-66**	82
***ent*-66**	49
66	79
68	26.5

* Data provided by Philip Kraft and Alain E. Alchenberger, Givaudan
Switzerland AG, Fragrance Research.

6.3   Physicochemical properties relevant to odour intensity

Odour molecules must be transmitted to the odour receptor in the gaseous state. The weaker the intermolecular attractive forces of a substance, the more readily a substance will exist in the gas phase. The greater the extent to which a substance exists in the gas phase the higher the vapour pressure of that substance.

Vapour pressure values can be used to estimate the probability that a substance will possess favourable volatility as a fragrance. The vapour pressure of a substance is the pressure exerted at dynamic equilibrium between gas and liquid states of a substance. Vapour pressure increases exponentially with temperature according to the following formula:

$$\textbf{Log p = -0.05223a/T + b}$$

p is the vapour pressure

T is the absolute temperature

a and b are constants

When the vapour pressure of a substance equals the surrounding atmospheric pressure, the boiling point of that substance is reached [8]. A typical vapour pressure curve as a function of temperature is presented in Figure 6.3.
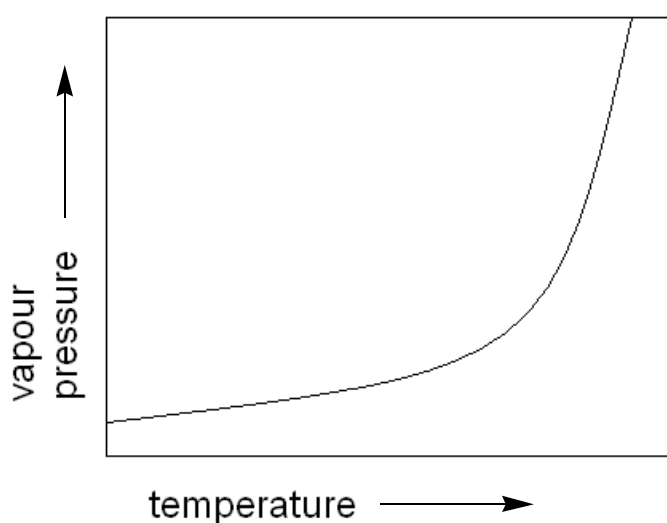
Figure 6.3 Exponential curve depicting the relationship between vapour pressure and increasing temperature for a substance

A linear calibration relationship exists when ln P is plotted against 1/T, with a negative slope equal to $-\Delta Hvap/R$. Heats of vapourisation values can be derived from the slope of the line, just as temperatures or vapour pressures can be read or extrapolated from the line. The enthalpy of vapourisation and the vapour pressure of a substance can be related by the Clausius-Clapeyron equation [9] by substituting ΔH_{vap} into the equation above:

$$\textbf{Ln P = -}\Delta\textbf{H}_{\textbf{vap}}\textbf{/RT + c}$$

T is the absolute temperature

R is the gas constant ($8.314 J.mol^{-1}.K^{-1}$)

ΔH_{vap} is the enthalpy of vapourisation per mole of substance

C is a constant.

This equation can also be written as:

$$p = p° \exp[-\Delta H / R(1/T - 1/T°)]$$

p° is a known vapour pressure

T° is the known temperature (K)

T is the temperature for the vapour pressure to be calculated

p is the vapour pressure at a given temperature.

At a given temperature, the higher the vapour pressure, the more potent the odour of that substance is likely to be, if functional and conformational characteristics comply. The fragrant compound cineole has a vapour pressure of 2 mmHg (at 25°C) [10], which is comparatively high in the context of fragrance properties, and is reiterated by its potent odour properties. Many musk compounds exhibit volatility and odour potency 5 orders of magnitude (~0.4 mmHg) smaller than this [10]. The vapour pressure of **1** is predicted at a lower value than expected considering the measured intensity threshold (0.031ng/L). Taking the vapour pressure of **1** as a relative standard, we can draw conclusions on the predicted vapour pressures for the rest of the data set in combination with the empirical olfactory observations presented in Table 6.3, Table 6.4, Table 6.6 and Table 6.7. Referring to Table 6.2, the vapour pressures calculated predict that **67**, **69**, **70**, **74**, **23** and **25** would exhibit the most potent odours of the set.

Table 6.2 Some physical parameters of energy optimised benzodioxepine(on)e models [11] [12]

	Structure	LogP (n-octanol/water partition coefficient)	Boiling Point (°C)*	Vapour pressure (mmHg)+	Enthalpy of Vapourisation (± 3.0) (kJ/mol)
1		0.74	305 ± 41	0.00083	55
23		0.74	298 ± 39	0.0013	54
24		0.46	317 ± 42	0.00039	56
25		0.32	284 ± 29	0.0029	52
26		0.28	377 ± 42	0.0000067	62
27		0.22	364 ± 42	0.000017	61
28		2.2	323 ± 42	0.00026	56
29		1.4	393 ± 31	0.0000020	64
65		1.3	354 ± 41	0.000012	63
66		1.1	305 ± 41	0.00035	58
67		2.4	295 ± 40	0.0027	51
68		1.6	355± 42	0.000032	60
69		2.4	246 ± 25	0.044	46
70		2.9	265 ± 25	0.015	48
71		1.7	311 ± 41	0.00057	55
72		3.6	410 ± 44	0.00000058	66
73		2.4	329 ± 41	0.00017	57
74		0.6	284 ± 39	0.0029	52

* at 760 mmHg

+ at 25°C

The data presented in Table 6.2 were all derived from computational calculations with ACD I-Lab and Chem3D. If the vapour pressure and boiling point data were considered independently from logP and enthalpy of vapourisation values, all of the aforementioned odourants are shown to be stronger in odour than **1**. Compound **22** was found to exhibit a weak odour both at room temperature (blotter) and at its boiling points (GC-O). Compounds **69**, **70** and **25** exhibited moderate odour potency at room temperature but increasingly potent with application of heat. Compound **23** was also moderate at room temperature and then clearly detectable with heat, however a small degree weaker in odour than **69**, **70** and **25** from the olfactory port.

When atmospheric temperature (T) increases, vapour pressure (Ln P) increases, and the heat required for vapourisation (ΔH_{vap}) will therefore decrease. The less heat energy required to vapourise one mole of a substance, the more readily that substance will exist in the gas phase and the greater its potential as an odourant. Bearing in mind the large error associated with the predicted ΔH_{vap} values ($\pm$ 3.0 kJ/mol) and the small deviation in values, it would be inaccurate to make any definitive conclusions other than highlighting that the values complement the trends exhibited by the vapour pressure and boiling point data.

The potency and substantivity (longevity) of an odourant are dependent on a few physicochemical parameters. At a constant concentration, a plot of temperature vs odour potency (as distinguished from odour intensity) would be unique for each substance, as depicted inFigure 6.4. Some may remain level as their detectability remains level (A), others may increase gradually perhaps over a wider temperature range (B), and others may increase rapidly and then level out (C). Note that sensory adaptation is not relevant here, as the data points would be derived at separate intervals at increasing temperatures.
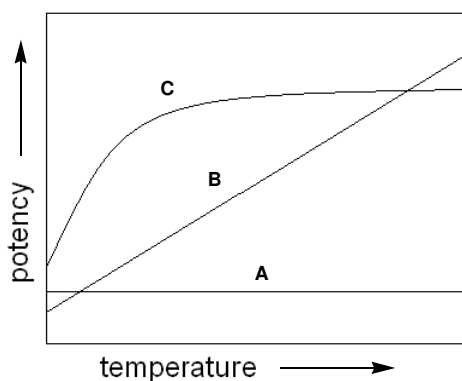

Figure 6.4 Examples of odourant potency levels with increasing temperature

Odour potency is directly linked to volatility. Volatility is intimately linked with the molecular mass of an odourant, however other factors also contribute, including polarity. The n-octanol-water partition coefficient (logP) provides an indication of molecular polarity encompassing intermolecular forces such as dipole-dipole energies, dispersion forces and potential hydrogen bonding. LogP values close to 1 provide the best predictive power equating to a powerful odourant. As logP rises beyond 2-3 (increasingly lipophilic), the odour becomes weak and indiscriminate. Less than 1 (increasingly hydrophilic) the odour becomes barely detectable or non-existent, as illustrated in Chapter 1, Section 1.3.5. Compound **1** evidently exhibits an ideal logP value, which is confirmed by its potent odour. Based on these observations, compound **74**, and potentially **65**, **66**, and **29** should exhibit the most potent odours. Surprisingly, compounds **65** and **66** and **29** were reported as weak odourants, and **27** relatively weak. Compound **74** exhibited a stronger odour than most others in the group. Displacement of the aromatic methyl with an aromatic *t*-butyl introduced one of the strongest odourant compounds of the group (**28**) (as confirmed by its intensity threshold), along with introduction of bromine *ortho* to the methyl (**23, 68**). The clear oils of **69**, **70** and **73** emanated some of the strongest odours of the group, more so with the application of heat, and also demonstrated the highest tenacity in conjunction with **28** and **68**. The logP value of 2.4, 2.9 and 2.4 respectively, particularly for the former two, demonstrates their higher lipophilicity. This alludes to the possibility of the bonding olfactory receptor type possessing increased affinity for hydrophobicity through presence of hydrophobic pockets. Perhaps the degree of polarity on the heterocyclic ring of **1** is limited to a carbonyl when considering introduction of oxygenated functionality. The weakening in odour of compounds **65**-**67** and **71**-**72**, and **22** with a methyl ester, support this proposal. The logP value for compound **23** was predictably calculated to match that of **1** with the only structural change a movement of the aromatic methyl from the *meta* to the *ortho* position. This movement resulted in a decrease in odour potency, so the *meta*-position seems to be the most powerful in relation to substitution for odour activity.

6.4 Qualitative data: olfactory odour descriptors
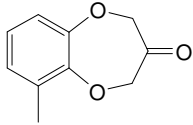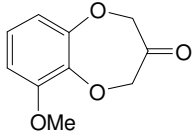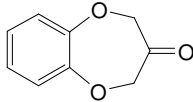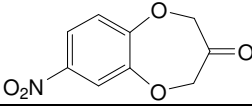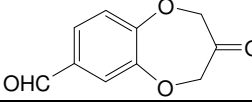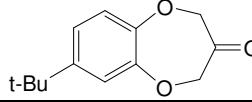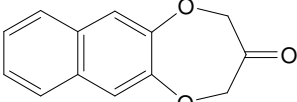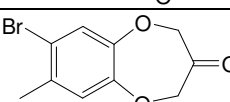
Comparison of GC-O and blotter methods for qualitative analysis revealed the applicability of both. GC-O is effective in removing trace impurities from the odour detected, as demonstrated in comparing the two results for compound **66** where residual yeast character is detected in the blotter analysis from the experimental method. Blotter methods allow assessment of the full accord capabilities of a fragrant compound from top

(initial perception) to base (after 1-2 hours), and reveals the tenacity of the odourant (after 24 hours). Slightly different odour aspects may also arise from the increased temperatures required in the GC-O method.

Increased or rapid oven temperature programs can be utilized for faster elution of peaks for olfactory work with GC-O. However as sample matrix complexity increases, so does co-elution of components leading to erroneous olfactory analysis. Temperature programs should incorporate a period around the maximum temperature limit to ensure all odour-active residues have been removed from the column prior to the next run. The professional analysis provided here is compared with the data derived by novice olfactory panelists for all analogues synthesized, followed by a graphical representation of the professional olfactory characteristics for clarity. Discrepancy between non-professional feedback and professional data is not necessarily attributable to false recognition by the un-trained panel. In most cases it is merely a lack of expansive knowledge of established olfactory linguistics. For this specific reason it is informative to compare a diverse collective of olfactory evaluation for a given odourant. The consumer is a novice, and would generate more basic cognitive impressions of an odourant when analyzing a fragrant consumer product. However, professional olfactory analysis is fine-tuned over years of experience and evidently invaluable to odour assessment and characterisation.

6.4.1   Benzodioxepinone analogues 23-29, 68

Table 6.3 Benzodioxepinone analogue olfactory data (**23-29**, **68**)-blotter analysis

	Compound	Qualitative olfactory data[a]
23		Fresh, floral-aldehydic odour of green and woody-marine tonality
24		Sweet-spicy, green-marine, floral, slightly earthy, walnut-like nuances, relatively weak
25		Green-floral, balsamic odour in the direction of Peru and Tolu balsam resinoid, a slight marine salty aspect
26		Fruity-spicy, balsamic odour with a slight woody inflection and a distant powdery-vanillic sweetness, weak
27		Sweet, powdery scent reminiscent of vanilla with a spicy-balsamic undertone
28		Fresh, marine, ozony odour, a green and walnut-like nuance, slightly floral
29		Oily, floral-green, and a slightly metallic odour, a very weak watery-floral, Calone-like inflection, weak
68		Marine-ozony, ethereal, walnut-like odour, with salty aspects and a floral-fruity, geranium-like inflection, slightly earthy

a) Data provided by Philip Kraft and Alain E. Alchenberger, Givaudan

Switzerland AG, Fragrance Research using compounds synthesised by the present research.

Table 6.4 Benzodioxepinone analogue olfactory data (23-29, 68)-GC-O analysis

Compound	Collective qualitative data: olfactory descriptors
23	Marine, mint, citrus
24	Marine, musty, green, vanilla, earthy
25	Sweet, creamy soda, buttery, slightly salty
26	Alcoholic, sweet
27	Leafy, woody, sandalwood, lavender, eucalyptus
28	Marine, floral, vanilla
29	Lemon, pepper, young fresh wood
68	Salty, fresh wood, green, leafy

[*] Data derived from four panellists, RMIT University

Both GC-O and blotter assessments revealed green and marine tonalities for compound **24**. The odour of Peru and Tolu balsam typically exhibit rich sweetness, so the mention of these in Table 6.3 complies with the generalised sweet note in Table 6.4. Both groups detected a slight salty aspect for compound **25**, and both parties detected sweet aspects for compound **26**. The spicy-balsamic odour recorded (Table 6.3) could easily be equivalent to the Australian recognition of a eucalypt inflection (Table 6.4). Both panels perceived marine and floral nuances for **28**. Comparison of the descriptors for compound **29** reveals a common recognition of saltiness. In conjunction, the geranium odour noted in Table 6.3 could likely correspond to the green and leafy aspects presented in Table 6.4.

Table 6.5 Graphical depiction of olfactory characteristics of compounds **23-29**, **68**, black: present, grey: present but weak (based on **Table 6.3**)

Compound		23	24	25	26	27	28	29	75
6.4.1.1.1	R^1	Me	OMe	H	H	H	H	H	H
	R^2	H	H	H	NO_2	CHO	^tBu	C_6H_4 (*face*)	Me
	R^3	H	H	H	H	H	H	-	Br
marine		■	■	▨			■	▨	■
green		■	■	■			▨	■	■
floral		■	▨	■			▨	■	■
aldehyde		■							
woody/earthy		■	■						
nutty			■				■		■
fruity					■				■
vanillic					■	■			
balsamic					■	▨			
metallic								▨	
salty									■
oily								■	
spicy					■				

Table 6.5 demonstrates that a large portion of the synthesised analogues maintained the original marine odour attribute of **1**, namely **23**, **24**, **28** and **68** and to a lesser extent **26** and **27**. In all cases the odour threshold was increased compared to **1**, indicated by a low perceived potency for the range. Aromaticity, particularly as benzylic functionality, as for

72, is prevalent in compounds used for their fragrant properties. The patent released by Pfizer allocated a general olfactory assessment of "watermelon green" to a range of benzodioxepinone compounds including **25** and **28** of this manuscript. Compound **25** and **29** exhibit similar odour profiles concordant with their comparable molecular attributes: a benzene and a naphthalene respectively. The green note is preserved, however the marine aspect is weakened for both structures, indicating the importance of aromatic substitution to the typical Calone 1951® olfactory character. Interestingly complete absence of substitution converts the fragrance emanated to a sweet array by reference to balsam of Peru and Tolu. The nitro and formyl derivatives **26** and **27** both displayed individual olfactory characteristics. The marine character is completely removed in both cases, with introduction of fruity, sweet, balsamic tonalities, with a hint of spiciness for **26**. The presence of vanilla in the accord of analogue **27** is rationalised in comparison with Heliotropin (Figure 6.5), with smaller ring size and absence of a ketone moiety Heliotropin possesses a strong aldehydic, vanilla fragrance.
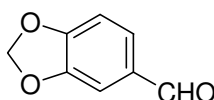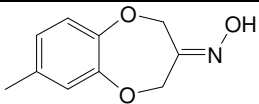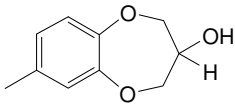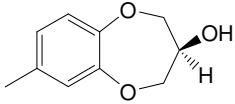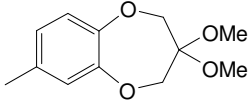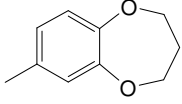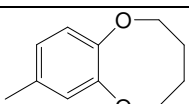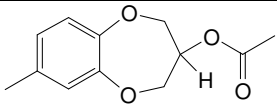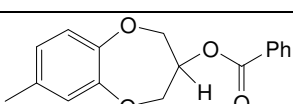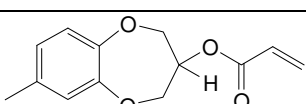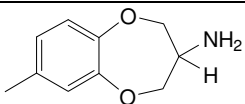
Figure 6.5 Piperonal (Heliotropin)

The steric bulk introduced by *t*-butyl and bromine groups (**28** and **68**), and the methoxy group in the *ortho* position of **24** may contribute to the walnut/nutty inflections perceived. Compound **68** serves as an interesting comparison, understandably maintaining the marine aspect as the entire molecular skeleton of **1** is preserved for this analogue. The marine odour is steered in a more salty direction, accompanied by floral notes, as also often detected in the headspace from **1**. To preserve the characteristic Calone 1951® odour, substitution is not restricted to the *meta*-position as demonstrated when comparing compounds **23**, **24**, **27** and **29**. The type of functionality present on the ring, rather than positioning, is more active in deconstructing the marine odour character, exhibited by the qualitative assessment of **25**, **26** and **27**.

6.4.2   Benzodioxepine analogues 65-67, 69-74

Table 6.6 Benzodioxepine analogue olfactory data (**65-67, 69**-**74**)-blotter analysis

Compound		Qualitative olfactory data[a]
65		Fresh, marine-ozony odour with a green nuance, slightly aldehydic, weak
rac- **66**		Marine, ozony, aldehydic, fruity-floral nuances, weak
ent- **66**		Food-like and yeast-type character, and a fishy, butyric and valeric nuance, weak
67		Marine, ozony, watery, floral-green facets and a metallic character, weak
69		Naphthalinic, balsamic-sweet, spicy-medical odour in the direction of guaiacol, green-floral, vanilla-type nuances
70		Sweet, powdery, balsamic, aromatic odour in the direction of origanum and thyme oil, a slightly woody and marine inflection and slight spicy nuances
71		Floral-balsamic, slightly green, spicy and smoky facets, with a woody inflection, weak
72		Salty, green with spicy-balsamic, slight floral-marine, weak
73		Chemical, fruity, green and garlic-like, marine, woody and smoky-leathery inflections
74		Marine, green-mossy, with medicinal, animalic and slightly woody facets

[a] Data provided by Philip Kraft and Alain E. Alchenberger, Givaudan Switzerland AG, Fragrance Research by blotter analysis.

Table 6.7 Benzodioxepinone analogue olfactory data (**65**-**67**, **69**-**74**)-GC-O analysis

Compound	Collective qualitative data: olfactory descriptors
65	Port, alcohol, syrup, nutty, woody, caramel, rich, sweet
rac-**66**	Weak, icing sugar, sweet, vanilla, lemon rind, cinnamon, slight wood, slight green
ent-**66**	Sweet, sugary, candy, estery, coconut, methanol, slight mint
67	Weak, green, bergamot, marine, fresh, grass, slight floral
69	Woody, estery, coconut, tropical, cherry, sarsaparilla
70	Sweet, vanilla
71[+]	Fresh, balsamic vinegar, unripe fruit, mustard, horseradish, slight aniseed
72[+]	Weak, chemical, methanol with a sweet inflection
73[+]	Rubbery, plastic, slight woody
74	Slight marine, dirt-like, fishy

[+] Summarised GC-O data from four panellists, RMIT University

+ Blotter analysis only

As an illustration the spicy medical odour detected in Table 6.6 could be the same attribute perceived as a sarsaparilla-type odour in Table 6.7. Likewise the descriptor list for compound **71** is a good example of recognition of the same odour defined differently; the odour of balsamic and horseradish would be reasonably difficult to discriminate in the absence of visual or verbal clues. Both parties detected the animalic notes for **74** and similarly, preservation of the marine character for **67** was recognised by both. The term 'chemical' is a broad descriptor and can often overlap with medicinal, alcoholic and naphthalinic. The denotation 'sweet' is likewise multi-faceted, and 'fresh' not easily defined with more specific terminology, however an odour can be undeniably 'fresh'.

Upon attempted distillation of **70**, the glassware was left smelling potently of rich vanilla for many days proving the tenacity of the fragrance. The heating conditions of the distillation were replicated (50-80°C/0.5 mmHg) for both **69** and **70** and headspace analysis (t_R: 12.03, 13.27 min respectively) confirmed the purity, stability and odour preservation of both compounds. No decomposition products or polymerised material were evident at higher temperatures. Unfortunately this enhancement of odour was not reported upon prolonged analysis at ambient temperatures by blotter. Nevertheless heat-

resistant, especially heat-enhanced odourants in the absence of significant co-decomposition are novel.

Magnolan® presents another hetero di-oxygenated species with an aromatic component in the form of a benzene ring. This compound exhibits a floral, rose odour character. Interestingly the racemate (Figure 6.6) features an additional marine nuance [13]. Comparing this structure to the discoveries made from our SOR analysis, we can conclude that the heteroatom oxygens contribute a marine inflection in the absence of the ketone.

Figure 6.6 Magnolan®
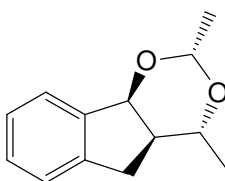
It was suspected very early on that the carbonyl moiety was essential to the unique odour attributes exhibited by Calone 1951®. This became increasingly evident as more analogues were evaluated for their olfactory properties. Exposed ketones are generally reactive, and olfactory interaction is no exception by evidence gathered from potent odour compounds containing a ketone moiety.

Table 6.8 Graphical depiction of olfactory characteristics of compounds **65-67, 69-74**, black: present, grey: present but weak (based on Table 6.6)

Compound	65	66	67	69	70	71	72	73	74
R^1	NOH	OH	OMe	H	H	O_2CMe	O_2CPh	O_2CCHCH_2	NH_2
R^2		H	OMe	H	H	H	H	H	H
n				1	2				
marine	■	■	■		▨	▨	▨	▨	■
ozone	■	■	■			▨	▨		
green	▨		▨	▨	▨	▨	■	■	■
aldehyde	▨	■							
floral		▨	▨	▨	■	▨			
fruity		▨	▨					■	■
chemical				■	■			■	■
spicy				■	▨	▨	■		
balsamic				■	■	■	■		
woody					▨	▨		▨	▨
herbal				■					
smoky						▨	▨	▨	▨
salty							■		
garlic								■	
metallic		▨							
sweet				■	■				
medicinal				■	■				▨
animalic									▨

Referring to Table 6.8 a few olfactory-based conclusions can be drawn. Maintaining an electron rich oxygen moiety with altered connectivity and hybridisation allowed assessment of how C-3 substitution alters the familiar marine odour character of the parent species. The marine tonality remains detectable upon removal of the carbonyl, in addition more dominant accords begin to arise such as aldehydic, sweet, and floral-fruity. Most notable is the transition from a potent odour (0.031ng/L) [14] to an undeniably weak odour for both compounds **65** and **66**. It seems the olfactory receptor binding site pocket is quite specifically delineated for a ketone on the cyclic portion, with an sp^2 to sp^3 conversion perhaps contributing to the potent-weak alteration of the odour intensity. Products **65-67** demonstrate that replacement of the cyclic ketone with functionality of similar electronegativity but differing connectivity results in a dramatic decrease in intensity. As oxime groups are effective at binding glyco-compounds and peptides [15] one would predict **65** as a potent odour analogue. This was not the case, and our observation suggests that the introduction of the hydroxyl substituent at the polar region of

the molecule may generally result in a perceptible weakening of the odour. The slightly higher odour potency of **66** and **67** with sp³ hydroxy and acetal substituents respectively suggests the receptor binding pocket exhibits conformational selectivity.

Absence of functionality on the ether ring of **69** and **70** introduces a perceptible sweet nuance to the accord, with the larger cyclic portion of **70** providing a slight increase in spiciness. Compound **69**, the C-3 methylene analogue of **1**, was completely devoid of marine character, drawing a direct correlation between C-3 substitution and marine odour. The 8-membered ring (compound **70**) features a marine nuance, although MM2 and PM3 energy minimised models of **70** suggest a non-planar ring conformation unlike 7-membered variants **65**-**67**, **69** and **71-73**. Synthesis of **71**-**73** allowed geometric considerations when contemplating olfactory changes from the introduction of steric bulk on the oxygenated portion of the ring. Replacement of the ketone with a carboxylic methyl (**71**) or benzyl (**72**) ester weakens overall olfactory properties. As an exception, **73** possessed moderate-strong odour potency, possibly explained by the terminal vinyl group. The presence of allyl and vinyl groups typically result in odour-active compounds, such as the strong fruity herbal-green odour of allyl ionone (Figure 6.7).
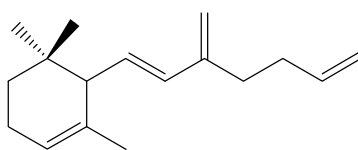
Figure 6.7 Allyl α-ionone

Despite contrasting R groups, the acyl attachments of **71**-**73** altered perceived qualitative characteristics by introduction of more pronounced green, spicy-herby and smoky connotations. It is worth noting the contrast in molecular make-up, yet collective balsamic odour attribute of acetylated and benzylated derivatives **71** and **73**, and alicyclic compounds **69** and **70**. With a molecular weight of 284 the benzoyl analogue, **72**, borders on the molecular weight limit of 300 for an odourant molecule, providing further reasoning for the decreased potency.

Primary and secondary amines are prevalent as food components and less utilised in perfumery. The medicinal, animalic nuances for compound **74** were therefore expected for the amine analogue. Amines are typically potent odourants, although odour activity becomes increasingly indiscriminate as molecular size increases. In the absence of the oxygen functionality, an sp² oxygen is replaced with an sp³ primary amine for **74**, further

illustrating the correlation of marine character to small C-3 substituents. In conjunction with compounds **65**-**67**, compound **74** unexpectedly preserves the marine character.

6.5 Conformational considerations

Fragrance chemistry research has repeatedly revealed that in conjunction with functional group classification, the constitutional nature of a molecule plays a significant role in olfactory receptor recognition and hence the odour emanated from a particular compound.

Computational chemistry is based on quantum mechanical (QM) methods. QM methods predict that spatial distribution of atoms is based on the corresponding energies of component nuclei and electrons. These potential energies (charges) and motions govern the relationship between the substructures. The simplest basis for QM theory is the Schrödinger equation:

$$H\psi = E\psi$$

where H is the Hamiltonian operator

ψ is the electronic wave function, incorporating electron motion and position

e is the energy associated with a particular electron [12]

which is applied to 1 electron-1 nucleus systems. The states of an electron form orbitals associated with that atom. These states can be overlapping to form orbitals of different character. When normalized, the square of the wave function denotes the probability of an electron existing in a particular state.

$$\int \Psi^2(r)dr = 1$$

where r = radius (x, y and z)

These probabilities then represent the atomic orbitals and their energies. The forces of interaction of a molecule can also be termed the potential energy surfaces (PES) of a molecule, and semi-empirical (SE) QM methods aim to calculate these. PES outcomes and the resulting structural and chemical information vary depending on the SE method chosen. Geometry optimization is achieved via SE methods that aim for a molecular conformation where the net forces of the molecule sum to zero [12].

Energy minimized structures provide the optimal geometry of a given molecule taking implicit limitations of the applied computational method into consideration. By modifying the atomic coordinates the favourable geometry of the molecule is the most likely conformation that the molecule adopts in space. Computational modelling can be segregated into two main categories, each based on a different energy framework, *ab initio* and semi-empirical. *Ab initio* is undeniably more advanced and reliable, however the inherent complexity means that SE can be more appropriate particularly in the case of simple organic molecules such as those presented here. Both methods present individual advantages and limitations, and some forces such as dispersion forces are not as yet captured accurately by either method. Most SE methods exclude valence electrons from the energy calculations, whereas *ab initio* involve all nuclei and electrons for the zero-point iterations. With SE methods some factors are approximates or completely omitted, however SE makes up for this by thorough parameterisation. Parameterisation involves a relative standard, such as experimental data or an *ab intitio* construct, allowing SE methods to generate more accurate parameters.

SE methods compute energies based on thermodynamic (heat of formation) values. Even alongside the existence of *ab initio*, SE methods are often preferable for generation of molecular geometry. Due to the lack of extensive basis functions for SE calculations general forces such as dispersion and van der Waals are not accurately reported. The Austin Model 1 (AM1) and Parameterisation Method 3 (PM3) are two of the more advanced and specialized SE systems. Both have superseded MNDO methods in the SE family. MNDO was a MOPAC program first released in 1983 [16]. MNDO, AM1 and PM3 are all classified as Neglect of Diatomic Differential Overlap (NDDO) systems developed by Dewar and colleagues [16]. AM1 can struggle with optimization of halogen atoms, and nitrogen parameterisation may be inaccurate. A high degree of charge localization can detrimentally affect heat of formation estimations, and hydrogen bonds can adopt distorted orientation. Overall PM3 is more advanced than AM1, for example heats of formation values are found to be more precise. Hydrogen bond angles are more accurately predicted, however hydrogen bond energies derived with AM1 have been found to be more exact. Non-bonded distances can be underestimated, although on average PM3 predicts bond lengths and bond energies more accurately than AM1 [12].

A molecule has only one attainable global energy minimum, which can probably be termed the absolute minimum. However, dependent on the initial conformation a number of other local minima can be reached that the selected potential energy function can deem

as the absolute minimum energy conformer. Energy changes are duplicated until a favourable minimal energy gradient between increments is reached. This corresponds to iterative determination of energy derivatives and resultant geometrical optimization. Accuracy of optimization can therefore be achieved by manipulation of the energy gradient. A 'saddle point' is a higher energy molecular geometry of the PES in the vicinity of two low energy minima. At this point the slope of the surface is zero. To eradicate the chance of minimization resulting in a saddle point a molecular dynamics simulation can be run prior to SE energy optimization. Molecular dynamics (MM2) combines kinetic simulation with thermodynamic control based on Newtonian law. In contrast to heat of formation derivatives calculated by SE, molecular dynamics computes algebraically-derived energy values that represent the difference between conformations.

6.5.1   A comparative study with conformational data by Archer and Claret [17]

Configuration can play a large part in determining odour character and potency. We noticed with SE models generated with Chem3D V8.0 (MM2 and PM3 optimised) that aromatic substitution of the benzodioxepinone system has a significant influence over the geometric conformation the heterocyclic ring adopts. The dependence of perceptible 1D NMR shift differences of benzodioxepinones, **23-29, 68**, on functional group class and positioning supported this. Archer and Claret [18] published results on angle of twist (θ) along the bond between the aromatic ring and the heteroaromatic oxygen atoms by extinction coefficient UV absorption readings indicative of $\pi \rightarrow \pi^*$ transitions. Their modelling investigations led to the conclusion that the heterocyclic portion of the benzodioxepinone skeleton preferred either a more stable, rigid chair form or a flexible skewed pseudo twist-boat conformation. They state conversion to the boat conformation is only adopted by a negligible percentage of the compound due to steric constraints.

Compound **22** features similar odour characteristics to **1** only weaker. The low potency is surprising considering the prevalence of methyl ester functionality in odour-active compounds. Enolisation of either of the two carbonyls of **22** (Figure 6.8) and potentially the cyclic ketone carbonyl of **23-29, 68** would be evident by the enol proton appearing as a singlet shifted further downfield than the keto-tautomer. Higher coupling constants for the methylene protons would also result. The OCH_2 signals are split into AB quartets by asymmetrical substitution at C-3.
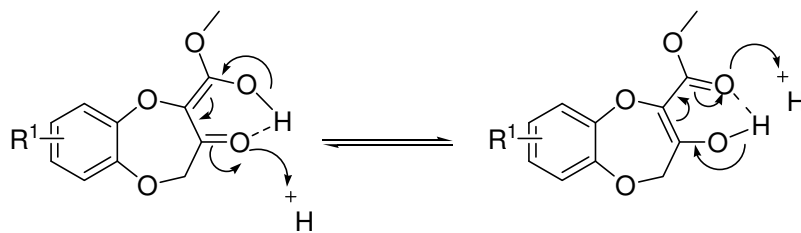
Figure 6.8 Keto-enol tautomerism of 3,4-Dihydro-7-methyl-3-oxo-2*H*-1,5-benzodioxepine-2-carboxylate

Archer and Claret noticed in an aprotic solvent (CCl$_4$) the β-keto ester intermediate adopts a chair conformation stabilised by intramolecular H-bonding, with enolisation of approximately 20% of the compound. Conversely in an alternative aprotic solvent, DMSO, suppression of the enol form occurs, recognised through conversion of the AB quartet of the methylene to a singlet. They claim the β-keto-ester is stabilised to a boat conformation. Our basic modelling confirmed a chair conformation with the heteroatom oxygen atoms lying planar with the aromatic ring (Figure 6.9).
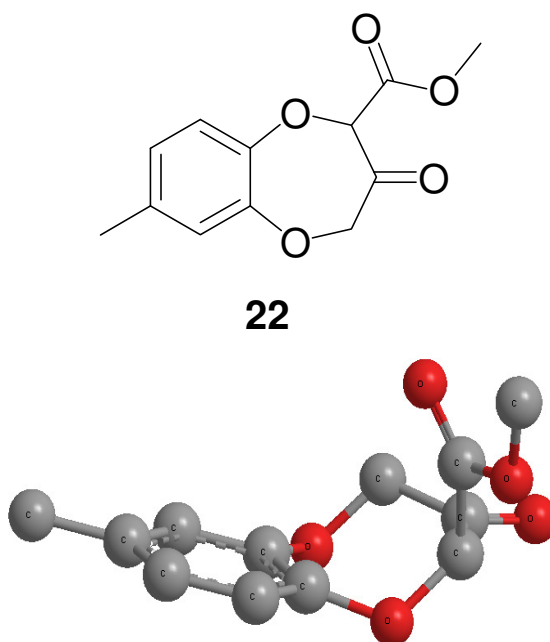

22

Figure 6.9 3,4-Dihydro-methyl 7-methyl-3-oxo-2*H*-1,5-benzodioxepine-2-carboxylate (**22**)

Archer and Claret analysed angle of twists via extinction coefficients of benzodioxepine compounds of ring size 5-7 carbons with various aromatic substitutions of the C–7 and C–8 positions including bromine, nitro, methyl and acetyl groups and concluded that no correlation existed between ring size and angle of twist for these compounds, however made no further conclusions. From the shift differences for equivalent functionalities in

our NMR results (see Chapter 2) and modelling discoveries we postulate that aromatic functional group substitution can have a significant effect on heterocyclic ring conformation of the benzodioxepinone skeleton.

Archer and Claret analysed aromatic-substituted cyclopropane compounds, those featured that are common to our research include *ortho*-methyl (**23**), *meta*-Me (**1**), *meta*-Br (**68**), and pyro (**25**). No correlation between ring size (n = 1-3) and extinction coefficient was noticed for the nitro derivative. They reported that 1,4-benzodioxan (shown in Figure 6.10) adopts a skew conformation and the 3,4-dihydro-2*H*-1,5-benzodioxepin (**25**) conformer adopts chair geometry.
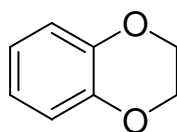

Figure 6.10 1,4-Benzodioxane

In conjunction the eight-membered tetrahydrobenzodioxocin (**70**) takes on a symmetrical skew conformation and the homologous 7-membered heterocyclic ring undergoes conformational interconversion via a boat form. An increase in absorption value may result from the introduction of a non-polar substituent in the 3-position, which they state would encourage the molecule to adopt the skew conformation. Introduction of polar substituents in the same position means dipole interactions must also be attributed to the overall conformational preference of the molecule.

Interestingly they also studied the spiro benzodioxepine, later synthesised by Jamrozik and colleagues in 1994 (see Chapter 3, Section 3.1), and found that both heterocyclic rings of the structure prefer to adopt a chair conformation.

6.5.2   MM2 (molecular mechanics) and PM3 (MOPAC) optimised conformational models

A selection of exemplar models have been chosen from the conformational models derived with SE methods for the data set of benzodioxepin(on)es synthesised. Hydrogen atoms are excluded.

The presence of an electron-donating substituent in the *meta*-position (**1**, **28**) or the *ortho*-position (**23**, **24**) generally results in a planar conformation as that shown in Figure 6.10. The heterocyclic oxygen atoms providing the only true non-planar deviation at a bond angle of 115Å for *meta*-methyl (**1**), *ortho*-methyl (**23**), and *meta-t*-butyl (**28**) analogues. Conformer **24** with an *ortho*-methoxy group deviates slightly at 114Å. In the absence of aromatic substitution, analogue **25** also adopts the chair-type conformation, likewise featuring an oxygen bond angle of 115Å. Introduction of a bromine substituent (**68**) has minimal effect on the rigid chair conformation adopted by **1**, also exhibiting a bond angle of 115Å at the heterocyclic oxygen atoms. The varied odour characteristics of **68** indicate that the olfactory receptor site also perceives the aromatic section of the molecule.
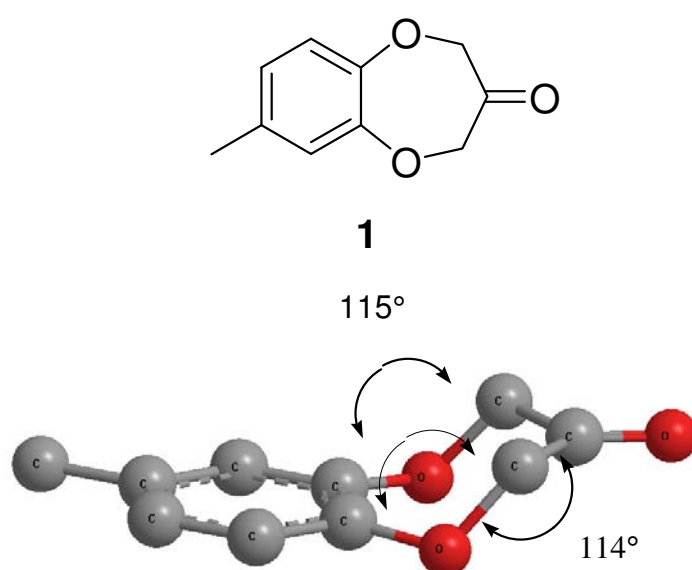

1

115°

114°

Figure 6.11 Semi-empirical energy-minimised conformational model of **1**

The molecular conformation presented in Figure 6.11 reveals why **1**, **68**, **24**, and to a degree **25** easily exist as crystalline solids. Interestingly at 97% purity **23** readily solidifies below approximately ≤5°C, however exists as clear oil at room temperature.

Energy-optimised models of **1**, **23-28**, **68**, **71**, **73** all featured hetero-aromatic oxygen atoms that adopted a similar angle of direction within the group. By superimposing the two heteroatom oxygens (the planar aromatic ring directly perpendicular to the plane of the page) the oxy-carbons adopt the same directional bond angle as the formyl derivative depicted in Figure 6.14. All compounds of this group exhibit a bond angle of 115° other than **24** with an angle of 114°.

Analogue **66** adopts a peculiar configuration, resembling a scorpion tail (Figure 6.12). Comparison of this geometry to that depicted in Figure 6.18 (**71-73**), indicates that introduction of steric bulk on the hydroxy oxygen preserves the twist conformation as opposed to analogue **66** locking the structure into the geometry shown.
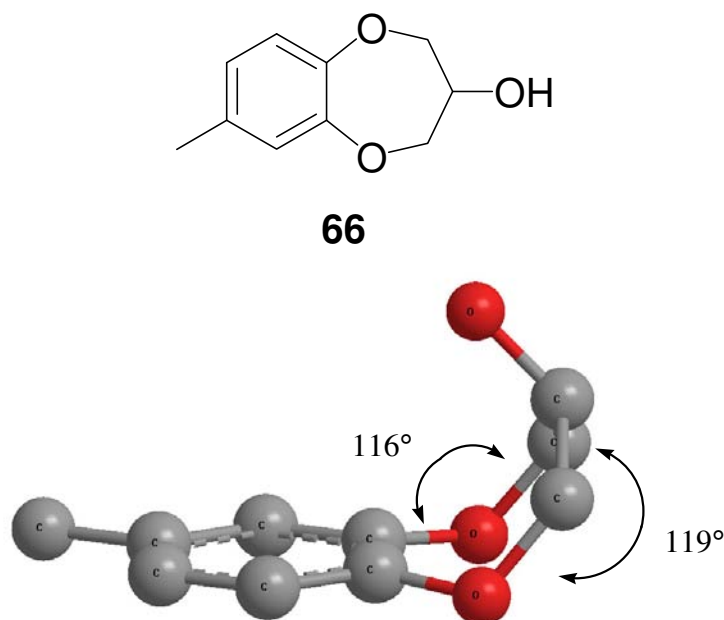

66

Figure 6.12 Semi-empirical energy-minimised conformational model of **66**

This configuration provides more reasoning for the evident decrease in olfactory character of **66** in comparison to **1**. A conformation such as that presented in Figure 6.12 can be equivalent to steric bulk, as the configuration translates to restricted accessibility within the binding pocket, possibly minimising the number of receptors able to detect the molecule and hence weakening the odour.

The influence of planarity from the aromatic ring of **66** on the conformation of the heterocyclic ring becomes evident on analysis of structure **29** (Figure 6.13). Conformer **29** resembles **66** with slight asymmetry in angle. Strangely compounds **66** and **29** do not share any distinct olfactory characteristics other than floral and marine notes detected at room temperature, and woody facets detected with GC-O.
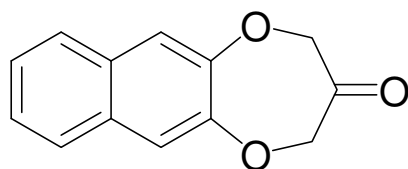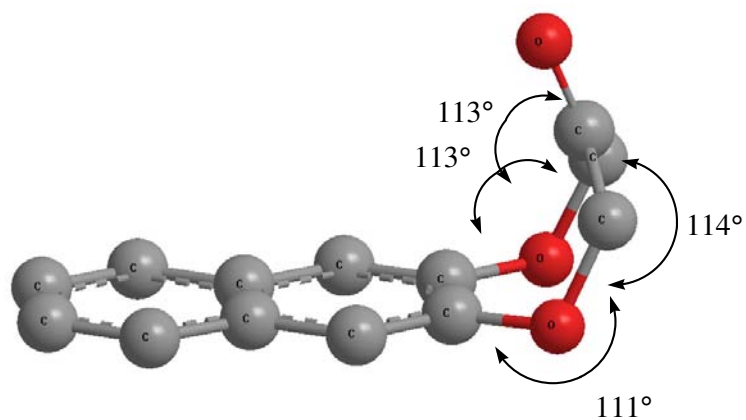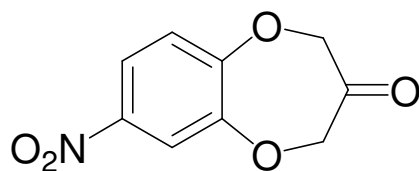
29

Figure 6.13 Semi-empirical energy-minimised conformational model of **29**

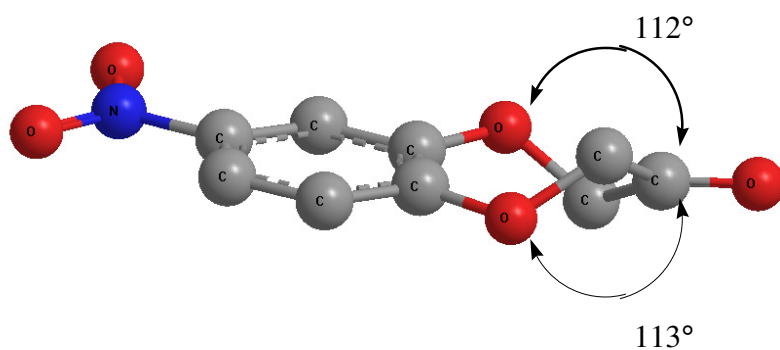Introduction of a *meta*-nitro substituent (Figure 6.14) causes the molecule to adopt skew conformation.

26

Figure 6.14 Semi-empirical energy-minimised conformational model of **26**

The pseudo-twist configuration of compound **26** features oxygen atoms that lie planar with the aromatic ring, with both oxy-carbons and the carbonyl angled in the same direction. The direction of the oxy-carbons of the heterocyclic ring occurs *anti* at 112° and 113°.

The formyl derivative (**27**) shown in Figure 6.15 adopted a chair conformation similar to the ED analogues, in apparent contrast to the twist conformation assumed by its EW counterpart, **26**. Chemically and physically, analogues **26** and **27** are completely alike as demonstrated by their reactivity in our experimental research, however the distinction in conformation is concordant with the differences in blotter and GC-O olfactory evaluation between the two compounds.
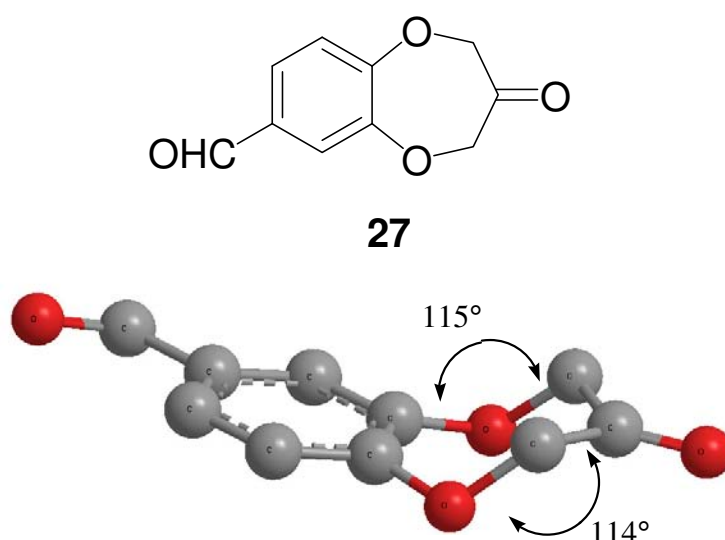

27

Figure 6.15 Semi-empirical energy-minimised conformational model of **27**

Conformer **69** (Figure 6.16) adopts a similar configuration to that of **70** (Figure 6.17), as expected in light of Archer and Claret's discoveries, an additional carbon in the cyclic structure results in pseudo twist-boat geometry.

69
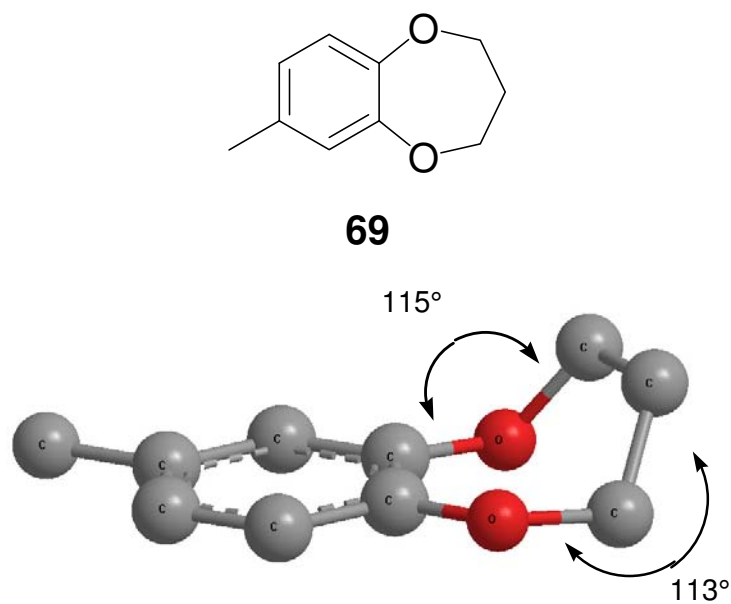
Figure 6.16 Semi-empirical energy-minimised conformational model of **69**

Comparative to other benzodioxepines, **69** and **70** are undeniably similar in odour character. Table 6.3 and Table 6.4 reveal that at ambient temperature, the sweet characteristics of **69** seem to be more prominent, whereas with heating the rich vanilla character of **70** is more pronounced.
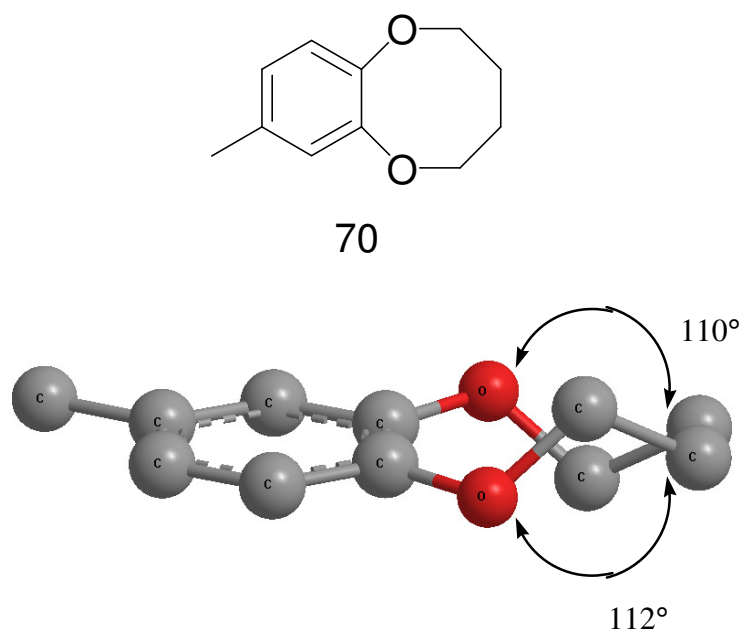

70

Figure 6.17 Semi-empirical energy-minimised conformational model of **70**

This skew conformation demonstrated by **69** and **70**, similar to **26** seems synonymous with the introduction of balsamic, fruity, spicy, sweet and slightly woody odour modalities and weakening of the marine, ozone type inflections.

For compounds **67**, **74**, **72**, **69**, **70**, **26** and **65** the heterocyclic oxygens can be superimposed and the aliphatic ring methylenes (oxy-carbons) adopt bond angles in opposing directions by approximately the same magnitude, best illustrated in Figure 6.14 or Figure 6.16. For **65**, **67** and **74** both *anti* angles orient at 113°. The benzoyl group causes *anti* ring geometry unlike **71** and **73**, featuring angles 112° and 114°. With absence of the carbonyl, such as for **69**, the ring converts from a symmetrical chair to pseudo twist with opposing angles of 113° and 114°. The eight-membered benzodioxecine exhibits equivalent *anti* angles of 110°. Introduction of an aromatic nitro group deflects the angles at 112° and 113°. The geometry prediction for **74** and **26** may not be completely accurate due to a decreased compatibility of SE methods for nitrogen-derived functional groups.
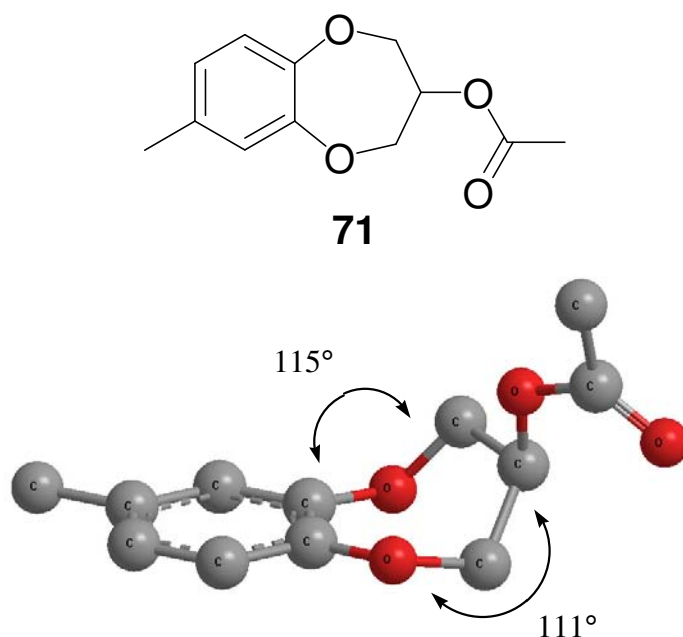

71

Figure 6.18 Semi-empirical energy-minimised conformational model of **71**

The conformation adopted by **69**, with no C-3 substitution suggests that these structures have maintained the configuration of the parent compound, **1**, and makes apparent that substitution introduced at this position bears minimal influence on geometry, unless the

substitution introduces significant steric bulk as in the form of a phenyl group with **72** leading to geometry resembling **70** and **26**. At ambient temperature **71** (Figure 6.18), **72** and **73** maintain a green aspect to the odour emitted. Woody and smoky inflections are introduced to **71** and **73**, however **71** and **72** share common floral and balsamic notes. Overall Table 6.3 reveals individual odour profiles for **71**, **72** and **73**.

6.6   Conclusion

Overall, ^{1}H and ^{13}C NMR assignments largely correspond with the trends observed for the predicted configurations adopted by the above structures. Some unexpected exceptions to this were, for example, the conformation of structure **29**, which one would expect to resemble structure **1** due to the planarity of the aromatic region and which NMR assignments support, however the predicted structure is much more closely related to **66**.

Structures **26** and **27** both correspond closely to the structure of **1** with the exception of the type of substituent present on the aromatic ring. It is therefore interesting that the ^{1}H methylene shifts of **27** more closely match **1** ($\sim$ 4.7 ppm) as does its predicted conformation. Structure **26** on the other hand has methylene shifts appearing further downfield ($\sim$ 4.9 ppm) and whose configuration mirrors the more flexible structure of **70**. This is most likely due to the stronger resonance of the nitro and hence the protons of **26** will be more deshielded.

The C-3 carbon of both structures **69** and **71** are sp^3 hybridised although the secondary nature of **71** would explain the lower field deshielded ^{1}H and ^{13}C signals. J1 splitting for the protons of the C-2 and C-4 methylenes of **71** is much greater as a result, indicated by the higher coupling constant ($J1$ = 12.8 Hz) in comparison with **69** (J = ~5.2 Hz).

Please refer to Tables 2.6 and 4.2 for a broader summary of relevant ^{1}H and ^{13}C assignments provided for comparison with the geometric models predicted in this chapter.

Odour potency aside, the benzodioxepine(on)e data set provides a favourable array of marine-based odourant molecules. The intensity thresholds and odour potency in general was disappointing, however the odour characters provided valuable information for marine-odour analogues from which further syntheses can be designed. Conclusions from correlating vapour pressure predictions with odour activity and generation of SE-

optimised conformers allude to the high stereospecificity of the receptor site delineated for detection of **1**. The blotter analysis provided kindly by Philip Kraft and Alain Alchenberger is the initial step in an intensive assessment for odourant applicability. When a multi-step comprehensive odour evaluation isn't feasible, the choice of evaluation should be based on the potential application of the odourant, eg. incorporation into washing powders would demand a higher degree of heat resistance, and if possible the odourant should be tested over a temperature range.

6.7 References

[1] J. Boeckh, Odor Specificity and Reaction Range of a Single Olfactory Receptor Cell. Theor. Odor Odor Meas. Proc. (1968) 213-226.

[2] M.G. Beets, The Molecular Parameters of Olfactory Response. Pharmacol. Rev. 22(1) (1970) 1-34.

[3] S. Firestein, C. Picco, A. Menini, The Relation Between Stimulus and Response in Olfactory Receptor Cells of the Tiger Salamander. J. Physiol. (Oxford, U.K.) 468 (1993) 1-10.

[4] S.P. Firestein, C.; Menini, A., The Relation Between Stimulus and Response in Olfactory Receptor Cells of the Tiger Salamander. J. Physiol. (Oxford, U.K.) 468 (1993) 1-10.

[5] L. Turin, A Spectroscopic Mechanism for Primary Olfactory Reception. Chem. Senses 21(6) (1996) 773-791.

[6] M. Talbot, The Holographic Universe, Harper Collins Publishers, Great Britain, 1996, p. 18.

[7] P. Kraft, J.A. Bajgrowicz, C. Denis, G. Frater, Odds and Trends: Recent Developments in the Chemistry of Odorants. Angew. Chem., Int. Ed. 39(17) (2000) 2980-3010.

[8] T.L.B.H.E.L.J.B.E. Burston, Chemistry. The Central Science, Prentice-Hall International, New Jersey, U.S.A., 1997, p. 402.

[9] T.L. Brown, H.E. LeMay Jr., B.E. Burston, Chemistry. The Central Science, Prentice-Hall International, New Jersey, U.S.A., 1997, p. 402.

[10] K.D. Perring, in: D. H. P. C. S. Sell (Ed.), The Chemistry of Fragrances, The Royal Society of Chemistry, Cambridge, U.K., 1999, pp. 188-201.

[11] Advanced Chemistry Development. ACD/I-Lab, V8.02.

[12] Chem3D. CambridgeSoft, V8.0.

[13] A. Abate, E. Brenna, G. Fronza, C. Fuganti, S. Ronzani, S. Serra, Enzyme-mediated Preparation of Chiral 1,3-Dioxane Odorants. Helv. Chim. Acta 86(3) (2003) 592-606.

[14] P. Kraft, W. Eichenberger, Conception, Characterization and Correlation of New Marine Odorants. Eur. J. Org. Chem.(19) (2003) 3735-3743.

[15] S. Vonhoff, T.D. Heightman, A. Vasella, Inhibition of Glycosidases by Lactam Oximes. Influence of the Aglycon in Disaccharide Analogs. Helv. Chim. Acta 81(9) (1998) 1710-1725.

[16] K.B. Lipkowitz, D.B. Boyd, Reviews in Computational Chemistry, Vol. 2, VCH Publishers, U.S.A., 1991, p. Chapter 8.

[17] A.W. Archer, P.A. Claret, D.F. Hayman, The Conformation of 3,4-Dihydro-2*H*-1,5-benzodioxepin, and its Derivatives as Determined from their Ultraviolet Absorption Spectra. J. Chem. Soc. B: Phys. Org. 6 (1971) 1231-1240.

[18] A.W.C. Archer, P. A.; Hayman, D. F., The Conformation of 3,4-Dihydro-2*H*-1,5-benzodioxepin, and its Derivatives as Determined from their Ultraviolet Absorption Spectra. J. Chem. Soc. B: Phys. Org. 6 (1971) 1231-1240.

7   Experimental Procedures

Molecular model calculations were performed using Density Functional Theory, as implemented in the Dmol^3 program package. The PBE function was used in combination with the DNP basis set (Double Numerical plus Polarisation). All calculations were all-electron and spin-restricted. Each model was charge neutral. The geometry of each model was optimised, without constraints. Electron density maps, HOMOs and LUMOs were calculated for the relaxed structures.

Microwave experiments were performed in a prototype microwave applicator "MDV2.4" and 0-700 W variable power microwave source (2m172) [1]. IR: Perkin-Elmer Spectrum 2000 Fourier transform IR spectrophotometer. NMR: Bruker Avance 300 (300 MHz) spectrometer, Varian Gemini 200 (200 MHz) spectrometer, referenced to TMS with the solvent resonance as the internal standard ($CHCl_3$: 7.26 ppm) unless otherwise stated. MS: Hewlett Packard 6890 GC with BPX-5 column/5973 Mass Selective Detector. Semi preparative HPLC: Varian Prostar (Model 210), with Phenomenex column (250 x 10 mm, 5u ODS (3)). Separation was achieved using $MeCN:H_2O$ (33:67) at 3.5 mL/min flow rate, with UV-Vis detection. FC: Merck Silica gel 60 (0.040-0.063µm). TLC: Merck Kieselgel 60 F_{254} (particle size 5-40 µm, layer thickness 0.2 mm on aluminium, 20 × 20 cm); visualisation: UV   254 nm. Optical Rotation: Carlzeiss Jena Circle Polarimeter, 32-G580c, 200mm cell, instrument error: 100% EtOH, α = -0.3°. Potassium *tert*-butoxide and methyl bromoacetate were supplied by Merck. Otherwise, all reagents were obtained from Aldrich Chemical Co. and used without further purification. THF was dried over CaH_2, followed by distillation from Na/benzophenone. DMF was dried over CaH_2, followed by distillation onto molecular sieves (4Å). NMR data reported in the procedural section were derived from the Bruker Avance XWin software and MestRe-C$^©$ 2.3a. NMR spectra labels were derived with MestRe-C$^©$ 2.3a software only.

7.1 General Procedure A for Preparation of Calone 1951® (1) and Analogues

7.1.1 Preparation of 1

Methyl 2-[2-(2-methoxy-2-oxoethoxy)-4-methylphenoxy] acetate (**21**)

Conventional method: Ground, oven-dried K_2CO_3 (9.00 g, 65.12 mmol) and methyl bromoacetate (6.0 mL, 63.38 mmol) were added sequentially to a solution of **23** (2.00 g, 16.11 mmol) in anhydrous DMF (100 mL). The solution was heated to 120°C for 2 hr then the hot mixture was poured into ice/H_2O (200 mL) and extracted with DCM (3 × 100 mL). The combined organic portions were washed with 5% aqueous NaOH (2 × 50 mL) followed by H_2O (2 × 50 ml) and dried over $MgSO_4$. Concentration *in vacuo* yielded yellow oil which was purified by vacuum column chromatography through a short silica gel column, initially washed with pentane then eluted with EtOAc:pentane with a 1:9-3:7 gradient. Evaporation was followed by bulb distillation to afford **21** as a white solid (3.37 g, 78%), m.p. 43-44°C.

Microwave procedure: Reagents were combined as in the conventional procedure and the solution was irradiated for 4 min at 200 W under a nitrogen atmosphere. Work-up of the reaction mixture was performed according to the conventional procedure providing **21** in good yield (3.60 g, 83%).

3,4-Dihydro-methyl 7-methyl-3-oxo-2H-1,5-benzodioxepine-2-carboxylate (**22**)

Under an inert atmosphere, a solution of **21** (3.72 g, 13.88 mmol) in anhydrous THF (35 mL) was added over 5 minutes to a stirring mixture of KO^{t}Bu (3.11 g, 27.71 mmol) in anhydrous THF (35 mL) cooled in an ice/H_2O bath. The reaction solution was then transferred to an oil bath at 70°C and heated for 30 minutes before quenching in a stirred mixture of HCl (200 mL, 0.2M) in ice (200 g) The acidic solution was extracted with DCM (3 × 100 mL) and the combined organic layers were washed with H_2O (2 × 150 mL). Concentration in vacuo provided **22** as viscous yellow-brown oil (3.00 g, 92%) consisting of a mixture of regioisomers and required storage at -20°C. After prolonged storage, purification by column chromatography on silica gel (hexane:EtOAc, 1:1) was necessary prior to use.

7-Methyl-2*H*-1,5-benzodioxepin-3(4*H*)-one (**1**)

To a solution of **22** (1.00 g, 4.24 mmol) in EtOH (10 mL) was added 2M HCl (50 mL) and the solution heated at 90°C with stirring in an oil bath. After 2 hr the reaction mixture was poured into ice/H_2O (100 mL) and extracted with DCM (3 × 100 mL). The combined organic extracts were washed with H_2O (1 × 200 mL) then dried over $MgSO_4$ and concentrated *in vacuo* to leave a brown semi-solid. Bulb distillation (0.5mmHg/70°C) provided **1** as a crystalline white solid (0.59 g, 78%), m.p. 38-39°C (lit. 38-40°C [35]).

7.1.2   Preparation of 23

Methyl 2-[2-(2-methoxy-2-oxoethoxy)-3-methylphenoxy] acetate (**21a**)

Conventional procedure: Similar to **21**, the **23** protocol involves reaction of **20a** (1.00 g, 8.05 mmol) to form **21a**. Purification involved bulb distillation (160°C/0.4mmHg) twice, which gave the product as clear pale yellow oil (1.99 g, 92%).

Microwave procedure: Following the irradiation procedure outlined for **21**, **20a** (0.50 g, 4.03 mmol) was employed as substrate to form **21a**. Purification by vacuum column chromatography through a short silica gel column, initially washed with pentane then eluted with EtOAc:pentane using a 1:9-3:7 gradient, followed by bulb distillation (180°C/0.5mmHg) to yield a clear/pale yellow oil (0.39 g, 36%). IR (neat), ν (cm^{-1}): 3002m, 2955s, 2853m, 2112w, 1774s, 1749s, 1646w, 1604m, 1587m, 1488s, 1440s, 1380m, 1304m, 1262m, 1183m, 1114m, 1070m, 1027m. ^{1}H NMR (300MHz, CDCl$_3$): δ: 6.89-6.60 (3H, m, H-4', -5', -6'), 4.69 (2H, s, 1''-CH$_2$), 4.60 (2H, s, 2-CH$_2$), 3.74 (3H, s, 3''-OMe), 3.72 (3H, s, 3-OMe), 2.28 (3H, s, Ar-Me); ^{13}C NMR (75MHz, CDCl$_3$): δ : 169.9 (2''-CO), 168.9 (1-CO), 149.8 (C-1'), 145.9 (C-2'), 132.3 (C-3'), 124.1 (C-4'), 123.7 (C-5'), 111.5 (C-6'), 69.0 (1''-CH$_2$), 65.6 (2-CH$_2$), 51.6 (3-, 3''-OMe), 15.8 (Ar-Me). EIMS *m/z*: 268 (M$^{+\bullet}$, 16.4%), 209 (4.6), 207 (3.3), 195 (10.6), 176 (11.3), 163 (12.5), 149 (14.6), 135 (75.5), 121 (3.2), 109 (16.6), 91 (18.9), 77 (20.8), 65 (16.6), 63 (5.5), 59 (9.4), 51 (10.0), 45 (100).

3,4-Dihydro-methyl 6/9-methyl-3-oxo-2*H*-1,5-benzodioxepine-2-carboxylate (**22a**)

Compound **21a** (1.00 g, 3.73 mmol) was reacted according to the procedure outlined to give **22a** (0.72 g, 82%) as a caramel-coloured oil. IR (neat), ν (cm^{-1}): 3474m, 2956s, 2572w, 1742s, 1677m, 1632w, 1594m, 1477s, 1440s, 1337m, 1274s, 1250m, 1217s, 1202s, 1100s, 1071m, 1045m. ^{1}H NMR (300MHz, CDCl$_3$): δ : *regioisomer 1*: 6.93-6.83 (3H, m, H-7, -8, -9), 5.36 (1H, s, H-2), 4.81 (1H, d, *J* = 16.7 Hz, H-4$_A$), 4.62 (1H, d, *J* =

16.7 Hz, H-4$_B$), 3.86 (3H, s, 1-OMe), 2.22 (3H, s, Ar-Me); *regioisomer 2*: 6.93-6.83 (3H, m, H-7, -8, -9), 5.37 (1H, s, H-4), 4.87 (1H, d, *J* = 16.7 Hz, H-2$_A$), 4.56 (1H, d, *J* = 16.7 Hz, H-2$_B$), 3.85 (3H, s, OMe), 2.28 (3H, s, Ar-Me); ^{13}C NMR (75MHz, CDCl$_3$): δ : *regioisomer 1*: 199.7 (C-3), 165.4 (CO$_2$), 147.1 (C-9a), 145.9 (C-5a), 130.7 (C-6), 125.2 (C-7), 124.0 (C-8), 118.1 (C-9), 81.8 (C-2), 76.4 (C-4), 52.9 (OMe), 15.9 (Ar-Me); *regioisomer 2*: 199.6 (C-3), 165.4 (CO$_2$), 147.3 (C-9a), 145.4 (C-5a), 130.0 (C-6), 126.4 (C-7), 122.8 (C-8), 118.8 (C-9), 81.8 (C-4), 76.4 (C-2), 58.4 (OMe), 18.2 (Ar-Me). EIMS *m/z*: 236 (M$^{+\bullet}$, 100%), 204 (4.5), 177 (21.9), 149 (66.2), 135 (47.6), 121 (22.5), 105 (4.8), 94 (46.7), 77 (27.8), 66 (33.8), 51 (13.5), 39 (18.0).

6-Methyl-2*H*-1,5-benzodioxepin-3(4*H*)-one (**23**)

Compound **22a** (1.02 g, 4.32 mmol) was reacted according to the procedure for **1** to yield a brown oil (0.56 g, 72%) which was bulb distilled under vacuum (0.2mmHg/50-60°C) to afford **23** as a clear oil (0.11 g, 14%). IR (KBr), ν (cm^{-1}): 3024w, 2964w, 2939w, 2906w, 2839w, 1790m, 1738s, 1613w, 1592m, 1492m, 1475s, 1440m, 1419w, 1380w, 1324m, 1296m, 1274s, 1258s, 1205m, 1191m, 1101s, 1080m. ^{1}H NMR (300MHz, CDCl$_3$): δ: 6.86 (3H, broad s, H-7, -8, -9), 4.74 (2H, s, H-4), 4.70 (2H, s, H-2), 2.23 (3H, s, Ar-Me); ^{13}C NMR (75MHz, CDCl$_3$): δ: 205.1 (C-3), 148.4 (C-9a), 146.9 (C-5a), 130.4 (C-6), 125.4 (C-7), 123.0 (C-8), 118.6 (C-9), 75.6 (C-4), 75.5 (C-2), 16.1 (Ar-Me). EIMS *m/z*: 178 (M$^{+\bullet}$, 100%), 150 (5.2), 135 (32.0), 122 (2.3), 108 (4.8), 94 (82.1), 77 (17.0), 66 (76.6), 51 (16.8), 39 (19.2).

7.1.3   Preparation of 24

Methyl 2-[2-methoxy-6-(2-methoxy-2-oxoethoxy)phenoxy] acetate (**21b**)

Conventional procedure: Following the conventional procedure outlined in **21**, **20b** (2.51 g, 17.9 mmol) was esterified to form **21b**. Purification involved bulb distillation (190°C/0.5mmHg) performed twice to give clear oil (3.35 g, 66%).

Microwave procedure: Following the irradiation procedure outlined for **21**, **20b** (0.50 g, 3.57 mmol) was reacted to form **21b**. Purification by vacuum column chromatography through a short silica gel column, initially washed with pentane then eluted with EtOAc:pentane using a 1:9-3:7 gradient, followed by bulb distillation (190°C/0.5mmHg) to yield a clear oil (0.46 g, 45%). IR (KBr), ν (cm^{-1}): 2954w, 2918w, 2843w, 1757s, 1602m, 1499m, 1479s, 1445m, 1397w, 1387w, 1306m, 1259m, 1217s, 1182m, 1125s, 1093m, 1069m. ^{1}H NMR (300MHz, CDCl$_3$): δ: 6.94-6.45 (3H, m, H-4', -5', -6'), 4.65 (2H, s, 1''-

CH$_2$), 4.64 (2H, s, 2-CH$_2$), 3.79 (3H, s, Ar-OMe), 3.75 (3H, s, 3''-OMe), 3.72 (3H, s, 3-OMe); ^{13}C NMR (75MHz, CDCl$_3$): δ: 169.4 (1-CO), 169.1 (2''-CO), 153.3 (C-1'), 151.2 (C-3'), 137.3 (C-2'), 123.8 (C-5'), 107.8 (C-4'), 106.7 (C-6'), 69.5 (2-CH$_2$), 66.6 (1''-CH$_2$), 56.1 (Ar-OMe), 51.6 (3-OMe), 51.6 (3''-OMe).   EIMS *m/z*: 284 (M$^{+\bullet}$, 84.7%), 252 (2.0), 211 (64.0), 192 (11.8), 165 (20.2), 153 (86.8), 137 (9.2), 125 (40.0), 107 (29.2), 95 (32.0), 77 (15.0), 65 (12.0), 51 (15.6), 45 (100).

3,4-Dihydro-methyl 6/9-methoxy-3-oxo-2*H*-1,5-benzodioxepine-2-carboxylate (**22b**)

Compound **21b** (3.32 g, 11.69 mmol) was reacted according to the procedure for **22**. Trituration with EtOH provided **22b** as a white crystalline solid (2.50 g, 85%). m.p. 117-119 °C. IR (KBr), ν (cm^{-1}): 2962m, 2897w, 2847w, 1767s, 1741s, 1596m, 1486s, 1473s, 1441m, 1435m, 1416w, 1345m, 1319m, 1277s, 1259m, 1246m, 1214s, 1204s, 1176s, 1105s, 1080s, 1068m, 1034m. ^{1}H NMR (300MHz, CDCl$_3$): δ: 6.92-6.60 (3H, m, H-7, -8, -9), 5.36 (1H, s, H-2), 4.75 (1H, d, *J* = 16.6 Hz, H-4$_A$), 4.54 (1H, d, *J*= 16.6 Hz, H-4$_B$), 3.88 (3H, s, Ar-OMe), 3.84 (3H, s, 1-OMe); ^{13}C NMR (75MHz, CDCl$_3$): δ: 198.9 (C-3), 164.9 (CO$_2$), 150.9 (C-9a), 148.3 (C-6), 137.0 (C-5a), 122.6 (C-8), 113.4 (C-7), 108.0 (C-9), 82.4 (C-2), 76.9 (C-4), 56.4 (Ar-OMe), 52.9 (1-OMe). EIMS *m/z*: 252 (M$^{+\bullet}$, 97.3%), 209 (16.2), 193 (15.0), 165 (27.8), 151 (29.9), 137 (9.2), 110 (46.1), 95 (100), 79 (18.6), 65 (16.4), 51 (31.3), 39 (53.3).

6-Methoxy-2*H*-1,5-benzodioxepin-3(4*H*)-one (**24**)

Compound **22b** (1.10 g, 4.36 mmol) was solubilized in minimal EtOH/DCM (2:1), and reacted according to the procedure for **1** for 2.5 hr. Aqueous work-up involved neutralisation with NaHCO$_3$ prior to extraction, with final concentration affording white crystals (0.81 g, 95%), m.p. 130-132 °C. IR (KBr), ν (cm^{-1}): 3030w, 2962m, 2897w, 2847w, 1767s, 1740s, 1596m, 1486s, 1474s, 1441m, 1435m, 1415w, 1345w, 1319m, 1277m, 1259m, 1247m, 1214s, 1204s, 1176m, 1105s, 1080m, 1068m, 1034w. ^{1}H NMR (300MHz, CDCl$_3$): δ: 6.94-6.62 (3H, m, H-7, -8, -9), 4.87 (2H, s, H-4), 4.73 (2H, s, H-2), 3.87 (3H, s, Ar-OMe); ^{13}C NMR (75MHz, CDCl$_3$): δ: 204.2 (C-3), 151.5 (C-6), 149.4 (C-9a), 138.4 (C-5a), 122.9 (C-8), 113.1 (C-7), 106.7 (C-9), 76.2 (C-2), 75.6 (C-4), 56.3 (Ar-OMe). EIMS *m/z*: 194 (M$^{+\bullet}$, 100%), 166 (1.6), 151 (63.1), 137 (3.5), 123 (4.9), 110 (32.3), 107 (18.0), 95 (75.0), 79 (9.8), 77 (4.9), 65 (10.1), 51 (15.4), 39 (20.9). High Resolution Mass Spectrum (HRESI) Found [M + 1]$^{+\bullet}$, 195.0650. C$_{10}$H$_{10}$O$_4$ [M + H]$^{+\bullet}$ requires 195.0657.

7.1.4 Preparation of 25

Methyl 2-[2-(2-methoxy-2-oxoethoxy)phenoxy] acetate (**21c**)

Conventional procedure: Pyrocatechol **20c** (0.50 g, 4.54 mmol) was reacted according to the procedure outlined for **21** to form **21c**. Bulb distillation (180°C/0.05mmHg) performed twice afforded the product as a white solid (1.01 g, 88%), m.p. 44-48°C.

Microwave procedure: Following the irradiation procedure outlined for **21**, **20c** (2.00 g, 18.16 mmol) was reacted to form **21c**. Bulb distillation (160°C/0.5mmHg) performed twice provided the product as a white solid (2.24 g, 48%), m.p. 44-48°C. IR (KBr), ν (cm^{-1}): 3012w, 2961m, 1752s, 1708w, 1596m, 1507s, 1456m, 1434m, 1372m, 1334m, 1275m, 1233s, 1197s, 1180s, 1163m, 1138s, 1088w, 1068m, 1020w. ^{1}H NMR (300MHz, CDCl$_3$): δ: 6.94-6.86 (4H, m, H-3', -4', -5', -6'), 4.71 (4H, s, 1''-, 2-CH$_2$), 3.77 (6H, s, 3-, 3''-OMe); ^{13}C NMR (75MHz, CDCl$_3$): δ: 169.3 (1-, 2''-CO), 147.9 (C-1', -2'), 122.6 (C-4', -5'), 115.3 (C-3', -6'), 66.5 (1''-, 2-CH$_2$), 52.1 (3-, 3''-OMe). EIMS m/z: 254 (M$^{+\bullet}$, 32.0%), 222 (2.3), 193 (9.8), 162 (33.0), 149 (2.8), 135 (14.2), 121 (29.5), 107 (2.1), 95 (9.9), 77 (16.4), 63 (7.7), 52 (10.2), 45 (100).

3,4-Dihydro-methyl 3-oxo-2*H*-1,5-benzodioxepine-2-carboxylate (**22c**)

Compound **21c** (3.65 g, 14.37 mmol) was reacted according to the procedure for **22** to give **22c** as pale brown oil (2.78 g, 87%). IR (neat), ν (cm^{-1}): 3472m, 2956m, 1746s, 1682m, 1634w, 1594m, 1494s, 1456m, 1439s, 1396w, 1338m, 1273s, 1250m, 1228s, 1157m, 1106m, 1081m, 1025m. ^{1}H NMR (300MHz, CDCl$_3$): δ: 7.11-6.95 (4H, m, H-6, -7, -8, -9), 5.36 (1H, s, H-2), 4.82 (1H, d, J = 16.8 Hz, H-4$_A$), 4.60 (1H, d, J = 16.8 Hz, H-4$_B$), 3.85 (3H, s, OMe); ^{13}C NMR (75MHz, CDCl$_3$): δ: 199.3 (C-3), 165.2 (CO$_2$), 147.2 (C-5a), 147.0 (C-9a), 125.0 (C-7), 123.6 (C-9), 121.4 (C-8), 120.5 (C-6), 81.8 (C-2), 76.8 (C-4), 52.9 (OMe). EIMS m/z: 222 (M$^{+\bullet}$, 99.4%), 190 (6.3), 163 (16.7), 146 (3.0), 135 (100), 121 (61.0), 107 (23.7), 92 (4.2) 91 (4.0), 80 (52.5), 77 (38.5), 69 (10.8), 65 (26.0), 63 (26.0), 52 (41.5), 43 (30.5).

2*H*-1,5-Benzodioxepin-3(4*H*)-one (**25**)

Compound **22c** (0.65 g, 2.93 mmol) was reacted according to the procedure for **1** in EtOH/DCM (2:1) to give a yellow-brown residue (0.45 g, 94%). Trituration of the semi solid residue with DCM provided **25** as a white crystalline solid (0.05 g, 10%), m.p. 64-65°C. IR (KBr), ν (cm^{-1}): 3408w, 2957m, 1741s, 1631m, 1586w, 1495s, 1459w, 1303m, 1263s, 1181w, 1153w, 1097m, 1052s, 1025m. ^{1}H NMR (300MHz, CDCl$_3$): δ: 6.90 (4H, s, H-6, -7, -8, -9), 4.08 (4H, s, H-2, -4); ^{13}C NMR (75MHz, (CD$_3$)$_2$CO): δ: 204.3 (C-3), 152.2

(C-5a, -9a), 124.9 (C-7, -8), 122.7 (C-6, -9), 79.4 (C-2, -4). EIMS *m/z*: 164 (M$^{+\bullet}$, 100%), 136 (2.0), 121 (27.3), 108 (9.6), 94 (2.6), 80 (75.4), 63 (12.8), 52 (27.5), 32 (22.4).

7.1.5   Preparation of 26

Methyl 2-[2-(2-methoxy-2-oxoethoxy)-4-nitrophenoxy] acetate (**21d**)

Conventional method: Nitrocatechol **20d** (0.50 g, 3.22 mmol) was reacted according to the procedure previously outlined [8] to form **21**. Purification by vacuum column chromatography through a short silica gel column, initially washed with pentane then eluted with EtOAc:pentane using a 1:9-3:7 gradient, followed by bulb distillation (215°C/0.1mmHg) provided **21d** a bright yellow solid (0.51 g, 53%).

Microwave method: Preparation using irradiation heating methods with **20d** (0.50 g, 3.22 mmol) as discussed in this manuscript provided **21d** in (0.71 g, 74%), m.p. 84-86°C.

 IR (KBr), ν (cm^{-1}):   3087w, 2960w, 1757s, 1590w, 1520m, 1505m, 1437w, 1373w, 1347m, 1309w, 1286m, 1242w, 1207s, 1174m, 1145w, 1109m, 1085m, 1062m. ^{1}H NMR (300MHz, CDCl$_3$): δ: 7.93-6.85 (3H, m, H-3', -5', -6'), 4.83 (2H, s, 2-CH$_2$), 4.80 (2H, s, 1''-CH$_2$), 3.82 (3H, s, 3-OMe), 3.81 (3H, s, 3''-OMe); ^{13}C NMR (75MHz, CDCl$_3$): δ: 168.3 (1-CO), 168.1 (2''-CO), 153.0 (C-1'), 147.4 (C-2'), 142.2 (C-4'), 118.7 (C-6'), 113.0 (C-5'), 109.8 (C-3'), 66.1 (2-CH$_2$), 66.0 (1''-CH$_2$), 52.5 (3-OMe), 52.4 (3''-OMe). EIMS *m/z*: 299 (M$^{+\bullet}$, 22.0%), 267 (9.7), 240 (10.2), 207 (4.7), 194 (8.2), 180 (15.4), 166 (16.3), 151 (3.0), 135 (4.8), 120 (5.9), 107 (5.3), 92 (2.8), 79 (16.6), 63 (9.5), 51 (13.4), 45 (100), 30 (3.0).

3,4-Dihydro-methyl 7/8-nitro-3-oxo-2*H*-1,5-benzodioxepine-2-carboxylate (**22d**)

Compound **22d** (0.71 g, 2.37 mmol) was reacted according to the procedure for **22** to provide crude **22d** as bright red/yellow oil (0.43 g, 68%). Pure **22d** was not isolated from the complex mixture. IR (neat), ν (cm^{-1}): 3413m, 2924s, 2725w, 2255w, 2128w, 1740m, 1645m, 1590w, 1519m, 1460s, 1376m, 1342m, 1278m, 1051s, 1026s, 1005s. EIMS *m/z*: 267 (M$^{+\bullet}$, 100%), 235 (11.1), 207 (22.2), 194 (5.6), 180 (7.6), 166 (28.8), 162 (9.9), 149 (7.7), 134 (65.8), 119 (20.8), 107 (24.2), 101 (6.8), 92 (15.8), 79 (53.4), 77 (17.8), 75 (32.2), 69 (18.9), 65 (11.4), 63 (31.2), 59 (32.4), 53 (23.0), 51 (48.1), 45 (38.1), 39 (13.8).

7-Nitro-2*H*-1,5-benzodioxepin-3(4*H*)-one (**26**)

Compound **22d** (0.81 g, 3.03 mmol) was reacted according to the procedure outlined for **1** for 2.5 hr to give a brown semi-solid (0.28 g). The sample was purified by semi-preparative HPLC (t$_R$ = 11.7 min, λ$_{max}$ = 239 nm, 311 nm) to afford **26** as orange oil (16

mg, 2%). IR (KBr), ν (cm⁻¹): 3452w, 3080w, 2925w, 2853w, 1801w, 1736s, 1587m, 1517s, 1491m, 1429w, 1346s, 1315m, 1274s, 1176w, 1122w, 1098w, 1080w, 1036m. ^{1}H NMR (300MHz, CDCl$_3$): δ: 8.03-7.11 (3H, m, H-6, -8, -9), 4.98 (2H, s, H-2), 4.91 (2H, s, H-4); ^{13}C NMR (75MHz, CDCl$_3$): δ: 202.1 (C-3), 153.7 (C-9a), 147.9 (C-5a), 143.3 (C-7), 121.3 (C-9), 119.8 (C-8), 117.6 (C-6), 76.3 (C-4), 75.3 (C-2). EIMS m/z: 209 (M$^{+•}$, 100%), 193 (2.3), 167 (4.1), 166 (3.5), 163 (3.5), 151 (14.1), 135 (15.0), 120 (4.0), 107 (55.3), 105 (7.9), 90 (2.8), 79 (37.1), 77 (12.3), 75 (14.1), 63 (11.9), 51 (22.8). High Resolution Mass Spectrum (HRESI) Found [M]$^{+•}$, 209.0325. C$_9$H$_7$O$_5$N [M]$^{+•}$ requires 209. 0324.

7.1.6 Preparation of 27

Methyl 2-[4-formyl-2-(2-methoxy-2-oxoethoxy)phenoxy] acetate (**21e**)

Formylcatechol **20e** (1.00 g, 7.24 mmol) was reacted under microwave irradiation according to the procedure previously outlined [8] to form **21e**, which was twice purified by bulb distillation (210°C/0.1mmHg) to give a white solid (1.61 g, 79%). Preparation using conventional heating methods as discussed in this manuscript provided **21e** in 55%, m.p. 84-86°C. IR (KBr), ν (cm⁻¹): 2957w, 1765m, 1751s, 1682m, 1598m, 1588m, 1520m, 1442m, 1428m, 1404w, 1392w, 1380w, 1340m, 1332m, 1290m, 1218s, 1175m, 1133s, 1080w, 1060m. ^{1}H NMR (300MHz, CDCl$_3$): δ: 9.83 (1H, s, Ar-CHO), 7.50-6.91 (3H, m, H-3', -5', -6'), 4.81 (2H, s, 2-CH$_2$), 4.78 (2H, s, 1''-CH$_2$), 3.80 (6H, s, 3-, 3''-OMe); ^{13}C NMR (75MHz, CDCl$_3$): δ: 190.4 (Ar-CHO), 168.4 (1-, 2''-CO), 152.8 (C-1'), 148.1 (C-2'), 131.0 (C-4'), 126.9 (C-5'), 113.3 (C-6'), 112.6 (C-3'), 65.9 (1''-, 2-CH$_2$), 52.3 (3-, 3''-OMe). EIMS m/z: 282 (M$^{+•}$, 37.8%), 250 (11.4), 223 (7.3), 193 (3.7), 177 (4.7), 163 (18.1), 149 (35.3), 135 (4.1), 119 (8.4), 105 (4.7), 95 (6.2), 77 (11.3), 63 (8.1), 51 (10.1), 45 (100).

3,4-Dihydro-methyl 7/8-formyl-3-oxo-2H-1,5-benzodioxepine-2-carboxylate (**22e**)

Compound **21e** (0.30 g, 1.06 mmol) was reacted according to the procedure for **22** yielding crude **22e** as yellow oil (0.13 g, 50%). Pure **22e** was not isolated from the complex mixture. IR (neat), ν (cm⁻¹): 3425m, 2956m, 2361w, 1742s, 1688m, 1599m, 1509m, 1440m, 1276s, 1212s, 1163m, 1130m, 1063m. EIMS m/z: 250 (M$^{+•}$, not observed), 178 (55.7), 149 (100), 121 (25.3), 108 (0.5), 103 (1.0), 91 (5.8), 79 (6.5), 63 (14.3), 51 (12.0), 42 (7.6).

3,4-Dihydro-3-Oxo-2*H*-1,5-benzodioxepine-7-carbaldehyde (**27**)

Compound **22e** (0.17 g, 0.68 mmol) was reacted according to the procedure given for **1**. Extraction of the reaction solution was performed without $NaHCO_3$ neutralisation to afford yellow oil (0.11g, 85%). The sample was purified by semi preparative HPLC (t_R = 7.8 min, λ_{max} = 270 nm) to afford **27** as a yellow semi-solid (12 mg, 11%). IR (KBr), ν (cm^{-1}): 3437b, 3041w, 2923w, 2852w, 2836w, 2735w, 1802w, 1736s, 1704w, 1683s, 1605w, 1575s, 1508m, 1438w, 1421w, 1383w, 1359w, 1341w, 1314m, 1299m, 1283s, 1269s, 1236w, 1208w, 1162w, 1109w, 1044m, 1027w, 1017w. ^1H NMR (300MHz, $CDCl_3$): δ: 9.85 (1H, s, Ar-CHO), 7.53-7.50 (2H, m, H-6, -8), 7.10 (1H, d, *J* = 8.8 Hz, H-9), 4.79 (2H, s, H-2), 4.71 (2H, s, H-4); ^{13}C NMR (75MHz, $CDCl_3$): δ: 203.0 (C-3), 190.2 (Ar-CHO), 153.5 (C-9a), 148.6 (C-5a), 132.4 (C-7), 126.0 (C-8), 122.7 (C-9), 121.6 (C-6), 76.1 (C-4), 75.2 (C-2). EIMS *m/z*: 192 (M$^{+\bullet}$, 100%), 163 (80.6), 149 (5.9), 135 (13.2), 121 (4.8), 108 (15.3), 91 (3.7), 79 (25.9), 63 (12.3), 51 (19.3), 42 (5.9), 39 (5.4).

7.1.7 Preparation of 28

Methyl 2-[4-(*tert*-butyl)-2-(2-methoxy-2-oxoethoxy)phenoxy] acetate (**21f**)

t-Butylcatechol **20f** (1.00 g, 6.02 mmol) was reacted following the procedure outlined for **21**. Bulb distillation (190°C/0.3mmHg) performed twice afforded **21f** as clear oil (1.40 g, 75%). Preparation using microwave irradiation as discussed in this manuscript provided **21f** in 65%. IR (neat), ν (cm^{-1}): 2908s, 2956s, 2870m, 2111w, 1762s, 1608m, 1592m, 1583m, 1510s, 1440s, 1414m, 1376m, 1364m, 1294s, 1201s, 1153s, 1110m, 1068s, 1028m, 1005m. ^1H NMR (300MHz, $CDCl_3$): δ: 6.96-6.77 (3H, m, H-3', -5', -6'), 4.72 (2H, s, 2-CH$_2$), 4.68 (2H, s, 1''-CH$_2$), 3.78 (6H, s, 3-, 3''-OMe), 1.26 (9H, s, Ar-^{t}Bu); ^{13}C NMR (75MHz, $CDCl_3$): δ: 169.5 (1-, 2''-CO), 147.3 (C-1'), 145.9 (C-2', -4'), 119.4 (C-5'), 114.9 (C-6'), 114.2 (C-3'), 67.2 (2-CH$_2$), 66.7 (1''-CH$_2$), 52.1 (3-OMe), 52.0 (3''-OMe), 34.3 (C$_q$(Ar-^{t}Bu)), 31.3 (Ar-^{t}Bu). EIMS *m/z*: 310 (M$^{+\bullet}$, 23.1%), 295 (100), 222 (2.2), 205 (0.8), 191 (1.0), 177 (4.2), 163 (11.5), 149 (2.7), 133 (4.9), 121 (1.8), 117 (2.4), 105 (3.9), 91 (5.7), 77 (5.2), 65 (1.8), 59 (2.4), 51 (1.3), 45 (32.4).

3,4-Dihydro-methyl 7/8-(*tert*-butyl)-3-oxo-2*H*-1,5-benzodioxepine-2-carboxylate (**22f**)

Compound **21f** (2.42 g, 7.81 mmol) was reacted according to the procedure for **22** to provide **22f** as clear brown oil (1.89 g, 87%). IR (neat), ν (cm^{-1}): 3456m, 2958s, 2870s, 2566m, 2085w, 1741s, 1582m, 1504s, 1473m, 1437s, 1414s, 1364m, 1269s, 1206s, 1149s, 1126s, 1102m, 1079m. ^1H NMR (300MHz, $CDCl_3$): δ: *regioisomer 1*: 7.11-6.94

(3H, m, H-6, -8, -9), 5.40 (1H, s, H-2), 4.82 (1H, d, J = 16.4 Hz, H-4$_A$), 4.60 (1H, d, J = 16.6 Hz, H-4$_B$), 3.87 (3H, s, OMe), 1.28 (9H, s, Ar-^{t}Bu); *regioisomer 2*: 7.11-6.94 (3H, m, H-6, -8, -9), 5.36 (1H, s, H-2), 4.81 (1H, d, J = 17.1 Hz, H-4$_A$), 4.58 (1H, d, J = 16.8 Hz, H-4$_B$), 3.86 (3H, s, OMe), 1.28 (9H, s, Ar-^{t}Bu); ^{13}C NMR (75MHz, CDCl$_3$): δ: *regioisomer 1*: 199.6 (C-3), 165.5 (CO$_2$), 148.5 (C-9a), 146.4 (C-5a), 144.5 (C-7), 120.8 (C-8), 119.8 (C-9), 117.5 (C-6), 81.7 (C-2), 76.7 (C-4), 52.9 (OMe), 34.4 (C$_q$(Ar-^{t}Bu)), 31.3 (Ar-^{t}Bu); *regioisomer 2*: 199.6 (C-3), 165.4 (CO$_2$), 147.2 (C-9a), 145.7 (C-5a), 144.8 (C-7), 121.8 (C-8), 120.6 (C-9), 118.2 (C-6), 81.9 (C-4), 76.8 (C-2), 52.9 (OMe), 34.2 (C$_q$(Ar-^{t}Bu)), 31.3 (Ar-^{t}Bu). EIMS m/z: 278 (M$^{+•}$, 22.5%), 263 (100), 235 (4.8), 219 (3.0), 205 (6.1), 191 (3.4), 175 (4.8), 163 (2.6), 147 (3.8), 133 (2.5), 121 (2.8), 115 (4.2), 105 (3.2), 91 (6.1), 77 (4.7), 65 (1.7), 55 (2.1), 41 (2.5), 32 (4.6).

7-(*tert*-Butyl)-2*H*-1,5-benzodioxepin-3(4*H*)-one (**28**)

Compound **22f** (1.24 g, 4.46 mmol) was reacted according to the procedure outlined for **1** for 2.5 hr with the aqueous work up involving neutralisation with aq NaHCO$_3$ prior to extraction to provide brown oil. The residue was bulb distilled (0.2mmHg/100-105°C) to give a white crystalline solid (0.82 g, 84%), m.p. 66-68 °C. IR (KBr), ν (cm^{-1}): 2965s, 2950m, 2901m, 2868m, 1791w, 1742s, 1577m, 1504s, 1477m, 1461m, 1438m, 1424m, 1409m, 1394w, 1367w, 1359w, 1347w, 1300s, 1274s, 1248m, 1206m, 1189m, 1127m, 1098w, 1045s. ^{1}H NMR (300MHz, CDCl$_3$): δ: 7.02-6.79 (3H, m, H-6, -8, -9), 4.72 (2H, s, H-2), 4.69 (2H, s, H-4), 1.26 (9H, s, Ar-^{t}Bu); ^{13}C NMR (75MHz, CDCl$_3$): δ: 204.9 (C-3), 147.6 (C-9a), 147.4 (C-5a), 145.8 (C-7), 120.7 (C-8), 120.3 (C-9), 117.8 (C-6), 75.7 (C-2), 75.6 (C-4), 34.3 (C$_q$(Ar-^{t}Bu), 31.3 (Ar-^{t}Bu). EIMS m/z: 220 (M$^{+•}$, 25.8%), 205 (100), 177 (11.4), 149 (3.5), 135 (3.9), 121 (4.1), 105 (3.7), 91 (6.8), 77 (7.1), 6.5 (2.8), 55 (2.4), 41 (3.5).

7.1.8   Preparation of 29

5,8-Dihydro-methyl 2-{[3-(2-methoxy-2-oxoethoxy)-2-naphthalenyl]oxy} acetate (**21g**)

The dihydroxy naphthalene **20g** (2.00 g, 12.49 mmol) was reacted to form **21g** according to the procedure outlined for **21**. Purification was achieved by continuous trituration with DCM until an ivory solid appears (3.56 g, 96%), m.p. 78-80 °C. The irradiation method as discussed for **21**, generated **21g** in 75% yield. IR (KBr), ν (cm^{-1}): 2975w, 2953m, 1751s, 1737s, 1629w, 1603w, 1585w, 1510m, 1488s, 1460m, 1447m, 1436m, 1410w, 1380m, 1339w, 1284s, 1247s, 1228s, 1189m, 1168s, 1123m, 1078w, 1047m, 1034w, 1024m. ^{1}H

NMR (300MHz, CDCl$_3$): δ: 7.67 (2H, dd, J1 = 6.1 Hz, J2 = 3.1 Hz, H-5', -8'), 7.35 (2H, dd, J1 = 6.1 Hz, J2 = 3.5 Hz, H-6', -7'), 7.12 (2H, s, H-1', -4'), 4.83 (4H, s, 1''-, 2-CH$_2$), 3.82 (6H, s, 3-, 3''-OMe); ^{13}C NMR (75MHz, CDCl$_3$): δ: 169.1 (1-, 2''-CO), 147.7 (C-2', -3'), 129.5 (C-4a, -8a), 126.5 (C-5', -8'), 124.8 (C-6', -7'), 109.6 (C-1', -4'), 66.2 (1''-, 2-CH$_2$), 52.3 (3-, 3''-OMe). EIMS m/z: 304 (M$^{+\bullet}$, 100%), 272 (7.6), 243 (23.4), 213 (8.0), 203 (5.4), 185 (26.4), 171 (87.0), 147 (5.6), 127 (25.6), 115 (35.7), 102 (24.7), 88 (6.1), 76 (6.0), 63 (5.6), 45 (67.0).

3,4,7,10-Tetrahydro-methyl-3-oxo-2H-naphtho[2,3-b][1,4]dioxepine-2-carboxylate (**22g**)
Compound **21g** (1.39 g, 4.57 mmol) was reacted according to the procedure for **22** to produce **22g** as caramel brown oil (1.16 g, 93%). A portion of this sample was purified by semi preparative HPLC (t_R = 29.9 min, λ$_{max}$ = 230 nm) to give **22g** as a light brown oil (21 mg, 2%). IR (KBr), ν (cm^{-1}): 3453m, 3056w, 2954w, 1744s, 1635w, 1602w, 1505s, 1469s, 1363m, 1277s, 1225s, 1172s, 1117m, 1072m, 1024m. ^{1}H NMR (300MHz, CDCl$_3$): δ: 7.70 (2H, dd, J1 = 6.0 Hz, J2 = 3.2 Hz, H-7, -10), 7.54 (1H, s, H-11), 7.45 (1H, s, H-6), 7.39 (2H, dd, J1 = 6.7 Hz, J2 = 3.1 Hz, H-8, H-9), 5.41 (1H, s, H-2), 4.96 (1H, d, J = 17.1 Hz, H-4$_A$), 4.81 (1H, d, J = 17.1 Hz, H-4$_B$), 3.86 (3H, s, OMe); ^{13}C NMR (75MHz, CDCl$_3$): δ: 199.5 (C-3), 165.3 (CO$_2$), 147.2 (C-11a), 146.5 (C-5a), 131.0 (C-10a), 130.0 (C-6a), 125.7 (C-8), 125.3 (C-9), 126.7 (C-10), 126.8 (C-7), 118.0 (C-11), 116.7 (C-6), 81.7 (C-2), 76.5 (C-4), 53.0 (OMe). EIMS m/z: 272 (M$^{+\bullet}$, 3.4%), 243 (12.0), 213 (5.1), 185 (17.2), 171 (60.7), 157 (2.3), 147 (3.4), 127 (19.2), 115 (27.9), 102 (19.7), 88 (5.6), 76 (5.5), 63 (5.6), 45 (100).

7,10-Dihydro-2H-naphtho[2,3-b][1,4]dioxepin-3(4H)-one (**29**)
Compound **22g** (0.33 g, 1.21 mmol) was solubilized in minimal EtOH/EtOAc (2:1) and reacted according to the procedure given for **1** for 2.5 hr. Quenching of the reaction solution in aq NaHCO$_3$ and work-up as described for **1** gave a brown semi-solid (0.17 g, 65%). A portion of the sample was purified by semi preparative HPLC (t_R = 15.1 min, λ$_{max}$ = 230 nm) to give **22g** as a light brown crystalline solid (18 mg, 7%), m.p. 70-72°C. IR (KBr), ν (cm^{-1}): 3442m, 2960s, 2925s, 2854s, 1737m, 1599w, 1504m, 1470m, 1413w, 1363m, 1330w, 1289m, 1262s, 1169w, 1151w, 1098m, 1046s, 1030s. ^{1}H NMR (300MHz, CDCl$_3$): δ: 7.51 (2H, dd, J1 = 6.4 Hz, J2 = 3.2 Hz, H-7, -10), 7.19 (2H, dd, J1 = 6.4 Hz, J2 = 3.1 Hz, H-8, -9), 7.07 (2H, s, H-6, -11), 4.60 (4H, s, H-2, -4); ^{13}C NMR (75MHz, CDCl$_3$): δ: 204.8 (C-3), 148.2 (C-5a, -11a), 130.4 (C-6a, -10a), 126.7 (C-7, -10), 125.4 (C-8, -9), 117.2 (C-11, -6), 75.4 (C-2, -4). EIMS m/z: 214 (M$^{+\bullet}$, 100%), 186 (5.6), 171 (58.1), 160 (4.5), 142 (1.9), 130 (32.7), 114 (31.9), 102 (62.9), 88 (11.8), 76 (14.6), 63 (19.8), 51

(16.3), 39 (6.6). High Resolution Mass Spectrum (HRESI) Found [M + H]$^{+\bullet}$, 215.0715. C$_{13}$H$_{10}$O$_3$ [M + H]$^{+\bullet}$ requires 215.0629.

7.2 Preparation of a THP-protected Alkylating Agent, 2-[2-Bromo-1-(chloromethyl)ethoxy]tetrahydro-2H-pyran (58)

1-Bromo-3-chloro-2-propanol (**62**)

A 48% HBr solution (28.3 g, 170 mmol) was added dropwise to neat epichlorohydrin (15.0 g, 162 mmol) over a period of 2 hr with rapid stirring. The solution was stirred for an additional 45 min then dissolved in Et$_2$O (150 mL) and washed with saturated NaHCO$_3$ solution (3 × 50 mL). The ethereal layer was dried over MgSO$_4$, evaporated and distilled under vacuum (54-56°C/5mmHg) to yield **62** as clear oil (20.0 g, 71%). IR (neat), ν (cm^{-1}): 3380bs, 2961m, 2894w, 1625w, 1426s, 1382m, 1344m, 1295m, 1261s, 1225m, 1135m, 1088s, 1067s, 1039s. ^{1}H NMR (300MHz, CDCl$_3$): δ: 4.03 (1H, quint., J = 5.3 Hz, H-2), 3.70 (2H, d, J = 5.7 Hz, H-3), 3.56 (2H, d, J = 5.3 Hz, H-1), 2.64 (1H, s, OH); ^{13}C NMR (75MHz, CDCl$_3$): δ: 70.3 (C-2), 46.4 (C-3), 34.7 (C-1). ^{1}H,^{1}H COSY (CDCl$_3$): 3.98 (H-2) × 3.63 (H-3), 3.98 (H-2) × 3.51 (H-1), 3.65 (H-1, -3) × 2.58 (OH). ^{1}H,^{13}C HMQC (CDCl$_3$): H-2 × C-2 (70.5), H-3 × C-3 (46.7), H-1 × C-1 (34.9). EIMS m/z: 172 (M$^{+\bullet}$, not observed), 125 (96.2%), 123 (100), 95 (5.7), 93 (5.6), 81 (17.7), 79 (49.9).

[2-Bromo-1-(chloromethyl)ethoxy](trimethyl)silane (**63**)

TMSCl (13.13 g, mmol) was added to **62** (5.00 g, mmol) in Et$_2$O (100 mL) and allowed to stir at room temperature for 2 hours. The crude mixture was distilled under vacuum 49-50°C/0.5 mmHg) to yield **63** as clear oil (4.90 g, 73%). ^{1}H NMR (300MHz, CDCl$_3$): δ: 3.37-3.30 (4H, m, Cl-CH$_2$, Br-CH$_2$), 3.21-3.20 (1H, m, CH), 0.18 (9H, s, Si(CH$_3$)$_3$); ^{13}C NMR (75MHz, CDCl$_3$): δ: 71.8 (CH), 46.5 (Cl-CH$_2$), 34.5 (Br-CH$_2$), 0.11 (Si(CH$_3$)$_3$). EIMS m/z: 231 (M$^{+\bullet}$, 49.1%), 229 (37.4%), 197 (26.3), 195 (29.3), 174.9 (2.5), 172.9 (1.8), 151.1 (28.1), 139.0 (40.7), 137.0 (39.8), 123.0 (3.5), 109.0 (2.8), 95.1 (38.2), 93.1 (100.0), 75.1 (10.7), 73.1 (70.1), 57.1 (11.9).

2-[2-Bromo-1-(chloromethyl)ethoxy]tetrahydro-2*H*-pyran (**58**)

The alcohol **62** (10.0 g, 57.66 mmol) was added neat to 3,4-dihydro-2*H*-pyran (5.30 g, 63.00 mmol) followed by a catalytic amount of P$_2$O$_5$ (0.10 g, 0.35 mmol). The solution was warmed to 60°C in a water bath for 1 hr then allowed to reach ambient temperature and stirred for an additional hour. The resulting mixture was dissolved in ether (150 mL)

and washed with saturated NaHCO$_3$ solution (3 × 50 mL). The ethereal layer was dried over MgSO$_4$, evaporated and distilled under vacuum (101-102°C/50 mmHg) to yield (**58**) as clear oil (13.5 g, 91%). IR (neat), ν (cm^{-1}): 2940m, 2868w, 2853w, 1437w, 1395w, 1382w, 1344w, 1323w, 1284w, 1261w, 1199m, 1178w, 1148w, 1122m, 1075m, 1054s, 1029s. ^{1}H NMR (300MHz, CDCl$_3$): δ: 4.78-4.77 (1H, m, H-2), 4.06-3.98 (1H, m, CH), 3.92-3.48 (2H, m, H-6), 3.83-3.48 (4H, m, Cl-CH$_2$, Br-CH$_2$), 1.82-1.50 (6H, m, H-3, -4, -5); ^{13}C NMR (75MHz, CDCl$_3$): δ: 98.8 (C-2), 75.5 (CH), 62.7 (C-6), 44.2 (Cl-CH$_2$), 31.9 (Br-CH$_2$), 30.50 (C-3), 25.2 (C-5), 19.2 (C-4). ^{1}H,^{13}C HMQC (CDCl$_3$): H-2' × C-2' (99.1), H-1 × CH-1 (75.6), H-6' × C-6' (62.7), H-1$_A$ × 1-CH$_2$ (44.7), H-1$_B$ × 1-CH$_2$ (44.6), H-2 × C-2 (32.4), H-3' × C-3' (30.3), H-5' × C-5' (25.3), H-4' × C-4' (19.2). EIMS *m/z*: 257 (M$^{+•}$, 9.7%), 255 (7.6), 209 (2.0), 207 (2.1), 203 (2.2), 202 (1.6), 201 (1.8), 200 (2.7), 157 (16.2), 155 (12.5), 137 (3.7), 135 (3.8), 121 (5.1), 101 (3.7), 95 (2.7), 93 (2.4), 85 (100), 77 (5.8), 75 (17.7), 67 (6.7), 56 (20.0).

7.3   General Procedure B for Preparation of Calone 1951® (1) and Analogues

7.3.1   Preparation of 1

3,4-Dihydro-7-methyl-3-(tetrahydro-2*H*-pyran-2-yloxy)-2*H*-1,5-benzodioxepine (**60**)
Ground oven-dried K$_2$CO$_3$ (2.22 g, 16.06 mmol) was added in one portion to a solution of **20** (0.50 g, 4.03 mmol) in DMF. The solution was heated to 100°C and a solution of **58** (0.70 g, 2.72 mmol) in DMF was added dropwise over 30 min and the solution stirred at 120°C for 24 hours. The hot solution was poured into a stirred ice/H$_2$O (200 mL) mixture and saturated with NaCl before extraction with DCM (3 × 75 mL). The combined organic layer washed with H$_2$O (2 × 100 mL) then dried over MgSO$_4$. Concentration under vacuum yielded (0.98 g, 92%) as deep brown viscous oil. IR (neat), ν (cm^{-1}): 3436b, 3031w, 2942s, 2871s, 2738w, 2660w, 2578w, 2251w, 2227w, 2052w, 2017w, 1871w, 1724w, 1614w, 1579m, 1505s, 1455m, 1442m, 1415w, 1381w, 1355m, 1305s, 1262s, 1201s, 1185m, 1150m, 1128s, 1075s, 1034s. ^{1}H NMR (300MHz, CDCl$_3$): δ: 6.91-6.66 (3H, m, H-6, -8, -9), 4.74 (1H, t, H-2', *J* = 3.5 Hz), 4.42-4.00 (5H, m, H-2, -3, -4), 3.93-3.86 (1H, m, H-6$_A$'), 3.57-3.50 (1H, m, H-6$_B$'), 2.23 (3H, s, Ar-Me), 1.89-1.50 (6H, m, H-3', -4', -5'); ^{13}C NMR (75MHz, CDCl$_3$): δ: 149.6 (C-9a), 147.8 (C-5a), 132.7 (C-7), 124.4 (C-8), 123.4 (C-9), 121.2 (C-6), 98.4 (C-2'), 74.4 (C-3), 73.0 (C-4), 72.1 (C-2), 62.7 (C-6'), 30.7 (C-3'), 25.3 (C-5'), 20.5 (Ar-Me), 19.41 (C-4'). ^{1}H,^{1}H COSY (CDCl$_3$): 4.66 (H-2') × 1.61 (H-

3'), 3.81 (H-6$_B$') × 3.45 (H-6$_A$'), 3.81 (H-6') × 1.49 (H-5'). ^{1}H,^{13}C HMQC (CDCl$_3$): H-3 × C-3 (74.5), H-4 × C-4 (73.4), H-2 × C-2 (72.1), H-6' × C-6' (62.7). EIMS *m/z*: 264 (M$^{+\bullet}$, 76.9%), 236 (3.4), 208 (4.0), 206 (1.6), 180 (20.5), 162 (22.3), 149 (7.5), 135 (35.5), 10.6 (133.1), 124 (8.5), 123 (8.6), 105 (6.9), 99 (5.8), 91 (7.1), 85 (100), 77 (10.3), 67.1 (19.4), 57 (23.1), 55 (10.1).

3,4-Dihydro-7-methyl-2*H*-1,5-benzodioxepin-3-ol (**61**)

Vanadium pentoxide (14 mg, 0.11 mmol) was added to a 30% hydrogen peroxide solution (0.90 mL) and the mixture stirred at 0°C for 10 min. The catalyst mixture was then added to a solution of **60** (0.50 g, 1.89 mmol) in CH$_3$CN (20 mL) and heated at 70°C for 15-20 min, or until the solution ceased effervescing and took on a dark green colour. The CH$_3$CN was removed by rotary evaporation and the crude material solubilised in 2M NaHCO$_3$ solution (50 mL). Extraction of the product was achieved with DCM (3 × 40 mL), the organic portions washed with saturated NaHCO$_3$ solution (1 × 60 mL). Concentration under vacuum yielded an opaque resin, which solidified upon cooling to give **61** as a white solid (0.26 g, 76%), m.p. 56-58°C. IR (KBr), ν (cm^{-1}): 3210b, 3083m, 2988m, 2961m, 2922m, 2866m, 2714w, 1611w, 1578m, 1509s, 1443m, 1414w, 1383w, 1360w, 1344s, 1300s, 1290s, 1275s, 1261s, 1202m, 1151m, 1137s, 1116m, 1103w, 1042s. ^{1}H NMR (300MHz, CDCl$_3$): δ: 6.89 (1H, d, *J* = 8.1 Hz, H-9), 6.80 (1H, s, H-6), 6.78 (1H, d, *J* = 8.1 Hz, H-8), 4.35-4.25 (2H, m, H-2$_A$, -4$_A$), 4.08-3.99 (3H, m, H-4$_B$, -3, -2$_B$), 2.78 (1H, s, OH), 2.24 (3H, s, Ar-Me); ^{13}C NMR (75MHz, CDCl$_3$): δ: 150.2 (C-9a), 148.3 (C-5a), 133.0 (C-7), 123.7 (C-8), 121.5 (C-9), 120.7 (C-6), 74.6 (C-2), 74.4 (C-4), 69.1 (C-3), 20.3 (Ar-Me). ^{1}H,^{1}H COSY (CDCl$_3$): 4.30 (H-2$_A$) × 4.03 (H-2$_B$), 4.30 (H-4$_A$) × 4.03 (H-4$_B$). ^{1}H,^{13}C HMQC (CDCl$_3$): H-2 (2H) × C-2 (74.5), H-4 (2H) × C-4 (74.4), H-3 (1H) × C-3 (69.2). EIMS *m/z*: 180 (M$^{+\bullet}$, 100%), 161 (2.0), 149 (10.6), 135 (50.9), 123 (28.1), 109 (11.2), 107 (4.8), 106 (4.7), 95 (7.9), 94 (9.2), 91 (10.1), 78 (12.6), 77 (14.1), 66 (9.9), 65 (6.5) 57 (2.2), 51 (5.9).

7-Methyl-2*H*-1,5-benzodioxepin-3(4*H*)-one (**1**)

To an aqueous solution of KOH (4%, 20 mL), KMnO$_4$ (1.75 g, 11.07 mmol) at 0-5°C was added to **61** (0.40 g, 2.22 mmol) in one portion. The reaction solution was allowed to stir for 2.5 hr, the MnO$_2$ was removed by vacuum filtration and the filter cake washed with Et$_2$O (2 × 20 mL). The filtrate was acidified with dropwise addition of concentrated HCl to pH 2, and then extracted with Et$_2$O (3 × 30 mL). The combined organic portions were washed with saturated NaHCO$_3$ (1 × 50 mL), dried over MgSO$_4$ and concentrated to yield a yellow resin that was purified by bulb distillation (0.5mmHg/70°C) to provide **1** a crystalline white solid (0.35 g, 87%), m.p. 38-39°C (lit. 38-40°C [35]). IR (KBr), ν (cm^{-1}):

3448w, 3057w, 2991w, 2920w, 2859w, 1742s, 1614w, 1582w, 1506s, 1466w, 1435m, 1414w, 1303s, 1265s, 1207m, 1150m, 1119m, 1053s. ^{1}H NMR (300MHz, CDCl$_3$): δ: 6.90-6.75 (3H, m, H-6, -8, -9), 4.70 (2H, s, H-4), 4.67 (2H, s, H-2), 2.27 (3H, s, Ar-Me); ^{13}C NMR (75MHz, CDCl$_3$): δ: 204.8 (C-3), 147.9 (C-9a), 146.1 (C-5a), 133.8 (C-7), 124.3 (C-8), 121.2 (C-9), 120.6 (C-6), 75.8 (C-2), 75.5 (C-4), 20.5 (Ar-Me). EIMS *m/z*: 178 (M$^{+•}$, 100%), 150 (2.4), 149 (2.6), 135 (24.2), 122 (6.1), 108 (8.5), 94 (89.2), 91 (17.5), 89 (12.4), 77 (16.6), 66 (73.9), 63 (13.6), 51 (18.0), 39 (20.8).

7.3.2   Preparation of 23

3,4-Dihydro-6-methyl-3-(tetrahydro-2*H*-pyran-2-yloxy)-2*H*-1,5-benzodioxepine (**60a**)

Methylcatechol **20a** (0.50 g, 4.03 mmol) was reacted according to the procedure outlined for **60** to yield **60a** as brown viscous oil (0.95 g, 90%). IR (neat), ν (cm^{-1}): 3452b, 3075w, 3017w, 2943s, 2870s, 2739w, 1906w, 1835w, 1724w, 1649w, 1624w, 1593m, 1477s, 1455m, 1440m, 1402w, 1379w, 1355m, 1302s, 1272s, 1248m, 1194s, 1159m, 1128s, 1084s, 1034s. ^{1}H NMR (300MHz, CDCl$_3$): δ: 6.77 (3H, s, H-7, -8, -9), 4.75 (1H, apparent t, H-2'), 4.45-4.23 (5H, m, H-2, -3, -4), 3.95-3.87 (1H, m, H-6$_A$'), 3.57-3.50 (1H, m, H-6$_B$'), 2.21 (3H, s, Ar-Me), 1.90-1.51 (6H, m, H-3', -4', -5'); ^{13}C NMR (75MHz, CDCl$_3$): δ: 150.0 (C-9a), 148.5 (C-5a), 130.0 (C-6), 124.4 (C-7), 122.0 (C-8), 118.4 (C-9), 98.4 (C-2'), 74.4 (C-3), 72.9 (C-2), 71.9 (C-4), 62.7 (C-6'), 30.7 (C-3'), 25.3 (C-5'), 19.5 (C-4'), 16.2 (Ar-Me). EIMS *m/z*: 264 (M$^{+•}$, 57.7%), 236 (5.8), 208 (3.1), 206 (1.4), 180 (13.9), 162 (21.0), 149 (8.1), 135 (38.1), 124 (5.5), 123 (6.0), 105 (5.5), 99 (5.0), 94 (4.8), 91 (7.1), 85 (100), 77 (9.6), 67 (18.1), 57 (22.3), 55 (8.1).

3,4-Dihydro-6-methyl-2*H*-1,5-benzodioxepin-3-ol (**61a**)

Compound **60a** (0.70 g, 2.65 mmol) was deprotected according to the procedure for **61** to give clear oil, which solidified to a white solid upon cooling (0.41 g, 85%), m.p. 34-38°C. IR (KBr), ν (cm^{-1}): 3265b, 2964m, 2920m, 2860w, 1589w, 1528w, 1477s, 1438m, 1377w, 1343w, 1292s, 1278s, 1247m, 1196s, 1161w, 1138s, 1087s, 1045s, 1011m. ^{1}H NMR (300MHz, CDCl$_3$): δ: 6.86 (3H, s, H-7, -8, -9), 4.35-4.25 (1H, m, H-3), 4.08-3.99 (4H, m, H-2, -4), 2.60 (1H, broad s, OH), 2.24 (3H, s, Ar-Me); ^{13}C NMR (75MHz, CDCl$_3$): δ: 151.4 (C-9a), 149.7 (C-5a), 131.0 (C-6), 125.5 (C-7), 123.2 (C-8), 119.2 (C-9), 74.8 (C-2), 74.4 (C-4), 69.7 (C-3), 16.1 (Ar-Me). EIMS *m/z*: 180 (M$^{+•}$, 100%), 161 (2.6), 149 (16.3), 136 (22.1), 135 (62.5), 124 (21.2), 123 (24.0), 109 (12.4), 107 (4.4), 105 (4.8), 95 (5.1), 94 (8.5), 91 (11.8), 89 (2.5), 78 (11.1), 77 (16.4), 66 (11.4), 57 (2.7), 52 (4.8), 51 (6.6).

6-Methyl-2*H*-1,5-benzodioxepin-3(4*H*)-one (**23**)

Compound **61a** (0.40 g, 2.22 mmol) was oxidised according to the procedure for **1** producing a yellow resin, purified by bulb distillation (0.2mmHg/50-60°C) to give **23** as clear oil (0.22 g, 56%).

7.3.3   Preparation of 24

3,4-Dihydro-6-methoxy-3-(tetrahydro-2*H*-pyran-2-yloxy)-2*H*-1,5-benzodioxepine (**60b**)

Methoxycatechol **20b** (0.50 g, 3.57 mmol) was reacted according to the procedure **60** to yield **60b** as brown viscous oil (0.91 g, 91%). IR (neat), ν (cm^{-1}): 3436b, 2944s, 2873m, 2853m, 2744w, 2251w, 1673m, 1652m, 1598m, 1588m, 1489s, 1476s, 1456m, 1441m, 1387w, 1356w, 1311m, 1273m, 1248m, 1202s, 1183w, 1162w, 1119s, 1103s, 1077s, 1093s, 1024s. ^{1}H NMR (300MHz, CDCl$_3$): δ: 6.87-6.78 (1H, m, H-8), 6.62-6.51 (2H, m, H-7, -9), 4.96-4.43 (2H, m, H-2$_A$, -4$_A$), 4.56-4.04 (3H, m, H-2$_B$, -3, -4$_B$), 5.10 (1H, t, J = 3.5 Hz, H-2'), 3.84 (3H, s, Ar-OMe), 3.56-3.49 (2H, m, H-6'), 1.87-1.53 (6H, m, H-3', -4', -5'); ^{13}C NMR (75MHz, CDCl$_3$): δ: 151.2 (C-6), 143.9 (C-9a), 139.8 (C-5a), 120.6 (C-8), 113.2 (C-9), 110.4 (C-7), 98.0 (C-2'), 74.1 (C-3), 72.3 (C-2), 70.2 (C-4), 62.9 (C-6'), 56.1 (Ar-OMe), 30.7 (C-3'), 25.3 (C-5'), 23.2 (C-4'). EIMS *m/z*: 280 (M$^{+\bullet}$, 49.9%), 252 (13.5), 224 (4.2), 196 (29.2), 178 (18.3), 165 (6.9), 151 (35.8), 149 (11.0), 140 (12.3), 125 (5.1), 107 (14.2), 95 (18.5), 85 (100), 77 (5.3), 67 (20.0), 57 (28.6), 55 (15.1), 51 (6.0).

3,4-Dihydro-6-methoxy-2*H*-1,5-benzodioxepin-3-ol (**61b**)

Compound **60b** (0.77 g, 2.75 mmol) was reacted according to the procedure for **61** to provide **61b** as yellow resin (0.41 g, 76%). IR (neat), ν (cm^{-1}): 3459b, 3099w, 2941m, 2840w, 1721m, 1646w, 1598m, 1588m, 1489s, 1475s, 1442m, 1361w, 1321w, 1304w, 1272s, 1249s, 1207m, 1183m, 1092s, 1076s, 1029m. ^{1}H NMR (300MHz, CDCl$_3$): δ: 6.92-6.86 (1H, t, J = 8.3 Hz, H-8), 6.67-6.61 (2H, m, H-7, -9), 4.41-4.26 (2H, m, H-4$_A$, -2$_A$), 4.16-4.09 (3H, m, H-4$_B$, -3, -2$_B$), 3.86 (3H, s, Ar-OMe), 2.01 (1H, broad s, OH); ^{13}C NMR (75MHz, CDCl$_3$): δ: 152.3 (C-6), 151.9 (C-9a), 140.8 (C-5a), 122.9 (C-8), 113.7 (C-9), 107.0 (C-7), 75.2 (C-2), 74.9 (C-4), 69.7 (C-3), 56.3 (Ar-OMe). EIMS *m/z*: 196 (M$^{+\bullet}$, 100%), 177 (1.4), 165 (9.5), 151 (38.2), 140 (24.6), 125 (14.9), 110 (11.5), 107 (26.2), 95 (21.5), 93 (170), 81 (4.3), 77 (5.3), 68 (2.4), 66 (2.1), 6.3 (3.1), 57 (4.1), 55 (4.3), 51 (10.7).

6-Methoxy-2*H*-1,5-benzodioxepin-3(4*H*)-one (**24**)

Compound **61b** (0.40 g, 2.04 mmol) was reacted according to the procedure for **1** to afford a yellow resin which was bulb distilled (0.2mmHg/65°C) to furnish clear crystals (0.34 g, 87%).

7.3.4 Preparation of 25

3,4-Dihydro-3-(tetrahydro-2*H*-pyran-2-yloxy)-2*H*-1,5-benzodioxepine (**60c**)

Pyrocatechol **20c** (0.50 g, 4.54 mmol) was reacted according to the procedure for **60** to afford yellow-brown viscous oil (0.99 g, 87%). IR (neat), ν (cm^{-1}): 3436b, 3069w, 3036w, 2942s, 2871m, 2852m, 2741w, 2661w, 2223w, 1932w, 1737w, 1600w, 1583m, 1492s, 1464m, 1455m, 1442w, 1403w, 1379w, 1356w, 1303s, 1258s, 1248s, 1202w, 1181w, 1160m, 1122m, 1104m, 1074s, 1043s, 1022s. ^{1}H NMR (300MHz, CDCl$_3$): δ: 7.01-6.86 (4H, m, H-6, -7, -8, -9), 4.74 (1H, t, *J* = 3.6 Hz, H-2'), 4.45-4.10 (5H, m, H-2, -3, -4), 3.94-3.87 (1H, m, H-6$_A$'), 3.57-3.50 (1H, m, H-6$_B$'), 1.89-1.50 (6H, H-3', -4', -5'); ^{13}C NMR (75MHz, (CD$_3$)$_2$CO): δ: 150.0 (C-5a, -9a), 124.0 (C-8), 122.9 (C-7), 121.5 (C-6), 120.8 (C-9), 98.5 (C-2'), 74.4 (C-3), 73.1 (C-2), 72.0 (C-4), 62.7 (C-6'), 30.8 (C-3'), 25.3 (C-5'), 19.4 (C-4'). EIMS *m/z*: 250 (M$^{+\bullet}$, 42.8%), 222 (1.6), 194 (2.0), 166 (17.8), 148 (23.3), 135 (7.1), 121 (36.6), 109 (4.7), 107 (1.4), 103 (1.2), 99 (5.2), 91 (4.4), 85 (100), 77 (6.6), 67.1 (15.2), 57 (18.3), 55 (11.3).

3,4-Dihydro-2*H*-1,5-benzodioxepin-3-ol (**61c**)

Compound **60c** (0.82 g, 3.28 mmol) was deprotected according to the procedure for **61** to provide clear oil, which partially solidified upon cooling to a white semi-solid. Evaporative crystallisation from Et$_2$O/pentane gave **61c** as clear crystals (0.49 g, 91%), m.p. 48-50°C. IR (KBr), ν (cm^{-1}): 3266b, 2964w, 2917w, 2856w, 1594w, 1579w, 1523w, 1494m, 1455w, 1402w, 1375w, 1261s, 1182w, 1132m, 1098m, 1040s, 1019s. ^{1}H NMR (300MHz, CDCl$_3$): δ: 7.04-6.94 (4H, m, H-6, -7, -8, -9), 4.31-4.26 (2H, m, H-4$_A$, -2$_A$), 4.12-4.07 (3H, m, H-4$_B$, -3, -2$_B$), 2.61 (1H, broad s, OH); ^{13}C NMR (75MHz, CDCl$_3$): δ: 151.1 (C-5a, -9a), 124.0 (C-7, -8), 121.6 (C-6, -9), 74.8 (C-2, -4), 69.7 (C-3). EIMS *m/z*: 166 (M$^{+\bullet}$, 100%), 147 (2.9), 135 (19.5), 122 (25.8), 121 (76.8), 110 (30.5), 109 (12.3), 95 (14.6), 81 (9.4), 77 (14.0), 63 (12.8), 52 (9.4).

2*H*-1,5-Benzodioxepin-3(4*H*)-one (**25**)

Compound **61c** (0.39 g, 2.35 mmol) was oxidised according to procedure for **1** to provide pale yellow oil, which was eluted through a short silica column with DCM to provide clear oil, which crystallised (0.23 g, 60%), m.p. 64-65°C.

7.3.5   Preparation of 26

3,4-Dihydro-7-nitro-3-(tetrahydro-2*H*-pyran-2-yloxy)-2*H*-1,5-benzodioxepine (**60d**)

Nitrocatechol **20d** (0.50 g, 3.22 mmol) was reacted according to the procedure for **60** yielding **60d** as deep orange viscous oil (0.81 g, 85%). IR (neat), ν (cm^{-1}): 3428b, 3081w, 2945s, 2870m, 2605w, 2243w, 1994w, 1809s, 1720w, 1586m, 1520s, 1494m, 1463w, 1424w, 1347s, 1322m, 1281s, 1265s, 1202w, 1182w, 1159w, 1123s, 1073s, 1033s. ^{1}H NMR (300MHz, CDCl$_3$): δ: 7.80-7.77 (2H, m, H-8, -6), 7.00-6.97 (1H, m, H-9), 4.71 (1H, apparent t, H-2'), 4.54-4.27 (5H, m, H-2, -3, -4), 3.92-3.84 (1H, m, H-6$_A$'), 3.57-3.50 (1H, m, H-6$_B$'), 1.86-1.51 (6H, m, H-3', -4', -5'); ^{13}C NMR (75MHz, CDCl$_3$): δ: 155.5 (C-9a), 149.5 (C-5a), 142.6 (C-7), 120.8 (C-9), 118.8 (C-8), 116.9 (C-6), 98.9 (C-2'), 74.4 (C-3), 73.0 (C-2), 72.1 (C-4), 62.8 (C-6'), 30.6 (C-3'), 25.1 (C-5'), 19.4 (C-4'). EIMS *m/z*: 295 (M$^{+\bullet}$, 11.2%), 211 (18.7), 193 (19.0), 180 (1.4), 166 (12.4), 147 (2.6), 134 (1.2), 120 (4.5), 107 (1.9), 91 (3.0), 85 (100), 79 (4.7), 67 (10.3), 63 (2.8), 57 (10.9), 55 (4.3), 51 (3.2).

3,4-Dihydro-7-nitro-2*H*-1,5-benzodioxepin-3-ol (**61d**)

Compound **60d** (0.76 g, 2.57 mmol) was deprotected according to the procedure for **61**. The yellow resin was crystallized from Et$_2$O to provide **61d** as pale yellow solid (0.28 g, 52%), m.p. 74-78°C. IR (KBr), ν (cm^{-1}): 3453b, 3105w, 3076w, 2953w, 1802w, 1721w, 1587w, 1518s, 1496m, 1466w, 1422w, 1351s, 1325m, 1283s, 1270m, 1186w, 1126w, 1103w, 1077m, 1020m. ^{1}H NMR (300MHz, CDCl$_3$): δ: 7.87-7.82 (2H, m, H-6, -8), 7.05 (1H, d, *J* = 8.7 Hz, H-9), 4.36-4.21 (5H, m, H-2, -3, -4), 2.12 (1H, broad s, OH); ^{13}C NMR (75MHz, CDCl$_3$): δ: 155.9 (C-9a), 150.1 (C-5a), 143.2 (C-7), 121.5 (C-9), 119.4 (C-8), 117.5 (C-6), 74.9 (C-2), 74.6 (C-4), 69.0 (C-3). EIMS *m/z*: 211 (M$^{+\bullet}$, 100%), 192 (2.4), 180 (13.9), 167 (10.6), 166 (10.6), 155 (8.8), 152 (3.9), 137 (11.6), 134 (5.5), 121 (11.0), 107 (19.9), 94 (4.2), 91 (6.0), 79 (15.0), 77 (4.1), 75 (4.4), 65 (16.3), 63 (16.1), 57 (14.9), 51 (12.6).

7-Nitro-2*H*-1,5-benzodioxepin-3(4*H*)-one (**26**)

At –78 °C under a N$_2$ atmosphere DMSO (0.42 g, 5.37 mmol) in DCM (5 mL) was added dropwise over 20 min to oxalyl chloride (0.34 g, 2.68 mmol) in DCM (40 mL) and the mixture stirred for 15 min. Compound **61d** (0.25 g, 1.18 mmol) in DCM (5 mL) was added dropwise over 30 min followed by stirring at –78 °C for 90 min. TEA (0.68 g, 6.72 mmol) was then added dropwise over 15 min and the solution stirred for a further 2 hr at –78 °C. Aqueous THF (10 mL, 1:1 H$_2$O/THF) was added while maintaining the temperature of the reaction below -60°C. The reaction solution was then allowed to reach 0°C followed by addition of DCM (40 mL). The organic mixture was washed with 2M HCl (2 × 60 mL), dried over MgSO$_4$ and concentrated by rotary evaporation. The crude resin was crystallised from MeCN to form **26** as a bright yellow semi-solid (0.21 g, 84%), m.p. 110-112 °C.

7.3.6 Preparation of 27

3,4-Dihydro-3-(tetrahydro-2*H*-pyran-2-yloxy)-2*H*-1,5-benzodioxepine-7-carbaldehyde (**60e**)

Formylcatechol **20e** (0.50 g, 3.62 mmol) was reacted according to the procedure for **60** to give **60e** as caramel brown viscous oil (0.74 g, 74%). IR (neat), ν (cm^{-1}): 3422b, 3063w, 2943m, 2869m, 2733w, 1803w, 1686s, 1601s, 1573m, 1501s, 1432m, 1389w, 1356w, 1316m, 1281s, 1201w, 1158m, 1127s, 1074s, 1033s. ^{1}H NMR (300MHz, CDCl$_3$): δ: 9.77 (1H, s, Ar-CHO), 7.42-6.95 (3H, m, H-6, -8, -9), 4.72 (1H, apparent t, H-2'), 4.59-4.22 (5H, m, H-4, -3, -2), 4.01-3.78 (1H, m, H-6$_A$'), 3.56-3.51 (1H, m, H-6$_B$'), 1.80-1.18 (6H, m, H-5', -4', -3'); ^{13}C NMR (75MHz, CDCl$_3$): δ: 190.6 (Ar-CHO), 155.3 (C-9a), 150.1 (C-5a), 131.7 (C-7), 125.2 (C-8), 121.4 (C-9), 121.3 (C-6), 98.7 (C-2'), 74.0 (C-3), 72.9 (C-2), 72.0 (C-4), 62.8 (C-6'), 30.7 (C-3'), 25.2 (C-5'), 19.5 (C-4'). EIMS *m/z*: 278 (M$^{+•}$, 21.7%), 250 (1.0), 222 (2.2), 194 (30.4), 176 (19.2), 164 (15.7), 149 (30.1), 137 (4.2), 121 (3.0), 119 (4.2), 113 (2.9), 109 (2.1), 105 (1.1), 103 (1.2), 99 (1.2), 93 (1.2), 91 (5.0), 85 (100), 79 (5.0), 67 (12.7), 57.1 (14.4), 55 (6.6), 51 (3.3).

3,4-Dihydro-3-hydroxy-2*H*-1,5-benzodioxepine-7-carbaldehdye (**61e**)

Compound **60e** (0.56 g, 2.01 mmol) was deprotected according to the procedure for **61** to yield **61e** as yellow resin (0.35 g, 89%). IR (neat), ν cm^{-1}: 3440b, 3078w, 2939m, 2856m, 2735w, 2620w, 1794w, 1731m, 1688s, 1599s, 1588m, 1574m, 1505s, 1434s, 1394w, 1359w, 1338w, 1317m, 1280s, 1169m, 1138m, 1099w, 1035m. ^{1}H NMR (300MHz,

CDCl$_3$): δ: 9.82 (1H, s, Ar-CHO), 7.47-7.45 (2H, m, H-6, -8), 7.06 (1H, d, J = 8.8 Hz, H-9), 4.32-4.14 (5H, m, H-2, -3, -4), 2.87 (1H, broad s, OH); ^{13}C NMR (75MHz, CDCl$_3$): δ: 190.6 (Ar-CHO), 155.8 (C-9a), 150.8 (C-5a), 132.2 (C-7), 125.7 (C-8), 122.6 (C-9), 121.8 (C-6), 74.7 (C-2), 74.5 (C-4), 69.1 (C-3). EIMS m/z: 194 (M$^{+\bullet}$, 100%), 175 (3.2), 163 (16.9), 149 (65.2), 137 (21.3), 121 (13.3), 119 (5.7), 109 (6.0), 105 (3.1), 95 (5.7), 91 (5.3), 79 (8.3), 77 (7.6), 65 (8.9), 63 (11.4), 57 (7.2), 51 (8.8).

3,4-Dihydro-3-oxo-2H-1,5-benzodioxepine-7-carbaldehyde (**27**)

Compound **61e** (0.25 g, 1.29 mmol) was reacted according to the procedure outlined for **26**. The crude resin was crystallised from MeCN to form **27** as a white solid (0.13 g, 52%), m.p. 110-112 °C.

7.3.7   Preparation of 28

3,4-Dihydro-7-(*tert*-butyl)-3-(tetrahydro-2H-pyran-2-yloxy)-2H-1,5-benzodioxepine (**60f**)

t-Butylcatechol **20f** (0.50 g, 3.01 mmol) was reacted according to procedure for **60** to give **60f** as light brown viscous oil (0.90 g, 98%). IR (neat), ν (cm^{-1}): 3435b, 3039w, 2952s, 2870m, 2741w, 2662w, 1727w, 1625w, 1613w, 1574m, 1505s, 1463m, 1455m, 1442w, 1412w, 1393w, 1363w, 1355w, 1306s, 1274m, 1263m, 1239m, 1202m, 1185w, 1161w, 1122s, 1097w, 1076s, 1034s, 1023m. ^{1}H NMR (300MHz, CDCl$_3$): δ: 6.96-6.86 (3H, m, H-6, -8, -9), 4.74 (1H, t, J = 2.8 Hz, H-2'), 4.46-4.21 (5H, m, H-2, -3, -4), 3.95-3.86 (1H, m, H-6$_A$'), 3.57-3.49 (1H, m, H-6$_B$'), 1.90-1.43 (6H, m, H-3', -4', -5'), 1.26 (9H, s, Ar-^{t}Bu); ^{13}C NMR (75MHz, CDCl$_3$): δ: 147.5 (C-9a), 146.3 (C-5a, C-7), 120.9 (C-8), 120.1 (C-9), 119.7 (C-6), 98.4 (C-2'), 74.5 (C-3), 73.0 (C-2), 71.9 (C-4), 62.6 (C-6'), 34.1 (C$_q$(Ar-^{t}Bu)), 31.3 (Ar-^{t}Bu), 30.8 (C-3'), 25.3 (C-5'), 19.4 (C-4'). EIMS m/z: 306 (M$^{+\bullet}$, 76.6%), 291 (57.6), 263 (3.5), 261 (2.5), 250 (1.9), 248 (1.0), 235 (12.7), 222 (19.1), 207 (81.3), 204 (5.0), 193 (4.9), 189 (23.8), 177 (11.7), 163 (6.2), 161 (6.1), 151 (9.7), 147 (3.5), 133 (9.7), 121 (4.2), 119 (3.9), 117 (2.8), 115 (2.9), 105 (12.1), 91 (12.5), 85 (100), 77 (11.2), 67 (16.8), 57 (25.1), 55 (16.8), 51 (35.8).

3,4-Dihydro-7(*tert*-butyl)-2H-1,5-benzodioxepin-3-ol (**61f**)

Compound **60f** (0.80 g, 2.61 mmol) was deprotected according to the procedure for **61** to furnish **61f** as a white solid (0.47 g, 81%), m.p. 48-50°C. IR (KBr), ν (cm^{-1}): 3459b, 2962m, 2866w, 1578w, 1503s, 1460w, 1447w, 1409m, 1390w, 1364w, 1311s, 1274s, 1252m, 1236s, 1204w, 1184w, 1118m, 1090m, 1057m, 1042s, 1022m. ^{1}H NMR

(300MHz, CDCl$_3$): δ: 7.04-6.95 (3H, m, H-6, -8, -9), 4.32-4.23 (2H, m, H-2$_A$, -4$_A$), 4.09-4.04 (3H, m, H-2$_B$, -3, -4$_B$), 2.70 (1H, apparent s, OH), 1.27 (9H, s, Ar-^{t}Bu); ^{13}C NMR (75MHz, CDCl$_3$): δ: 150.4 (C-9a), 148.5 (C-5a), 147.5 (C-7), 120.9 (C-8), 120.8 (C-9), 118.6 (C-6), 74.7 (C-2, -4), 69.7 (C-3), 34.2 (C$_q$(Ar-^{t}Bu), 31.3 (Ar-^{t}Bu). EIMS m/z: 222 (M$^{+\bullet}$, 29.0%), 207 (100), 163 (3.8), 151 (9.1), 133 (4.6), 123 (5.1), 105 (6.8), 91 (4.9), 77 (6.3), 65 (2.1).

7-(*tert*-Butyl)-2*H*-1,5-benzodioxepin-3(4*H*)-one (**28**)

Compound **61f** (0.41 g, 1.85 mmol) was oxidised according to the procedure for **1** to give clear oil, which was purified by bulb distillation (0.2mmHg/100-105°C) providing **28** as crystalline solid (0.30 g, 73%), m.p. 66-68°C.

7.3.8   Preparation of 29

3,4,7,10-Tetrahydro-3-(tetrahydro-2*H*-pyran-2-yloxy)-2*H*-naphtho[2,3-*b*][1,4]dioxepine (**60g**)

Dihydroxynaphthalene **20g** (0.50 g, 3.12 mmol) was reacted according to the procedure for **60** to provide **60g** as brown viscous oil (0.77 g, 82%). IR (neat), ν (cm^{-1}): 3331b, 3056w, 2943s, 2870m, 1708m, 1670s, 1631w, 1602w, 1503s, 1472s, 1453s, 1386m, 1359m, 1290s, 1260s, 1247s, 1201m, 1172m, 1159m, 1125s, 1074s, 1031s. ^{1}H NMR (300MHz, CDCl$_3$): δ: 7.67-7.61 (2H, m, H-7, -10), 7.36 (2H, s, H-6, -11), 7.33-7.30 (2H, m, H-8, -9), 4.77 (1H, apparent t, H-2'), 4.51-4.30 (5H, m, H-2, -3, -4), 4.05-3.83 (1H, m, H-6$_A$'), 3.59-3.44 (1H, m, H-6$_B$'), 1.90-1.20 (6H, m, H-3', -4', -5'); ^{13}C NMR (75MHz, CDCl$_3$): δ: 151.1 (C-11a), 150.2 (C-5a), 130.2 (C-6a, -10a), 126.5 (C-7, -10), 124.8 (C-8, -9), 116.9 (C-6, -11), 98.5 (C-2'), 74.6 (C-3), 73.0 (C-2), 71.9 (C-4), 62.7 (C-6'), 30.7 (C-3'), 25.3 (C-5'), 19.4 (C-4'). EIMS m/z: 300 (M$^{+\bullet}$, 64.6%), 272 (14.3), 244 (7.8), 216 (30.8), 198 (16.7), 185 (10.3), 181 (2.2), 171 (43.6), 169 (13.6), 160 (18.4), 141 (9.0), 131 (11.5), 128 (10.6), 127 (14.5), 115 (22.3), 114 (16.8), 102 (22.4), 85 (100), 77 (3.9), 76 (4.0), 67 (17.9), 57 (28.3), 55 (11.2).

3,4,7,10-Tetrahydro-2*H*-naphtho[2,3-*b*][1,4]dioxepin-3-ol (**61g**)

Compound **60g** (0.65 g, 2.17 mmol) was deprotected according to the procedure for **61**. Crystallisation of the residue from MTBE yielded **61g** as a red solid (0.34 g, 73%), m.p. 79-80°C. IR (KBr), ν (cm^{-1}): 3420b, 3056w, 2925w, 1777w, 1726m, 1627w, 1598m, 1503s, 1474m, 1458w, 1445w, 1432w, 1394w, 1360m, 1341w, 1289m, 1263s, 1173m, 1151w, 1109m, 1069w, 1031s. ^{1}H NMR (300MHz, CDCl$_3$): δ: 7.71-7.68 (2H, m, H-7, -10),

7.46 (2H, s, H-6, -11), 7.39-7.36 (2H, m, H-8, -9), 4.41-4.36 (2H, m, H-2$_A$, -4$_A$), 4.14-4.09 (3H, m, H-2$_B$, -3, -4$_B$), 2.30 (1H, apparent s, OH); ^{13}C NMR (75MHz, CDCl$_3$): δ: 151.1 (C-5a, -11a), 130.7 (C-6a, -10a), 126.8 (C-7, -10), 125.3 (C-8, -9), 118.1 (C-6, -11), 75.3 (C-2, -4), 69.8 (C-3). EIMS m/z: 216 (M$^{+•}$, 100%), 197 (1.5), 185 (12.8), 172 (16.4), 171 (31.6), 160 (33.4), 145 (5.0), 131 (16.0), 127 (13.3), 115 (22.0), 114 (22.9), 102 (12.6), 88 (5.3), 77 (3.9), 76 (3.6), 63 (3.9).

7,10-Dihydro-2*H*-naphtho[2,3-*b*][1,4]dioxepin-3(4*H*)-one (**29**)

Compound **61g** (0.31 g, 1.43 mmol) was oxidised according to procedure for **1** to provide **29** as grey-white solid (0.19g, 61%), m.p. 70-74°C.

7.4   Preparation of Analogues 65-74

7-Methyl-2*H*-1,5-benzodioxepin-3(4*H*)-one oxime (**65**)

Benzodioxepinone **1** (3.00 g, 16.85 mmol) was dissolved in a solution of MeCN (60 mL) and H$_2$O (20 mL). Sodium acetate (2.07 g, 25.00 mmol) was added followed by hydroxylamine hydrochloride (1.37 g, 19.71 mmol) and the reaction mixture allowed to stir at 50°C for 24 hr or until reaction was complete as indicated by GC-MS. The clear reaction solution was poured into ice/H$_2$O (300 mL) and the white precipitate was isolated by vacuum filtration. The filter cake was washed with ice cold H$_2$O (2 × 50mL) to furnish **65** as a fluffy white solid (3.05 g, 94%), m.p. 98-100°C. IR (KBr), ν (cm^{-1}): 3289m, 3026w, 2921m, 2858w, 1582w, 1509s, 1448m, 1422m, 1358w, 1311s, 1266m, 1204m, 1151w, 1115m, 1056m, 1028m, 1001m. ^{1}H NMR (300MHz, CDCl$_3$): δ: 6.89-6.66 (3H, m, H-6, H-8, H-9), 5.05 (2H, s, H-4, *α-isomer*), 5.03 (2H, s, H-4, β-isomer), 4.91 (2H, s, H-2, *α-isomer*), 4.88 (2H, s, H-2, β-isomer), 2.24 (3H, s, Ar-Me), OH (not observed); ^{13}C NMR (75MHz, CDCl$_3$): δ: *α-isomer*: 157.3 (C-3), 146.9 (C-9a), 145.0 (C-5a), 132.2 (C-7), 125.1 (C-8), 122.5 (C-9), 119.6 (C-6), 68.7 (C-2), 68.3 (C-4), 20.3 (Ar-Me); *β-isomer*: 157.3 (C-3), 148.3 (C-9a), 146.5 (C-5a), 134.6 (C-7), 122.9 (C-8), 122.0 (C-9), 120.2 (C-6), 68.4 (C-2), 68.1 (C-4), 20.6 (Ar-Me). ^{1}H,^{13}C HMQC (CDCl$_3$): H-4 × C-4 (68.4), H-2 × C-2 (68.2). ^{1}H,^{13}C HMBC (CDCl$_3$): H-2, -4 (*α-isomer*)) × C-9a (146.9), C-5a (145.8), H-2, -4 (*β-isomer*) × C-9a (148.4), C-5a (147.5). EIMS m/z: 193 (M$^{+•}$, 100%), 176 (53.7), 148 (48.9), 135 (17.1), 123 (26.0), 121 (13.9), 105 (5.5), 95 (16.3) 77 (14.1), 66 (15.4), 54 (7.1), 39 (8.7). High Resolution Mass Spectrum (HRESI) Found [M]$^{+•}$, 194.0812. C$_{10}$H$_{12}$NO$_3$ [M + H] $^{+•}$ requires 194.0817.

3,4-Dihydro-7-methyl-2*H*-1,5-benzodioxepin-3-ol (**rac-66**)

To a suspension of **1** (1.00 g, 5.62 mmol) in H_2O (20 mL), MeOH (40 mL) was added until **1** completely solubilised. $NaBH_4$ (0.42 g, 11.10 mmol) was added portion-wise with cooling in an ice bath. The reaction solution was left to stir at ambient temperature for 4 hours and then quenched with 0.1 M HCl solution (150 mL). The solution was then extracted with DCM (3 × 50 mL). The combined organic phases were washed with H_2O (2 × 100 mL) then dried over $MgSO_4$ and the solvent was evaporated under reduced pressure to leave **66** as a low melting white solid (0.90 g, 89%), m.p. 56-58°C, α = -0.7°, $[\alpha]_D$ = -8.3° (*c* = 0.02, EtOH).

3,4-Dihydro-(*R/S*)-7-methyl-2*H*-1,5-benzodioxepin-3-ol (**ent-66**)

A mixture of glucose powder (3.0 g, 16.65 mmol) in phosphate buffer (50 mL) was added to baker's yeast (6.0 g) suspended in H_2O (120 mL). The solution was left to stir at 30ºC for 30 min. 7-Methyl-2H-1,5-benzodioxepin-3(4*H*)-one (0.5 g, 2.81 mmol) previously dissolved in EtOH:DMSO (5:5 mL) was added dropwise to the reaction mixture and left to stir at 30ºC. After 4 hours complete reduction was confirmed by GC-MS. The baker's yeast was removed by vacuum filtration, the filtrate was extracted with EtOAc (3 × 70 mL) and washed with H_2O (5 × 200mL). The combined organic layers were dried over $MgSO_4$ and concentrated by rotary evaporation to yield an opaque solution which solidified to an ivory solid upon cooling (0.35 g, 70%), m.p. 58-60°C, α = -4.8°, $[\alpha]_D$ = -120° (*c* = 0.02, EtOH). IR (KBr), ν (cm^{-1}): 3210b, 3083m, 2988m, 2961m, 2922m, 2866m, 2714w, 1611w, 1578m, 1509s, 1443m, 1414w, 1383w, 1360w, 1344s, 1300s, 1290s, 1275s, 1261s, 1202m, 1151m, 1137s, 1116m, 1103w, 1042s. ^{1}H NMR (300MHz, CDCl$_3$): δ: 6.89 (1H, d, *J* = 8.1 Hz, H-9), 6.80 (1H, s, H-6), 6.78 (1H, d, *J* = 8.1 Hz, H-8), 4.25 (2H, m, H-2$_A$, -4$_A$), 4.04 (3H, m, H-2$_B$, -3, -4$_B$), 2.24 (3H, s, Ar-Me), 1.33 (1H, s, OH); ^{13}C NMR (75MHz, CDCl$_3$): δ: 150.2 (C-9a), 148.3 (C-5a), 133.0 (C-7), 123.7 (C-8), 121.5 (C-9), 120.7 (C-6), 74.6 (C-2), 74.4 (C-4), 69.1 (C-3), 20.3 (Ar-Me). ^{1}H,^{1}H COSY (CDCl$_3$): 4.18 (H-2$_A$, -4$_A$) × 3.94 (H-2$_B$, -3, -4$_B$). EIMS *m/z*: 180 (M$^{+\bullet}$, 100%), 149 (11.2), 135 (47.6), 123 (27.3), 109 (10.6), 94 (8.45), 91 (9.0), 77 (12.0), 66 (8.2), 51 (5.0), 39 (4.4). High Resolution Mass Spectrum (HRESI) Found [M + Na]$^{+\bullet}$, 203.0682. $C_{10}H_{12}O_3Na$ [M + Na]$^{+\bullet}$ requires 203.0684.

3,4-Dihydro-3,3-dimethoxy-7-methyl-2*H*-1,5-benzodioxepine (**67**)

Trimethyl orthoformate (2.46 mL, 22.48 mmol) was added to a solution of **1** (0.40 g, 2.25 mmol) in $MeNO_2$ (20 mL) cooled to 0°C. A catalytic portion of MeOH (0.90 mL, 22.19 mmol) was added, followed by the dropwise addition of trifluoromethane sulphonic acid

(0.04 mL, 0.45 mmol) and the reaction mixture heated to 100°C under an inert atmosphere (N_2) for 3 hours. The clear purple solution was cooled to ambient temperature then poured into saturated $NaHCO_3$ solution (100 mL). The aqueous mixture was extracted with Et_2O (3 × 40 mL) and the combined organic extracts were washed with H_2O (1 × 75 mL) then dried over $MgSO_4$. Concentration under vacuum afforded transparent yellow oil that was purified using bulb distillation (0.2mmHg/80-90°C) to give **22** as colourless oil (0.36 g, 72%). IR (KBr), ν (cm^{-1}): 2925s, 2856s, 2730w, 1867w, 1743w, 1615w, 1583w, 1505m, 1460s, 1377m, 1305m, 1270m, 1165m, 1146m, 1121w, 1092m, 1071m, 1025w. ^{1}H NMR (300MHz, CDCl$_3$): δ: 6.67-6.83 (3H, m, H-6, H-8, H-9), 4.20 (2H, s, H-2), 4.19 (2H, s, H-4), 3.33 (6H, s, 1-, 2-OMe), 2.23 (3H, s, Ar-Me); ^{13}C NMR (75MHz, CDCl$_3$): δ: 149.1 (C-9a), 147.2 (C-5a), 132.8 (C-7), 123.5 (C-8), 120.9 (C-6), 120.2 (C-9), 100.8 (C-3), 71.7 (C-2), 71.5 (C-4), 48.6 (1-, 2-OMe), 20.4 (Ar-Me). EIMS *m/z*: 224 (M$^{+\bullet}$, 100%), 193 (7.7), 179 (11.2), 165 (4.2), 163 (5.2), 161 (3.2), 149 (35.9), 135 (86.7), 119 (40.0), 105 (19.1), 91 (33.7), 71 (22.2), 59 (7.0), 45 (23.7). High Resolution Mass Spectrum (HRESI) Found [M + Na]$^{+\bullet}$, 247.0946. $C_{12}H_{16}O_4Na$ [M + Na]$^{+\bullet}$ requires 247.0946.

7-Bromo-8-methyl-2*H*-1,5-benzodioxepin-3(4*H*)-one (**68**)

Sodium bromate (2.54g, 16.83 mmol) was added to **1** (1.00 g, 5.62 mmol) dissolved in cyclohexane:H_2O (40:30mL). Sodium metabisulphite (0.98 g, 5.15 mmol) solubilized in H_2O (10 mL) was added dropwise to the solution, which was left to stir at 50°C for 8 hours. The deep yellow solution was quenched with ice/H_2O (250 mL), extracted with Et_2O (3 × 100 mL) and combined organic portions washed with H_2O (2 × 200 mL). The organic layer was dried over $MgSO_4$ and concentrated under reduced pressure to give a pale yellow powdery solid (1.23 g, 85%), m.p. 88-90°C. IR (KBr), ν (cm^{-1}): 2930w, 2900w, 1737s, 1602w, 1566m, 1480s, 1451m, 1428m, 1416m, 1378w, 1294s, 1266m, 1230w, 1178m, 1152s, 1052s, 1036s. ^{1}H NMR (300MHz, CDCl$_3$): δ: 7.17 (1H, s, H-6), 6.87 (1H, s, H-9), 4.67 (2H, s, H-2), 4.66 (2H, s, H-4), 2.28 (3H, s, Ar-Me); ^{13}C NMR (75MHz, CDCl$_3$): δ: 203.8 (C-3), 147.3 (C-9a), 146.6 (C-5a), 133.3 (C-8), 124.2 (C-6), 122.3 (C-9), 117.4 (C-7), 75.7 (C-2), 75.5 (C-4), 21.9 (Ar-Me). EIMS *m/z*: 258 (M$^{+\bullet}$, 89.4%), 257 (10.5), 256 (91.7), 215 (12.3), 213 (12.3), 202 (3.5), 200 (3.6), 174 (25.5), 172 (27.7), 149 (30.5), 135 (4.8), 121 (6.5), 105 (2.9), 93 (100), 77 (18.3), 65 (14.0), 51 (12.3), 39 (10.3). High Resolution Mass Spectrum (HRESI) Found [M]$^{+\bullet}$, 256.9812. $C_{10}H_9O_3Br$ [M + H]$^{+\bullet}$ requires 256.9813.

3,4-Dihydro-7-methyl-2*H*-1,5-benzodioxepine (**69**)

Ground, oven-dried K_2CO_3 (3.34g, 24.15 mmol) and 1,3-dibromopropane (2.45 mL, 24.13 mmol) were added sequentially to a solution of 4-methyl catechol (1.0 g, 8.05 mmol) in anhydrous DMF (50 mL). The solution was irradiated under N_2 (200 W, 2 min) with vigorous stirring. Upon cooling (15 min), the solution was poured into ice/H_2O (200 mL). The aqueous solution was extracted with DCM (3 × 100 mL) and the combined organic extracts were washed with 5% aqueous NaOH (2 × 50 mL) followed by H_2O (2 × 50 ml). The organic layer was dried over $MgSO_4$ and concentrated *in vacuo* to provide crude yellow oil. The crude material was dissolved in MeCN (12.0 mL) with TEA (6.0 mL) and stirred at ambient temperature for 48 hrs. The ammonium bromide salts were removed using a syringe filter (0.45 μm), and the remaining residue stored at -20°C until no more precipitate was formed. Flash chromatography was employed on the remaining residue using n-heptane to give **69** (0.73 g, 55%) as colourless oil.

Reactions conducted using conventional oil bath heating for 2 hr at 120°C, followed by work-up according to the above procedure provided compound **70** in 78% yield.

Alternatively, sodium metal (0.19 g, 8.26 mmol) was added to ethylene glycol monobutyl ether (20 mL). Upon complete solubilization, the addition of 4-methyl catechol (0.50 g, 4.03 mmol) was followed by 1,3-dibromopropane 0.85 mL, 8.37 mmol). The reaction mixture was placed in an oil bath at 115°C and left until GC-MS had confirmed all 4-methyl catechol had been consumed. Once cooled to ambient temperature solid NaBr was removed by gravity filtration. The resulting mother liquor was subject to column chromatography on silica gel flushed with heptane. Purification of **69** or **70** was achieved by elution with a solvent gradient of 2:98-10:90 DCM:heptane. Compound **69** was obtained as clear oil (0.25 g, 38%). IR (neat), ν (cm^{-1}): 3031w, 2953m, 2867m, 1865w, 1726w, 1613w, 1578m, 1505s, 1461m, 1416m, 1388m, 1360w, 1349w, 1305s, 1260s, 1232w, 1201m, 1149m, 1117m, 1102m, 1054s. ^{1}H NMR (300MHz, ($CDCl_3$): δ: 6.92-6.70 (3H, m, H-6, H-8, H-9), 4.10 (2H, t, *J* = 5.3 Hz, H-2), 4.08 (2H, t, *J* = 5.1 Hz, H-4), 2.21 (3H, s, 1-Me), 2.11 (2H, quint., *J* = 5.5 Hz, H-3); ^{13}C NMR (75MHz, ($CDCl_3$): δ: 153.2 (C-9a), 151.3 (C-5a), 134.6 (C-7), 125.5 (C-8), 123.8 (C-9), 123.1 (C-6), 72.4 (C-2), 72.3 (C-4), 34.1 (C-3), 21.5 (Ar-Me). ^{1}H,^{1}H COSY ($CDCl_3$): 3.96 (H-2, -4) × 1.97 (H-3). ^{1}H,^{1}H *J*-resolved: 4.22 (t, H-4, *J* = 5.4 Hz), 4.18 (t, H-2, *J* = 5.1 Hz), 2.16 (quint., H-3, *J* = 5.55 Hz). ^{1}H,^{13}C HMQC ($CDCl_3$): H-2, -4 × C-2, -4 (70.4), H-3 × C-3 (32.1). EIMS *m/z*: 164 (M$^{+•}$, 100%), 135 (85.2), 123 (26.5), 108 (11.4), 94 (26.7), 77 (19.1), 66 (35.4), 51 (16.4), 39 (30.1).

2,3,4,5-Tetrahydro-8-methyl-1,6-benzodioxocine (**70**)

K$_2$CO$_3$ (3.34g, 24.20 mmol), **20** (1.0 g, 8.06 mmol), and 1,4-dibromobutane 2.86 mL, 23.95 mmol) were added sequentially to DMF (50 mL) and the mixture was heated to 120ºC for 2 hr. Workup was followed according to the procedure given for **69** to give crude yellow oil. The crude material was treated with TEA as for **69**, then subject to flash chromatography eluting with n-heptane to 5:95 DCM:heptane gradient to afford **70** (0.93 g, 65%) as a clear pale yellow oil.

Reaction involving microwave irradiation according to the procedure for **69** provided **70** in 24% yield. IR (neat), ν (cm^{-1}): 2925w, 2867w, 1360w, 2342w, 1726w, 1613w, 1578w, 1504s, 1470w, 1444w, 1382w, 1304s, 1255m, 1230m, 1194w, 1153w, 1118w, 1085w, 1055w, 1006w. ^{1}H NMR (300MHz, CDCl$_3$): δ: 6.87-6.72 (3H, m, H-7, H-9, H-10), 4.29 (2H, t, J = 5.5 Hz, H-2), 4.21 (2H, t, J = 5.5 Hz, H-5), 2.26 (3H, s, Ar-Me), 1.88 (4H, m, H-3, H-4); ^{13}C NMR (75MHz, CDCl$_3$): δ: 149.5 (C-10a), 146.6 (C-6a), 133.5 (C-8), 123.8 (C-9), 122.6 (C-10), 122.3 (C-7), 73.1 (C-2), 72.2 (C-5), 27.3 (C-4), 26.4 (C-3), 20.6 (Ar-Me). ^{1}H,^{1}H COSY (CDCl$_3$): 4.23 (H-5) × 1.82 (H-4), 3.96 (H-2) × 1.95 (H-3). ^{1}H,^{13}C HMQC (CDCl$_3$): H-2 × C-2 (73.2 ppm), H-5 × C-5 (74.5), H-4 × C-4 (28.0), H-3 × C-3 (26.6). EIMS m/z: 178 (M$^{+\bullet}$, 100%), 150 (2.3), 135 (75.2), 124 (100), 106 (11.8), 94 (16.6), 78 (38.8), 66 (47.9), 55 (96.0), 39 (73.2).

3,4-Dihydro-7-methyl-2*H*-1,5-benzodioxepin-3-yl acetate (**71**)

TEA (0.20 mL, 1.43 mmol) was added to a solution of **66** (0.20 g, 1.11 mmol) in anhydrous Et$_2$O (20 mL). Acetyl chloride (0.097 mL, 1.36 mmol) was added dropwise and the reaction mixture left to stir at ambient temperature for 2 hours. The precipitate was removed by vacuum filtration and the filtrate dissolved in Et$_2$O (50 mL) and washed with aq. 2M HCl (3 × 50 mL) and saturated aq NaHCO$_3$ (3 × 50 mL). The organic extracts were combined and dried over MgSO$_4$, then concentrated under vacuum to afford **71** as a low melting yellow solid (0.22 g, 88%) in >95% purity by GC-MS, m.p. 43-44°C. IR (KBr), ν (cm^{-1}): 2969m, 2947w, 2926w, 1736s, 1694w, 1579w, 1509m, 1445m, 1396w, 1379m, 1338w, 1296m, 1276m, 1252s, 1206m, 1154w, 1109m, 1056s, 1028m. ^{1}H NMR (300MHz, CDCl$_3$): δ: 6.83 (1H, d, J = 8.1 Hz, H-9), 6.76 (1H, s, H-6), 6.71 (1H, d, J = 8.1 Hz, H-8), 5.26 (1H, tt, J1 = 5.1 Hz, J2 = 4.3 Hz, H-3), 4.37 (1H, dd, J1 = 12.8 Hz, J2 = 4.3 Hz, H-2$_A$), 4.35 (1H, dd, J1 = 12.8 Hz, J2= 4.3 Hz, H-2$_B$), 4.28 (1H, dd, J1 = 12.8 Hz, J2 = 5.1 Hz, H-4$_A$), 4.26 (1H, dd, J1 = 12.8 Hz, J2 = 5.1 Hz, H-4$_B$), 2.24 (3H, s, Ar-Me), 2.13 (3H, s, CO-Me); ^{13}C NMR (75MHz, CDCl$_3$): δ: 170.3 (CO), 149.4 (C-9a), 147.5 (C-5a),

133.2 (C-7), 123.8 (C-8), 121.2 (C-9), 120.5 (C-6), 71.5 (C-3), 71.4 (C-2), 71.2 (C-4), 20.9 (CO-Me), 20.4 (Ar-Me). ^{1}H,^{1}H COSY (CDCl$_3$): 5.17 (H-3) × 4.23 (H-2, -4). ^{1}H,^{13}C HMQC (CDCl$_3$): H-3 × C-3 (71.6), H-2, -4 × C-2, -4 (71.4), H-2' x CH3-2' (20.5). EIMS m/z: 222 (M$^{+\bullet}$, 23.1%), 162 (46.1), 161 (38.9), 149 (6.5), 135 (51.8), 133 (5.9), 124 (12.7), 123 (10.0), 105 (8.3), 94 (17.1), 91 (13.7), 77 (18.7), 66 (25.5), 51 (12.6), 43 (100), 39 (24.5).

3,4-Dihydro-7-methyl-2H-1,5-benzodioxepin-3-yl benzoate (**72**)

Benzoyl chloride (0.142 mL, 1.22 mmol) was reacted with **66** following the procedure described for the preparation of **71** to afford **72** as a low melting white solid (0.14 g, 44%) in >95% purity by GC-MS, m.p. 54-56°C. IR (KBr), ν (cm^{-1}): 2931w, 1714s, 1613w, 1601w, 1582m, 1506s, 1463m, 1450m, 1416w, 1392w, 1361w, 1331m, 1308m, 1287s, 1264s, 1253s, 1209m, 1195m, 1174m, 1151m, 1117s, 1085m, 1070m, 1041m, 1033m. ^{1}H NMR (300MHz, CDCl$_3$): δ: 8.10 (1H, s, H-2'), 8.10 (1H, s, H-6'), 7.59 (1H, t, J = 7.3 Hz, H-4'), 7.45 (2H, t, J = 7.8 Hz, H-3', -5'), 6.86 (1H, d, J = 8.1 Hz, H-9), 6.79 (1H, s, H-6), 6.73 (1H, d, J = 8.1 Hz, H-8), 5.53 (1H, tt, $J1$ = 5.1 Hz, $J2$ = 4.3 Hz, H-3), 4.51 (1H, dd, $J1$ = 12.8 Hz, $J2$ = 4.3 Hz, H-2$_A$), 4.50 (1H, dd, $J1$ = 12.8 Hz, $J2$ = 4.3 Hz, H-2$_B$), 4.43 (1H, dd, $J1$ = 12.8 Hz, $J2$ = 5.1 Hz, H-4$_A$), 4.42 (1H, dd, $J1$ = 12.8 Hz, $J2$ = 5.1 Hz, H-4$_B$), 2.26 (3H, s, Ar-Me); ^{13}C NMR (75MHz, CDCl$_3$): δ: 165.8 (CO), 149.4 (C-9a), 147.6 (C-5a), 133.4 (C-4'), 133.2 (C-7), 129.8 (C-6'), 129.5 (C-2'), 128.4 (C-3', -5'), 123.8 (C-8), 121.2 (C-6), 120.5 (C-9), 71.9 (C-3), 71.6 (C-2), 71.3 (C-4), 20.5 (Ar-Me). ^{1}H,^{1}H COSY (CDCl$_3$): 8.01 (H-2', -6') × 7.38 (H-3', -5'), 7.52 (H-4') × 7.38 (H-3', -5'), 5.45 (H-3) × 4.40 (H-2, -4), 4.45 (H-4) × 4.33 (H-2). ^{1}H,^{13}C HMQC (CDCl$_3$): H-2', -6' × C-2', -6' (129.8), H-4' × C-4' (133.5), H-3', -5' × C-3', -5' (128.5), H-3 × C-3 (72.1), H-2, -4 × C-2, -4 (71.7). EIMS m/z: 284 (M$^{+\bullet}$, 48.8%), 162 (100), 149 (3.2), 135 (32.0), 123 (2.7), 105 (70.9), 94 (7.0), 77 (40.2), 66 (7.4), 51 (7.7), 39 (3.8).

3,4-Dihydro-7-methyl-2H-1,5-benzodioxepin-3-yl prop-2-enoate (**73**)

Acryloyl chloride (0.099 mL, 1.22 mmol) was reacted with **66** following the procedure outlined for **71**, to yield **73** a clear pale yellow oil (0.057 g, 22%) in >95% purity by GC-MS. IR (neat), ν (cm^{-1}): 3106w, 3036m, 1955w, 1873w, 1732s, 1635m, 1619w, 1581m, 1505s, 1462w, 1445w, 1406s, 1306s, 1295s, 1259s, 1185s, 1150m, 1115m, 1075m, 1050s, 1012m. ^{1}H NMR (300MHz, CDCl$_3$): δ: 6.83 (1H, d, J = 8.1 Hz, H-9), 6.76 (1H, s, H-6), 6.72 (1H, d, J = 8.1 Hz, H-8), 6.49 (1H, d, J = 17.3 Hz, H-3$_A$'), 6.18 (1H, dd, $J1_{trans}$ = 17.3 Hz, $J2_{cis}$ = 10.4 Hz, H-2'), 5.90 (1H, d, J = 10.4 Hz, H-3$_B$'), 5.35 (1H, tt, $J1$ = 5.1 Hz, $J2$ = 4.3 Hz, H-3), 4.34 (1H, dd, $J1$ = 12.8 Hz, $J2$ = 4.3 Hz, H-2$_A$), 4.33 (1H, dd, $J1$ = 12.8 Hz, $J2$ = 4.3 Hz, H-2$_B$), 4.25 (1H, dd, $J1$ = 12.8 Hz, $J2$ = 5.1 Hz, H-4$_A$), 4.23 (1H, dd, $J1$ = 12.8

Hz, $J2$ = 5.1 Hz, H-4$_B$), 2.24 (3H, s, Ar-Me); ^{13}C NMR (75MHz, CDCl$_3$): δ: 165.4 (CO-1'), 149.3 (C-9a), 147.5 (C-5a), 133.2 (C-3'), 132.0 (C-7), 127.8 (C-2'), 123.8 (C-8), 121.2 (C-9), 120.5 (C-6), 71.5 (C-3), 71.4 (C-2), 71.2 (C-4), 20.4 (Ar-Me). ^{1}H,^{1}H COSY (CDCl3): 6.43 (H-3$_A$') × 6.11 (H-2'), 6.14 (H-2') × 5.85 (H-3$_B$'), 5.28 (H-3) × 4.30 (H-2$_A$, -4$_A$). ^{1}H,^{13}C HMQC (CDCl3): H-3$_B$' × C-3' (133.1), H-3$_A$' × C-3' (130.9), H-2' × C-2' (128.4), H-3 × C-3 (71.6), H-2 × C-2 (70.5), H-4 × C-4 (70.2). EIMS m/z: 234 (M$^{+•}$, 66.5%), 162 (100), 149 (8.3), 135 (54.5), 123 (56.0), 105 (7.6), 94 (13.4), 77 (10.5), 66 (13.4), 55 (44.9), 39 (6.3).

3,4-Dihydro-7-methyl-2H-1,5-benzodioxepin-3-amine (**74**)

Under a dry nitrogen atmosphere NaBH$_4$ (1.64 g, 43.33 mmol) was added portion wise to freshly distilled TiCl$_4$ (2.39 mL, 21.79 mmol) in anhydrous DME (100 mL) at 0°C. The blue solution was stirred for 10 min followed by the addition of **65** (1.0 g, 5.18 mmol), then the mixture was warmed to ambient temperature and allowed to stir for 24 hr. The reaction was quenched in ice/H$_2$O (200 mL) then washed with DCM (5 × 50 mL). The aqueous portion was then basified to pH 8 and extracted with DCM (3 × 70 mL). The combined organic extracts were dried over MgSO$_4$ and concentrated under vacuum to give a yellow resin that was subjected to semi preparative HPLC (t_R = 10.2 min, λ_{max} = 231, 275 nm) to afford **74** as a clear oil (0.50 g, 54%). IR (neat), ν (cm^{-1}): 3361w, 3295m, 3033w, 2925m, 2878w, 1612w, 1578w, 1505m, 1459w, 1417w, 1394w, 1373w, 1305m, 1260m, 1202w, 1148w, 1114w, 1091w, 1033m. ^{1}H NMR (300MHz, CDCl$_3$): δ: 6.89-6.71 (3H, m, H-6, -8, -9), 4.14 (2H, broad s, NH$_2$), 4.32-3.97 (5H, m, H-2, -3, -4), 2.24 (3H, s, Ar-Me); ^{13}C NMR (75MHz, CDCl$_3$): δ: 150.5 (C-9a), 148.7 (C-5a), 133.9 (C-7), 124.1 (C-8), 121.8 (C-9), 121.0 (C-6), 74.1 (C-2), 74.0 (C-4), 50.7 (C-3), 20.5 (Ar-Me). ^{1}H,^{1}H COSY (CDCl$_3$): 4.16 (H-2$_A$) × 3.27 (H-2$_B$), 4.16 (H-4$_A$) × 3.27 (H-4$_B$), 4.13 (H-4, -2) × 3.96 (H-3). ^{1}H,^{13}C HMQC (CDCl$_3$): H-2, -4 × C-4, -2 (74.0), H-3 × C-3 (52.0). EIMS m/z: 179 (M$^{+•}$, 65.5%), 162 (19.2), 151 (20.6), 150 (57.2), 135 (100), 123 (7.1), 121 (9.3), 105 (7.3), 91 (12.9), 78 (17.9), 77 (19.8), 66 (8.7), 65 (8.8), 63 (5.7), 56 (34.7), 51 (11.1). High Resolution Mass Spectrum (HRESI) Found [M]$^{+•}$, 180.1017. C$_{10}$H$_{14}$NO$_2$ [M + H]$^{+•}$ requires 180.1024.

7.5   Preparation   of   Crude   2,5-Dihydro-8-methyl-1,6-benzodioxocine (77)

1,2-Bis(allyloxy)-4-methyl benzene (**75**)
4-Methyl catechol **20** (0.50 g, 4.03 mmol) was solubilized in anhydrous DMF (50 mL), to which ground oven-dried K_2CO_3 (1.67 g, 12.1 mmol) and allyl bromide (1.95 g, 16.0 mmol) were added. The reaction solution was heated at 80°C for 2 hr. The solution was quenched in ice/H_2O (150 mL) and extracted with DCM (3 × 50 mL). The combined extracts were washed with brine (2 × 50 mL) and concentrated under vacuum. The crude residue was solubilized in MeCN (6.0 mL), followed by addition of TEA (2.0 mL) and stirred at ambient temperature for 24 hr to remove excess allyl bromide. The solid material was removed with a syringe filter (0.45 µm), and the remaining residue stored at -20°C to allow final bromide salts to precipitate. Once the remaining precipitate had been removed by syringe filter, the TEA was removed with rotary evaporation to yield **75** as clear pale yellow oil (0.81 g, 99%).

2,5-Dihydro-8-methyl-1,6-benzodioxocine (**77**)
Grubb's catalyst (0.025 g, 0.029 mmol) solubilized in anhydrous benzene (10 mL) was added to **75** (0.50 g, 2.45 mmol) dissolved in anhydrous benzene (30 mL) under N_2. The reaction mixture was left to stir at 50°C and monitored by GC-MS. Upon completion the excess solvent was removed under vacuum. The solution was run through a short column (SiO_2) using DCM:pentane at a gradient of 2:98-10:90 with vacuum elution. The collected fractions provided **77** as clear oil (0.36 g, 83%).

7.6   Synthetic Steps Towards Preparation of (5aR,9aR)-7-Methylhexahydro-2H-1,5-benzodioxepin-3(4H)-one (88)

7,8-Dioxaspiro[4.5]decane-1,4,6,9-tetrone (disuccinoyl peroxide) (**93**)
Succinic anhydride (**92**) (2.0 g, 26.3 mmol) was combined with 30% hydrogen peroxide (20 mL) solution and the mixture was stirred vigorously in an oil bath at 70°C for 0.5 hr. The reaction solution was allowed to reach room temperature to encourage formation of the white precipitate product. The solid precipitate was filtered under vacuum and washed with ice cold H_2O (5 × 10 mL) and ice cold Et_2O (3 × 10 mL) to give purified **93** (0.98 g, 19%).

(1*R*,2*R*)-4-Methyl-1,2-cyclohexanediol (**88**)

Method 1: Disuccinoyl peroxide (**93**) (0.34 g, 1.72 mmol) was added to cyclic olefin **94** (0.10 g, 1.04 mmol) in H_2O (10 mL) containing Sorbitan trioleate (Span 85) (1.5 mg). The mixture was stirred vigorously for 24 hr at 50°C in an oil bath. The reaction mixture was poured into a 10% $NaHCO_3$ solution (20 mL) and extracted with DCM (4 × 15 mL). The combined organic extracts were washed with H_2O (1 × 20 mL) and concentrated in vacuo to leave clear yellow oil. The yellow residue was crystallised from EtOAc: Et_2O with evaporative methods to leave clear crystals of purified **60** (21 mg, 14%).

Method 2: *m*-Chloroperbenzoic acid (0.33 g, 1.94 mmol) in DCM was added dropwise over 0.5 hr to a stirred solution of **59** (0.15 g, 1.56 mmol) in DCM held at 0°C in an ice bath. The reaction solution was left to stir at ambient temperature for 5 day after which the solid precipitate was removed by filtration. The precipitate was washed with 5% KOH solution, and the filtrate was concentrated under vacuum to leave purified **60** as white crystalline solid (41 mg, 18%).

7.7 Preparation of crude 5*H*-1,4-benzodioxepin-3(2*H*)-one (98)

Methyl 2-(2-formylphenoxy)acetate (**96**)

Ground oven-dried K_2CO_3 (23.7 g, 171.6 mmol) and methyl bromoacetate (15.79 mL, 171.2 mmol) were added to salicylaldehyde (6 mL) in anhydrous DMF (40 mL). The solution was heated at 90°C for 1 hr under N_2 and then quenched in ice/H_2O (100 mL). The reaction solution was then extracted with DCM (3 × 40 mL), and the combined organic extracts were washed with brine (2 × 40 mL). Excess solvent and reagents were removed under vacuum (0.5 mmHg) with gentle heating in a H_2O bath (30°C) to leave a beige-coloured residue (9.60 g, 86%) that solidified upon cooling.

Methyl 2-[2-(hydroxymethyl)phenoxy]acetate (**97**)

$NaBH_4$ (0.30 g) was added to **96** (1.57 g) dissolved in a solution of H_2O (30 mL) and MeOH (10 mL). The solution was placed in an ice/H_2O bath and left to stir vigourously for 2 hr.

5*H*-1,4-benzodioxepin-3(2*H*)-one (**98**)

Addition of KO^{t}Bu (1.1 eq) to **41** in THF at 70°C failed to induce cyclisation. GC-MS monitoring of the reaction over 1 hr revealed formation of a range of cleavage products from **41**.

Aqueous HCl (2M) (40 mL) was added to the reaction solution of **97** and the mixture was stirred for 1 hr at ambient temperature. The reaction solution was added to ice/H$_2$O (40 mL) and extracted with DCM. The organic portions were combined and washed with brine (1 × 50 mL) and H$_2$O (4 × 40 mL). The organic layer was then concentrated *in vacuo* to leave clear pale yellow oil (1.12 g, 84%). Impurities 2-[2-(hydroxymethyl)phenoxy]acetaldehyde, **100** and 2-[2-(hydroxymethyl)phenoxy]-1-ethanol, **101** were also formed. These two compounds were not isolated, however the degree of formation of these can be seen in GC trace shown in Figure 4.32.

7.8   Chromatographic Separations

7.8.1   Semi-Preparative High Performance Liquid Chromatography (HPLC)

HPLC fractions were collected using a Varian Prostar, Model 210 system on a Phenomenex analytical column with dimensions of 250 × 10 mm with prodigy 5 micron ODS (3), 100A. The samples were run at a pressure of 2900 psi with a flow rate of 3.0 mL/min in MeCN:H$_2$O (33:77).

7.8.2   Instrument Conditions for GC-qMS

Instrument 1:

GC-qMS was performed on a Hewlett Packard 5890 GC system equipped with a Hewlett Packard 5970 mass selective detector. The sample was run on a BPX5 (5% phenyl polysilphenylene-siloxane) capillary column with dimensions of 30 m × 0.25 mm I.D. × 0.25 μm d$_f$. The oven was held at 50°C for 10 min then increased to 300°C at 20°C/min and held for 10 min. Samples were injected manually with a 1 μL syringe. Helium was used as carrier gas at a flow rate of 1.0 mL/min and a split ratio of 50:1. For all analyses the transfer line temperature was 260°C.

Instrument 2:

GC-qMS was performed on an Agilent HP6890 system equipped with a HP5973 mass selective detector (Agilent Technologies, Burwood, Australia) with an Agilent 7683 Series autosampler (Agilent Technologies, Palo Alto, CA, USA). The sample was run on a BPX5 (5% phenyl polysilphenylene-siloxane) capillary column with dimensions of 30 m $\times$ 0.25 mm I.D. $\times$ 0.25 μm d_f. The oven was held at 50°C for 5 min then increased to 300°C at 20°C/min and held for 10 min. The injected sample volume was 1 μL with a split ratio of 50:1. Helium was used as carrier gas at a flow rate of 1.0 mL/min. For all analyses the transfer line temperature was 260°C. The source temperature was 230°C with a mass scan range of m/z 30-550 at a data acquisition rate of 20 cycles/sec (Hz). The detector (electron multiplier) voltage was 2 kV with ionisation energy of 70 eV. Selected ion monitoring (SIM; 178, 149, 135, 122, 94, 77 m/z ions selected) mode was run at a data acquisition rate of 8.33 Hz.

7.8.3   Instrument Conditions for GC×GC-TOFMS

An Agilent HP6890 GC (Agilent Technologies, Burwood, Australia) with Chemstation data system to program modulation was interfaced to the Pegasus III time-of-flight mass spectrometer (TOFMS) (LECO, ST Joseph, MI, USA) for mass spectral data. Injection methods employed an Agilent 7683 Series autosampler (Agilent Technologies, Palo Alto, CA, USA). The primary column was a 30 m x 0.25 mm I.D. x 0.25 μm d_f BPX5 (5% phenyl polysilphenylene-siloxane) capillary directly coupled to a secondary BP20 column 1 m x 0.1 mm I.D. x 0.1 mm d_f (polyethylene glycol) capillary, both from SGE International, Ringwood, Australia. The GC oven temperature was programmed from 50°C (held for 5 min) to 250°C at a rate of 20°C/min, which was held for 10 min. The detector voltage for electron impact ionisation was set at 70 eV. The ion source temperature was set at 200°C to acquire ions in the mass range 45-5000 m/z at 50 spectra/s. Samples (1 μL) were injected at 250°C using split conditions (10:1) with helium as carrier gas and a flow rate of 1 mL/min.

The primary and secondary columns were connected via a transfer line with zero dead volume (SGE International, Ringwood, Australia) operated at 260°C. The 6890GC was retrofitted with an Everest model Longitudinally Modulated Cryogenic System (LMCS)

(Chromatography Concepts, Doncaster, Australia). Modulation period (P_M) was set at 5 seconds.

7.8.4 Sample Preparation for qGC-MS and GCxGC-TOFMS

The Cool Water Woman perfume was purchased and stored at room temperature. Calone 1951® is a solid compound and was stored at 4°C. The Calone 1951® standard was analysed at 10% dilution in analytical (AR) grade hexane. The perfume sample was analysed at 10% dilution in analytical (AR) grade hexane, and with a 10% Calone 1951® spike addition.

7.8.5 GCxGC-TOFMS Software

Importation of the raw data matrix was achieved using the ASCII (.csv) format. Origin (Microcal Software, Northampton, MA) was used to convert the original ASCII file to a conventional chromatogram trace. 2D-GC converter (Chromatography Concepts) software enabled importation into Transform (Fortner Research, Boulder, USA) to generate the 2D contour plot. ChromaTOF™ software (LECO) was used for peak integration and identification of peaks and referenced to the mass spectra from NIST (1998) and Wiley (7th Edition, 2000) libraries.

7.8.6 Gas Chromatography-Olfactometry

GC (FID)-olfactometry analyses were performed using a Hewlett Packard HP6890 gas chromatography system with an olfactometry sniffer port (SGE International ODO-II model). Separation was on a 30 m × 0.19 mm ID × 0.25 μm d_f BPX5 capillary column. The temperature program was 70°C held for 3 min, then 10°C/min to 250°C. Total run time was 28 min at constant flow of 1.0 mL/min. Hydrogen was used as the carrier gas. Injection volumes were 1μL (10-20% in acetone). The injector temperature was 250°C at a split ratio of 50:1. The FID detector:sniffer port split ratio was 1:1. The humidified air eluting from the sniffer port was maintained at 50°C.

Four un-trained panellists performed the olfactory analyses. Panellists sniffed an 8-minute window (4 minutes either side) around the retention time corresponding to the

identified compound and recorded their odour descriptor (free choice profiling) and intensity (strong, medium, weak) observations. Odour descriptors were initially offered to subjects, however it was found that this had a placebo-type influence and the descriptors offered by the subjects was suitable. Prior to quantitative evaluation all compounds were identified by qGC-MS, and the purity and retention times validated by GC-FID. Samples were analysed at 10% (v/v) in HPLC-grade acetone. Purity of all compounds analysed was >95%, most >99%. Blotter analysis was performed at 10% in dipropylene glycol, sniffed at 4 hr and 24 hr.

7.8.7 Headspace Gas Chromatography (H-GC)

GC-qMS was performed on an Agilent HP5890 system equipped with a HP5970 mass selective detector (Agilent Technologies, Burwood, Australia). The sample was run on a BPX5 (5% phenyl polysilphenylene-siloxane) capillary column with dimensions of 30 m $\times$ 0.25 mm I.D. $\times$ 0.25 μm d_f. The oven was held at 50°C for 5 min then increased to 300°C at 10°C/min and held for 10 min with no solvent delay. A 0.1 mL gas-tight syringe was used to inject 0.05 mL of headspace gas at a split ratio of 50:1. Helium was used as carrier gas at a flow rate of 1.0 mL/min. For all analyses the transfer line temperature was 260°C. The source temperature was 230°C with a mass scan range of m/z 30-550 at a data acquisition rate of 20 cycles/sec (Hz).

7.8.8 Experimental Protocol: Geometric models

CambridgeSoft Chem3D Ultra was used for generation of energy-minimised structures. The original structure generated from Chem3D was energy minimised using the MM2 force field with thermodynamic control set at 1.0 Kcal/atom/ps and the target temperature at 300 K. The structure was then optimised using semi-empirical PM3 with restricted parameters (closed shell) and assumed Mulliken charges. The PM3 system was set to run on heat of formation calculations at an RMS gradient of 0.100.

7.9   References

[1] A.M.   Lingham,   M.,   Provided   on   trial   by   Warlock   Engineering: www.warlock.com.au/chemreactor.htm. (2002-2006).

8   Conclusion and Recommendation for Further Work

Contributions from a variety of disciplines render olfactory research and fragrance chemistry an ever-expanding field of research. The valuable contributions from fragrance syntheses to discoveries at the molecular level of olfactory activity are evident. As SAR has persisted as a mainstay in drug research, so too will SOR in fragrance chemistry. Comprehensive olfactory evaluation inclusive, this thesis has aimed at contributing to the molecular databank of accessible novel fragrant compounds.

The literature review presented in Chapter 1 covers the scope of research discoveries in olfactory perception, and the attributes required by a molecule to be eligible as an odourant. Progress in genetics, physiology and chemistry has led to the understanding of the structure and function of olfactory processes. In the context of the favourable properties exemplified as primary for odour-activity in the introductory chapters, synthetic manipulations of the benzodioxepinone skeleton aimed to comply with these requirements to increase the chances of discovering molecular properties conducive for a prime odourant. The scope of functional group investigation was broad in order to test the limitations of olfactory perception.

The overall syntheses presented in this manuscript were divided into two broad categories: aromatic substituents and polar functional group variation. Chapters 2 and 3 focused on various aromatic substitutions for testing functional group locale and properties. Chapter 2 implemented a synthetic strategy based on literature methodology (Procedure A). As detailed it was discovered that diversity in aromatic substitution affected the physicochemical make-up of the entire benzodioxepinone structure through characterization studies including NMR and SE modelling. As a result success of the original synthetic scheme was selective and therefore an alternative synthetic methodology was applied. The novel mechanistic approach introduced (Procedure B) derived successful results and broad synthetic applicability as assessed in Chapter 3. Chapters 2 and 3 also presented a comparative study between the two schemes and a summated assessment of yields and purity levels. It was determined that the initial methodology can be applied to obtain select benzodioxepinone targets in high yields and purity and the devised methodology can be applied more broadly to obtain a wider scope of benzodioxepinone ring-closure products in competitive yields and purities. The

success achieved with Procedure B in application to compounds with aromatic electron-withdrawing groups was particularly conducive as that was specifically where the original synthetic strategy was hindered.

Chapter 4 explored syntheses to produce derivatives from alterations of the heterocyclic carbonyl for exploration of differences in polarity.

Research presented in Chapter 5 utilised GCxGC for detection of Calone 1951® in a commercial fragrance as a case study for this pioneering and sensitive technique for separation and identification of components in complex materials such as fragrances.

Chapter 6 presents the collated olfactory characteristics derived for the analogues synthesized in Chapters 2, 3 and 4 assessed by professionals (Philip Kraft, Alain Alchenberger) in the field of fragrance chemistry. These results are presented with conclusions drawn based on geometry and some generalized physicochemical parameters. More specifically Chapter 6 provides a critical assessment of two methods of olfactory evaluation, GCO and blotter analysis. Overall the most beneficial analysis incorporates both methods to test and evaluate the odourant. For efficient analyses under time constraints, the method should be selected in light of an understanding of the potential applications for the odourant and the properties of the fragrant compound to be exploited.

A synthetic area not thoroughly explored in this manuscript and proposed for future research involves the exploration of proton-donor, proton-acceptor regions within an accessible distance to each other as reported by Guenther and Wolfgang. Introduction of bi-functionality is informative when mono-functional equivalents have been assessed. Reports on the odour-activity noticed by Guenther and Wolfgang provide an interesting base to further explore the benzodioxepinone arena.

Research presented in Section 4.3.3 demonstrates that attempts to place sulfur heteroatoms into the benzodioxepinone structure is arduous and ineffective, primarily due to the increased number of oxidation state possibilities for sulfur, which can hinder formation of a benzodioxepine configuration. As an alternative, nitrogen heteroatoms could be incorporated to form a diazepin system as shown in Scheme 8.1.
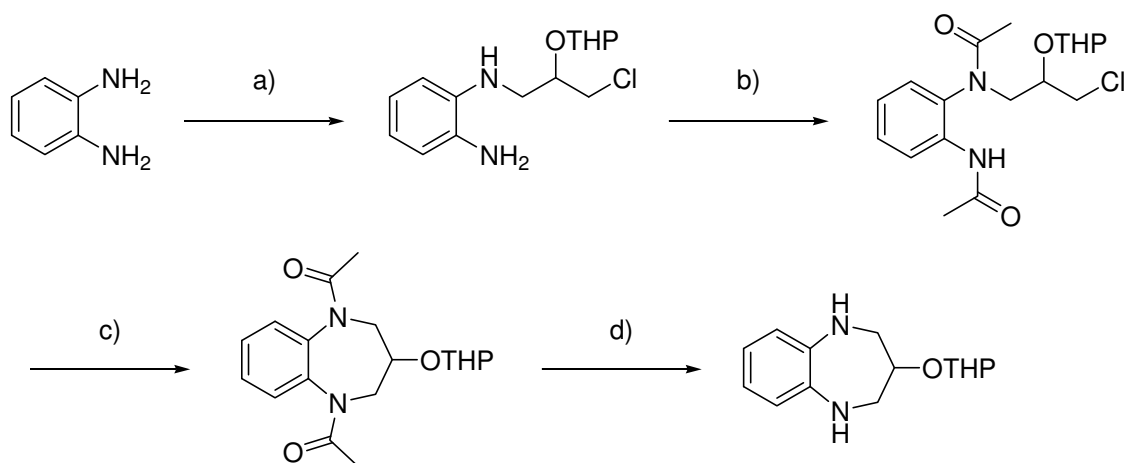
Scheme 8.1 Proposed pathway to 1,2,4,5-tetrahydro-3*H*-1,5-benzodiazepin-3-one: a) LDA, **62**, THF; b) Ac$_2$O, DCM ; c) LDA, THF; d) HCl, aq. EtOH

The research presented in this thesis has proven that substitution at the carbonyl carbon of Calone 1951® provides analogues with high odour thresholds, chiral and non-chiral inclusive. Exploration of the influence and effect of chirality adjacent to the benzene ring would provide desirable substrates for odour intensity analyses, in conjunction with odour character. Implementation of a variation of the THP-protected synthesis presented in Chapter 4 applied to the cyclohexane product (**62**) from Section 4.3.4 would result in an interesting optically active analogue as presented in Scheme 8.2.
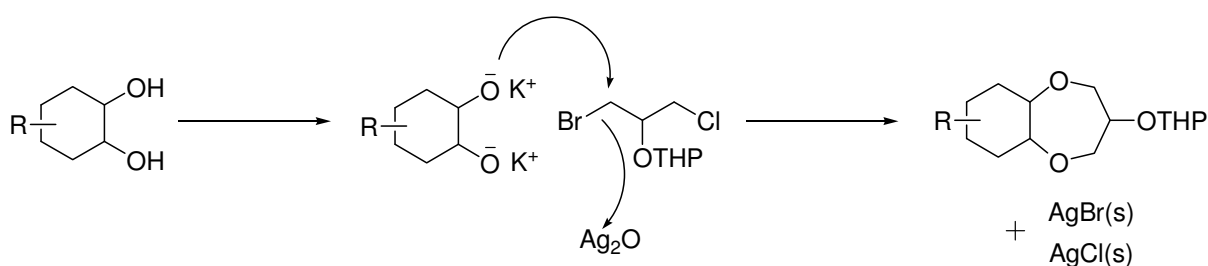
Scheme 8.2 Proposed pathway to hexahydro-2*H*-1,5-benzodioxepin-3(4*H*)-one: KH, Ag$_2$O, DMF

In light of the discoveries by researchers such as Turin, testing his proposals would have provided an interesting experimental critique to the data published by Turin. Comprehensive IR data (normal IR and far-IR) was obtained for each compound within the bendioxepinone group, however limited access to relevant software hindered further progress in this area. Comparisons made with Raman spectra would be informative, in conjunction with odourant activity and temperature correlations.

Appendices

Appendix 1

Proposed major fragment ions from soft ionization of **21** and derivatives of **21** (70eV), EI mass spectrum of **21c**
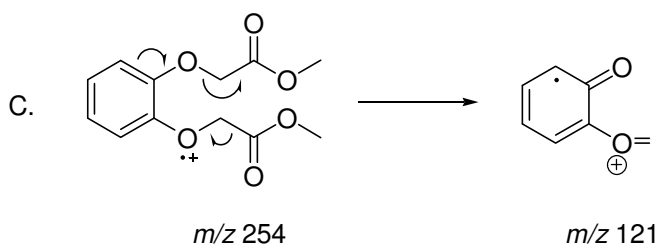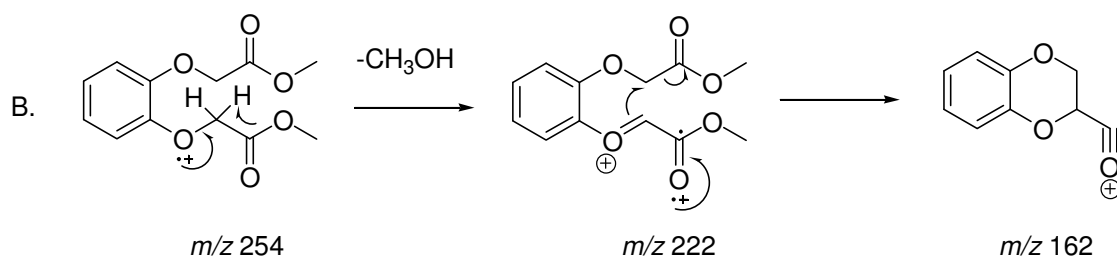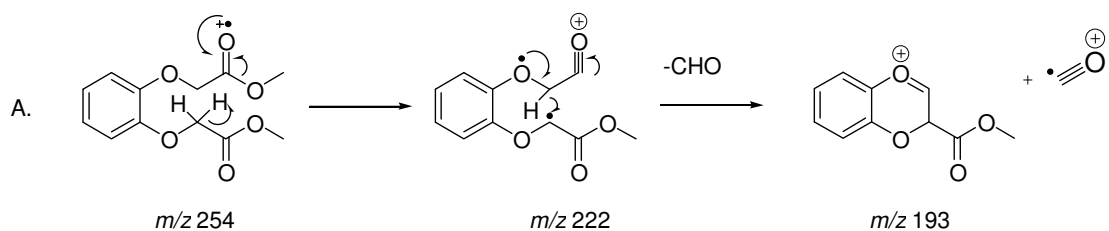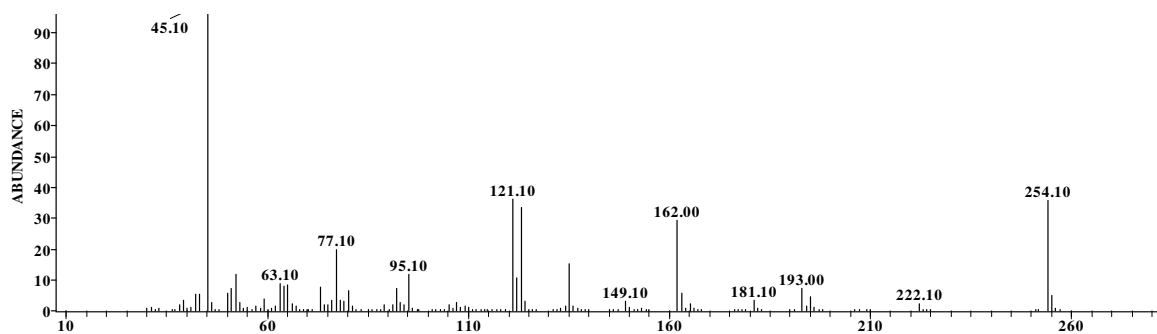
Appendix 2

^{1}H,^{13}C HMQC of **21a**
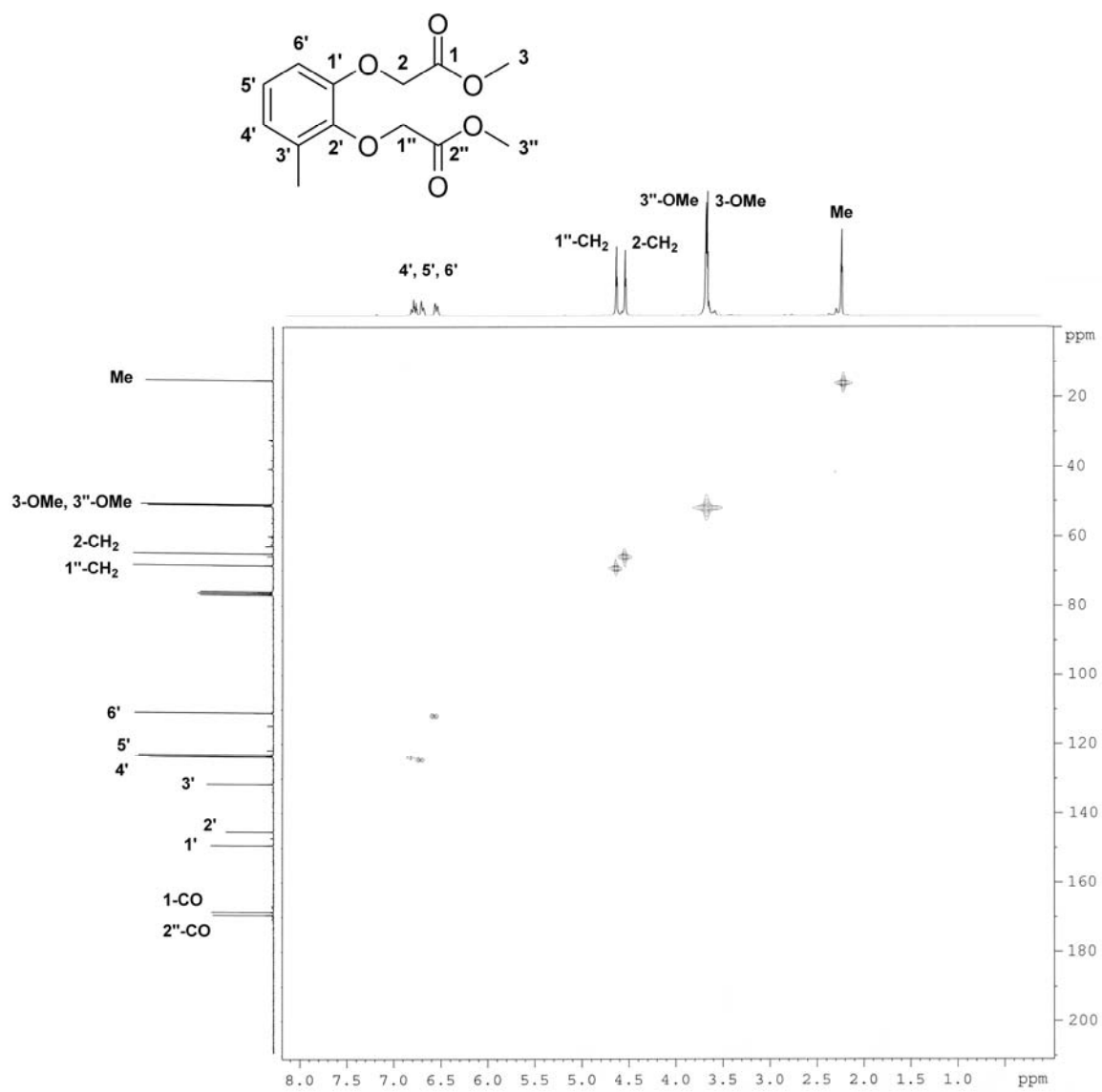
Appendix 3

^{1}H and ^{13}C spectra of **21b**
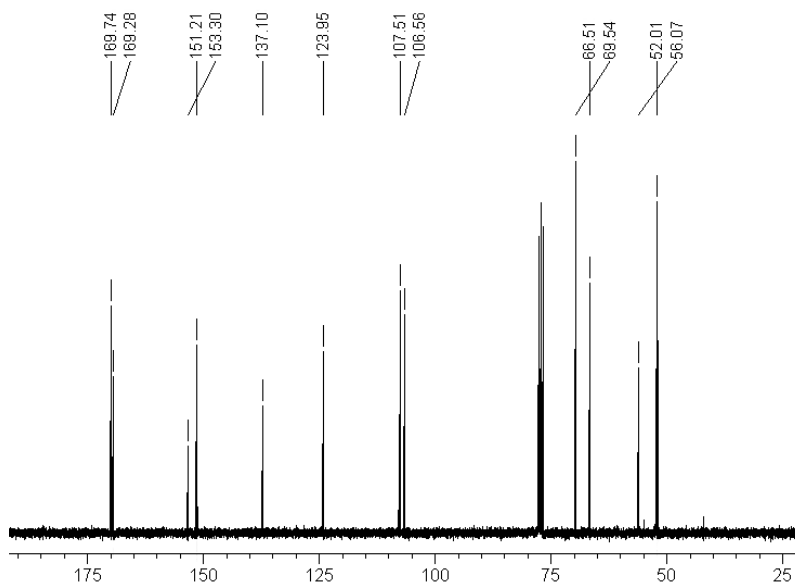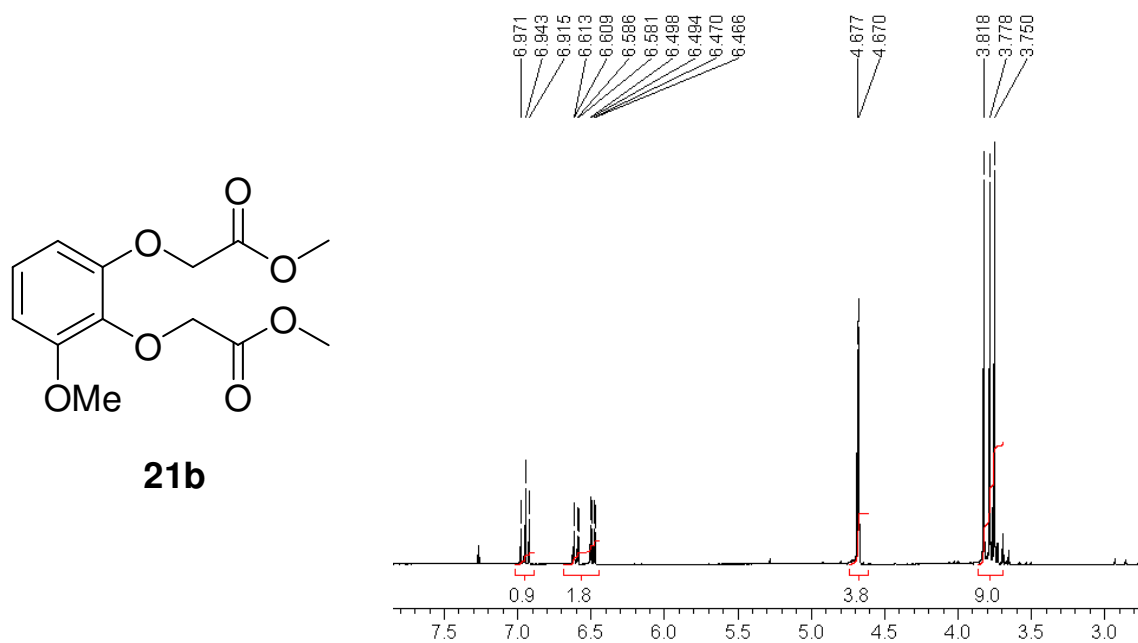
EI mass spectrum and $^1H,^{13}C$ HMQC spectrum of **21b**

^{1}H,^{13}C HMBC of **21b**

254
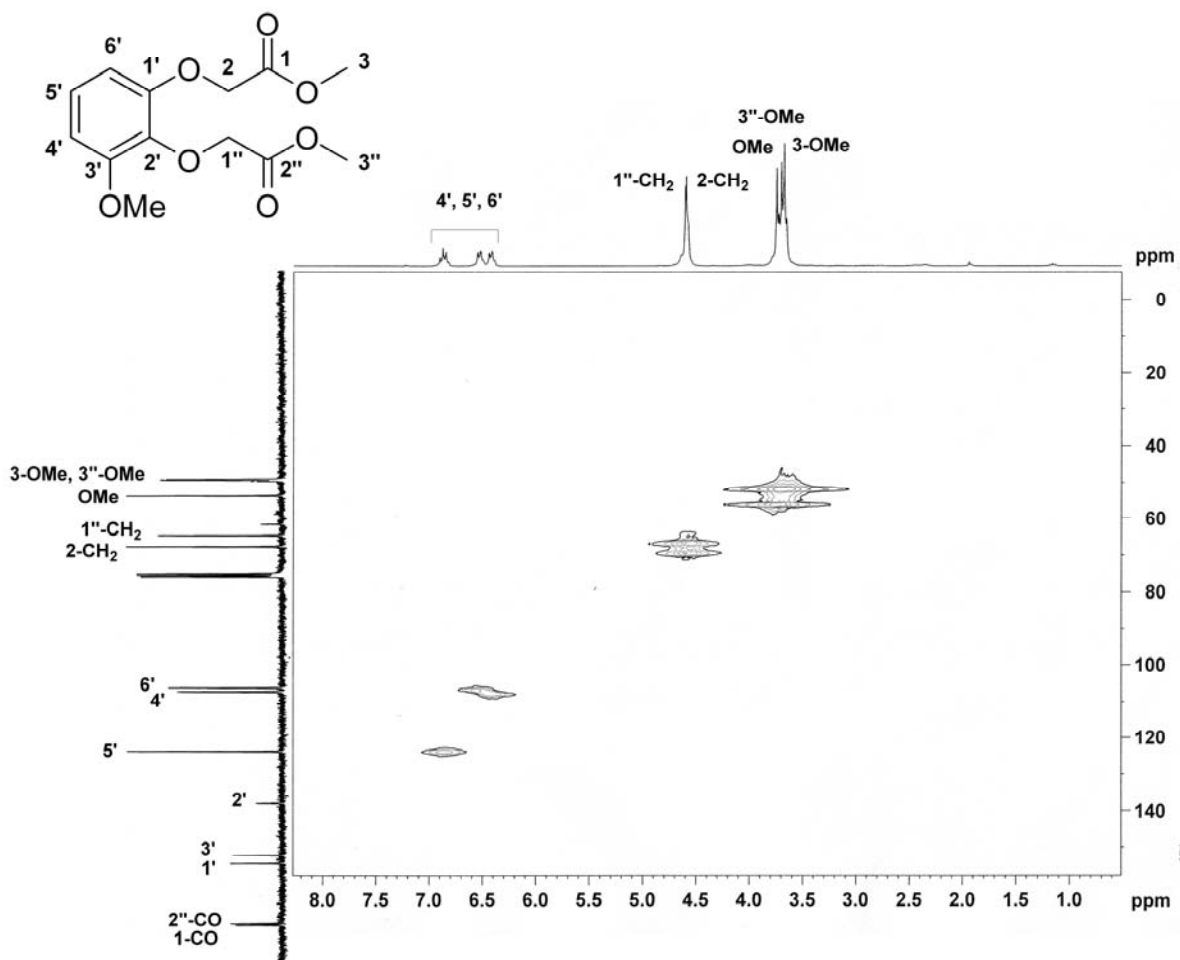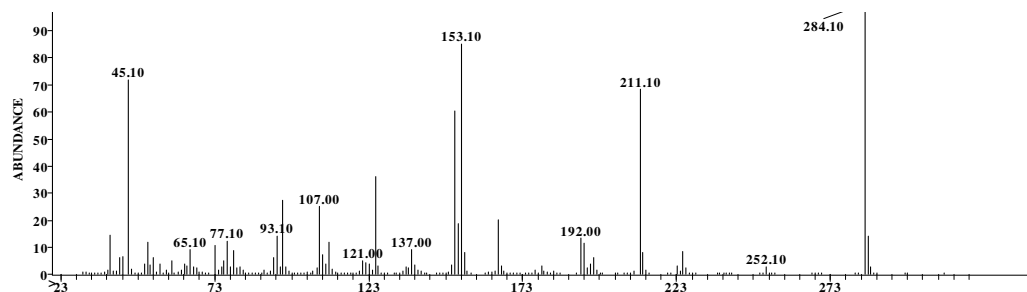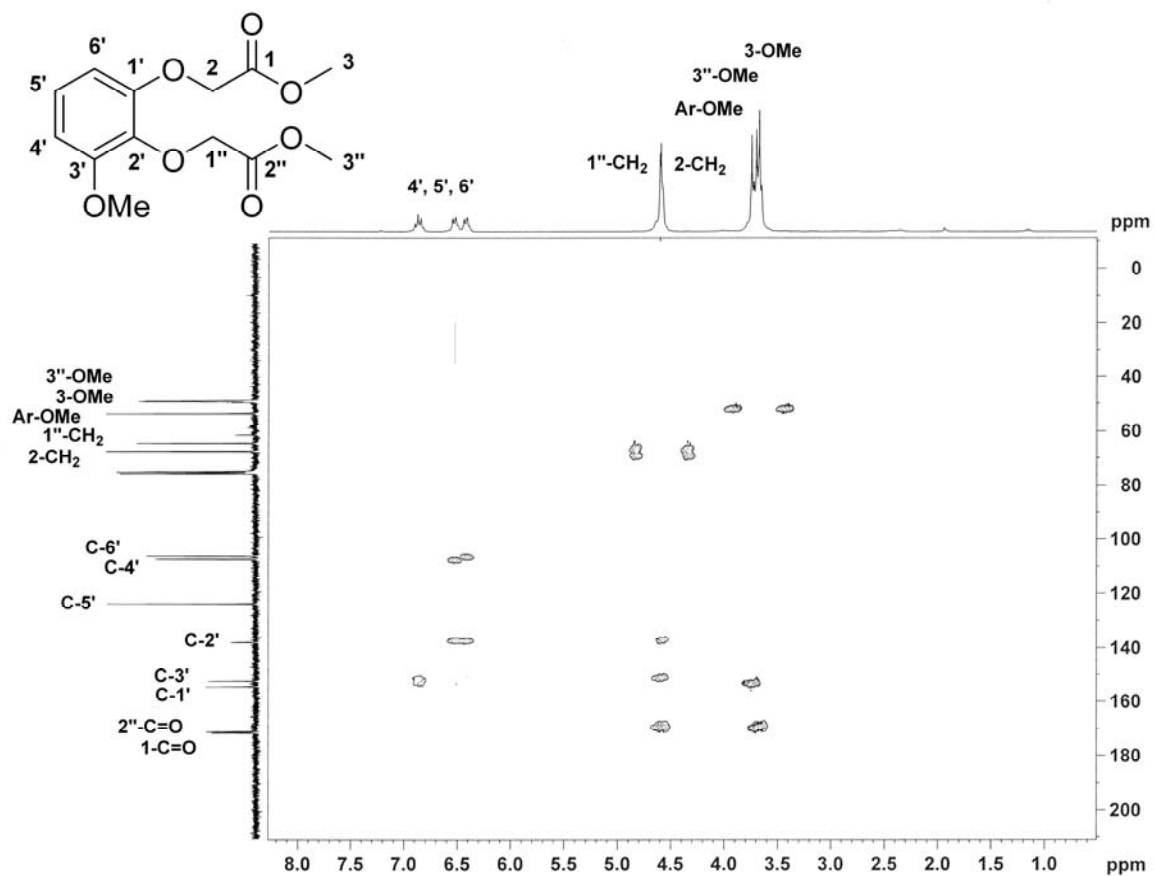
Appendix 4

^{1}H and ^{13}C NMR spectra of **22b**
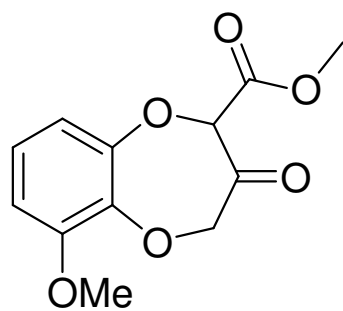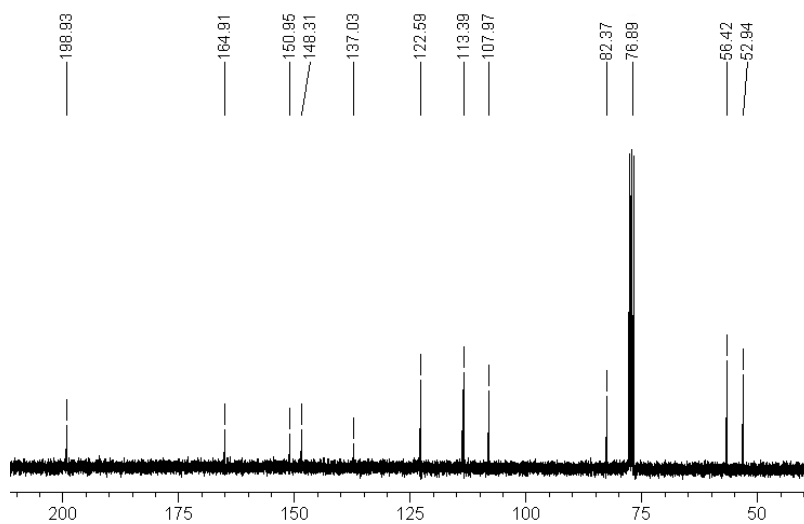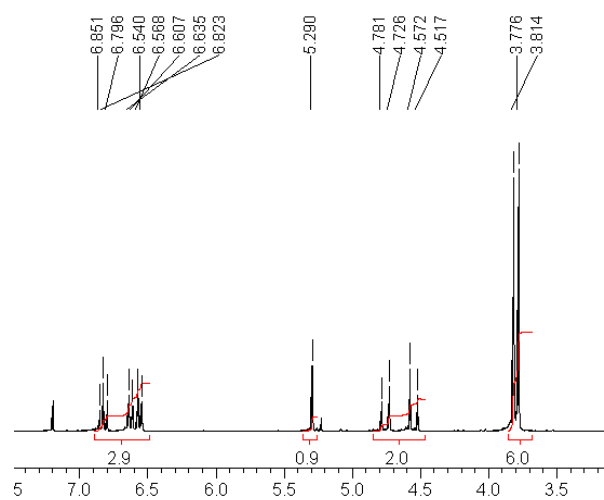
22b
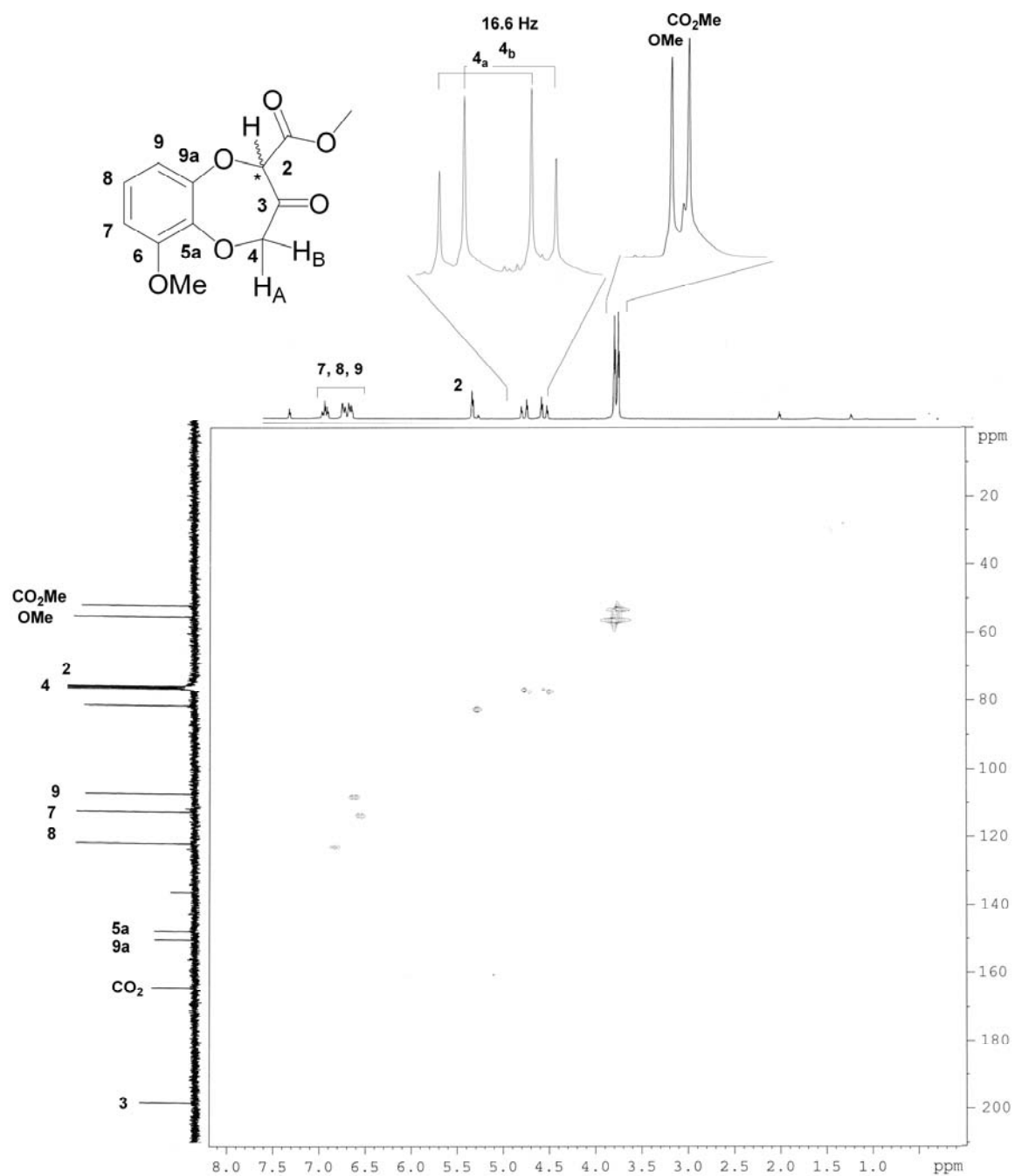
Appendix 5

Proposed soft ionization of **1** and derivatives of **1, 23-29** (70eV), EI mass spectrum of **25**

25
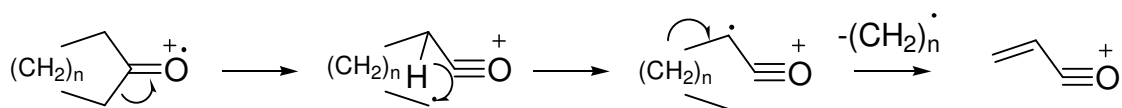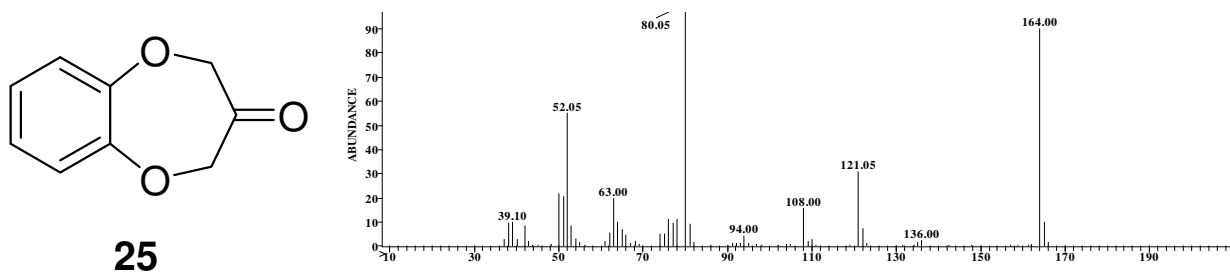
Appendix 6

Proposed soft ionisation of **62** (70eV)

m/z 123

m/z 79

m/z 93/95
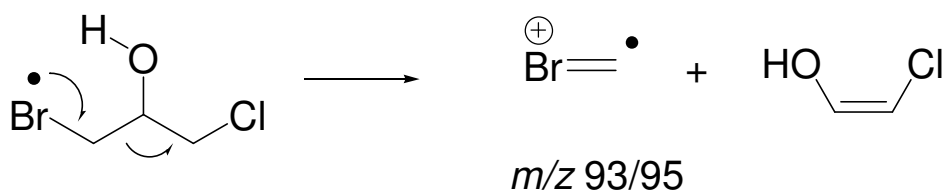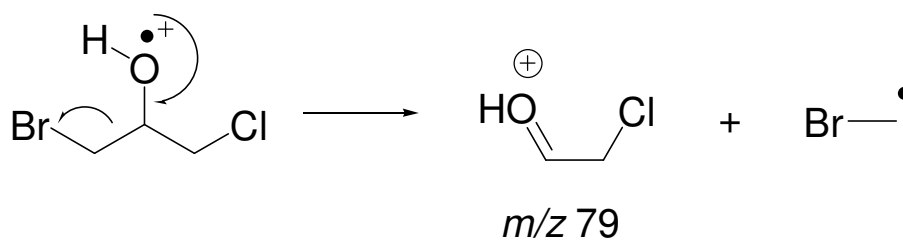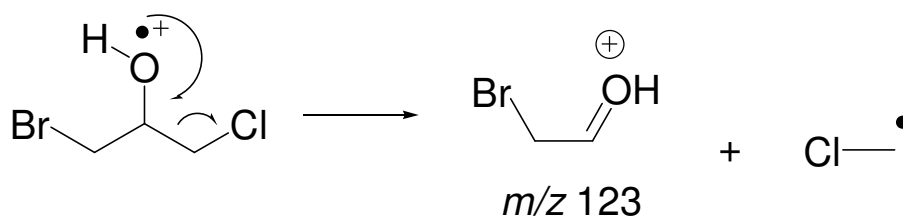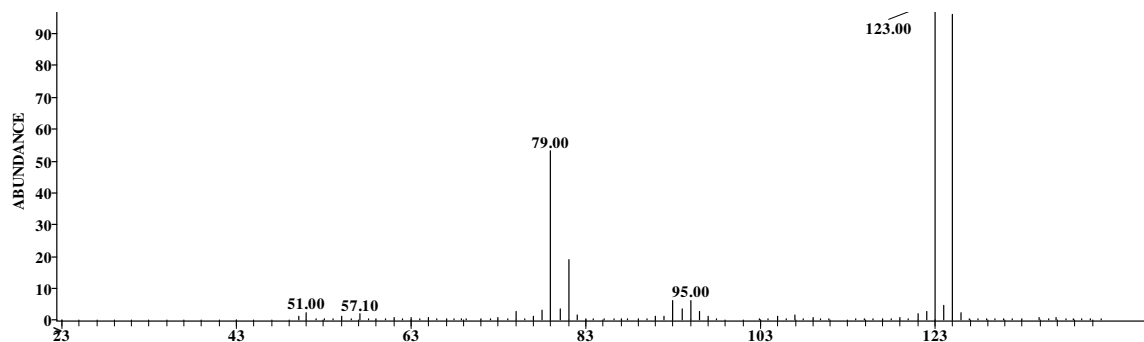
¹H and ¹³C spectra of **62**

62
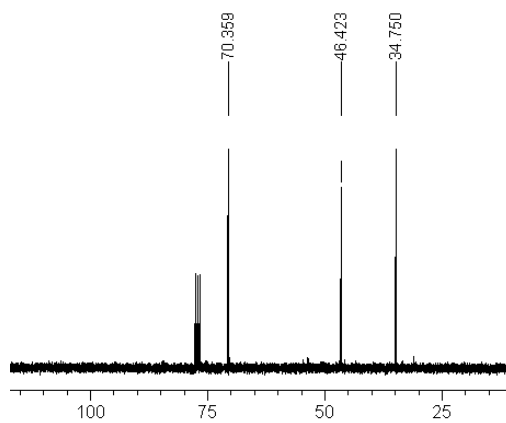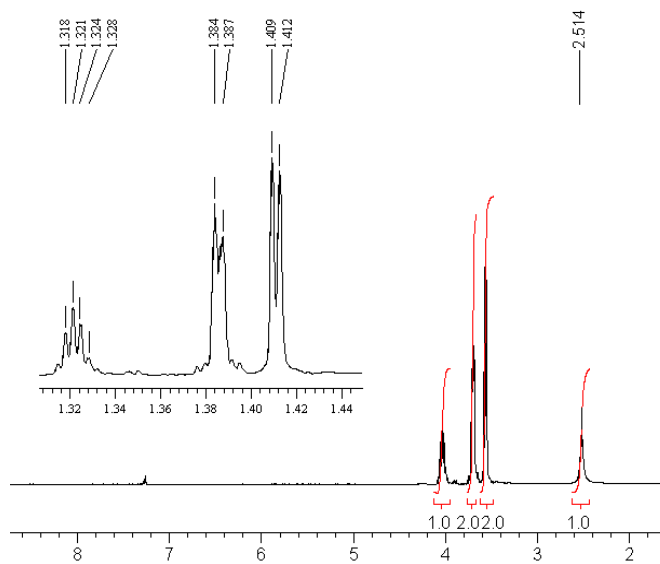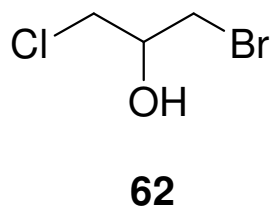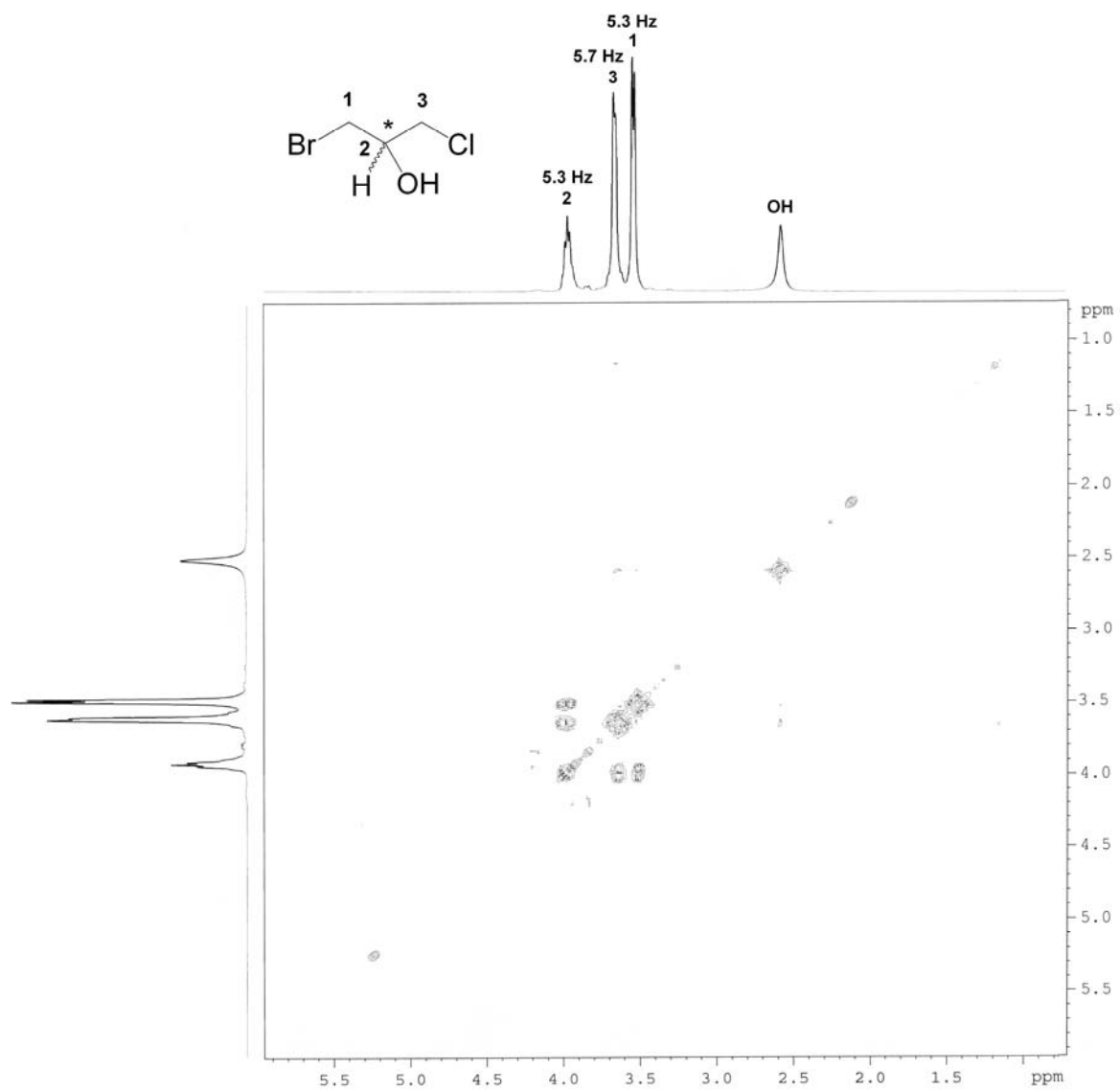
COSY spectrum of **62**
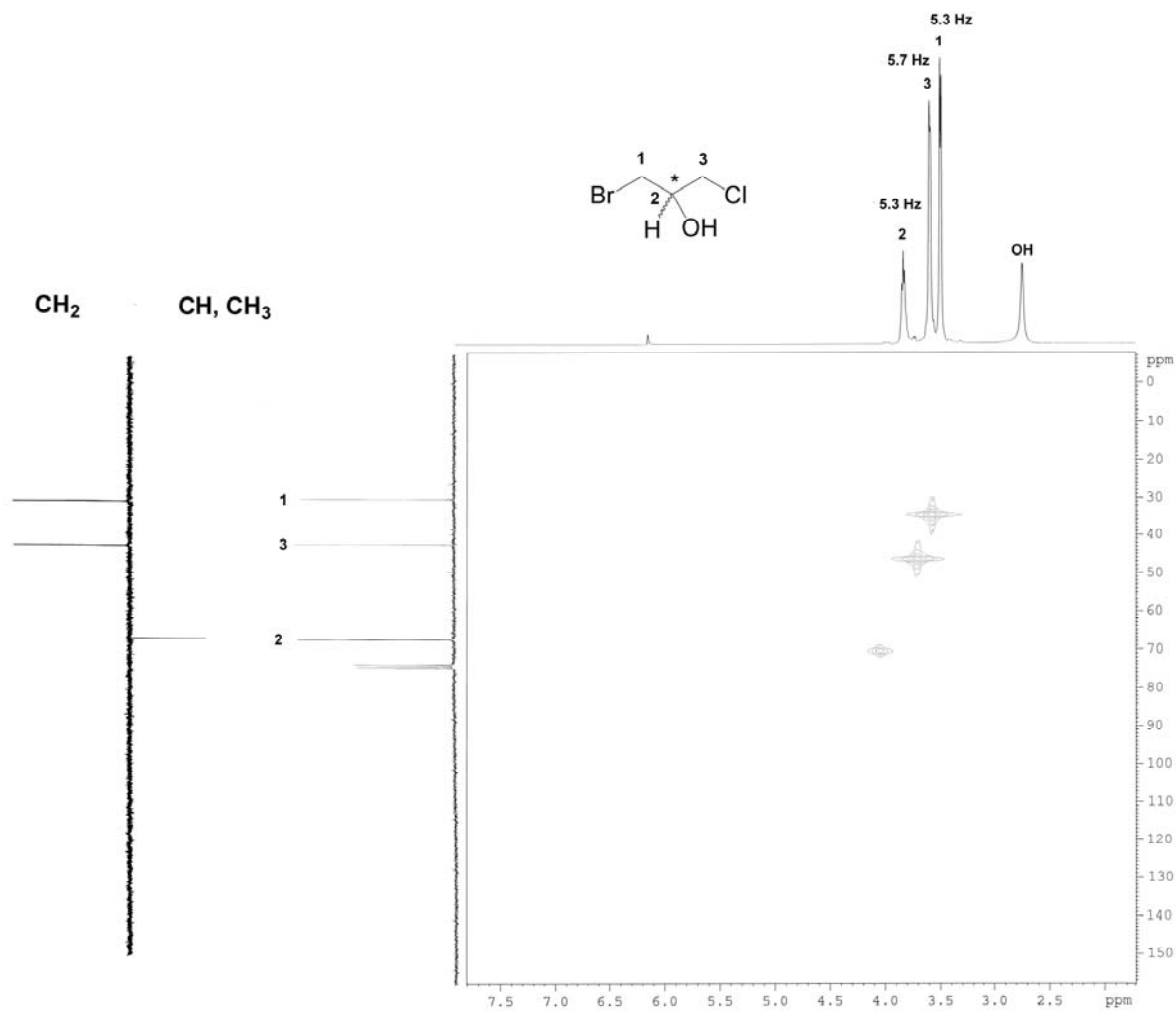
Appendix 7

^{1}H and ^{13}C NMR spectra of 63
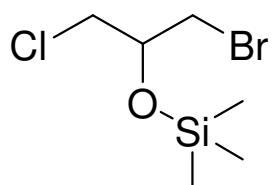
63
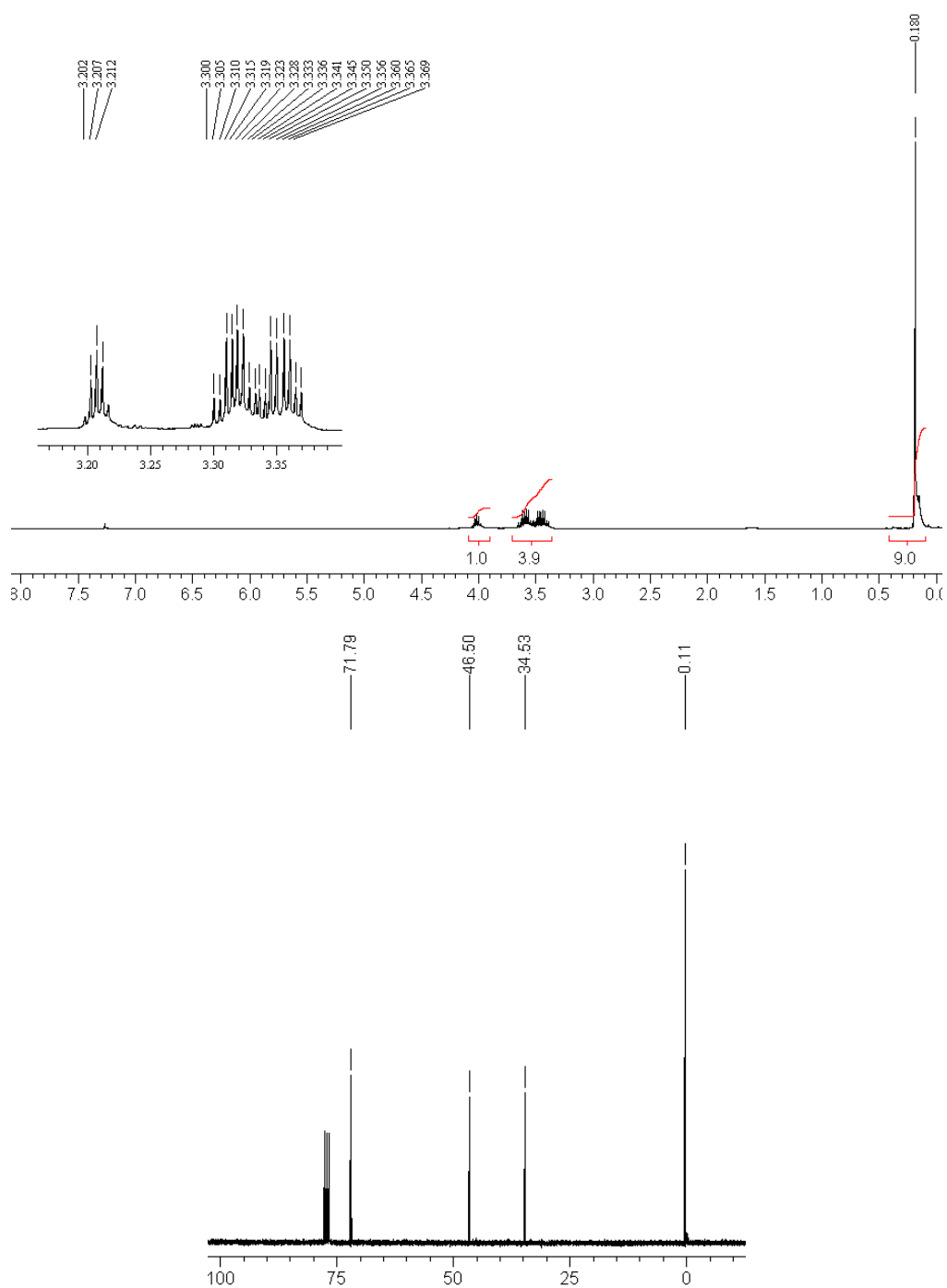
Quadrupole GC-MS of **63**

63
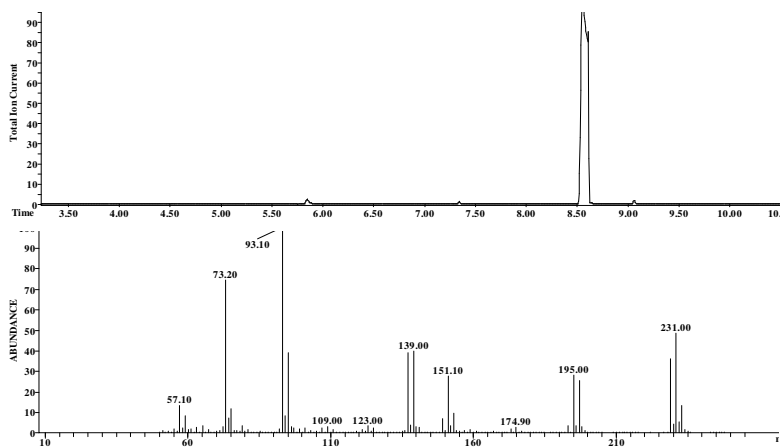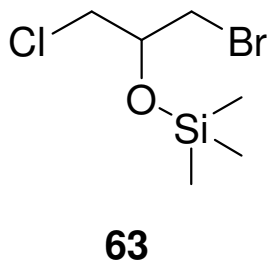
Appendix 8

^{1}H and ^{13}C spectra of **58**
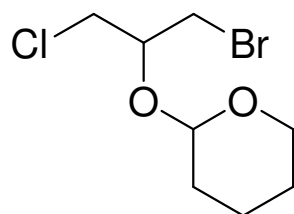
58
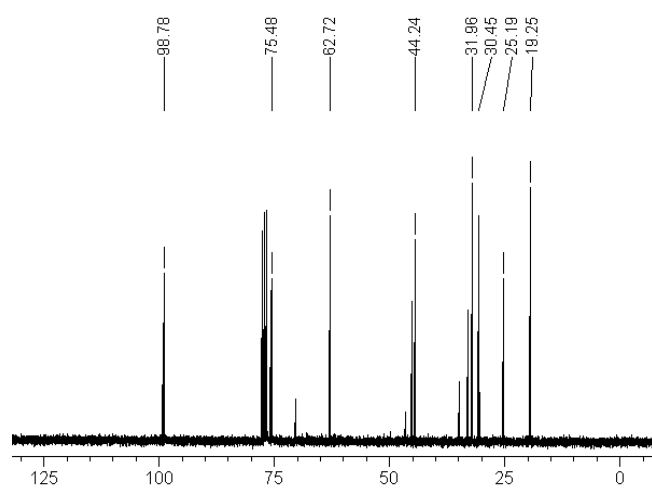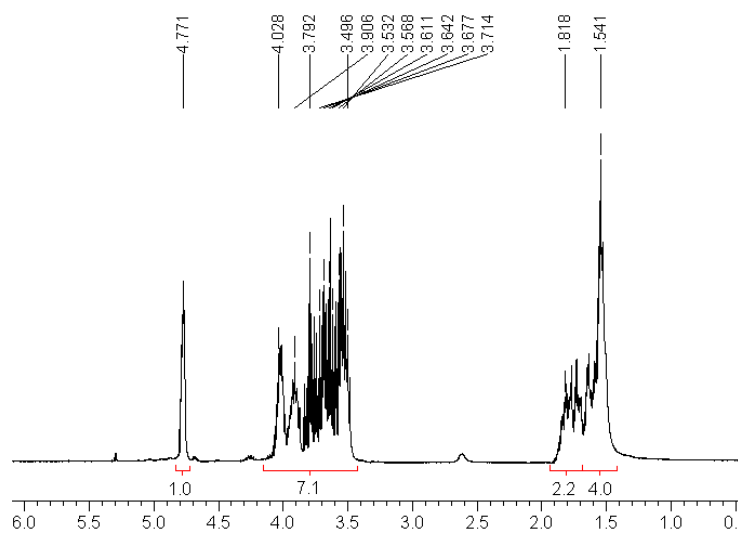
COSY spectrum of **58**
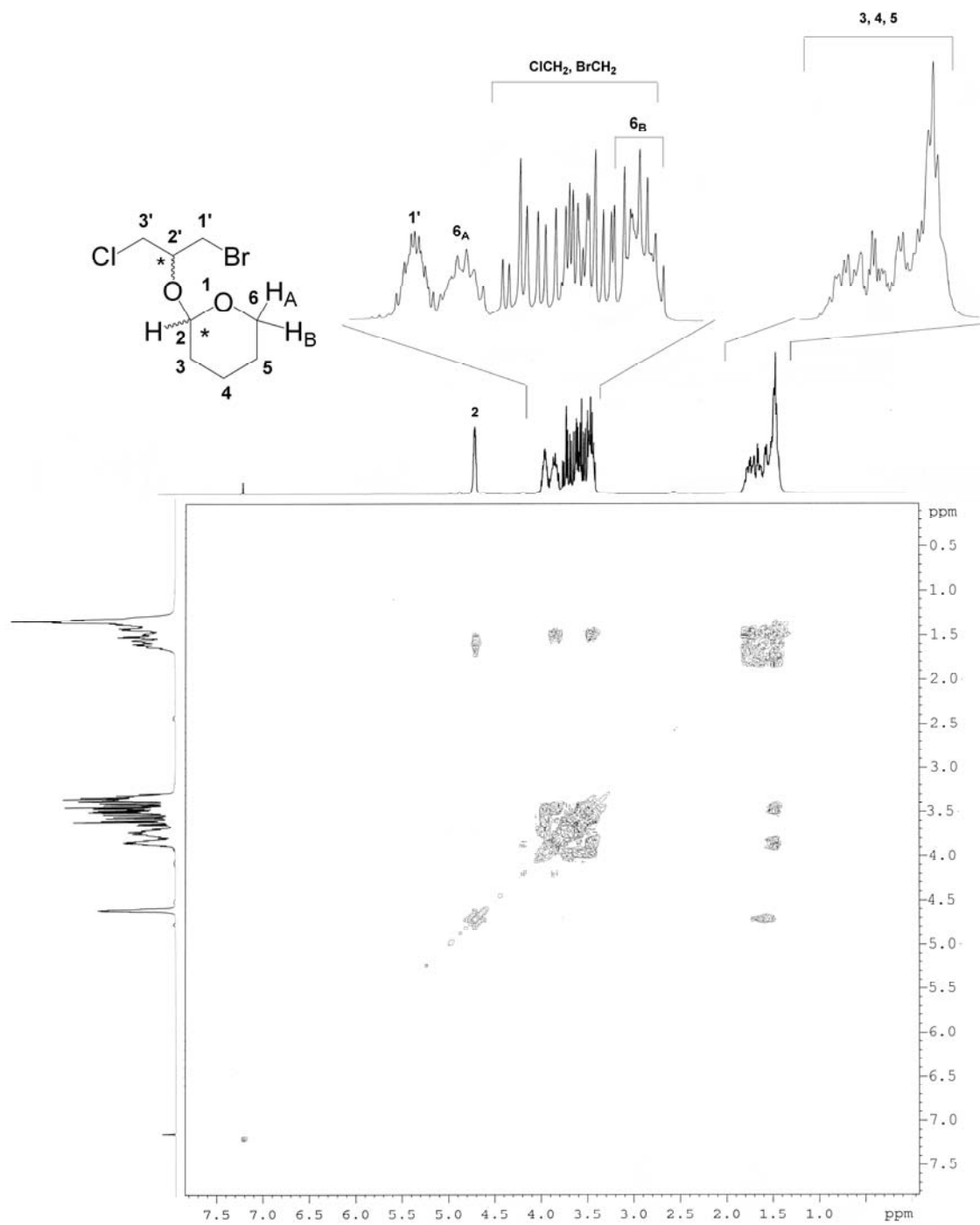
Appendix 9

^{1}H and ^{13}C spectra of **60a**

60a
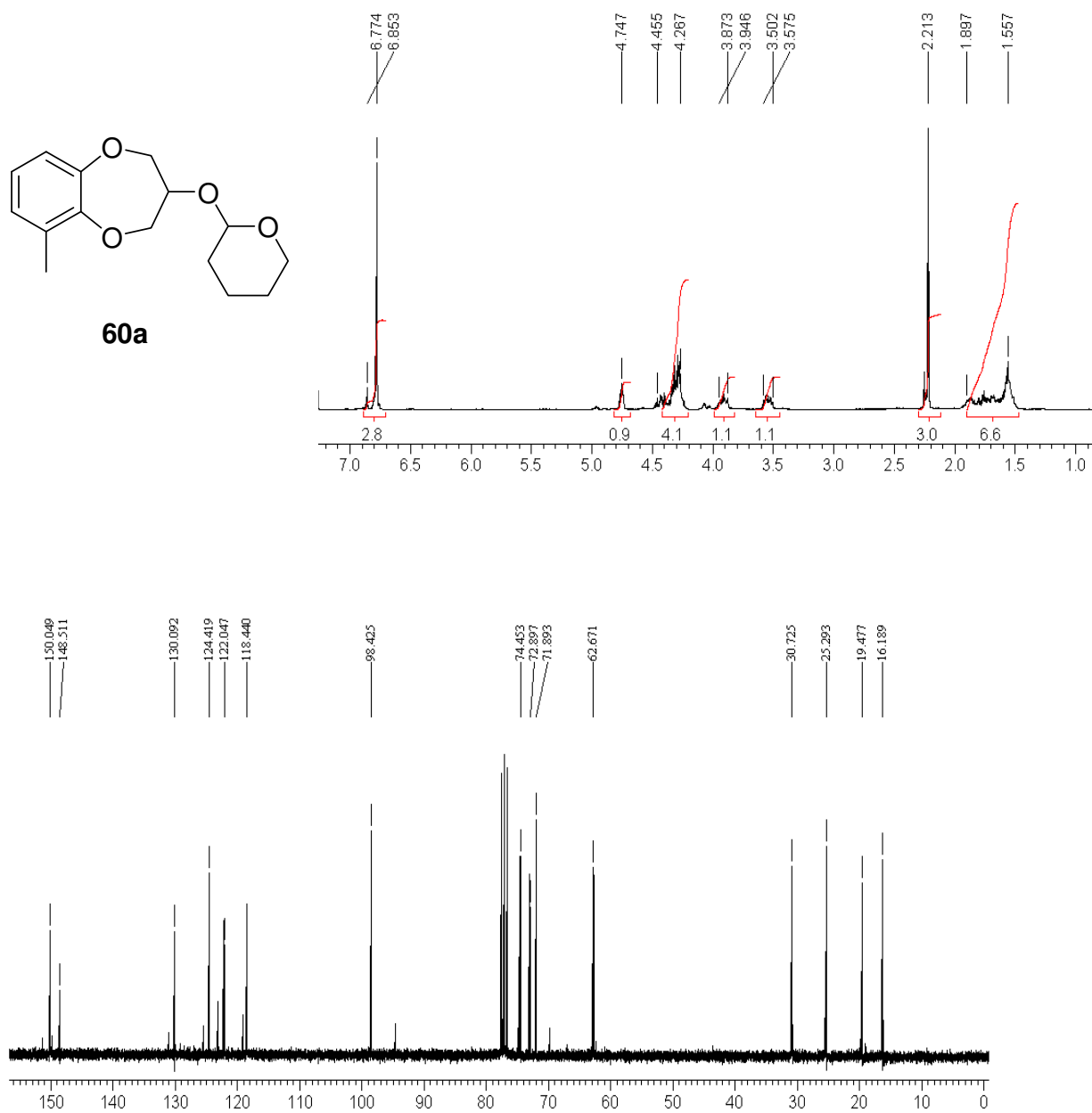
Quadrupole GC-MS of **60a**
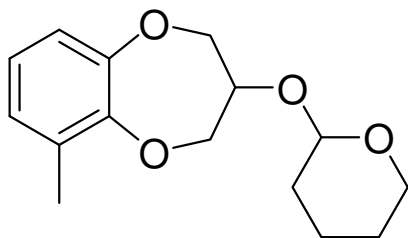
60a
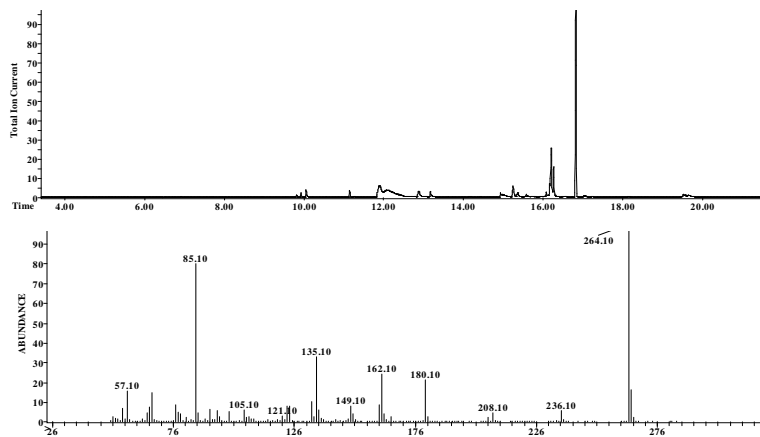
COSY spectrum of **60a**
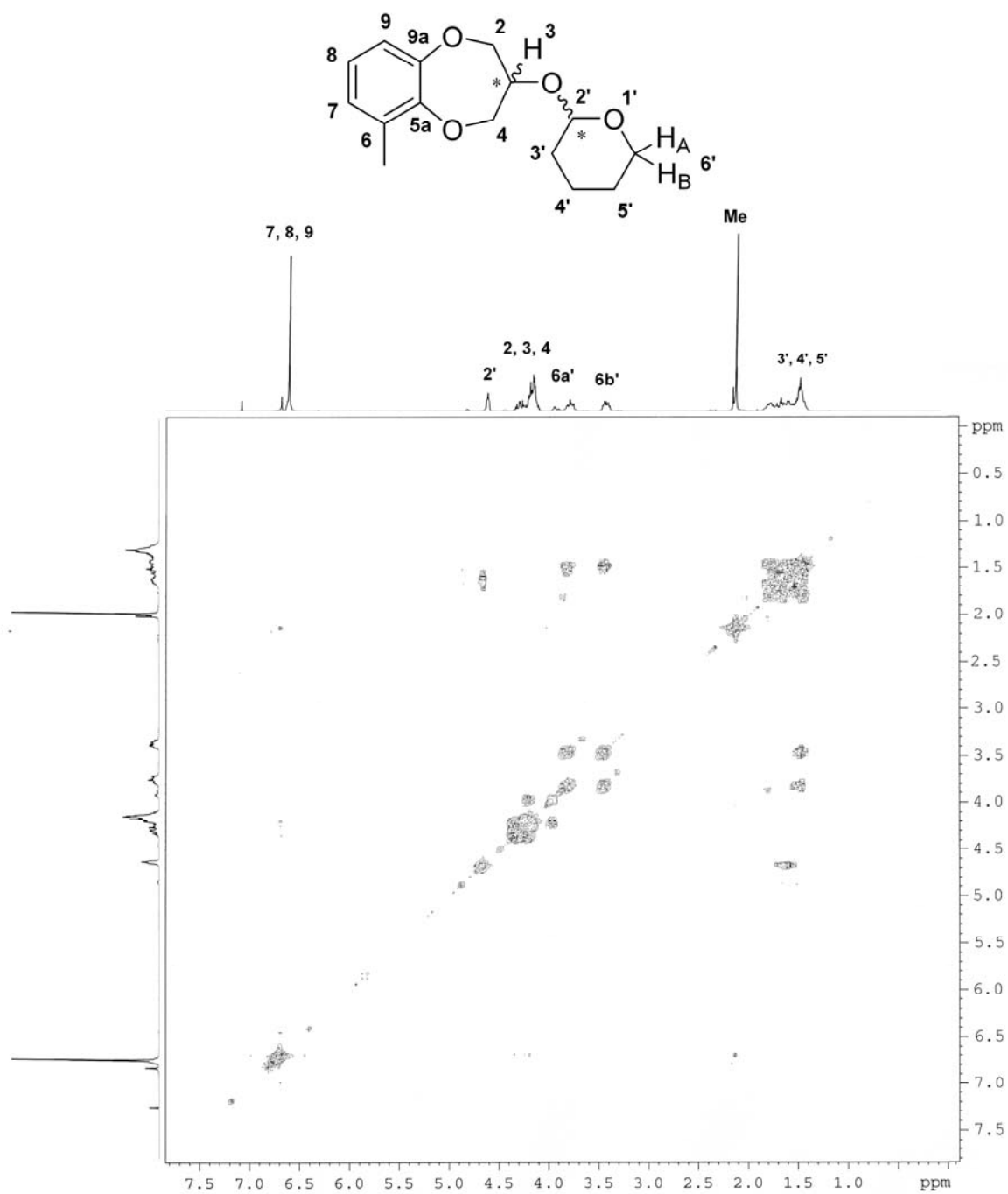
¹H,¹³C HMQC spectrum of **60a**
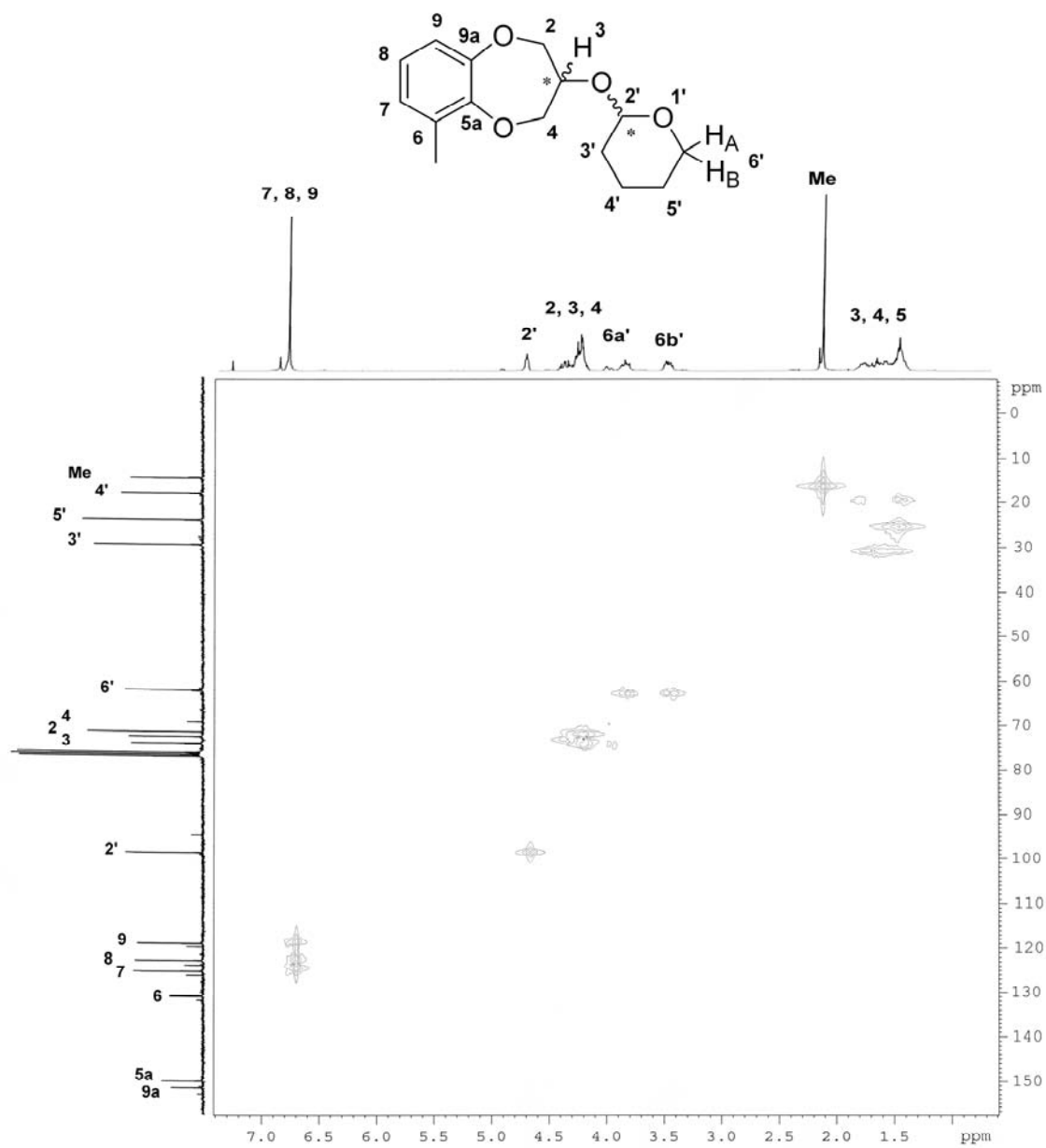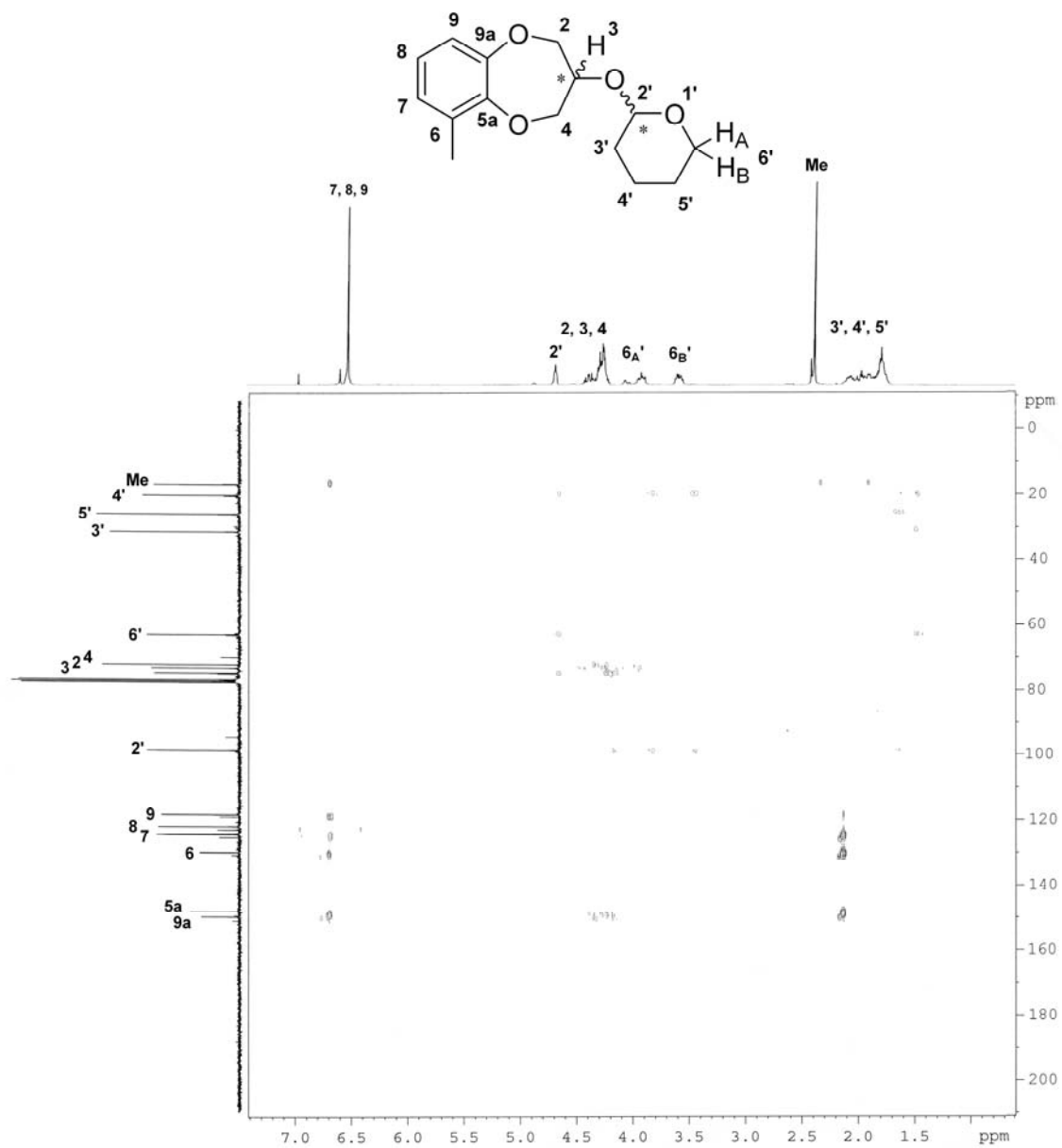
Appendix 10

^{1}H and ^{13}C spectra of **60d**
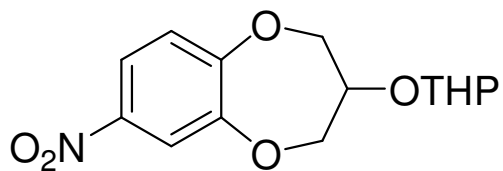
50d
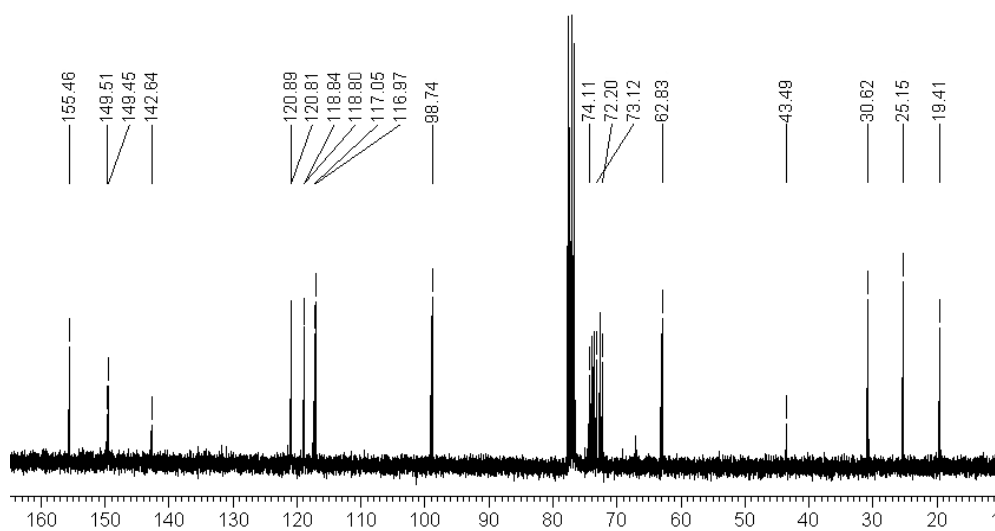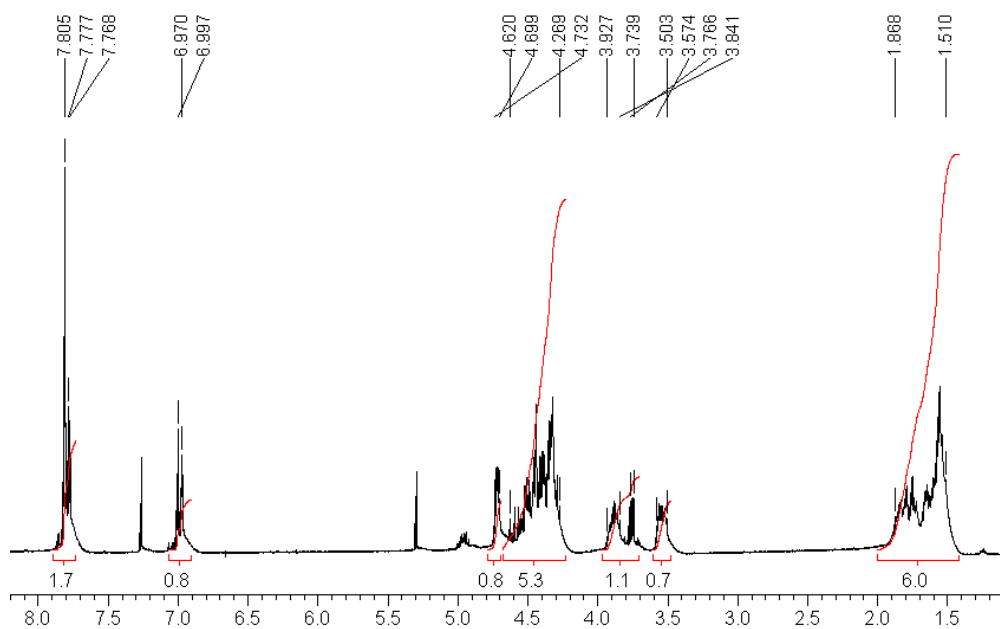
¹H,¹³C HMBC spectrum of **60d**
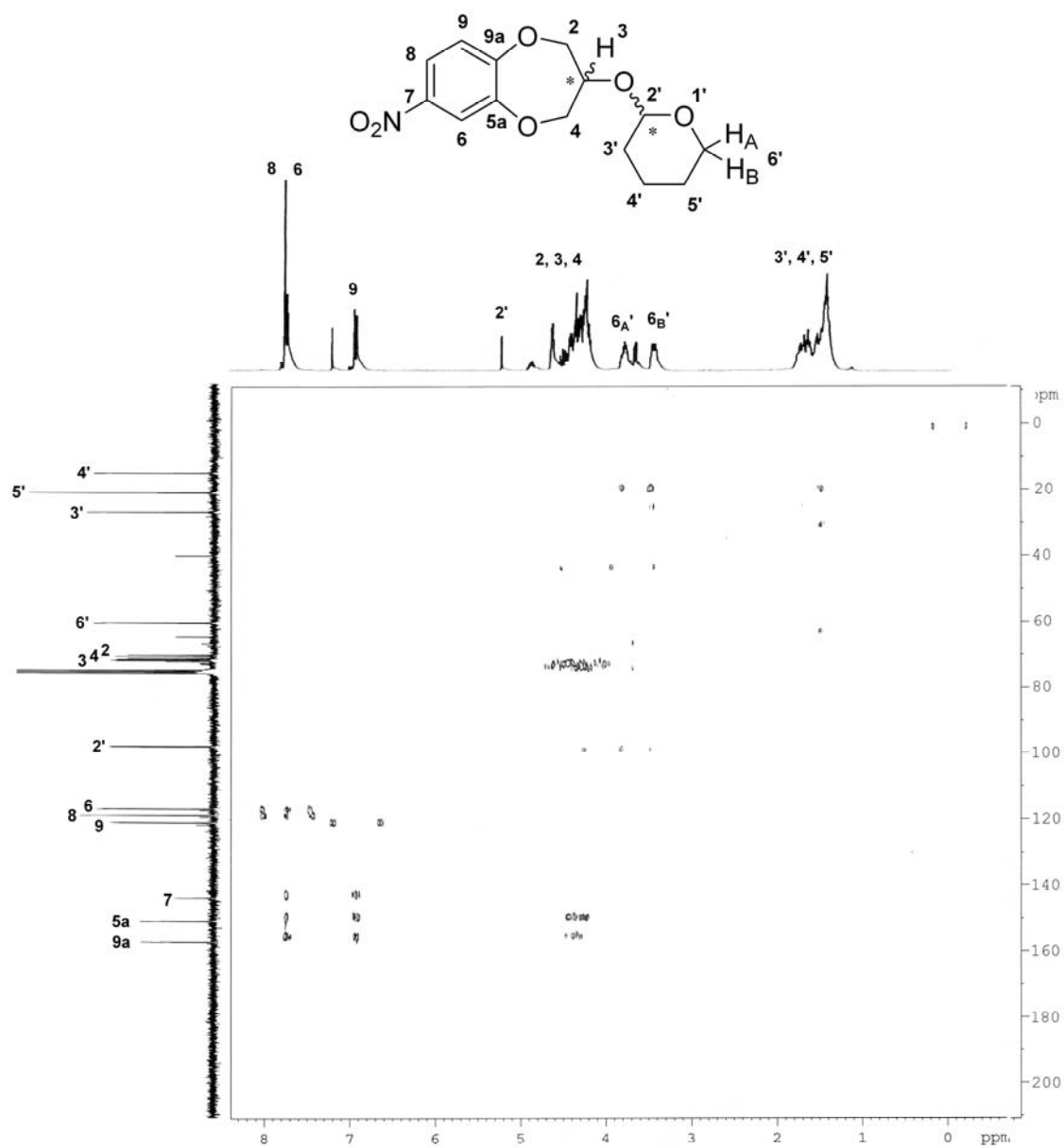
Appendix 11

^{1}H and ^{13}C spectra of **61a**
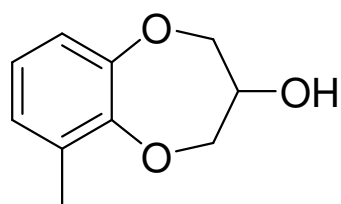
61a
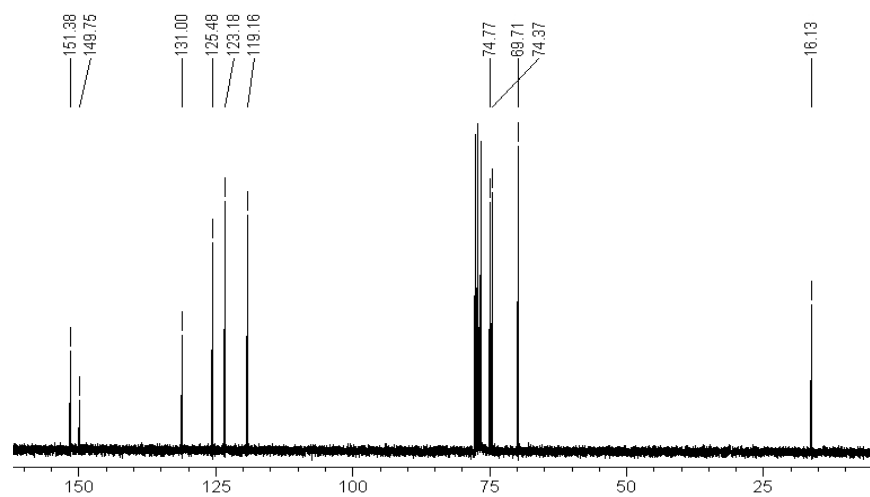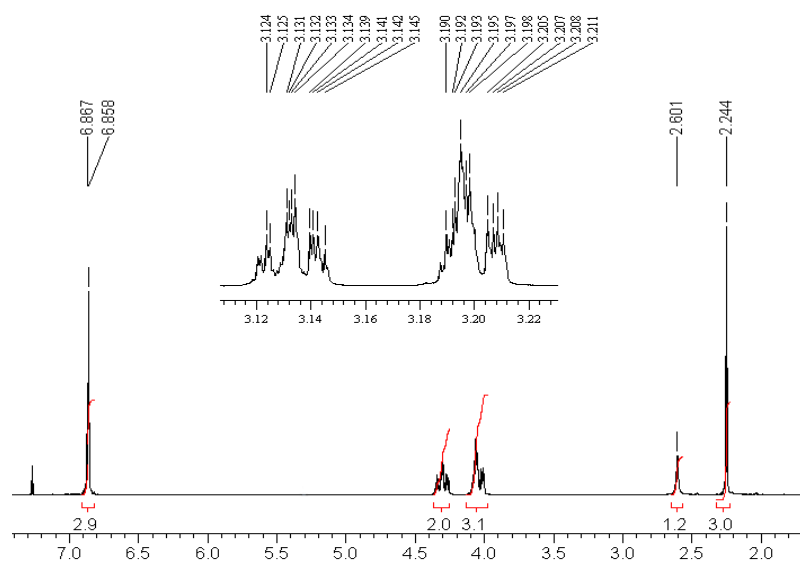
Quadrupole GC-MS of **61a**
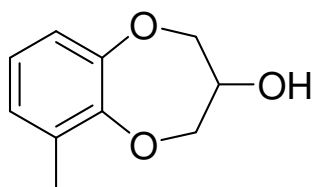
61a
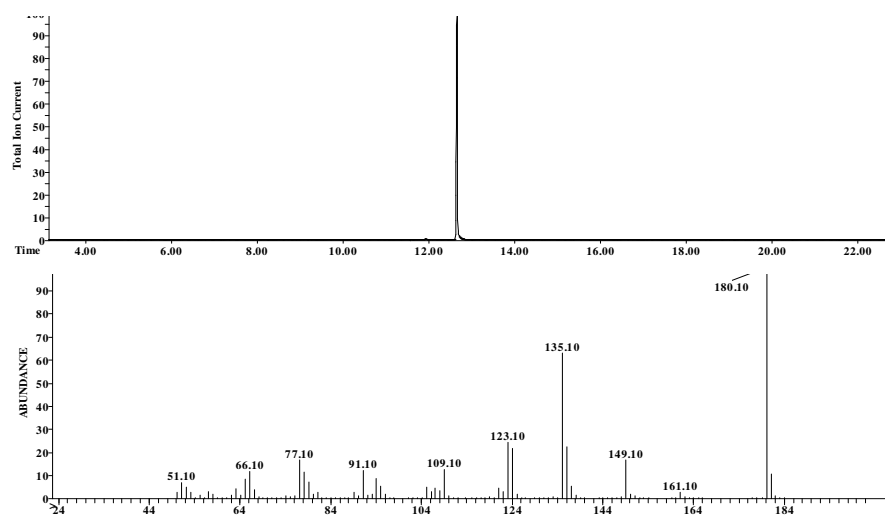
COSY spectrum of **61a**
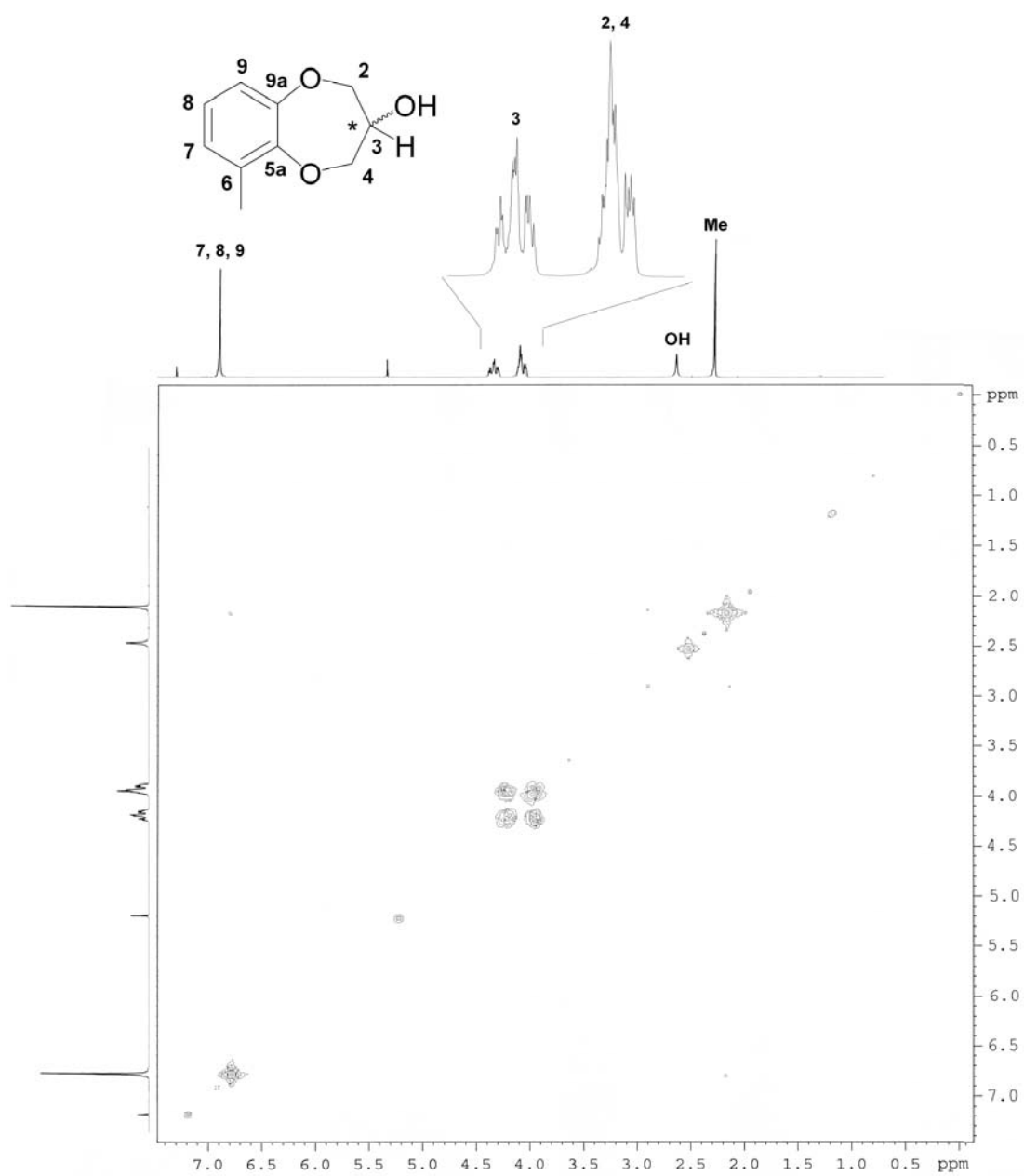
¹H,¹³C HMQC of **61a**
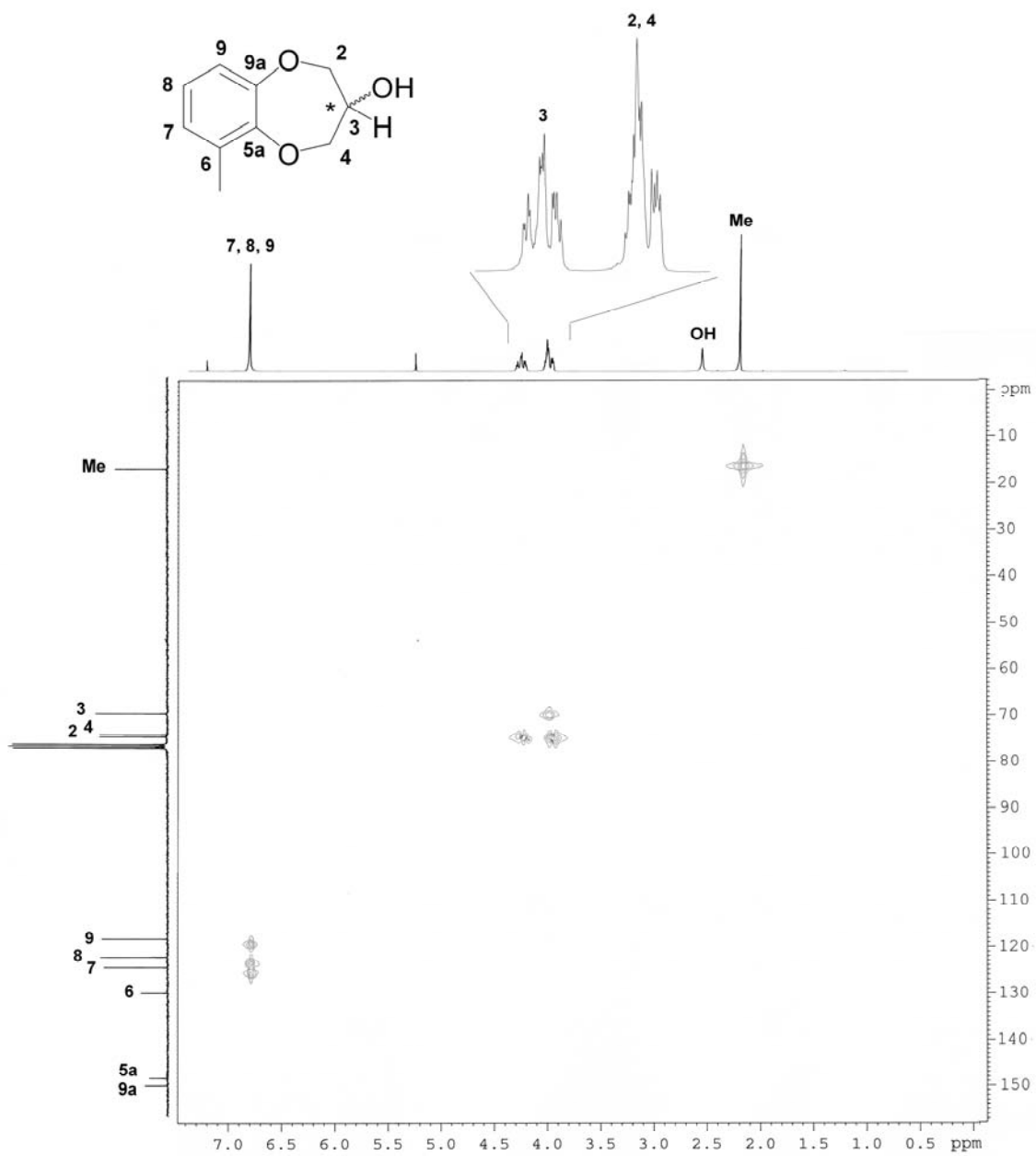
Appendix 12

COSY spectrum of **61d**
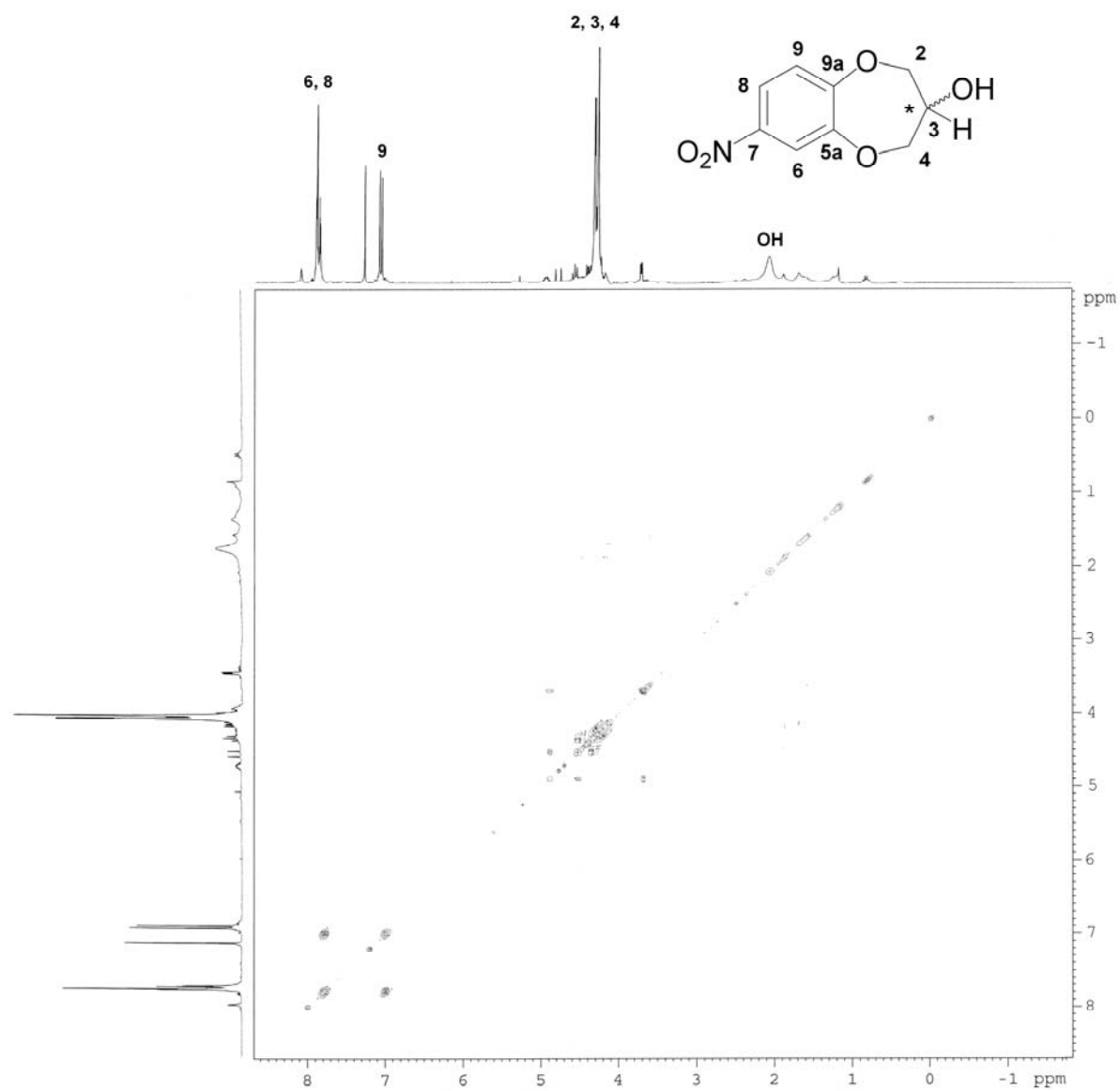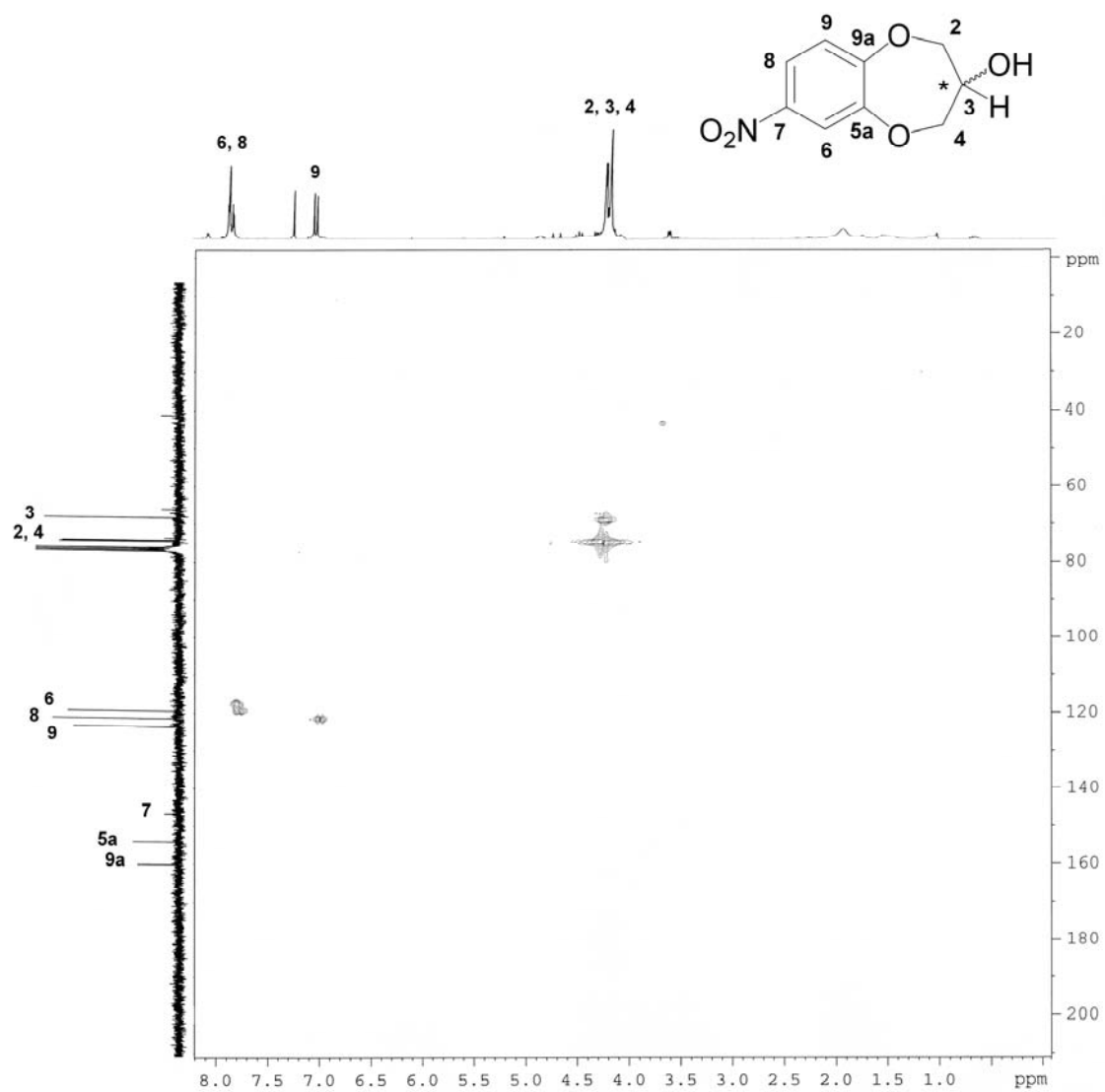
Appendix 13

^{1}H,^{1}H COSY of **24**
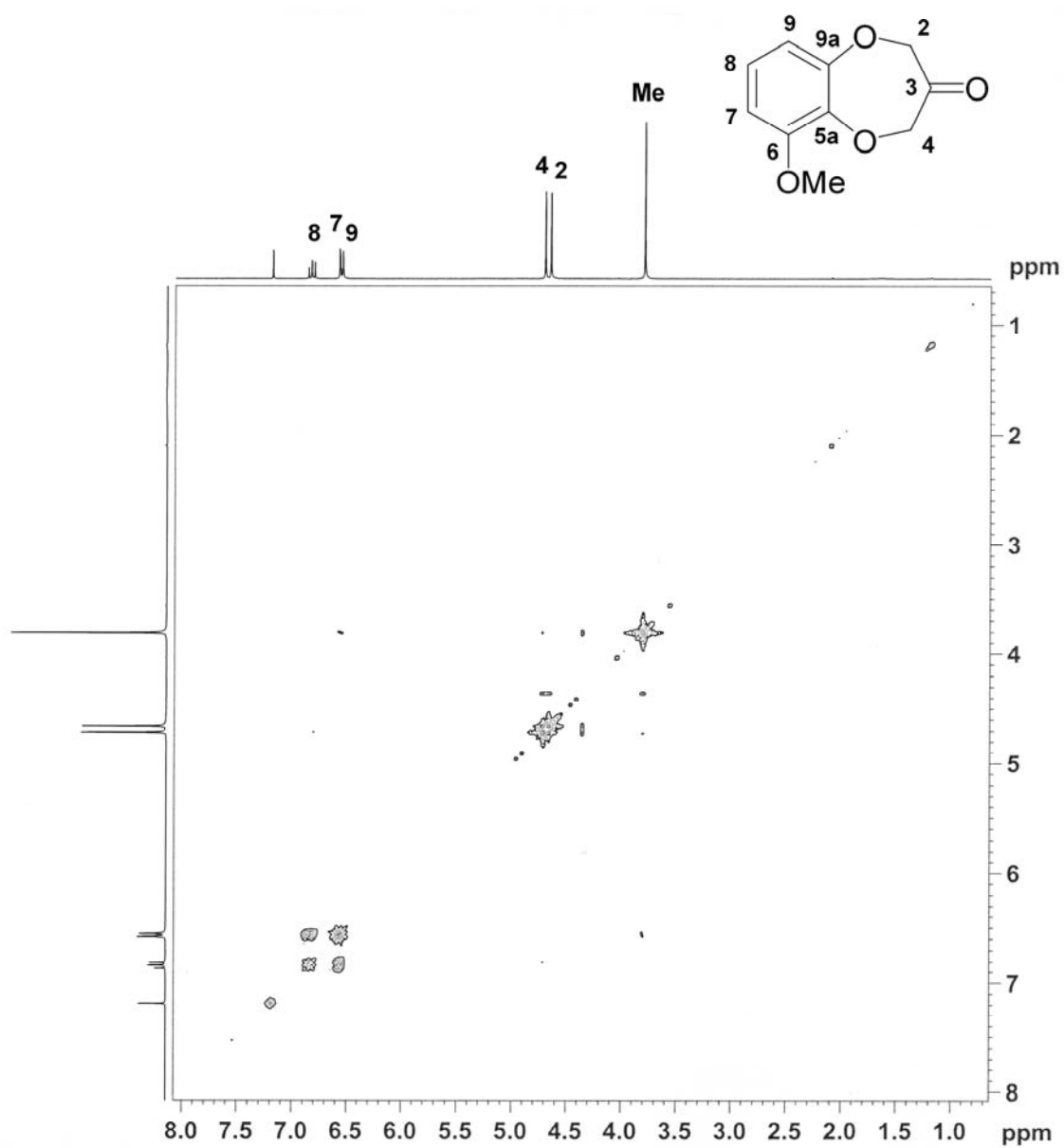
Appendix 14

^{1}H,^{13}C HMQC of **26**
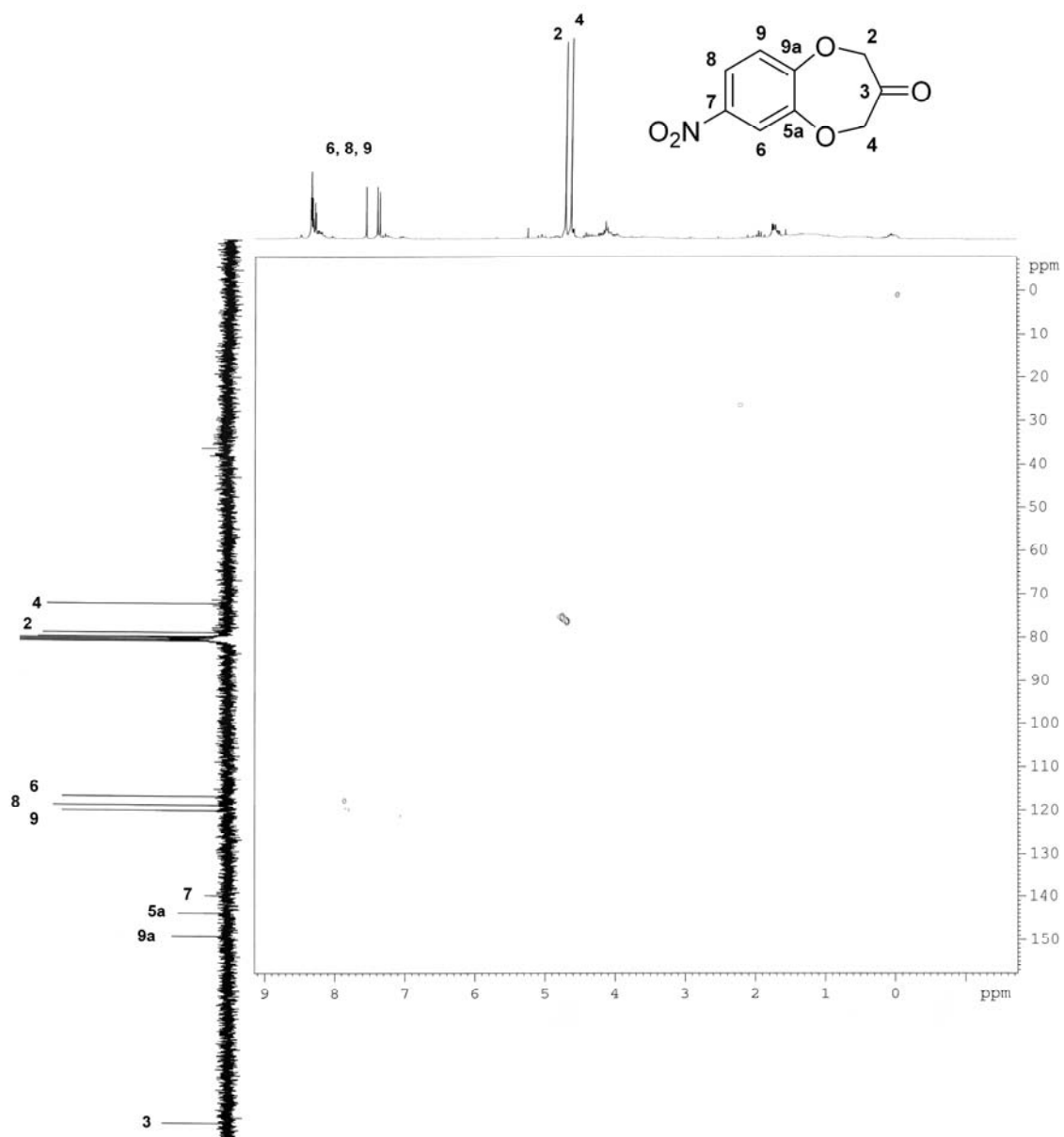
¹H,¹³C HMBC spectrum of **26**
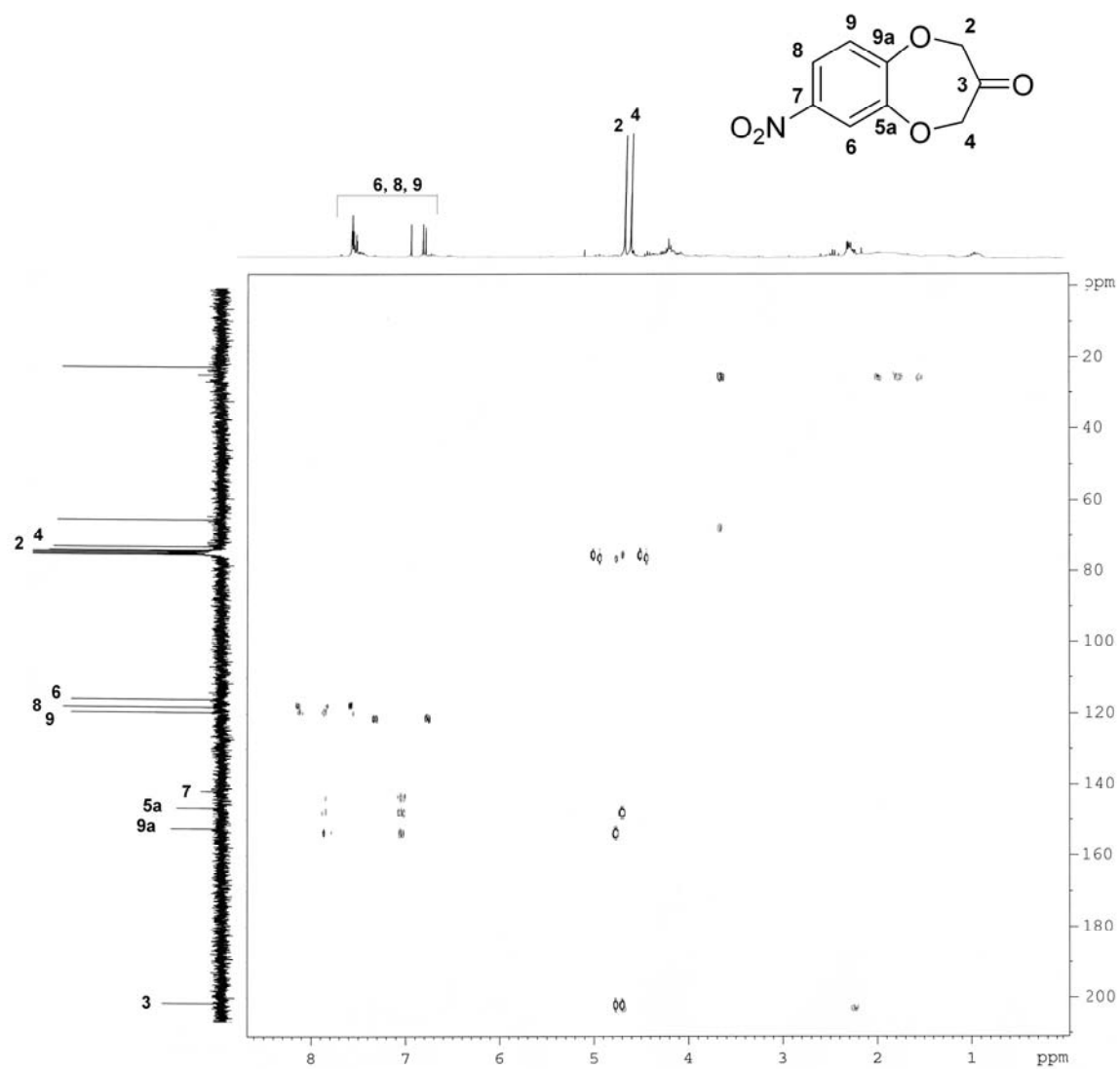
Appendix 15

65
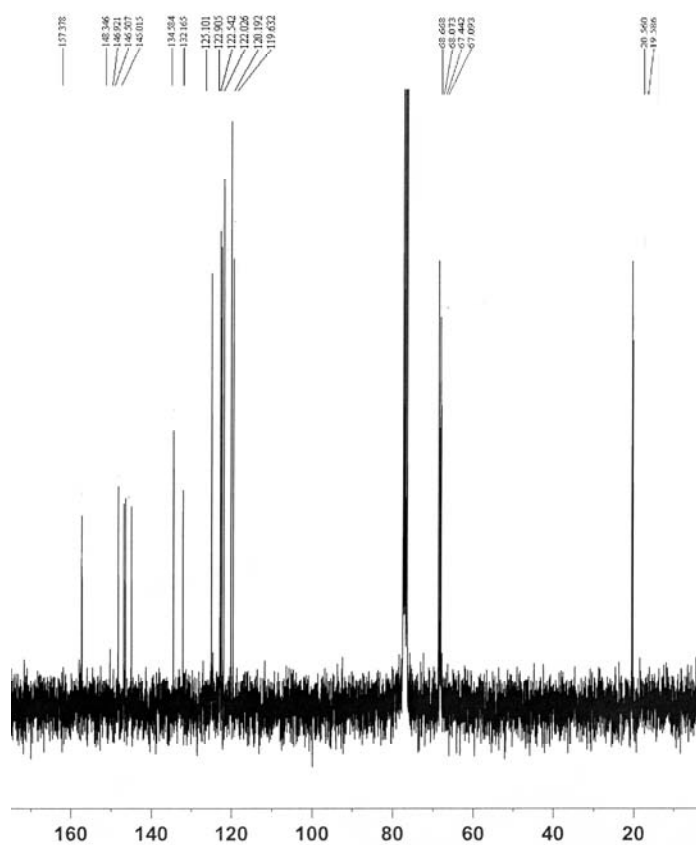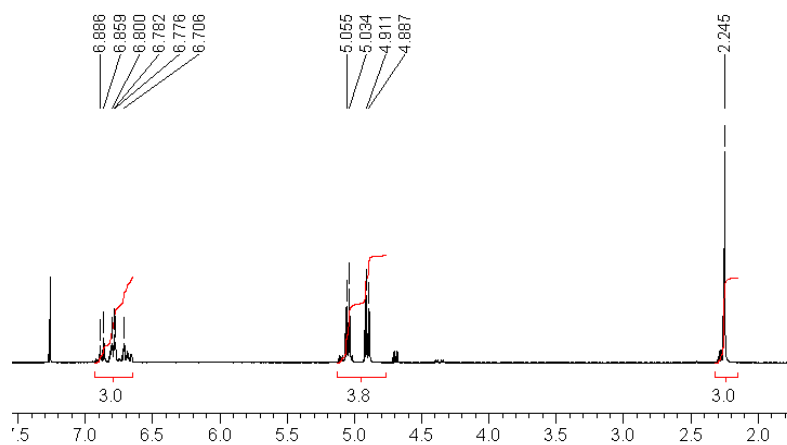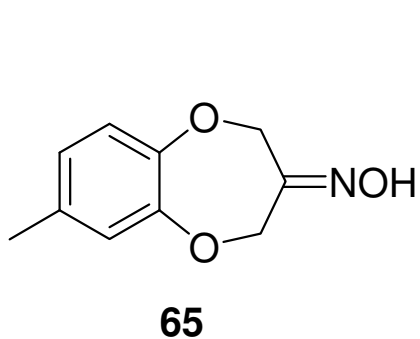
^{1}H,^{1}H COSY of **65**
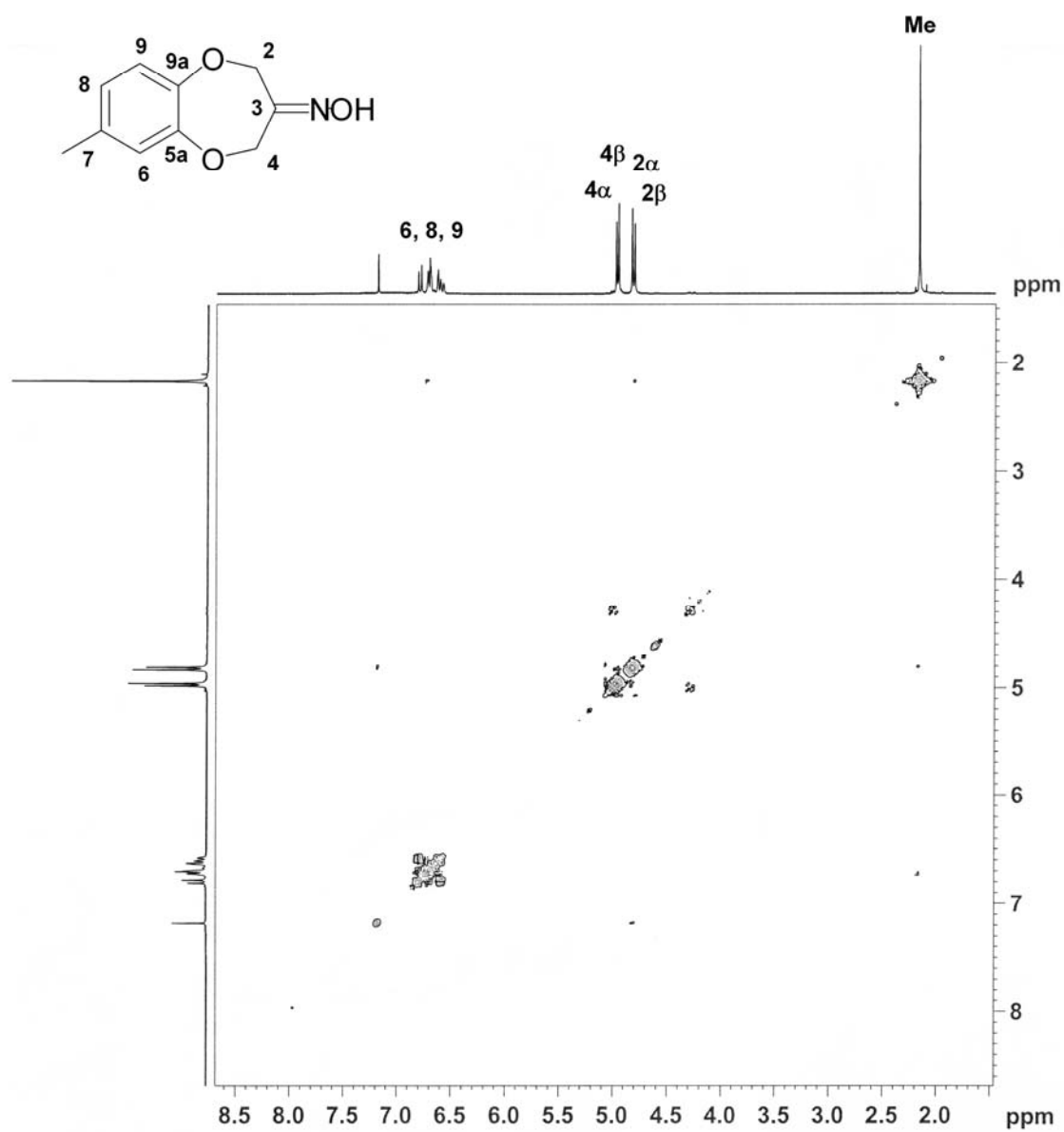
Appendix 16

^{1}H, and ^{13}C NMR of **66**

66
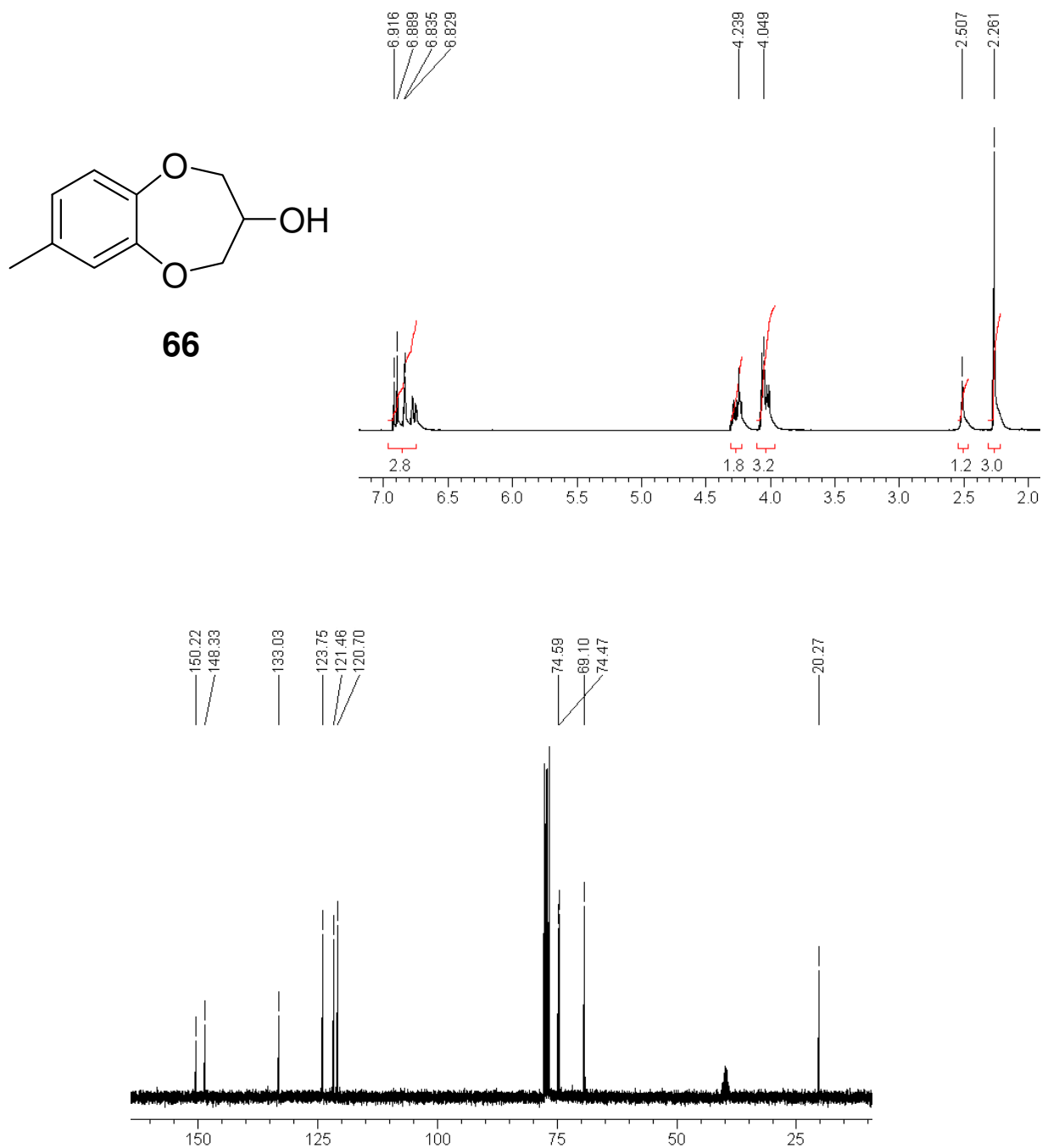
COSY spectrum of **66**
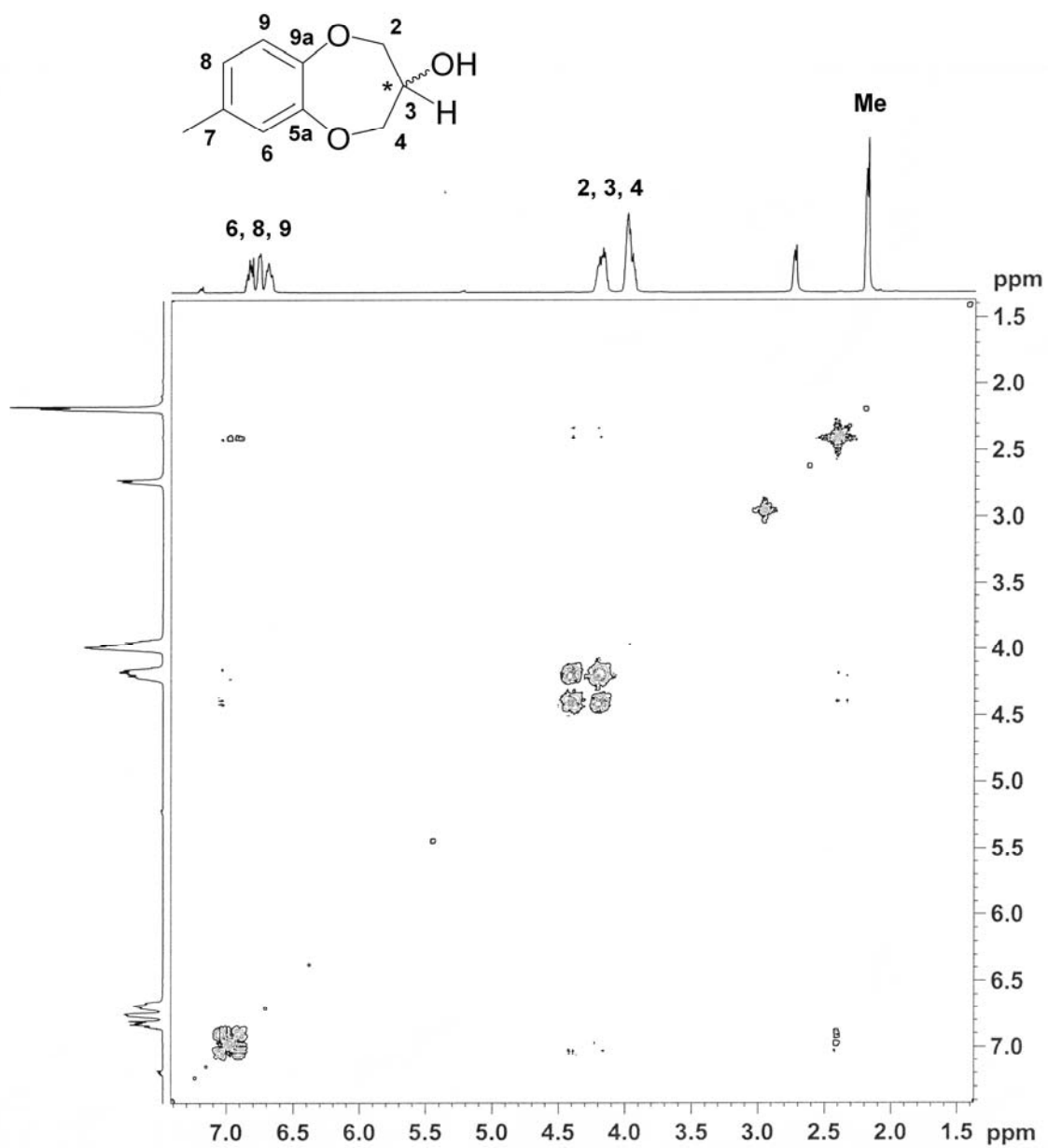
J-resolved spectrum of **66**
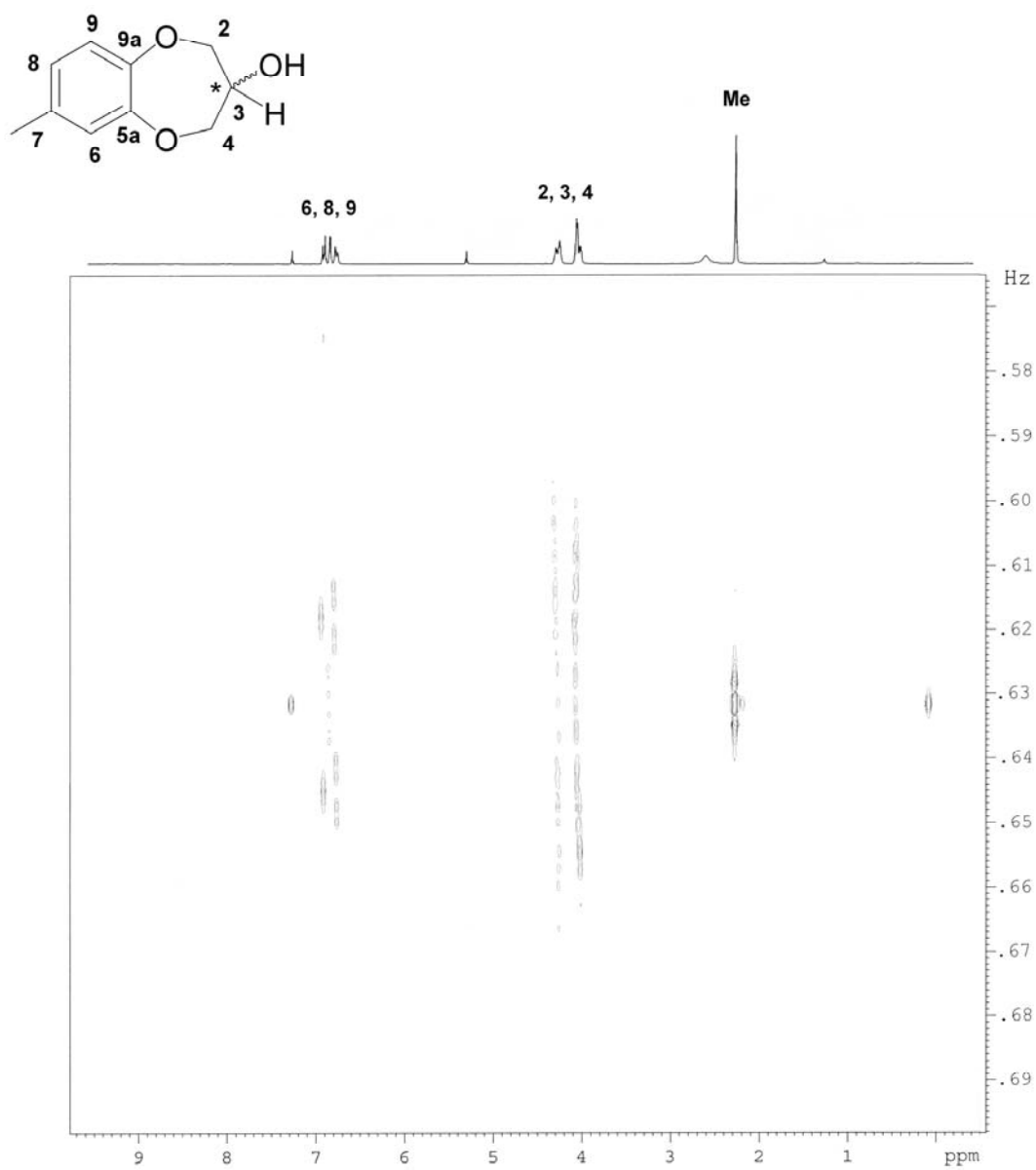
Appendix 17
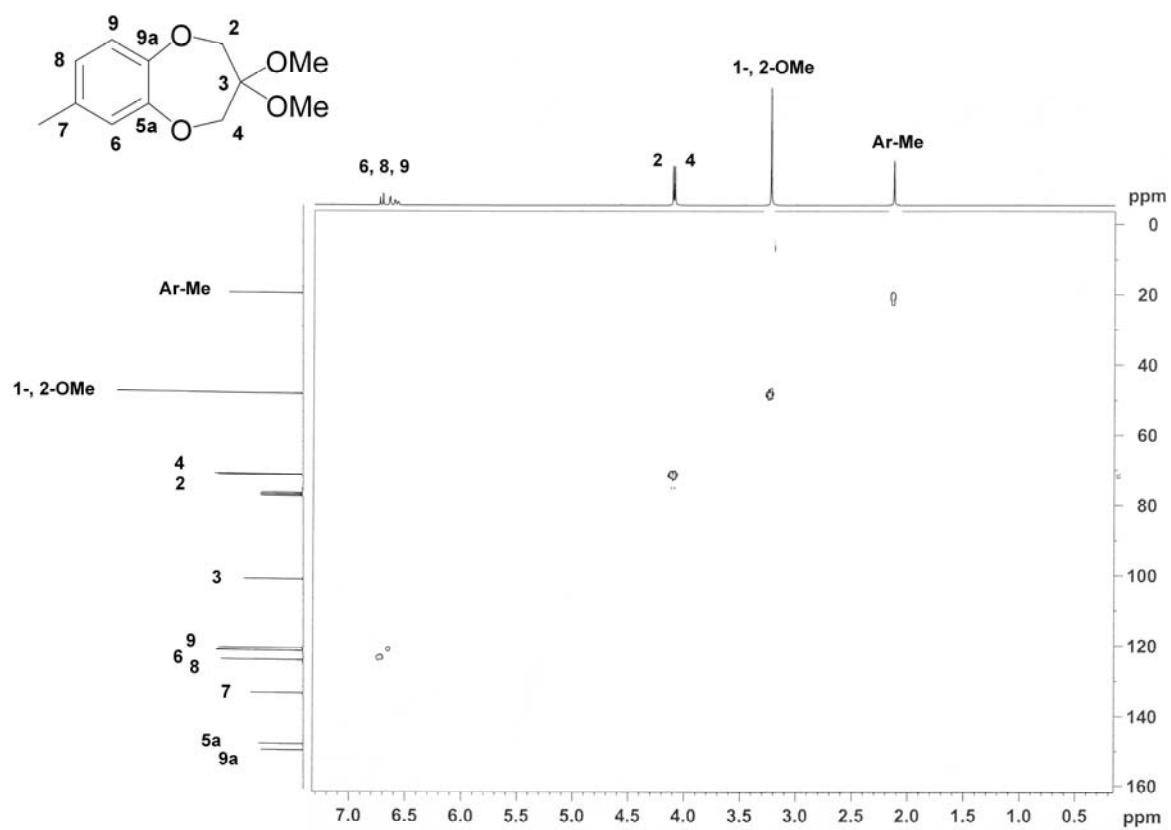
^{1}H,^{13}C HMQC of **67**
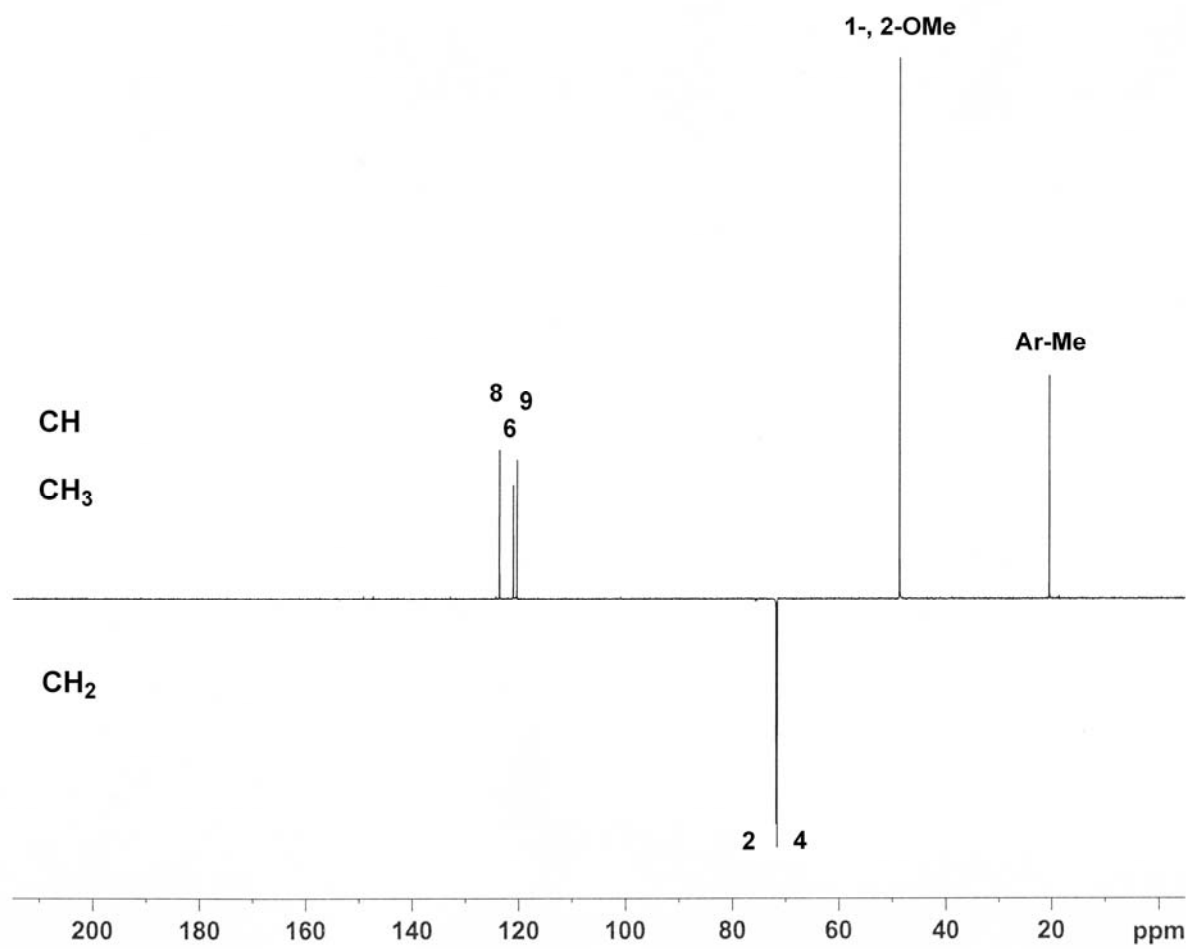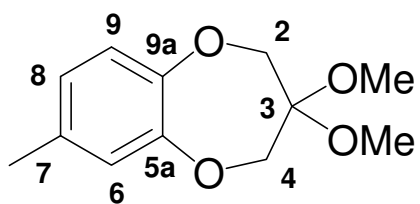
Appendix 18

^{1}H and ^{13}C spectrum of **68**

68
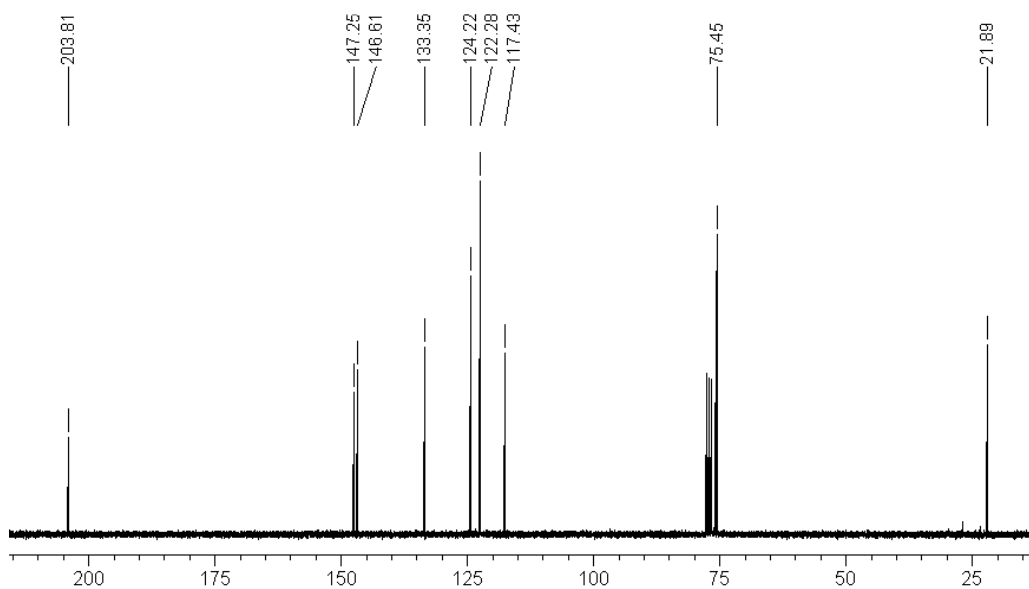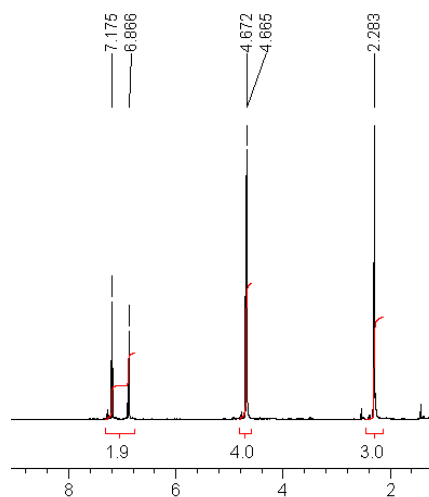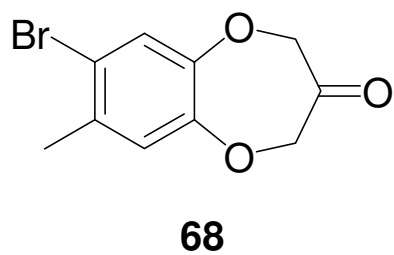
¹H,¹³C HMBC spectrum of **68**
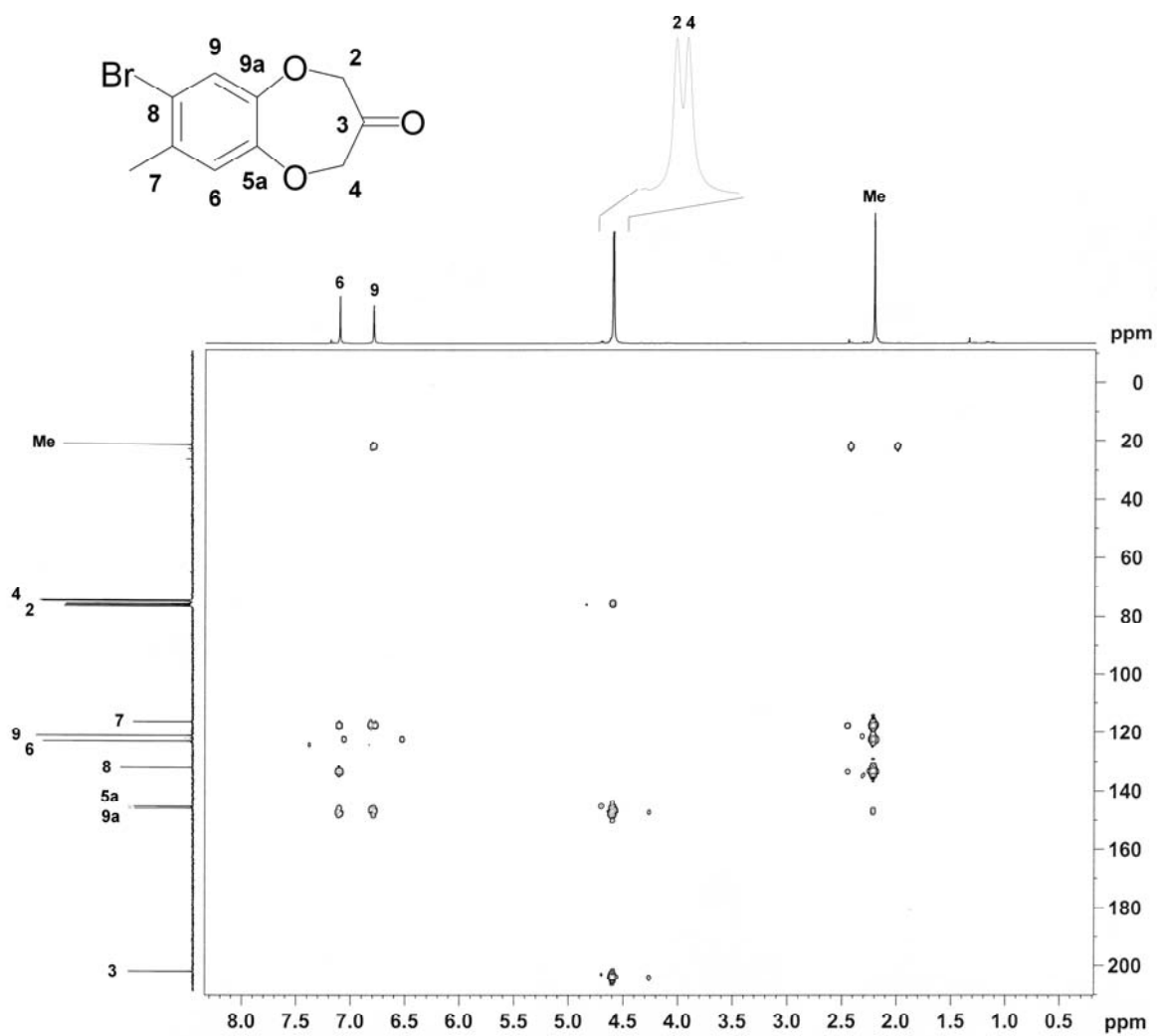
Appendix 19

^{1}H and ^{13}C of **69**

69
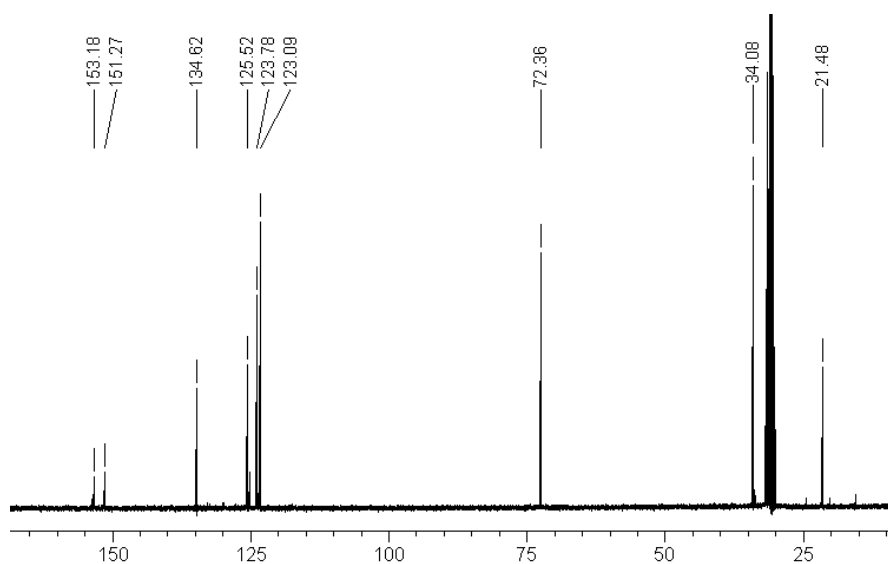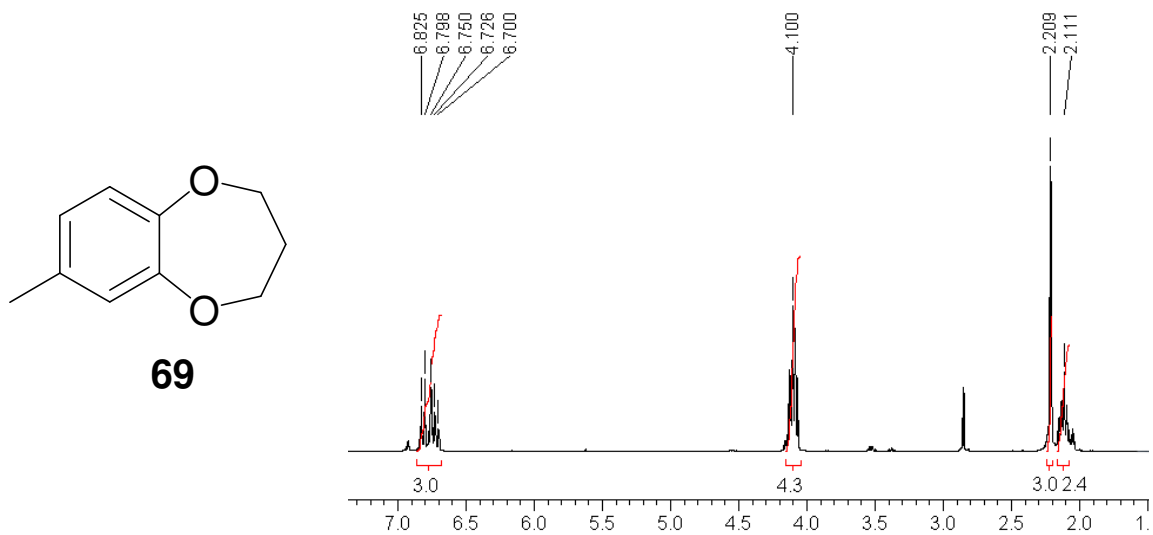
COSY of **69**
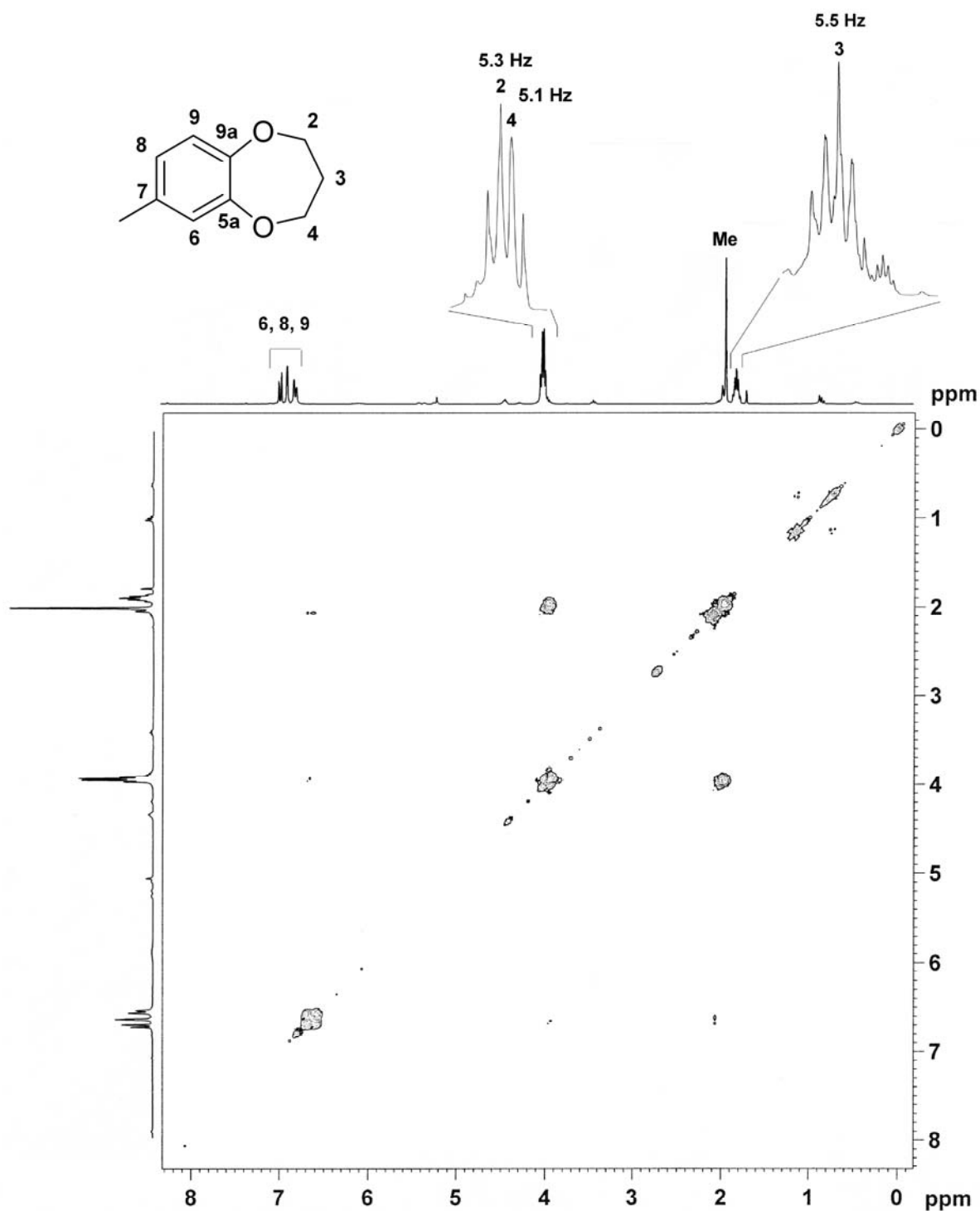
^{1}H,^{13}C HMQC of **69**
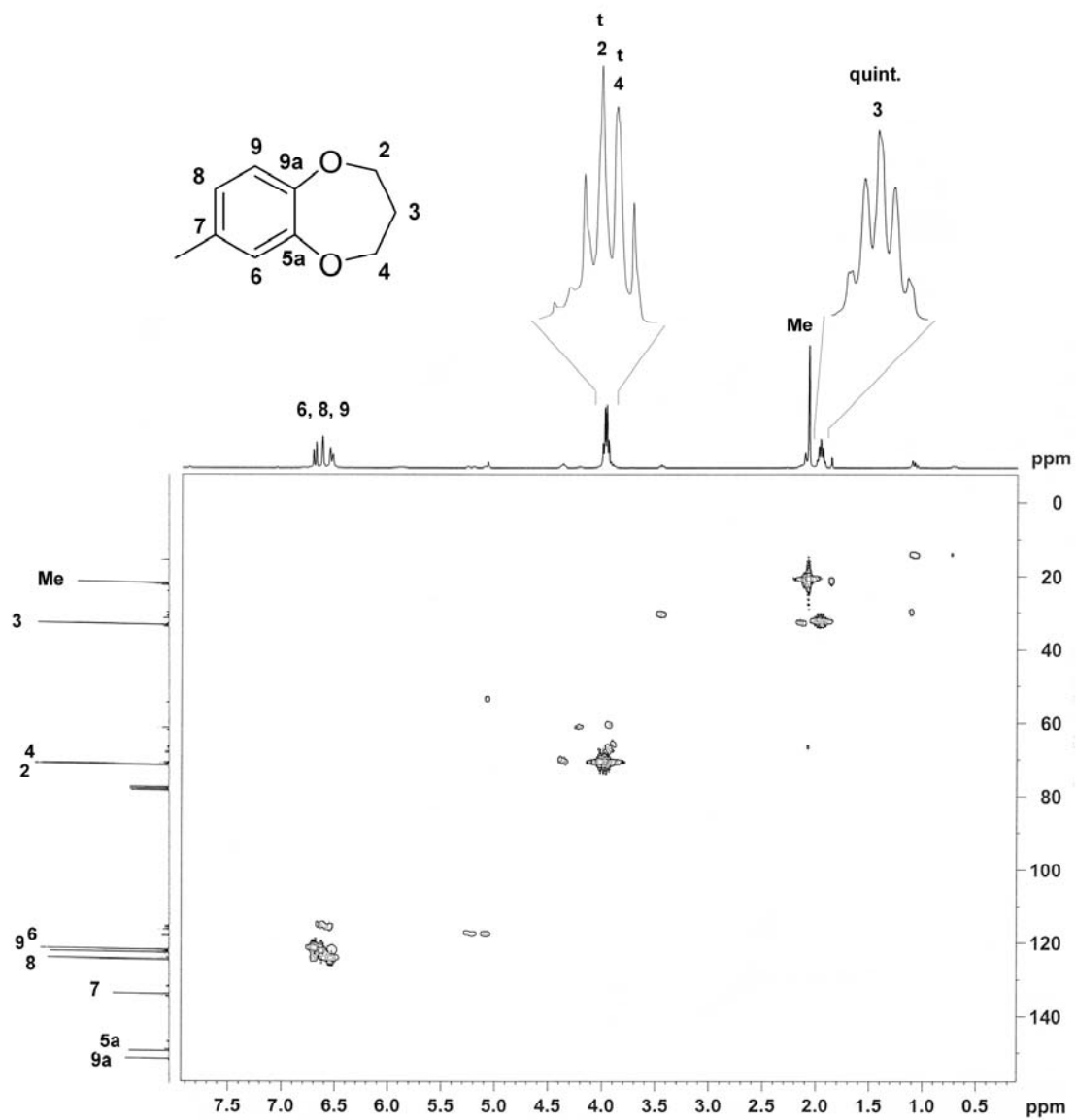
Appendix 20

^{1}H (d$_6$-acetone) and ^{13}C (CDCl$_3$) spectra of **70**

70
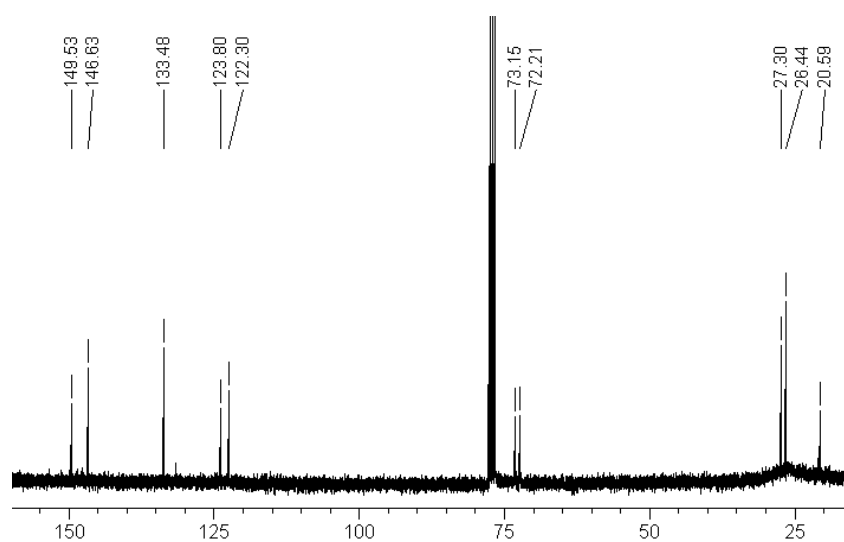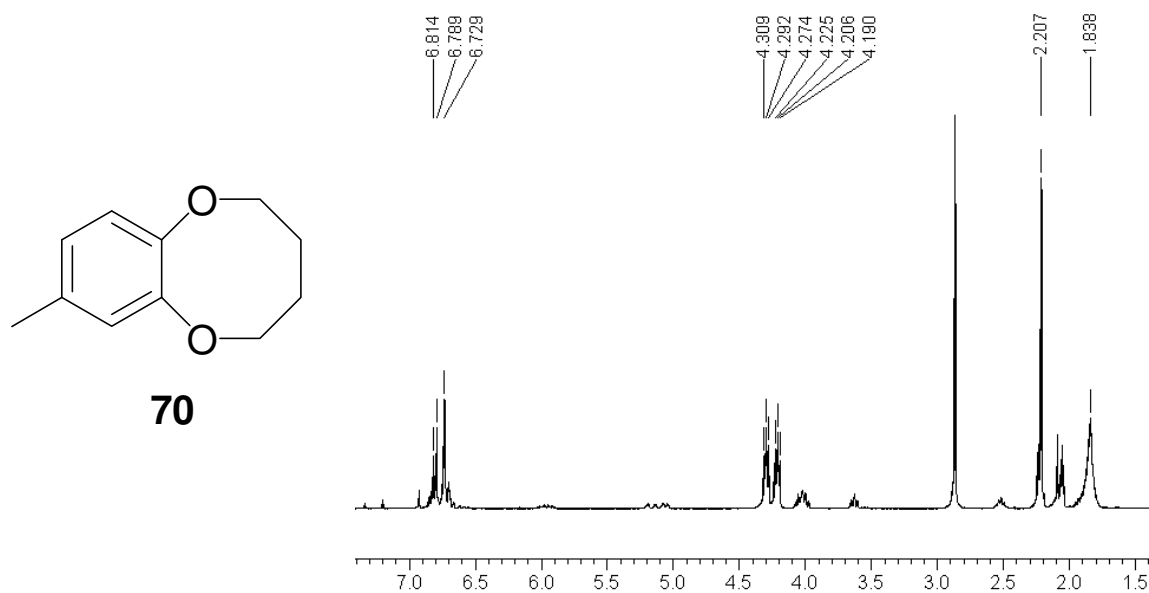
¹H,¹³C HMQC spectrum of **70**
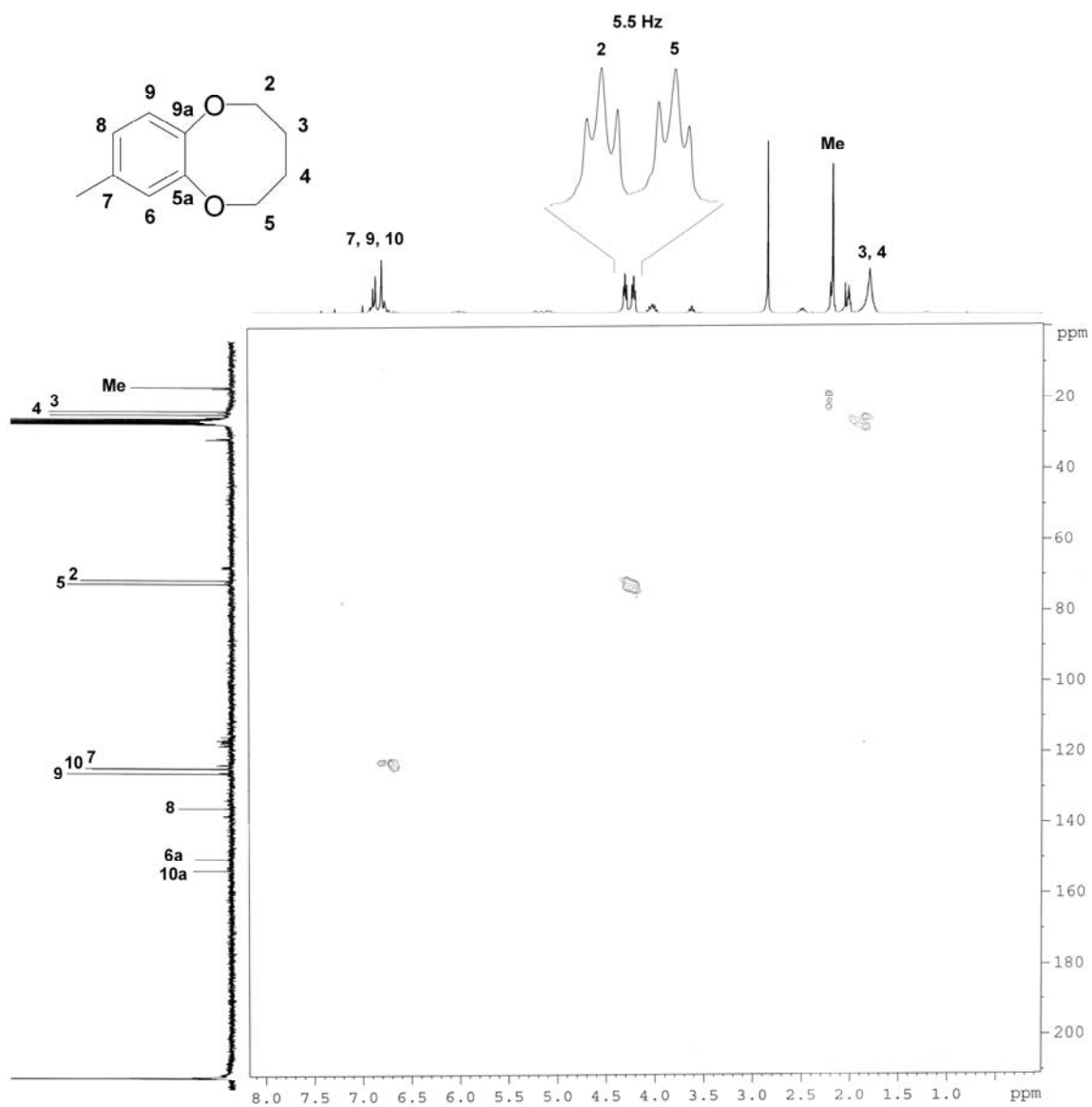
¹H *J*-resolved spectra of **70**
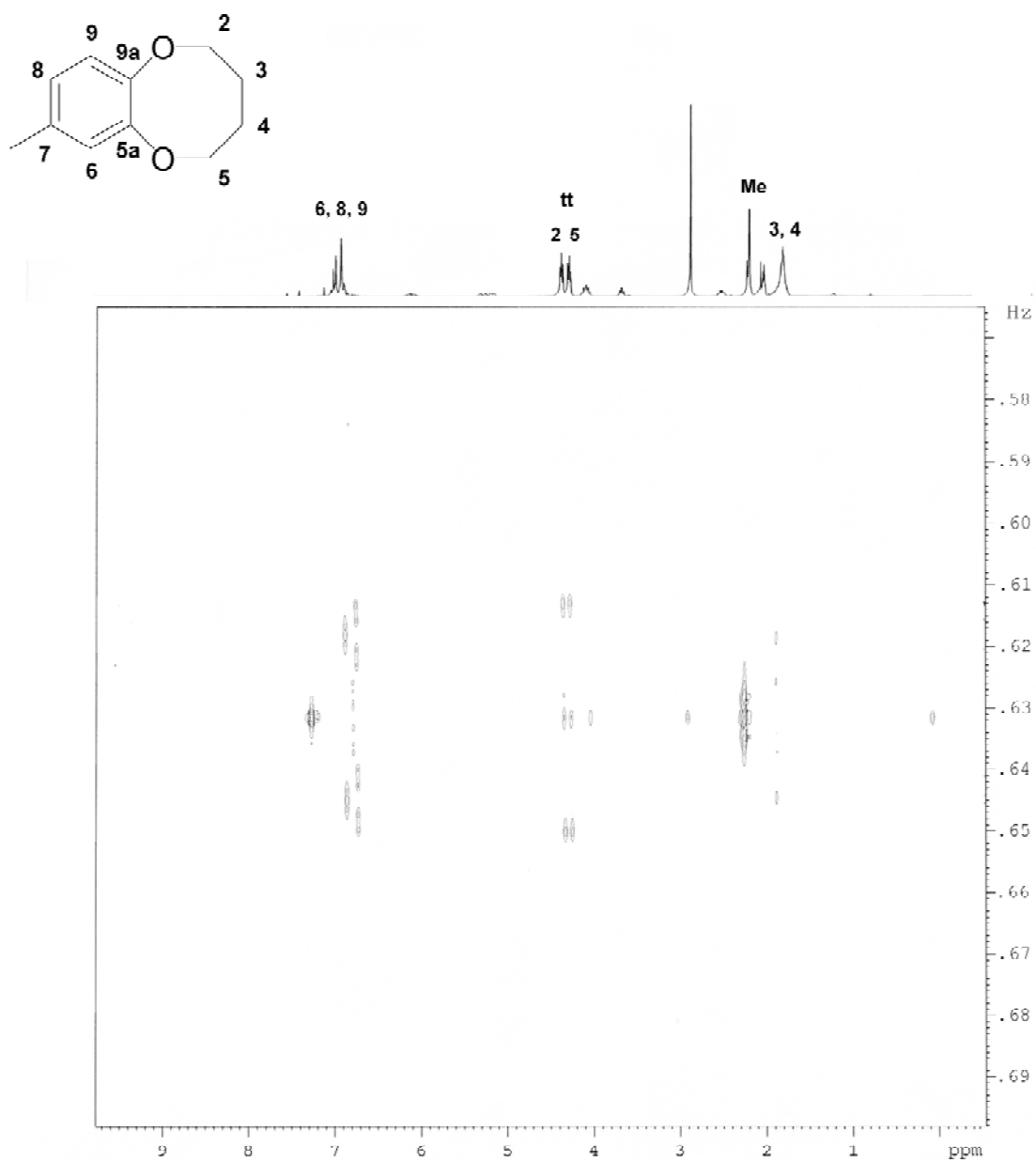
Appendix 21

<superscript>1</superscript>H and <superscript>13</superscript>C spectra of **71**
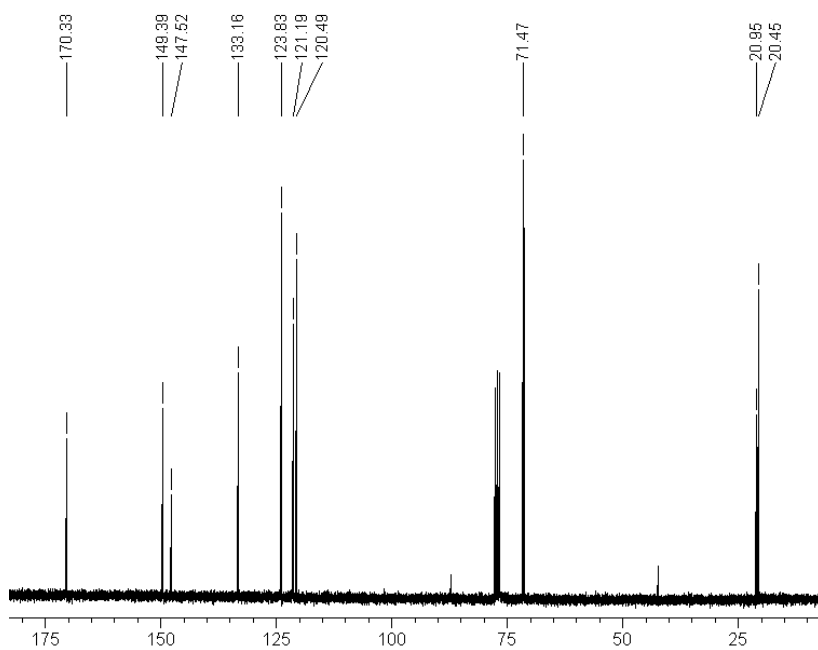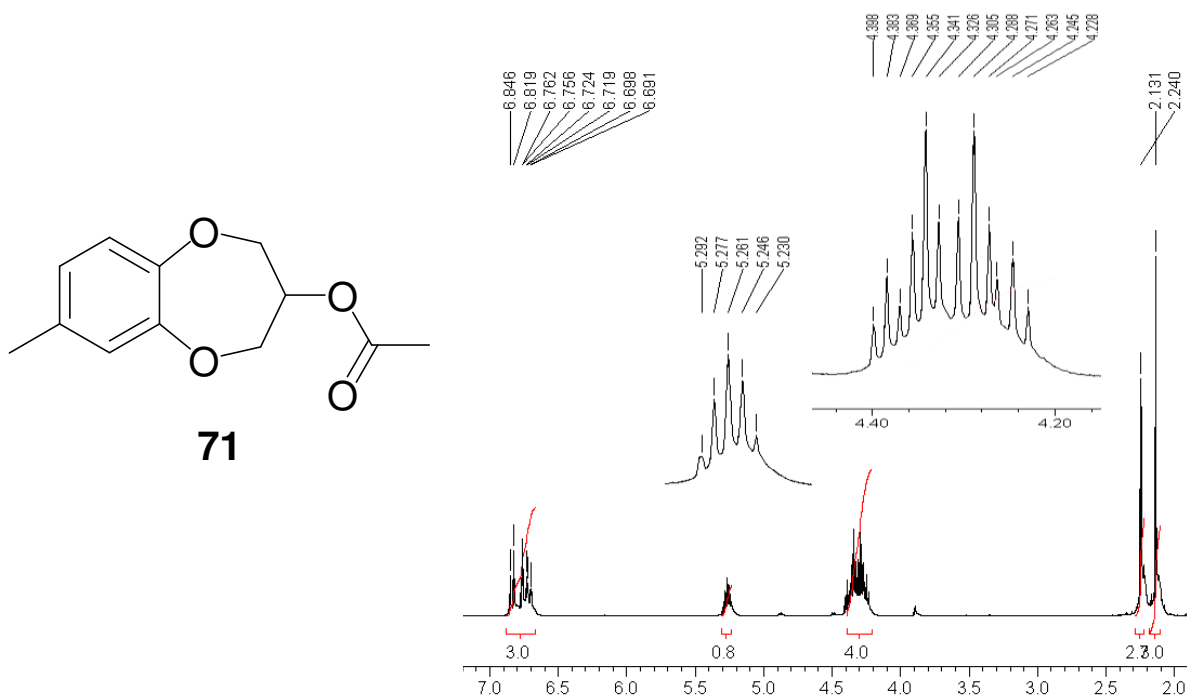
COSY spectrum of **71**
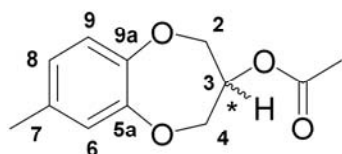
3   5.1, 4.3 Hz

2_A, 2_B 12.8, 4.3 Hz

4_A, 4_B 12.8, 5.1 Hz
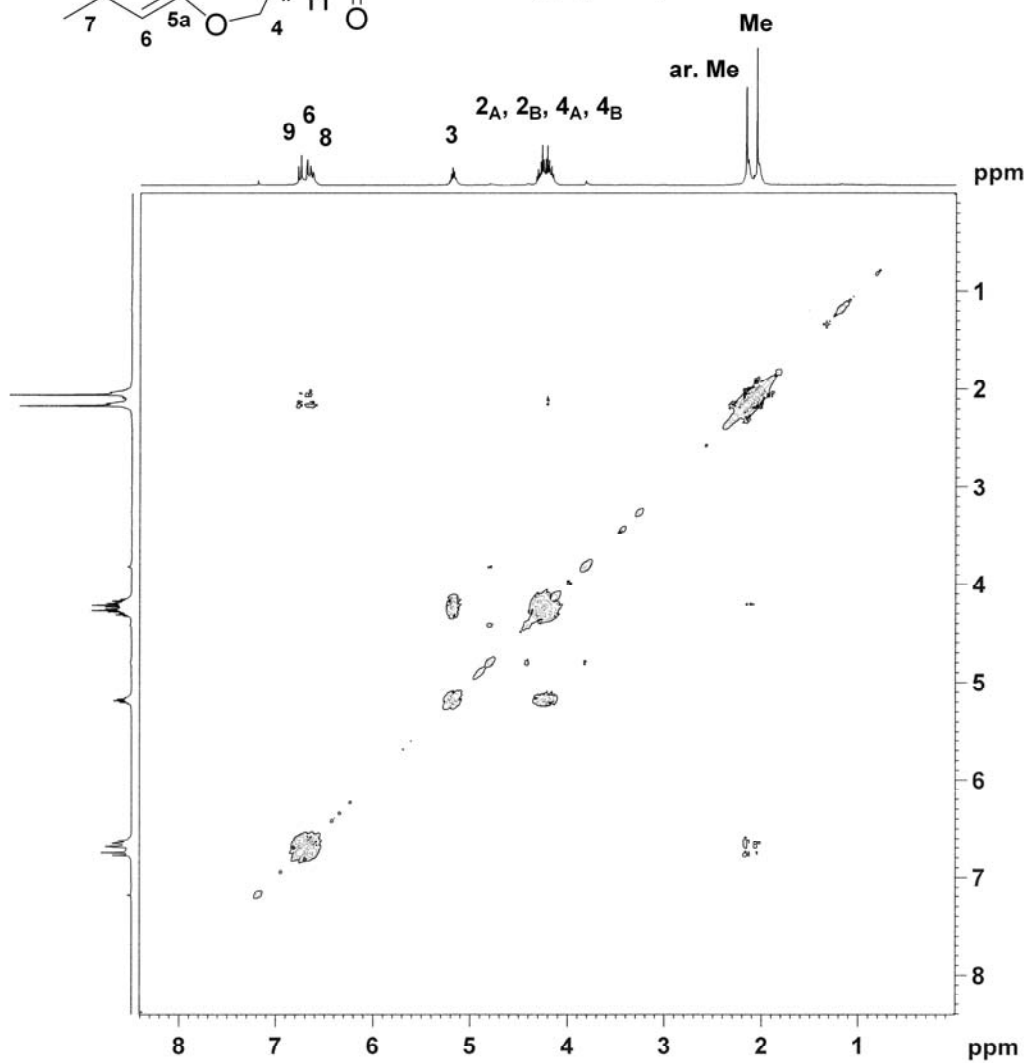
# ^{1}H,^{13}C HMQC spectrum of **71**
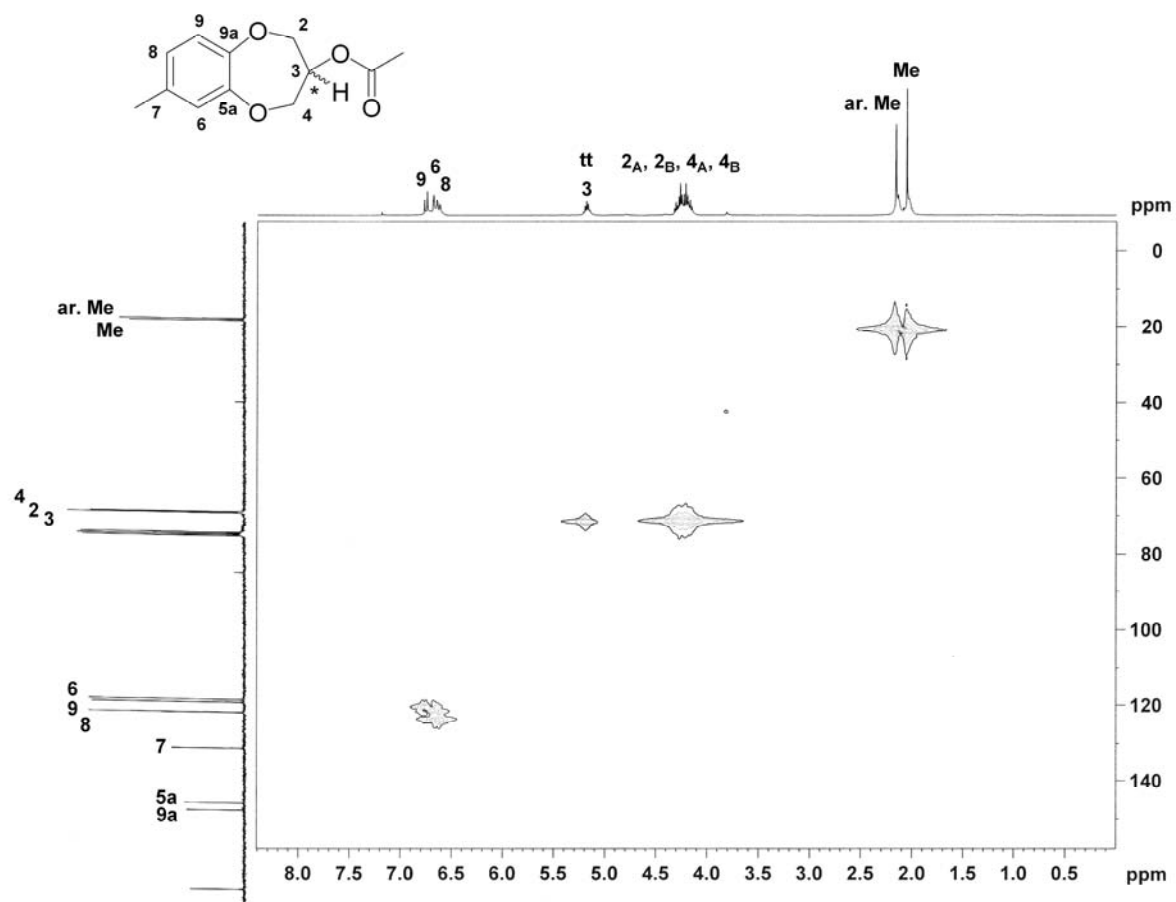
Appendix 22

^{1}H and ^{13}C NMR spectra of **72**

72
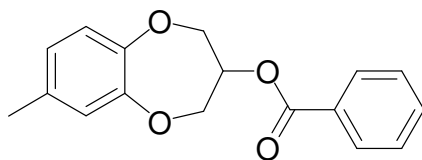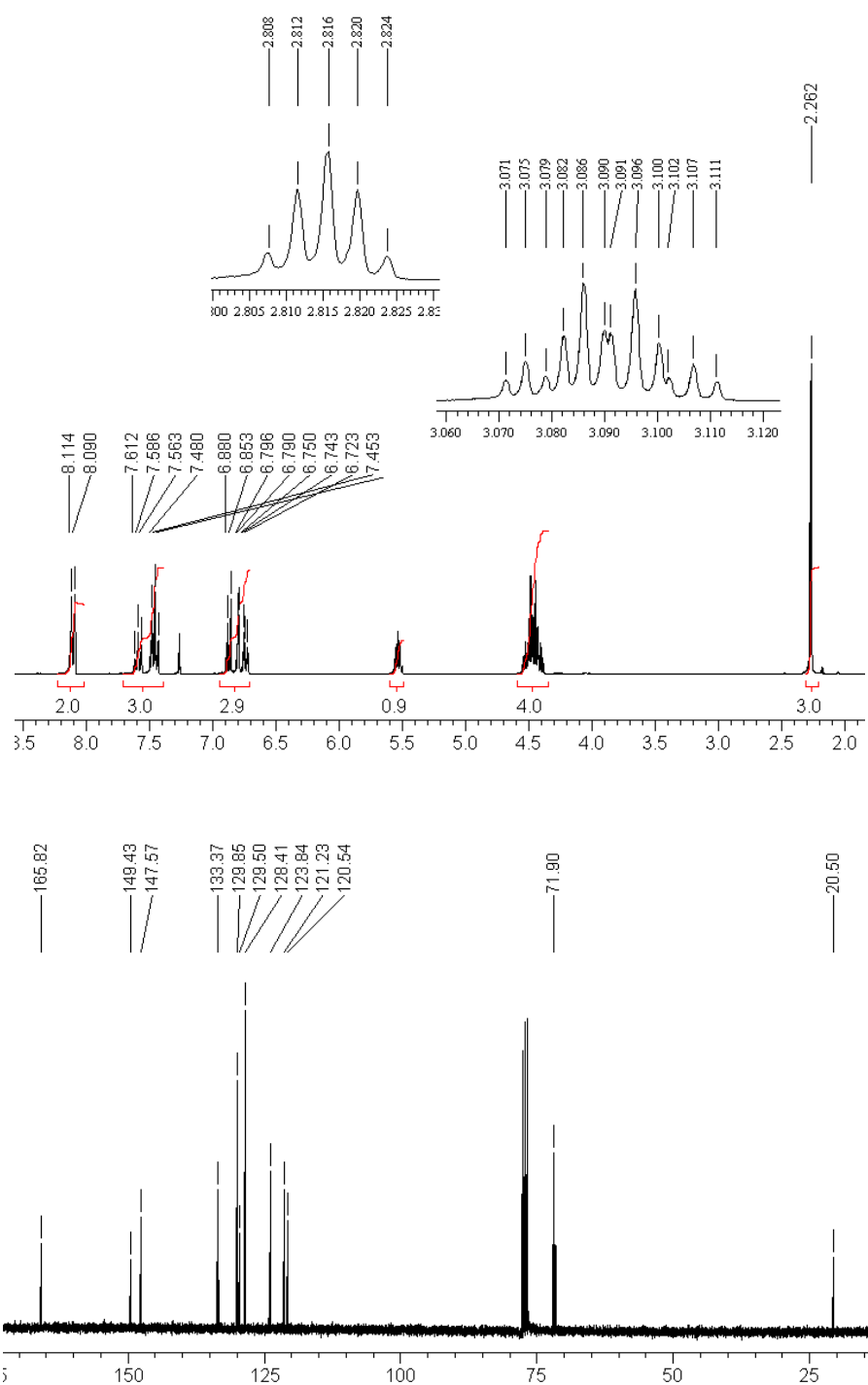
EI mass spectrum and COSY of **72**

3 5.1, 4.3 Hz
2$_A$, 2$_B$ 12.8, 4.3 Hz
4$_A$, 4$_B$ 12.8, 5.1 Hz
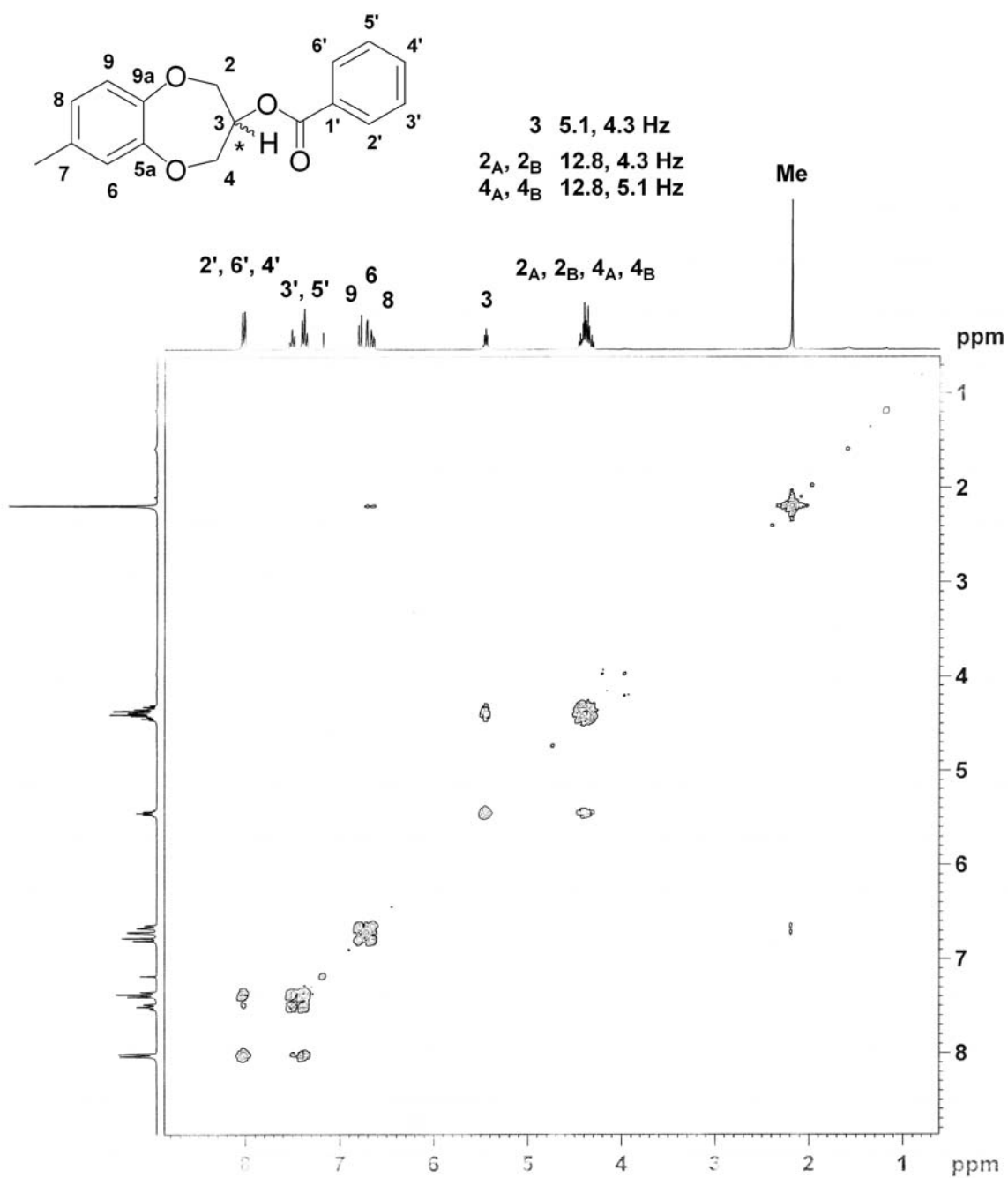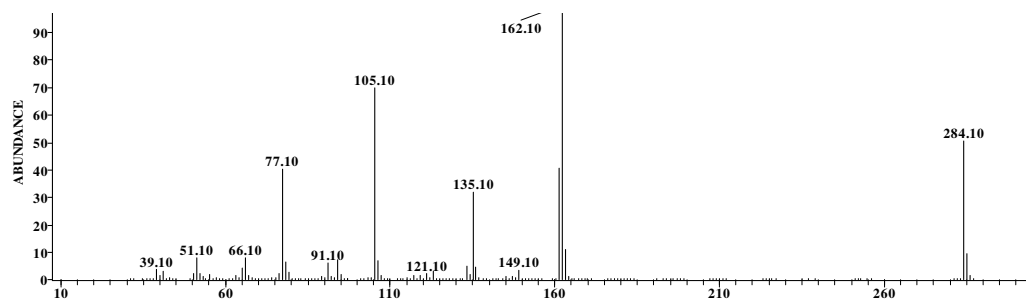
^{1}H,^{13}C HMQC spectrum of **72**
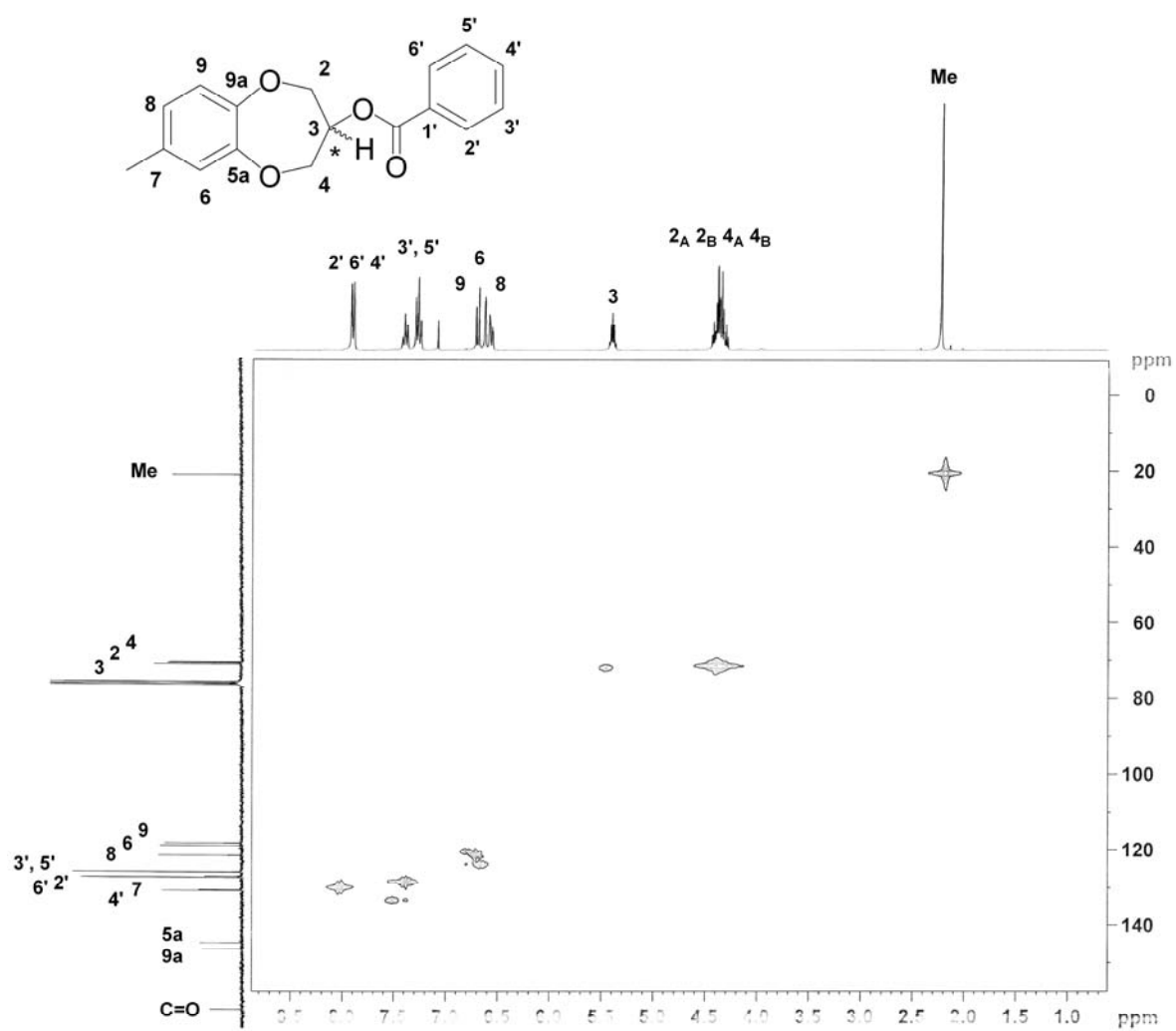
Appendix 23

^{1}H and ^{13}C spectra of **73**

73

^{1}H *J*-resolved spectrum of **73**

2'	17.3, 10.4 Hz
3$_{A'\,trans}$	17.3 Hz
3$_{B'\,cis}$	10.4 Hz
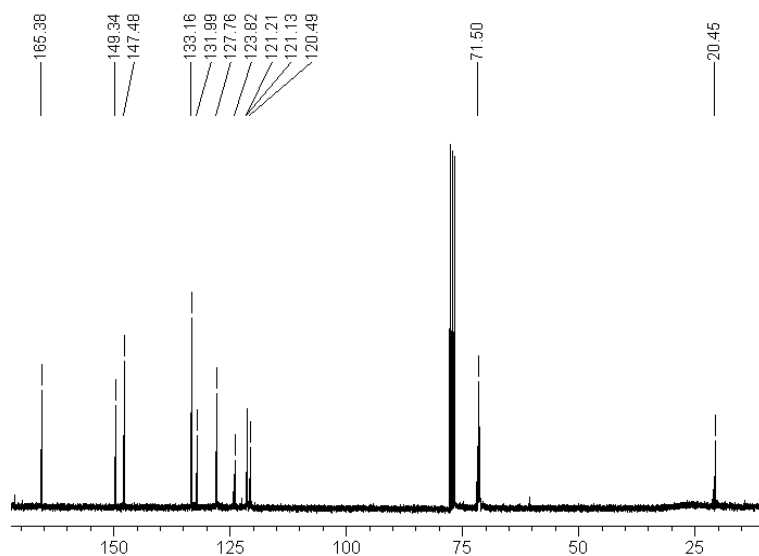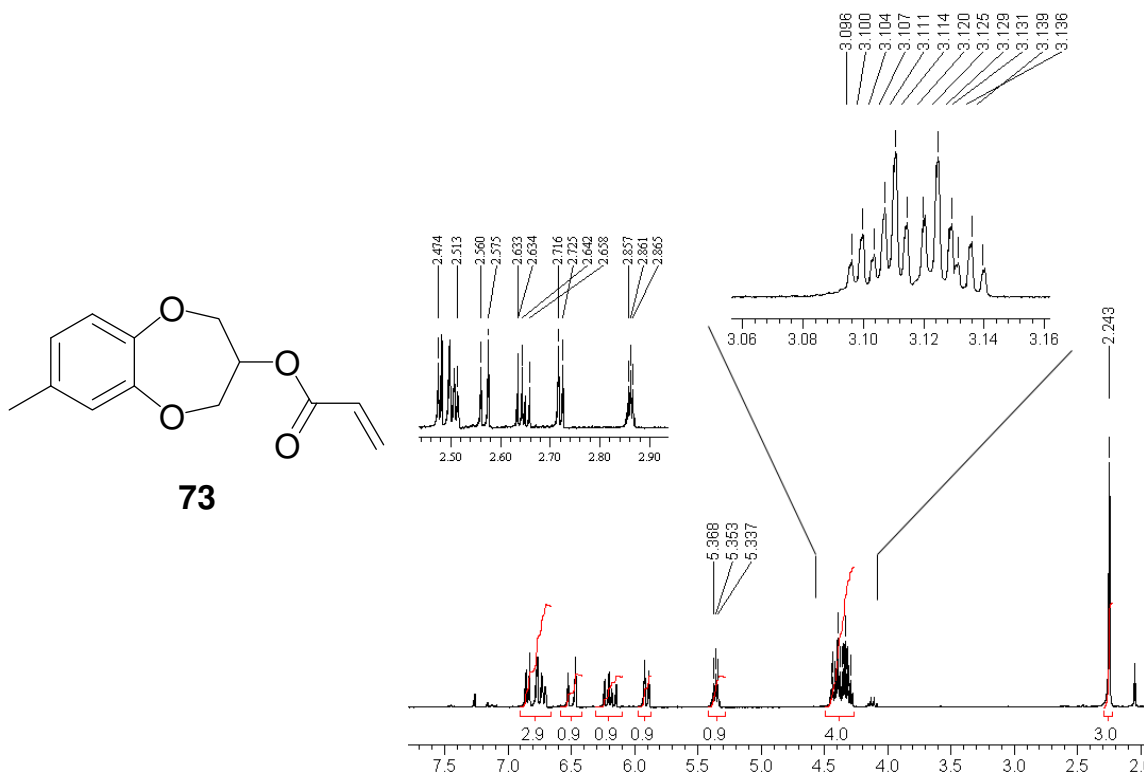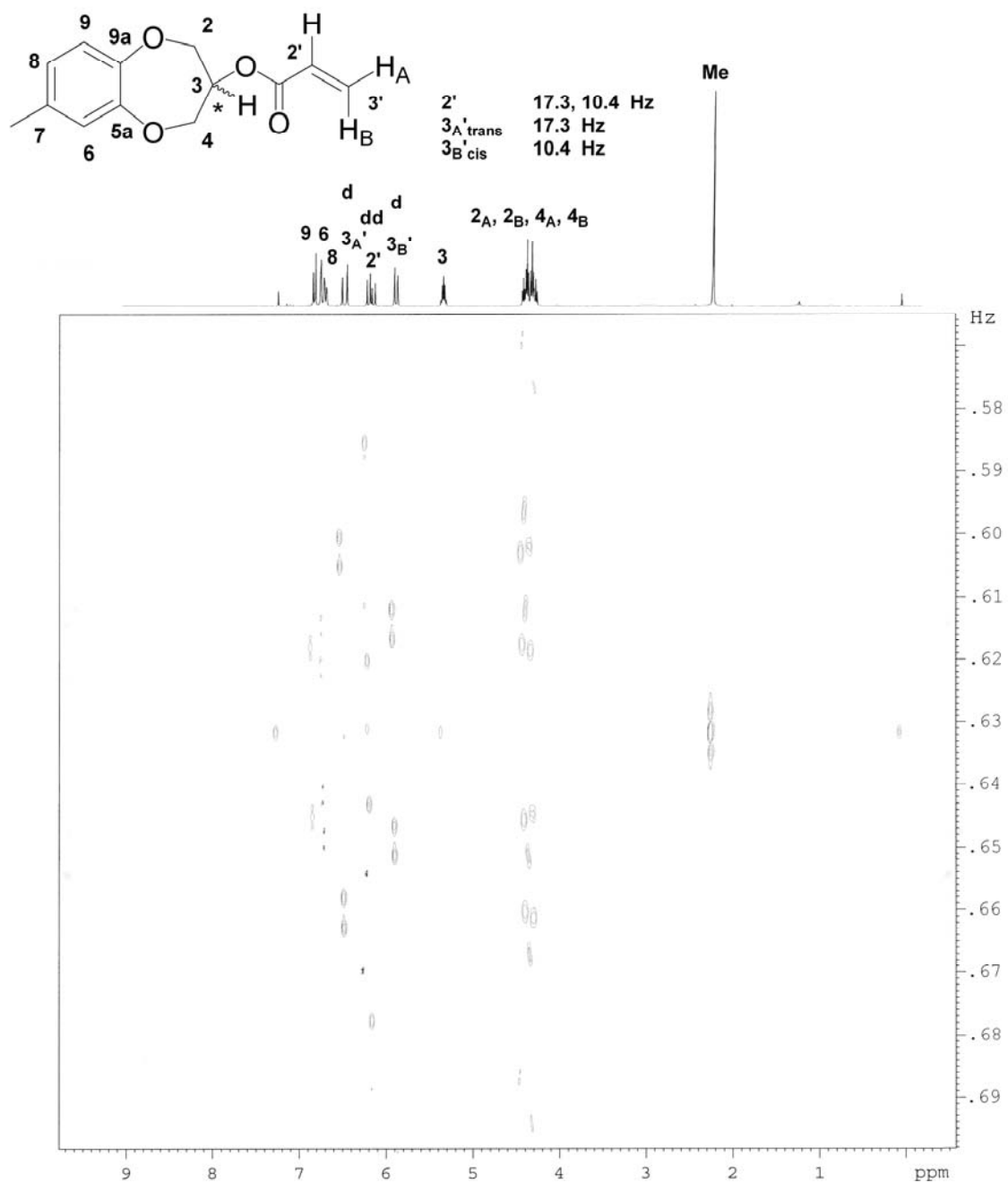
DEPT135 spectrum of **73**
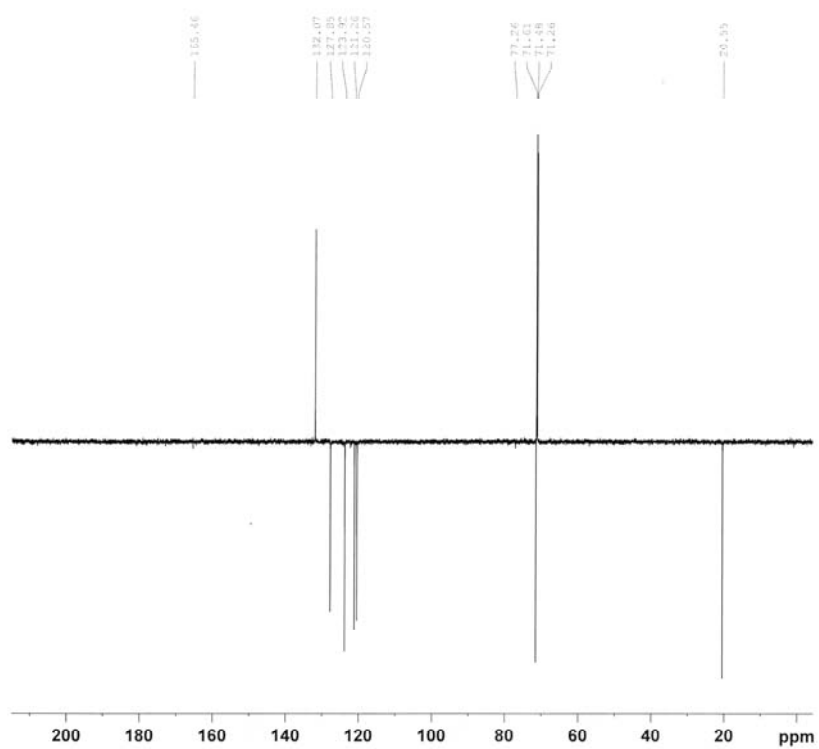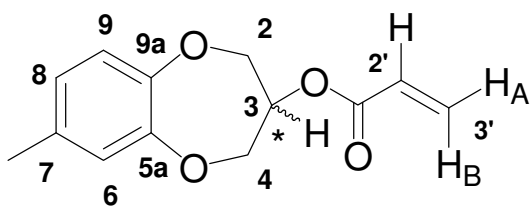
Appendix 24

¹H and ¹³C spectra of **74**
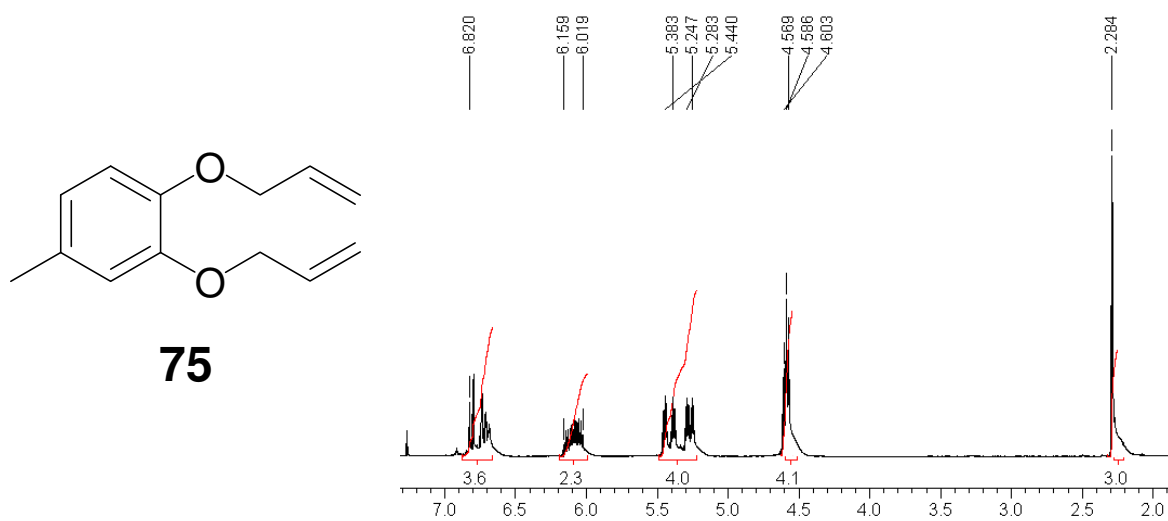

74
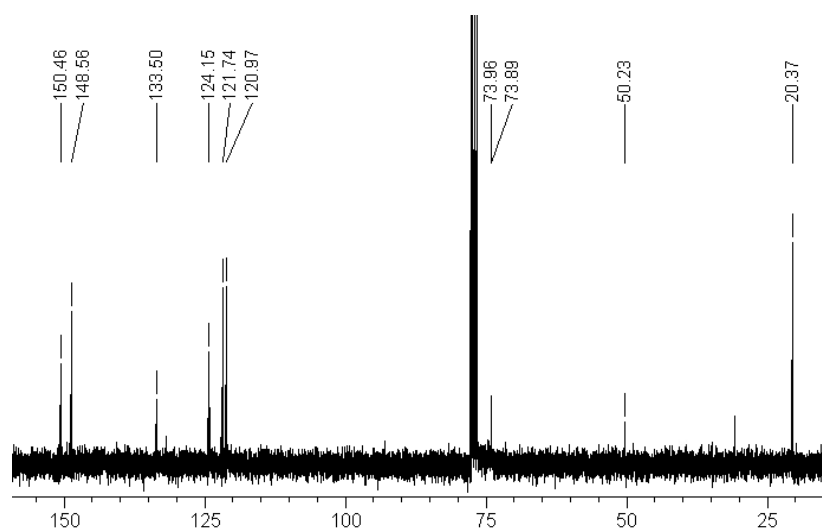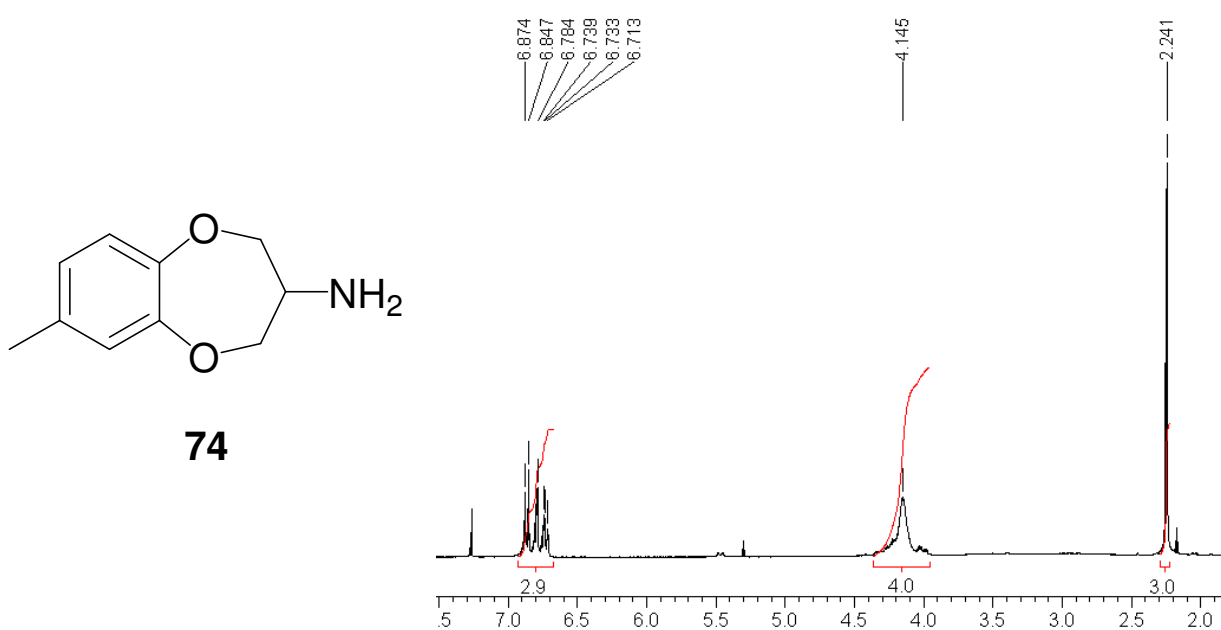
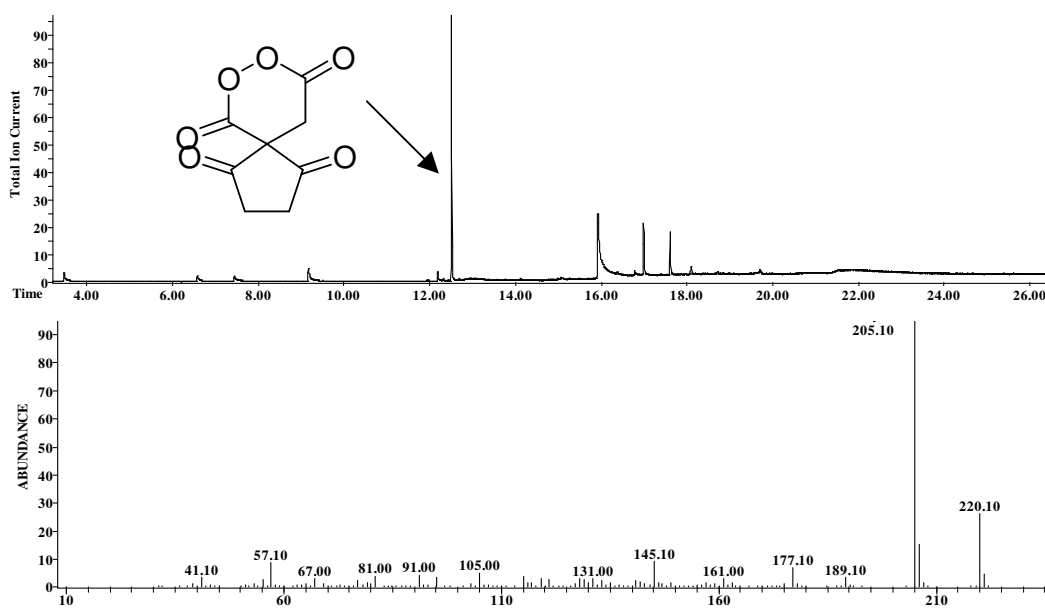¹H *J*-resolved spectrum of **74**
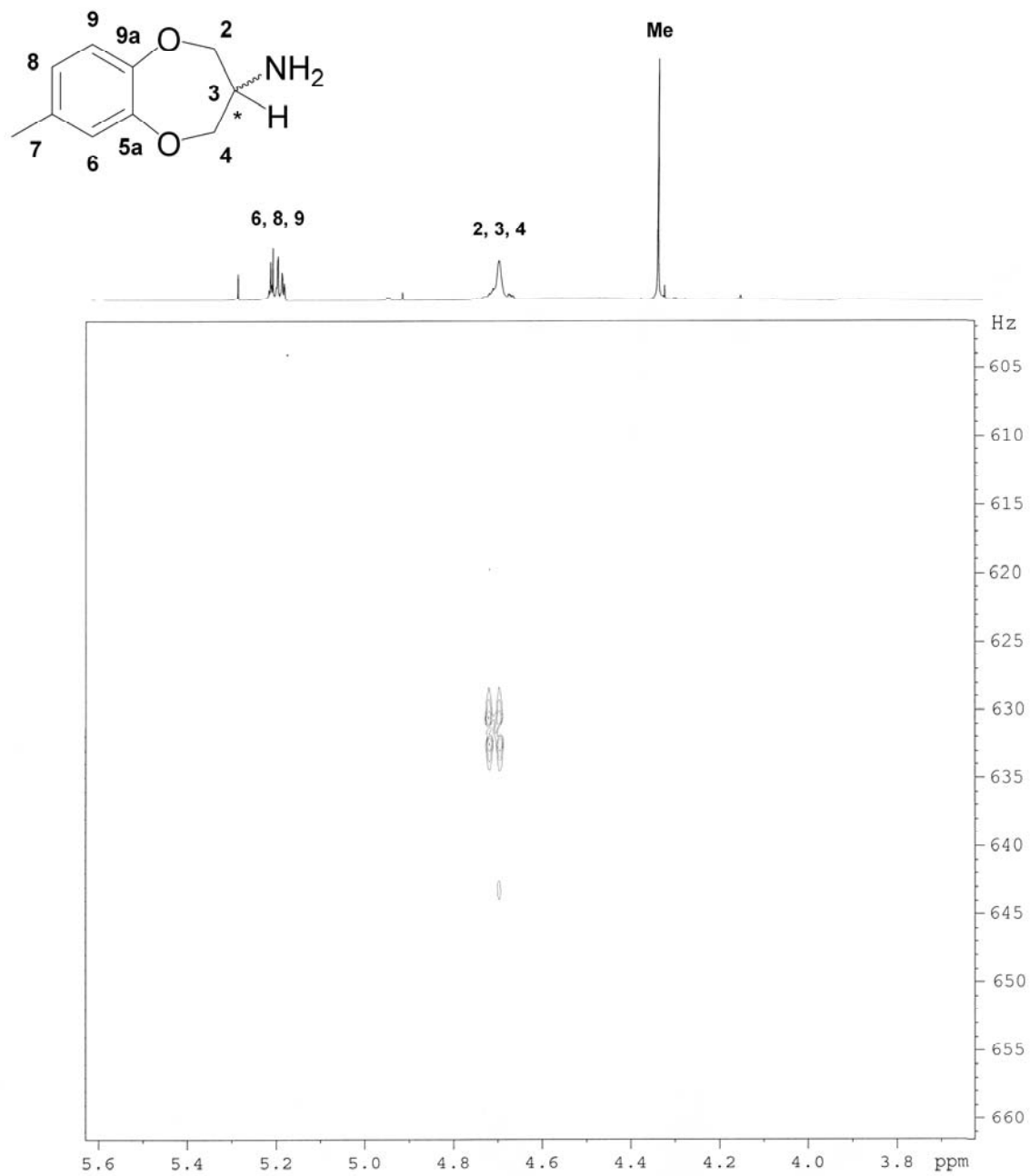
Appendix 25

^{1}H and ^{13}C spectra of **75**
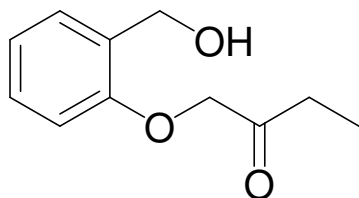
75
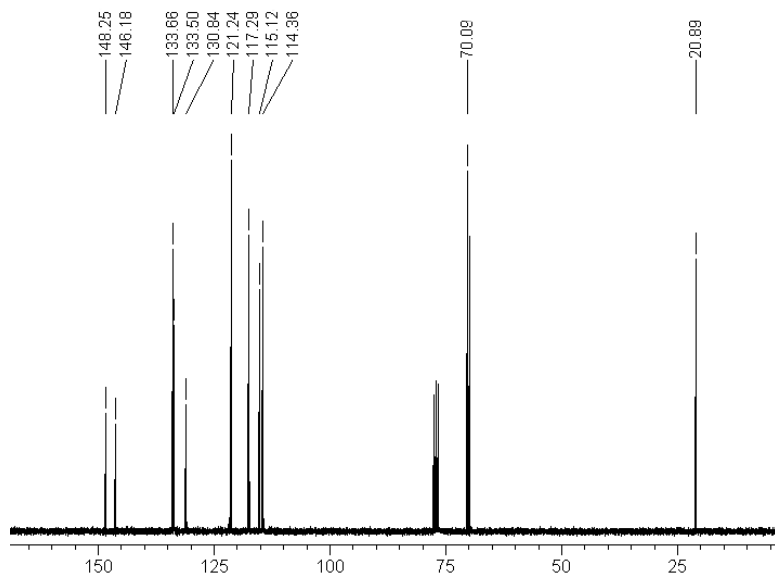
Appendix 26

Quadrupole GC-MS of disuccinoyl peroxide (7,8-dioxaspiro[4.5]decane-1,4,6,9-tetrone (**93**)

Appendix 27

¹H and ¹³C NMR spectra of ethyl 2-[2-(hydroxymethyl)phenoxy]acetate (**97**)

97